Underground Reservoirs: Fluid Production and Injection
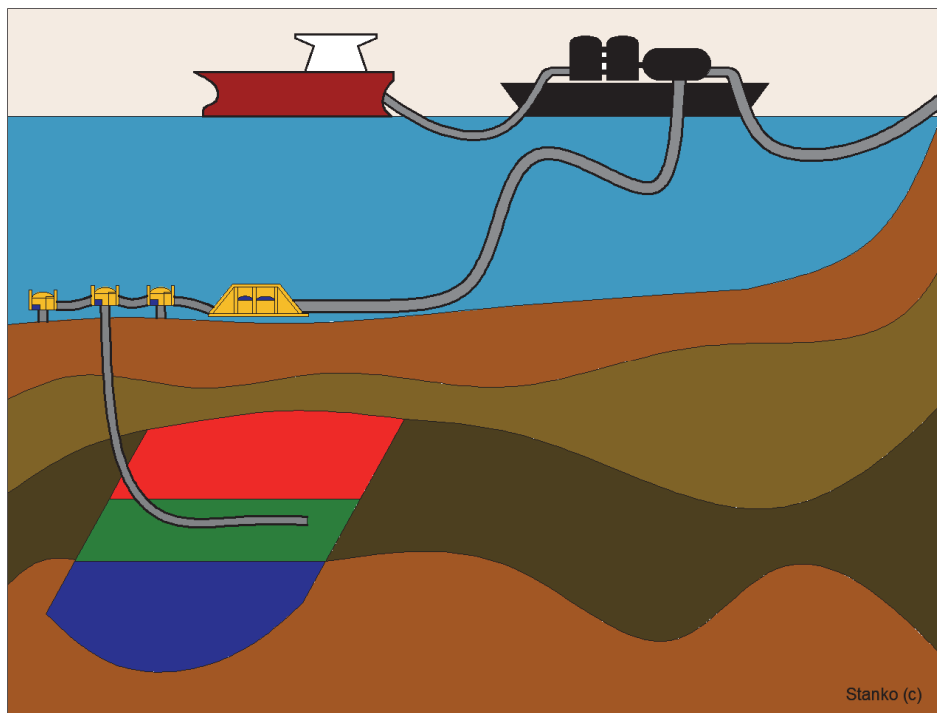
Stanko (c)

Compendium

Prof. Milan Stanko

PREFACE

These notes address, hopefully in a simple manner, a variety of topics on production performance of oil and gas fields.

The notes are given as compendium for the master-level courses Field Development and Operations (TPG4230) and Production Wells (TPG4245) taught at the Department of Geoscience and Petroleum of the Norwegian University of Science and Technology (NTNU) in Trondheim, Norway. The course TPG4230 was designed in 2007 by Prof. Michael Golan and teaches and integrates a variety of multi-disciplinary petroleum engineering topics used in the development and management of hydrocarbon reservoirs and fields.

The lectures of the courses are video-recorded and are available on my YouTube channel, under the following link[1]. Each lecture has in the description links to my handwritten notes and exercise class files that were discussed. The videos of the production wells course are available in this link[2].

These notes will be updated often, and more material will be added with time. Be aware that references might be incomplete. If you have any comments or find errors, I appreciate you sending me an email at milan.stanko(at)ntnu.no. Equation usage is intentionally reduced to a minimum as expressions are usually provided in class or are available in other sources.

I appreciate and acknowledge the contribution, corrections, time and support of Prof. Michael Golan and Prof. Curtis H. Whitson. Many of the ideas presented in the document are based on their work and their way of thinking.

I appreciate the help and contributions of Ruben Ensalzado regarding document formatting, editing, re-writing numerous equations and general quality control.

Prof. Milan Stanko

---

[1] https://www.youtube.com/channel/UCWMfsCe1NQMgx4UZWrVvFgA

[2] https://www.youtube.com/playlist?list=PLXfmJjG2tXbpjx6bezD4famP9YtVFEXqw

CONTENTS

LIST OF FIGURES

1. FIELD PERFORMANCE

The flow interaction between reservoir and production system defines the most important output of an oil and gas asset: the production profile (the produced flow rates of oil or gas with time). The production profile is one of the most important performance indicators of a field as it defines the revenue profile thus allowing to compute the economic value of the asset.

The production profile is typically computed and predicted using analytical or numerical models (e.g. simulators) that represent accurately the reservoir and production system. The fundamental idea is to produce several times a "virtual field" testing different alternatives (e.g. production strategies, enhanced recovery methods, etc.) to determine which one provides the best economic value. Once the best alternative is determined, the production strategy is executed on the real asset.

This analysis is usually performed multiple times both during the field design phase and in the operational phase. In the field design phase, the main goal is to compare different production and development strategies and architectures. The numerical models are not yet fully defined and there are lot of uncertainties in the input data. For an existing asset, it is usually used to foresee future problems, to evaluate the implementation of Improved Oil Recovery (IOR) methods, drilling additional wells, among others. The numerical model is very well defined and the historical production data has been used to reduce uncertainties in the models[3] and improve their predictability.

The two systems (reservoir and production system) are governed by different physical phenomena. However, the field performance is defined by the interaction between them. When seen from the reservoir side, the production system defines the back-pressure acting on the sand-face of the wells. When seen from the production system side, the reservoir defines the amounts of fluids coming into the well and the formation deliverability.

1.1. RESERVOIR

The reservoir is a heterogeneous porous media that contains oil, gas and water under pressure and where wells have been drilled and completed. The wellbores are at a pressure lower than reservoir pressure which causes the migration of fluid from the neighboring porous media to the wells. The flow deliverability of the formation depends, among other things, on the pressure at the wellbore, the rock properties, the average reservoir pressure, fluid properties, flow restrictions in the vicinity of the wellbore, extension and shape of the drainage area. The deliverability of the reservoir will be typically reduced with time as fluids are drained from it, the average pressure declines and the distribution and saturation of fluids in the reservoir changes.

A simplistic but useful analogy of a reservoir system is a tank with fluid under pressure inside. The well is a small exit port with a restriction. The average reservoir pressure (i.e. the tank pressure, p_R) drives fluid from the tank to the wellbore (p_{wf}, pressure at the exit). The restriction represents the pressure losses that are generated when the fluid flows through the formation towards the well. When fluid is drained from the tank (formation) the tank pressure (reservoir pressure) is reduced, thus reducing the flow rate that the tank can deliver at a fixed wellbore pressure.

---

[3] Reservoir models are typically history matched to production data. Production system models are typically tuned with pressure, temperature and rate measurements along the production system.
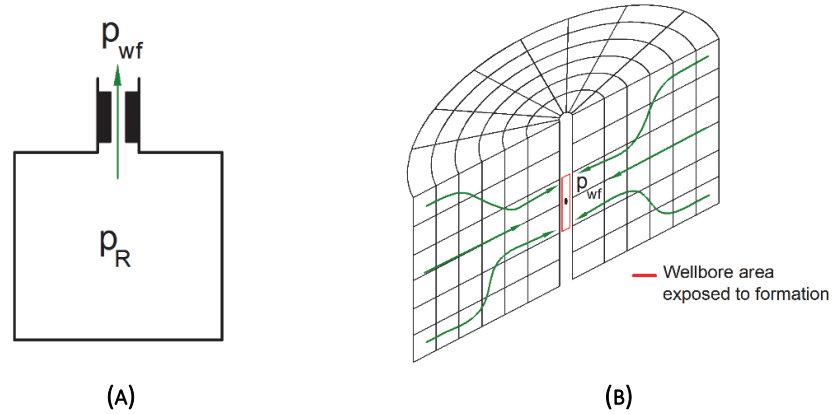
FIGURE 1-1. (A) TANK ANALOGY OF A (B) RESERVOIR SYSTEM

The main time scale of interest for field-life studies is in the range of days-weeks-months-years. Even though there are also short transient events in the scale of hours, minutes and seconds (e.g. when the bottom-hole well conditions are changed suddenly, the well is closed for a period of time due to intervention, etc.) these events are usually ignored. This is because they occur over a short period of time and thus they do not usually affect the overall performance of the field (production, recovery factor, reservoir pressure, etc.).

The depletion performance of the reservoir is typically predicted using three approaches:

· Material balance
· Decline curve analysis
· Reservoir simulation

The second approach will not be discussed in this section.

In material balance, the reservoir is represented by a tank with oil, gas and water under pressure (Figure 1-2). Calculations are executed in a stepwise manner where the amount of oil or gas produced from the reservoir is given as an input and the new saturation of fluids and pressure inside the tank are calculated by applying conservation of mass in the tank. The producing gas oil ratio or water cut of the produced fluids can be predicted using the change of the phase mobilities due to changes in phase saturation.
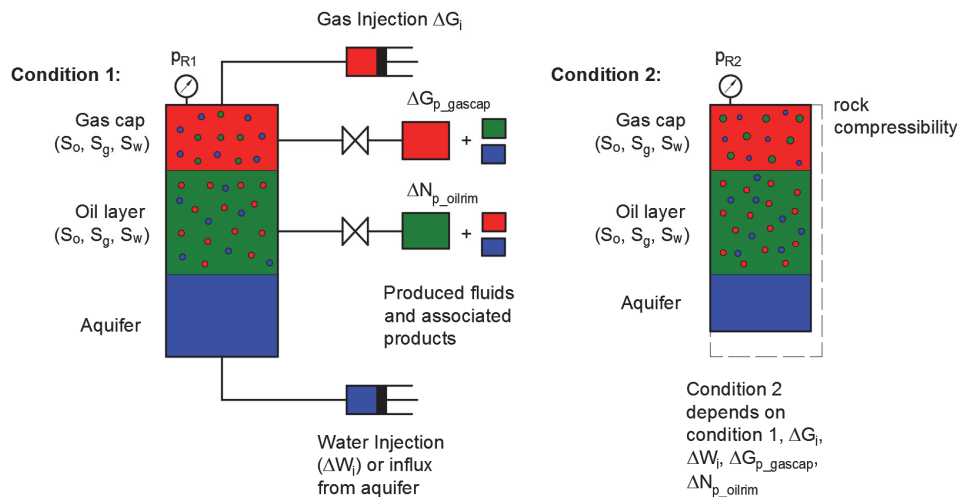
FIGURE 1-2. GRAPHICAL DEPICTION OF THE MATERIAL BALANCE APPROACH

A material balance model requires the oil (or gas) cumulative production as an input and thus cannot be used to predict the production output of the reservoir with time. For that purpose, an additional model must be provided to quantify the pressure drop between reservoir and a downstream condition (e.g. bottom-hole pressure). This model is often an Inflow Performance Relationship curve.

A reservoir simulator is used when it is important to consider the spatial (2D or 3D) variation of properties (e.g. pressure, saturation) in the reservoir with time. The reservoir model consists of a numerical discretization of the porous media where mass conservation is applied in every sub-volume. The flow between cells is described using an expression for pressure drop in porous media (e.g. Darcy's Law). Pressure or rate boundary conditions are applied on the cells where the wells are, and no flow conditions are typically applied at the outer edges of the reservoir.

The model uses as input the initial distribution of pressure, porosities, permeabilities, fluid saturations, and it computes the time evolution of pressure, oil, gas and water saturation. The simulation is controlled with both a target rate and a minimum pressure at the well boundaries provided at each time step. The computation is carried out in a stepwise manner, outputting results for pre-specified time intervals.

During the solving process, the minimum pressure given is imposed on the well boundary. If the rate computed is higher than the target rate specified, then the target rate is feasible. A series of iterations are then made trying several pressure values until one value is found that gives exactly the target rate specified. On the other hand, if the rate obtained is below the target rate, the target rate is not feasible, and the well boundary condition is the minimum pressure.

Depending on the complexity of the field, in some cases it is possible to use only the reservoir simulator to predict its performance and neglect the rest of the production system. For example, in a field where each well is producing to its own separator close to the wellhead, including tubing pressure drop tables in a reservoir model provides an exact approximation of the field performance.

In reservoir simulation, the grid does not typically capture the near-wellbore region in detail. The well usually traverses through several blocks and the block size is much bigger than the wellbore radius. In consequence, an IPR-like equation (often called well index or WI) must be used; this equation relates the formation oil, water and gas with the pressure difference between the block where the well is placed and the wellbore pressure.

1.2. PRODUCTION SYSTEM (SURFACE NETWORK)

The production system is the assembly of wells, pipes, valves, pumps, meters that have the function of transporting fluids from the reservoir to the processing facilities in a controlled manner. When the fluid travels from the reservoir(s) (source) to the separator(s) (sink), it must overcome energy losses (e.g. pressure and temperature drop) and sometimes "compete" with other fluids in transportation conduits.

In contrast with the reservoir, the field-life analysis of a production system is performed assuming that changes in reservoir deliverability are slow enough so that the system progresses continuously from one steady-state to another. Therefore, the analysis is usually performed at a given point in time, ignoring all past and all present conditions and using only the **current** deliverability of the reservoir. Other possible quick transients such as slugging, intermittent production, etc. are not part of the scope of a field-life analysis.

In models of the production system, the well inflow at a particular time "t" is usually represented by an IPR equation (Inflow performance relationship, see Figure 1-3 for some examples). The IPR is typically a smooth, monotonic, downwards curve that provides the bottom-hole pressure that must be applied at the sand face to deliver a specific standard condition flow rate. This approach is usually a good approximation to reservoir deliverability.

IPR for undersaturated oil	IPR for saturated oil/gas
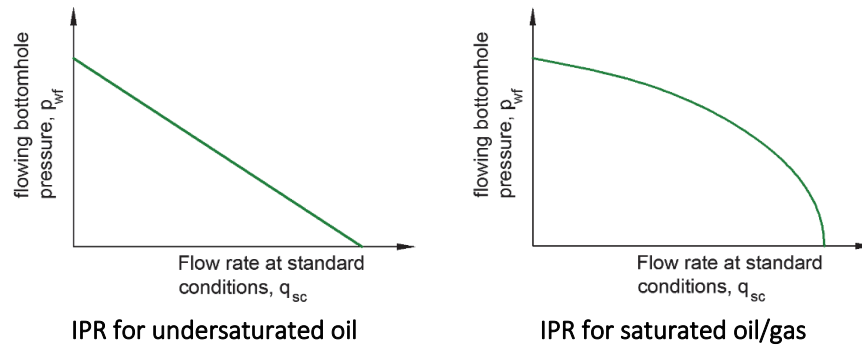
FIGURE 1-3. IPR CURVE

The IPR curves come typically from recent well tests, by using analytical equations together with limited field data, or generated by a reservoir simulator.

The produced rates, pressures and temperatures at time "t" are calculated by performing a flow equilibrium calculation in the production system. This involves solving simultaneously mass, momentum and energy conservation equations for all elements in the system (conduits, flowlines, pipelines, valves, pumps, etc). Pipelines are typically discretized in segments. The boundary conditions upstream are the IPRs, (i.e. the wells' inflows) and downstream the pressure(s) of the separator(s).

When there is adjustable equipment in the production system (e.g. adjustable chokes, pumps, gas lift injection) there is usually a variety of "feasible" equilibrium rates that the system can produce. For example, in a system with a choked well, the rate of the well can vary depending if the choke is fully open, fully closed or something in between. If the well has an electric submersible pump (ESP) then a variety of operational rates can be achieved by changing the pump rotational speed.

1.3. COUPLING RESERVOIR MODELS AND MODELS OF THE PRODUCTION SYSTEM

As mentioned earlier, the production profile of the field should be computed considering the interaction between the reservoir and production system. Figure 1-4 shows a possible way to couple a material balance (MB) model of the reservoir with a model of the production system to obtain the production profile of the field.
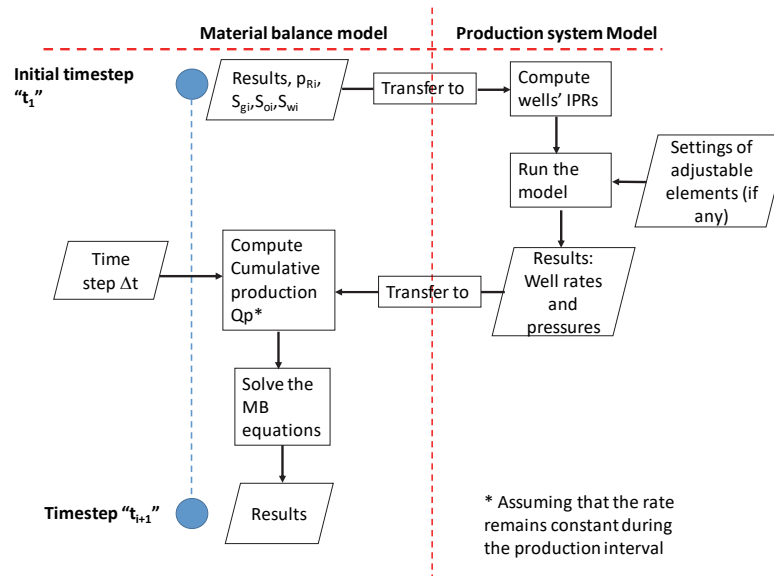
FIGURE 1-4. TIME STEP OF AN EXPLICIT COUPLING SCHEME BETWEEN A MATERIAL BALANCE MODEL AND A MODEL OF THE PRODUCTION SYSTEM TO PREDICT PRODUCTION PROFILE

Since the model of the production system is steady-state, the changes associated with reservoir depletion are introduced by modifying the IPRs in every time step (based on the output from the reservoir model). In this particular case, the IPR is recalculated in every time step using the reservoir pressure and the mobility of the oil and gas phases (calculating relative permeability from the saturation).

When using a reservoir simulation model, the IPR curves are often generated by the reservoir simulator and transferred to the network model. An example of this methodology is shown in Figure 1-5.
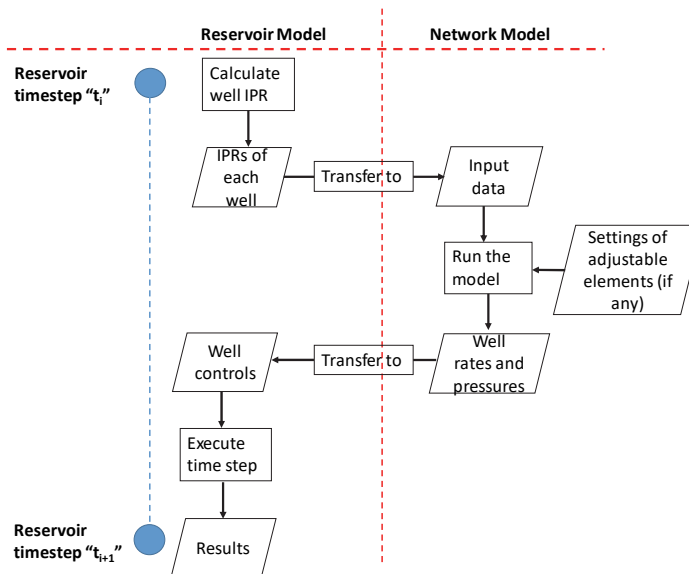
FIGURE 1-5. EXPLICIT COUPLING BETWEEN A RESERVOIR SIMULATION AND A MODEL OF THE PRODUCTION SYSTEM

There are multiple approaches to couple reservoir and production system models. The two approaches discussed before are explicit because, for a given time step, rates are calculated only once in the network model and then imposed in the reservoir model. The rates are then assumed to remain constant during the time interval specified. However, this is seldom the case because of the reduction of reservoir pressure when fluids are produced. A workaround frequently applied to reduce this inaccuracy is to reduce the length of the

time step. Explicit coupling strategies sometimes cause instabilities in the solution (oscillating production rates with time). The reduction of time step length often eliminates this problem.

Explicit coupling strategies are suitable when the models of reservoir and production system are available in two separate computational routines (often black box commercial packages) and are maintained and used separately (e.g. by different departments within the company). An explicit coupling minimizes the required transfer of information between models in every time step.

Other coupling approaches and a detailed discussion about coupling models or the reservoir and the production system are discussed in detail by Barroux[1-1].

1.4.   PRODUCTION POTENTIAL

For a particular time "t" there will be either a unique rate that the field can produce (if there are no adjustable elements in the system of they have a fixed setting) or a maximum rate that the field can produce (if there are adjustable elements). We will refer to this unique or maximum rate that the field can produce at a given point in time as: "production potential".

For example, if the well has an adjustable choke the maximum rate is most likely achieved when the choke is fully open. If the well has an electric submersible pump (ESP) then the maximum rate is probably achieved when the pump rotational speed is highest. If adjustable elements are present in the system, it is usually possible to produce any rate lower than the maximum rate by regulating such elements.

The production potential is different from the "well potential" variable printed in every time step by the reservoir simulator. The well potential is the producing rate obtained when the minimum bottom-hole pressure is applied on the well boundary.

To illustrate how these two concepts are different, consider a single well system in which wellhead pressure is kept constant. The well potential of the reservoir simulator is estimated using a constant bottom-hole pressure as shown in Figure 1-6.b, only taking into account the reservoir deliverability (inflow performance relationship). The production potential is calculated by performing a hydraulic equilibrium calculation at the bottom-hole intersecting the IPR and tubing performance relationship (TPR) shown in Figure 1-6a. These two values will be equal only when the minimum bottom-hole pressure specified equals the equilibrium bottom-hole pressure (in the fig. when $p_R = p_{R3}$). For the other IPRs however, the production potential is over-predicted.
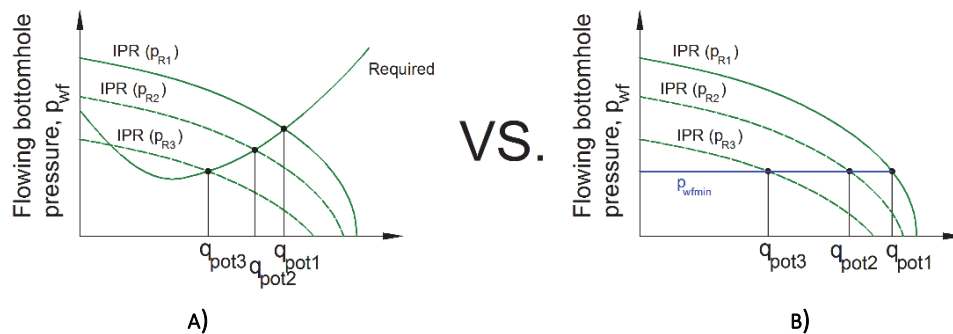
FIGURE 1-6. (B) WELL POTENTIAL CALCULATION VS. (A) PRODUCTION POTENTIAL CALCULATION

As time progresses, the production potential of the production system will also change, mainly due to two types of changes: changes in the inflow (IPR) and changes to the production system.

A strategy commonly used in reservoir management when producing the field in plateau mode is to allocate production to individual wells using their potential. At a given time, the well and field potential are calculated, and well split factor are computed by dividing the individual well production potential by the field production potential. Then, the rate to be produced by each well is calculated by multiplying the field plateau rate by the individual well split factor.

In a producing field, the reservoir deliverability follows a trend with depletion similar to reservoir pressure, i.e. is reduced with time. This is not only due to reservoir pressure decline, but for example, in an oil well, an increase of the well's producing GOR and WC will reduce the oil productivity as well. Changes in reservoir deliverability affect all components of the production system downstream the reservoir, for example if the well producing gas oil ratio (GOR) changes, then pressure losses will change in all downstream conduits.

Some examples of changes to the production system are man-made changes in the pipeline diameter, lowering separator pressure, modification of choke opening, changes in well completion, installation of artificial lift, well stimulation or fracking, etc. Other changes are reduction of the conduits' cross section due to scale deposition, wax deposition, etc. When the modification is abrupt and occurs at one point in time, the production potential will display a discontinuity at the particular cumulative production where the change is introduced (as shown in Figure 1-7).
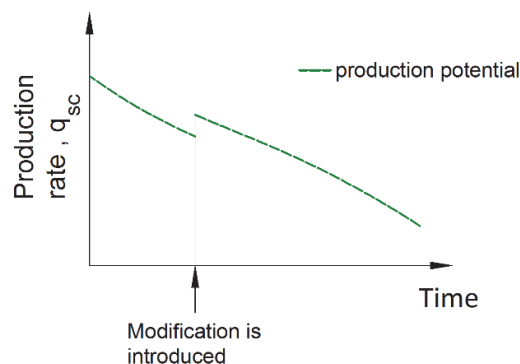
FIGURE 1-7. PRODUCTION POTENTIAL BEHAVIOR VS. TIME WHEN A PRODUCTION ENHANCEMENT MODIFICATION IS PERFORMED IN THE SYSTEM

The decrease in reservoir deliverability causes a decrease in production potential with time. Changes in the production system can increase or decrease the production potential with time, depending on the type of change as explained in the previous paragraph.

1.5. PRODUCTION SCHEDULING

There are two main types of production offtake in a field: period with fixed production rate (plateau mode) or declining production (decline mode). In plateau mode, as the name indicates, the field or well is produced at a constant rate for a given period (lower than the production potential). However, as the production potential is typically reduced with time, there comes a time when the field rate is the same as the production potential. After that moment, the field will not be able to sustain the plateau rate and its production starts to decline (e.g. following the production potential curve). This is shown in Figure 1-8.
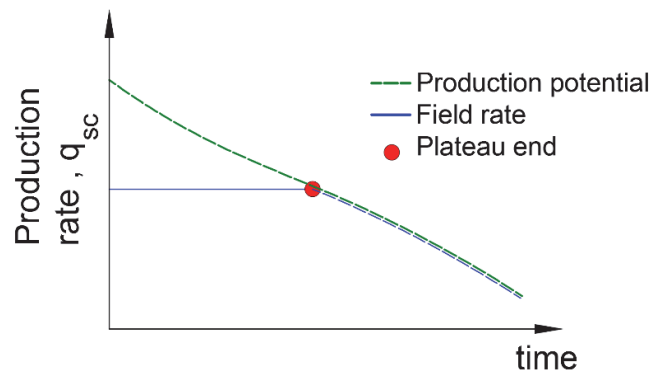
FIGURE 1-8. PLATEAU PRODUCTION MODE

This production mode is typically employed for standalone field developments with dedicated processing facilities or when there are contractual production obligations (e.g. gas contracts). This is usually the outtake strategy that yields the best economic value for the project. Producing more at an early stage (like in decline mode) increases revenue but the CAPEX investment becomes excessive due to the increased size of the processing facilities and offshore structure.

In decline mode, as the name indicates, production rates typically decline with time (as shown in Figure 1-9). In principle, the objective is to produce as much as possible as early as possible (i.e. always produce at the production potential of the system). However, the production rates might be sometimes lower than the production potential but follow a similar decline with time. This may occur for example when there are additional operational constraints that impede reaching the production potential, e.g. maximum flow rate to avoid sand production, gas coning, water coning, maximum drawdown in the formation.

It can also occur when the adjustable equipment is operated at a constant setting or there are non-trivial settings (unknown to the field operator) of the adjustable equipment that yield maximum production (e.g. a particular gas-lift rate that yields optimum oil production).
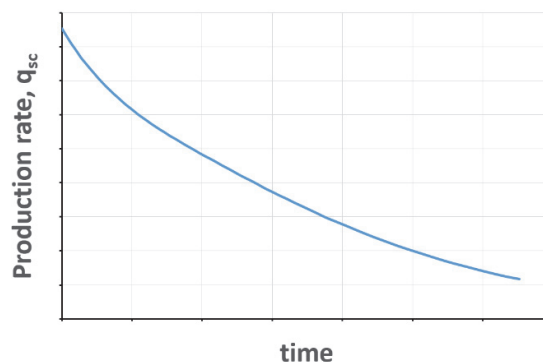
FIGURE 1-9. PRODUCTION PROFILE OBTAINED WHEN OPERATING IN DECLINE MODE

This production mode is employed typically for satellite fields that will use the spare capacity of the processing facilities of a neighboring mature field.

Figure 1-10 shows the production profile of the single well production system producing in plateau mode and producing at the production potential from the beginning. Both systems are being produced until the same ultimate amount of gas or oil is recovered (Q_{PU}).

Fixing a constant plateau rate causes that the time to abandonment is considerably prolonged when compared to the open choke case. However, the total amount of oil or gas recovered is the same (i.e. blue and violet areas are the same). A lower plateau rate will give an even longer time to abandonment.
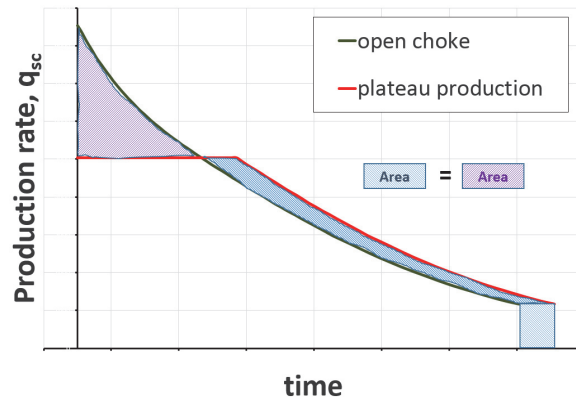
FIGURE 1-10. PRODUCTION RATE BEHAVIOR VS CUMULATIVE PRODUCTION FOR OPEN CHOKE AND CONSTANT RATE

1.5.1. EARLY AND UNEXPECTED PLATEAU DROP-OFF DUE TO BOTTLENECKING OF PROCESSING FACILITIES

Consider we are currently in the development stage of an oil and gas field. The production profiles in time of oil, gas, water, liquid (water and oil), water cut and gas oil ratio given in Figure 1-14 have been generated using computer simulators, are considered the most likely to occur and will be used as basis for system design.
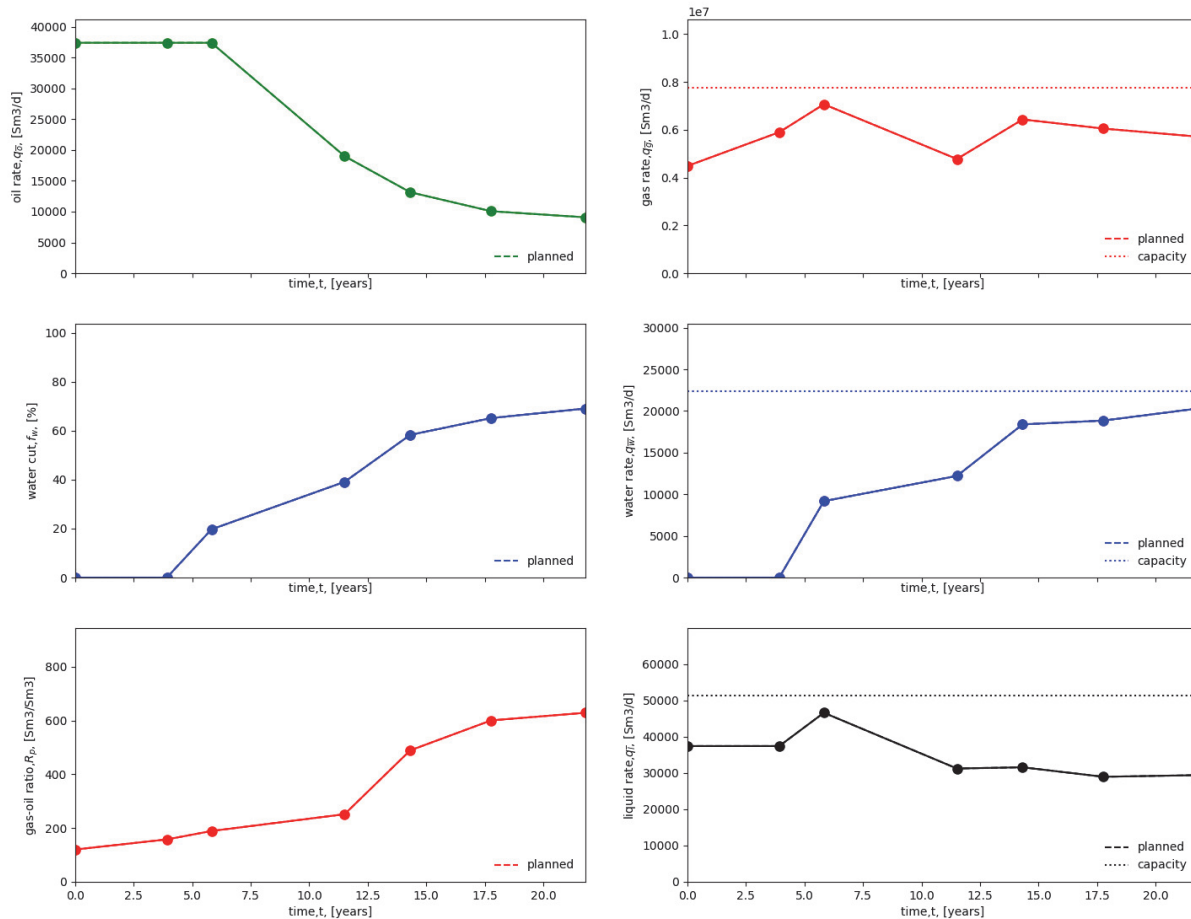
FIGURE 1-11. PREDICTED PRODUCTION PROFILES OF OIL, GAS, WATER, LIQUID, WATER CUT AND GAS-OIL RATIO AND TOPSIDE PROCESSING CAPACITIES CHOSEN.

These profiles are subsequently used for the design of the topside processing facilities. In this design process, maximum processing capacities of gas, water and liquid are set, including a safety margin (discontinuous

horizontal lines shown in the plots on the column to the right in the figure). These values are used to size processing equipment such as separators, pumps, compressors, hydrocyclones, etc.

The prediction of production profiles is usually highly uncertain, both in the design and operational phase, due to the high uncertainty in reservoir characteristics and other parameters that are input to the software used to generate production profiles. Consider now we are some years in production and the water cut has increased earlier than what was originally predicted, as indicated in Figure 1-12 (left column, middle figure, the first three dots are the actual field water cut, while the discontinuous line gives the original prediction, **we are currently on the third dot**). As it can be seen in the middle and lower plots on the right column, the water and liquid rate exceed their processing capacity, so it is impossible for the field to process the rates produced.
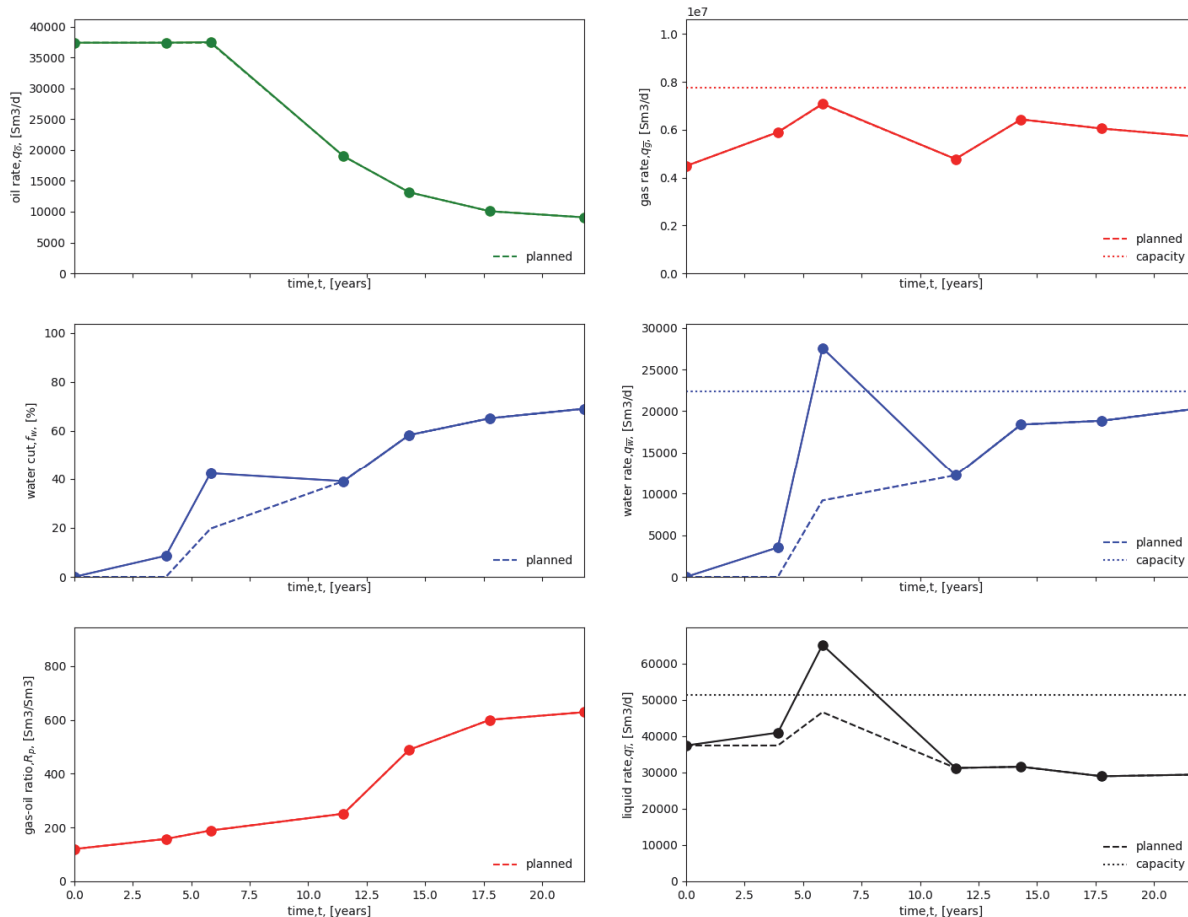
FIGURE 1-12. PREDICTED AND ACTUAL PRODUCTION PROFILES OF OIL, GAS, WATER, LIQUID, WATER CUT AND GAS-OIL RATIO AND TOPSIDE PROCESSING CAPACITIES CHOSEN (ACTUAL ARE UP TO THE FIRST THREE DOTS FROM LEFT TO RIGHT)

A quick, pragmatic, but painful solution to this problem is to reduce the field oil rate at that time, as indicated in Figure 1-13. Instead of continuing in plateau, field managers are forced to choke back oil production until the water and liquid production are within the processing capacities of the topside facilities. We commonly say in this situation that the field or processing facilities are "bottlenecked", i.e. some unit is operating at capacity, and this hinders from producing more hydrocarbons.
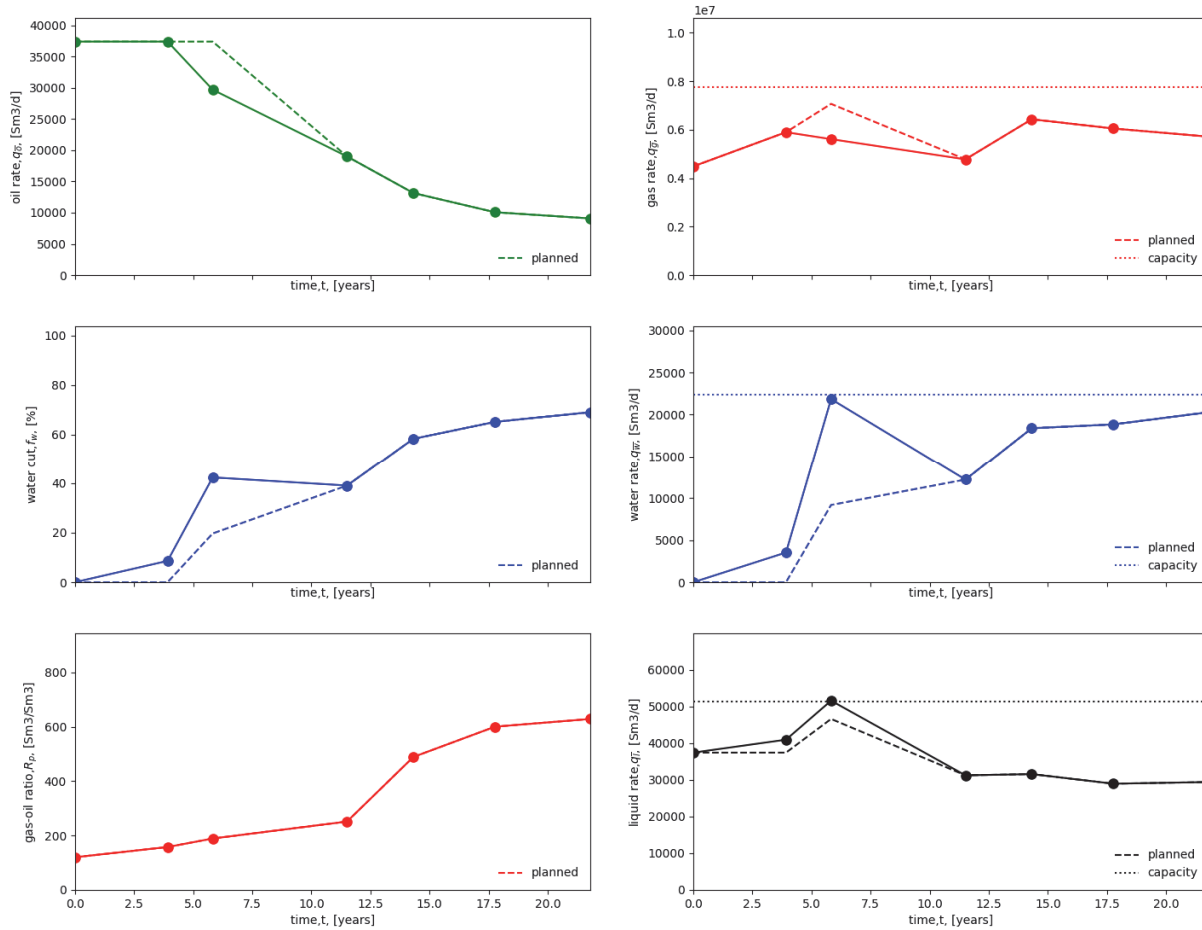
FIGURE 1-13. PREDICTED AND ACTUAL PRODUCTION PROFILES OF OIL, GAS, WATER, LIQUID, WATER CUT AND GAS-OIL RATIO AND TOPSIDE PROCESSING CAPACITIES CHOSEN. ADJUSTMENT OF OIL PLATEAU RATE TO MEET WATER AND LIQUID PROCESSING CAPACITIES.

Some solutions to avoid dropping off plateau early are to expand the capacity of the processing facilities (not always feasible due to space constraints and high cost), or selectively choke wells that have high water cut to reduce water production without losing too much oil.

1.6.   RELATIONSHIP BETWEEN PRODUCTION POTENTIAL AND CUMULATIVE PRODUCTION

As mentioned earlier, the production potential partly depends on the deliverability of the formation. In reality, the reservoir deliverability (IPR) does not depend on time but mainly on the amount of fluid that has been withdrawn from the reservoir since the initial condition to time t:

$$Q_P = \int_0^t q_{sc}(t) \cdot dt$$

EQ. 1-1

Q_P represents amounts of oil or gas and it is called cumulative production.

Figure 1-14 shows the Well IPR curve (flowing bottom-hole pressure vs flow rate) for 3 increasing values of cumulative production. Note that the IPR of the formation is reduced if more fluids have been produced from the reservoir.
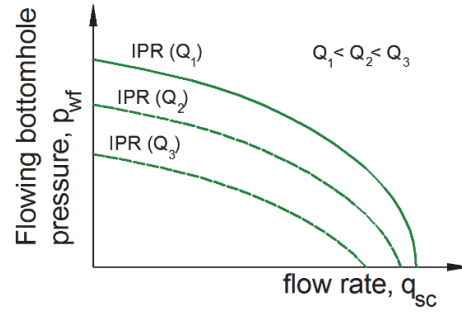
FIGURE 1-14. CHANGES OF IPR WITH CUMULATIVE PRODUCTION

This implies that **the production potential at a given point in time is mainly dependent on the how much fluid has been produced up to that point in time**.

If a method of estimating well IPR vs. cumulative production is available, the computation of the production potential curve using numerical models is straightforward.

Example 1: Consider a production system consisting of an undersaturated oil reservoir with an underlying aquifer with volume V_a and a number of identical wells N_w. The pressure will decline according to Eq. 1-2:

$$p_R = p_i - N_p \cdot A \qquad \text{EQ. 1-2}$$

With A being:

$$A = \frac{B_o}{\left[N \cdot B_{o,i} \cdot \left(c_o + \frac{c_w \cdot S_w + c_f}{S_o}\right) + V_a \cdot \phi_a \cdot (c_w + c_f) \cdot B_w\right]} \qquad \text{EQ. 1-3}$$

The rate of a single well can be expressed as:

$$q_{o,well} = J \cdot (p_R - p_{wf}) \qquad \text{EQ. 1-4}$$

If the well has some sort of artificial lift method installed such as an electric submersible pump, usually the maximum well rate will be achieved when the flowing bottom-hole pressure is lowered to a minimum value:

$$q_{o,well\ max} = J \cdot (p_R - p_{wf,min}) \qquad \text{EQ. 1-5}$$

Considering the number of wells and that the effect of the flow commingling in the surface network does not affect the individual well performance, then the field maximum rate can be expressed as:

$$q_{o,field\ max} = N_w \cdot J \cdot (p_R - p_{wf,min}) \qquad \text{EQ. 1-6}$$

Substituting Eq. 1-2 in Eq. 1-6:

$$q_{o,field\ max} = N_w \cdot J \cdot (p_i - N_p \cdot A - p_{wf,min}) \qquad \text{EQ. 1-7}$$

Expanding the terms and grouping:

$$q_{o,field\ max} = -N_w \cdot J \cdot N_p \cdot A + N_w \cdot J \cdot (p_i - p_{wf,min}) \qquad \text{EQ. 1-8}$$

Renaming terms:

$$q_{o,field\ max} = q_{pp} \qquad \text{EQ. 1-9}$$

$$q_{ppo,field} = N_w \cdot J \cdot \left(p_i - p_{wf,min}\right)$$

EQ. 1-10

$$a = N_w \cdot J \cdot A$$

EQ. 1-11

Finally, the production potential is given by the following expression:

$$q_{pp} = -a \cdot N_p + q_{ppo,field}$$

EQ. 1-12

The production potential of the system will approximately follow the smooth, downwards and continuous trend shown in Figure 1-15.
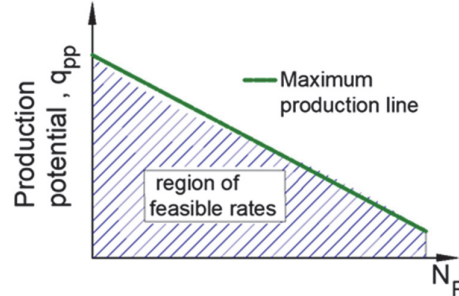
FIGURE 1-15. PRODUCTION RATE BEHAVIOR VS CUMULATIVE PRODUCTION FOR OPEN CHOKE SHOWING THE REGION OF FEASIBLE RATES

Example 2: Consider a production system where there are N_w identical wells producing from a common dry gas reservoir, each one with their own separator and flowline. The dry gas tank material balance equation is:

$$p_R = \frac{Z_R \cdot p_i}{Z_i} \cdot \left(1 - \frac{G_p}{G}\right)$$

EQ. 1-13

The production of a single well can be expressed with the low-pressure backpressure equation as a function of the field rate (q_f), the total number of wells (N_w):

$$\frac{q_f}{N_w} = C \cdot \left(p_R{}^2 - p_{wf}{}^2\right)^n$$

EQ. 1-14

The dry gas tubing equation is:

$$\frac{q_f}{N_w} = C_T \cdot \left(\frac{p_{wf}{}^2}{e^s} - p_{wh}{}^2\right)^{0.5}$$

EQ. 1-15

Finally, the flowline equation (assuming horizontal flowline):

$$\frac{q_f}{N_w} = C_{fl} \cdot \left(p_{wh}{}^2 - p_{sep}{}^2\right)^{0.5}$$

EQ. 1-16

To compound everything in one equation, one follows the procedure:

1. Clearing $p_{wh}{}^2$ from Eq. 1-16, then substituting in Eq. 1-15.
2. Clear $p_{wf}{}^2$ from the equation found in step 1 and substitute in Eq. 1-14.
3. Clear p_R from the equation found in step 2 and substitute in Eq. 1-13. This gives:

$$\left(\left(\frac{q_f}{N_w \cdot C}\right)^{\frac{1}{n}} + e^s \cdot \left(\frac{q_f}{N_w \cdot C_T}\right)^2 + e^s \cdot \left(\frac{q_f}{N_w \cdot C_{fl}}\right)^2 + e^s \cdot p_{sep}{}^2\right)^{0.5} = \frac{Z_R \cdot p_i}{Z_i} \cdot \left(1 - \frac{G_p}{G}\right) \qquad \text{EQ. 1-17}$$

Eq. 1-17 is plotted in Figure 1-16 using the following input:

- Number of wells, $N_w = 5, 10, 15$
- Backpressure coefficient, $C = 1000 \ Sm^3/bar^{2 \cdot n}$
- Backpressure exponent, $n = 1$
- Tubing elevation coefficient, $s = 0.155$
- Tubing coefficient, $C_T = 4.03 \cdot 10^4 \ Sm^3/bar$
- Flowline coefficient, $C_{fl} = 2.83 \cdot 10^4 \ Sm^3/bar$
- Separator pressure, $p_{sep} = 30 \ bara$
- Initial reservoir pressure, $p_i = 276 \ bara$
- Gas deviation factor calculated with the correlation of Hall and Yarborough, T = 92 °C and gas specific gravity 0.5.
- Initial gas in place $G = 2.7 \cdot 10^{11} \ Sm^3$
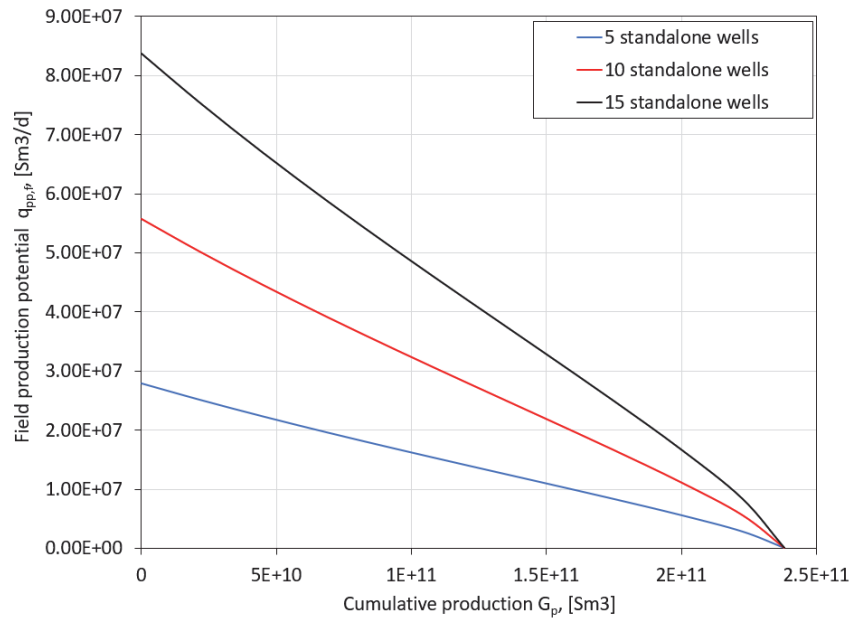
FIGURE 1-16. FIELD PRODUCTION POTENTIAL VS CUMULATIVE PRODUCTION FOR DRY GAS RESERVOIR WITH STANDALONE WELLS

When more wells are used in the system, the production potential is higher. The effect is proportional, due to the fact that well are standalone, and adding a new well does not interfere or affect the performance of other wells.

Figure 1-17 shows the dimensionless production potential of the field versus recovery factor. The dimensionless production potential has been found by dividing each field production potential curve by its maximum production potential (i.e. the production potential at $G_p = 0 \ Sm^3$) and the cumulative production by the initial gas in place. Surprisingly, the curves for all number of wells fall on top of each other.
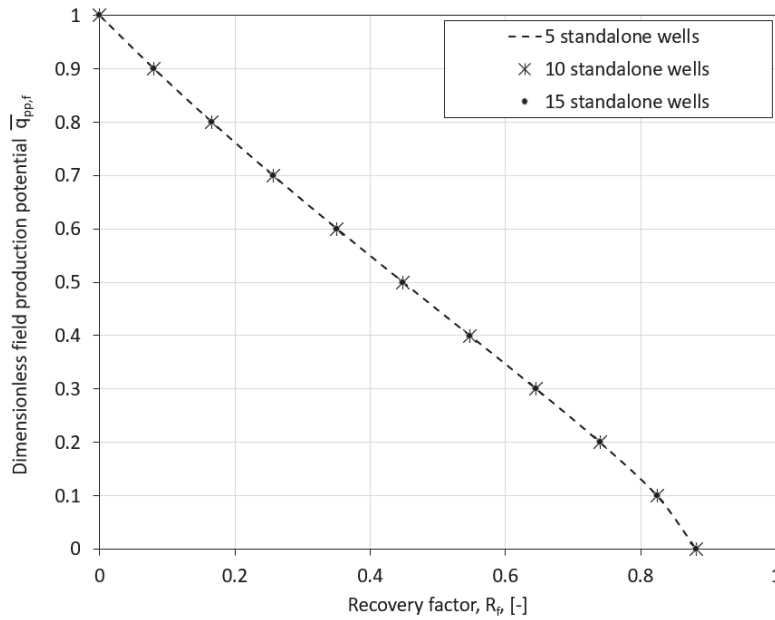
FIGURE 1-17. DIMENSIONLESS FIELD PRODUCTION POTENTIAL VS RECOVERY FACTOR FOR DRY GAS RESERVOIR WITH STANDALONE WELLS

The dimensionless production potential curve in Figure 1-17 remains unchanged if the amount of gas in place is increased or decreased. Figure 1-18 shows the dimensionless production potential of the field estimated with variations of ±50% on the backpressure coefficient, tubing coefficient, flowline coefficient and varying separator pressure. These variations cause modest changes in the curve.
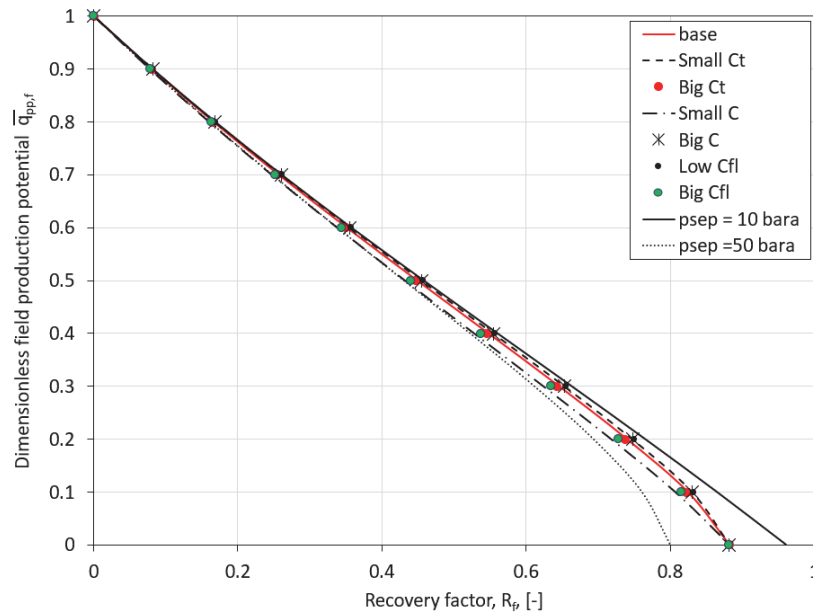
FIGURE 1-18. DIMENSIONLESS FIELD PRODUCTION POTENTIAL VS RECOVERY FACTOR FOR DRY GAS RESERVOIR WITH STANDALONE WELLS, SENSITIVITY STUDY ON SYSTEM PROPERTIES

An approximate equation to describe the relationship between field dimensionless production potential and recovery factor is:

$$\bar{q}_{pp,f} = \left(1 - \alpha \cdot R_f\right)$$

EQ. 1-18

Where α is a constant that can be calculated from data (in this case $\alpha = 1.14$)

Example 3: Consider a production system where there are N_w identical wells producing from a common dry gas reservoir, but they are grouped in N_t templates (where each template has a number of $N_{w,t}$ wells). There are identical flowlines from each template to a common junction, and one long pipeline from the junction to the separator. The dry gas tank material balance equation is:

$$p_R = \frac{Z_R \cdot p_i}{Z_i} \cdot \left(1 - \frac{G_p}{G}\right)$$

EQ. 1-19

The production of a single well can be expressed with the field rate (q_f), the total number of wells per template ($N_{w,t}$), the total number of wells and the low-pressure backpressure equation:

$$\frac{q_f}{N_{w,t} \cdot N_t} = C \cdot \left(p_R{}^2 - p_{wf}{}^2\right)^n$$

EQ. 1-20

The dry gas tubing equation is:

$$\frac{q_f}{N_{w,t} \cdot N_t} = C_T \cdot \left(\frac{p_{wf}{}^2}{e^s} - p_{wh}{}^2\right)^{0.5}$$

EQ. 1-21

The flowline equation (assuming horizontal flowline):

$$\frac{q_f}{N_t} = C_{fl} \cdot \left(p_{wh}{}^2 - p_{junc}{}^2\right)^{0.5}$$

EQ. 1-22

The pipeline equation (assuming horizontal pipeline):

$$q_f = C_{pl} \cdot \left(p_{junc}{}^2 - p_{sep}{}^2\right)^{0.5}$$

EQ. 1-23

To compound everything in one equation, one follows the procedure:

1. Clearing $p_{junc}{}^2$ from Eq. 1-23, then substituting in Eq. 1-22.
2. Clear $p_{wh}{}^2$ from the equation found in step 1 and substitute in Eq. 1-21.
3. Clear $p_{wf}{}^2$ from the equation found in step 2 and substitute in Eq. 1-20.
4. Clear p_R from the equation found in step 3 and substitute in Eq. 1-19. This gives:

$$\left(\left(\left(\frac{q_f}{N_{w,t} \cdot N_t \cdot C}\right)^{\frac{1}{n}} + e^s \cdot \left(\frac{q_f}{N_{w,t} \cdot N_t \cdot C_T}\right)^2 + e^s \cdot \left(\frac{q_f}{C_{pl}}\right)^2 + e^s \cdot p_{sep}{}^2 + e^s \right.\right.$$

EQ. 1-24

$$\left.\left. \cdot \left(\frac{q_f}{C_{fl} \cdot N_t}\right)^2 \right)^{0.5}\right) = \frac{Z_R \cdot p_i}{Z_i} \cdot \left(1 - \frac{G_p}{G}\right)$$

In this case, wells interfere and affect the performance of each other. It was found that the field maximum rate at initial time ($q_{ppo,field}$) is a function of the number of wells (N_{wells}) and the maximum well rate at initial time ($q_{ppo,well}$, assuming flowing alone):

$$q_{ppo,field} = q_{ppo,well} \cdot N_{wells} \cdot F^{(N_{wells}-1)}$$

EQ. 1-25

In this equation, F is a factor tuned to data (for the case presented F= 0.9412).

To evaluate the effect of the gathering system on the production potential curve, the expressions for standalone wells (Eq. 1-17), network[4] wells (Eq. 1-24) and considering IPR only (with fixed bottom-hole pressure of 120 bara) are plotted in Figure 1-19. The network doesn't affect significantly the dimensionless field production potential curve when compared to the standalone case but excluding the system downstream the well bottom-hole does.
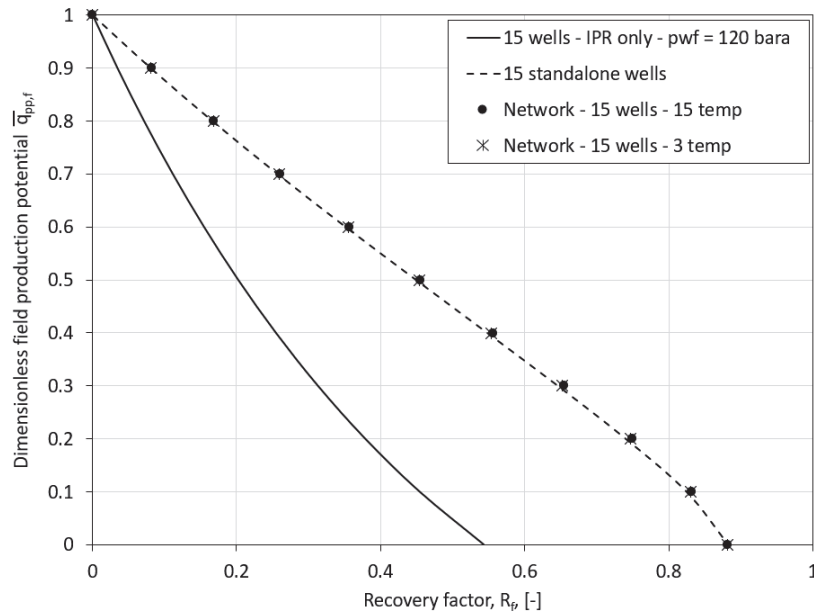
FIGURE 1-19. DIMENSIONLESS FIELD PRODUCTION POTENTIAL VS RECOVERY FACTOR FOR DRY GAS RESERVOIR WITH STANDALONE WELLS, NETWORK WELLS AND CONSIDERING IPR ONLY.

Example 4: Figure 1-20 shows the dimensionless field production potential vs. recovery factor for several cases. All cases had a surface gathering network transporting production to the processing facilities coupled with the reservoir model.

---

[4] Using flowline coefficient C_{fl} = 2.83 10^5 Sm^3/bar and pipeline coefficient C_{pl} = 2.75 10^5 Sm^3/bar
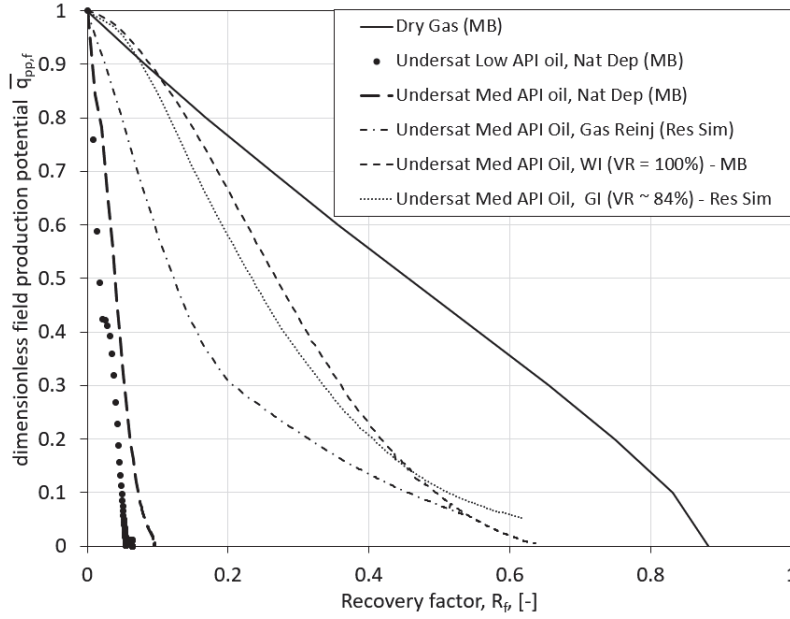
FIGURE 1-20. DIMENSIONLESS FIELD PRODUCTION POTENTIAL VS RECOVERY FACTOR FOR SEVERAL PRODUCTION SYSTEMS.

More details about the cases, modeling assumptions and results can be found in Stanko [1-4].

A general continuous equation to reproduce most of these curves is a fifth order polynomial:

$$\bar{q}_{pp} = a_5 \cdot \left(R_f\right)^5 + a_4 \cdot \left(R_f\right)^4 + a_3 \cdot \left(R_f\right)^3 + a_2 \cdot \left(R_f\right)^2 + a_1 \cdot R_f + 1 \qquad \text{EQ. 1-26}$$

If, on the other hand, the curves have some discontinuity or do not fit well to a continuous function, then a piece-wise linear approximation can be a more suitable alternative:

$$\bar{q}_{pp} = \begin{cases} \dfrac{\bar{q}_{pp,0} - \bar{q}_{pp,1}}{R_{f,0} - R_{f,1}} \cdot \left(R_f - R_{f,1}\right) + \bar{q}_{pp,1} & if \quad R_{f,0} \leq R_f < R_{f,1} \\[2mm] \dfrac{\bar{q}_{pp,1} - \bar{q}_{pp,2}}{R_{f,1} - R_{f,2}} \cdot \left(R_f - R_{f,2}\right) + \bar{q}_{pp,2} & if \quad R_{f,1} \leq R_f < R_{f,2} \\[2mm] \dfrac{\bar{q}_{pp,2} - \bar{q}_{pp,3}}{R_{f,2} - R_{f,3}} \cdot \left(R_f - R_{f,3}\right) + \bar{q}_{pp,3} & if \quad R_{f,2} \leq R_f < R_{f,3} \\[1mm] \quad\quad\quad\quad ... & \\[1mm] \dfrac{\bar{q}_{pp,N-1} - \bar{q}_{pp,N}}{R_{f,N-1} - R_{f,N}} \cdot \left(R_f - R_{f,N}\right) + \bar{q}_{pp,N} & if \quad R_{f,N-1} \leq R_f \leq R_{f,N} \end{cases} \qquad \text{EQ. 1-27}$$

Where $\left(\bar{q}_{pp,i}, R_{f,i}\right)$ are data point pairs, and there is a total of "N" point pairs.

The curves of production potential versus cumulative production of a production system can be computed from these curves by multiplying $\bar{q}_{pp}$ by the maximum production of the system at recovery factor equal zero ($q_{ppo,field}$), and by substituting recovery factor by Q_p/Q. To update the curves of production potential in time, if, for example, at some point in time, a new well is drilled, then the value of $q_{ppo,field}$ must be updated accordingly.

1.7. PRODUCTION SCHEDULING AND PLANNING USING PRODUCTION POTENTIAL CURVE

The production potential curve versus cumulative production can be used to perform production scheduling and planning without recurring to perform coupled runs of reservoir and production models. This is because

by expressing the production potential as a function of cumulative production, the time dependency has been removed. To ilustrate this, three examples will be presented and discussed next.

Example 1: Undersaturated oil reservoir with an underlying aquifer with volume V_a and a number of identical wells N_w.

Let us assume the field will be produced at a plateau rate $(q_{p,f})$ initially and then it will enter in decline. The plateau will end when the field production potential becomes equal to the field plateau rate $(q_{p,f})$

$$q_{p,f} = -a \cdot N_P^* + q_{ppo}$$

EQ. 1-28

Then, the plateau duration can be calculated with the cumulative production N_P^*

$$t_p = \frac{N_p^*}{q_{p,f}} = \frac{q_{p,f} - q_{ppo}}{-q_{p,f} \cdot a} = \left(\frac{q_{ppo}}{q_{p,f}} - 1\right) \cdot \frac{1}{a}$$

EQ. 1-29

After the plateau, the field will produce at potential:

$$q_f = q_{pp,f} = -a \cdot N_p + q_{ppo}$$

EQ. 1-30

Expanding the definition of cumulative production:

$$q_f = -a \cdot \left(N_p^* + \int_{t_p}^{t} q_f \cdot dt\right) + q_{ppo}$$

EQ. 1-31

Substituting the definition of N_P^*

$$q_f = -a \cdot \int_{t_p}^{t} q_f \cdot dt - a \cdot \frac{q_{p_f} - q_{ppo}}{-m} + q_{ppo}$$

EQ. 1-32

Simplifying:

$$q_f = -a \cdot \int_{t_p}^{t} q_f \cdot dt + q_{p\_f}$$

EQ. 1-33

A solution to this equation is:

$$q_f = q_{p,f} \cdot e^{-a \cdot (t - t_p)}$$

EQ. 1-34

Therefore, if the production potential displays a linear behavior with respect to cumulative production, the production profile post-plateau has an exponential behavior with time. The coefficient of the exponential function, that dictates the rate decline depends both on the decline characteristics of the reservoir (A), the flow "resistance" in the formation (and in principle, in the tubing and surface flowlines) and the number of wells. If the number of wells is increased, the decline will become more pronounced.

The field production profile is given by the following equations:

$$for\ t < t_p \qquad\qquad q_f = q_{p,f}$$

EQ. 1-35

$$for\ t \geq t_p \qquad\qquad q_f = q_{p,f} \cdot e^{-a \cdot (t - t_p)}$$

EQ. 1-36

<u>Example 2:</u> Plateau mode production

Consider the production strategy proposed in Figure 1-21a. The production potential curve has been divided in three parts that will be produced at constant rate. The production rates are feasible because they fall below the production potential line. Figure 1-21b. shows the production profile calculated from Figure 1-21a. As the reservoir is produced with constant rate periods, it is simple to estimate the duration of each period by dividing the cumulative production of the period by the period rate.
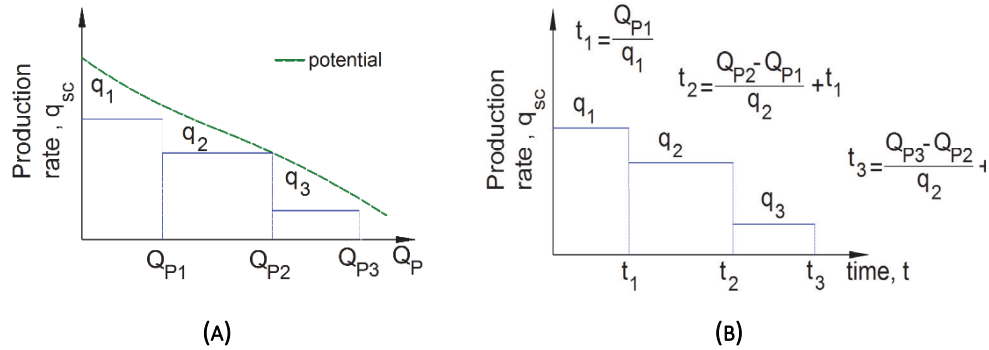
FIGURE 1-21. PLATEAU MODE PRODUCTION

For a few simple cases (e.g. dry gas, undersaturated oil) an analytical expression of the production potential q_{pp} can be found. However, in general, for the majority of cases (e.g. saturated oil, gas condensate) this is not possible. The production potential must then be calculated by running a simulation of coupled reservoir and production models at maximum rate and record the field rate and the cumulative production Q_p. This process yields a collection of points.

For cases where the production potential is not linear, it is usually not practical to solve analytically for the plateau duration and post-plateau field rate as presented in the previous examples. If an analytical expression is available, plateau duration can be estimated by substituting the desired plateau rate and solve the equation (usually with a root solving method) for the cumulative production at plateau end Q_p^*. If a collection of points is available, Q_p^* can be found by interpolating on the table. With Q_p^* and plateau rate, one can then calculate plateau duration.

The post-plateau field rate can be estimated by dividing the post-plateau period in a series of discrete time steps and expressing the cumulative production at time t_i using the trapezoidal rule for numerical integration:

$$Q_p(t_i) = 0.5 \cdot \big(q(t_i) + q(t_{i-1})\big) \cdot (t_i - t_{i-1}) + Q_p(t_{i-1})$$ EQ. 1-37

All rates in the post-plateau period should fall on the production potential curve, i.e.

$$q(t_i) = f\big(Q_p(t_i)\big)$$ EQ. 1-38

Eq. 1-37 and Eq. 1-38 must be solved simultaneously for each time step t_i and departing from plateau end. If the production potential is available as a collection of points, Eq. 1-38 means interpolation.

<u>Example 3:</u> Production potential of a system with two standalone wells

Consider a field with two (2) standalone wells, and that the production potential of each well can be expressed as a function of the cumulative production of each individual well:

$$q_{pp}^i = f(Q_p^i)$$ EQ. 1-39

In this case the production profile can be computed separately for each well from the production potential curve and then add them up to obtain the field production profile. Note that the field production potential for a given field cumulative production is not unique. This is because there are different ways to achieve the same field cumulative production (e.g. in a two well system, produce more from well 1 than 2, produce equal, or produce more from well 2 than 1).

As an example, consider the production system with 2 standalone wells shown in Figure 1-22a. The production potential of each well is presented in Figure 1-22b. Wells will be produced at constant rate initially, with plateau rates q_{P1} and q_{P2} and, when the plateau rate is no longer feasible, they will be produced at the production potential.

(A)   (B)
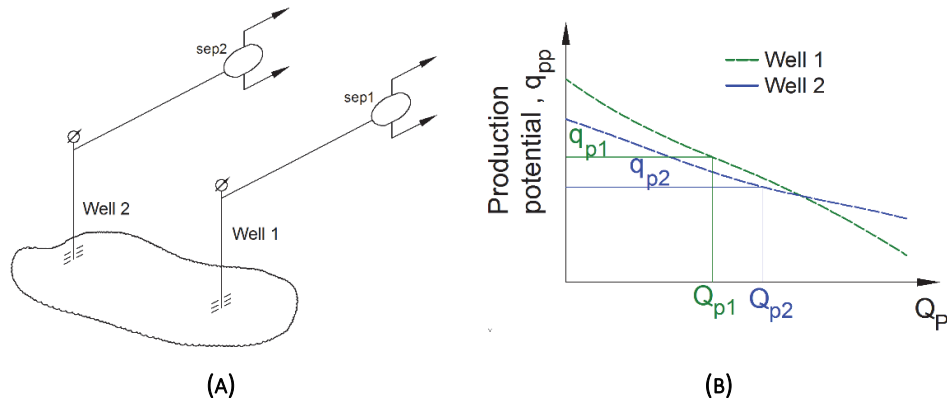
FIGURE 1-22. EXAMPLE CASE: 2 STANDALONE WELLS

The plateau duration of each well can be very easily calculated by intersecting the individual plateau rate with the production potential curve of each well. This yields a plateau duration of $t_{p1} = Q_{P1}/q_{P1}$, for well 1 and $t_{p2} = Q_{P2}/q_{P2}$ for well 2. After the plateau ends, the production profile of each well follows the potential.

A typical reservoir management problem consists of how to define well rates to maximize field plateau duration when a fixed field rate is desired. If individual well plateau rates are to be kept constant, this can be achieved by finding the plateau rates for which the plateau end occurs at the same time. If the production potential curves are straight lines the following procedure is suitable:

The production potential curve for well 1:

$$q_{pp1} = -a_1 \cdot Q_{p1} + q_{ppo1}$$

EQ. 1-40

The cumulative production at which the production potential (q_{pp1}) is equal to the plateau rate (q_{p1}), i.e. Q_{Pp1}, is:

$$Q_{Pp1} = \frac{q_{ppo1} - q_{p1}}{a_1}$$

EQ. 1-41

Similarly, for well 2:

$$Q_{Pp2} = \frac{q_{ppo2} - q_{p2}}{a_2}$$

EQ. 1-42

Then the plateau duration has to be the same for both wells:

$$t_{p1} = \frac{Q_{Pp1}}{q_{p1}}; \ t_{p2} = \frac{Q_{Pp2}}{q_{p2}}$$

EQ. 1-43

Substituting Eq. 1-41 and Eq. 1-42 in Eq. 1-43:

$$\frac{q_{ppo1} - q_{p1}}{a_1 \cdot q_{p1}} = \frac{q_{ppo2} - q_{p2}}{a_2 \cdot q_{p2}}$$

EQ. 1-44

$$\frac{q_{ppo1}}{q_{p1}} - 1 = \frac{a_1}{a_2} \cdot \left(\frac{q_{ppo2}}{q_{p2}} - 1 \right)$$

EQ. 1-45

Eq. 1-45 has two unknowns, therefore one more equation is needed. Clearing q_{p2} from the expression of the total plateau rate:

$$q_{p2} = q_p - q_{p1}$$

EQ. 1-46

Substituting Eq. 1-46 in Eq. 1-45 yields:

$$q_{p1}^2 \cdot (a_1 - a_2) + q_{p1} \cdot \left(q_{ppo1} \cdot a_2 + q_p \cdot a_2 - q_p \cdot a_1 + q_{ppo2} \cdot a_1 \right) - q_{ppo1} \cdot a_2 \cdot q_p = 0$$

EQ. 1-47

Eq. 1-47 can be solved with the quadratic formula to find q_{p1}:

$$a = (a_1 - a_2)$$

EQ. 1-48

$$b = q_{ppo1} \cdot a_2 + q_p \cdot a_2 - q_p \cdot a_1 + q_{ppo2} \cdot a_1$$

EQ. 1-49

$$c = -q_{ppo1} \cdot a_2 \cdot q_p$$

EQ. 1-50

$$q_{p1} = \frac{-b \pm \sqrt{b^2 - 4 \cdot a \cdot c}}{2 \cdot a}$$

EQ. 1-51

Note that the main constraints used to solve this problem were that both wells must produce in plateau mode with a constant rate and then will enter in decline at the same time. However, there are infinite alternatives to produce the field at plateau rate as shown in Figure 1-23 and each option will yield a different field plateau duration.

(A)   (B)

(C)   (D)
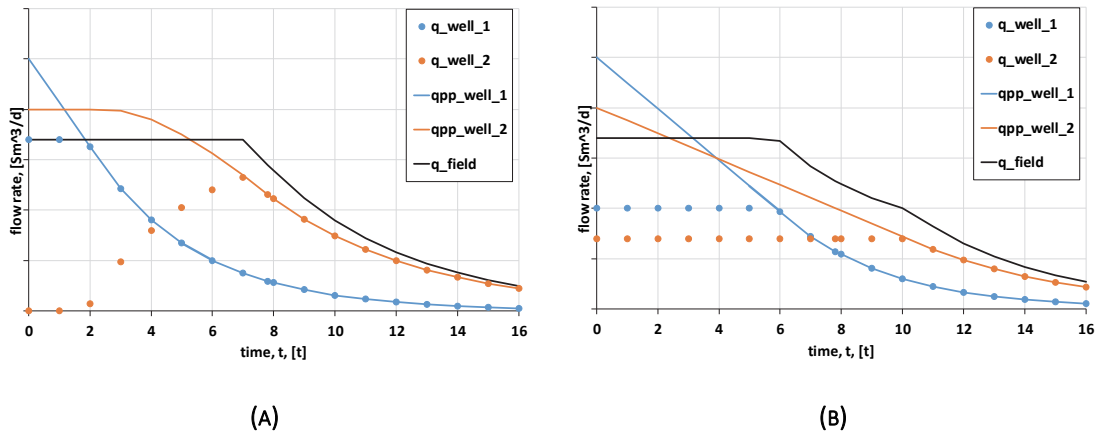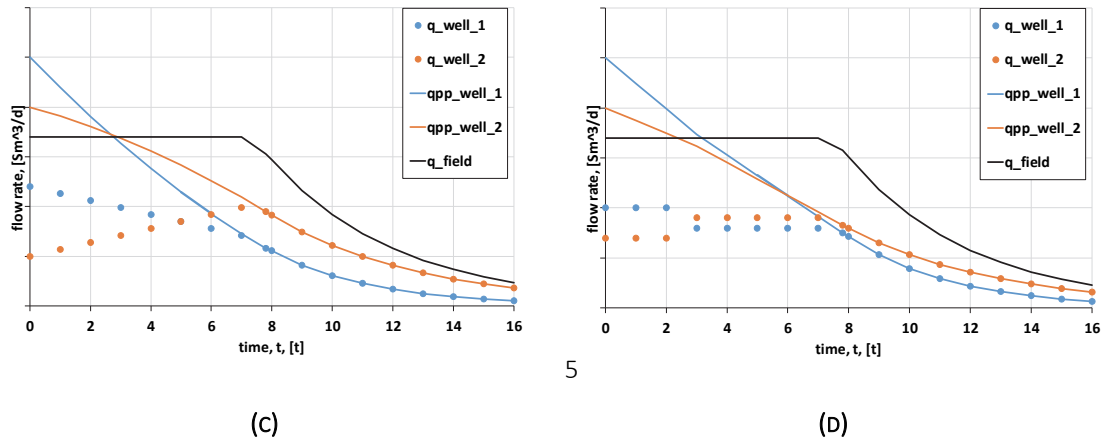
FIGURE 1-23. 4 DIFFERENT ALTERNATIVES TO PRODUCE THE TWO WELLS SYSTEM IN PLATEAU MODE

1.8. EFFECT OF ARRIVAL PRESSURE (AKA. SINK PRESSURE OR SEPARATOR PRESSURE) ON DIMENSIONLESS PRODUCTION POTENTIAL CURVE

Case 1. Standalone dry gas wells:

As it was shown in Figure 1-18, modest changes to separator pressure have modest effects on the curve of dimensionless production potential. Namely, it changes the value of recovery factor at zero dimensionless production potential consequently changing the curve for lower values of dimensionless production potential (or equivalently, high values of recovery factor). For practical applications, one will abandon the field at much higher values of dimensionless production potentials (or, equivalently, at lower recovery factors) therefore, deviations of the curve of dimensionless production potential on that region are of little importance.

To evaluate more in detail the effect of separator pressure on the curve of dimensionless production potential, new calculations were performed allowing bigger variations in separator pressure (1-150 bara, initial reservoir pressure is 276 bara) for the same case presented in Figure 1-18 (5 standalone dry gas wells). Results are shown in Figure 1-24. Above separator pressures of 60 bara, there starts to be significant variations to the curve of dimensionless production potential even for high values of dimensionless production potential (and low recovery factors).
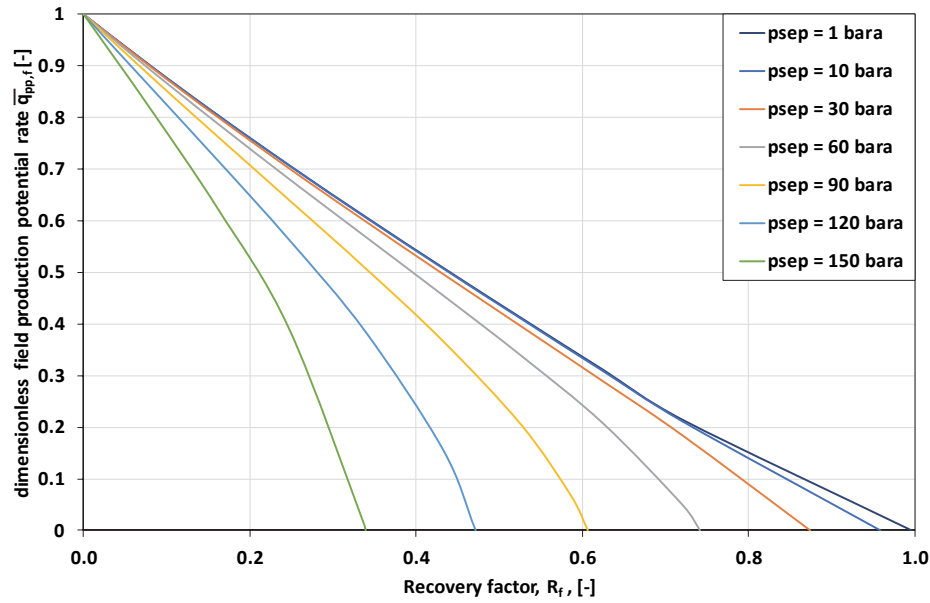
FIGURE 1-24. DIMENSIONLESS FIELD PRODUCTION POTENTIAL VS RECOVERY FACTOR FOR DRY GAS RESERVOIR WITH STANDALONE WELLS. EFFECT OF SEPARATOR PRESSURE CHANGES FROM 1 TO 150 BARA.

For this case it seems a valid approach to capture the effect of separator pressure on the curve of dimensionless field production potential is to use the second order polynomial:

$$\bar{q}_{pp,f} = a \cdot R_f{}^2 + b \cdot R_f + 1 \qquad \text{EQ. 1-52}$$

with a and b functions of separator pressure (in this case a third-degree polynomial and a second-degree polynomial fit best respectively).

To find the field production potential one must multiply the dimensionless production potential by the maximum field production at initial time ($q_{ppo,f}$), which depends on the separator pressure. In this case, the behavior between $q_{ppo,f}$ versus p_{sep} at initial time can be approximated by a quadratic equation:

$$q_{ppo,f} = q_{ppo,ref} \cdot \left(1 + c \cdot \left(\frac{p_{sep}}{p_{sep,ref}}\right) + d \cdot \left(\frac{p_{sep}}{p_{sep,ref}}\right)^2\right) \qquad \text{EQ. 1-53}$$

Where $q_{ppo,ref}$ can be set to, for example, field rate for the lowest separator pressure at initial time, and $p_{sep,ref}$ can be set to, for example, the static pressure computed at the separator assuming shut-in field at initial time. This equation was derived in a similar way to the normalization approach followed to generate the dimensionless production potential curve.

Therefore, a full analytical model proposed to find field production potential when separator pressure is varying with time is:

$$q_{ppo,f} = q_{ppo,ref} \cdot \left(1 + c \cdot \left(\frac{p_{sep}}{p_{sep,ref}}\right) + d \cdot \left(\frac{p_{sep}}{p_{sep,ref}}\right)^2\right) \cdot \left(a \cdot R_f{}^2 + b \cdot R_f + 1\right) \qquad \text{EQ. 1-54}$$

This equation could be used to model and estimate production profile in time for systems where fields/groups of wells producing from the same reservoir units are connected to a common tie-in (manifold) point that has a varying pressure (for example that connects to a common flowline and produced further,

e.g. to a separator). To perform the computations for this imagined case, the curve of the flowline needs to be available to compute pressure of the tie-in point as a function of total gas rate in time.

Case 2. Undersaturated oil reservoir with aquifer undergoing water injection with gas-lifted network wells

A study on separator pressure effect on the curve of dimensionless production potential was performed on the base case of study case 2 presented by Stanko [1-4] (details are provided in the article). The base case considered that the production of the two subsea well clusters (one with 4 and another with 3 wells) is commingled subsea in a manifold and then transported to the surface separator using a 400 m deep riser. The riser was removed for the calculations performed here, and the pressured varied was the subsea manifold pressure, which is the most downstream point considered in the model. Results are shown in Figure 1-25. Ignoring the riser and varying the subsea manifold pressure have a modest effect (max 10% deviation) on the curve of dimensionless production potential.
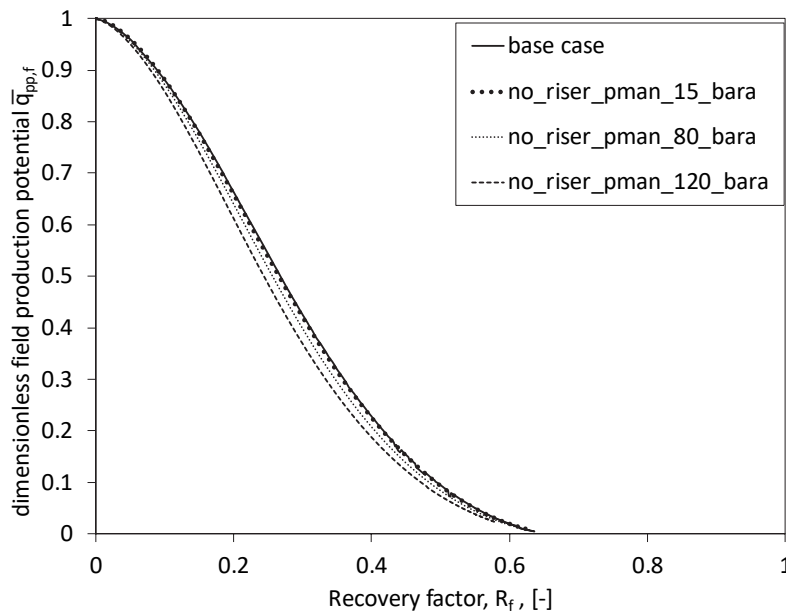
FIGURE 1-25. DIMENSIONLESS FIELD PRODUCTION POTENTIAL VS RECOVERY FACTOR FOR UNDERSATURATED OIL RESERVOIR WITH AQUIFER UNDERGOING WATER INJECTION WITH GAS-LIFTED NETWORK WELLS. SUBSEA MANIFOLD PRESSURED VARIED FROM 15 TO 120 BARA.

Similar to case 1, for this case it was also found that the relationship between the field production potential at initial time $q_{ppo,f}$ versus $p_{manifold}$ can be approximated by a quadratic equation (Eq. 1-53), with d = -0.60 and c = -0.37.

Case 3. Naturally depleted undersaturated oil reservoir with aquifer and gas-lifted network wells

A study on separator pressure effect on the curve of dimensionless production potential was performed on the natural depletion case (2.13) of study case 2 presented by Stanko [1-4] (details are provided in the article). It is similar to the base case presented earlier but considering natural depletion instead of water injection. Similarly to the previous case, it is considered that the production of the two subsea well clusters (one with 4 and another with 3 wells) is commingled subsea in a manifold and then transported to the surface separator using a 400 m deep riser. The riser was removed for the calculations performed here, and the pressured varied was the subsea manifold pressure, which is the most downstream point considered in the model. Results are shown in Figure 1-26. Ignoring the riser and varying the subsea manifold pressure have a significant effect on the curve of dimensionless production potential.
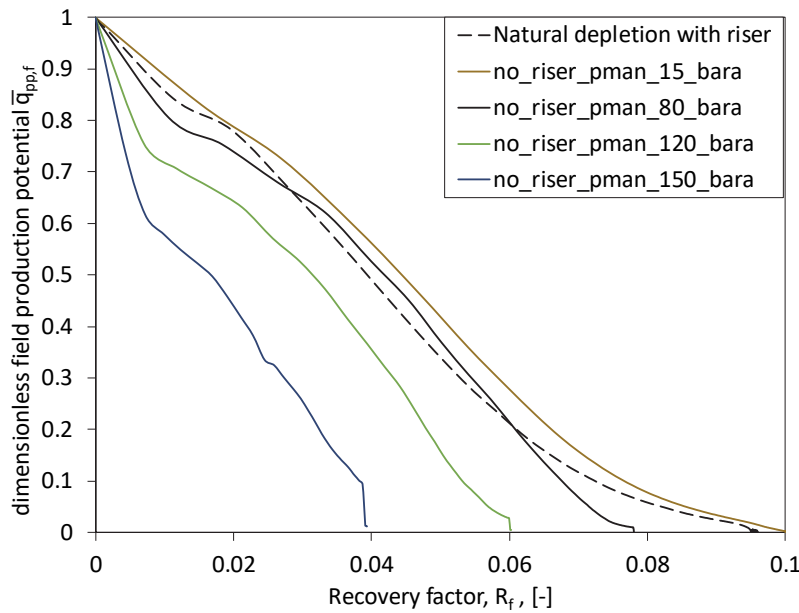
FIGURE 1-26. DIMENSIONLESS FIELD PRODUCTION POTENTIAL VS RECOVERY FACTOR FOR NATURALLY DEPLETED UNDERSATURATED OIL RESERVOIR WITH AQUIFER WITH GAS-LIFTED NETWORK WELLS. SUBSEA MANIFOLD PRESSURED VARIED FROM 15 TO 150 BARA.

1.9.   APPLICABILITY OF THE PRODUCTION POTENTIAL CONCEPT IN REAL FIELDS AND MULTI-WELL PRODUCTION SYSTEMS

The production potential concept is valid only when the reservoir (or well) producing GOR, WC, reservoir pressure and IPR can be safely predicted as a function of its cumulative production and the near well transient period (infinite acting) is short.

This concept can be used to design and predict the production profile of the field. For example, in early stages of field planning an assumption typically made is that all wells are identical. In consequence, the production potential of the field is just the multiplication of the number of wells time the production potential of a single well. This approach is often used to estimate roughly the number of wells that are required to produce the field rate for a desired time period. An example of this method is presented and discussed thoroughly by Van Dam [1-5].

For more complex cases, e.g. reservoirs that cannot be modeled with a material balance approach, an iterative approach is often used (without using the production potential method) where field models are run multiple times with different production rates and their results compared.

More details about the limitations and applications of production potential curves can be found in Stanko [1-4].

REFERENCES

[1-1] Barroux, C., Duchet-Suchaux, P., Samier, P. & Nabil, R. (2000). *Linking Reservoir and Surface Simulators: How to improve the Coupled Solutions*. SPE-65159. *European Petroleum Conference*. Paris: Society of Petroleum Engineers.

[1-2] Golan, M.; Whitson, C. H. (1986). *Well Performance*. Second Edition. Prentice-Hall Inc. Englewood Cliffs, New Jersey.

[1-3] Nind, T. (1964). *Principles of Oil Well Production*. McGraw-Hill.

[1-4] Stanko, M. (2021). *Observations on and use of curves of current dimensionless potential versus recovery factor calculated from models of hydrocarbon production systems*. Journal of Petroleum Science and Engineering. Volume 196. 108014. ISSN 0920-4105, https://doi.org/10.1016/j.petrol.2020.108014.

[1-5] Van Dam, J. (1986). *Planning of Optimum Production from a Natural Gas Field*. Journal of the Institute of Petroleum 54 (521).

2.   FLOW PERFORMANCE IN PRODUCTION SYSTEMS

The production system is the assembly of wells, pipes, valves, pumps, meters that have the function of transporting fluids from the reservoir to the processing facilities in a controlled manner. Formally, the processing facilities[5] should also be considered as part of the production system but they are excluded from the current discussion. This is because the primary separator pressure is usually kept constant (e.g. with a control system as shown in Figure 2-1) which decouples (in terms of flow and pressure dependence) the system upstream and downstream the separator.

pc ...pressure controller
llc ...liquid level controller
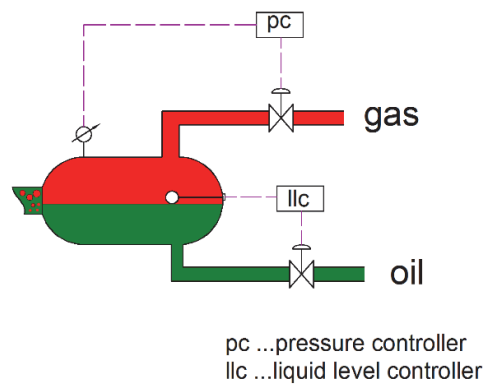
FIGURE 2-1. SIMPLIFIED LEVEL AND PRESSURE CONTROL SYSTEM IN A SEPARATOR

The layout and characteristics of the production system might vary significantly depending on the reservoir characteristics, its geographical location (offshore, onshore, remote access), the field development concept, the existence of neighboring fields, among others. However, it is possible to define two clear configurations: standalone wells (e.g. gas wells in domestic US) where each well is producing through their own pipeline to a separator (as in Figure 2-2a) or surface networks where well production is gathered by pipelines that transverse the field and converge in the main production facilities (as in Figure 2-2b).

(A)   (B)
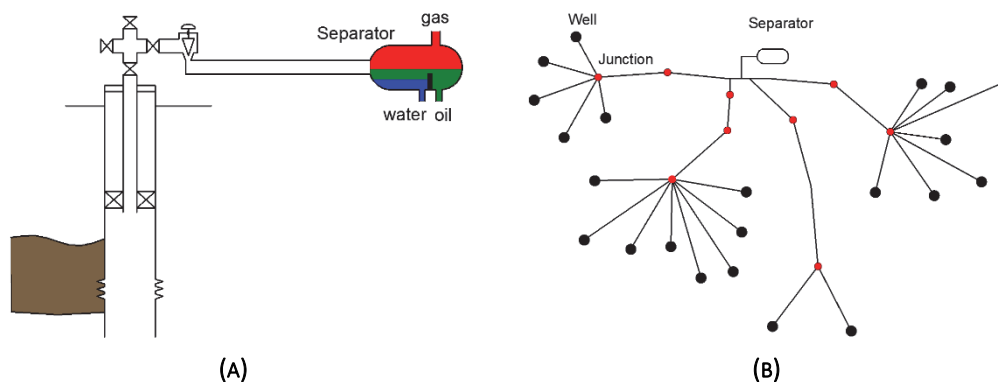
FIGURE 2-2. LAYOUT OF TWO PRODUCTION SYSTEMS

The surface connectivity between wells defines, to a great extension, the degree of flow interference between them (i.e. how the operating conditions in one well affect others).

When the fluid travels from the reservoir(s) (source) to the separator(s) (sink), it has to overcome energy losses (e.g. pressure drop) and sometimes "compete" with other fluids in the transportation pipes. A flow equilibrium

---

[5] An overview of typical parts of offshore oil and gas processing facilities is presented in Appendix E.

state is reached where the producing rates, pressures and temperatures of the system are a product of a balance between the capacity of each source and the existing energy losses/additions.

Numerical models are often used to understand and estimate the flow equilibrium state of production systems. The numerical model of a production system is usually a steady state representation that comprises from the well bottom-holes (source nodes) to the first stage separator(s) (sink nodes). The main purpose of this model is to compute the rates from each well and the pressure and temperature distribution in the production system.

The well inflow is typically represented by an IPR equation (Inflow performance relationship) that provides the bottom-hole pressure that has to be applied at the sand face to deliver a specific standard condition rate (see Figure 2-3). The IPR describes the reservoir deliverability for a given depletion state and assuming that a pseudo-steady state has been reached in the reservoir. Please note that the same well might be producing from different reservoir regions or have several laterals, so several IPRs might be required for the same well.

IPR for undersaturated oil   IPR for saturated oil/gas
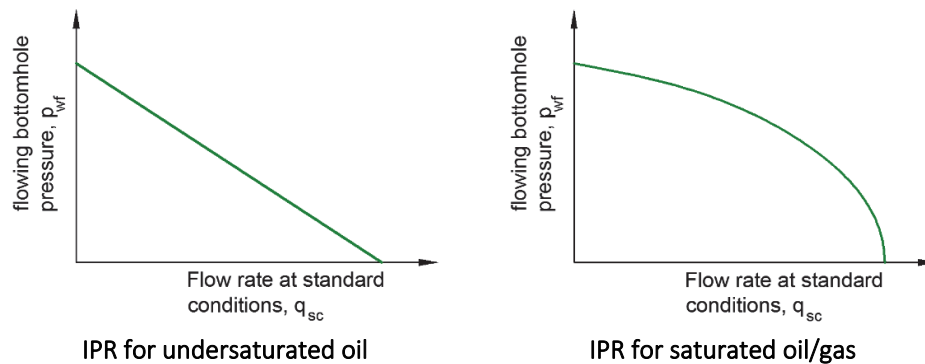
FIGURE 2-3. IPR CURVE

Flow in tubular conduits such as tubing, casing and pipelines is represented with equations that predict the temperature and pressure drops[6]. Usually, these equations use constant fluid properties, so a length discretization and a step-wise calculation has to be performed to capture fluid behavior. The separator is represented by a constant pressure value. Other elements, such as restrictions, chokes, valves, boosters, etc. have their own particular equations to predict pressure and temperature change according to the energy introduced or removed from the fluid.

These equations are usually derived by applying mass, momentum and energy conservation equations to the element or interest. The equations are further simplified to reduce the number of unknowns by introducing relationships between variables, empirical correlations, etc.

This set of equations that constitute the numerical model of the production system is solved simultaneously in an iterative manner (e.g. using a Newton method). They have to be solved simultaneously because the upstream or downstream conditions of one element are usually the downstream or upstream conditions of another element. The solving process is usually referred to as computing the flow equilibrium of the production system and usually consists on assuming and varying well rate(s) to minimize a pressure residual using a Newton method.

In a single well-pipeline-separator system (as in Figure 2-2a) the procedure might be as follows:

·   Assume well rate

---

[6] As an example, please refer to appendix A for the full development of the equation for gas flow in the tubing.

- Compute bottom-hole pressure from IPR equation.
- Compute separator pressure using bottom-hole pressure, well rate and pressure loss in tubing and pipeline.
- Compare if the separator pressure calculated is equal to the given separator pressure, if not, another well rate is tried.
- The process is repeated until the difference between the given and calculated separator pressure is minimal.

As an example, consider the production network of two wells shown in Figure 2-4.
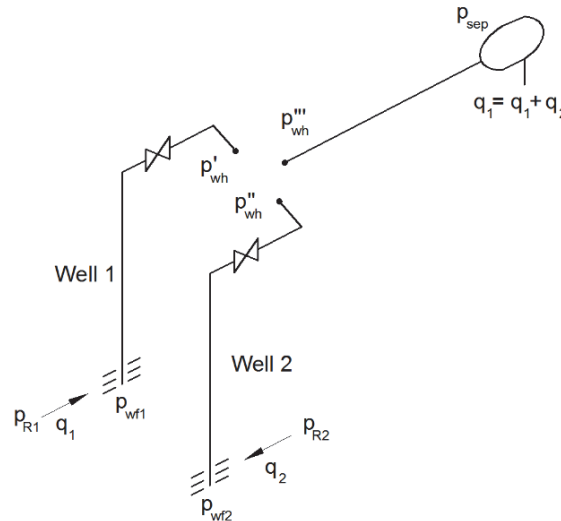
FIGURE 2-4. PRODUCTION NETWORK WITH TWO WELLS

A methodology for solving the flow equilibrium conditions of the system is the following:

- Assume a surface rate for both wells (q_1 and q_2)
- Use the inflow performance relationship of each well to calculate the operating bottom-hole pressures (p_{wf1} and p_{wf2}).
- Perform pipe pressure drop calculations from the bottom-hole of wells 1 and 2 to the wellhead points p'_{wh} and p''_{wh}.
- With the separator conditions, the sum of the two liquid rates calculate the wellhead pressure (p'''_{wh}).
- Iterate on the rate of each well until the three pressures (p'_{wh}, p''_{wh}, p'''_{wh}) are the same.

In the following discussions, the flow performance and equilibrium of a production system will be explained graphically using the available and required pressure curves. These concepts are similar to what is popularly known as "Nodal Analysis" and are based on the fact that, for a flowing system, the pressure at a given location must be the same if calculated countercurrent or concurrent **from a location with a fixed pressure**.

Please note that the graphical method is used just to understand the performance of the production system. Engineering calculations are made solving the system of equations (i.e. numerical model).

2.1.   INFLOW PERFORMANCE RELATIONSHIP

Consider the configuration shown in Figure 2-5. The cross section of a radial reservoir is shown, with a vertical well drilled in the center. Initially the well is closed so the pressure across the reservoir is constant and equal to p_{Ro}. The well is then put to production and the wellbore pressure is fixed to p_{wf}.
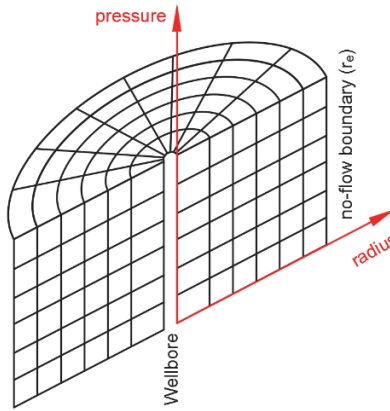
FIGURE 2-5. CROSS SECTION OF A VERTICAL WELL DEPICTING THE COORDINATE SYSTEM TO PLOT PRESSURE VERSUS RADIUS

Initially, at time t_1 only the vicinity of the well will experience a reduction in pressure because of flow towards the wellbore (shown in Figure 2-6). As time passes the pressure will be reduced farther away from the wellbore until it reaches the boundary r_e (t_3). With time, as the reservoir is depleted and the reservoir pressure falls, the pressure distribution will continue to change as shown in t_4. In this stage, it is usually valid that $\frac{\partial p}{\partial t} = constant$ at all radial positions.

The period from t_0 to t_3 is called infinite acting and the period after t_3 is called "stabilized flow" or pseudo steady state (pss), after the pressure changes have reached the outer boundary. If the boundary is not uniform, and the pressure changes take different times to reach all the boundaries, then there is an intermediate regime between infinite acting and pseudo steady state called "transient", in which pressure changes haven't reached yet all boundaries.
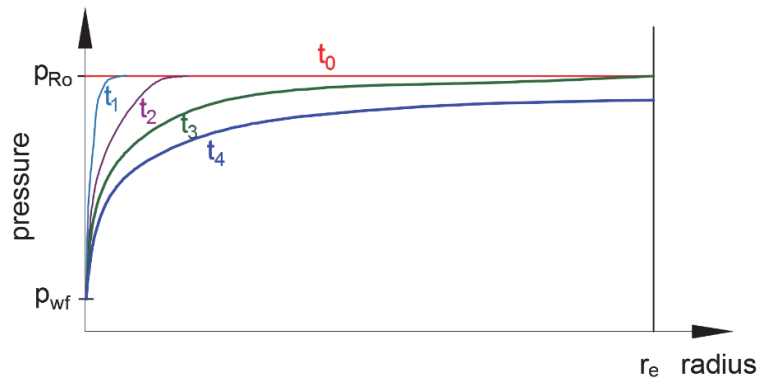
FIGURE 2-6. EVOLUTION OF PRESSURE ACROSS THE RESERVOIR WITH TIME WHEN PUT ON PRODUCTION

In some reservoirs, the pressure at the outer boundary is kept constant (e.g. due to water injection, aquifer support, etc.). For those cases, typically referred to as "steady-state production", it is assumed that the standard condition rate is constant for all radial positions.

The time required for the reservoir to enter the pseudo steady state (or alternatively, steady state) depends greatly on the reservoir characteristics, i.e. permeability, porosity, and properties of the fluid (i.e. viscosity, compressibility). It might take from a few hours to years.

An expression to estimate the required time (in hours) to reach pseudo-steady state or steady-state is given in Eq. 2-1 (for vertical wells and circular drainage area):

$$t = 281.3 \cdot \frac{\phi \cdot \mu \cdot c_t \cdot A}{k}$$

<div align="right">EQ. 2-1</div>

Where:

ϕ	Porosity [-]
μ	Fluid viscosity at reservoir conditions [cp]
c_t[7]	Total compressibility @ reservoir conditions [1/bar]
A	Drainage area [m^2]
k	Permeability [md]

TABLE 2-1. TIME REQUIRED TO PSS FOR A GAS RESERVOIR WITH THE CHARACTERISTICS[8] AND USING EQ. 2-1.

k	tpss		k	tpss
[md]	[h]		[md]	[h]
0.01	835 552.28		100	83.56
0.1	83 555.23		1 000	8.35
1	8 355.52		10 000	0.84
10	835.55			

For reservoirs with medium to high permeabilities, the well enters pseudo steady state or steady state in relatively short time (minutes, hours, days), thus most of the reservoir outtake will be performed under those regimes. Moreover, one can frequently remove the time dependence from the equations by relating it to depletion and using reservoir pressure instead.

For tight formations ($k < 1$ md) productivity in the transient regime must be considered when estimating the IPR. Therefore, time typically appears explicitly in these equations, together with an initial pressure.

Inflow performance relationship (IPR) expressions are typically derived by solving analytically the partial differential equations (PDE) of reservoir flow and introducing simplifications and assumptions. The derivation often yields an expression that relates reservoir and bottom-hole pressure with reservoir rates at the transient, steady state and pseudo-steady state regimes.

The IPR typically contains information about:

· Permeability and porosity of the formation
· Well drainage area, formation thickness
· Type of outer boundary – typically no flow or sometimes constant pressure (e.g. if injection from a neighboring well is being applied)
· Restricted flow to the wellbore (formation damage, stimulation, fracturing, perforation penetration, gravel pack, screens).
· Wellbore geometry
· Volume-averaged pressure of the drainage region (reservoir pressure)
· Variation of fluid properties with pressure (viscosity, relative permeability, formation volume factor)
· The convergence effect when fluids flows towards the wellbore.
· Oil, gas and water saturation in the drainage area.

---

[7] $c_t = c_f + (S_w \cdot c_w + S_g \cdot c_g + S_o \cdot c_o)$
[8] $\phi = 0.3$, $\mu = 0.012$ cp, $c_t = 7.3E\text{-}03$ bar^{-1}, $A = 1$ 130 973 m^2

In principle, there should be three independent IPRs, one for each phase that is produced from the formation (oil, gas and water). However, often the IPR is made for one of the phases (the main phase, oil or gas) and the other are expressed by using a ratio (gas oil ratio, GOR, water cut, WC). The ratio is often assumed to remain constant when rate is varied.

Steady state and pseudo steady state IPRs are usually applying integrating Darcy's law (steady state and laminar flow):

$$\frac{q}{A} = \frac{k}{\mu} \cdot \frac{\Delta p}{\Delta x}$$

EQ. 2-2

Or Forschheimer's (steady state and turbulent flow):

$$\frac{q}{A} + \left(\frac{q}{A}\right)^2 \cdot \beta \cdot \rho \cdot \frac{\mu}{k} = \frac{k}{\mu} \cdot \frac{\Delta p}{\Delta x}$$

EQ. 2-3

On the domain of interest. Note that in these equations, if the coordinate system points away from the well (for example when using a radial coordinate system) then a negative sign must be placed in from of the pressure gradient ($\frac{\Delta p}{\Delta x}$), since the pressure gradient is positive and rate flowing out of the well is considered to be negative. If one uses a sign convention in which the rate flowing out of the well is positive, the negative sign in front of the pressure gradient is not needed.

Often (e.g. when assuming a radial geometry) the resulting equations can be solved by variable separation, and integrating from wellbore to a location where reservoir pressure is located[9]. The local rate of the fluid q is expressed in terms of the standard conditions rate of the phase and black oil properties. All parameters that depend on pressure and all parameters that depend on geometry are integrated separately (one in space and one in pressure). Usually, fluid properties such as viscosity and black oil properties and permeabilities are included in the pressure integral.

The local rate at standard conditions is often assumed constant in the geometry. Formally speaking, this approximation is valid for steady state regimes but not for the pseudo steady state regime (since there is no flow at the boundary). In the pseudo-steady-state regime the mass flow of oil flowing towards the wellbore will increase gradually when approaching it. However, assuming a constant standards condition rate throughout the geometry is often a very good approximation, requiring some minor adjustments (for radial flow of undersaturated oil, the minor adjustment is the location of the reservoir pressure). This is because close to the wellbore is where most of the pressure drop occurs and there the difference between assuming a standard condition rate or a varying standard condition rate is minimal (the fluid contribution from the regions close to the well is small).

Issues like:

- formation damage due to invasion of mud during drilling
- area drainage shape
- partial penetration through the reservoir layer
- perforation
- sand control

---

[9] The location where reservoir pressure is located is used instead of the outer boundary, because one wishes the equation to result in terms of reservoir pressure, not in terms of the pressure of the outer boundary. This is because average reservoir pressure is practical to measure (e.g. using a shut-in test).

- wellbore deviation (and effect of permeability anisotropy, if there if flow contribution from different directions)
- fracking,

can usually be quantified by using the concept of "skin". Skin is a dimensionless form of the additional pressure drop the well experiences in the vicinity of the wellbore when non-idealities are present. Since the issues mentioned above usually occur very close to the wellbore, the rest of the IPR solution is not affected and only the value of the end point (wellbore pressure) must be adjusted to account for them.

When dealing with e.g. horizontal or inclined wells, it is often not possible to separate variables and integrate, since the resulting equations are more challenging. In these situations, luckily, equations of similar structure have been solved earlier for other disciplines (e.g. the Laplace equation using complex number theory), thus the analytical solutions can be applied to the equations at hand by analogy (e.g. making voltage analog to pressure and current analog to flow). The cases with boundaries (for example lateral along the well and upper and lower boundaries in a perfect horizontal well) are solved by placing imaginary mirror (or image wells) and using linear superposition.

In horizontal or inclined wells, the effect of permeability anisotropy is important since a significant part of the flow will come from the horizontal and vertical directions. A mathematical trick employed to be able to use solutions found for isotropic permeability is to apply a variable substitution on one of the geometric coordinates. In this way, the equations for anisotropic permeability cases can be converted to an equivalent coordinate system and become identical to the isotropic permeability equations. Some variable substitutions often used are that the effective thickness becomes $h_{eff} = \sqrt{\frac{k_h}{k_v}} \cdot h$ (having anisotropy is equivalent to

having a much thicker layer), $k_{eff} = \sqrt{k_h \cdot k_v}$ and wellbore radius $r_{w,eff} = r_w \cdot \left(\frac{\sqrt{\frac{k_h}{k_v}} + 1}{2} \right)$.

Most IPR equations typically end up with the following structure:

$$q = U \cdot \int_{p_{wf}}^{p_R} F(p) \cdot dp$$

<div align="right">EQ. 2-4</div>

Where the coefficient U is a function of reservoir rock properties, drainage geometry and non-ideal phenomena such as skin, partial penetration, etc. The pressure function $F(p)$ usually depends on fluid properties and on the relative permeability of the phase.

2.1.1. LIMITATIONS OF IPRS

Partial differential equations of flow in porous media have explicit solutions only for some idealized cases. If the partial differential equation is too complex, it usually must be solved numerically (like in a reservoir model). This makes it less attractive for using it in production calculations.

Having an analytical expression derived from the PDE is of great advantage because it allows:

- Quantifying the contribution and relevance of each parameter to well productivity and take corrective actions, if relevant
- Finding causes for reduced well performance (e.g. in theory, the well should produce "X", but in practice, the well is producing "Y", why?)
- Conducting well planning and completion design
- Predicting well productivity during the planning phase

· Predicting IPR with depletion by updating the equation parameters

However, it is always necessary to adjust the IPR obtained analytically with test data.

Some examples of inflow performance relationship equations are discussed next.

2.1.2. UNDERSATURATED, VERTICAL OIL WELL

The IPR expression for vertical undersaturated oil wells considering skin, radial drainage area and production in the pseudo-steady state regime is:

$$q_{\bar{o}} = \frac{2 \cdot \pi \cdot k \cdot h}{\left[ln\left(\frac{r_e}{r_w}\right) - 0.75 + s\right]} \cdot \int_{p_{wf}}^{p_R} \frac{1}{\mu_o \cdot B_o} dp \qquad \text{EQ. 2-5}$$

To use variables in practical metric units (thickness h in m, wellbore radius r_w in m, external boundary radius r_e in m , oil viscosity μ_o in cP, pressure p in bara, permeability k in md, to give oil rate in Sm³/d) we apply unit conversion:

$$q_{\bar{g}} \ in \ \left[\frac{m^3}{d}\right] = \left[\frac{86400 \ s}{d}\right] \cdot \frac{2 \cdot \pi \cdot \left[\frac{9.869233e - 16 \ m^2}{md}\right] \cdot h}{\left[ln\left(\frac{r_e}{r_w}\right) - 0.75 + s\right]}$$
$$\cdot \int_{p_{wf}}^{p_R} \frac{1}{\left[\frac{1.0e - 3 \ Pa \ s}{1 \ cP}\right] \cdot B_g} dp \left[\frac{1e5 \ Pa}{1 \ bara}\right] \qquad \text{EQ. 2-6}$$

Which gives:

$$q_{\bar{g}} = \frac{k \cdot h}{\left[ln\left(\frac{r_e}{r_w}\right) - 0.75 + s\right] \cdot 18.68} \cdot \int_{p_{wf}}^{p_R} \frac{1}{\mu_o \cdot B_o} dp \qquad \text{EQ. 2-7}$$

Here s is skin factor and B_o is the oil volume factor.

The product $B_o \cdot \mu_o$ is often linear with pressure (viscosity increases almost linearly with pressure, B_o decreases almost linearly with pressure), therefore, it's integration in pressure can be approximated by:

$$\int_{p_{wf}}^{p_R} \frac{1}{\mu_o \cdot B_o} dp = (p_R - p_{wf}) \cdot \left[\left(\frac{1}{\mu_o \cdot B_o}\right)_{@p_{wf}} + \left(\frac{1}{\mu_o \cdot B_o}\right)_{@p_R}\right] \cdot 0.5 \qquad \text{EQ. 2-8}$$

Then the solution of Eq. 2-19 gives:

$$q_{\bar{o}} = J\left(p_R - p_{wf}\right) \qquad \text{EQ. 2-9}$$

Where J, the productivity index, is:

$$J = \frac{k \cdot h}{18.68 \cdot \left[ln\left(\frac{r_e}{r_w}\right) - 0.75 + s\right]} \cdot \left(\frac{1}{\mu_o \cdot B_o}\right)_{@p_{av}} \qquad \text{EQ. 2-10}$$

Because the product $B_o \cdot \mu_o$ is linear then $\left[\left(\frac{1}{\mu_o \cdot B_o}\right)_{@p_{wf}} + \left(\frac{1}{\mu_o \cdot B_o}\right)_{@p_R}\right] \cdot 0.5 = \left(\frac{1}{\mu_o \cdot B_o}\right)_{@p_{av}}$.

The terms in the sum in the denominator of J represent, respectively from left to right, the effect of convergence ($ln\left(\frac{r_e}{r_w}\right)$), type of outer boundary (-0.75 if pseudo steady state, -0.5 if steady state), and skin effect. Usually, the term $ln\left(\frac{r_e}{r_w}\right)$ is an order of magnitude higher than the effect of the boundary.

Effect of depletion on undersaturated oil IPR

The colored lines and points in Figure 2-7 shows the IPRs calculated using Eq. 2-10 for an undersaturated oil well for reservoir pressures equal to 400, 300, 200 bara and several flowing bottom-hole pressures ranging from reservoir pressure to atmospheric pressure. While there are some variations of J due to flowing bottom-hole pressure and reservoir pressure, the variation is usually small, and J is often considered constant with depletion.
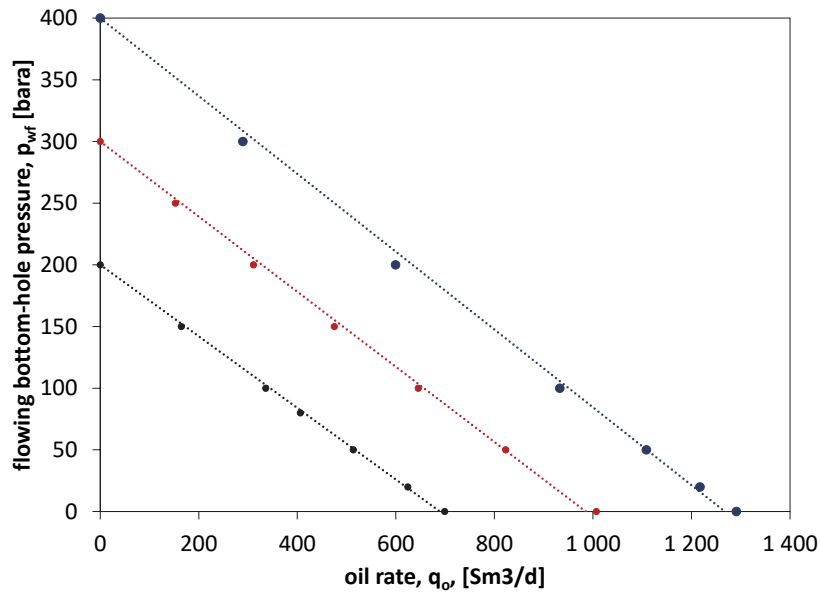
FIGURE 2-7. IPR PREDICTED BY EQ. 2. FOR UNDERSATURATED OIL WELL AND DIFFERENT RESERVOIR PRESSURES

EXERCISE: HORIZONTAL OR VERTICAL WELL?

You are considering drilling a well with wellbore radius (r_w) equal to 0.15 m in a undersaturated oil reservoir of thickness 40 m, with a horizontal permeability (k_H) equal to 15 md, and a permeability anisotropy ($\frac{k_H}{k_V}$) equal to 9. Determine how long should you make a horizontal well to have the same productivity index as a vertical well that is completed all through the reservoir thickness (h). Consider the reservoir has a length and width of 1500 m.

Additional information

Expressions for productivity index of vertical well and horizontal well to use for this task, (in units of $\frac{Sm3}{d}/bar$) are given below:

- Vertical undersaturated oil well perforated through all the reservoir thickness (h), neglecting boundary effect and skin.

$$J_{vertical\ well} = \frac{k_H \cdot h}{18.68 \cdot (\mu_o \cdot B_o)_{@p_{av}} \cdot \left[\ln\left(\frac{r_e}{r_w}\right)\right]}$$

Where permeability is in md, h in m, viscosity in cP and B_o in m³/Sm³

- Long[10], horizontal well of length L_w, located in the middle of the layer with thickness h, width D, in pseudo steady state:

$$J_{horizontal\ well} = \frac{k_H \cdot h}{6.22 \cdot (\mu_o \cdot B_o)_{@p_{av}} \cdot \left[\frac{\pi \cdot D}{2 \cdot L_w} + \frac{3 \cdot h \cdot \sqrt{\frac{k_H}{k_V}}}{L_w} \cdot \ln\left(\frac{h \cdot \sqrt{\frac{k_H}{k_V}}}{\pi \cdot r_w \cdot \left(1 + \sqrt{\frac{k_H}{k_V}}\right)}\right)\right]}$$

SOLUTION:

Making equal both analytical expressions gives:

$$\frac{k_H \cdot h}{18.68 \cdot (\mu_o \cdot B_o)_{@p_{av}} \cdot \left[\ln\left(\frac{r_e}{r_w}\right)\right]} = \frac{k_H \cdot h}{6.22 \cdot (\mu_o \cdot B_o)_{@p_{av}} \cdot \left[\frac{\pi \cdot D}{2 \cdot L_w} + \frac{3 \cdot h \cdot \sqrt{\frac{k_H}{k_V}}}{L_w} \cdot \ln\left(\frac{h \cdot \sqrt{\frac{k_H}{k_V}}}{\pi \cdot r_w \cdot \left(1 + \sqrt{\frac{k_H}{k_V}}\right)}\right)\right]}$$

Cancelling out common terms and clearing out the well length

$$L_w = \frac{\left[\frac{\pi \cdot D}{2} + 3 \cdot h \cdot \sqrt{\frac{k_H}{k_V}} \cdot \ln\left(\frac{h \cdot \sqrt{\frac{k_H}{k_V}}}{\pi \cdot r_w \cdot \left(1 + \sqrt{\frac{k_H}{k_V}}\right)}\right)\right]}{2.68 \cdot \left[\ln\left(\frac{r_e}{r_w}\right)\right]}$$

Substituting all factors, this gives $L_w = 156\ m$, i.e. In order to make the horizontal well more productive than the vertical well it has to be at least ca 4 times longer than the thickness of the reservoir.

IPR for water injector

The same model and reasoning employed for a undersaturated oil producer can be applied to a water injector. Starting from Darcy's equation in a radial isotropic reservoir, completed through the whole layer thickness "h"

$$\frac{q_w}{2 \cdot \pi \cdot r \cdot h} = -\frac{k}{\mu_w} \cdot \frac{dp}{dr} \qquad \text{EQ. 2-11}$$

A negative sign was added to the equation to obtain injection rates values which are positive. The coordinate system used here assumes that r increases when far from the wellbore. Since pressure decreases when far

---

[10] Long enough such that end effects can be ignored.

away from the wellbore, the pressure gradient is negative. If the negative sign is not added, this will give a negative injection rate.

Expressing the local flow rate of water in terms of the standard conditions rate:

$$\frac{q_{\bar{w}} \cdot B_w}{2 \cdot \pi \cdot r \cdot h} = -\frac{k}{\mu_w} \cdot \frac{dp}{dr}$$

EQ. 2-12

Separating variables

$$q_{\bar{w}} \cdot \frac{1}{r} = -\frac{2 \cdot \pi \cdot k \cdot h}{\mu_w \cdot B_w} \cdot dp$$

EQ. 2-13

Integrating each side:

$$q_{\bar{w}} \cdot \int_{r_w}^{r@p_R} \frac{1}{r} dr = q_{\bar{w}} \cdot ln\left(\frac{r@p_R}{r_w}\right) = -\frac{k \cdot h}{18.68} \cdot \int_{p_{wf}}^{p_R} \frac{1}{\mu_w \cdot B_w} dp$$

EQ. 2-14

For both injection and production cases, reservoir pressure will be located in the same radial position (Figure 2-8). If in pseudo steady state, this is at 0.47• r_e.
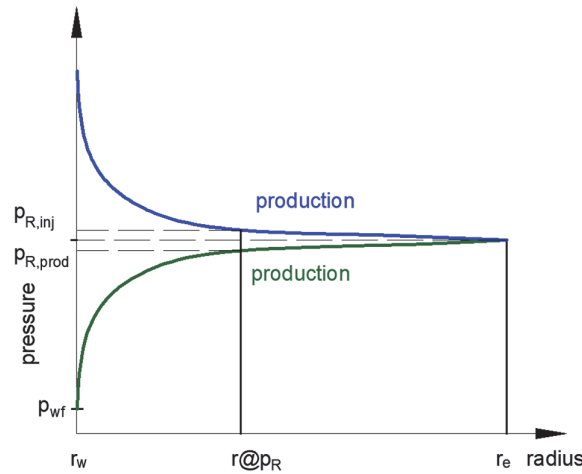
FIGURE 2-8. RADIAL PRESSURE DISTRIBUTION IN AN IDEAL VERTICAL WATER WELL IN PRODUCTION AND INJECTION MODE DEPICTING THE RADIAL LOCATION OF RESERVOIR PRESSURE DOES NOT CHANGE

$$ln\left(\frac{r@p_R}{r_w}\right) = ln\left(\frac{0.47 \cdot r_e}{r_w}\right) = ln\left(\frac{r_e}{r_w}\right) - 0.75$$

EQ. 2-15

Similar to the undersaturated oil case, the product $B_w \cdot \mu_w$ is often linear with pressure (viscosity increases almost linearly with pressure, B_w decreases almost linearly with pressure). Substituting in the equation gives.

$$q_{\bar{w}} = \frac{k \cdot h}{18.68 \cdot \left[ln\left(\frac{r_e}{r_w}\right) - 0.75\right]} \cdot \left(\frac{1}{\mu_w \cdot B_w}\right)_{@p_{av}} \cdot \left(p_{wf} - p_R\right)$$

EQ. 2-16

However, in this case the flow is entering the reservoir, and thus is in the same direction as the radial coordinate pointing outwards.

If there is skin, the injection bottom-hole pressure will be higher than the ideal, therefore

$$\left(p_{wf_{ideal}} - p_R\right) = q_{\bar{w}} \cdot \frac{18.68 \cdot \left[ln\left(\frac{r_e}{r_w}\right) - 0.75\right]}{k \cdot h} \cdot \left(\mu_w \cdot B_w\right)_{@p_{av}} \qquad \text{EQ. 2-17}$$

$$\left(p_{wf_{real}} - p_{wf_{ideal}}\right) = q_{\bar{w}} \cdot \frac{18.68}{k \cdot h} \cdot \left(\mu_w \cdot B_w\right)_{@p_{av}} \cdot s$$

Adding these two gives:

$$q_{\bar{w}} = \frac{k \cdot h}{18.68 \cdot \left[ln\left(\frac{r_e}{r_w}\right) - 0.75 + s\right]} \cdot \left(\frac{1}{\mu_w \cdot B_w}\right)_{@p_{av}} \cdot \left(p_{wf} - p_R\right) \qquad \text{EQ. 2-18}$$

Here the same logic as for undersaturated oil wells applies, positive skin requires a higher injection bottom-hole pressure to inject the same rate.

2.1.3. VERTICAL DRY GAS WELL

Assuming a vertical well with cylindrical drainage area, homogeneous formation, pseudo steady state flow, skin and considering rate dependent skin (turbulent flow), an analytical and general equation for flow of dry gas is (borrowing from the saturated oil case):

$$q_{\bar{g}} = \frac{k \cdot h}{18.68 \cdot \left[ln\left(\frac{r_e}{r_w}\right) - 0.75 + s\right]} \cdot \int_{p_{wf}}^{p_R} \frac{1}{\mu_g \cdot B_g} dp \qquad \text{EQ. 2-19}$$

Figure 2-9 shows the behavior of the term $\frac{1}{\mu_g \cdot B_g}$ versus pressure for dry gas of different specific gravities and at different temperatures. For low pressures it is usually linear, medium pressures it is nonlinear, and high pressures it is linear or constant.
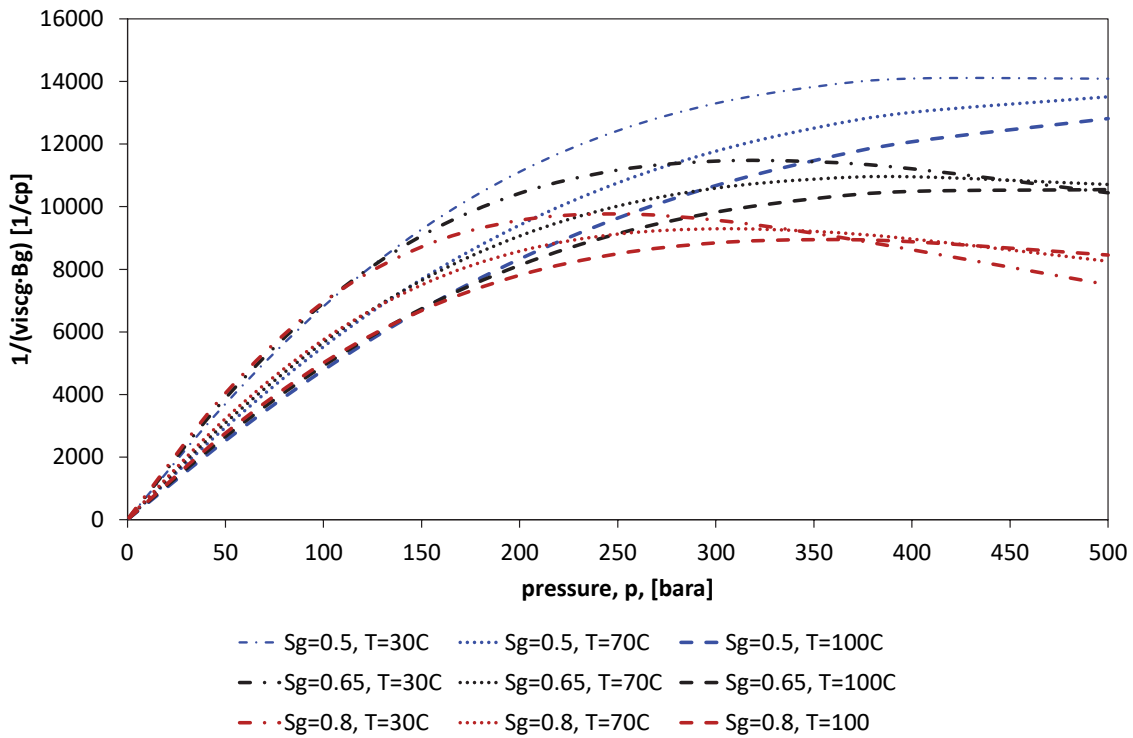
FIGURE 2-9. PRESSURE BEHAVIOR OF THE TERM $\frac{1}{\mu_g \cdot B_g}$ FOR NATURAL GAS WITH THREE VALUES OF SPECIFIC GRAVITY (0.5, 0.65, 0.8) AT THREE TEMPERATURES (30, 70 AND 100 °C).

If one expresses the gas volume factor with the real gas equation, the following expression is obtained:

$$q_{\bar{g}} = \frac{7.63 \cdot k \cdot h}{\left[ln\left(\frac{r_e}{r_w}\right) - 0.75 + s \right]} \cdot \frac{1}{T_R} \cdot 2 \cdot \int_{p_{wf}}^{p_R} \frac{p}{\mu_g \cdot Z} dp \qquad \text{EQ. 2-20}$$

With T_R in [K]. Defining:

$$m(p) = 2 \cdot \int_{p_{sc}}^{p} \frac{p}{\mu_g \cdot Z} dp \qquad \text{EQ. 2-21}$$

And applying this definition to Eq. 2-19 gives:

$$q_{\bar{g}} = \frac{7.63 \cdot k \cdot h}{\left[ln\left(\frac{r_e}{r_w}\right) - 0.75 + s \right]} \cdot \frac{1}{T_R} \left[m(p_R) - m(p_{wf}) \right] \qquad \text{EQ. 2-22}$$

Note that

$$\frac{\left[m(p_R) - m\left(p_{wf}\right) \right]}{2} \cdot \frac{T_{sc}}{T_R \cdot p_{sc}} = \int_{p_{wf}}^{p_R} \frac{1}{\mu_g \cdot B_g} dp \qquad \text{EQ. 2-23}$$

The term $\left[m(p_R) - m\left(p_{wf}\right) \right]$ simplifies to:

- $\frac{\left(p_R{}^2 - p_{wf}{}^2\right)}{\left(\mu_g \cdot Z\right)_{@p_R}}$ at low pressures (e.g. p_R and p_{wf} less than 140 bara), because the product $\frac{p}{\mu_g \cdot Z}$ is linear with pressure

- $\frac{2 \cdot p_R}{\left(\mu_g \cdot Z\right)_{@p_R}} \cdot \left(p_R - p_{wf}\right)$ at high pressures (e.g. p_R and p_{wf}. greater than 200 bara), because the product $\frac{p}{\mu_g \cdot Z}$ is often constant with pressure.

Turbulent flow

The flow of gas in the reservoir is often turbulent, thus it follows Forchheimer's equation, not Darcy's. To derive the IPR equation, we start from Forchheimer's equation in a radial isotropic reservoir, completed through the whole layer thickness "h"

$$\frac{\mu_g}{k} \cdot \frac{q_g}{2 \cdot \pi \cdot r \cdot h} + \rho_g \cdot \beta \cdot \left(\frac{q_g}{2 \cdot \pi \cdot r \cdot h}\right)^2 = \frac{dp}{dr} \qquad \text{EQ. 2-24}$$

Where β is a turbulence factor. A correlation for turbulence factor (in 1/m) (Janicek and Katz[2-9]) as a function of permeability (in md) is

$$\beta = \frac{18.04E9}{k^{1.25} \cdot \phi^{0.75}} \qquad \text{EQ. 2-25}$$

Expressing local rate of gas as $q_{\bar{g}} \cdot B_g$ and gas density as $\frac{\rho_{\bar{g}}}{B_g}$ gives

$$\frac{\mu_g}{k} \cdot \frac{q_{\bar{g}} \cdot B_g}{2 \cdot \pi \cdot r \cdot h} + \frac{\rho_{\bar{g}}}{B_g} \cdot \beta \cdot \frac{q_{\bar{g}}{}^2 \cdot B_g{}^2}{4 \cdot \pi^2 \cdot r^2 \cdot h^2} = \frac{dp}{dr} \qquad \text{EQ. 2-26}$$

Rearranging and simplifying terms:

$$\mu_g \cdot B_g \cdot \left(\frac{1}{k} \cdot \frac{q_{\bar{g}}}{2 \cdot \pi \cdot r \cdot h} + \rho_{\bar{g}} \cdot \frac{\beta}{\mu_g} \cdot \frac{q_{\bar{g}}^2}{4 \cdot \pi^2 \cdot r^2 \cdot h^2} \right) = \frac{dp}{dr}$$

EQ. 2-27

Separating variables:

$$\left(\frac{1}{k} \cdot \frac{q_{\bar{g}}}{2 \cdot \pi \cdot r \cdot h} + \rho_{\bar{g}} \cdot \frac{\beta}{\mu_g} \cdot \frac{q_{\bar{g}}^2}{4 \cdot \pi^2 \cdot r^2 \cdot h^2} \right) \cdot dr = \frac{dp}{\mu_g \cdot B_g}$$

EQ. 2-28

Integrating from wellbore to location of reservoir pressure gives

$$\frac{1}{k} \cdot \frac{q_{\bar{g}}}{2 \cdot \pi \cdot h} \cdot \left[ln\left(\frac{r_e}{r_w} \right) - 0.75 \right] + \rho_{\bar{g}} \cdot \frac{\beta}{\bar{\mu}_g} \cdot \frac{q_{\bar{g}}^2}{4 \cdot \pi^2 \cdot h^2} \cdot \left[\frac{1}{r_w} - \frac{1}{r_e} \right] = \int_{p_{wf}}^{p_R} \frac{1}{\mu_g \cdot B_g} dp$$

EQ. 2-29

Here $\bar{\mu}_g$ is an average gas viscosity between reservoir pressure location and wellbore.

Usually, r_e is much bigger than r_w, then the expression is simplified to:

$$\left[\frac{1}{2 \cdot \pi \cdot k \cdot h} \cdot \left(ln\left(\frac{r_e}{r_w} \right) - 0.75 \right) \right] \cdot q_{\bar{g}} + \left[\frac{\rho_{\bar{g}} \cdot \beta}{\bar{\mu}_g \cdot 4 \cdot \pi^2 \cdot h^2 \cdot r_w} \right] \cdot q_{\bar{g}}^2 = \int_{p_{wf}}^{p_R} \frac{1}{\mu_g \cdot B_g} dp$$

EQ. 2-30

The resulting equation is quadratic, thus clearing out the rate given reservoir and bottom-hole pressure is slightly more computationally expensive, as when compared against the expression obtained assuming Darcy flow.

In practical SI units the equation is:

$$\left[\frac{18.68}{k \cdot h} \cdot \left(ln\left(\frac{r_e}{r_w} \right) - 0.75 \right) \right] \cdot q_{\bar{g}} + \left[\frac{\rho_{\bar{g}} \cdot \beta}{\bar{\mu}_g \cdot h^2 \cdot r_w \cdot 2.947E16} \right] \cdot q_{\bar{g}}^2 = \int_{p_{wf}}^{p_R} \frac{1}{\mu_g \cdot B_g} dp$$

EQ. 2-31

To avoid solving the quadratic equation, Eq. 2-30 can be approximated further by:

- Rate-dependent skin (D).

Manipulating the quadratic equation

$$\left[ln\left(\frac{r_e}{r_w} \right) - 0.75 \right] \cdot q_{\bar{g}} + \left[\frac{k \cdot \rho_{\bar{g}} \cdot \beta \cdot q_{\bar{g}}}{\bar{\mu}_g \cdot 2 \cdot \pi \cdot h \cdot r_w} \right] \cdot q_{\bar{g}} = 2 \cdot \pi \cdot k \cdot h \cdot \int_{p_{wf}}^{p_R} \frac{1}{\mu_g \cdot B_g} dp$$

EQ. 2-32

Making $D = \frac{k \cdot \rho_{\bar{g}} \cdot \beta}{\bar{\mu}_g \cdot 2 \cdot \pi \cdot h \cdot r_w}$ and rearranging terms:

$$q_{\bar{g}} = \frac{2 \cdot \pi \cdot k \cdot h}{\left[ln\left(\frac{r_e}{r_w} \right) - 0.75 + D \cdot q_{\bar{g}} \right]} \cdot \int_{p_{wf}}^{p_R} \frac{1}{\mu_g \cdot B_g} dp$$

EQ. 2-33

Which is very similar to the original equation assuming Darcy flow, but including a rate-dependent skin.

- Adding an exponent n, which accounts for the presence of turbulent (n=0.5) or laminar (n=1) flow:

$$q_{\bar{g}} = C \cdot \left[m(p_R) - m(p_{wf}) \right]^n$$

EQ. 2-34

Effect of depletion on dry gas IPR

There is no need to correct for depletion the dry gas IPR.

2.1.1. INJECTION WELLS OF NATURAL GAS (E.G. FOR STORAGE), CO_2 OR H_2

The IPR derivation for a gas injection well is very similar to a dry gas producer, but, if we assume injection rates have a positive sign, a negative sign must be added to the equation.

$$q_{\bar{g}} = -\frac{2 \cdot \pi \cdot k \cdot h}{\left[ln\left(\frac{r_e}{r_w}\right) - 0.75 + s\right]} \cdot \int_{p_{wf}}^{p_R} \frac{1}{\mu_g \cdot B_g} dp$$

EQ. 2-35

This is because the radial coordinate system assumes that r increases when far from the wellbore, and since pressure decreases when far away from the wellbore, the pressure gradient is negative. If the negative sign is not added, this will give a negative injection rate.

Figure 2-10 shows the behavior of the term $\frac{1}{\mu_g \cdot B_g}$ with pressure for hydrogen, carbon dioxide and natural gas at different temperatures.
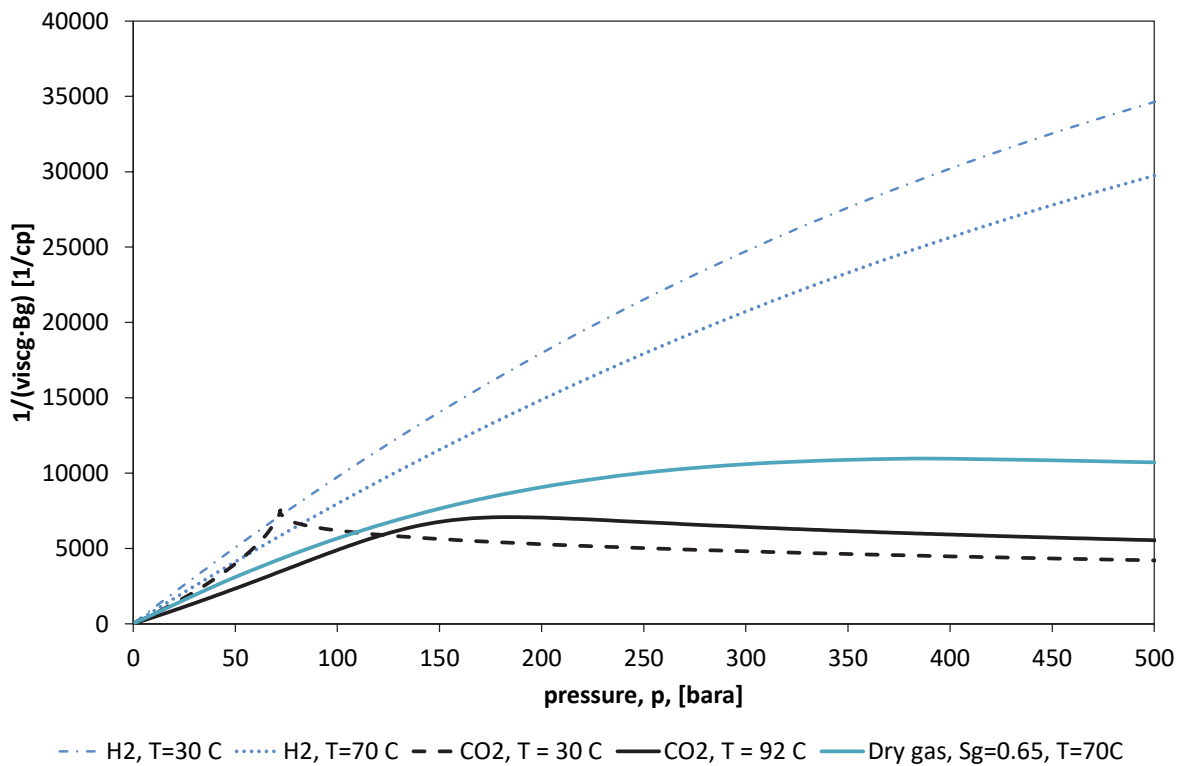
FIGURE 2-10. PRESSURE BEHAVIOR OF THE TERM $\frac{1}{\mu_g \cdot B_g}$ FOR PURE CO_2 AT TEMPERATURES OF 30 AND 92 °C, PURE H_2 AT TEMPERATURES OF 30 AND 70 °C AND NATURAL GAS WITH SPECIFIC GRAVITY 0.65 AND AT 70 °C.

For CO_2 injection, bottom-hole pressure and reservoir pressure are both usually high (e.g. above 200 bara), and then the $\frac{1}{\mu_g \cdot B_g}$ term can be assumed linear with pressure, then the expression is reduced to an expression similar to the saturated oil case:

$$q_{\bar{g}} = J \cdot \left(p_{wf} - p_R\right)$$

EQ. 2-36

2.1.2. SATURATED, VERTICAL OIL WELL

Assuming a vertical well with cylindrical drainage area, homogeneous formation, pseudo steady state flow, skin and considering rate dependent skin (turbulent flow), an analytical and general equation for flow of undersaturated and saturated oil with simultaneous flow of gas and water is:

$$q_{\bar{o}} = \frac{k \cdot h}{18.68 \cdot \left(ln\left(\frac{r_e}{r_w}\right) - 0.75 + s\right)} \int_{p_{wf}}^{p_R} \frac{k_{ro}}{\mu_o \cdot B_o} \, dp \qquad \text{EQ. 2-37}$$

Where the pressure function is:

$$F(p) = \frac{k_{ro}}{\mu_o \cdot B_o} \qquad \text{EQ. 2-38}$$

And U:

$$U = \frac{k \cdot h}{18.68 \cdot \left(ln\left(\frac{r_e}{r_w}\right) - 0.75 + s\right)} \qquad \text{EQ. 2-39}$$

If reservoir pressure is equal or below bubble point pressure ($p_R \le p_b$), a typical assumption (which is not always valid) to solve the pressure function integral is to consider the product $\frac{k_{ro}}{\mu_o \cdot B_o}$ linear with pressure below the bubble point. The pressure function can then be expressed as:

$$F(p) = \frac{k_{ro}}{\mu_o \cdot B_o} = \left(\frac{k_{ro}}{\mu_o \cdot B_o}\right)_{p=0} + \left[\left(\frac{k_{ro}}{\mu_o \cdot B_o}\right)_{p_R} - \left(\frac{k_{ro}}{\mu_o \cdot B_o}\right)_{p=0}\right] \cdot \frac{p}{p_R} \qquad \text{EQ. 2-40}$$

Or, equivalently:

$$F(p) = F(p = 0) + [F(p_R) - F(p = 0)] \cdot \frac{p}{p_R} \qquad \text{EQ. 2-41}$$

Therefore, the solution of the pressure function integral will have a linear term in addition to the quadratic term:

$$\int_{p_{wf}}^{p_R} F(p)dp = F(p = 0) \cdot (p_R - p_{wf}) + [F(p_R) - F(p = 0)] \cdot \frac{1}{p_R \cdot 2}\left(p_R{}^2 - p_{wf}{}^2\right) \qquad \text{EQ. 2-42}$$

Expanding terms:

$$\int_{p_{wf}}^{p_R} F(p)dp = F(p = 0) \cdot p_R - F(p = 0) \cdot p_{wf} + [F(p_R) - F(p = 0)] \cdot \frac{1}{p_R \cdot 2}\left(p_R{}^2 - p_{wf}{}^2\right) \qquad \text{EQ. 2-43}$$

$$\int_{p_{wf}}^{p_R} F(p)dp = F(p = 0) \cdot p_R - F(p = 0) \cdot p_{wf} + F(p_R) \cdot \frac{p_R}{2} - F(p_R) \cdot \frac{p_{wf}{}^2}{p_R \cdot 2} - F(p = 0) \cdot \frac{p_R}{2} \qquad \text{EQ. 2-44}$$
$$+ F(p = 0) \cdot \frac{p_{wf}{}^2}{p_R \cdot 2}$$

Grouping terms by pressure:

$$\int_{p_{wf}}^{p_R} F(p)dp = [F(p = 0) + F(p_R)] \cdot \frac{p_R}{2} - F(p = 0) \cdot p_{wf} - \frac{[F(p_R) - F(p = 0)]}{2} \cdot \frac{p_{wf}{}^2}{p_R} \qquad \text{EQ. 2-45}$$

Dividing by $[F(p = 0) + F(p_R)] \cdot \frac{p_R}{2}$

$$\frac{2}{[F(p = 0) + F(p_R)] \cdot p_R} \cdot \int_{p_{wf}}^{p_R} F(p)dp$$
$$= 1 - \frac{F(p = 0) \cdot 2}{[F(p = 0) + F(p_R)]} \cdot \frac{p_{wf}}{p_R} - \frac{[F(p_R) - F(p = 0)]}{[F(p = 0) + F(p_R)]} \cdot \left(\frac{p_{wf}}{p_R}\right)^2 \qquad \text{EQ. 2-46}$$

Defining a variable "V"

$$V = \frac{F(p=0) \cdot 2}{[F(p=0) + F(p_R)]}$$

EQ. 2-47

Therefore:

$$1 - V = \frac{F(p_R) - F(p=0)}{[F(p=0) + F(p_R)]}$$

EQ. 2-48

Substituting back in the integral of the pressure function:

$$\frac{2}{[F(p=0) + F(p_R)] \cdot p_R} \cdot \int_{p_{wf}}^{p_R} F(p) dp = 1 - V \cdot \frac{p_{wf}}{p_R} - (1-V) \cdot \left(\frac{p_{wf}}{p_R}\right)^2$$

EQ. 2-49

Substituting Eq. 2-49 back in the IPR equation:

$$q_{\bar{o}} = \frac{k \cdot h \cdot [F(p=0) + F(p_R)] \cdot p_R}{18.68 \cdot \left(ln\left(\frac{r_e}{r_w}\right) - 0.75 + s\right) \cdot 2} \left[1 - V \cdot \frac{p_{wf}}{p_R} - (1-V) \cdot \left(\frac{p_{wf}}{p_R}\right)^2\right]$$

EQ. 2-50

Making $q_{\bar{o},max}$:

$$q_{\bar{o},max} = \frac{k \cdot h \cdot [F(p=0) + F(p_R)] \cdot p_R}{18.68 \cdot \left(ln\left(\frac{r_e}{r_w}\right) - 0.75 + s\right) \cdot 2}$$

EQ. 2-51

The following expression is obtained:

$$q_{\bar{o}} = q_{\bar{o},max} \left[1 - V \cdot \frac{p_{wf}}{p_R} - (1-V) \cdot \left(\frac{p_{wf}}{p_R}\right)^2\right]$$

EQ. 2-52

Vogel found this same equation using data points generated with reservoir simulator, with V = 0.2.

Using Eq. 2-47, and assuming V = 0.2, $F(p=0)$ is then:

$$F(p=0) = \frac{F(p_R)}{9}$$

EQ. 2-53

Eq. 2-51 can then be further simplified:

$$q_{\bar{o},max} = \frac{k \cdot h \cdot \left[\frac{10}{9} \cdot F(p_R)\right] \cdot p_R}{18.68 \cdot \left(ln\left(\frac{r_e}{r_w}\right) - 0.75 + s\right) \cdot 2} = \frac{k \cdot h \cdot \left[\left(\frac{k_{ro}}{\mu_o \cdot B_o}\right)_{@p_R}\right] \cdot p_R}{18.68 \cdot \left(ln\left(\frac{r_e}{r_w}\right) - 0.75 + s\right) \cdot 1.8} = \frac{J}{1.8} \cdot pR$$

EQ. 2-54

Where J is the single-phase oil productivity index using properties at current reservoir pressure. It can be pointed out that $q_{\bar{o},max}$ is equal to the absolute open flow[11] of the well, calculated assuming an undersaturated oil well, divided by 1.8.

The backpressure equation, proposed by Fetkovich, is obtained if one applies V = 0 to Eq. 2-52. This assumes the pressure function $F(p)$ is a straight line between zero ("0") pressure and reservoir pressure.

$$q_{\bar{o}} = q_{\bar{o},max} \left[1 - \left(\frac{p_{wf}}{p_R}\right)^2\right]$$

EQ. 2-55

with $q_{\bar{o},max}$:

---

[11] AOF, oil rate at standard conditions when flowing bottom-hole pressure is zero bara.

$$q_{\bar{o},max} = \frac{k \cdot h \cdot [F(p_R)] \cdot p_R}{18.68 \cdot \left(ln\left(\frac{r_e}{r_w}\right) - 0.75 + s\right) \cdot 2} = \frac{k \cdot h \cdot \left[\left(\frac{k_{ro}}{\mu_o \cdot B_o}\right)_{@p_R}\right] \cdot p_R}{18.68 \cdot \left(ln\left(\frac{r_e}{r_w}\right) - 0.75 + s\right) \cdot 2} = \frac{J}{2} \cdot pR \qquad \text{EQ. 2-56}$$

Where J is the single-phase oil productivity index using properties at current reservoir pressure.

Eq. 2-55 can be rearranged to look similar to the backpressure equation for low-pressure dry gas wells:

$$q_{\bar{o}} = C\left[(p_R)^2 - (p_{wf})^2\right] \qquad \text{EQ. 2-57}$$

With $C = \frac{q_{\bar{o},max}}{p_R{}^2}$

To include high velocity effects (turbulent flow), a quadratic term can be included (e.g. Eq. 2-58 when using equation Eq. 2-55), or alternatively, an exponent n, accounting for the presence of turbulent (n=0.5) or laminar (n=1) flow (e.g. Eq. 2-59 when using equation Eq. 2-55).

$$q_{\bar{o}} + B \cdot q_{\bar{o}}{}^2 = q_{\bar{o},max}\left[1 - \left(\frac{p_{wf}}{p_R}\right)^2\right] \qquad \text{EQ. 2-58}$$

$$q_{\bar{o}} = q_{\bar{o},max}\left[1 - \left(\frac{p_{wf}}{p_R}\right)^2\right]^n \qquad \text{EQ. 2-59}$$

The IPR equations shown in this section can be used in two ways:

- If no test or field data is available, estimate IPR using the analytical expression. This will require geometric information, relative and absolute permeabilities, average oil saturation around the wellbore, fluid properties, etc. However, be aware that assuming $F(p)$ is linear with pressure is sometimes not adequate.
- If test data is available, tune the unknown parameters in the equation (e.g. $q_{\bar{o},max}$ and V if using Eq. 2-52) to match the results of the model to the test values. At least two test points are typically required. It is often reasonable to use V=0 or V=0.2.

Effect of depletion on saturated oil IPR

When the reservoir is being depleted, reservoir pressure will decrease below the bubble point pressure, and fluid properties and saturations around the wellbore will vary, and there will be simultaneous flows or gas, oil and water towards the wellbore[12]. Therefore, the IPR will also change.

In Eq. 2-52, both V and $q_{\bar{o},max}$ depend on the pressure function $F(p)$ and must be updated with depletion. However, in some cases, e.g. when using Vogel's or Fetkovich's equations, V is often left constant and only $q_{\bar{o},max}$ is updated with depletion[13].

As seem from Eq. 2-54 and Eq. 2-56, $q_{\bar{o},max}$ is often a function of reservoir pressure and the mobility evaluated at reservoir pressure. Therefore $q_{\bar{o},max}$ is often updated by scaling it by the ratio of new to old mobility and by the ratio of new to old reservoir pressure, as shown in Eq. 2-60.

---

[12] This is evidenced often by a variation in the producing GOR. Please refer to Appendix G for an expression for GOR variation with time.

[13] Astutik[2-1] in her master thesis generated IPRs using reservoir simulator for an oil well with gas and water coning. She obtained that V must be varied in time (from 0.85-0.39) to match properly the IPR curves computed. The behavior obtained for V versus reservoir pressure was non-monotonic.

$$q_{\bar{o},max,new} = q_{\bar{o},max,old} \cdot \left[\frac{\left(\frac{k_{ro}}{\mu_o \cdot B_o} \right)_{new} \cdot (p_R)_{new}}{\left(\frac{k_{ro}}{\mu_o \cdot B_o} \right)_{old} \cdot (p_R)_{old}} \right]$$ EQ. 2-60

2.1.3. COMPOSITE IPR: BOTH UNDERSATURATED AND SATURATED OIL

If reservoir pressure is above the bubble point pressure, but the flowing bottom-hole pressure is below the bubble point pressure ($p_{wf} \leq p_b \leq p_R$), then, a suitable equation is a composite IPR, linear above the bubble point:

If $p_{wf} \geq p_b$ then:

$$q_{\bar{o}} = J \cdot \left(p_R - p_{wf} \right) = J \cdot p_R \cdot \left(1 - \frac{p_{wf}}{p_R} \right)$$ EQ. 2-61

And using a suitable saturated oil IPR below the bubble point pressure, but using as reservoir pressure the bubble point pressure. To obtain the oil rate one must add the oil rate obtained from the undersaturated oil equation after substituting $p_{wf} = p_b$. For example, using Eq. 2-56:

for $p_{wf} < p_b$:

$$q_{\bar{o}} = \frac{J \cdot p_b}{2} \cdot \left(1 - \left(\frac{p_{wf}}{p_b} \right)^2 \right) + J \cdot p_R \cdot \left(1 - \frac{p_b}{p_R} \right)$$ EQ. 2-62

2.1.4. FLOW OF ASSOCIATED PRODUCTS IN AN OIL WELL: GAS AND WATER

With depletion, due to reservoir pressure reduction and neighboring injection, the saturation of gas and water around the wellbore will change and the gas and water mobility will increase or decrease, therefore, changing the producing GOR and WC.

If there is no gas coning from the gas cap nor water cusping from the water layer, then usually an IPR for the oil phase is used, and the gas and water rates are calculated with the producing GOR and WC. Therefore, it is typically assumed that GOR and WC remain constant for a given depletion state (or reservoir pressure) even though there might be variations with p_{wf} for a given reservoir pressure.

The flow of oil and water is sometimes modeled by using a "compound" liquid IPR equation. The liquid IPR is derived by writing two separate inflow performance relationships for oil and for water. For the case $p_R \geq p_b$:

$$q_{\bar{o}} = J_{oil} \cdot \left(p_R - p_{wf} \right)$$ EQ. 2-63
$$q_{\bar{o}} = J_{water} \cdot \left(p_R - p_{wf} \right)$$ EQ. 2-64

Adding these two equations gives:

$$q_{\bar{l}} = q_{\bar{o}} + q_{\bar{w}} = (J_{oil} + J_{water}) \cdot \left(p_R - p_{wf} \right) = J_l \cdot \left(p_R - p_{wf} \right)$$ EQ. 2-65

Substituting the definition of productivity index from Eq. 2-10 (assuming common reservoir thickness, drawdown and skin) gives:

$$J_l = \frac{k \cdot h}{18.68 \cdot \left[ln \left(\frac{r_e}{r_w} \right) - 0.75 + s \right]} \cdot \left(\frac{k_{ro}}{(\mu_o \cdot B_o)_{@p_{av}}} + \frac{k_{rw}}{(\mu_w \cdot B_w)_{@p_{av}}} \right)$$ EQ. 2-66

Based on this definition, the liquid productivity index of the well depends on the sum of the mobilities of oil and water. The relative permeabilities of water (k_{rw}) and oil (k_{ro}) depend on the average pore saturation of water (S_w) around the wellbore. When mostly water is flowing, the saturation of water is high and the relative permeability of water is high while the oil's is low. When mostly oil is flowing, the saturation of water is low

and the relative permeability of oil is high while the water's is low. Therefore, if the amount of water produced is high, the liquid productivity index should resemble a productivity index when only water is flowing. If the amount of water produced is low, the liquid productivity index should resemble a productivity index when only oil is flowing. As an example, Figure 2-11 below shows the variation of the liquid productivity index with produced water cut for a horizontal oil well (values calculated from data presented in Jurus et al[2-8]).
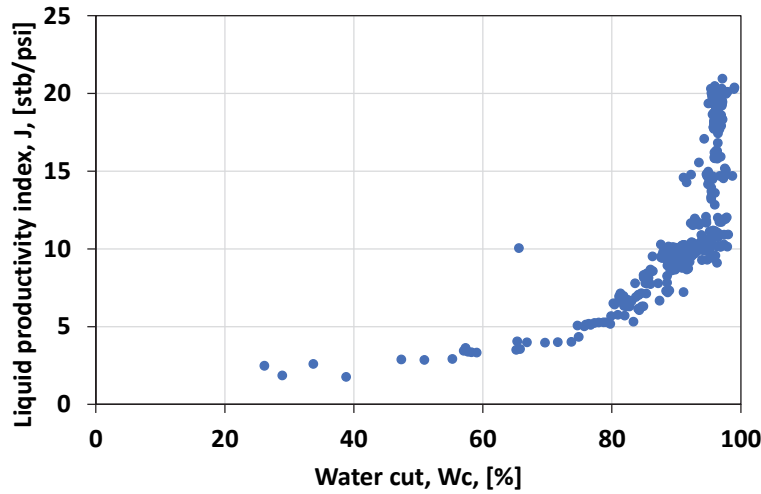
FIGURE 2-11. VALUE OF THE LIQUID PRODUCTIVITY INDEX AS A FUNCTION OF WATER CUT. VALUES CALCULATED FROM WELL TESTS IN A HORIZONTAL UNDERSATURATED VISCOUS OIL WELL WITH HYDRODYNAMIC AQUIFER.

Effect of depletion on liquid IPR

A new J_l can be found by using the expression:

$$J_{l,new} = J_{l,old} \cdot \frac{\left[\left(\frac{k_{ro}}{\mu_o \cdot B_o}\right)_{new} + \left(\frac{k_{rw}}{\mu_w \cdot B_w}\right)_{new}\right]}{\left[\left(\frac{k_{ro}}{\mu_o \cdot B_o}\right)_{old} + \left(\frac{k_{rw}}{\mu_w \cdot B_w}\right)_{old}\right]}$$

EQ. 2-67

2.1.5. IPR AND WATER OR GAS CONING

Coning from a gas cap or from the aquifer is usually established when the oil rate produced is greater than critical oil rate or, equivalently, when the flowing bottom-hole pressure is reduced below the critical bottom-hole pressure. The critical oil rate and critical bottom-hole pressure will depend strongly on the distance between the well and the water-oil contact or the gas-oil contact, among other parameters such as the vertical permeability.

Immediately after gas or water breakthrough occurs, the oil rate will be severely reduced (for example, Asheim reports ca 1/10 reduction in the oil rate in a well with water cusping in the Helder field). However, after some time the oil rate will stabilize, when the transient coning crest stops changing, and the well will then produce with a constant GOR or WC.

Analytical models indicate that the value of the stabilized GOR or WC depends on the ratio between the oil rate and the critical oil rate. Interestingly, the relationship is asymptotic, and there will be an oil rate above which the WC or GOR won't change significantly. For example, using the analytical steady-state model of Asheim for water coning from the aquifer to a horizontal, undersaturated oil well, the water ratio ($f_w = \frac{q_{\bar{w}}}{q_{\bar{o}}}$) has the upper limit:

$$f_{w,max} = \frac{\left(\frac{h_t}{h_e} - 1\right)}{\left(\frac{k_o \cdot \mu_w}{\mu_o \cdot k_w}\right)}$$

EQ. 2-68

Where:

h_t is the combined height of oil and water layers

h_e is the height of the oil layer

For cases where the critical oil rate is very low (e.g. with regular production rates 10 times higher) it will be almost impossible to produce the well without causing coning. However, in those situations the producing WC or GOR will most likely tend to remain constant despite changes in oil rates. Therefore, for these cases it is often possible to draw an IPR for oil (or total liquid) and calculate the gas (or water) with the stabilized values of GOR or WC. An example justifying this assumption is the work presented by Astutik[2-1] that studied an oil well with simultaneous coning of water and gas.

For cases where oil production rates are comparable to the critical oil rate (0-8 times larger) or where the pseudo steady state coning crest is not yet fully established, it is not possible to draw an IPR for one phase and find gas or water rates with the GOR and WC. More advanced models (or the use of a reservoir simulator) are usually required.

2.1.6. IPRs GENERATED WITH RESERVOIR SIMULATOR

IPRs can also be generated from a reservoir model. An example is the Vogel equation, which was derived from reservoir simulation results.

One common approach so derive IPR is to perform a numerical multi-rate well test. However, a disadvantage of this approach is that when the rate is changed, the reservoir will experience a transient. The rate should be recorded after the transient period has passed. An alternative procedure is presented by Astutik[2-1] (for reservoirs with a short transient regime):

- · Perform multiple runs of the reservoir model with different well flowing bottom-hole pressures.
- · Extract from the results of each run the oil, gas and water rates for several pre-specified reservoir pressures.
- · Group and plot all points that have the same reservoir pressure. This will give you the IPR at that specific reservoir pressure.

Graphically, the proposed procedure is equivalent to make a horizontal sweep in the IPR plot at constant flowing bottom-hole pressure, to collect the points at different reservoir pressures.
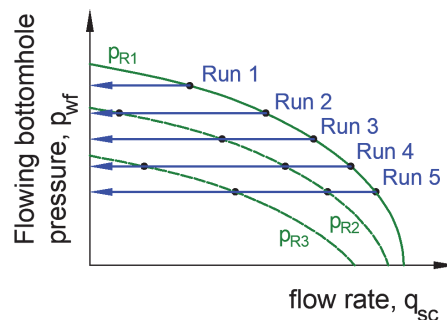
FIGURE 2-12. GRAPHIC ILLUSTRATION OF THE PROCESS TO ESTIMATE IPR WITH A RESERVOIR SIMULATOR ACCORDING TO ASTUTIK (2012)

2.2.   AVAILABLE AND REQUIRED PRESSURE FUNCTION

Consider the pipe shown in Figure 2-13. The pipe segment has an inlet "1" and an outlet "2". Assume that there is a single-phase fluid (e.g. gas, oil or water) flowing through the pipe with a standard-condition flow rate q_{sc} (i.e. a constant mass flow rate). In this setup, there are several calculation possibilities:

1.   The outlet and inlet pressures are given so the rate flowing through the pipe can be computed.
2.   The inlet pressure p_1 and the flow rate are given and it allows to compute the outlet pressure p_2, by performing concurrent pressure loss calculations.
3.   The outlet pressure p_2 and the flow rate are given and it allows to compute the inlet pressure p_1 by performing countercurrent pressure loss calculations.
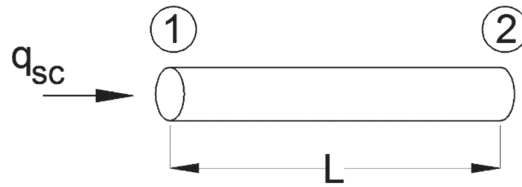
FIGURE 2-13. PIPE SEGMENT

If the inlet pressure p_1 is left constant, and the standard conditions rate is increased gradually from zero to an upper limit, the computed outlet pressures p_2 (computed with method 2) will display a monotonic concave curve behavior like the one shown in Figure 2-14. This curve is the "available pressure" curve.
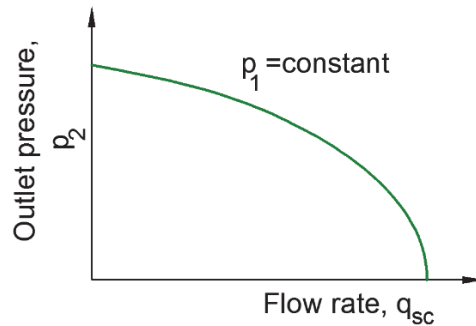
FIGURE 2-14. AVAILABLE PRESSURE AT PIPE OUTLET FOR DIFFERENT FLOW RATES AND FIXED INLET PRESSURE

If p_2 is left constant and the rate is varied from zero to an upper limit, the computed pressure p_1 (using method 3) will follow a convex curve behavior like the one shown in Figure 2-15. This curve is the "required pressure" curve.
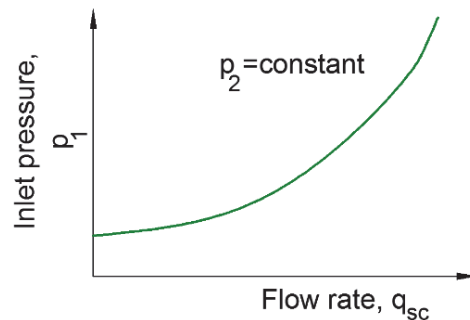
FIGURE 2-15. REQUIRED PRESSURE AT PIPE INLET FOR DIFFERENT FLOW RATES AND FIXED OUTLET PRESSURE

Note that the value of the curves at the origin (when there is no flow) is calculated using the hydrostatic fluid column only, thus it depends on the height difference between inlet and outlet (zero for this particular case,).

The available and required pressure curves concept can be extended to characterize the performance of complex parts of a production system (that include pipelines, reservoir, pumps, valves, etc.) and when a multiphase mixture (oil, gas and water) is flowing. For example, consider the well shown in Figure 2-16 that includes flow through porous media from reservoir to well bottom-hole, then pipe-flow in the casing and pipe-flow in tubing. Using the same logic presented earlier, the inlet to the well is the reservoir pressure (considered invariable for a given depletion state) and the outlet is the wellhead pressure. The available wellhead pressure curve (often referred to as wellhead performance relationship) will follow the same trend discussed before.
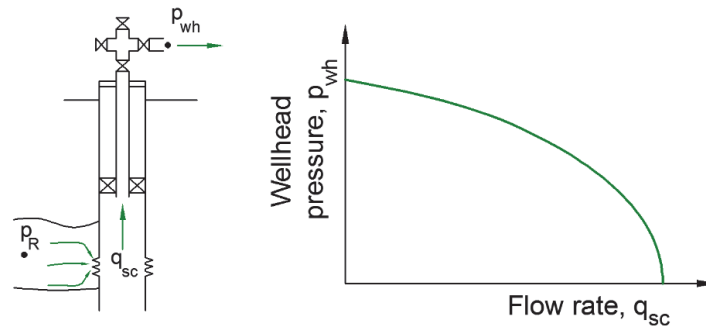
FIGURE 2-16. AVAILABLE WELLHEAD PRESSURE VS PRODUCED RATE

There is usually simultaneous flow of gas, oil and water in the well. The available and required pressure curves are usually built using the flow rate of the preferred hydrocarbon phase (oil or gas). The gas oil ratio (GOR) and water cut (WC, water surface rate divided by liquid surface rate) usually remain constant when the oil (or gas) flow rate is varied when building the curve. This means that available and required pressure curves can be built using the flow rate of any phase of preference, as the others are easily calculated with the GOR and WC.

If the GOR and WC change when varying the flow rate of the preferred hydrocarbon phase (e.g. due to water coning or gas cusping) an available wellhead pressure curve has to be constructed separately for each phase.

If a wellhead choke is included in the system and the flow through the choke is in the subcritical range, the curve is modified as shown in Figure 2-17. It indicates that, if the same rate is desired, a lower pressure p_2 has to be applied in the choked well case than with the no choke case (i.e. there are more pressure losses in the system).
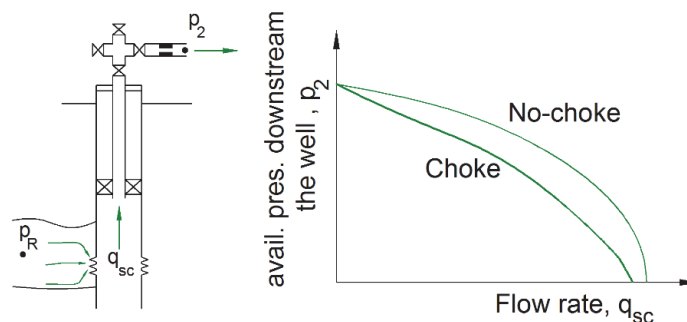
FIGURE 2-17. AVAILABLE WELLHEAD PRESSURE WITH CHOKE INCLUDED VS PRODUCED RATE

The required pressure curve can be computed in the same manner but countercurrent departing from a fixed downstream pressure point (i.e. separator). The curve shown in Figure 2-18 shows the pressure that has to be

exerted at the bottom-hole to flow a given rate through the tubing and pipeline. The curve represents the compound hydraulic performance of the tubing and pipeline (without considering the reservoir).
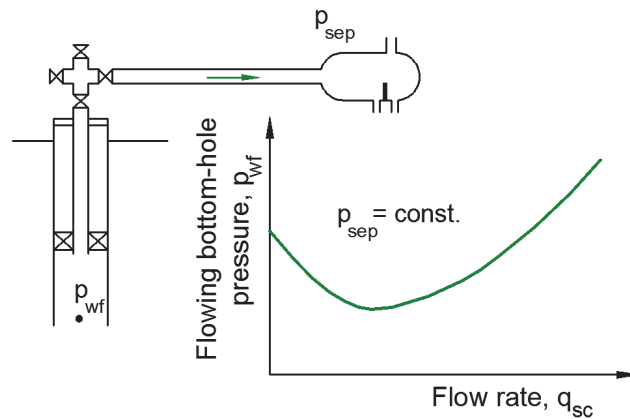
FIGURE 2-18. REQUIRED FLOWING BOTTOM-HOLE PRESSURE CURVE VS. PRODUCED RATE

The required pressure curve for simultaneous flow of gas, oil and water in a pipe usually displays the shape shown in Figure 2-18. The right part of the curve is a friction-dominated regime (high liquid and gas velocities) thus an increase in the flow rates give higher pressure drop. The left part of the curve is a gravity dominated regime (low liquid and gas velocities). For very low velocities, the gas travels faster than the liquid, reducing the cross-section flow area occupied by the gas thus yielding a mixture of the density very similar to the density of the liquid (1 in Figure 2-19). As the flow rate increases, the liquid begins to travel faster, reducing its flowing cross section area thus reducing the mixture density (2 in Figure 2-19).
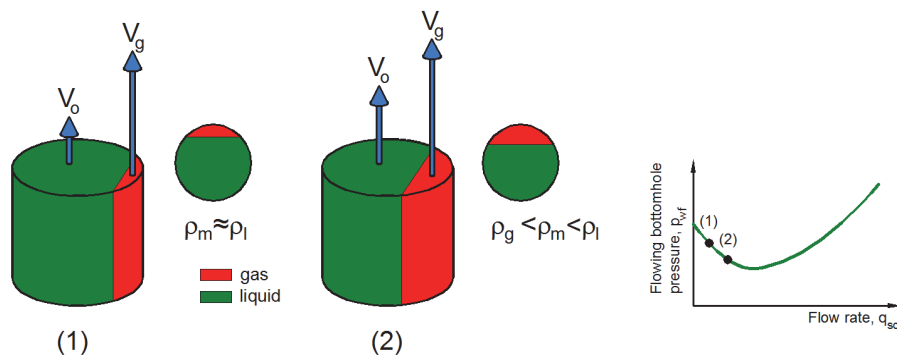
FIGURE 2-19. SCHEMATIC REPRESENTATION OF THE MIXTURE DENSITY VARIATION WITH SLIP BETWEEN GAS AND LIQUID VELOCITIES

In production systems there is simultaneous flow in pipes of two (oil and gas) or three phases (oil, gas and water). The amounts (mass flow rates) of oil and gas change along the production system due to the decrease in pressure and temperature. Usually in oil wells the amount of gas increases due to evolving gas out of solution and in gas producing systems the amount of liquid increases along the tubing due to condensation. However, the overall composition and total mass flow rate remains constant along the system starting in the reservoir near the wellbore to the surface, unless there is commingling of different streams or there are transient phenomena taking place (e.g. liquid accumulation).

An important part of the pressure drop in a production system occurs in the tubing, thus causing significant gas liberation from the oil and gas expansion, or, similarly, liquid condensation. In consequence, there are usually multiple flow patterns (phase distribution in the pipe) along the wellbore with different pressure and temperature gradients (as shown in Figure 2-20).

a) Typical flow patterns along the wellbore in an oil well   b) Typical flow patterns along the wellbore in a gas well
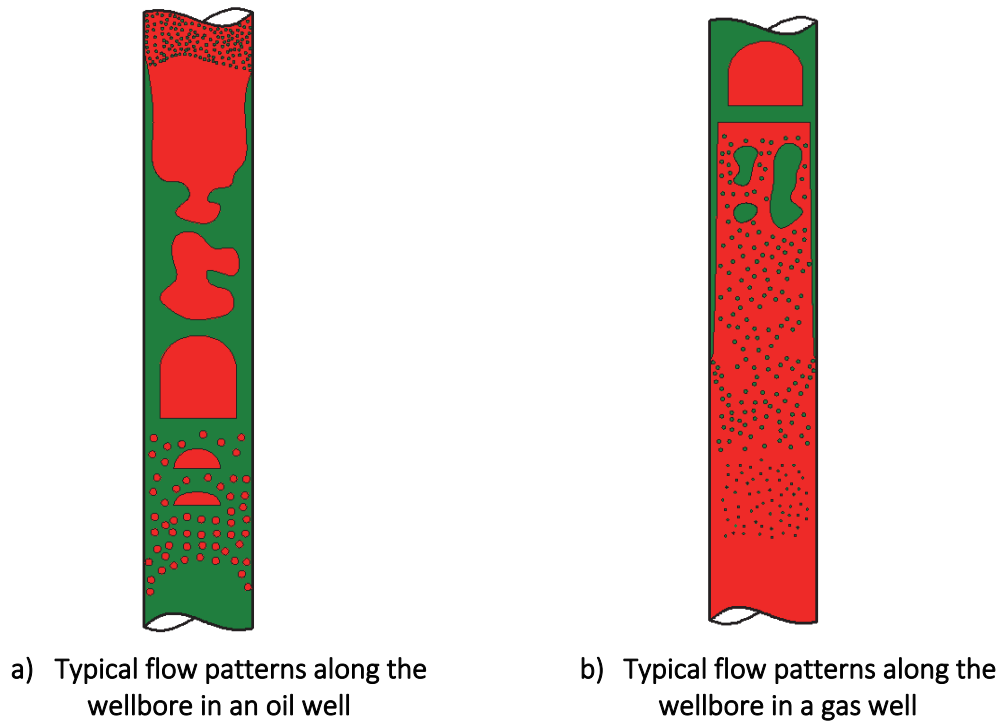
FIGURE 2-20. TYPICAL FLOW PATTERNS ALONG A WELLBORE AS PRESSURE AND TEMPERATURE DECREASE

COMPLETION BITE: TUBULARS

The conductor, casing and tubing are typically made of pipe sections (tubulars) that are threaded together. The tubulars used by the oil and gas industry can be of two types:

· API[14] tubulars: specified and must comply with standards, recommended practices and bulletins issued by the American Petroleum Institute (API).
· Non-API tubulars: designed and manufactured outside API specifications.

API tubulars for casing come in three length ranges: 16-25 ft, 25-34 ft and 34-38 ft. API tubulars for tubing come in two ranges: 20-24 ft and 28-32 ft. A pipe section usually refers to as a "joint"

A tag commonly used to refer to tubing and casing tubulars is shown below:

7''	-	32#	-	P-110	-	BTC/LTC
F01		F02		F03		F04

Where the fields F01, F02, F03 and F04 have the following information:

· F01: refers to the diameter (nominal or outer) of the pipe in inches. Diameters up to 4½ in are typically used for tubing (although higher diameters are often used, specially offshore). Diameters above 4½ in are typically used for casing.
· F02 refers to the weight per length of the pipe (given in pounds per foot or ppf)

---

[14] API: American Petroleum Institute

· F03 refers to the grade of the steel (yield strength of the material in 1000 psi).
· F04 refers to the thread connection type of the joint.

The "drift" is another important tubular specification that represents the maximum diameter of a cylindrical mandrel that can be passed without getting stuck inside the pipe. This is different from the pipe inner diameter (ID) due to ovalization, which is unavoidable in the manufacturing process. Drift must be taken into account when sending items through the tubular (completion tools, smaller tubulars, etc.)

Tubulars are joined together either by 1. machining them with a male-threaded end (pin) and female-threaded end (box) or 2. by machining them with male-threaded ends and using couplings. If using couplings, the coupling is usually threaded in the factory to one end of the joint before shipped to site (a process known as bucking).
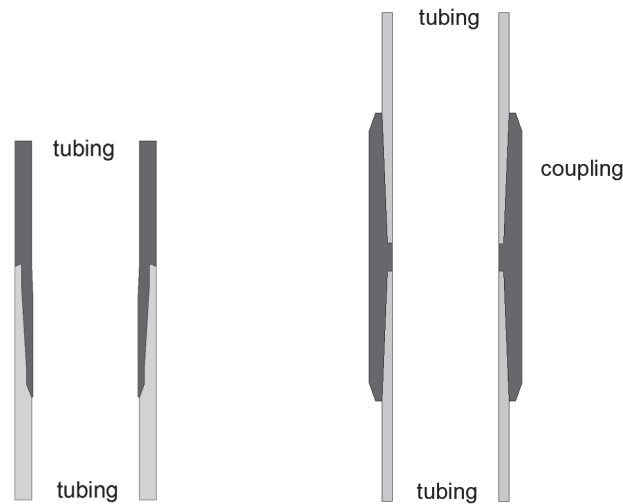
FIGURE 2-21. TWO JOINTS OF TUBING JOINED BY A COUPLING, OR AN INTEGRATED JOINT

The joints are threaded together (make-up) when running in-hole or before running in-hole (depending on the height and load capacity of the drilling rig, 2-3 joints can be threaded before hoisted and run in hole). There are several methods to "make-up" joints, but all of them consists on holding the string section that is inside the well (box), "stab" the suspended section (pin) into the lower section and rotate the suspended section until certain torque value is achieved.

Most of the methods to calculate pressure drop in multiphase flow are based on first identifying the flow pattern with some empirical or analytical criteria and use an associated pressure drop model (derived from mass and momentum conservation equations complemented with empirical correlations). In general, the information required to compute the pressure gradient (dP/dL) in multiphase flow at a certain PVT condition is:

· Local volumetric rates to compute superficial velocities of each phase (volume rate of the phase divided by pipe cross section area).
· Fluid properties: densities, viscosities, fluid-fluid interfacial tension.
· System properties: Pipe diameter (tubing or casing), roughness, inclination, wettability of the surface, entry effects (if any).

Due to the change in local volume rates and in flow patterns along the tubing, flowline or pipeline, it is necessary to perform the pressure drop calculations of the conduit by discretizing into segments.

The workflow, for the case of a single conduit transporting a standard flow rate of oil, gas and water and where the temperature of the fluid is known in advance, is the following:

· Discretize the conduit into segments.
· Define a starting point where p_0 and T_0 is known.
· Calculate local volume rates:
  o If using a compositional approach: 1) calculating total mass flow rate, 2) using a PVT model to calculate fluid properties at P and T.
  o If using a Black Oil (BO) approach: 1) converting from standard to local conditions using BO properties at P and T.; 2) using BO correlations or tables to determine other properties required (densities, viscosities, etc.).
· Compute superficial velocities
· Estimate pressure gradient ($dP/dL=c$) at the starting point using a multiphase flow model.
· Calculate the pressure in the next point in the conduit by solving numerically the equation Eq. 2-69 at the initial conditions p_0 and T_0.

$$\frac{dp}{dL} = c$$

Eq. 2-69

The numerical method to solve the equation may be explicit or implicit. An explicit 4th-order Runge-Kutta is suggested by the author.

· If the temperature is not given a priori and rather a temperature drop model is available, the numerical algorithm solves two functions simultaneously, one for pressure and one for temperature.

2.3.   FLOW EQUILIBRIUM IN PRODUCTION SYSTEMS

2.3.1. SINGLE WELL PRODUCTION SYSTEM

The production system usually has two boundaries where the pressure is fixed: reservoir pressure and separator pressure. To find the operating point, the following procedure is followed:

· Select a point of interest in the system
· Compute the available pressure curves considering the system upstream the point of interest down to the boundary node and
· Compute the required pressure curve considering the system downstream the point of interest up to the boundary node.
· Intersect the curves to find the operating flow rate.

Figure 2-22 shows the results of the process for a single well – separator system selecting the wellhead as the point of interest in the system. The available pressure curves include the pressure losses in reservoir and wellbore, while the required pressure curve includes the pressure losses in the pipeline keeping separator pressure constant.
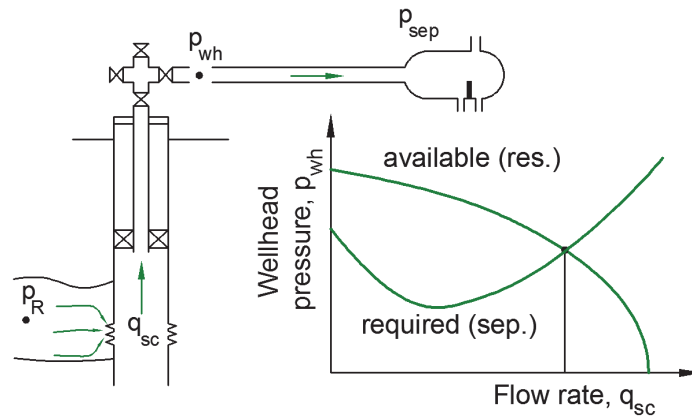
FIGURE 2-22. EQUILIBRIUM FLOW RATE OF THE SYSTEM CALCULATED BY INTERSECTING THE AVAILABLE PRESSURE CURVE CALCULATED FROM RESERVOIR AND THE REQUIRED PRESSURE CURVE FROM SEPARATOR

The production system often contains adjustable equipment such as chokes, ESPs, jet pumps, gas lift, Inflow control valves (ICV), that can operate at multiple operational settings (e.g. choke opening, ESP frequency, gas rate, valve opening). The settings of such equipment affect the available or required hydraulic performance of the system, thus the intersection point of the two curves. Figure 2-23 shows how the operating rate is reduced if the choke is fully open or 75% open.
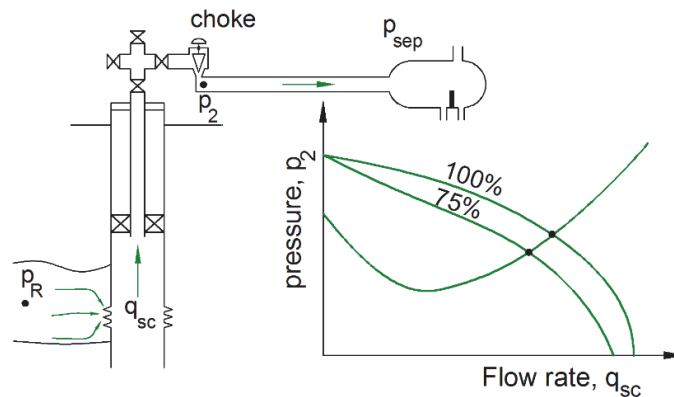
FIGURE 2-23. EQUILIBRIUM FLOW RATE OF THE SYSTEM FOR: FULLY OPEN CHOKE AND 75% OPEN CHOKE

Hydraulic equilibrium analysis can also be used for design purposes to determine the pressure difference that an adjustable equipment has to provide to achieve a specific rate. The analysis is carried out by removing the element from the system and defining the point of interest in the position where the element was. For example, in Figure 2-24 an adjustable choke is considered for installation in the system presented. If a rate below the natural intersection of the curves is desired, the graph allows to estimate the choke pressure drop required to achieve that rate.
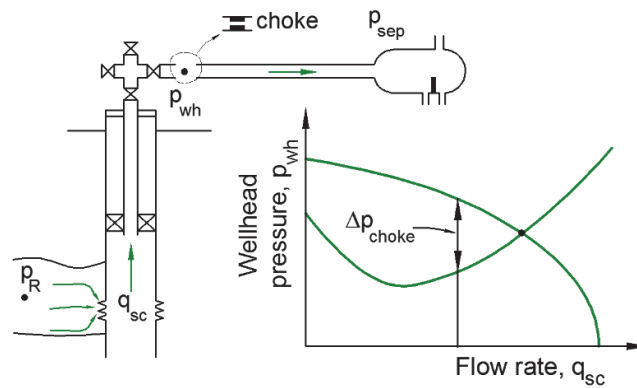
FIGURE 2-24. EQUILIBRIUM ANALYSIS EXCLUDING THE WELLHEAD CHOKE TO ESTIMATE CHOKE PRESSURE DROP TO ACHIEVE A
SPECIFIC FLOW RATE

This approach is useful also for ESP and general boosting design (e.g. selecting the inlet and outlet to the pump as the points of interest, e.g. Figure 2-25).
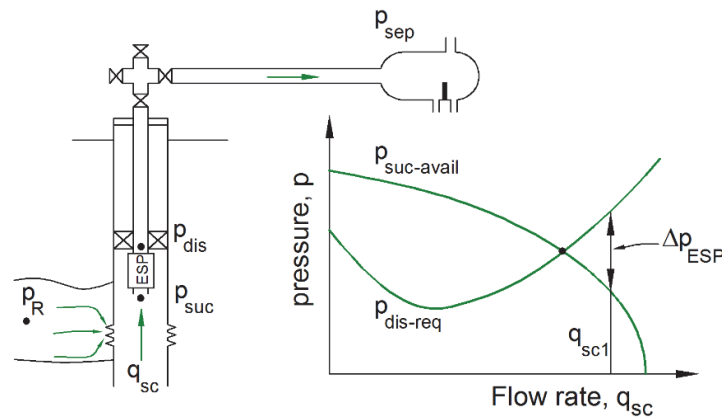
FIGURE 2-25. EQUILIBRIUM ANALYSIS EXCLUDING THE ESP TO ESTIMATE ESP PRESSURE BOOST TO ACHIEVE A SPECIFIC FLOW
RATE

This type of analysis is also relevant for some components that have a numerical model with poor predictability or with big uncertainties (e.g. multiphase boosters), in which case including it in the numerical model of the production system might give wrong results.

Please note that this approach does not allow to calculate the adjustable element setting (in the particular example choke opening) required to achieve the aforementioned pressure difference. For that, the performance curves of the equipment have to be used.

If a particular equipment is already available (e.g. installed in the well) or selected, then the performance curves are employed to verify if it is feasible to achieve the delta pressure and rate combination and to estimate the setting (choke opening or pump frequency) required to achieve that combination. If the operating condition is not feasible, the operating rate has to be modified.

If there is no particular equipment available or already installed in the well then, a screening is performed among commercially available equipment to determine which one delivers the required delta pressure and rate combination. The selection is made taking into account future changes in operating conditions, flexibility of the equipment, cost, among others.

The required and available pressure curves change with reservoir depletion and in consequence, the pressure difference required to produce the specified rate changes with time. In Figure 2-26, the required delta

pressure across the choke diminishes with time until the desired rate q_{SC1} is no longer feasible (a negative choke pressure drop is required, i.e. the choke has to be replaced by a booster).
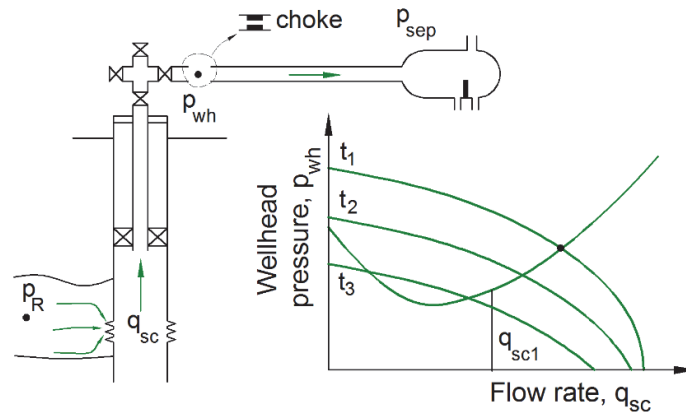
FIGURE 2-26. EQUILIBRIUM ANALYSIS EXCLUDING THE CHOKE TO ESTIMATE CHOKE PRESSURE DROP TO ACHIEVE A SPECIFIC FLOW RATE FOR DIFFERENT TIMES

2.3.2. OPERATIONAL ENVELOPE: CHOKE

A positive (fixed) choke or an adjustable choke at a given fixed opening will display the performance curve (pressure drop vs. rate) shown in Figure 2-27. Note that the inlet pressure, the GOR, WC are kept constant. The rate plotted is the surface rate of the preferred phase (e.g. oil or gas).
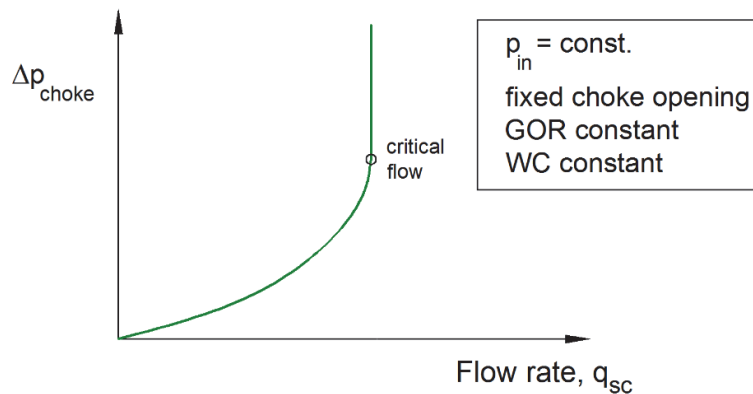
FIGURE 2-27.PERFORMANCE CURVE OF A CHOKE WITH FIXED OPENING

As expected, the pressure drop across the choke increases in a non − linear manner when the rate is increased. However, there is a point where it is not possible to increase the rate further (i.e. the pressure downstream the choke does not impact the rate flowing through the choke). This is because the fluid velocity at the throat of the choke has reached the sonic velocity (Figure 2-28), thus pressure changes downstream the choke do not affect the upstream conditions. This occurs typically when the pressure ratio is between 0.5-0.6.
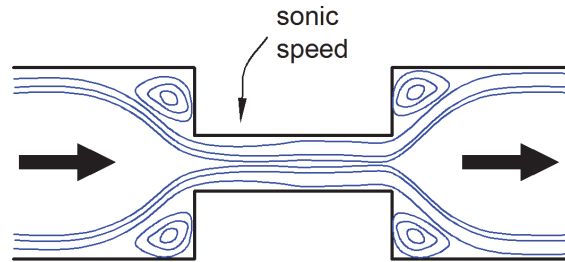
FIGURE 2-28. POSITIVE (FIXED) CHOKE IN CRITICAL REGIME (SONIC VELOCITY REACHED AT THE THROAT)

Figure 2-29 shows the behavior of pressure along the axis of a bean choke. Note that pressure drops suddenly when the flow encounters the contraction point. In gas-dominated flows this sudden pressure reduction can cause cooling (due to the Joule-Thomson effect), liquid condensation and ice formation (in the presence of free water).
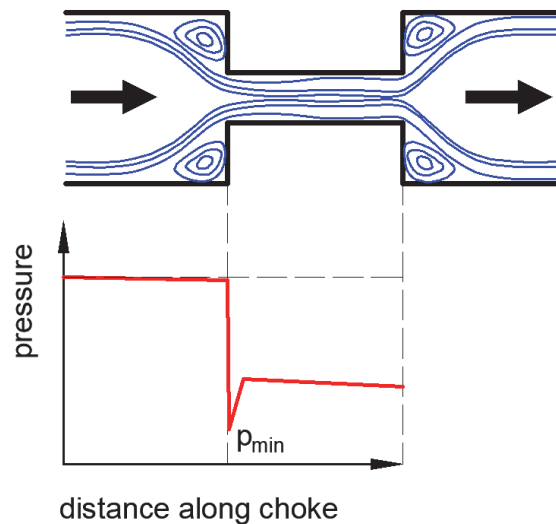
FIGURE 2-29. PRESSURE ALONG THE AXIS OF A BEAN CHOKE (BASED ON MEASUREMENTS BY KOURAKOS[2-19])

Figure 2-30 shows the performance curve of the choke when the inlet pressure is varied. The pressure drop at which the critical flow is reached increases proportionally with the inlet pressure: $\Delta p_c \approx p_{in} - 0.5\ p_{in} = p_{in}\ 0.5$.
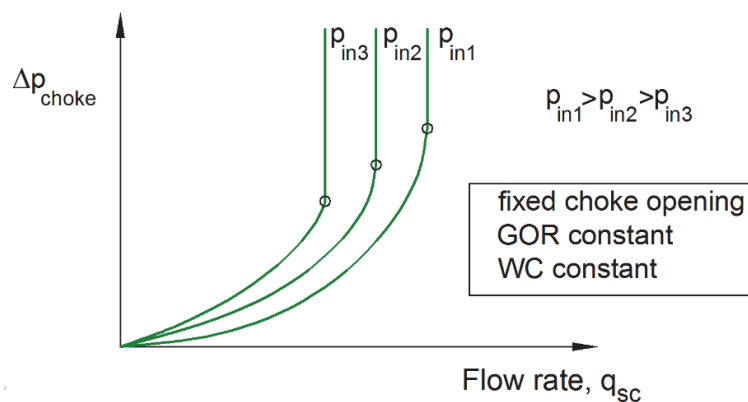
FIGURE 2-30. PERFORMANCE CURVE OF A CHOKE WITH FIXED OPENING

Changes in GOR and WC give a similar variation of the performance curve.

If the choke is adjustable, each choke opening will generate a curve like the one shown in Figure 2-27. A smaller opening will provide a larger pressure drop than a larger opening and critical flow will be reached at lower flow rates. The operational envelope of the choke for multiple choke openings is shown in Figure 2-31.
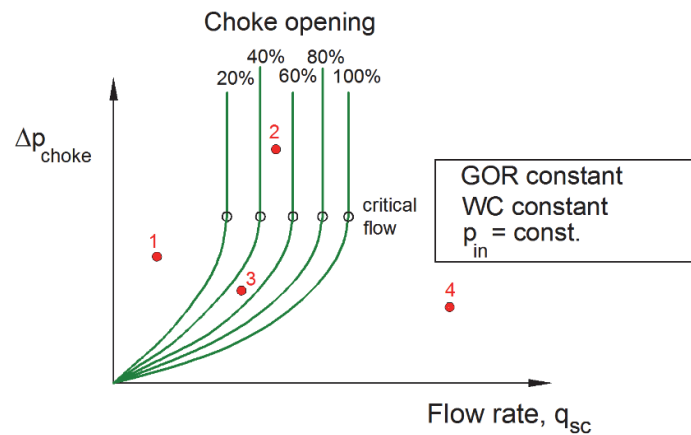
FIGURE 2-31. PERFORMANCE CURVE OF AN ADJUSTABLE CHOKE FOR SEVERAL CHOKE OPENINGS

Some fictitious "desired" operational conditions have been plotted on Figure 2-31 (with the same inlet pressure). Points 2 and 3 are feasible, as they fall in the center of the operating envelope of the choke. Point 2 will be operating in the critical range while point 3 will be operating in the subcritical range.

Point 4 falls outside of the choke envelope, which indicates that a larger choke is required for the application. Point 1 falls in the region of very small choke openings, thus it might be difficult to precisely achieve those operational conditions. A smaller choke should be considered for this application.

Note that, in Figure 2-31, for a constant pressure drop, there is an almost linear relationship between choke opening and flow rate. In reality, this relationship depends on the type of adjustable choke. Figure 2-32 shows, for adjustable chokes operating in the subcritical range, the flow rate through the choke (normalized by the flow rate at maximum opening) versus choke opening. The pressure drop and inlet pressure are kept constant.
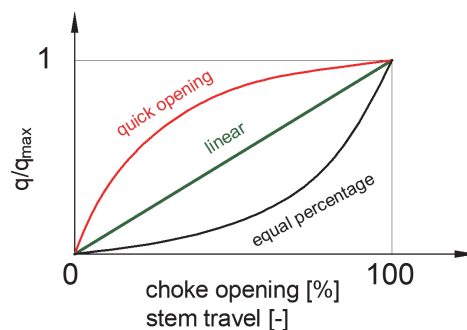
FIGURE 2-32. FLOW RATE ACROSS DIFFERENT TYPES OF ADJUSTABLE CHOKES WITH A FIXED PRESSURE DROP AND INLET PRESSURE

Chokes that follow the red curve belong to the type "quick opening" (e.g. needle and seat choke). In the low flow rate range, these chokes are very sensitive to the opening, making it difficult to achieve with accuracy the desired flow rate. They are however better at higher flow rates.

The black curve corresponds to "equal percentage" chokes (e.g. cage-type). In contrast with "quick opening" these chokes have a very good resolution for smaller openings but worsen for higher openings.

The green curve corresponds to linear type chokes. Disk chokes (Willis type) are normally near linear.

Consider the situation shown in Figure 2-33. A hydraulic equilibrium analysis is performed at the wellhead to determine required choke delta pressure to deliver a specific rate. The analysis is performed at two depletion times, 1 and 2. The required pressure curve remains constant with time but the available pressure curve is reduced due to the decrease in reservoir pressure. The pressure at the inlet to the choke and the choke delta pressure are estimated from the curve.
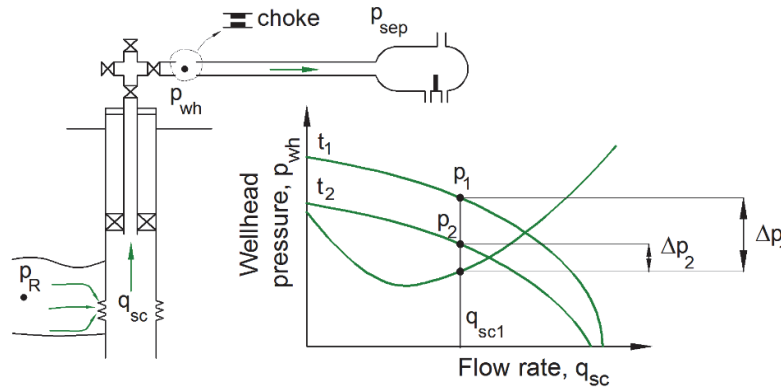
FIGURE 2-33. WELLHEAD EQUILIBRIUM ANALYSIS FOR CHOKE DESIGN FOR TWO DEPLETION STATES

Figure 2-34 shows the performance curve of a choke that has been selected for the application for the two inlet pressures given *p1* and *p2* and for multiple choke openings. Changes in choke opening have a greater impact in the performance curve than changes in inlet pressure.

Operating points 1 and 2 have been plotted on the figure (*Δp* and rate). At the operating conditions of point 1, the green performance curves are applicable. The choke is operating in the subcritical range and the choke opening required to achieve the given delta p is a value less than 60%. At the operating conditions of point 2 the blue performance curves are applicable. The choke is operating in the subcritical range and the choke opening required to achieve the given delta p is a value close to fully open (100%).
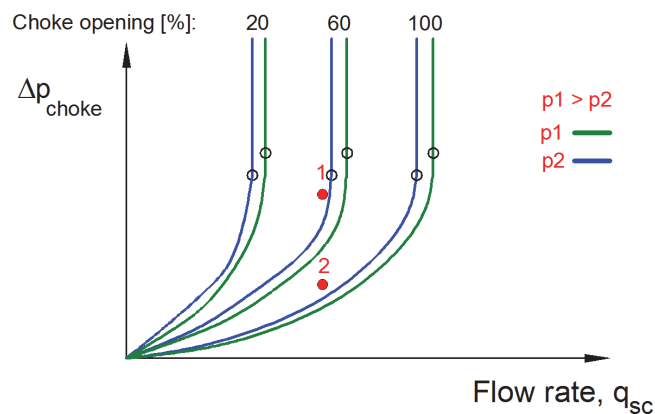
FIGURE 2-34. ADJUSTABLE CHOKE PERFORMANCE CURVE FOR DIFFERENT CHOKE OPENINGS AND TWO INLET PRESSURES

Choke modeling

Chokes, valves, leak paths are often modeled by integrating the differential version of the momentum equation between choke inlet and the throat and assuming there are no friction nor localized losses between

these two points. Due to the convergence of the flow, the effective throat cross-section area[15] is not exactly equal to the throat cross section area (A_{throat}), thus a correction factor (C) is introduced ($A_{throat,effective} = A_{throat} \cdot C$) and is varied such that model predicts measured data.

The one-dimensional momentum equation in differential form for liquid-gas flow, neglecting friction and localized losses is:

$$-dp = H_l \cdot \rho_g \cdot V_g \cdot dV_g + H_g \cdot \rho_l \cdot V_l \cdot dV_l$$

<div align="right">EQ. 2-70</div>

Or, equivalently:

$$-A \cdot dp = d(\dot{m}_g \cdot V_g + \dot{m}_l \cdot V_l)$$

<div align="right">EQ. 2-71</div>

If one assumes there is no slip between liquid and gas and the velocity is the mixture velocity, by integrating Eq. 2-70 between inlet and throat, and neglecting inlet velocity, one obtains:

$$-\int_{p_{inlet}}^{p_{throat}} \frac{1}{\rho_{m,homogeneous}} dp = \frac{(V_{m,throat})^2}{2}$$

<div align="right">EQ. 2-72</div>

Here mixture velocity at the throat $(V_{m,throat})$ is calculated using $A_{throat,effective}$. $\rho_{m,homogeneous}$ is the homogeneous mixture density:

$$\rho_m = \frac{1}{\dfrac{x}{\rho_g} + \dfrac{(1-x)}{\rho_l}}$$

<div align="right">EQ. 2-73</div>

Here x is gas mass fraction.

If one considers liquid and gas travel at different velocities, and neglecting inlet velocity, it is more convenient to integrate Eq. 2-71 than Eq. 2-70. One then obtains

$$-\int_{p_{inlet}}^{p_{throat}} \frac{1}{\rho_e} dp = \frac{\dot{m}^2}{2} \cdot \left[\frac{1}{\rho_{e,throat}^2 \cdot A_{throat,effective}^2}\right]$$

<div align="right">EQ. 2-74</div>

Where ρ_e is momentum density (Eq. D-26).

$$\frac{1}{\rho_e} = \left[\frac{x}{\rho_g} + \frac{S \cdot (1-x)}{\rho_l}\right] \cdot \left[x + \frac{(1-x)}{S}\right]$$

<div align="right">EQ. 2-75</div>

Here S is slip ratio (V_g/V_l).

The main issue when evaluating Eq. 2-72 or Eq. 2-74, to perform the integration and calculate conditions at the throat, is how to estimate liquid and gas density, gas mass fraction and slip versus pressure. This requires a pressure-temperature relationship, and modeling assumptions regarding slip and mass transfer.

---

[15] Often referred to as *vena contracta*

Mass transfer

Most mechanistic choke models used in petroleum engineering (e.g. Perkins[2-11], Sachdeva[2-12], Hydro[2-13], Al Safran[2-14]) use a "frozen flow" approach, where they assume there is no mass transfer in the choke, and use the inlet mass phase fraction. This assumption is maybe rooted in previous experimental work performed for quick depressurization of steam. For example, Moody[2-16] cites previous work of Edwards and O'Brien, Zaker and Wiedermann, Gallagher reporting that non-equilibrium states survive for less than one millisecond. Traveling distances from inlet to throat in the choke are usually short (e.g. around 10 cm) and fluid velocities are usually high (e.g. 20-100 m/s), giving traveling times in the order of magnitude of one millisecond.

A disadvantage of using a frozen flow assumption is that, if the choke inlet is in single phase liquid, no critical flow will ever be predicted, regardless of the values of pressure drop across the choke or throat opening, which could be contrary to what occurs in reality.

Thermodynamic equilibrium or non-equilibrium assumptions are used in other disciplines when developing valve/leak models, often giving a good match between model and experiments (Lorenzo et al[2-15], Darby[2-20]), which could indicate that comparing non-equilibrium survival time against transit time is an oversimplification.

Rigorous nonequilibrium modeling is not straightforward, as it often requires additional (often unknown or uncertain) information about interfacial area between the phases (e.g. flow pattern, bubble/droplet size), coefficients to estimate mass transfer, assignment of different temperatures for liquid and gas, etc.

Carstensen[2-18] implements frozen, equilibrium and non-equilibrium models, but reports a modest improvement in flow rate predictability.

Gas-liquid slip

Early mechanistic choke models used in petroleum engineering (e.g. Perkins, Sachdeva) assumed liquid and gas travel at the same velocity, while later models (e.g. Hydro, al Safran[16]) include slip and report a better match against measured data after adjusting the slip correlation.

Limited experimental data shows that there is slip between the phases in the choke. Vogrin[2-17] did experiments in contractions with air and water (which ensures mass transfer is negligible) and back-calculated slip from void fraction measured with gamma densitometers along the choke path. Slip values as high as 24 are reported. However, the highest gas mass fractions tested is of 0.143, and there were some repeatability issues in the experiments.

Temperature

Most mechanistic choke models assume an adiabatic-reversible contraction (i.e. isentropic process) from inlet to throat[17].

The models of Perkins, Sachdeva, Hydro, Al Safran use a pressure-gas density relationship derived by assuming adiabatic process, incompressible liquid, ideal gas and constant specific gas heat capacities at constant pressure and volume (calorically perfect gas). The derivation is given in Ros [2-10] and in Appendix B. Using a

---

[16] The model of al Safran has a small inconsistency because to represent the velocity term in the momentum equation homogeneous flow is assumed, but the density is calculated considering slip, using the holdup-averaged densities of liquid and gas.

[17] But the enthalpies of choke inlet and outlet are equal.

frozen flow approach together with this isentropic expansion allows to integrate the term $\int_{p_{inlet}}^{p_{throat}} \frac{1}{\rho} dp$ analytically, which is advantageous.

Throat/discharge coefficient

A big source of uncertainty in choke models is the choke coefficient (often referred to as the discharge coefficient C_d). The coefficient is correcting for the fact that, at the vena contracta, due to detachment of flow from the walls, the effective flow cross section area is smaller than the geometric throat area. This correction is sometimes called the contraction coefficient (C_c). The coefficient can also include other irreversibilities (e.g. friction and energy losses due to local recirculations). The value of C_d must be in the range (0,1]. It is usually low for viscous liquids and liquid flow, and high for gas-dominated flows. It is reported that it is a function of the choke geometry and the Reynolds number.

When measured data is available, a constant coefficient is often tuned to improve the match between model output and data. Table 2-2 shows values of the discharge coefficient used in some of the petroleum engineering choke models.

TABLE 2-2. VALUES OF DISCHARGE COEFFICIENT REPORTED IN PREVIOUS WORKS

Model	C_d value
Sachdeva	0.85
Perkins	0.826
Al Safran	0.7-0.75
Hydro	0.62 for orifice 0.45 for cage

Be aware the tuning of the choke coefficient could be compensating for incorrect or uncertain modeling assumptions.

As an example, data points (pressure values upstream and downstream the choke, mass flow and inlet temperature) were collected from the work by Schüller et al[2-13] for single phase flow of oil, gas and water. The value of the discharge coefficient was calculated from the single-phase choke equations presented in Appendix B. An associated error was calculated using derivative propagation considering that there is an error of 1 000 Pa in the pressure measurement and 0.01 kg/s in the mass flow measurements.

Resulting values of the discharge coefficient are plotted versus the Reynolds number calculated at the throat for oil, water and gas in Figure 2-35, Figure 2-36 for one size (11 mm) and two geometries (bean and cage). Results are similar for the other sizes (14 and 18 mm). The figures show that, the C_d somewhat increases with the Reynolds number, however the trend is non-monotonic. In most cases the non-monotonicity cannot solely be attributed to experimental error. The range of variation exhibited by the C_d is significant.
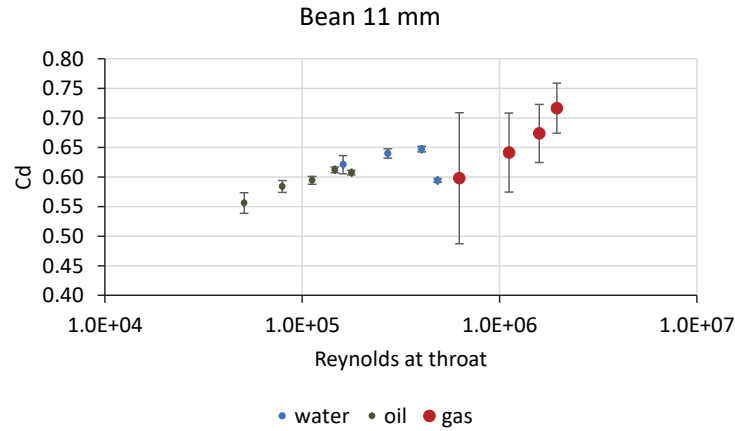
FIGURE 2-35. VALUES OF DISCHARGE COEFFICIENT CD AND ASSOCIATED ERROR VERSUS REYNOLDS NUMBER AT THE THROAT CALCULATED FROM THE DATA OF SCHÜLLER ET AL[2-13] FOR SINGLE PHASE FLOW OF WATER, OIL AND GAS FOR A BEAN CHOKE WITH THROAT DIAMETER OF 11 MM.
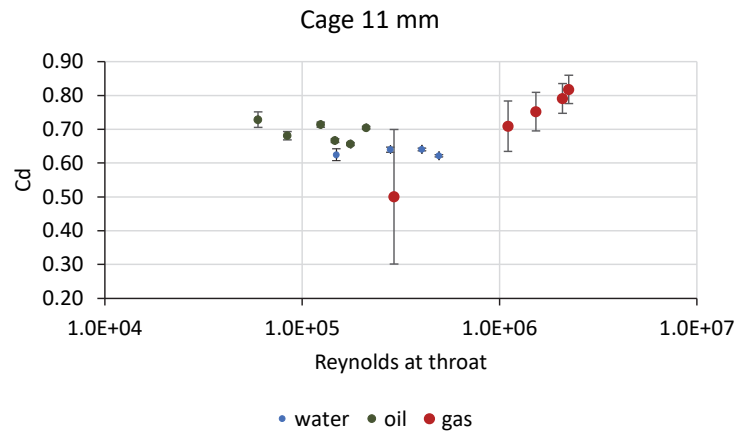
FIGURE 2-36. VALUES OF DISCHARGE COEFFICIENT CD AND ASSOCIATED ERROR VERSUS REYNOLDS NUMBER AT THE THROAT CALCULATED FROM THE DATA OF SCHÜLLER ET AL[2-13] FOR SINGLE PHASE FLOW OF WATER, OIL AND GAS FOR A CAGE CHOKE WITH THROAT DIAMETER OF 11 MM.

Figure 2-37 shows the average value of the discharge coefficient for each choke type. Colors indicate different fluids (red for gas, blue for water, green for oil). The error bars indicate maximum and minimum value encountered for that choke type and that fluid. The range of variation exhibited by the C_d is significant.
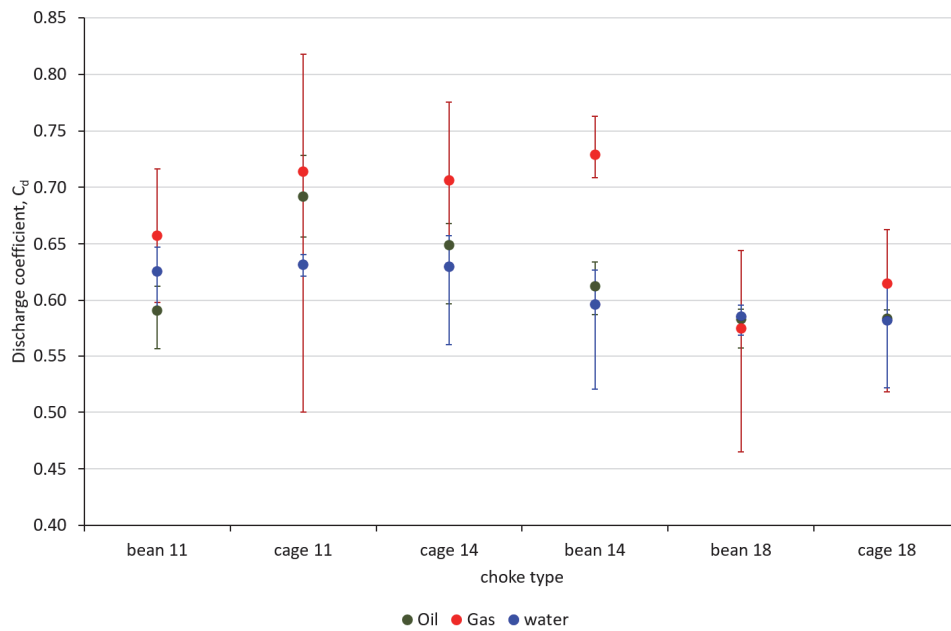
FIGURE 2-37. VALUES OF DISCHARGE COEFFICIENT CD VERSUS CHOKE TYPE, CALCULATED FROM THE DATA OF SCHÜLLER ET AL[2-13] FOR SINGLE PHASE FLOW OF WATER, OIL AND GAS. POINTS ARE AVERAGE VALUES, ERROR BARS DEPICT MAXIMUM AND MINIMUM VALUES

Based on the experimental data analyzed, the back-calculated discharge coefficient that satisfies the choke equation varies significantly with rate and type of fluid flowing through the choke. Therefore, it seems that assuming a constant C_d in a choke model could potentially give wrong results, since it is a proportionality constant directly multiplying the rate output of the choke model.

Keeping a constant C_d in a choke model could also require to (wrongly!) compensate by adjusting other model features to obtain the correct flow value.

However, Carstensen[2-18] proposed a variable C_d predictive model for in their choke model, and the accuracy was not significantly improved.

Challenges

Simply put, in choke modeling there are too many things that are unknown (e.g. mass transfer, slip) and it is difficult to verify if modeling assumptions are appropriate. One can get a good match by using a wrong modeling assumption that could be compensating for another wrong assumption. Moreover, a big simplification needed to apply the 1D momentum equation is assuming that the flow from inlet to throat is one-dimensional, with no localized losses.

Most authors of petroleum engineering choke models propose an equation and method and then tune to obtain best match with measured data, because the available literature or measured data is not detailed enough to verify the modeling assumptions.

As an example of the variability in results when using different modeling assumptions, consider the case presented in Table 2-3, where inlet pressure and outlet pressure are given. Two fluids are considered, an oil (Table 2-4) where properties where estimated with black oil correlations, and a gas (Table 2-5), where properties where estimated using an compositional equation of state. Choke calculations of oil rate (or mass flow rate) were performed for these two fluids. The slip correlation is taken from the Hydro model.

TABLE 2-3. VALUES OF VARIABLES INPUT TO THE NUMERICAL MODEL

Variable	Value
Inlet pressure, p_{in} [bara]	150
Inlet temperature, T_{in} [°C]	70
Outlet pressure, p_{out} [bara]	50
Throat diameter [m]	0.036

TABLE 2-4. PROPERTIES OF FLUID 1 – OIL

GOR [Sm3/Sm3]	400
WC [fraction]	0
Specific gravity of surface gas, $\gamma_{\bar{g}}$	0.8
Specific gravity of surface oil, $\gamma_{\bar{o}}$	0.871
Specific gravity of surface water, $\gamma_{\bar{w}}$	0.989

TABLE 2-5. COMPOSITION OF FLUID 2 – GAS

Component	Mole fraction [%]
Nitrogen	0.00524
Methane	0.83330
Carbon Dioxide	0.03140
Ethane	0.03140
Propane	0.02947
i-Butane	0.00539
N-Butane	0.00916
i-Pentane	0.00313
N-Pentane	0.00239
Hexanes	0.00099
Heptanes plus[18]	0.00282

Modeling assumptions and results for the oil case are presented in Table 2-6.

---

[18] The molecular weight of the heptanes plus is 182 and specific gravity 0.828

TABLE 2-6. MODELLING ASSUMPTIONS AND RESULTS – OIL CASE

Variable	Case-A	Case-B	Case-C	Case-D	Case-E	Case-F	Case-G
temperature	Ros[2-10]	Ros[2-10]	isothermal	isothermal	isothermal	energy equation	Ros[2-10]
mass transfer	No	no	no	equilibrium	equilibrium	No	no
slip	No	yes	no	yes	no	No	no
Throat area coefficient, C	1	1	1	1	1	1	0.8
critical pressure ratio	0.58	0.43	0.62	0.54	0.61	0.61	0.58
oil rate, [Sm3/d]	3561	4558	3316	3992	3370	3406	2844

Some observations are provided next:

- **Effect of slip:** Assuming or neglecting slip has a significant impact on the results (compare Cases A and B, and cases D and E, ca 20-30% difference in the value of oil rate).
- **Effect of temperature:** Assuming Ros[2-10], isothermal or energy equation[19] has a moderate impact on the results (compare cases A,C and F).
- **Effect of mass transfer:** assuming frozen flow or thermodynamic equilibrium has a small impact on the results (compare cases C and E).
- **Effect of throat area coefficient:** a 20% reduction in the throat area coefficient (1→0.8) as a big impact on the results (compare cases A and G).

Modeling assumptions and results for the gas case are presented in Table 2-7.

TABLE 2-7. MODELLING ASSUMPTIONS AND RESULTS – GAS CASE

Variable	Case-A	Case-B	Case-C	Case-D	Case-E	Case-F	Case-G
temperature	Ros[2-10]	Ros[2-10]	isothermal	isothermal	isothermal	energy equation	Ros[2-10]
mass transfer	No	no	no	equilibrium	equilibrium	No	no
slip	No	yes	no	yes	no	No	no
Throat area coefficient, C	1	1	1	1	1	1	0.8
critical pressure ratio	0.49	0.49	0.63	0.62	0.63	0.54	0.49
mass rate, [kg/s]	31.2	31.4	25.5	25.9	25.7	29.6	24.9

---

[19] Energy equation means solving the momentum and energy equations for liquid-gas flow stepwise in the choke from inlet to throat.

Some observations are provided next:

- **Effect of slip:** Assuming or neglecting slip has a small impact on the results (compare Cases A and B, and cases D and E).
- **Effect of temperature:** Assuming Ros[2-10], isothermal or energy equation has a significant impact on the results (ca 20%, compare cases A,C and F).
- **Effect of mass transfer:** assuming frozen flow or thermodynamic equilibrium has a small impact on the results (compare cases C and E).
- **Effect of throat area coefficient:** a 20% reduction in the throat area coefficient (1→0.8) as a significant impact on the results (compare cases A and G).

The main takeaways are:

- When modeling flow of oil-dominated flow through the choke, slip has a significant effect on the results. Mass transfer and temperature approaches have a reduced effect.
- When modeling flow of gas-dominated flow through the choke, temperature assumptions have a significant effect on the results. Mass transfer approaches and slip have a reduced effect.
- The throat area coefficient has a significant effect on the results.
- For a single component fluid, mass transfer modeling approaches could have an important effect on the results (Lorenzo et al[2-15]).

A simple choke model[20] and calculation modes

Consider Eq. 2-72[21] is our choke model.

$$-\int_{p_{inlet}}^{p_{throat}} \frac{1}{\rho_{m,homogeneous}} dp = \frac{\left(V_{m,throat}\right)^2}{2}$$

This equation can be used in three ways:

1. **Known information**: Inlet and outlet pressures, and fluid. **Unknown:** rate
2. **Known information**: Rate and outlet pressure, and fluid. **Unknown:** inlet pressure.
3. **Known information**: Rate and inlet pressure, and fluid. **Unknown:** outlet pressure.

This equation will be solved by computing the density integral numerically, but there are some considerations when dealing with the pressure boundaries. When operating in the subcritical regime, the pressure measured downstream the choke is usually employed to approximate the pressure at the throat, assuming there is very little pressure recovery after the throat. When operating in the critical regime, the pressure measured downstream the choke is lower than the pressure at the throat and initially unknown. The main challenge is that often is not known beforehand if the choke is operating in the critical or subcritical regime.

Figure 2-38 shows inverse values of density versus pressure for: 1) (red) gas, 2) (green) dead oil[22], 3) (orange) oil-gas mixture with saturation pressure around 150 bara. Values of fluid properties are calculated by assuming equilibrium and using the value of pressure and the entropy value of choke inlet conditions (400 bara, 80 °C). The density of the mixture is calculated by using expression Eq. 2-73 (homogeneous flow). Densities of liquid exhibit a modest variation with pressure when compared against gas and gas-oil mixtures.

---

[20] The approach discussed here is similar to the one presented by Darby[2-20].

[21] If slip is believed to be important, Eq. 2-74 can be used instead.

[22] Be aware oil density values are plotted on the secondary "y" axis.
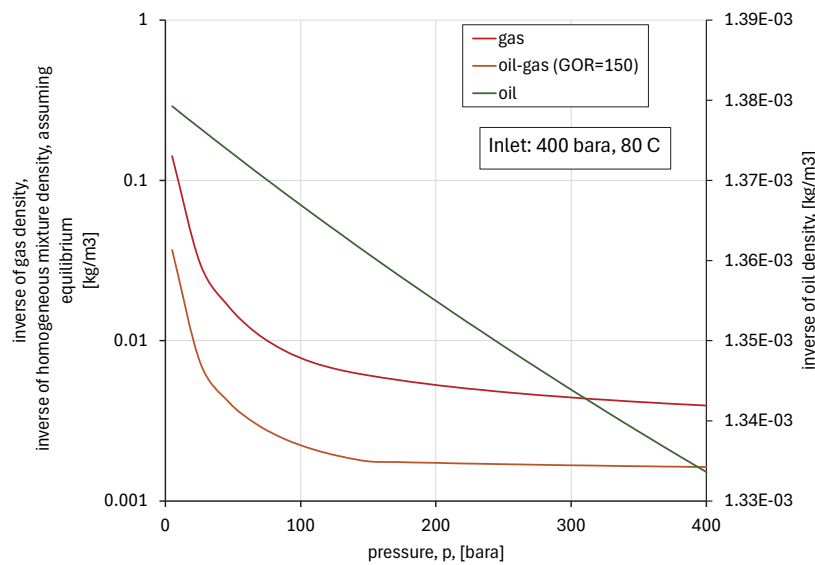
FIGURE 2-38. VALUES OF INVERSE OF DENSITY VERSUS PRESSURE FOR SINGLE PHASE OIL (GREEN), SINGLE PHASE GAS (RED), OIL-GAS MIXTURE (ORANGE). FLUID PROPERTIES HAVE BEEN CALCULATED USING PRESSURE AND ENTROPY OF INLET CONDITIONS, 400 BARA AND 80 °C. THE MIXTURE DENSITY IS CALCULATED ASSUMING HOMOGENEOUS FLOW AND EQUILIBRIUM CONDITIONS.

Figure 2-39 shows behavior of inverse of homogeneous mixture density for an oil and gas mixture using two calculations assumptions: the orange curve has been calculated using the pressure value and the entropy of inlet conditions (400 bara and 80 °C). The blue curve has been calculated using the pressure value and the temperature of inlet conditions (80 °C). For this case the difference is small, except at very low pressure values.
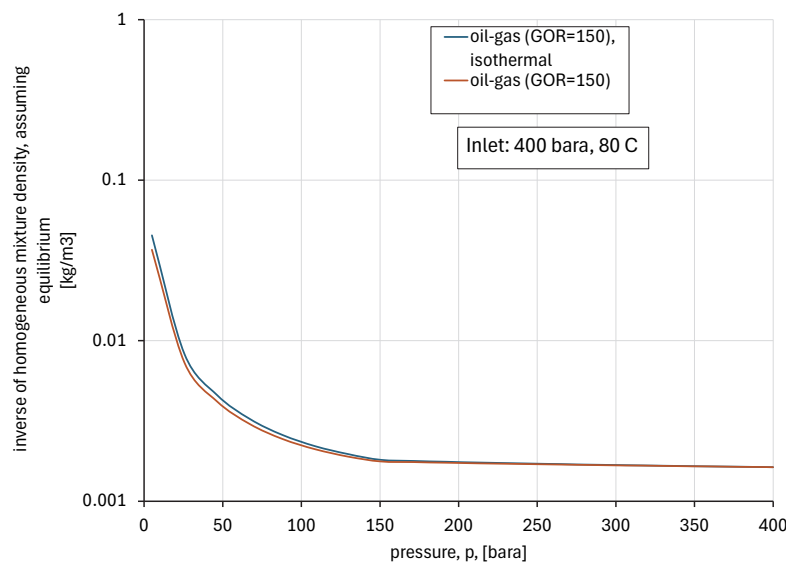
FIGURE 2-39. VALUES OF INVERSE OF HOMOGENEOUS MIXTURE DENSITY (CONSIDERING EQUILIBRIUM) VERSUS PRESSURE FOR OIL-GAS MIXTURE. FOR THE ORANGE CURVE, FLUID PROPERTIES HAVE BEEN CALCULATED USING PRESSURE AND ENTROPY OF INLET CONDITIONS, 400 BARA AND 80 C. FOR THE BLUE CURVE, FLUID PROPERTIES HAVE BEEN CALCULATED USING PRESSURE AND TEMPERATURE OF INLET CONDITIONS.

Figure 2-40 shows behavior of inverse of gas density two calculations assumptions: the red curve has been calculated using the pressure value and the entropy of inlet conditions (400 bara and 80 °C). The green curve

has been calculated using the pressure value and the temperature of inlet conditions (80 °C). The difference is significant.
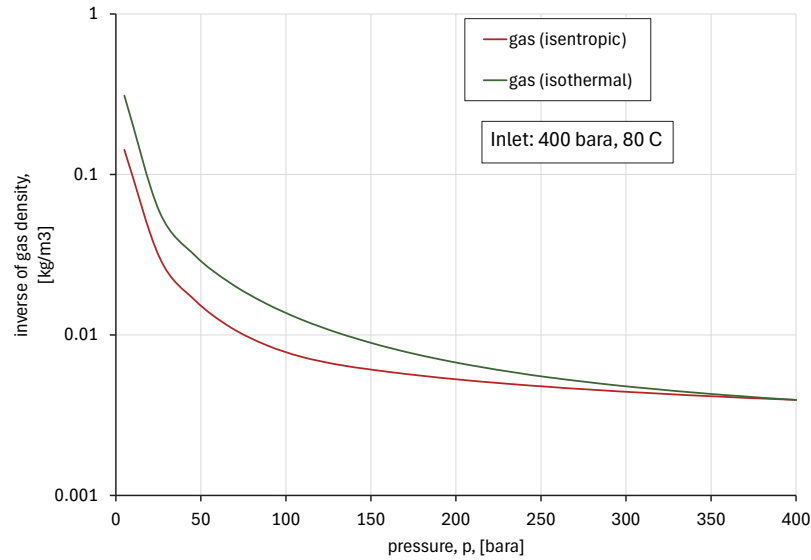
FIGURE 2-40. VALUES OF INVERSE OF GAS DENSITY VERSUS PRESSURE FOR GAS. FOR THE RED CURVE, FLUID PROPERTIES HAVE BEEN CALCULATED USING PRESSURE AND ENTROPY OF INLET CONDITIONS, 400 BARA AND 80 C. FOR THE GREEN CURVE, FLUID PROPERTIES HAVE BEEN CALCULATED USING PRESSURE AND TEMPERATURE OF INLET CONDITIONS.

Figure 2-41 shows behavior of inverse of homogeneous mixture density for an oil and gas mixture using the pressure value and the entropy of inlet conditions (60 bara and 80 °C). The blue curve has been calculated assuming equilibrium, while the green curve has been calculated assuming frozen flow, i.e. inlet mass fraction and liquid density, but varying gas density. The difference is considerable.
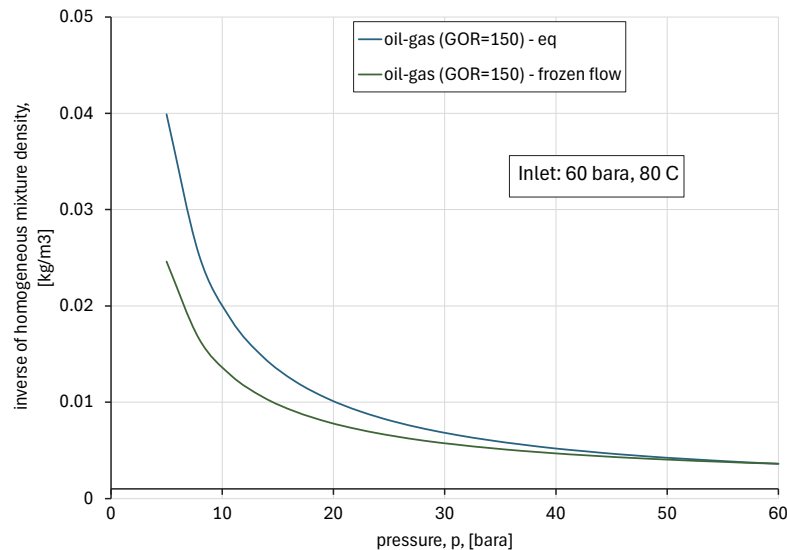
FIGURE 2-41. VALUES OF INVERSE OF HOMOGENEOUS MIXTURE DENSITY VERSUS PRESSURE FOR OIL-GAS MIXTURE. THE BLUE CURVE HAS BEEN CALCULATED ASSUMING EQUILIBRIUM, WHILE THE GREEN CURVE HAS BEEN CALCULATED ASSUMING FROZEN FLOW, I.E. INLET MASS FRACTION AND LIQUID DENSITY, BUT VARYING GAS DENSITY.

Figure 2-42 shows values of homogeneous mixture density (considering equilibrium) versus pressure for CO_2 using the pressure value and the entropy of inlet conditions (60 bara and 4 °C)
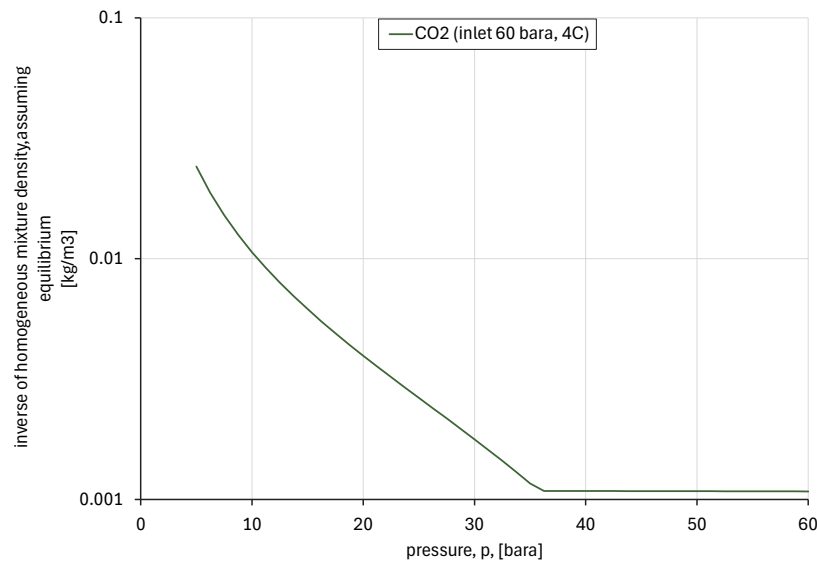
FIGURE 2-42. VALUES OF INVERSE OF HOMOGENEOUS MIXTURE DENSITY VERSUS PRESSURE FOR CO_2. CALCULATED ASSUMING EQUILIBRIUM, THE PRESSURE VALUE AND THE ENTROPY OF INLET CONDITIONS (60 BARA AND 4 °C).

Takeaways:

- For oil and gas mixtures, it seems assuming isothermal versus isentropic gives small differences.
- For gas, assuming isothermal versus isentropic gives significant differences.
- For oil and gas mixtures, assuming frozen flow or equilibrium gives modest differences.
- The inverse density term versus pressure exhibits a big variation versus pressure for gas or gas-liquid mixtures, while the variations are small for liquid. Finding a generic continuous analytical expression (like what is attempted by Carstensen[2-18]) seems difficult.

Calculation mode 1: rate estimation

This is the most common application of a choke model, for example for flow metering applications. The suggested calculation procedure is the following:

1. Create a "n"-size vector of pressures between inlet and outlet.
2. For each pressure element in the vector, estimate temperature. Either assume isothermal (use inlet temperature), or estimate using Eq. B-52 (approximation to isentropic expansion).
3. Calculate fluid properties (density of liquid and gas and gas mass fraction) for each member of the pressure vector. If more than two liquid phases are present, an equivalent liquid density must be calculated assuming e.g. a homogeneous liquid-liquid mixture. If frozen flow, the gas mass fraction is assumed to be constant and equal to the inlet value, while density of liquid and gas are updated.
4. Calculate mixture density for each member of the pressure vector.
5. Evaluate numerically the integral of the inverse of the mixture density starting from inlet pressure. Since it is not known if the choke is operating in the critical or subcritical regime, perform the integration stepwise, i.e. for each pressure element p_x in the vector calculate the cumulative integral between inlet and p_x. This assumes that we are in critical flow and the pressure p_x is the pressure at the throat. This assumption will be later checked.
   a. For each pressure p_x, calculate the velocity of the mixture at the throat by clearing out from Eq. 2-72. Then convert that velocity to mass flow (or oil, or gas rate) by using the expressions below.

$$V_{m,throat} = \frac{\frac{\dot{m}_{g,x}}{\rho_{g,x}} + \frac{\dot{m}_{l,x}}{\rho_{l,x}}}{A_{throat,effective}} = \frac{\dot{m} \cdot \left(\frac{x}{\rho_{g,x}} + \frac{1-x}{\rho_{l,x}}\right)}{A_{throat,effective}} = \frac{\dot{m} \cdot \frac{1}{\rho_{m,homogeneous,x}}}{A_{throat,effective}}$$

EQ. 2-76

$$\dot{m} = q_{\bar{o}} \cdot \rho_{\bar{o}} + q_{\bar{g}} \cdot \rho_{\bar{g}} + q_{\bar{w}} \cdot \rho_{\bar{w}} = q_{\bar{o}} \cdot \left(\rho_{\bar{o}} + R_p \cdot \rho_{\bar{g}} + \frac{W_c}{1 - W_c} \cdot \rho_{\bar{w}}\right)$$

EQ. 2-77

b. If at any pressure step $\dot{m}_X < \dot{m}_{x-1}$ this indicates that the choke is operating in the critical regime. A convergence routine can be triggered at this point to find the exact value of p_{throat} ($p_x < p_{throat} < p_{x-1}$) for which the value of $\dot{m}$ is maximum. However, if the pressure step is small enough, the value of $\dot{m}$ obtained without convergence is often satisfactory. Stop calculation and report $\dot{m}$ and p_{throat}.

c. If always $\dot{m}_X > \dot{m}_{x-1}$ up to $p_x = p_{outlet}$, then the choke is operating in the sub-critical regime.

To clarify why critical flow occurs in the equations, let's insert Eq. 2-76 in Eq. 2-72 and clear out the mass flow:

EQ. 2-78

$$\dot{m} = \frac{2 \cdot A_{throat,effective}}{\left(\frac{1}{\rho_{m,homogeneous,x}}\right)} \cdot \sqrt{-\int_{p_{inlet}}^{p_x} \frac{1}{\rho_{m,homogeneous}} dp}$$

The square root term is always increasing when the value of p_x goes down. But the inverse mixture density term also increases when the value of p_x goes down. Critical flow happens when the increase in the square root term is counteracted by the increase in the inverse mixture density term, giving a reduction in the mass flow.

Calculation mode 2: inlet pressure estimation

In this case, outlet pressure and rate are known, and one wishes to estimate inlet pressure. The main complexity in this case is that is not known a priori whether the outlet pressure provided is equal to throat pressure (subcritical regime) or lower (critical regime).

To study closer this case, let's consider an example with flow of dry gas through a choke, outlet pressure equal to 50 bara, inlet temperature 80 °C. Figure 2-43 shows the value of the residual of Eq. 2-72 for three values of standard conditions gas rate, and for several combinations of inlet pressure and throat pressure values, from 50 bara to 500 bara. Cases where inlet pressure is lower than throat pressure are discarded. For simplicity, the flow through the choke is assumed to be isothermal. The black line indicates inlet-throat pressure combinations where the residual is zero. There are multiple solutions to Eq. 2-72!

It can be seen that, if one assumes the choke is in the subcritical range (thus throat pressure is equal to 50 bara), there is no valid inlet pressure solution for the highest rate (a) but there are solutions for the medium (b) and low (c) rates.

The physical solution is the minimum point in the black curve. For almost all values of inlet pressure present in the black curve, there are two throat pressures that give a solution, a high value and a low value, except in the minimum point. As explained before in the calculation mode 1 case, for the flow to be in critical conditions, there must be a unique combination of inlet pressure and throat pressure that give maximum rate.

(a)

(b)

(c)
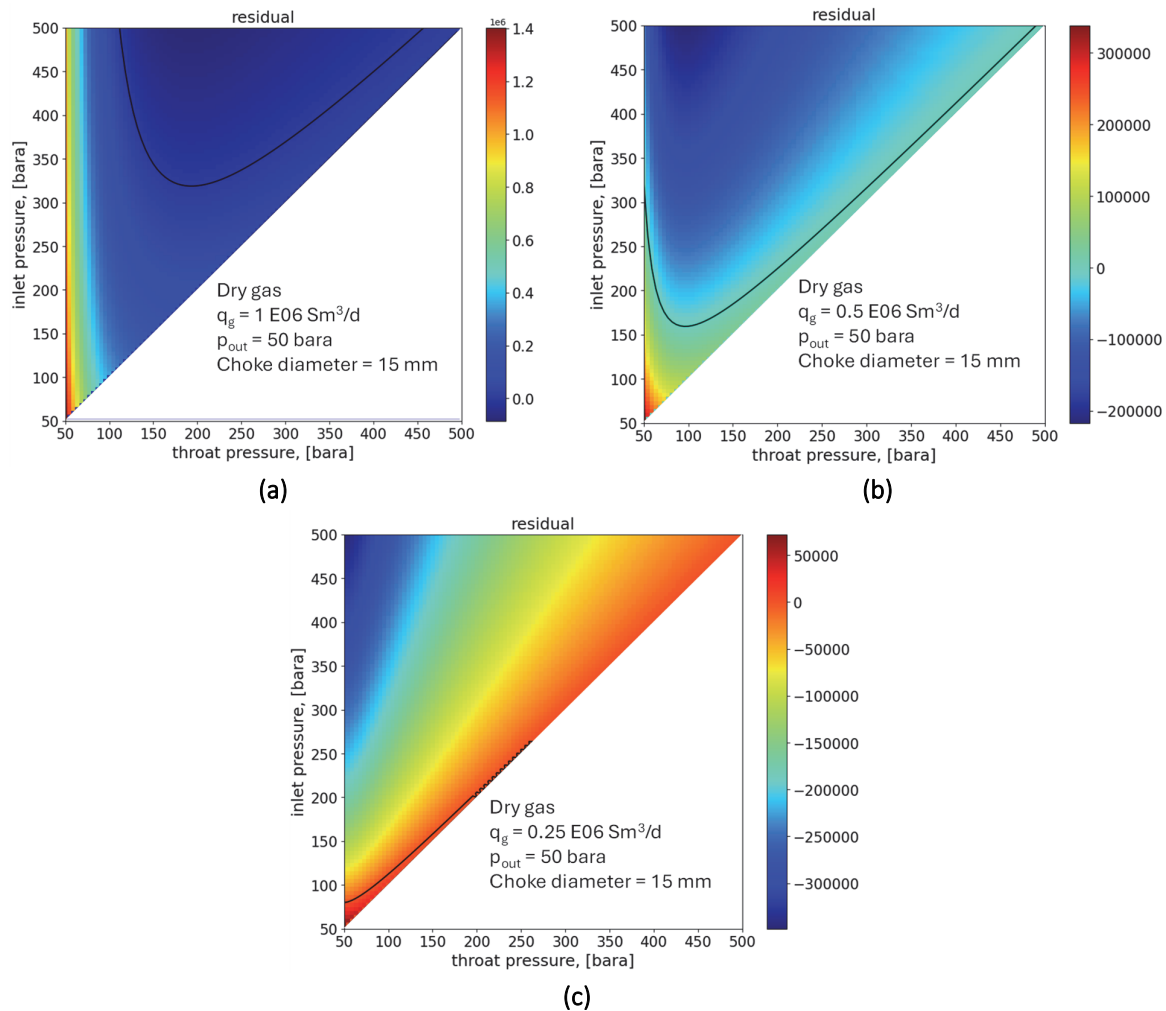
FIGURE 2-43. COLOR MAP OF THE VALUE OF THE RESIDUAL OF EQ. 2 76 FOR THREE VALUES OF STANDARD CONDITIONS GAS RATE, AND FOR SEVERAL COMBINATIONS OF INLET PRESSURE AND THROAT PRESSURE VALUES, FROM 50 BARA TO 500 BARA.

Let's consider another example with flow of oil through a choke, outlet pressure equal to 50 bara, inlet temperature 80 °C. Figure 2-43 shows the value of the residual of Eq. 2-72 for two values of GOR and a case with the presence of water and for several combinations of inlet pressure and throat pressure values, from 50 bara to 500 bara. Cases where inlet pressure is lower than throat pressure are discarded. For simplicity, the flow through the choke is assumed to be isothermal. The black line indicates inlet-throat pressure combinations where the residual is zero. There are multiple solutions to Eq. 2-72!
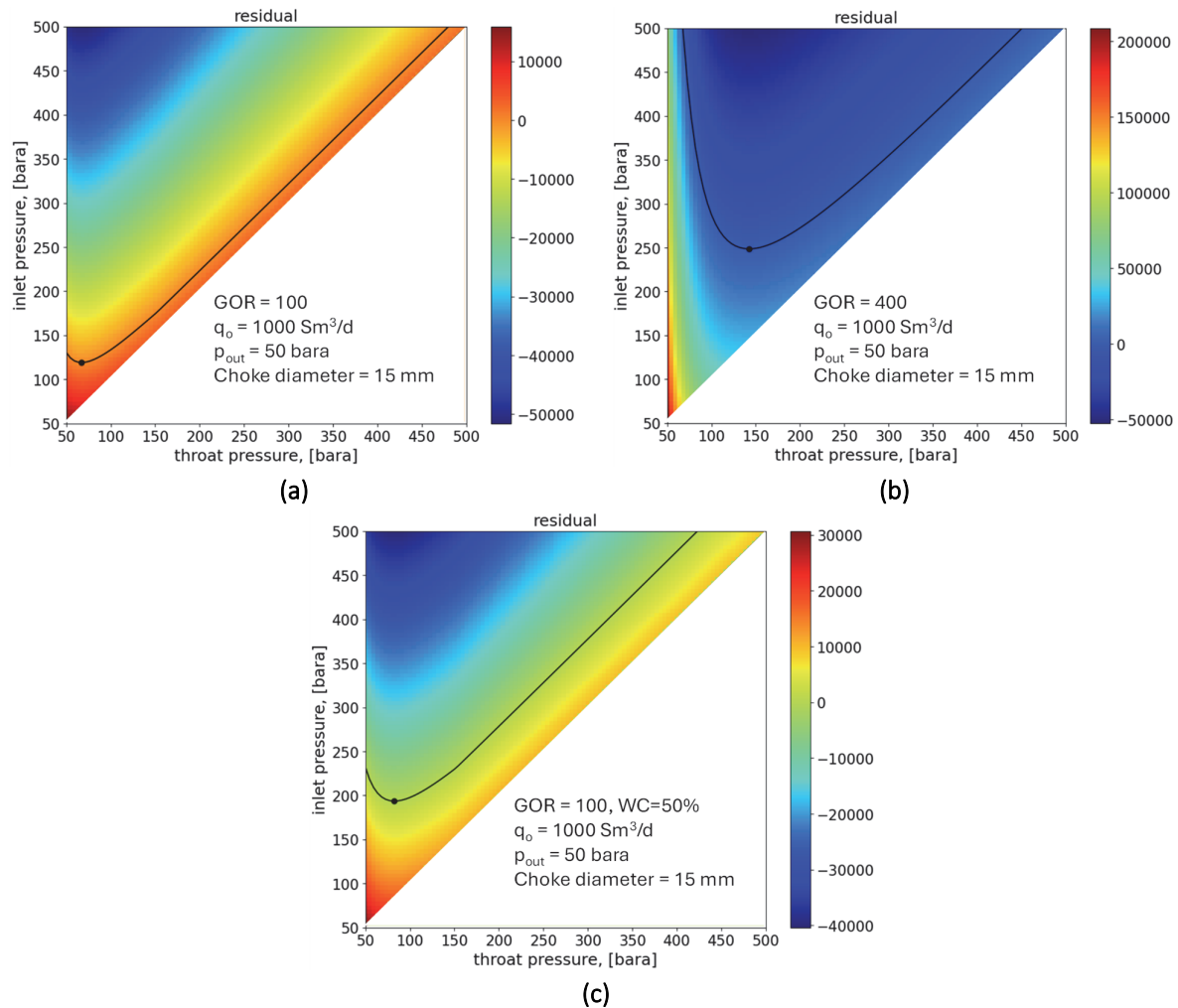
FIGURE 2-44. COLOR MAP OF THE VALUE OF THE RESIDUAL OF EQ. 2 76 FOR 1000 Sm^3/D OF OIL, OUTLET PRESSURE 50 BARA, 80 °C, CHOKE DIAMETER 15 MM, FOR GOR = 100 (A), GOR=400 (B) AND WC=50% (C).

2.3.3. BOOSTER

Boosters can be roughly split into two categories: in-well and out-of-well boosters. Within in-well boosters we have for example:

- Electric submersible pumps (ESP): multi-stage centrifugal pumps that are suitable for handling liquids or liquids with low amounts of gas. These pumps will be explained more in detail in section 2.3.4.
- Jet pumps: these are pumps without moving parts, consisting of a pipe surrounding a nozzle inside which a power fluid is accelerated, lowering the pressure and sucking the fluid in the annular space. These pumps are suitable for liquids, mixtures, or gasses. These pumps will be explained more in detail in section 2.3.6.
- Rod pumps: These are piston pumps where the periodic axial stroking of a piston moving up and down a chamber will sequentially open a valve located at the bottom to allow flow of fluids into the chamber and open a valve located at the top of the chamber to push fluids out of the chamber. These pumps are suitable for liquids.
- Progressive cavity pumps (PCP): These consist of a helical rotor that rotates inside a rubber (or metal) stator, where the movement of the rotor creates a chamber that moves from inlet to outlet, carrying the fluid. These pumps are usually suitable for liquids.

Within out of well boosters there are, for example:

- Single phase pumps: these are typically single or multi-stage centrifugal pumps, that are suitable for handling liquids or liquids with low amounts of gas. These pumps typically require a separation station upstream to remove the gas.
- Helico-axial pumps: these are typically multi-stage axial or semi-axial pumps. In these pumps the rotor blades are long and oriented almost perpendicular to the shaft, which promotes a good mixing of the phases and inhibits separation. These pumps are suitable for gas-liquid mixtures up to 80-90% gas volume fraction at the inlet.
- Twin-screw pumps: Typically consist of parallel screws. The movement of the screws creates a chamber that moves from inlet to outlet, carrying the fluid. These pumps are suitable for gas-liquid mixtures up to 90% gas volume fraction at the inlet.
- Wet gas compressors: they are typically multi-stage axial counter-rotating compressors. In this compressor both the rotor and stator resemble a rotor and rotate in opposite directions. Both have the dual function of accelerating the fluid and pressure recovery. These pumps are suitable for gas-liquid mixtures down to 80% gas volume fraction at the inlet.
- Dry gas compressors: they are typically multi-stage centrifugal compressors. They handle typically gas with very low content of liquid. These pumps typically require a separation station upstream to remove the liquid. These compressors will be explained more in detail in section 2.3.5.

Despite their differences, working principles and the type of fluids they handle, most of these boosters follow the same thermodynamic principles. The fluid power required by a boosting process is, using the 1st law of thermodynamics for open systems, equal to the enthalpy difference between inlet and outlet times the mass flow.

$$\dot{W} = \dot{m} \cdot (h_2 - h_1) = \dot{m} \cdot \Delta h$$

EQ. 2-79

It is common to express the enthalpy difference Δh as the enthalpy difference required by an ideal boosting process divided by the adiabatic efficiency ($\eta_{adiabatic}$).

$$\Delta h = \frac{\Delta h_{ideal}}{\eta_{adiabatic}}$$

EQ. 2-80

The ideal boosting process, that requires the least amount possible of energy, with no losses, irreversibilities nor heat exchange with the environment is the one performed at constant entropy (therefore $\Delta h_{ideal} = \Delta h_s$). The value of the adiabatic efficiency varies depending on the type of booster and the fluid it handles, but it can be roughly said that it lies between 0.3-0.8.

This equation indicates that to calculate the real compression power required, one should first compute the isentropic enthalpy difference and then compute the real enthalpy difference using the adiabatic efficiency.

Consider a situation where the fluid composition is known, the inlet pressure and temperature conditions are known, and the mass flow is known. Moreover, consider that the required outlet pressure is given (e.g. it has been estimated with a flow equilibrium analysis). With the composition, the inlet pressure and temperature, it is possible to compute the inlet specific enthalpy and entropy of the mixture. With this data, the outlet isentropic enthalpy can be calculated using the same inlet entropy and the required outlet pressure. With the isentropic enthalpy difference, and the adiabatic efficiency, one can then calculate the required boosting power. The outlet temperature can be computed by calculating first the actual enthalpy difference (using Eq. 2-80), then clearing out the outlet enthalpy and then using the outlet enthalpy and the outlet pressure to compute outlet temperature.

As an example of the procedure described above, consider the pressure-enthalpy diagram for Methane shown in Figure 2-45. This diagram has isotherms and iso-entropy lines over-imposed. Consider a compression

process from 50 bara to 100 bara, and inlet temperature 20 °C. The ideal compression process, that requires the least amount possible of energy, is the one that leads to a situation where the output has the same entropy as the inlet (blue point). The real compression process, however, is far from ideal and will lead to higher outlet temperatures than the isentropic (red point). In the case shown in the figure, is has been assumed that the compressor has an adiabatic efficiency of approximately 68%, i.e. the real enthalpy difference is roughly 1.46 times the isentropic.
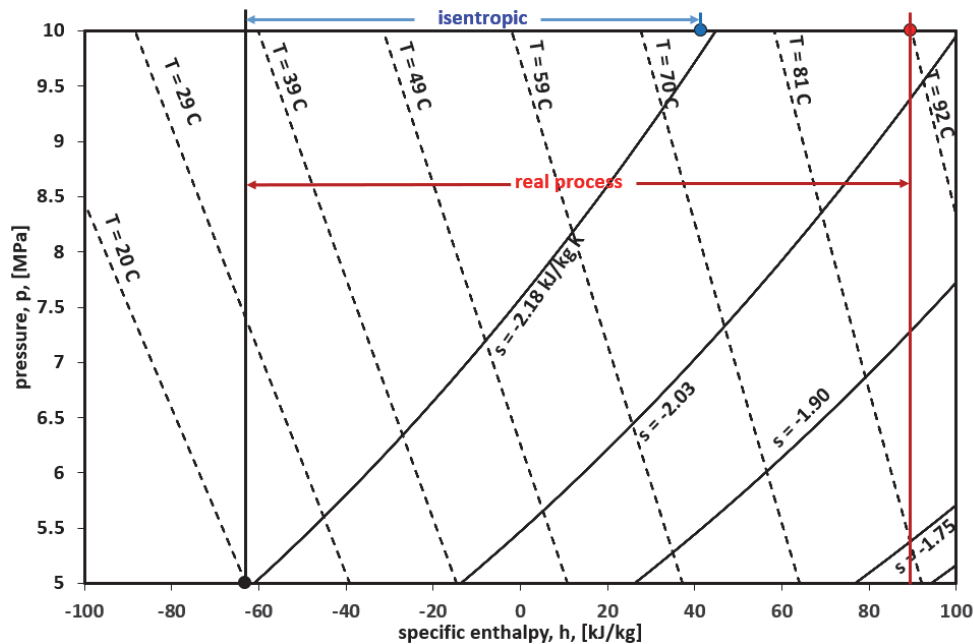
FIGURE 2-45. PRESSURE-ENTHALPY DIAGRAM FOR METHANE DEPICTING AN ISENTROPIC COMPRESSION PROCESS AND A REAL COMPRESSION PROCESS

The same procedure can be applied when the booster is handling liquid, a mixture of gas and liquid, or a gas. The only difference is that the thermodynamic behavior of the mixture will be different. Figure 2-46, Figure 2-47, Figure 2-48, Figure 2-49, and Figure 2-50 depict the pressure enthalpy diagrams of several fluids ranging from dead oil to methane, gradually increasing the producing GOR of the mixture. The plots have been made for a range of pressure and temperatures commonly encountered in the petroleum industry.
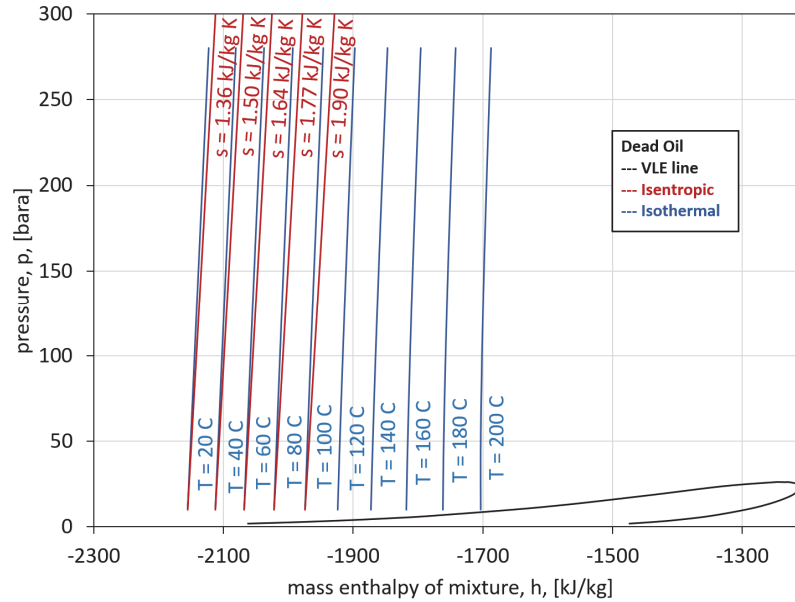
FIGURE 2-46. PRESSURE-ENTHALPY DIAGRAM FOR A DEAD OIL DEPICTING LINES OF ISO-TEMPERATURE AND ISO-ENTROPY

For the dead oil case, where for most of the operating region the fluid is liquid, it can be seen that the iso-temperature and the iso-entropy lines are almost vertical are very close to each other. This indicates that the ideal pumping process will lead to a minimal increase in temperature, and most of the enthalpy difference is due to the increase in pressure. It also indicates that one can achieve great pressure differences without investing much energy, because the lines have a big positive slope.

For a liquid, the enthalpy difference of two points with the same entropy can be approximated by:

$$\Delta h_s = \frac{\Delta p}{\rho}$$

EQ. 2-81

Substituting this expression in Eq. 2-79, to compute required boosting power, gives the familiar expression to estimate pump power consumption:

$$\dot{W} = \dot{m} \cdot \Delta h = \dot{m} \cdot \frac{\Delta h_s}{\eta_{adiabatic}} = q \cdot \frac{\Delta p}{\eta_{adiabatic}}$$

EQ. 2-82

Where q is the local rate at the inlet of the pump.
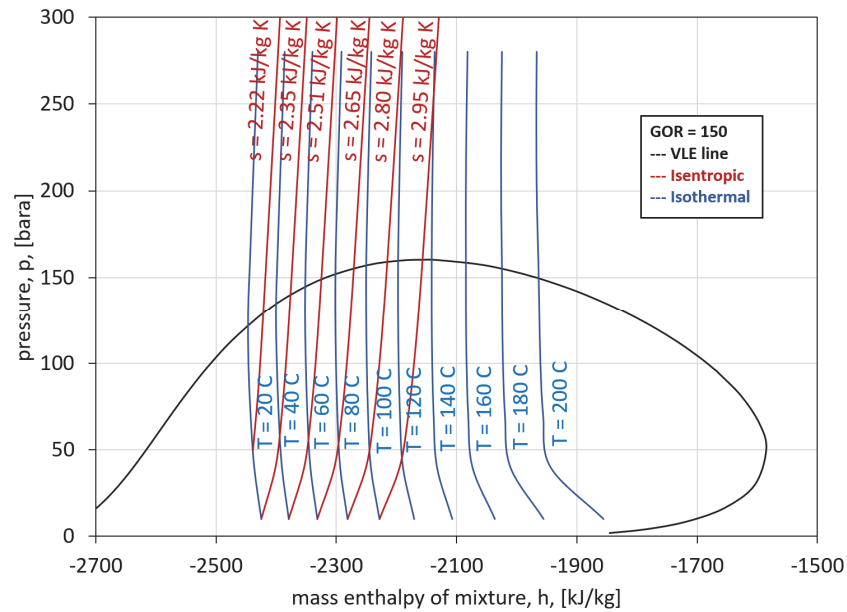
FIGURE 2-47. PRESSURE-ENTHALPY DIAGRAM FOR AN OIL WITH GOR = 150 DEPICTING LINES OF ISO-TEMPERATURE AND ISO-ENTROPY

When the GOR is increased, it can be seen that the iso-temperature lines will adopt a negative slope and the slope of the iso-entropy lines will be diminished, increasing the distance between them. This indicates that the ideal boosting process will lead to a significant increase in temperature (more significant the higher the GOR), and a significant part of the ideal enthalpy difference is due to the increase in temperature, besides pressure. It also indicates that to achieve great pressure differences more energy will be required. This is not a limitation of the booster, it is a consequence of the thermodynamic behavior of the fluid as it contains a bigger share of lighter components.
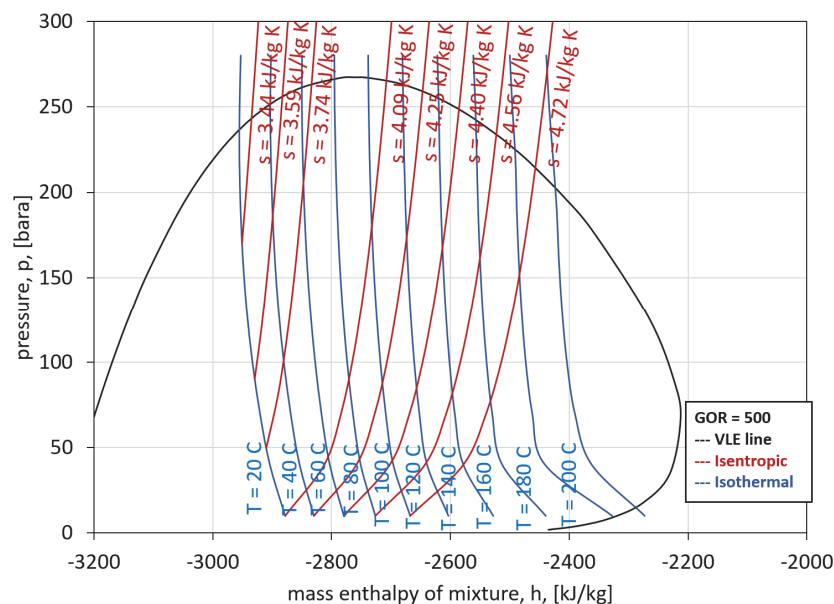
FIGURE 2-48. PRESSURE-ENTHALPY DIAGRAM FOR AN OIL WITH GOR=500 DEPICTING LINES OF ISO-TEMPERATURE AND ISO-ENTROPY
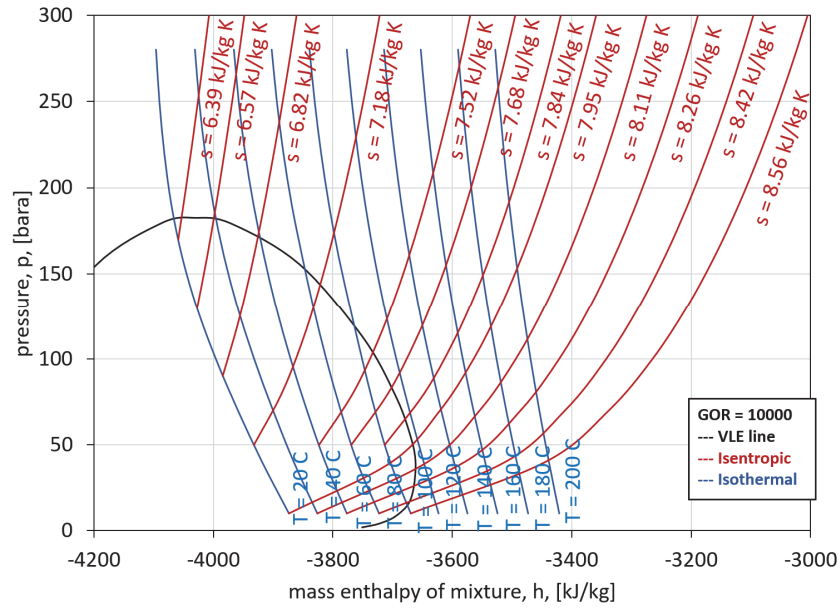
FIGURE 2-49. PRESSURE-ENTHALPY DIAGRAM FOR AN OIL WITH GOR=10 000 DEPICTING LINES OF ISO-TEMPERATURE AND ISO-ENTROPY
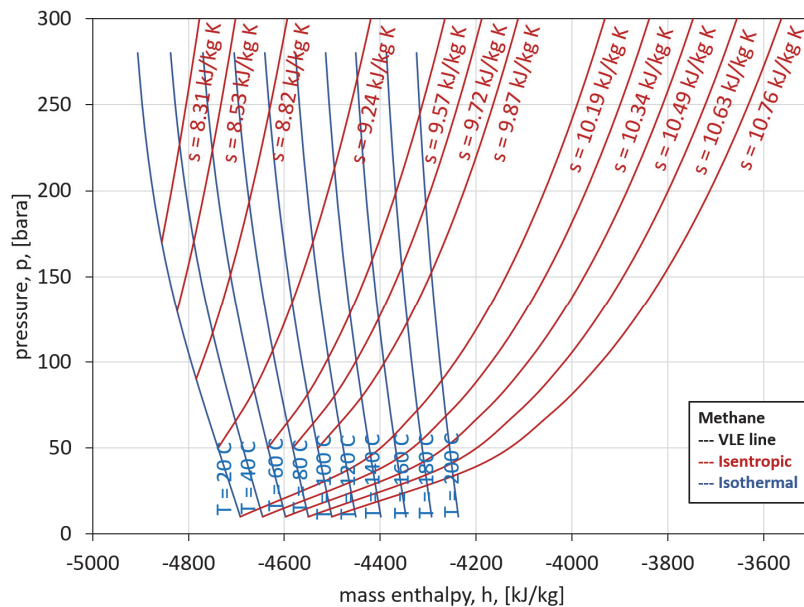
FIGURE 2-50. PRESSURE-ENTHALPY DIAGRAM FOR METHANE DEPICTING LINES OF ISO-TEMPERATURE AND ISO-ENTROPY

Exercise: Estimate required boosting power for different fluids

Consider that one needs to increase the pressure of 7 kg/s of fluid from 50 to 100 bara. The inlet temperature is 50 °C. Consider a fixed adiabatic booster efficiency equal to 0.6, and use the diagrams presented in Figure 2-46, Figure 2-47, Figure 2-48, Figure 2-49, and Figure 2-50. Calculate, for each fluid, the outlet temperature of the fluid, the outlet temperature of the fluid considering an isentropic expansion, and the total required boosting power.

We follow the steps (for each fluid):

- With the inlet temperature and inlet pressure locate the inlet point on the p-h diagram and read the inlet enthalpy.
- With the outlet pressure and assuming the output entropy is equal to the inlet entropy, read the outlet isentropic enthalpy from the p-h diagram.
- With the inlet enthalpy and the outlet isentropic enthalpy, calculate the ideal enthalpy difference.
- With the ideal enthalpy difference and using Eq. 2-80, compute the real enthalpy difference.
- With the real enthalpy difference and the mass flow and using Eq. 2-79, calculate the power required by the booster.
- With the real enthalpy difference and the inlet enthalpy, compute the outlet enthalpy.
- With the outlet enthalpy and the outlet pressure and the p-h diagram, read the outlet temperature.

The results of this process are shown in Table 2-8. When the content of gas increases, the power and outlet temperature increase significantly.

TABLE 2-8. REQUIRED BOOSTING POWER AND OUTLET TEMPERATURES WHEN BOOSTING 7 KG/S OF SEVERAL FLUIDS FROM 50 °C, 50 BARA TO 100 BARA, ASSUMING ADIABATIC EFFICIENCY OF 0.6

FLUID	h_{in}	$T_{out,s}$	Δh_s	Δh	Power	h_{out}	T_{out}
	[kJ/kg]	[C]	[kJ/kg]	[kJ/kg]	[kW]	[kJ/kg]	[C]
Dead Oil	-2086	51	8	13	87.9	-2074	53
GOR=150	-2369	58	14	23	164.0	-2346	62
GOR=500	-2834	70	34	56	393.3	-2778	78
GOR=10000	-3850	94	82	136	955.4	-3714	113
Methane	-4661	107	118	196	1371.2	-4465	135

Boosters typically have a maximum power capacity, dictated by the electric motor (or gas turbine) driving the shaft. The booster can be operated at that maximum power capacity or at lower values typically by regulating the rotational speed. Consider a booster operated at constant power $\dot{W}^*$, and the equation to compute the power of the booster provided earlier:

$$\dot{W}^* = \dot{m} \cdot \frac{\Delta h_s}{\eta_{adiabatic}}$$

EQ. 2-83

Eq. 2-83 specifies that the isentropic enthalpy difference and the mass flow have an inversely proportional relationship. This means the same fixed number $\dot{W}^*$ can be obtained either by a high mass flow rate and a low isentropic enthalpy difference, or a low mass flow rate and a high isentropic enthalpy difference. Therefore, an iso-power line in a booster performance plot depicting iso-entropic enthalpy difference versus mass flow should depict a hyperbola (Figure 2-51).
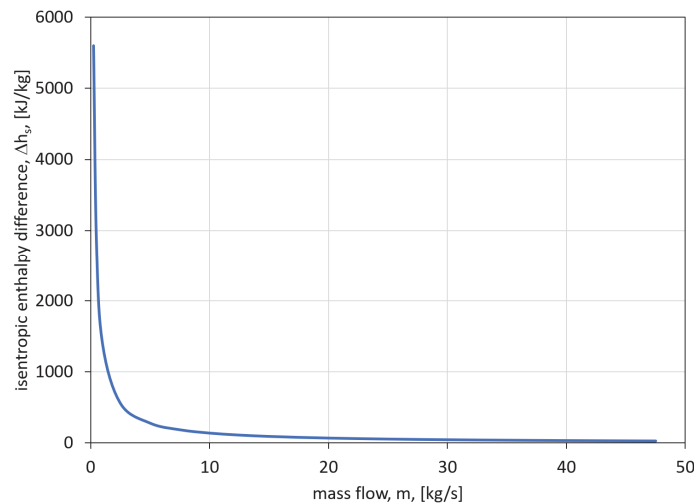
FIGURE 2-51. DIAGRAM OF ΔH_s VERSUS MASS FLOW FOR A BOOSTER OPERATING AT CONSTANT POWER OF 1.4 MW AND ASSUMING A CONSTANT ADIABATIC EFFICIENCY OF 1

However, in rotor-dynamic boosters such as centrifugal and axial pumps, compressors and multiphase boosters, the adiabatic efficiency is often a function of mass flow (or local flow rate at the inlet) as the blades and vanes are designed to handle optimally a specific amount of fluid with specific characteristics. These boosters have a peak of efficiency at a nominal value of rate above and below which the efficiency is reduced significantly. Because of this, the plot of iso-entropic enthalpy difference versus mass flow will not depict a hyperbola. Moreover, boosters typically have a mass flow operating range, and it is often not possible to operate outside of it, because it leads to low efficiency and failure. The isentropic enthalpy difference is strongly correlated with the pressure difference, and the mass flow rate with the local volumetric rate at inlet conditions. Therefore, the performance curve of pressure difference versus local volumetric rate at inlet conditions at constant power often depicts sort of a straight line with negative slope, due to the concave behavior of adiabatic efficiency with local rate at inlet.

2.3.4.   OPERATIONAL ENVELOPE: ELECTRIC SUBMERSIBLE PUMP

An electric submersible pump (ESP) operating with undersaturated oil, will display the performance curve shown in Figure 2-52. The performance curves have been plotted for several rotational speeds (f). The plot is made considering that the GOR, WC and fluid viscosity are constant. The maximum rotational speed is f_1 and the minimum rotational speed is f_5. For a fixed rotational speed if the rate is increased, the pressure boost provided by the pump diminishes.

Three lines have been drawn on the plot. To avoid decreased pump life, the pump should always operate between the minimum (down-thrust) and the maximum (up-thrust) lines. When the pump operates outside this range, there is poor efficiency and excessive wear in the washers (lower or upper) that support the pump impeller[23]. The line in violet color is the best efficiency line (BEL) and it is usually desirable to operate as close as possible to it. The hydraulic efficiency will typically be reduced if the rate is increased or decreased from this value.

---

[23]   In   floating-impeller   configurations,   the   shaft   induces   impeller   rotation   through   a   key (https://en.wikipedia.org/wiki/Key_(engineering)) , but the impeller is free to move axially (up or down) with respect to the shaft.
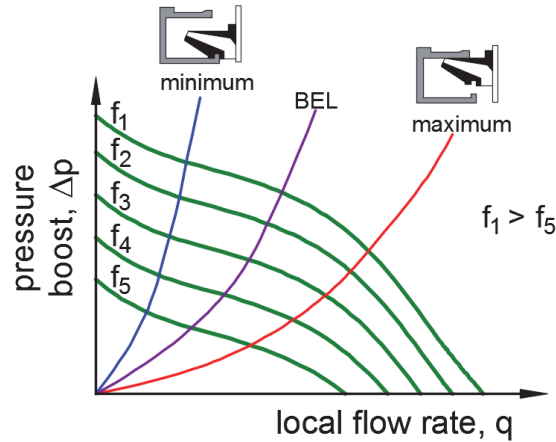
FIGURE 2-52. PUMP PERFORMANCE CURVE, DELTA PRESSURE VS LOCAL FLOW RATE

The feasible operating region of the ESP is defined by the up-thrust and down-thrust lines and the minimum and maximum rotational speed (which gives a trapezoidal-like operational region). Besides this operational constraint, additional constraints that are typically imposed on ESP operation are:

- The suction pressure to be above the bubble point pressure of the crude (often with a safety margin to avoid vaporization of the crude at the ESP inlet due to inlet losses). If this is not possible, a gas-liquid separator should be installed at the inlet and the gas should be produced through the annulus. In some cases, it is also possible to use impellers that are gas-tolerant and can be used for inlet gas volume fractions of up to 10%.
- The total power required (as given by Eq. 2-84) must be equal or less than the total capacity of the motor.

$$P = \frac{\Delta p \cdot q}{\eta_h \cdot \eta_m}$$ EQ. 2-84

Where:

P	Required hydraulic pumping power [W]
Δp	Pressure increase provided by the pump, [Pa]
q	Total volumetric rate at pump inlet conditions [m³/s]
η_h	Hydraulic efficiency [-]
η_m	Mechanical efficiency [-]

Viscosity greatly affects the performance (and hydraulic efficiency) of an ESP. Figure 2-53 shows how the ESP performance map changes when operating with water versus operating with a crude of 200 cP.
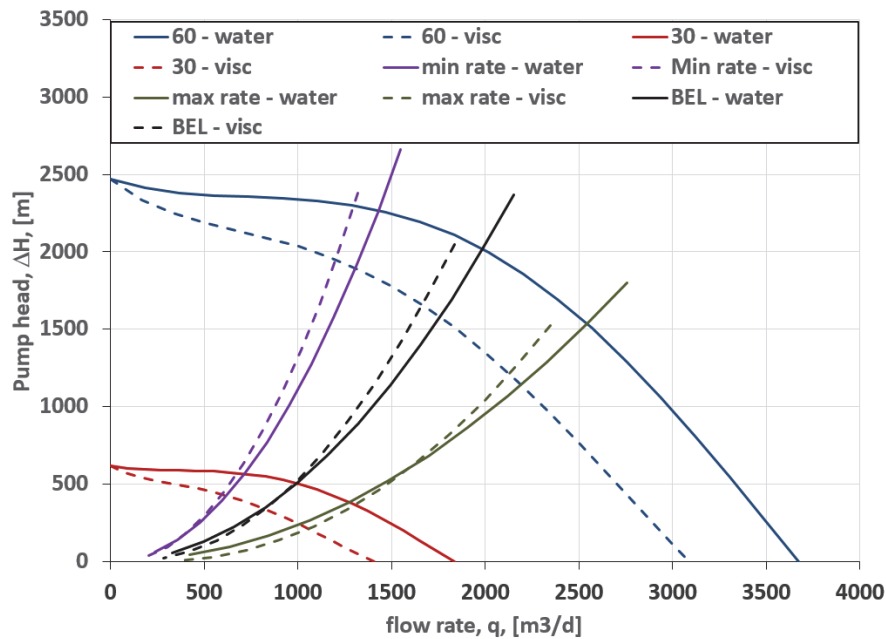
FIGURE 2-53. PUMP PERFORMANCE CURVE OPERATING WITH WATER OR WITH AN OIL OF 200 CP. PREDICTED WITH THE METHOD DESCRIBED IN THE STANDARD ANSI/HI 9.6.7-2010

When pumping oil-water mixtures, the effective viscosity of the mixture will depend on (among other things) the volume fraction of each phase. Therefore, in wells producing oil and water the viscosity will change with time when the water cut increases. It is important to take into account this time variation when selecting a suitable ESP pump for the application.

Density variations will also affect the pressure boost provided by the ESP. Although the operational map in terms of pump head (ΔH) is unaffected by density, the pressure boost is $\Delta p = \Delta H \cdot \rho$, thus it will change with changes in density.

Consider the situation shown in Figure 2-54. A hydraulic equilibrium analysis is performed at the pump suction and discharge to determine required pump delta pressure to deliver a specific rate at two depletion times, 1 and 2. The pressure at the inlet to the pump and the choke delta pressure are estimated from the curves.
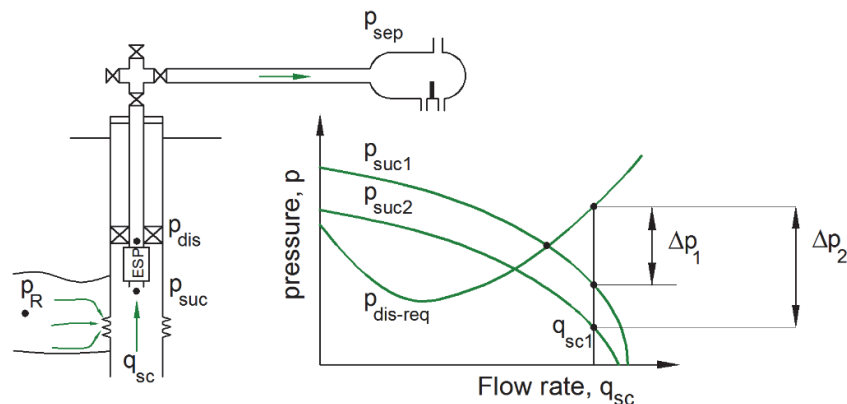
FIGURE 2-54. ESP EQUILIBRIUM ANALYSIS FOR ESP DESIGN FOR TWO DEPLETION STATES

Figure 2-55 shows the performance curve of an ESP that has been selected for the application for several rotational speeds. Operating points 1 and 2 have been plotted on the figure (Δp and rate). The ESP should operate at a frequency between f_4 and f_3 to produce point 1, and between f_1 and f_2 to produce point 2. As time

passes the delta pressure required by the pump will increase until the pump frequency reaches its maximum. At that moment, the rate should be reduced to move the operating point back into the pump operating envelope.
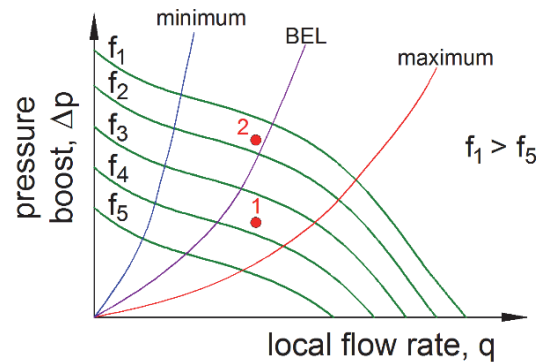
FIGURE 2-55. ESP PERFORMANCE CURVE WITH OPERATING POINTS OVERIMPOSED

2.3.5. OPERATIONAL ENVELOPE: DYNAMIC GAS COMPRESSOR

In systems with gas, compressors are sometimes used to provide additional energy to the fluid to overcome pressure losses in the surface pipe transportation system. The compressors used for this type of applications are centrifugal or axial compressors. Axial compressors are used for high rates and medium to low pressure boosts, and centrifugal compressors are used for low to medium rates and high-pressure boosts.

The pressure-enthalpy diagram for Methane is shown in Figure 2-56. Consider a compression process from 50 bara to 100 bara, and inlet temperature 20 °C. The ideal compression process, that requires the least amount possible of energy, with no losses or irreversibilities is the one performed at constant entropy (blue line in the plot).
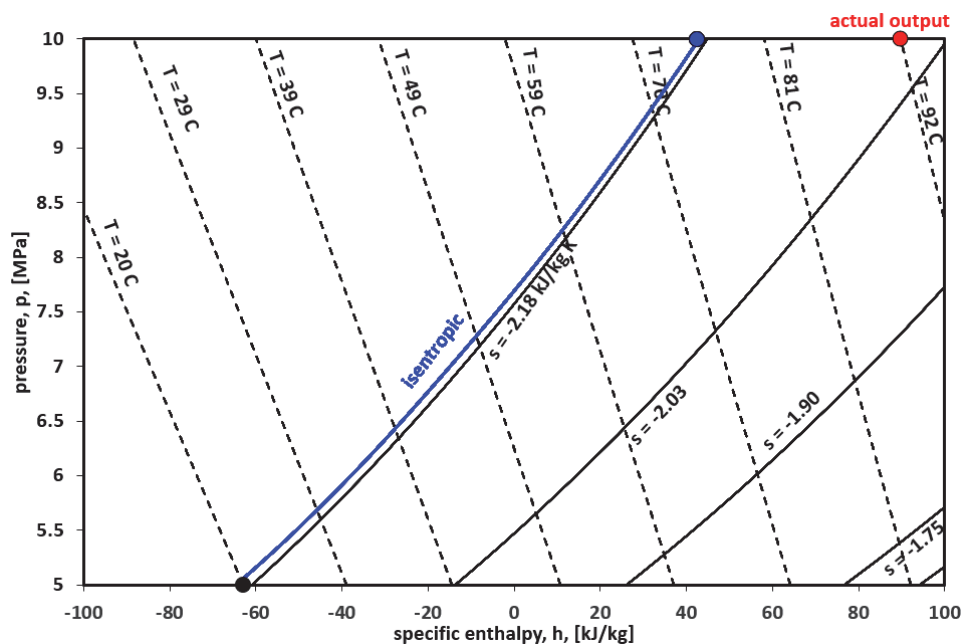
FIGURE 2-56. PRESSURE-ENTHALPY DIAGRAM FOR METHANE DEPICTING AN ISENTROPIC COMPRESSION PROCESS AND THE OUTPUT OF A REAL COMPRESSION PROCESS

The real compression process, however, is far from ideal and leads to higher outlet temperatures than the isentropic (see the red point in the figure labelled with "actual output"). The output of the real process can be

approximated using a polytropic process ($p\,v^n$ = *const*) where the polytropic exponent n represents the "efficiency" of the compression process. In the extreme when $n=k$ (ratio of specific heats Cp/Cv), the process is isentropic.

The outlet temperature of a polytropic process can be estimated with the expression below (with T input in absolute units, such as K):

$$T_{out} = T_{in} \cdot r_p^{\frac{n-1}{n}}$$

EQ. 2-85

For convenience, the polytropic exponent is expressed as a function of the polytropic efficiency η_p, a number between 0-1 (0-100%):

$$\eta_p = \frac{k-1}{k} \cdot \frac{n}{n-1}$$

EQ. 2-86

The polytropic efficiency typically varies as a function of the operational flow rate. For centrifugal compressors, it typically lies in the range 0.65-0.80.

The fluid power required by the polytropic compression process is equal to the enthalpy difference between inlet and outlet times the mass flow.

$$\dot{W} = \dot{m} \cdot (h_2 - h_1) = \dot{m} \cdot \Delta h$$

EQ. 2-87

The enthalpy difference is estimated using Eq. 2-88:

$$\Delta h = \frac{H_p \cdot g}{\eta_p}$$

EQ. 2-88

Where:

g Gravitational acceleration [m/s^2]

H_p Polytropic head, [m], given by:

$$H_p = \frac{T_{suc}}{g} \cdot Z_{av} \cdot R \cdot \frac{n}{n-1} \cdot \left(r_p^{\frac{n-1}{n}} - 1\right)$$

EQ. 2-89

Where:

T_{suc} Suction temperature [K]

Z_{av} Average gas deviation factor between compressor discharge and suction

R Specific gas constant [J/kg K]

n Polytropic exponent[24]

g Gravitational acceleration [m/s^2]

r_p Pressure ratio p_{dis}/p_{suc} [-]

The performance map of compressors is typically expressed in terms of the polytropic head versus the actual volumetric rate at the compressor suction. Figure 2-57 shows the performance map of a gas compressor. In a

---

[24] The compression of the gas in the compressor is approximated assuming that the process is polytropic ($p \cdot v^n$ = const). The polytropic exponent can be estimated from measured data.

similar way to the ESP, the polytropic head decreases when the rate increases. Higher rotating speeds increase the polytropic head.
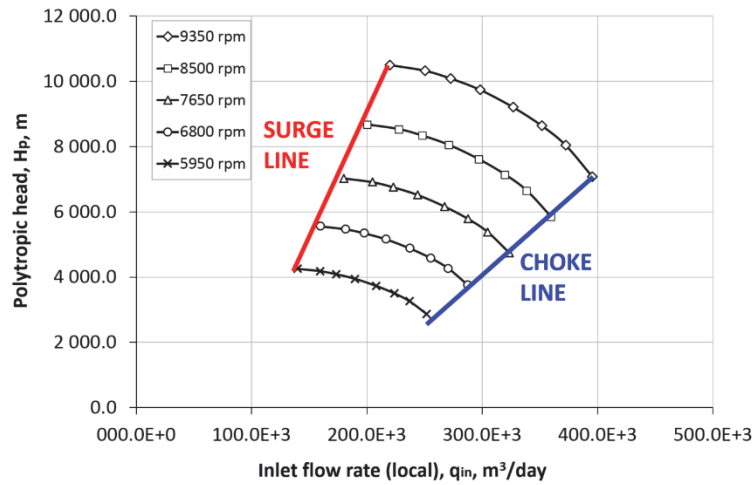
FIGURE 2-57. PERFORMANCE MAP OF A GAS COMPRESSOR

The map is contrained to the right by the choke line. In this region, the flow in the compressor reaches the sonic velocity and cannot be increased further. To the left surge becomes an issue. In surge the flow stops being steady and there is cyclic flow reversal at the discharge. This is because the polytropic head curve drops at rates below the surge line.

Consider a compressor with fixed suction pressure and a valve located at the exit. In the operational region to the right of the surge line if one chokes the valve at the discharge, the rate is reduced and the pressure delivered by the compressor matches the pressure upstream the valve. However, then the rate is reduced below the surge rate, the compressor is no longer able to deliver this pressure (due to the concavity of the curve) and the discharge pressure becomes higher than the pressure the compressor can deliver. This causes flow reversal. With the flow reversal, the pressure at the discharge decreases and falls within the compressor curve again. The rate increases again and the cycle is repeated.

The performance map of a compressor will vary mainly with the inlet temperature, the molecular weight of the gas (M) and the heat capacity ratio[25] ($k = C_p/C_v$). If the curves at test conditions are known[26], the following expressions can be used to correct them and estimate the performance under different conditions:

$$q_{new} = q_{test} \cdot \sqrt{\frac{k_{new}}{k_{test}}} \cdot \sqrt{\frac{M_{test}}{M_{new}}} \cdot \sqrt{\frac{T_{new}}{T_{test}}} \qquad \text{EQ. 2-90}$$

$$H_{p,new} = H_{p,test} \cdot \frac{k_{new}}{k_{test}} \cdot \frac{M_{test}}{M_{new}} \cdot \frac{T_{new}}{T_{test}} \qquad \text{EQ. 2-91}$$

To avoid having a collection of curves each time these variables change, often the operating point is converted to the test conditions using Eq. 2-86 and Eq. 2-87, and are plotted on the test performance map.

Besides the constraint that the operating points must fall on the compressor performance map, there are some additional constraints that must be considered:

---

[25] A empirical expression to estimate k is k= $1.30 - 0.31 \cdot (\gamma_g - 0.55)$
[26] Typically, 1 atm and 15.56 ºC at the suction

· The required compression power (P) must be less than the power capacity of the driving motor. The total required power can be computed with Eq. 2-92.

$$P = \frac{\Delta h \cdot \dot{m}}{\eta_m}$$ EQ. 2-92

Where:

$\dot{m}$ Mass flow [kg/s]

η_m Mechanical efficiency [-]

· The temperature at the discharge must be kept below a maximum allowable value. This is usually due to temperature limits in the compressor seals and safeguard the integrity of the downstream piping. In systems where chemicals are injected (e.g. hydrate inhibitor), the temperature should also be kept below the vaporization temperature of the chemical, to ensure its effectiveness.
· The pressure at the suction must be above a minimum allowable value (typically due to rotor balancing, forces on the shaft and to maintain the effectiveness of seals).

2.3.6. OPERATIONAL ENVELOPE: JET PUMP

A Jet pump, or ejector, is a device without moving parts in which a high-pressure source fluid is injected to the main fluid stream through a nozzle. Due to the high speed the high-pressure fluid achieves in the nozzle, its pressure is reduced significantly and creates a sucking effect. The suction side of the jet-pump is then connected to this location (Figure 2-58). The high-pressure fluid is usually single-phase gas or liquid (oil or water).
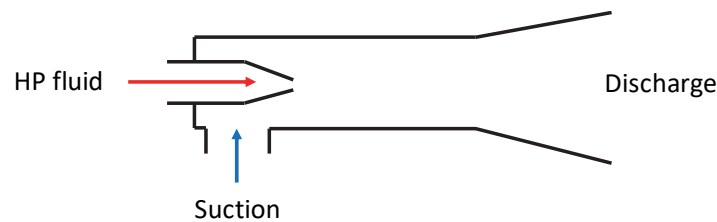
FIGURE 2-58. SIMPLIFIED SCHEMATIC OF A JET PUMP

A jet pump displays the performance shown in Figure 2-59 (taken from Beg and Sarshar[2-7]). The x axis shows the mass flow ratio between suction and injection fluid, r_m. The y axis shows the pressure ratio between discharge and suction, r_p. There are several curves for different values of r_{pi} which is the pressure ratio between injection fluid pressure and suction. For a given r_{pi}, if one increases the mass flow ratio r_m (injects less fluid) the possible pressure ratio to achieve between discharge and suction is reduced. If one increases the r_{pi} keeping the mass flow ratio fixed, a higher r_p is achieved.
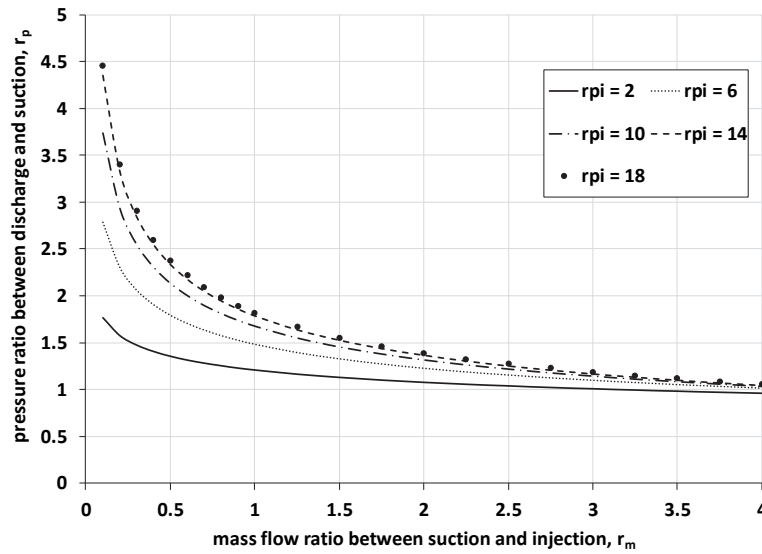
FIGURE 2-59. PERFORMANCE PLOT OF A JET PUMP (TAKEN FROM BEG AND SARSHAR[2-7])

An equation to represent this performance is:

$$r_p = a \cdot (r_m)^b$$

EQ. 2-93

Where "a" and "b" are functions of r_{pi} (e.g. polynomials).

A procedure to determine the operational conditions of a production system with a jet pump is the following:

- Excluding the jet pump, compute the available pressure at the suction (using only the system upstream the pump) and the required pressure at the discharge (using only the system downstream the pump) to deliver a desired rate q.
- With these values compute r_p and r_{pi} (with the injection pressure known). Read from the chart the required mass flow ratio r_m, using the appropiate curve of r_{pi} .
- Compute the required mass flow of injection fluid. Subsequently, compute again the required pressure at the discharge of the pump with the desired rate q and the mass flow of injection fluid.
- The process is then repeated until the required mass flow ratio r_m does not change from iteration to iteration.

2.4.   FLOW EQUILIBRIUM IN PRODUCTION NETWORKS

In a production network the operating conditions in one well affect, to some degree, others, therefore all possible hydraulic interactions have to be accounted for when computing its hydraulic performance.

The graphical procedure is very rarely used to explain equilibrium calculations of a production network. This is because, for most cases, pipeline available and required pressure curves depend on the sum of rates of multiple wells, making it difficult to perform a graphical intersection with the single well pressure curves. Additionally, the inlet and outlet pressure of pipelines are initially unknown (unless the end of the pipe is the separator), so the available or required pressure curve have to be redrawn for every inlet or outlet pressure value assumed.

For these reasons the flow performance analysis of production networks is almost exclusively performed using computerized routines and software. However, most of the observations given for the single well production system are applicable to the network case.

Consider as an example the case shown in Figure 2-60 where there is a production system with three wells, a pipeline and a separator. The point is interest is defined as the junction where the production of the three wells is commingled. The available pressure curve is calculated for each well from the reservoir to the junction and the required pressure curve is calculated for the pipeline from the separator to the junction.
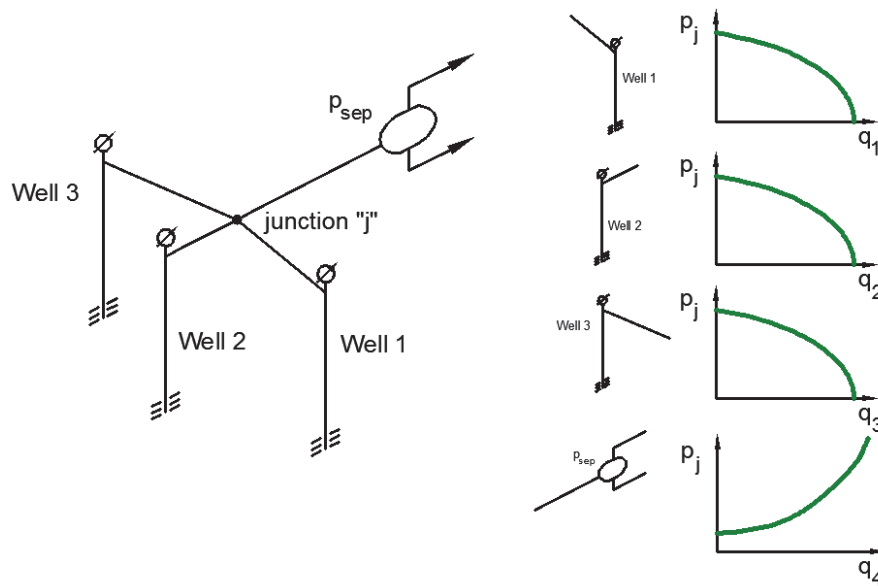
FIGURE 2-60. PRODUCTION NETWORK WITH 3 WELLS. AVAILABLE JUNCTION PRESSURE CURVE FOR THREE WELLS AND REQUIRED JUNCTION PRESSURE CURVE FOR THE PIPELINE

To deal with the fact that all available and required pressure curves are drawn with different rates (well 1, 2, 3, 4 and pipeline) an iterative process has to be performed to find the equilibrium rate of each well:

1. Assume a junction pressure
2. Read q_1, q_2, q_3 and q_4 from the available and required pressure curves.
3. Verify that $q_1 + q_2 + q_3 = q_4$. If yes, the assumed junction pressure is the real operating pressure. Else, go back to step 1.

The mass conservation equation at the junction is checked to verify that the operating junction pressure is physically consistent.

It is also possible to assume an equilibrium rate for each well and then check that the junction pressure is the same for all wells and pipeline. However, this is a bit more cumbersome as three variables have to be guessed instead of one.

It is perhaps more practical to regard the production network as the mathematical function shown in Figure 2-61. The network model takes as input: properties of the production system, settings of the adjustable elements and provides as output the well rates.
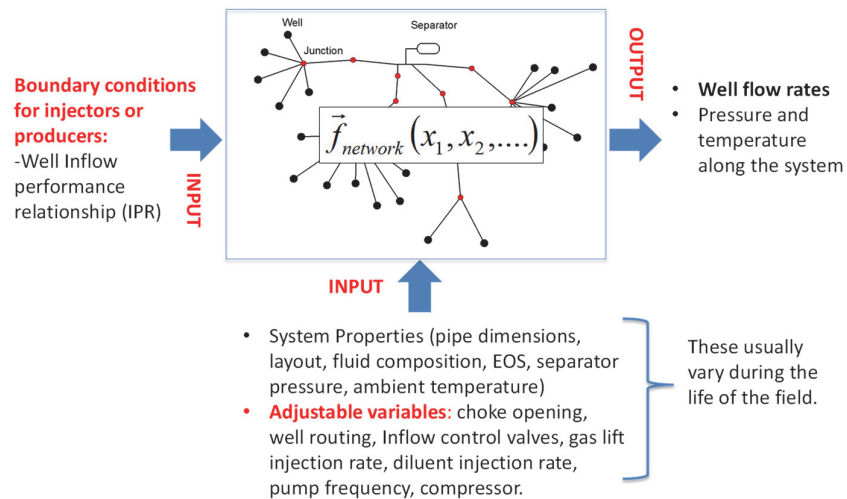
FIGURE 2-61. DEPICTION OF THE PRODUCTION NETWORK MODEL AS A MATHEMATICAL FUNCTION

As mentioned before, if there are adjustable elements in the production network, the solution will depend on the settings of such adjustable elements. Consider, for example, the case of two wells and a pipeline presented in Figure 2-62.
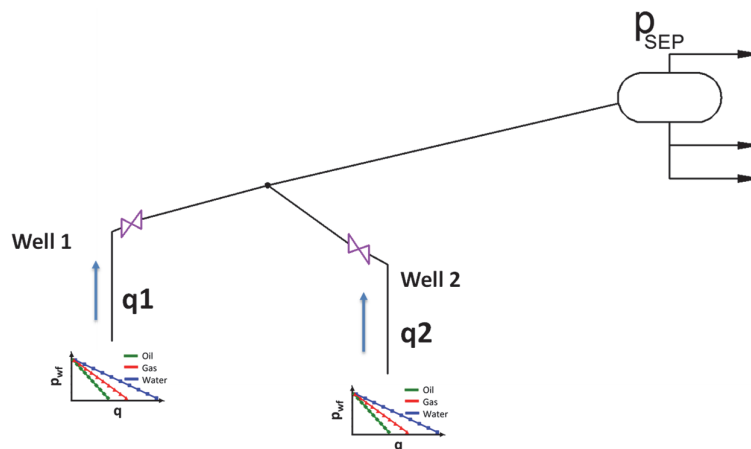
FIGURE 2-62. PRODUCTION NETWORK WITH 2 WELLS

If there are no adjustable elements in the system, the network model function provides a unique combination of rates q_1 and q_2 as the solution of the network. However, if each well has an adjustable wellhead choke, the solution of the network model function becomes dependent on the choke settings. Figure 2-63 presents a plot where flow rates of well 1 are plotted in axis "y" and flow rates of well 2 are plotted on axis "x". When both chokes are open, the unique combination of rates mentioned earlier is obtained (central red point in Figure 2-63). When well 2 is closed, well 1 will be producing alone in the network and the network model solution yields the point in the y axis. When well 1 is closed, the network solution yields the point on the x axis.
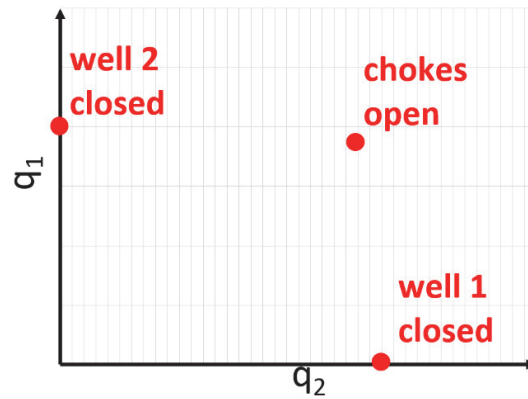
FIGURE 2-63. WELL FLOW RATE SOLUTIONS FOR NO CHOKE, WELL 1 CLOSED, AND WELL 2 CLOSED

If the network is solved repeatedly for multiple combinations of choke openings, it is possible to create a map shown in Figure 2-64 that shows which well rate combinations are achievable by choking and which are not. Figure 2-64 has been generated for a production system of two gas wells equipped with wellhead chokes and discharging to a common pipeline and separator.
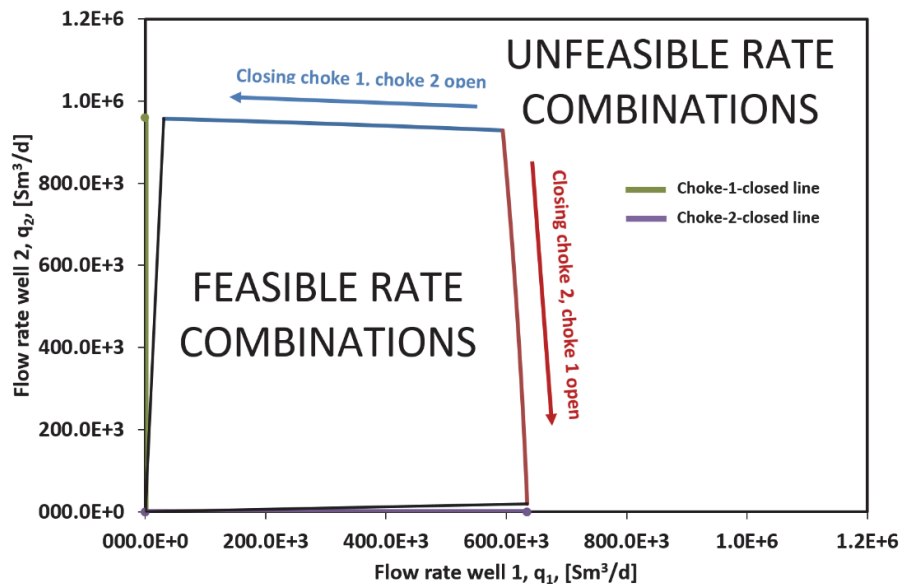
FIGURE 2-64. WELL FLOW RATE DOMAIN SOLUTION FOR THE PRODUCTION SYSTEM WITH 2 WELLS

An interactive calculator is available here https://www.desmos.com/calculator/k6yktvzvfu for the reader to use and visualize the effect of several system parameters on the operational rates (intersection).

Note that there are two small unfeasible operational regions very close to the x and y axis (the green and violet lines correspond to well standalone production in the network). For example, when choke 1 is left open and choke 2 is gradually closed (red line), there will be a point when well 2 cannot physically produce anymore (and its production becomes zero). This is because the rate of well 2 becomes too small when compared with the rate of well 1. At that point, if the choke of well 1 is closed slightly (i.e. q_1 is reduced), then well 2 will be able to flow again. This is how the black lines in the drawing (bottom and left bounds of the feasibility region) were calculated.

The feasible operational region for a system of 3 wells discharging to a common flowline is shown in Figure 2-65 a, enclosed by 3 surfaces (one per each well). The operating point is where all surfaces intersect. Figure 2-65 b shows the effect of choking well 1.

a) Wellhead chokes fully open   b) Wellhead choke of well 1 = 50 bar, 2 and 3 fully open
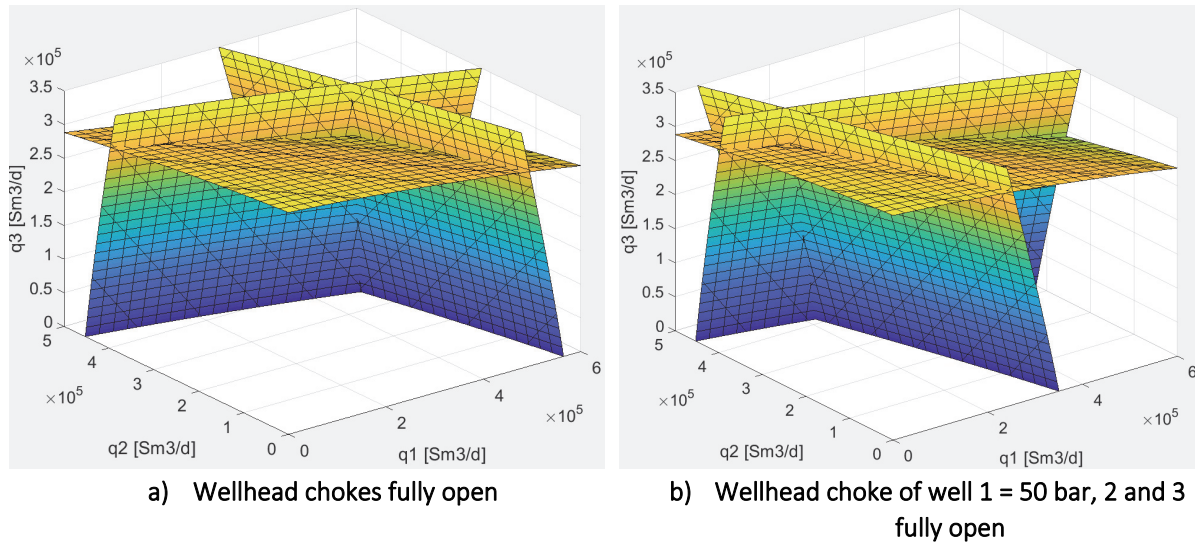
FIGURE 2-65. WELL FLOW RATE DOMAIN SOLUTION FOR THE PRODUCTION SYSTEM WITH 3 WELLS

Keep in mind this peculiarity of production networks. If there are no adjustable elements, or the adjustable elements have a fixed setting, there is one unique solution to the production network. However, if there are adjustable elements in the system, there is usually a variety of operational conditions that can be achieved.

2.4.1. SOLVING NETWORK HYDRAULIC EQUILIBRIUM FIXING WELL RATES

As in the case of the single well production system, it is also possible to solve the network fixing a rate in single or multiple wells and removing some adjustable elements. In this operational mode, the network model is used to verify if is physically possible to produce the specified rates and to estimate pressure change that the adjustable element has to provide.

Consider as an example, the two well network shown in Figure 2-66. Each well is equipped with a wellhead choke. Assume that the location downstream the chokes is very close to the junction p_j, such as all pressures (downstream choke 1, downstream choke 2 and junction) can be considered identical. Note the **chokes are ignored when performing the analysis**.
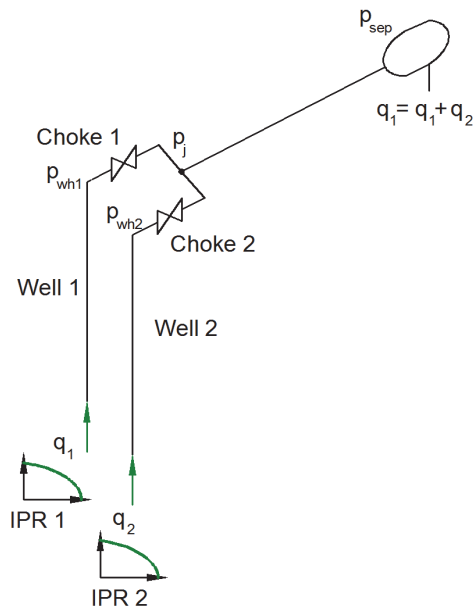
FIGURE 2-66. WELL FLOW RATE DOMAIN SOLUTION FOR THE PRODUCTION SYSTEM WITH 2 WELLS

By fixing the rate, the bottom-hole pressure of each well can be calculated with the IPR. With the bottom-hole pressure and the rate, it is possible to compute pressure drop concurrent up to wellhead (upstream the chokes). At the same time, with the well rates and separator pressure, it is possible to compute junction pressure by performing counter-current pressure drop calculations.

If $p_{wh1} > p_j$ and $p_{wh2} > p_j$ then it is physically possible to produce the rate and the chokes pressure drop can be estimated. If, on the other hand, the wellhead pressures are lower than junction pressure, the well rate is not feasible and it has to be reduced to a lower value. To calculate the well feasible rate, the choke delta pressure has to be set to 0 ($p_{wh} = p_j$) and the hydraulic equilibrium rate calculated.

This type of analysis can also be done with other adjustable equipment such as ESPs, compressors and boosters.

2.4.2. DOWNHOLE NETWORKS

Networks can also exist in wells, e.g. when wells are multi-lateral, multi-layer or multi-section. As an example, consider the horizontal wellbore presented in Figure 2-67. the horizontal section is open hole, drilled in the oil layer and swellable packers have been installed along the liner to "split" the wellbore in sections. Each section is equipped with a sliding sleeve, which can be activated to allow or close communication between the annulus and the inside of the liner.
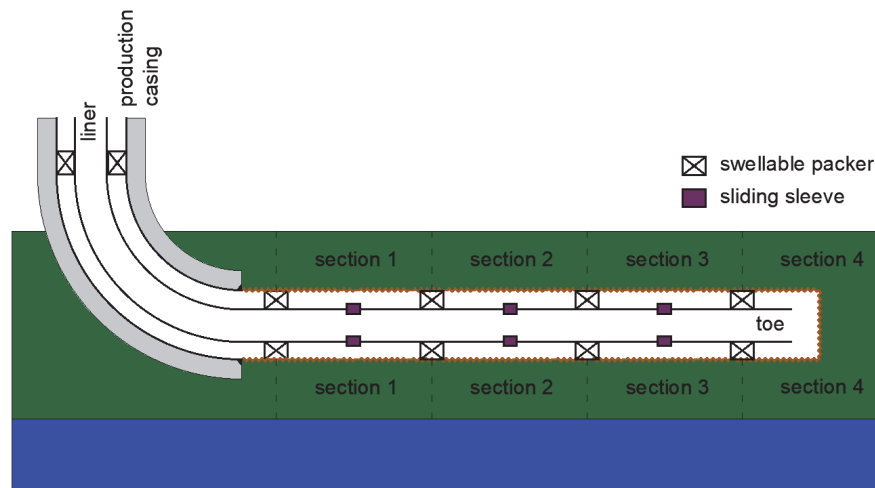
FIGURE 2-67. HORIZONTAL WELLBORE WITH SEVERAL SECTIONS DELIMITED BY PACKERS

The system shown above can be represented by the equivalent line diagram:
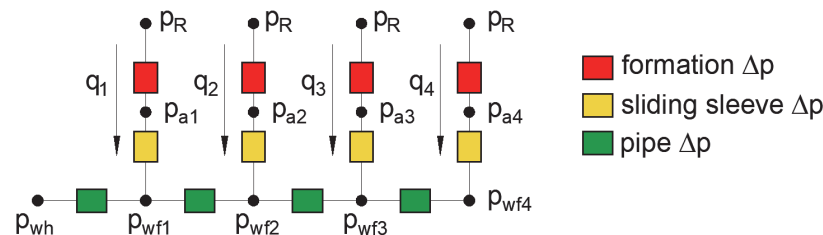
FIGURE 2-68. EQUIVALENT LINE DIAGRAM REPRESENTING A SECTIONED HORIZONTAL WELLBORE

One can use network calculations, just like in surface gathering systems to estimate how much will each section produce. In the case that the production is uneven (i.e. significantly different from each section), this might lead to coning from the aquifer. This occurs typically at the sections closer to the heel, because the flowing

bottomhole pressure is lower. To avoid this problem, sometimes an Inflow control Device (ICD) is placed on the liner wall of the section to increase artificially the pressure drop.

COMPLETION BITE: SLIDING SLEEVE

A sliding sleeve is a pipe section threaded to the tubing that is used to establish or stop communication at will between the inside of the tubing and the annulus (annular space between tubing-casing). Sliding sleeves are typically used to isolate or connect zones in a well.

The figure below shows the main elements of a sliding sleeve. It consists of two concentric pipe sections, the outer, which is screwed as part of the production string, and the inner, which can move up or down.
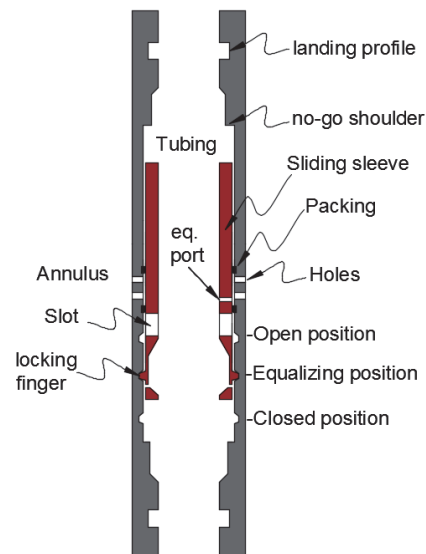
FIGURE 2-69. GENERIC SLIDING SLEEVE CONFIGURATION

Locking fingers lock on the grooves to hold in the housing the sleeve position. When the sleeve is pressed downwards or upwards, the locking fingers will contract when coming out of the groove, and will expand after reaching the next groove as shown in the figure below.
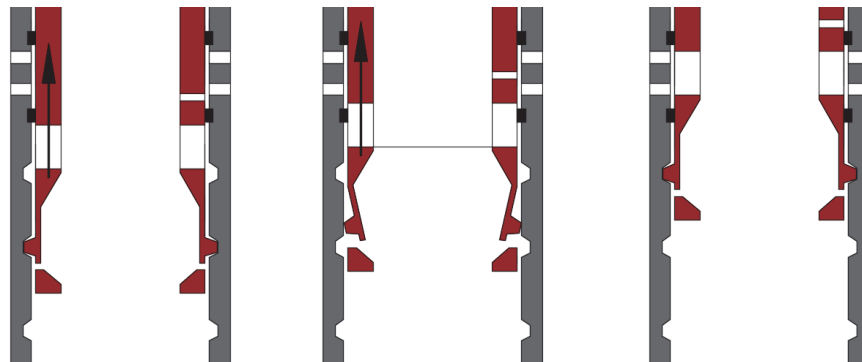
FIGURE 2-70. DETAILS OF THE LOCKING MECHANISM OF THE SLEEVE
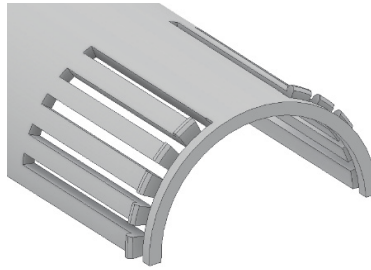
FIGURE 2-71. DETAILS OF THE LOCKING FINGERS ON THE SLEEVE THAT RETRACT AND EXPAND WHEN RECIPROCATED AXIALLY INSIDE THE SLEEVE

Sliding sleeves typically have three positions (although they can have more, depending on the application): open, closed and equalizing. When the sleeve is in the open position, the slots in the sleeve are aligned with the holes in the housing.

SHIFTING PROCEDURE

There are several methods to shift sleeves. The most common is by using wireline (slickline). The general sequence to shift the sleeve using slickline is shown below. In the first step, the shifting tool is lowered into the sleeve and jarred down until the collet of the shifting tool is locked into the landing profile of the sleeve.
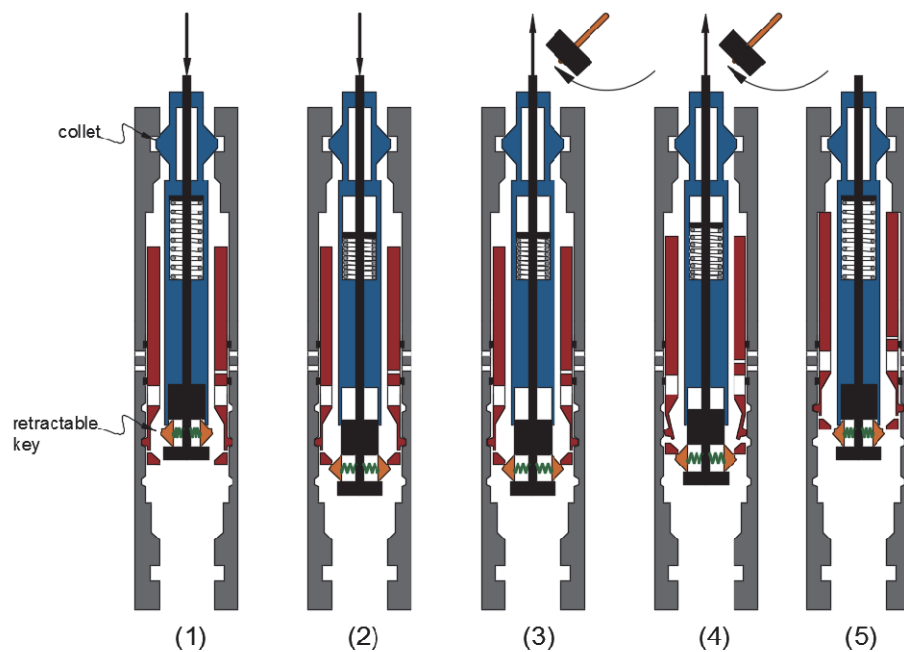
FIGURE 2-72. SHIFTING SEQUENCE OF A SLIDING SLEEVE USING SLICKLINE

In the second step, the wireline is further lowered until the retractable keys of the shifting tool are deployed and sit on the slower end of the sleeve. After this, the wireline is jarred up, to displace the sleeve from the lower position to the upper position (steps 3-5).

REFERENCES

[2-1] Astutik, W. (2012). *IPR modeling for coning wells*. Thesis for the degree of Master of Science. Norwegian University of Science and Technology. Trondheim.

[2-2] Crafton, J. Dyal, V. (1976). *An Iterative Solution for the Gas Pipeline Network Problem*. SPE-6032. Annual Fall Technical Conference and Exhibition of the SPE of AIME. Society of Petroleum Engineers. New Orleans

[2-3] Golan, M., Whitson, C. H. (1986). *Well Performance*. Second Edition. Prentice-Hall Inc

[2-4] Litvak, M., Darlow, B. (1995). *Surface Network and Well Tubing head Pressure Constraints in Compositional Simulation*. SPE-29125. *Symposium on Reservoir Simulation*. Society of Petroleum Engineers. San Antonio.

[2-5] Tian, S., Adewumi, M. *A New Algorithm for Analyzing and Designing Two Phase Flow Pipeline Networks* Paper 28177 presented at the 1993 AIChE spring National Meeting, Texas. 1993.

[2-6] Whitson, C. H. (1983). *Reservoir Well Performance and Predicting Deliverability*. SPE12518.

[2-7] Beg, N., Sarshar, Sacha. (2014). Engineers' Handbook on Surface Jet pumps for Enhanced oil and gas production. Caltec Limited.

[2-8] Jurus, W.; Stanko, M.; Parra, A.; Golan, M. Simplified Near Wellbore Reservoir Simulation To Predict the Performance of Viscous Oil Horizontal Well with Water Coning from an Active Aquifer. SPE Latin American and Caribbean Petroleum Engineering Conference; 2015-11-18 - 2015-11-20.

[2-9] Janicek, J. D., Katz, D.L. Applications of Unsteady State Gas Flow Calculations. Preprint from Res. Conf., U. of Michigan (June 20, 1955)

[2-10] Ros, N.C.J. An analysis of critical simultaneous gas/liquid flow through a restriction and its application to flowmetering. Appl. sci. Res. 9, 374 (1960). https://doi.org/10.1007/BF00382215

[2-11] Perkins, T.K. (1993) Critical and Subcritical Flow of Multiphase Mixtures Through Chokes, SPE Drilling & Completion, SPE-20633-PA, 8(4): 271-276. https://doi.org/10.2118/20633-PA

[2-12] Sachdeva, R., Schmidt, Z., Brill, J.P., and Blais, R.M. (1986) Two-Phase Flow Through Chokes, 61st Annual Technical Conference and Exhibition of the Society of Petroleum Engineers, SPE-15657-MS. https://doi.org/10.2118/15657-MS

[2-13] Schüller, R. B., Solbakken, T., and Selmer-Olsen, S. (2003) Evaluation of Multiphase Flow Rate Models for Chokes Under Subcritical Oil/Gas/Water Flow Conditions, SPE Production & Facilities, SPE-84961-PA, 18(3): 170-181. https://doi.org/10.2118/84961-PA

[2-14] Al-Safran, E.M. and Kelkar, M.G. (2009) Predictions of Two-Phase Critical Flow Boundary and Mass Flow Rate Across Chokes, SPE Production & Operations, SPE- 109243-PA, 24(2): 249-256. https://doi.org/10.2118/109243-PA

[2-15] M De Lorenzo, P Lafon, JM Seynhaeve, Y Bartosiewicz. Benchmark of Delayed Equilibrium Model (DEM) and classic two-phase critical flow models against experimental data. - International Journal of Multiphase Flow, 2017.

[2-16] Moody, Frederick J.. "Maximum discharge rate of liquid-vapor mixtures from vessels." , Sep. 1975. https://doi.org/10.2172/7309475

[2-17] Vogrin, Jr., Joseph A. (1963). An experimental investigation of two-phase, two-component flow in a horizontal, converging-diverging nozzle. https://doi.org/10.2172/4637255

[2-18] Carstensen, Carl-Martin and Kanstad, Stig Kåre, Multiphase Flow Through Chokes - An Evaluation of Frozen, Equilibrium, and Nonequilibrium Flow Models (March 21, 2022). Journal of Petroleum Science and Engineering, Volume 215, Part A, August 2022, 110402, Available at SSRN: https://ssrn.com/abstract=4497848

[2-19] Kourakos, V. Experimental study and modeling of single- and two-phase flow in singular geometries and safety relief valves. PhD thesis. 2011.

[2-20] Darby, Ron. (2005). Size safety-relief valves for any conditions. Chemical Engineering -New York-Mcgraw Hill Incorporated then Chemical Week Publishing Llc-. 112.

3.   PRODUCTION OPTIMIZATION

In the industry, "Production optimization" is a wide term that englobes detecting opportunities to increase field oil or gas production, cost reduction and implementing solutions to materialize them. The main principle is to introduce small cost-effective changes to improve the production system. Roughly speaking, the potential increase in production that can be achieved by executing optimization lies someplace between 1-30%.

Some actions that are typically executed to perform production optimization are:

- Detect locations in the system with abnormally high-pressure loss and flow restrictions
- Verification of equipment design conditions vs actual operating conditions
- Identification and addressing fluid sources that have disadvantageous characteristics (e.g. high water cut, high H_2S content)
- Identify and correct system malfunctions and non-intended behavior
- Analyze and improve the logistics and planning of maintenance, replacement and installation of equipment or in the execution of field activities.
- Review the occurrence of failures and recognize patterns
- Calibration of instrumentation
- Identification of operational constraints (e.g. water handling capacity, power capacity)
- Observe and analyze the response of the system when changes are introduced
- Find control settings of equipment that give a production higher than current (or, preferably, that give maximum production possible)
- Identify bottlenecks
- Identifying and monitoring key performance indicators (KPIs)

Some tools that are typically used for performing these actions are historic measured and reported data, instrumentation readings, experiences reported by field operators and in-house or commercial numerical simulators.

However, formally speaking, the term "optimization" is wrongly used to characterize most of the activities described above. In mathematics, optimization refers to find or determine the maximum or minimum value of a function that is dependent on input parameters while honoring constraints. In practical production optimization checks are seldom made to verify if the corrections and changes introduced in the system are in fact the "best" possible alternative. Therefore, a better term to use to englobe most of the activities mentioned above might be "production effectivization".

In this chapter only one case of production optimization is discussed: finding control values in the system that maximize an indicator of economic or system health. Some typical indicators are: oil and gas production rates, revenue, net present value, ultimate recovery, cumulative production, inverse of lifting costs. The optimization formulation usually includes multiple operational constraints.

3.1.   OPTIMIZING A PRODUCTION SYSTEM

An existing or in-planning production system has usually adjustable elements, design features that are yet undecided upon or production and drilling schedules that are modifiable in time. It is usually desirable to find the particular setting or values of such elements that provides the most attractive operational conditions within the resources available. The definition of "most attractive operational conditions" depends on the particular application, the field architecture, the resources available, but it is usually to produce maximum oil, gas production or revenue (usually called the main objective function) while honoring multiple operational constraints. Some typical constraints are keeping water production within processing capacity, oil and gas

within sale specs, electrical power available, injection gas capacity. In most cases, constraints can become limiting factors that impede to reach an optimum value of the objective function.

The search for optimum operational conditions of the production system is typically performed by using model-based mathematical optimization. The model must be accurate enough to predict appropriately the operating conditions of the production system (taking into account uncertainty in measured data). Otherwise, any analysis based on the model has limited applicability and usability. Intuitively speaking, the numerical model is a "surrogate" of the real production system and it can be run with multiple variations of its controls to find better operating conditions than the current.

Figure 3-1 shows a simplified scheme designed to close the gap between the output of the model and the measured variables of the real system. The main task of the data assimilation algorithm is to receive the output from sensors and change parameters in the model until the difference between the output of the model and the measured variables is minimized. The parameters in the model are typically properties of the network that have a high uncertainty (e.g. IPRs) or empirical factors employed by the multiphase pressure drop correlations. The data assimilation algorithm might also quality control and process (clean, average, validate, aggregate) the data points that come from the sensors.
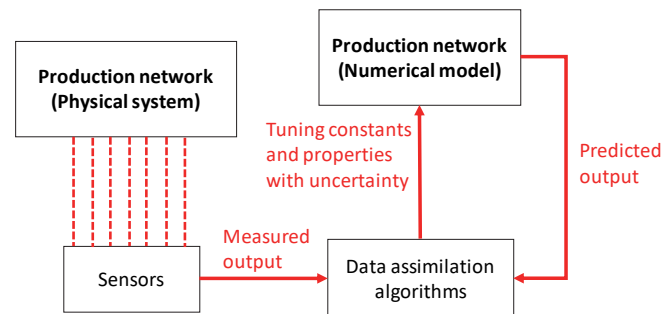
FIGURE 3-1. DATA ASSIMILATION PROCESS FOR THE NETWORK MODEL (ADAPTED FROM BARROS ET AL, 2015[3-3])

Using the model has the advantage that it can be queried multiple times to get operational data (in most cases) quicker than with the real system. Additionally, and depending on the type of model (black box or open), it is possible to have access to the underlying equations which is a requirement for some optimization algorithms.

Production optimization is often executed in three-time scales: very short term, short-term (which also englobes real time) and long-term (months-years).

Short-term optimization often focuses on finding optimum controls for a given point in time (a particular day or week), often assuming that the system is at a pseudo steady-state condition (e.g. for a given depletion state). There is data available to tune the model. Models typically used are well, gathering system and processing plant. Typical optimization objectives are oil, condensate or gas production, revenue. Typical optimization variables are: choke and valve opening, gas lift rates, pump frequency, well routing.

In long-term optimization the objective is to find optimal control values along time that optimize an indicator compounded in time (e.g. cumulative production, recovery factor net present value of the project). Typical control variables are well placement, well rates, well status, number of wells, well routing. Models typically used are reservoir models often integrated with well, network, processing facilities and economic. Models are usually highly uncertain.

In some production systems there is often a conflict between short-term and long-term optimization, because the short-term optimization is oblivious to the effect changes can cause in the future on the system. For example, in an oil-rim reservoir with an underlying aquifer and ESP-lifted wells, a short-term optimization in

each time step would probably advice to increase the frequency of ESPs, to produce as much as possible. However, a long-term optimization will probably give more conservative ESP frequency values because it will cause early water breakthrough and reduce ultimate recovery.

In very-short term optimization the time scale is in seconds, minutes and hours. The objective function is typically to maximize production, revenue, but it can also be to reduce and mitigate fluctuations (for example inhibit severe slugging in a well by controlling a choke). Typical objective variables are valve opening, gas lift rates, pump frequency. It can be deployed using transient or steady state models, but it can also be deployed directly on the physical system.

For some types of production system, e.g. single choked well, or single ESP-lifted well, finding the optimum conditions is a trivial process, just opening the choke to its maximum (Figure 3-2), or increasing the ESP frequency to its maximum yields maximum oil production. For this type of cases the optimum point is defined when operational constraints are met (e.g. power capacity feeding the ESP, sand production in the well, maximum associated water produced etc.).
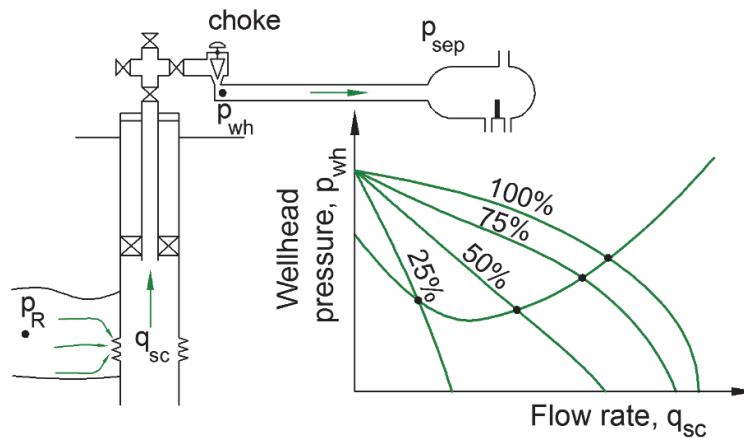
FIGURE 3-2. EQUILIBRIUM FLOW RATE OF THE SYSTEM FOR: FULLY OPEN CHOKE, 75%, 50% AND 25% OPEN CHOKE

For other cases, e.g. gas lifted wells, diluent lifted wells, systems with jet pumps, networks with chokes or ESPs, etc. there is usually a specific setting that yields optimum operational conditions. Three cases are discussed next to exemplify these situations. Additionally, a long-term production optimization case is presented in section 5.2.3.

3.1.1. CASE 1: GAS-LIFTED WELLS

Figure 3-3 shows a well with a gas lift valve installed in it. The plot to the right shows: 1) pressures (at bottom-hole, located in the tubing directly in front of the discharge of the gas lift valve) required to flow against separator pressure for several well oil rates and 2) pressures obtained when the fluid flows from the reservoir to the same location for several well oil rates. The first curve is affected by the amount of gas injected while the second doesn't.

 When no gas is injected (i.e. the GOR is the formation GOR), the natural equilibrium oil rate is given by the intersection between the available (green) and required (magenta) pressure curves (please note that the bottom-hole pressure is plotted vs. oil rate). However, when gas is injected through the valve, the GOR of the tubing and pipeline changes, thus changing the required pressure curve and the intersection point.

When gas is injected in the tubing, the density of the flowing mixture is reduced thus yielding less gravitational pressure losses. However, the velocity of the mixture increases thus yielding more frictional pressure losses. When low amounts of gas are injected, the reduction of gravitational pressure losses is higher than the

increment of frictional pressure losses thus yielding a reduction of pressure in the tubing. However, when the amount of gas injected is higher, the frictional pressure losses are higher than the reduction of gravitational losses thus yielding an increase of pressure in the tubing. This change of trend is shown in Figure 3-4.
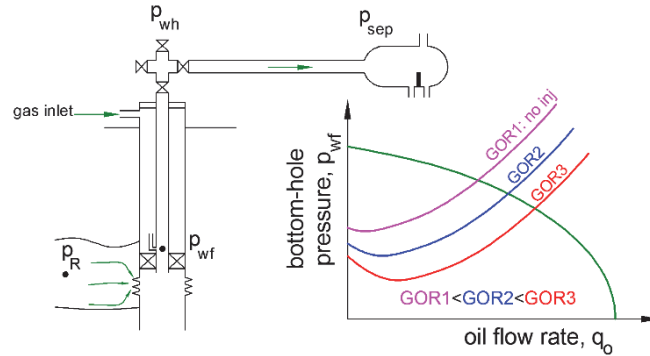
FIGURE 3-3. NATURAL EQUILIBRIUM POINT CALCULATED FOR WELL WITH NO GAS LIFT INJECTION AND WITH GAS INJECTION
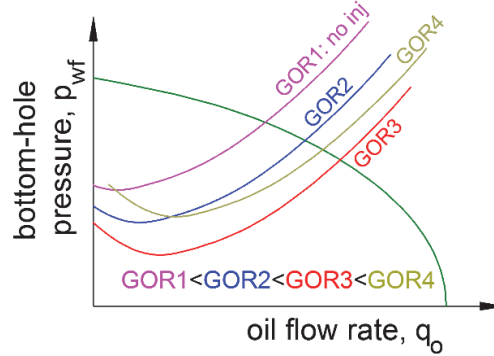
FIGURE 3-4. NATURAL EQUILIBRIUM POINTS CALCULATED FOR DIFFERENT AMOUNTS OF GAS LIFT INJECTED

The oil equilibrium rates for several gas lift rates are plotted in Figure 3-5. This concave curve is called gas-lift performance relationship. The maximum oil production is highlighted in red, where the derivative of reservoir oil production with respect to gas lift rate is equal to zero.
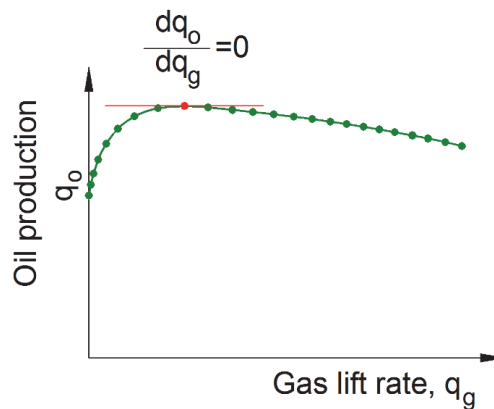
FIGURE 3-5. GAS-LIFT PERFORMANCE RELATIONSHIP

If maximum oil production is desired, the optimum gas injection rate is the x component of the red dot in Figure 3-5. However, there might be gas capacity constraints such as there is not enough gas capacity to deliver this rate. For a single well problem, the optimum gas lift rate can be easily found by plotting the gas lift performance curve and performing a visual inspection.

COMPLETION BITE: GAS-LIFT VALVE

Gas lift valves are deployed in a device called gas lift mandrel (as shown in Figure 3-6) that is threaded to the tubing. There are two main types of mandrels, retrievable and conventional.
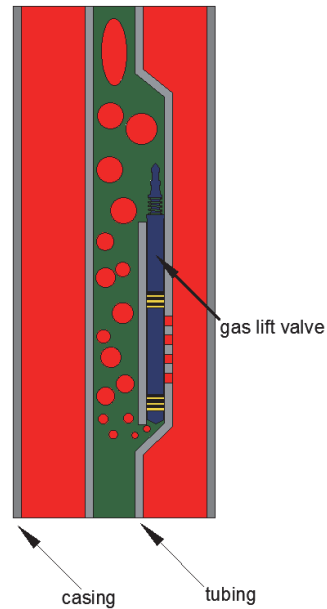
FIGURE 3-6. MANDREL TYPES USED TO DEPLOY GAS-LIFT VALVES

In the case a retrievable mandrel is used, gas-lift valves can be installed and retrieved at will using wireline or coiled tubing. The process to lock the gas-lift valve in the mandrel pocket is shown in Figure 3-7.
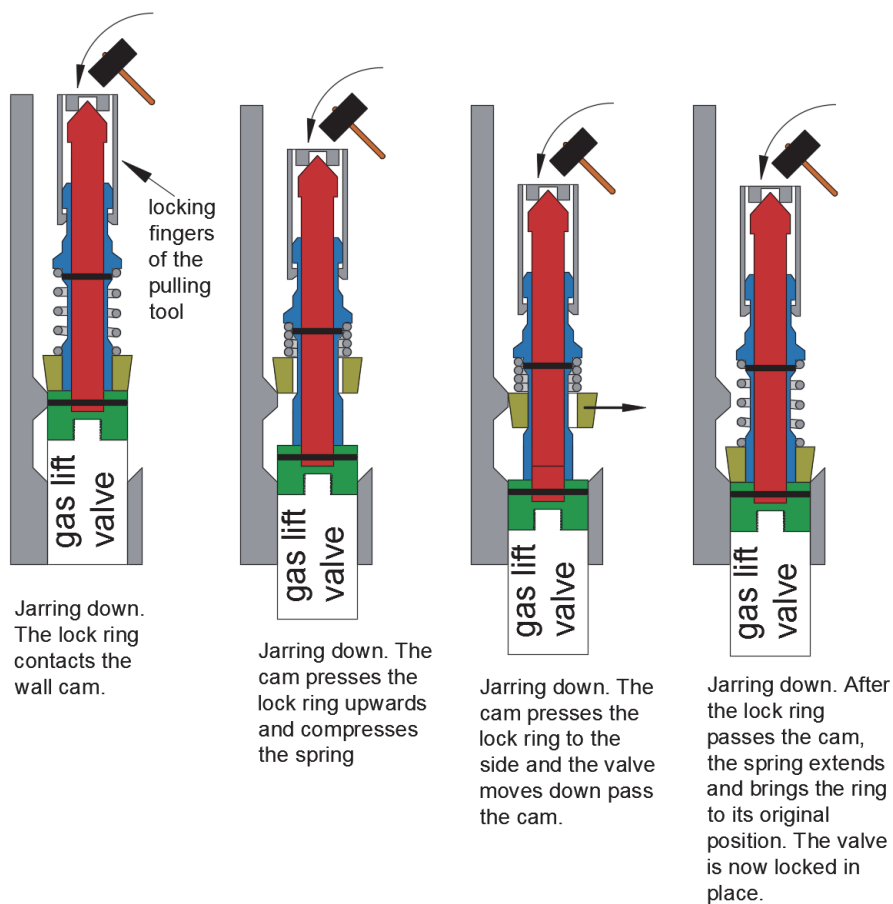
FIGURE 3-7. LOCKING PROCESS OF THE GAS LIFT VALVE IN THE MANDREL POCKET

The process to retrieve the gas-lift valve from the pocket is shown in Figure 3-8.
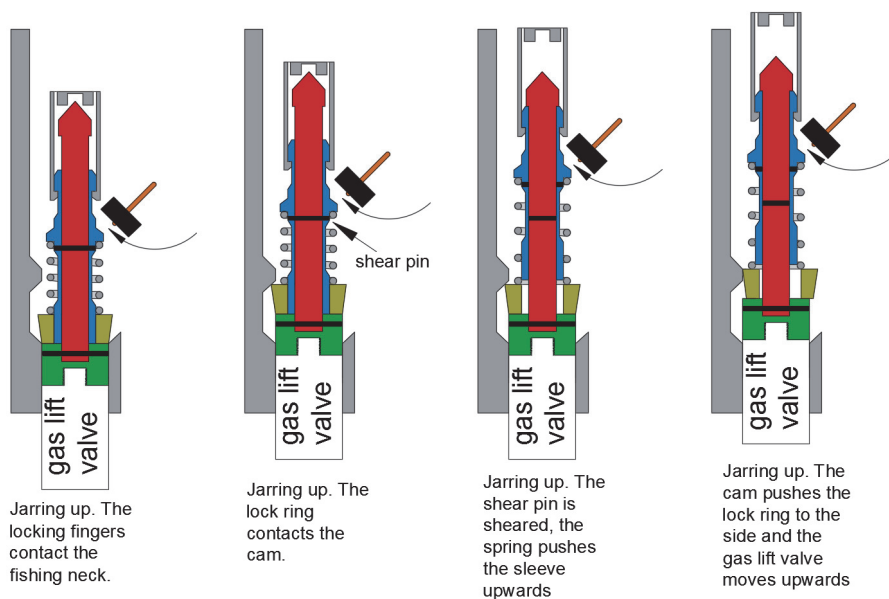
FIGURE 3-8. SEQUENCE TO RETRIEVE A GAS-LIFT VALVE FROM THE MANDREL POCKET

Consider two gas lifted wells that are producing to a production separator. Consider further that the two wells are independent from each other such that the reservoir oil production of each well is only a function of the well's gas injection rate $q_o = f(q_{g,inj})$. The behavior is approximated with the polynomial expression shown below:

$$q_o = f(q_{g,inj}) = a \cdot q_{g,inj}{}^4 + b \cdot q_{g,inj}{}^3 + c \cdot q_{g,inj}{}^2 + d \cdot q_{g,inj} + e$$

EQ. 3-1

The values of the coefficients for the two well are taken from Pavlov et al[3-5] and are shown in Table 3-1. The values of gas injection rate are input in 1E03 Sm^3/d and the oil rates are in Sm^3/d.

TABLE 3-1. POLYNOMIAL COEFFICIENTS

Coefficient	Well 1	Well 2
a [(Sm3/d)$^{-3}$]	-3.9E-7	-1.3E-7
b [(Sm3/d)$^{-2}$]	2.1E-4	1.0E-4
c [(Sm3/d)$^{-1}$]	-4.3E-2	-2.8E-2
d	3.7	3.1
e [Sm3/d]	12.0	-17.0

Figure 3-9 shows a color map of the total oil production for several combinations of gas-lift rates injected in wells 1 and 2 (axis x and y respectively). Contour lines are drawn at constant values of total oil rate. The maximum is achieved when one injects approximately 100 1E3 Sm3/d in both wells.
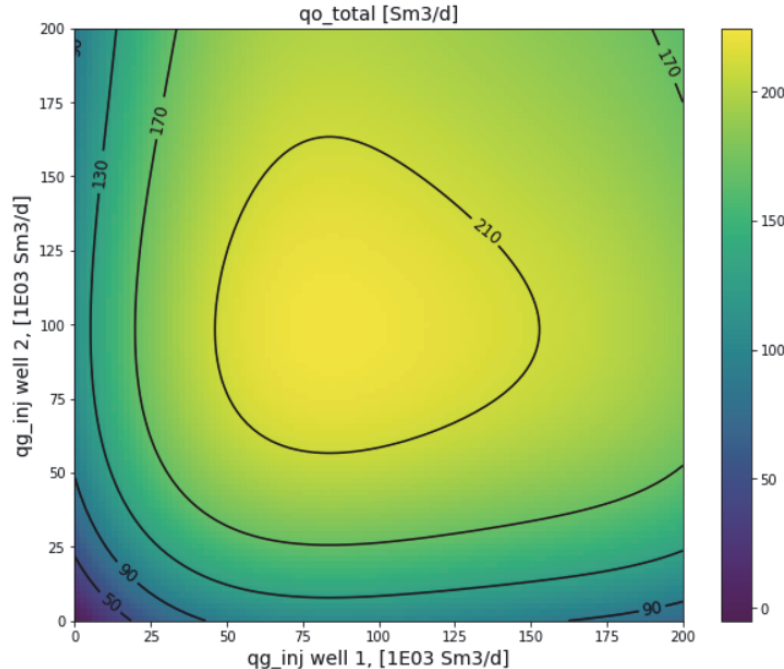
FIGURE 3-9. COLORMAP AND CONTOUR LINES OF TOTAL OIL PRODUCTION AS A FUNCTION OF LIFT-GAS INJECTED IN WELLS 1 AND 2

If there is a limitation in the total amount of gas available to inject, i.e. $q_{g,inj,1} + q_{g,inj,2} \leq q_{g,inj,total}$ this condition will reduce the feasible area of operation of Figure 3-9. Figure 3-10 shows lines (in red) of constant $q_{g,inj,total}$. The feasible area of operation will therefore be below the line. If the amount of gas available is

enough to reach the maximum point, then this is the best operating point. If the amount of gas is not enough, then, for this particular case, the best is when similar gas lift rates are injected in both wells.
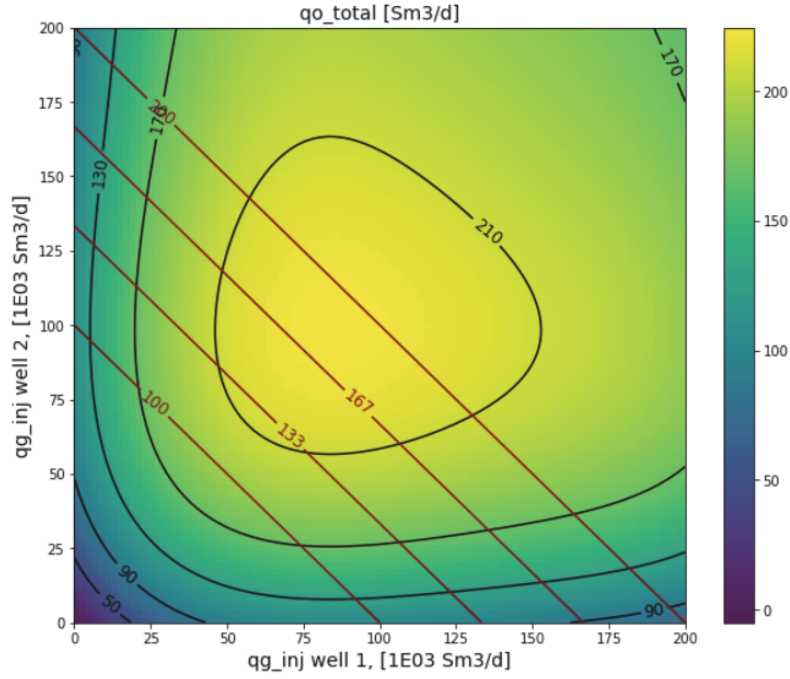
FIGURE 3-10. COLOR MAP AND CONTOUR LINES OF OIL PRODUCTION AS A FUNCTION OF LIFT-GAS INJECTED IN WELLS 1 AND 2. CONTOUR LINES OF TOTAL AVAILABLE GAS-LIFT RATE.

Mathematical procedure to find the optimal gas lift injection rate

The total oil production function (F) is the sum of the individual well oil production (f_i). The total number of wells is N.

$$F(q_{g,inj1}, q_{g,inj2}, q_{g,inj3}, \dots) = \sum_{i=1}^{N} f_i(q_{g,inji})$$

EQ. 3-2

F is a multivariate (N) additively separable scalar function. In order to include the limitation on injection gas available ($\sum q_{g,inj} \leq q_{g,inj\ TOT}$), the Lagrange function is created:

$$L(q_{g,inj1}, q_{g,inj2}, q_{g,inj3}, \dots) = \sum_{i=1}^{N} f_i(q_{g,inji}) - \lambda \cdot (\sum_{i=1}^{N} q_{g,inji} - q_{g,inj\ TOT})$$

EQ. 3-3

A necessary condition for this function to be maximum is that the elements of its gradient must be equal to zero (Eq. 3-4) and when the additional conditions (Eq. 3-5, Eq. 3-6, Eq. 3-7) are met:

$$\frac{\partial L(q_{g,inj1}, q_{g,inj2}, q_{g,inj3}, \dots)}{\partial q_{g,inji}} = \frac{\partial f_i(q_{g,inji})}{\partial q_{g,inji}} - \lambda = 0 \Rightarrow \frac{\partial f_i(q_{g,inji})}{\partial} = \lambda$$

EQ. 3-4

$$\lambda \cdot \left(\sum_{i=1}^{N} q_{g,inji} - q_{g,injTOT} \right) = 0$$

EQ. 3-5

$$\lambda \geq 0$$

EQ. 3-6

$$\sum_{i=1}^{N} q_{g,inji} < q_{g,injTOT}$$

<div align="right">EQ. 3-7</div>

There are two possible solutions:

Solution 1:	$\lambda = 0, \dfrac{\partial f_i(q_{g,inj})}{\partial q_{g,inj}} = 0$	All the wells are operating in their maximum. Valid only if there is enough gas available ($\sum q_{g,inj} \leq q_{g,inj\ TOT}$)
Solution 2:	$\lambda > 0, \dfrac{\partial f_i(q_{g,inj})}{\partial q_{g,inj}} = \lambda$	All wells are operating at the same gradient in the gas lift performance curve. Valid only if all the gas available is used ($\sum q_{g,inj}$ - $q_{g,inj\ TOT} = 0$)

Other cases of gas-lift optimization with different objective variables and constraints are presented in Appendix H.

3.1.2. CASE 2: TWO GAS WELLS EQUIPPED WITH WELLHEAD CHOKES

Consider the production system shown in Figure 3-11 with two dry gas wells with wellhead chokes. The production of the two wells is commingled and sent to a separator through a pipeline.
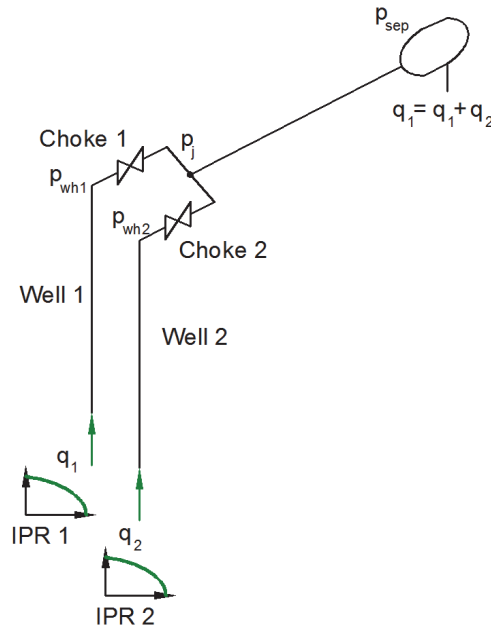
FIGURE 3-11. PRODUCTION SYSTEM WITH TWO DRY GAS WELLS

This production system has been discussed previously. The feasible operational region achievable by adjusting the wellhead chokes is shown in Figure 3-12.
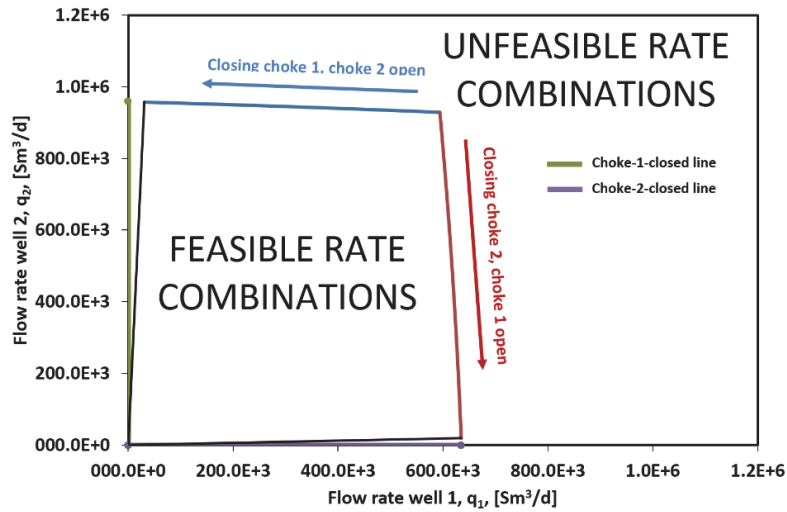
FIGURE 3-12. WELL FLOW RATE DOMAIN SOLUTION FOR THE PRODUCTION SYSTEM WITH 2 WELLS

It is of interest to evaluate if there is a particular choke opening combination that yields maximum total gas rate. As a first step, the objective function (total rate $q_T = q_1 + q_2$) is inspected visually by plotting it in a x,y,z plot (Figure 3-13) vs q_1 and q_2 for the flow rate ranges estimated in Figure 3-12 ($0 < q_1 < 6.5.10^5\ Sm^3/d$ and $0 < q_2 < 1.0.10^6\ Sm^3/d$). If the feasible operational region is not taken into account, the maximum will be located where there is an equal rate distribution between wells 1 and 2.
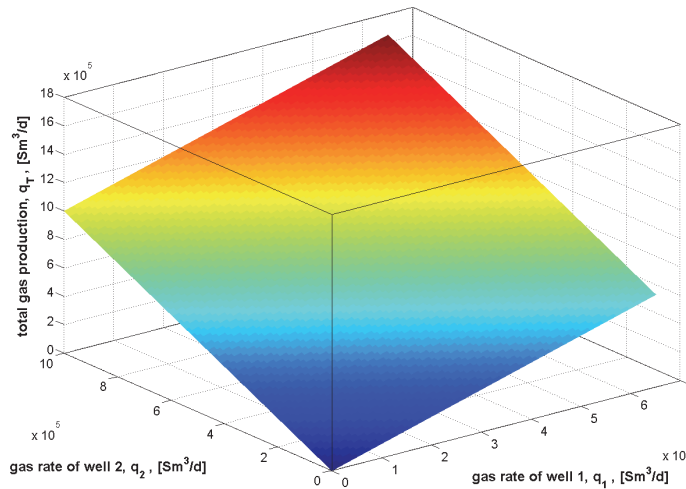
FIGURE 3-13. TOTAL GAS PRODUCTION AS A FUNCTION OF WELL 1 AND WELL 2 RATES

However, not all rate combinations plotted in Figure 3-13 are feasible. In fact there is only a limited operational region achievable by choking (presented in Figure 3-12). In Figure 3-14 the bounds that define the feasible region have been imposed in Figure 3-13. The maximum total gas flow rate is obtained when the two chokes are fully open.
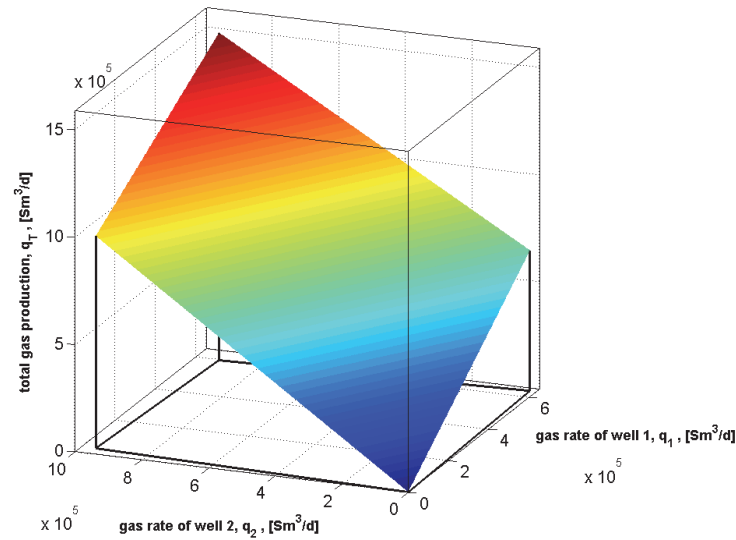
FIGURE 3-14. TOTAL GAS PRODUCTION PLOTTED ON THE FEASIBILITY REGION

Note that to obtain a maximum different from the open choke condition, the feasibility area has to be skewed considerably towards one of the wells. See as an example the modified feasible operational region shown in Figure 3-15 (where well 2 has a higher deliverability than well 1) and the resulting total gas flow rate function in Figure 3-16. Please note that the maximum occurs now when well 1 is almost completely choked and well 2 is fully open.
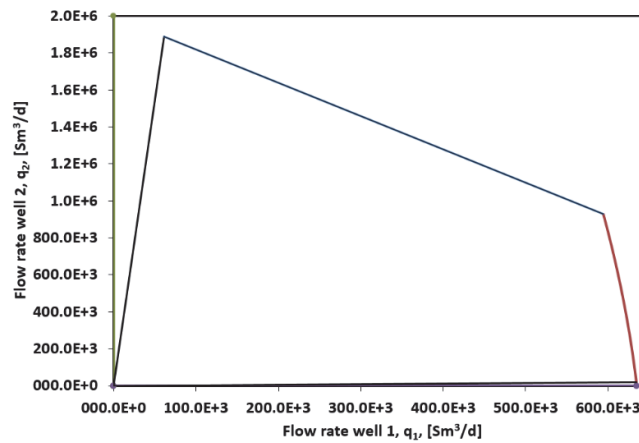
FIGURE 3-15. WELL FLOW RATE DOMAIN SOLUTION FOR THE PRODUCTION SYSTEM WITH 2 WELLS. WELL 2 HAS A HIGHER DELIVERABILITY THAN WELL 1
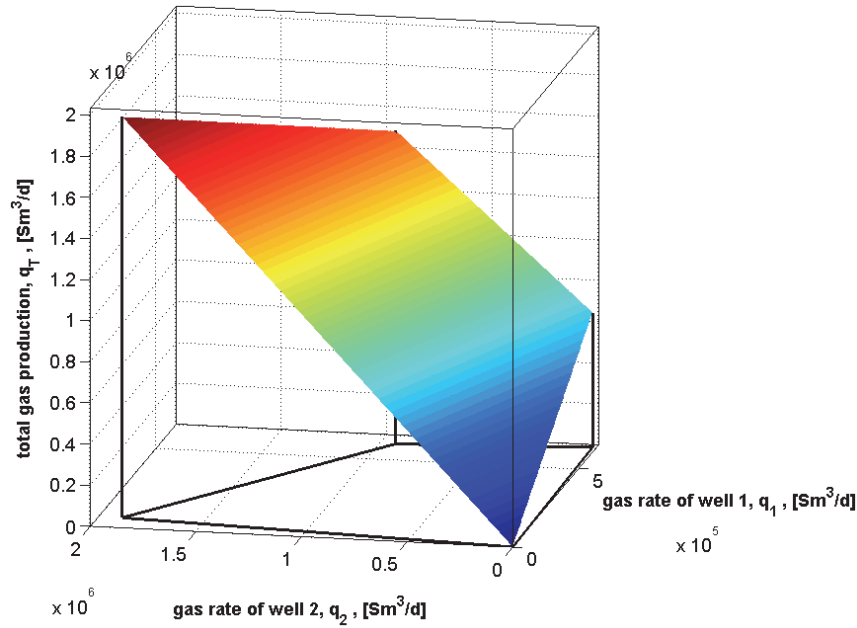
FIGURE 3-16. TOTAL GAS PRODUCTION PLOTTED ON THE FEASIBILITY REGION

Generally speaking, the shape of the bounds of the feasibility region define where the maximum will be located. In the simple case presented, two gas wells discharging to a common pipeline, the bounds are fairly linear, thus tending only to three possible solutions:

· Fully open the choke of the most productive well and close the other
· Open fully both chokes
· Maximum total rate is a plateau that can be achieved by leaving open the most productive well and choking (with any opening) the least productive well

The shape of the bounds of the feasibility region (linear, parabolic etc) depends on the characteristics of the production system and have to be calculated and taken into account for each specific case.

3.1.3. CASE 3: TWO ESP-LIFTED WELLS

Consider the network shown in Figure 3-17 with two ESP-lifted wells producing with different water cut (the full details of the system can be found in Stanko and Golan[3-6]). Well 1 has a producing water cut of 50% and well 2 has a producing water cut of 90%. The ESPs can be operated at frequencies between 30-60 Hz and it is required to find the optimum combination that yields maximum total oil production.
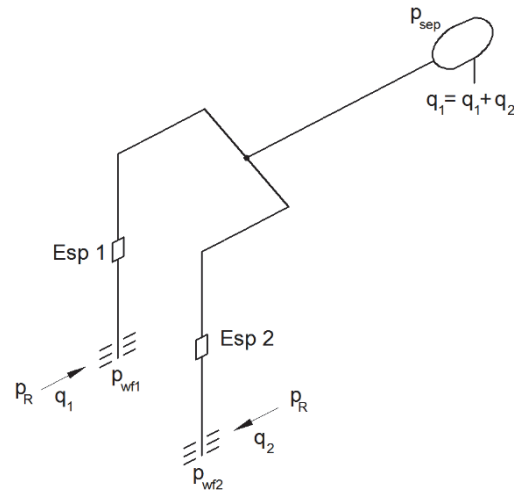
FIGURE 3-17. TWO ESP-LIFTED WELLS WITH COMMON WELLHEAD MANIFOLD DISCHARGING TO A PIPELINE

In order to find graphically the optimum ESP setting, multiple calculations of the hydraulic equilibrium of the system were made for different combinations of ESP frequency of wells 1 and 2. The results are shown in the color map of Figure 3-18. The color scale represents total oil production and the x and y axis represent the frequency of wells 1 and 2 respectively. It is possible to see that the frequency of ESP 1 has a higher impact in the total oil production. The best combination of ESP frequencies is $f_1 = 60\ Hz$ and $f_2 = 42\ Hz$.
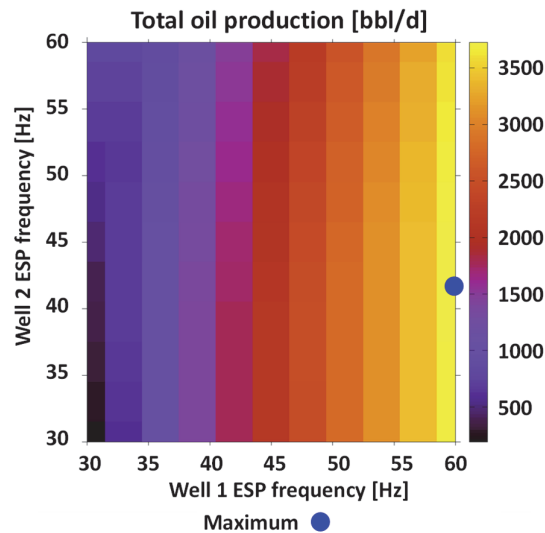
FIGURE 3-18. TOTAL OIL PRODUCTION COLOR MAP FOR THE COMPLETE ESP FREQUENCY RANGE OF WELLS 1 AND 2

Automatic search for optimal operating conditions of the production system

The search for optimum operational conditions of the production system is typically performed by using an optimization technique and not by brute-force inspection as presented in the cases earlier. The brute-force inspection is useful to understand the problem and the interdependence between objective function, variables and constraints, but in the general case (multi-variate) it is impossible to create such plots.

There are mainly two types of optimization: parametric (or static) optimization and dynamic optimization. In static optimization, the same techniques to maximize or minimize a mathematical function (e.g. f(x,y)) are applied but on the model of the production system. The model can be a long-term model (e.g. a reservoir model) or a short-term model (network and well).

In dynamic optimization, control techniques are used to optimize a model, the physical system or a combination of both. Most control techniques work on a time-step basis, i.e. sequentially reading variation of variables, computing new settings of adjustable variables and applying them on the system. For example, in an oil-gas separator with a level controller, the control loop reads the liquid level, and outputs the valve opening to apply on the liquid exit line. This logic can be applied in optimization, for example by driving the derivative of the objective with respect to the variable to zero in time.

Control techniques usually require a transient model. However, a steady state model can also be used, where the model is evaluated at each time step.

The optimization technique to employ depends on the optimization problem and the characteristics of the production system. The problems are commonly continuous (the variation of the adjustable element setting is usually continuous), constrained and non-linear (behavior of the objective function). Although there are also linear, integer problems.

Non-linear optimization methods are roughly classified in two groups: 1) gradient-based and 2) derivative free techniques.

Gradient-based, as its name indicates, are techniques that use gradient information to estimate a search direction and calculate the next operational conditions to evaluate. In this type of methods, it is timesaving to have available analytical expressions for gradients. Otherwise (when working with black-box models) gradients can be estimated numerically using finite differences, but it is usually inefficient for large systems because it requires multiple evaluations of the model on each iteration. An animation of a derivative-based method (Newton's method) is available here:

https://demonstrations.wolfram.com/MinimizingTheRosenbrockFunction/

Derivative-free techniques perform multiple evaluations on the model and use certain some logic to generate the next operational points to evaluate. The logic employed depends on depends on the method (examples are: evolutionary algorithms, pattern search, genetic algorithms, etc.) but it typically consists in using the best solutions found in one iteration to generate new operational points to test in the next iteration.

An animation of the Nelder-Mead method is available here:

https://www.optimization101.org/p/nlp7.html

An animation of a genetic algorithm is available here:

https://demonstrations.wolfram.com/GlobalMinimumOfASurface

And an animation of a pattern-search algorithm is available here:

https://en.wikipedia.org/wiki/Pattern_search_(optimization)

Linear problems use other family of methods like the Simplex algorithm. An animated example of a linear problem is given here:

https://www.optimization101.org/p/lp1.html

An animated example of the Simplex algorithm applied to the linear problem is:

https://www.optimization101.org/p/lp3.html

An animated example of the Simplex algorithm and the branch and Bound algorithm to solve a linear problem with integer variables is available here:

https://www.optimization101.org/p/ip3.html

Constraints can be included in the optimization by using Lagrange multipliers, barrier functions. Non-linear functions can be linearized by applying piece-wise linear interpolation (split the function in ranges and use a linear trend line for each range). However, to avoid using logical operators (if-like statement to check in which range a variable x is) that are often incompatible with optimization algorithms, additional variables are included, such as SOS2 (special ordered set of type 2).

Formulation of the optimization problem

An optimization formulation should contain the following elements:

- Objective
- Decision variables
- Constraints

There are usually two ways to "pose" optimization problems: one is to solve both optimization and modeling simultaneously and the other is to solve them sequentially. The first alternative is more suitable for models where there is access to the underlying equations and solving computational routines. In these cases, it is usually possible to use gradient-based methods that require estimations of the Hessian.

The second alternative is more suitable for black box models, where there is no access to the underlying equations and computational routines. In these models it is usually favorable to estimate gradients numerically by perturbing the model several times or to use heuristic optimization algorithm.

To exemplify the difference, consider the following case shown in Figure 3-19 with two ESP-lifted wells producing to a common pipeline and separator.
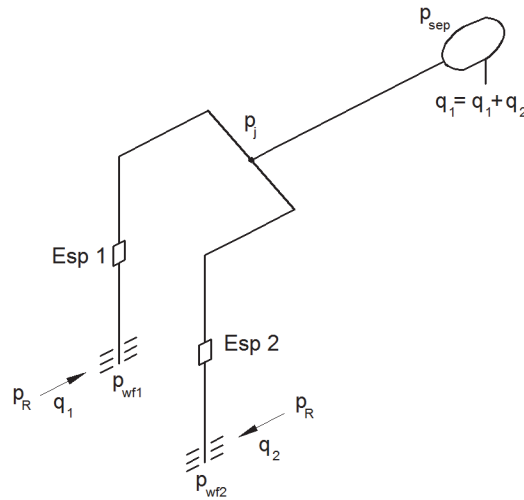
FIGURE 3-19. TWO ESP-LIFTED WELLS WITH COMMON WELLHEAD MANIFOLD DISCHARGING TO A PIPELINE.

One possible mathematical formulation to find the hydraulic equilibrium of the system is to solve the set of equations:

$$p_j = F_1(q_1, f_1)$$
$$p_j = F_2(q_2, f_2)$$
$$p_j = F_3(q_1, q_2)$$

EQ. 3-8

Or, equivalently, to minimize: EQ. 3-9

$$\varepsilon(q_1, f_1, q_2, f_2) = [F_1(q_1, f_1) - F_2(q_2, f_2)]^2 + [F_2(q_2, f_2) - F_3(q_1, q_2)]^2 = 0$$

Where:

q_1, q_2 Rates of wells 1 and 2, unknown variables @ standard conditions

p_i, p_j Junction pressure, unknown variable

F_1 Pressure drop function for well 1 representing the compound pressure change from reservoir, tubing, pump, tubing and flowline

$F_2,$ Pressure drop function for well 2 representing the compound pressure change from reservoir, tubing, pump, tubing and flowline

F_3 Pressure drop function for the pipeline, representing the pressure loss in the pipeline.

f_1, f_2 Rotational speed of ESP pumps 1 and 2 respectively.

For given frequencies of the ESP pumps, it is possible to solve the system of equations (e.g. using a Newton method) and find the equilibrium rates q_1 and q_2.

Let's say now that one wishes to find out ESP frequencies for wells 1 and 2 that maximize the separator rate $q_1 + q_2$, subject to the constraint that f_1, f_2 must be within the operational range of (30-70 Hz).

If one employs the first method described above to solve this problem, then one must use two sequential loops:
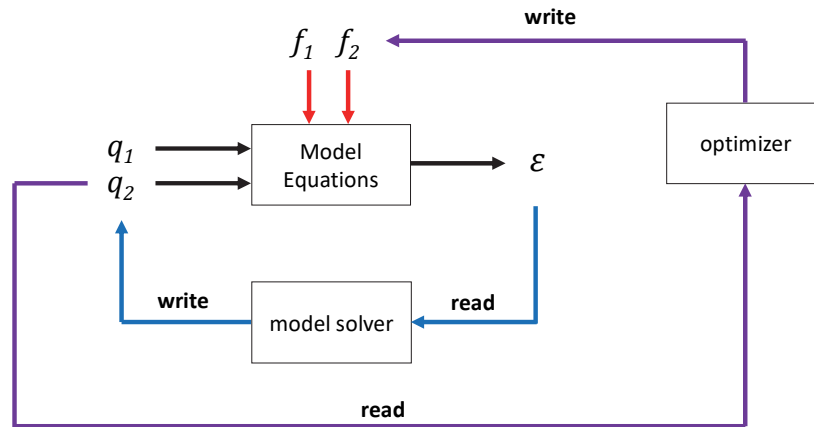
FIGURE 3-20. TWO ESP-LIFTED WELLS WITH COMMON WELLHEAD MANIFOLD DISCHARGING TO A PIPELINE.

Where, in each iteration of the optimization loop, it is necessary to solve the model once, or several times.

If one employs the second method described above to solve this problem, then a way to formulate the optimization problem is the following:

Maximize: $q_1 + q_2$

By changing: f_1, f_2, q_1, q_2

Subjected to the constraints: $[F_1(q_1, f_1) - F_2(q_2, f_2)]^2 + [F_2(q_2, f_2) - F_3(q_1, q_2)]^2 = 0$

$$30\ Hz \leq f_1, f_2 \leq 70\ Hz$$

Note that solving the hydraulic equilibrium of the network has been added as a constraint. This means that any optimal solution found has to be a feasible operating condition in the numerical model of the network.

This strategy is used often when optimizing production networks. This optimization problem can be solved with any suitable method, e.g. a gradient-based method.

Differences in the formulation

The complexity of the optimization problem can sometimes depend on the decision variables chosen. For example, and using the case presented earlier of two ESP lifted wells in a network, an optimization formulation of optimizer and model together which provides a non-linear formulation is:

Maximize: $q_1 + q_2$

By changing: f_1, f_2, q_1, q_2

Subjected to the constraints: $[F_1(q_1, f_1) - F_2(q_2, f_2)]^2 + [F_2(q_2, f_2) - F_3(q_1, q_2)]^2 = 0$

$$30\ Hz \le f_1, f_2 \le 70\ Hz$$

The problem is non-linear, because functions F_1, F_2, F_3. are non-linear.

However, by using the model, it is possible to compute the feasible operational rate region of the system, by running all combinations of pump frequencies f_1, f_2. Consider the results are similar to the one shown in Figure 3-21.
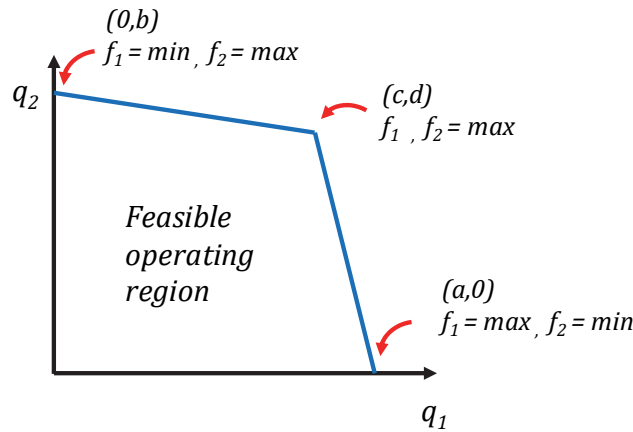
FIGURE 3-21. FEASIBLE OPERATING REGION OF A SYSTEM WITH TWO ESP-LIFTED WELLS WITH COMMON WELLHEAD MANIFOLD DISCHARGING TO A PIPELINE.

Therefore, if the values of a,b,c and d are known a priori and if the boundaries are linear, the original non-linear optimization problem can be re-formulated as a linear optimization problem by:

Maximize: $q_1 + q_2$

By changing: q_1, q_2

Subjected to the constraints:
$$q_2 \le b - \frac{b-d}{c} q_1$$

$$q_1 \le a + \frac{a-c}{d} q_2$$

By performing a priori model evaluations, it is possible to remove the non-linearity.

3.2.   Issues hindering the industrial scale adoption of model-based production optimization

The industry has been somewhat slow in accepting, adopting and implementing model-bases optimization solutions. This can be partly attributed to the following reasons:

3.2.1.   Foreign from the field's reality

Before embarking on a model-based production optimization project It is always relevant to ask the question: is optimization really necessary for this particular case? To execute production optimization entails extensive use of human, computational resources and time so it is always best to be 100% sure that it is strictly necessary for the particular case.

Also, is it actually possible to change the decision settings? Is the equipment or actuator functional and available? Am I allowed to operate the control element? Is the actuator response time compatible with the optimization workflow?

When formulating the optimization problem, it is crucial to deeply understand (as much as possible) the underlying physical system. Furthermore, to identify the most important variables, objectives and constraints and to avoid overcomplicating the problem. This might be sometimes difficult to distill properly during communications between engineers partly due to lack of understanding of the underlying issues. The lack of subsequent communication between the optimization engineer and the field operator worsens further the problem.

3.2.2.   Models uncertainty

The uncertainty associated with the numerical models is usually high and there is limited confidence on their results (this is especially applicable to the case of reservoir models). This raises doubts about the applicability of the optimum operational controls found and creates resistance and skepticism on the side of operators. It is always good practice to vary the system parameters (e.g. with a probabilistic sampling method) and quantify the effect it has on the optimum solution.

3.2.3.   Non-sustainability of the proposed solutions

Some factors that contribute to the lack of sustainability of the solutions are:

- Lack of expertise on the industry side to understand the basics of the solution provided by consultants or vendors.
- Ease of use. Not understanding the solution added to difficulties using it often lead to abandoning it.
- The usage of self-programmed surrogate models that are not easily scalable and maintained. Many engineers often prefer commercial software where their maintenance, upgrade and troubleshooting are delegated to a third-party company.
- Lack of ownership by the industrial partner.

In the area of production optimization, sometimes it is very difficult to develop general solutions and platforms that are suitable for the majority of field cases encountered. That is why field engineers should always understand to a great degree the optimization solutions provided by external consultants and vendors.

REFERENCES

[3-1] Alarcon, G. A., Torres, C. F. & Gomez, L. E. (2002). Global optimization of gas allocation to a group of wells in artificial lift using nonlinear constrained programming. *Journal of Energy Resources Technology* 124 (4).

[3-2] Khan Academy (2018) *Lagrange Multipliers, examples*. Article retrieved from: https://www.khanacademy.org/math/multivariable-calculus/applications-of-multivariable-derivatives/constrained-optimization/a/lagrange-multipliers-examples.

[3-3] Barros, E.G.D., Van den Hof, P.M.J., Jansen, J.D. (2015). Value of Information in Closed-Loop Reservoir Management. *Computational Geosciences* 20 (3).

[3-4] *Simplex Optimization method*. Article retrieved from: http://www.chem.uoa.gr/applets/AppletSimplex/Appl_Simplex2.html

[3-5] Pavlov, A., Haring, M., Fjalestad, K. (2017). *Practical extremum-seeking control for gas lifted oil production*. 2017 IEEE 56th Annual Conference on Decision and Control.

[3-6] Stanko, M., Golan, M. (2015). *Exploring the Potential of Model-Based Optimization in Oil Production Gathering Networks with ESP-Produced High Water Cut wells.* 2Presented at the 17th International Conference on Multiphase Production Technology, Cannes, France, 10-12 June, BHR-2015-J2.

4.   FLUID BEHAVIOR TREATMENT IN OIL AND GAS PRODUCTION SYSTEMS

There are two main methodologies to characterize and quantify fluid behavior: Black oil and compositional. In the Black Oil (BO) approach three phases are considered: oil (liquid phase), gas (gaseous phase) and water (liquid phase) and a set of variables are employed to relate the volumetric amounts of the phases at standard conditions with the volumetric amounts at any pressure and temperature condition. The compositional approach employs an equation of state (EOS) and the molar composition to estimate fluid properties (determining numerically the number of phases and calculating their properties).

The BO model can be regarded as a subset of the compositional model where only two components are used: oil and gas (in most cases water can be treated independently assuming that it does not partition in oil or gas).

The BO approach is still the preferred choice of engineers in the petroleum industry because it is more "practical" (involves tangible amounts measured in the field) and it is faster than performing time consuming EOS calculations.

In the past, BO properties were generated from correlations developed for particular fluids and applied to other cases by using tuning parameters (e.g. typical approach used in commercial software for analysis of production systems). Nowadays, the generalized procedure is to develop an EOS to characterize oil and gas fluid behavior and then generate BO properties using this EOS. The BO parameters are pre-computed and stored in tables that can later be used as needed by engineers (e.g. in simulators).

The typical workflow to characterize a reservoir fluid is roughly as follows:

- **Sampling:** a representative sample of the producing fluid is taken. This can be done in three typical locations in the production system:
  - Formation/Well bottom-hole (oil and gas).
  - Test Separator (oil and gas separately). They are later recombined depending on the individual rates.
  - Wellhead
- **Determine fluid composition:** e.g. using gas chromatography.
- **Perform laboratory tests**
  - CCE Constant composition expansion
  - DLE differential liberation experiment
  - CVD Constant volume depletion
  - MSF Multistage separator experiment
- **Develop a PVT model**. Development of a physically consistent EOS that represents all the laboratory tests considering the uncertainties associated to each test and the uncertainties in compositions, and particularly the properties and amounts of heavy components. Pseudo-components are typically employed to represent groups of heavy components (e.g. C7 and above). The properties of such pseudo-components are adjusted such that they represent properly the original composition.

4.1.   THE BLACK OIL MODEL

To simplify the discussion and the introduction of concepts, an initial assumption will be made that **the overall composition of the fluid stream under study is constant**. This is generally not true because in a production system there is mixing of streams with different compositions, the amounts of oil and gas produced by the wells change in time due to depletion, gas conning, injection, etc. On a later section, once the basic concepts are discussed, the consideration is removed.

This chapter does not discuss the presence of water (e.g. gas solubility in water) or the definition and estimation of its BO properties. Please refer to Chapter 9 of Whitson[4-1] for details on the topic.

The BO model is based on the situation when oil and gas at local p and T conditions are brought **separately** to standard conditions by passing them through the surface process (P) existing in the field (Figure 4-1).
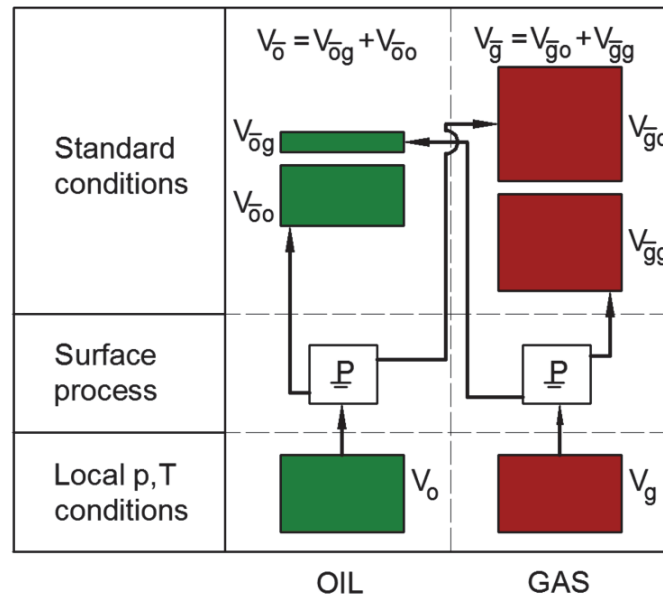
FIGURE 4-1. SCHEMATIC REPRESENTATION OF THE FLASHING OF OIL AND GAS AT LOCAL CONDITIONS TO STANDARD CONDITIONS

Where the subscripts are:

$\bar{g}$	surface gas component
$\bar{o}$	surface oil component
g	gas phase @ (p,T)
o	oil phase @ (p,T)

Surface oil ($V_{\bar{o}}$) will be generated from gas phase ($V_{\bar{o}g}$) and from oil phase ($V_{\bar{o}o}$) and surface gas ($V_{\bar{g}}$) will be generated from gas phase ($V_{\bar{g}g}$) and from oil phase ($V_{\bar{g}o}$). Four BO parameters, p and T dependent, are then defined to relate these 4 quantities with the local oil (V_o) and gas (V_g) volume and are summarized in Table 4-1. These BO parameters are not strict thermodynamic properties, as their values depend on the reference standard conditions employed (in SPE for instance it is 60°F and 1 atm), the surface process and the composition.

TABLE 4-1. BO PARAMETERS

BO Variable	Definition
Oil Volume Factor	$B_o(p,T) = \dfrac{V_o(p,T)}{V_{\bar{o}o}}$
Gas Volume Factor	$B_g(p,T) = \dfrac{V_g(p,T)}{V_{\bar{g}g}}$
Solution Gas Oil Ratio	$R_s(p,T) = \dfrac{V_{\bar{g}o}}{V_{\bar{o}o}}$
Solution Oil Gas ratio	$r_s(p,T) = \dfrac{V_{\bar{o}g}}{V_{\bar{g}g}}$

These parameters constitute what is known as the "modified" BO formulation. The traditional BO formulation does not include the Solution Oil Gas Ratio r_s (often called r_v). This parameter is important when dealing with volatile oils and gas condensate fluids.

There are other BO properties that are often recorded at p, T such as oil viscosity (μ_o), gas viscosity (μ_g), oil-gas interfacial tension (σ_{og}). These parameters are often required to perform numerical pressure and temperature drop calculations in reservoir and production systems.

Note that when the fluid is taken to standard conditions through a specific surface process it will always give the same GOR and the same oil and gas specific gravities at standard conditions (γ_o and γ_g) despite the local p and T conditions. This is the reason why the GOR, γ_g and γ_o are often used to characterize a given fluid.

For certain local p, T conditions, there might be only one phase in equilibrium (oil or gas). In that case, the BO properties of the non-existing phase are undefined.

Black oil parameters are usually computed using PVT software with a composition, an EOS (properly tuned to lab data), and the surface process existing on the field (usually described as a series of separators). The workflow is presented in Figure 4-2 and is roughly as follows:

- Take an arbitrary number of moles of the seed composition (z_i) to p and T conditions and separate the oil and gas and store the values of local volumes. The oil will have a composition x_i and the gas a composition y_i.
- Take the oil and gas separately through the surface process. At the output gather surface oil and all surface gas and register the standard conditions volumes.
- Compute BO parameters for the combination of p and T.
- Repeat for several combinations of p and T.
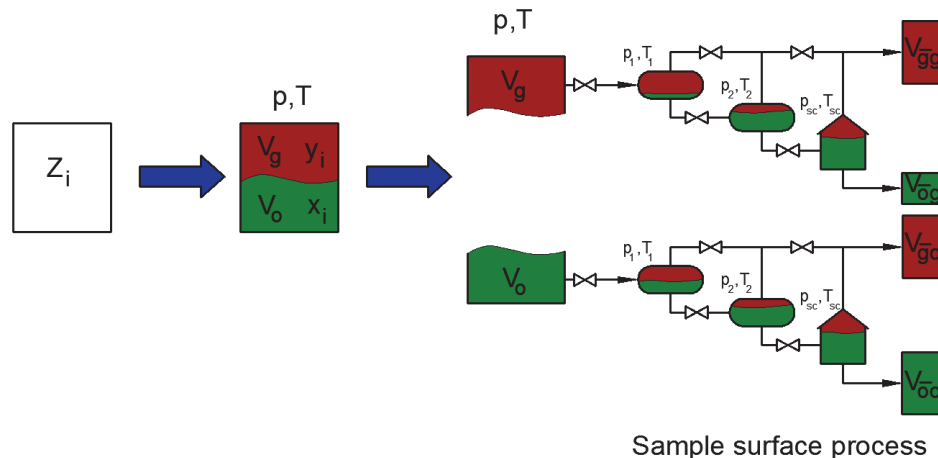
FIGURE 4-2. SCHEMATIC OF THE PROCESS TO GENERATE BO PROPERTIES

The higher and lower limits for p and T depend on what the BO properties are going to be used for. For simulations of the reservoir and production system, BO properties have to be generated for the highest and lowest pressure and temperature expected. However, these values might be unknown a priori as they are usually a result of the calculations or numerical models that use the BO properties.

It is not failsafe to generate BO properties just between the initial reservoir pressure and temperature and the first stage separator pressure and temperature. For example, when compression or pumping exists on the field, pressure and temperature might reach values above reservoir pressure (e.g. at the compressor or pump discharge) or below separator pressure (e.g. at the compressor or pump suction).

If the pressure of interest p for which it is desired to generate BO properties is within the range of the pressure values of the surface process, usually all separators (or equipment) that operate above the pressure p are neglected in the surface process.

BO parameters are usually stored in a set of tables, where each one contains the variation with pressure for a fixed temperature. Reservoir or production simulators perform linear (or bilinear) interpolation in these tables to obtain BO properties at specific p and T conditions.

Figure 4-3 presents a sketch of the variation of the BO properties versus pressure for a fixed temperature (e.g. Reservoir) of the hydrocarbon mixture shown in Figure 4-4. At the given temperature, single phase oil will be formed for pressures equal or greater than the bubble point pressure.
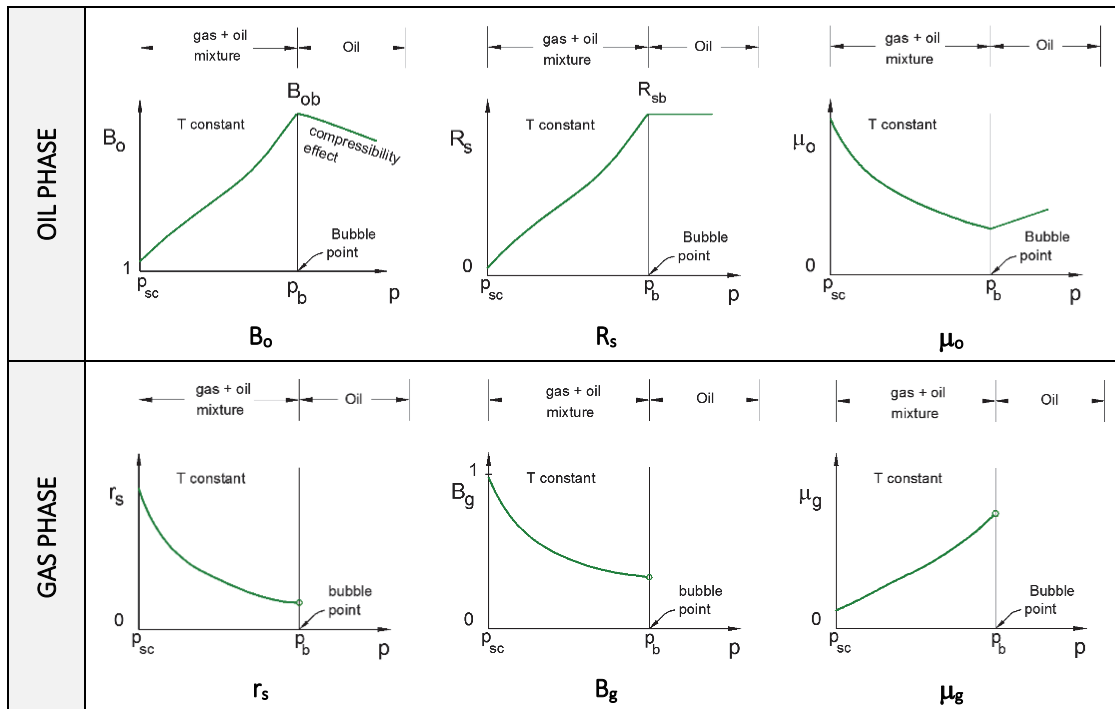
FIGURE 4-3. BEHAVIOR OF BO PARAMETERS VS. PRESSURE FOR A FIXED TEMPERATURE
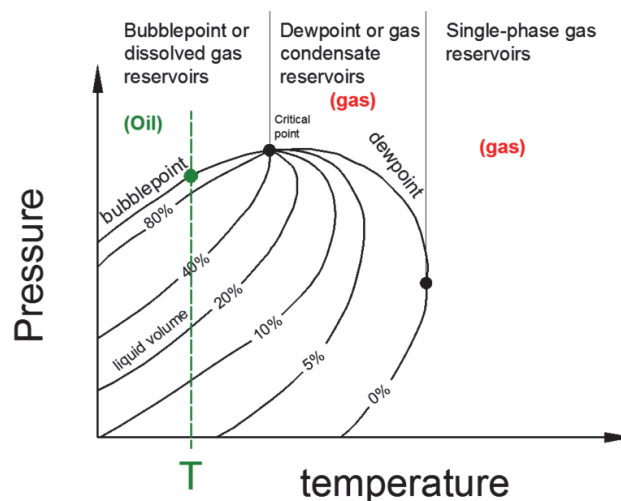
FIGURE 4-4. PHASE DIAGRAM OF THE HYDROCARBON MIXTURE USED IN FIGURE 4-3

For almost all parameters, there is a change of trend in the curve when the fluid changes from a mixture to single phase oil. The solution gas-oil ratio (R_s) remains constant as there is no more free gas in the system to go into the oil. The value of the oil volume factor (B_o) diminishes with pressure above the bubble point due to the liquid compressibility. The BO properties of the gas (r_s, B_g and μ_g) become undefined for pressures at and higher than the bubble point pressure, due to the fact that there is no gas phase at those pressure conditions.

Figure 4-5 presents a sketch of the variation of the BO properties of versus pressure for a fixed temperature of the hydrocarbon mixture shown in Figure 4-6. The temperature is greater than the temperature shown used in Figure 4-5 such as gas will be formed at pressures equal or greater than the dew point pressure.
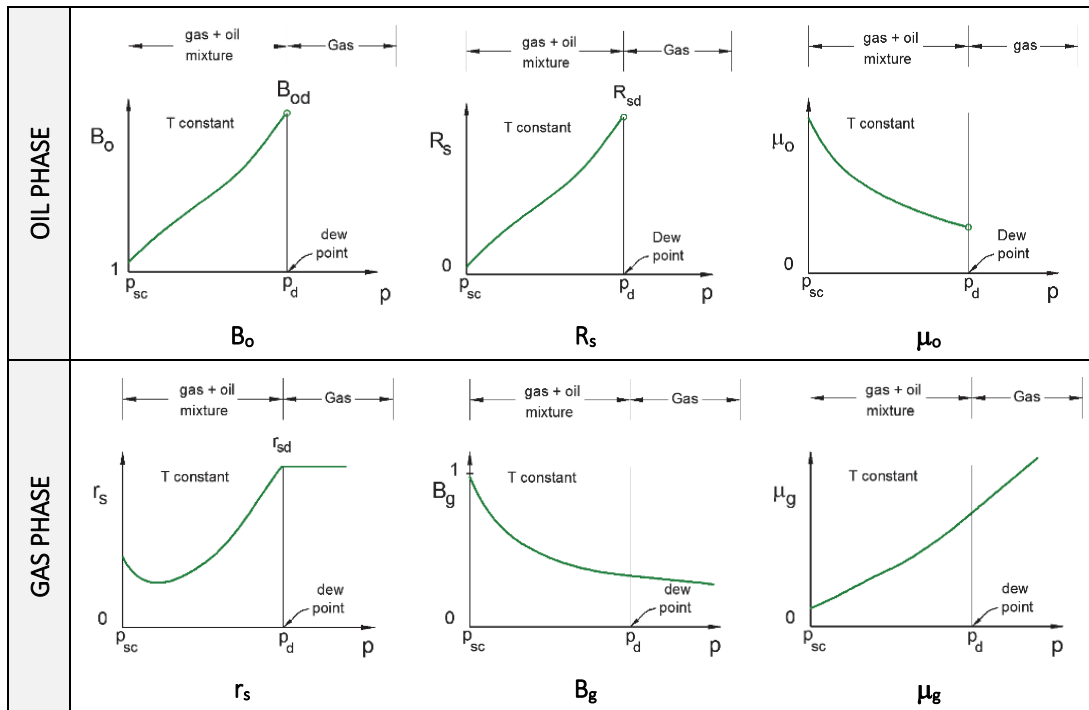
FIGURE 4-5. BEHAVIOR OF BO PARAMETERS VS. PRESSURE FOR A FIXED TEMPERATURE
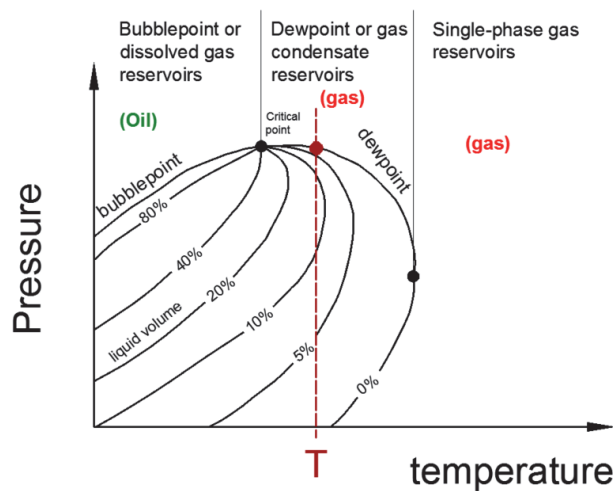
FIGURE 4-6. PHASE DIAGRAM OF THE HYDROCARBON MIXTURE USED IN FIGURE 4-5

When the fluid changes from a mixture to single phase gas the solution oil-gas ratio (r_s) remains constant as there is no more free oil in the system to go into the gas. The BO properties of the oil (R_s and B_o) become

undefined for pressures at and higher than the dew point pressure, due to the fact that there are no volumes of oil at those pressure conditions.

4.2.   VARIATION OF BO PROPERTIES WITH TEMPERATURE

For engineering analysis of production systems, it is important to capture the variation of BO properties with both pressure and temperature. The variation of the solution gas-oil ratio (R_s) with pressure is presented in Figure 4-7 for three temperatures. The phase envelope of the fluid is presented in Figure 4-8.
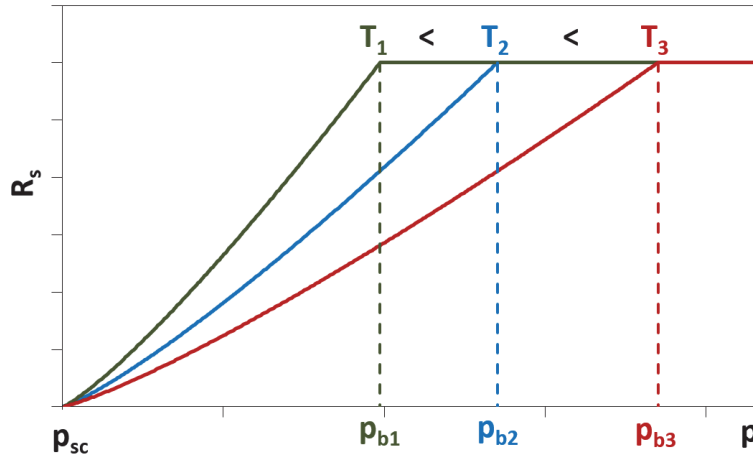
FIGURE 4-7. SOLUTION GAS OIL BEHAVIOR WITH PRESSURE FOR THREE TEMPERATURES
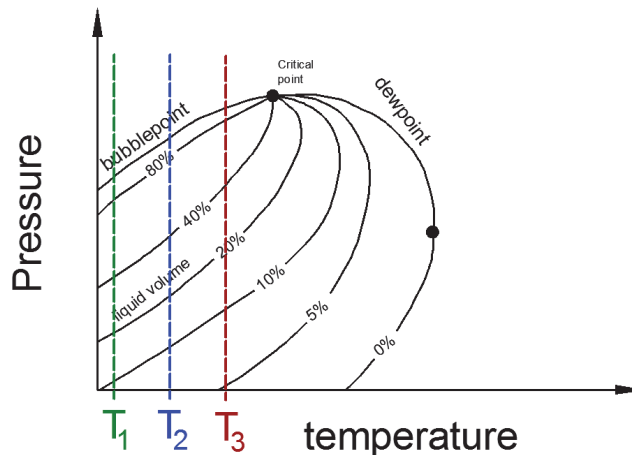
FIGURE 4-8. PHASE DIAGRAM OF THE HYDROCARBON MIXTURE USED IN FIGURE 4-7

When the temperature increases, the bubble point pressure also increases, however the value of the solution gas-oil ratio at the bubble point is the same for all temperatures. This is due to the fact that, once the local conditions correspond to single phase oil, it does not matter what temperature does it have, it will always liberate the same amount of gas when brought to standard conditions.

At a given pressure, the solution gas-oil ratio will be higher for a low temperature compared with a high temperature.

The variation of the Oil volume factor (B_o) and Gas volume factor (B_g) with pressure are presented in Figure 4-9 and Figure 4-10 for three temperatures. Remember that, when the bubble point pressure is reached, there is no more free gas, therefore, B_g is undefined.

140
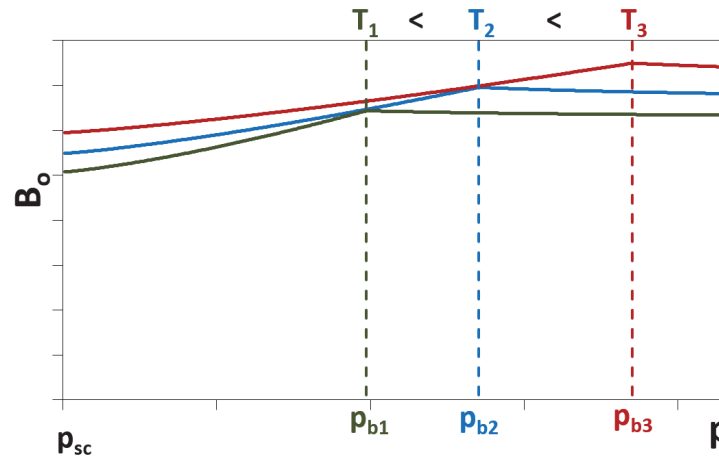
FIGURE 4-9. OIL VOLUME FACTOR BEHAVIOR WITH PRESSURE FOR THREE TEMPERATURES
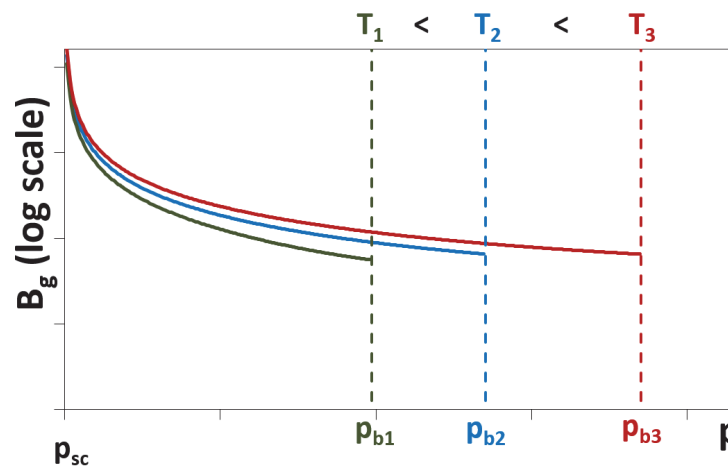
FIGURE 4-10. GAS VOLUME FACTOR BEHAVIOR WITH PRESSURE FOR THREE TEMPERATURES

The variation of the solution oil-gas ratio (r_s) with pressure is presented in Figure 4-11 for three temperatures. The phase envelope of the fluid is presented in Figure 4-12.

For the particular case shown, the dew point pressure decreases with temperature however the value of the Solution oil-gas ratio at the dew point is the same for all temperatures. This is due to the fact that, once the local conditions correspond to single phase gas, it does not matter what temperature does it have, it will always liberate the same amount of oil when brought to standard conditions.

At a given pressure, the solution oil-gas ratio will be higher for a high temperature compared with a low temperature.
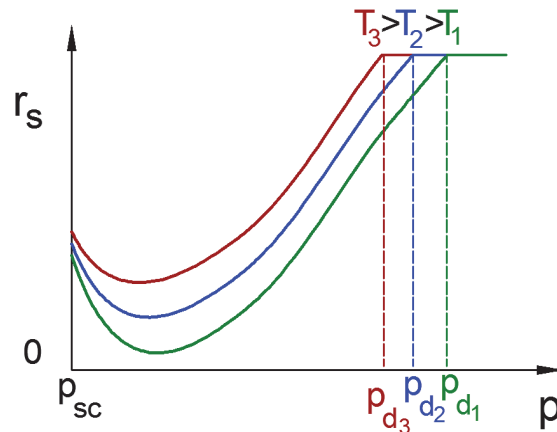
FIGURE 4-11. SOLUTION OIL-GAS RATIO WITH PRESSURE FOR THREE TEMPERATURES
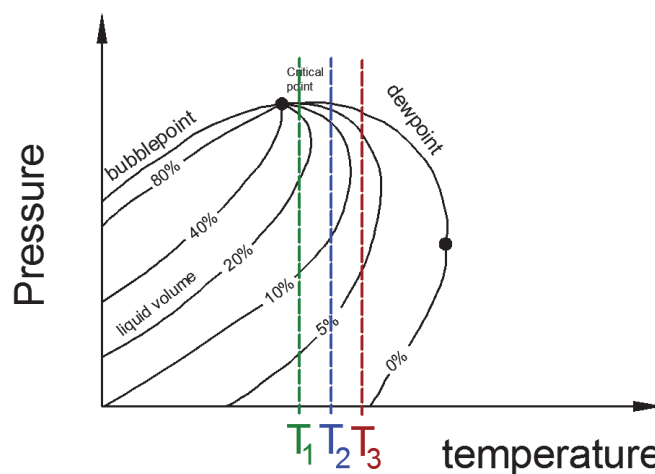
FIGURE 4-12. PHASE DIAGRAM OF THE HYDROCARBON MIXTURE USED IN FIGURE 4-12

4.3.   VARIATION OF BO PROPERTIES WITH COMPOSITION

When a fluid of certain composition is taken to standard conditions through a specific surface process it produces a unique value of gas-oil ratio (GOR) and unique values of oil and gas specific gravities at standard conditions (γ_g and γ_o). Therefore, a change in GOR is always a safe indicator of changes in the composition.

Note that the GOR of the stream is always equal to the saturation R_s of the mixture, or to the saturation $1/r_s$ (depending if the temperature of study is below the critical temperature of the mixture or above, as the cases shown in Figure 4-4 and Figure 4-6).

In the development done in the previous sections the molar composition of the fluid was kept constant when generating BO properties (this composition typically comes from well samples). However, this is seldom the case as in a production system there is mixing of streams with different compositions, the well producing GOR (or the GOR in each cell of the reservoir model) typically changes in time due to depletion, gas conning, gas injection, etc.

Changes in GOR will affect black oil properties. An example of this is shown in Figure 4-13[27].

---

[27] Here the new compositions for each GOR have been generated using compositions of separator gas and oil and the procedure highlighted in section 4.6.
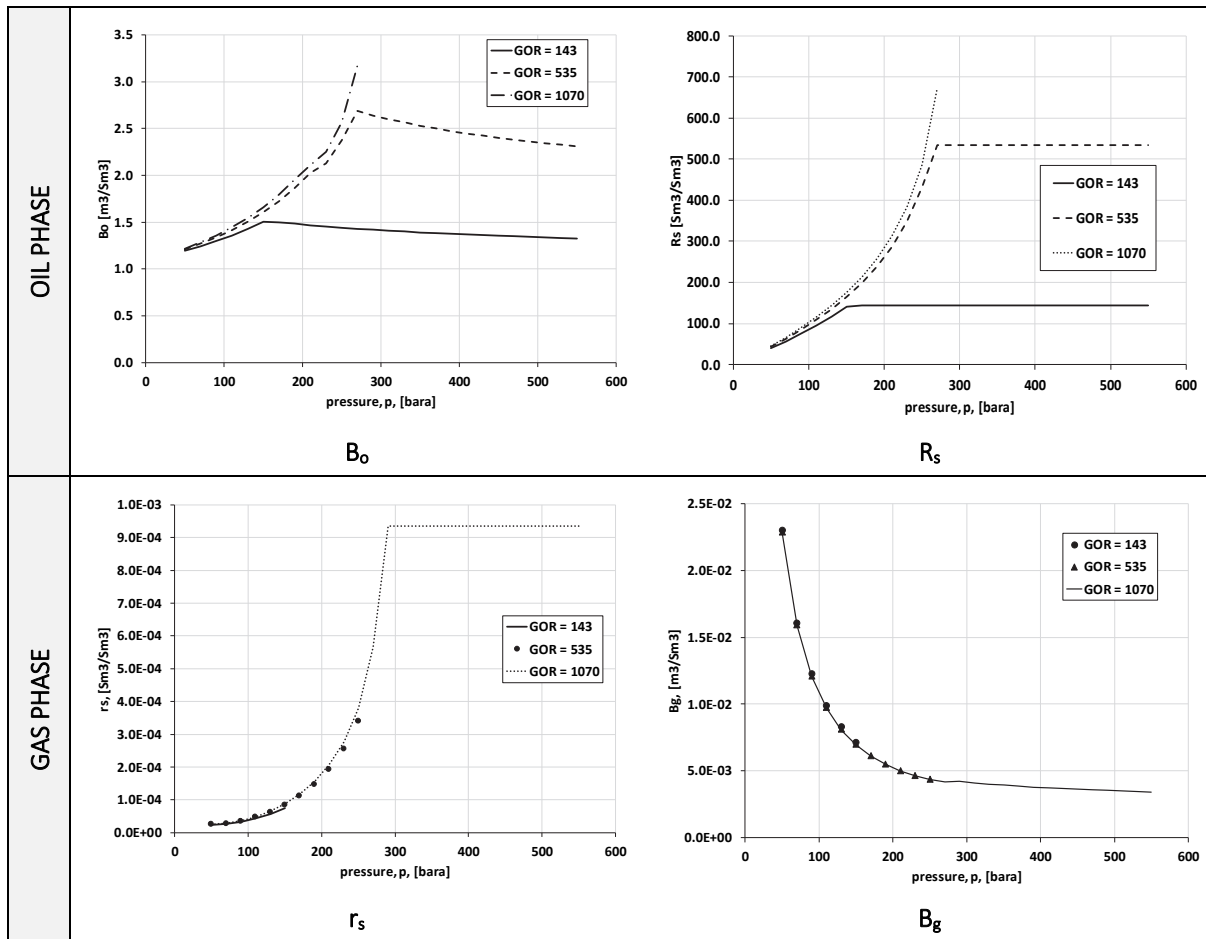
FIGURE 4-13. BLACK OIL PROPERTIES ESTIMATED FOR DIFFERENT COMPOSITIONS (GOR). NOTE THAT FOR GOR=1070, THE FLUID IS NOT ANYMORE AN OIL BUT A GAS IN UNDERSATURATED CONDITIONS.

In situations where a variation of GOR is expected, one must generate black oil tables as a function of GOR, in addition to pressure and temperature. A tri-linear interpolation is used to find black oil properties for a given GOR, p and T.

Saturation pressure (bubble point pressure and dew point pressure) are sometimes used instead of GOR.

When a GOR and p and T conditions are provided to estimate BO properties, the first analysis to perform is to determine if the fluid is in saturated or undersaturated conditions. A robust approach to do this is to precompute, at constant temperature, for a large range of GORs (i.e. compositions), the bubble point pressure (or dew point pressure) and the bubble point R_{sb} (or the dew point r_{sd}, depending if at the given temperature the undersaturated fluid is gas or oil). The R_{sb} and $1/r_{sd}$ are plotted vs p_b and p_d (Figure 4-14).
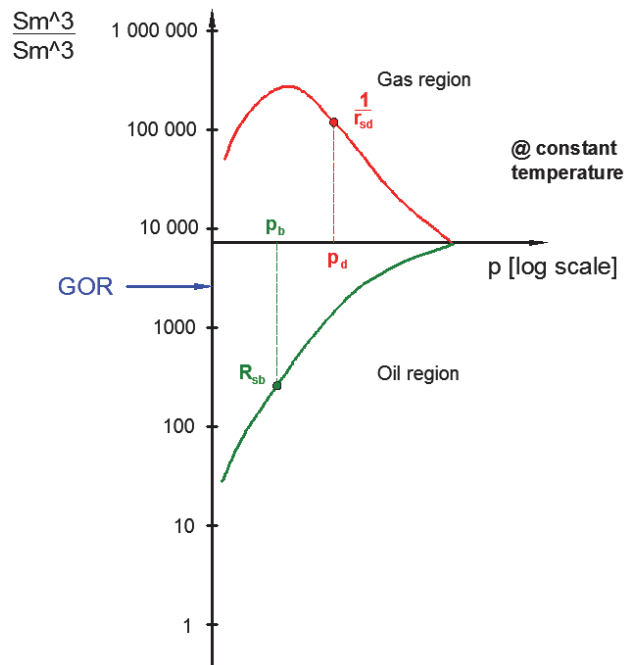
FIGURE 4-14. R_s AND $1/r_s$ VS p COMPUTED FOR SEVERAL GORS AT CONSTANT TEMPERATURE

With the given GOR one can enter on the y axis (arrow in blue in Figure 4-14) and identify if the undersaturated fluid is gas or oil and read on the x axis the p_b or p_d. If the given pressure is less than the saturation pressure, then the fluid is in saturated conditions and saturated properties have to be used. If the pressure is greater than the saturation pressure, then the fluid is in undersaturated conditions, and undersaturated properties should be used with the given GOR.

In general, for the following cases:

·   The reservoir is undergoing gas injection
·   The reservoir is undergoing gas recycling
·   The production system commingles production of pay-zones with different compositions
·   The reservoir has compositional heterogeneities (e.g. with depth or region)

It is usually necessary either to use a compositional model or to separate the reservoir or production system in sections with constant composition and build a BO table for each composition. If an analysis requires mixing or commingling fluids from different compositions then an equivalent black oil table has to be developed depending on the mixing ratio or a compositional approach should be used.

However, when the fluid stream is a combination of gas and oil from reservoir oil, **or** gas and oil from reservoir gas, **it might still be possible to use a common black oil table** for all resulting compositions (albeit with some modifications).

Consider as an example an oil well as the one shown in Figure 4-15. The well will produce more and more gas with depletion as the pressure diminishes around the well bore and the gas mobility increases (an expression to compute the producing GOR is provided in Appendix G). Figure 4-16 shows how the phase envelope of the well stream changes as the GOR increases.
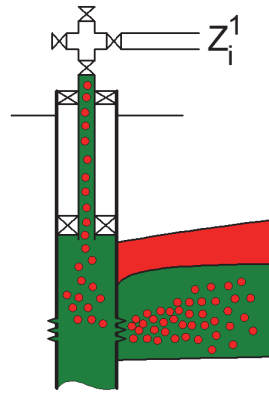
FIGURE 4-15. OIL WELL
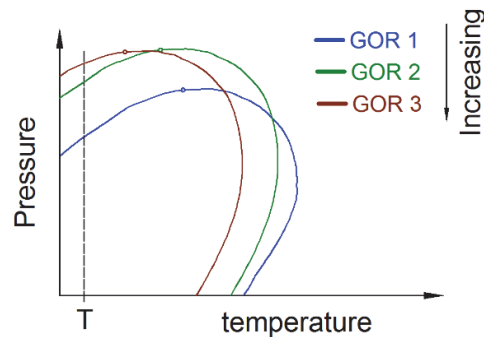
FIGURE 4-16. VARIATION OF THE PHASE ENVELOPE WITH CHANGES IN COMPOSITION (GOR)

In this case it could be possible to use a unique black oil table for the complete life of the well.

The original composition has an initial R_{si} (or r_{si}, depending on the type of fluid) that is equal to the GOR. The GOR can change in two possible ways:

- The new GOR (GOR$_2$) is lower than the initial GOR (GOR$_1$). In this case, one can expand the original fluid composition to the saturation pressure that gives R_s = GOR$_{new}$ (black arrow shown in Figure 4-17) and use this composition for the generation of new black oil properties:
  - o For pressures below this saturation pressure (region marked with the letter "S" in Figure 4-17), the saturated BO properties of this composition will be identical to those found with the original fluid composition, therefore, it is not necessary to estimate them.
  - o For pressures above this saturation pressure (region marked with the letter "U" in Figure 4-17), the undersaturated properties will be different from those of the original composition and must be computed.
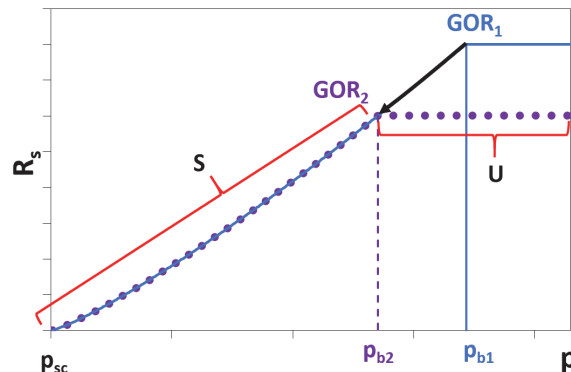
FIGURE 4-17. R_s VARIATION WITH COMPOSITION WHEN THE NEW GOR IS LOWER THAN THE ORIGINAL GOR

- The new GOR (GOR_2) is higher than the initial GOR (GOR_1). In this case one must estimate a new composition for this new GOR to estimate black oil properties. One approach that can be used to do this is to:
  - Extract the composition of the incipient gas at the saturation pressure of the original composition
  - Add this incipient gas to the original composition until the saturation pressure of the resulting mixture is equal to the critical pressure of the resulting mixture

The saturated black oil properties for GOR values higher than the original mixture GOR are found by expanding the new mixture between its saturation pressure (critical pressure) and the saturation pressure of the original mixture. The saturated black oil properties for GOR values below the GOR of the original mixture will be equal to those of the original mixture and it is not necessary to estimate them.

Figure 4-18 shows the R_s behavior versus pressure plotted for the composition of the well at an early time "1" and a later time "2" with higher GOR. The saturated R_s values (for $p < p_{b1}$) are the same for both times, but the saturation R_s, (GOR) has changed.
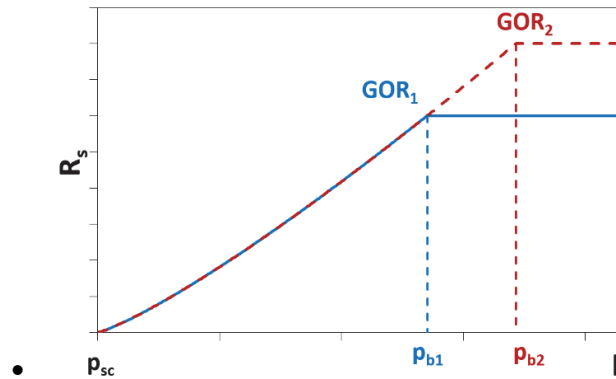
FIGURE 4-18. R_s VARIATION WITH COMPOSITION WHEN THE NEW GOR IS HIGHER THAN THE ORIGINAL GOR

The undersaturated properties for GOR values between the GOR value of the original and the new mixture are found by expanding the new mixture to a saturation pressure that gives the desired GOR value, and then using the resulting composition of the saturation oil and gas to compute undersaturated black oil properties.

A note when using BO correlations

If BO properties are generated using BO correlations, the behavior of properties estimated at other GORs will be as discussed above.

A comment on BO tables

BO tables (e.g. those used in reservoir simulators) usually have two parts. One provides values of BO properties in the saturation region (continuous lines in Figure 4-19) and one that provides BO property values for the undersaturated region at multiple GORs.
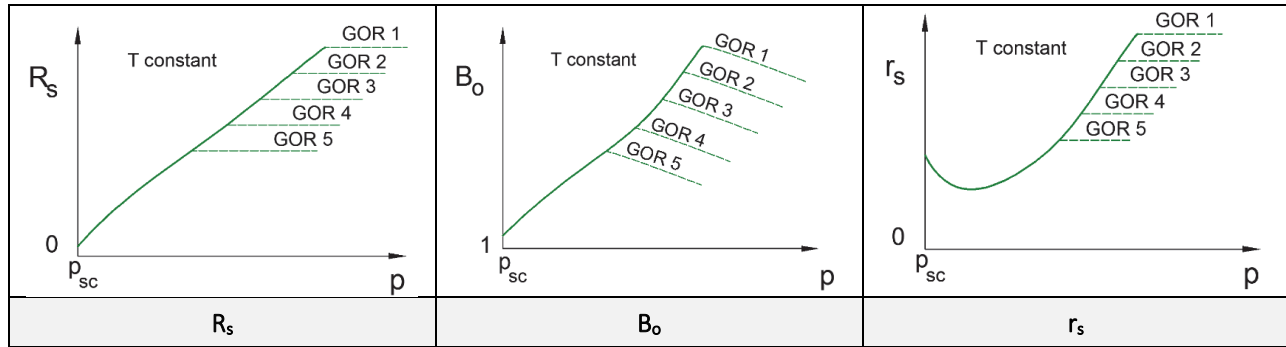
FIGURE 4-19. VARIATION OF MAIN BO PARAMETERS WITH COMPOSITION WHEN MORE GAS FLOWS INTO THE WELLBORE

4.4.   BO CORRELATIONS

There are many correlations for BO parameters of the oil phase developed for particular fields, fluids and regions. Typically, these correlations are accurate only if the fluid of interest and pressure and temperature conditions are similar to those for which the correlations were developed. As an example, Table 4-1 shows some expressions for p_b, R_S, B_o, B_g and r_s.

TABLE 4-2. SELECTED CORRELATIONS FOR BO PARAMETERS

PROPERTY	CORRELATION	AUTHOR
Bubble pressure	$p_b = 1.995 \cdot \left(\dfrac{R_S}{\gamma_g}\right)^{0.83} \cdot 10^{0.001643 \cdot T - 0.0125 \cdot \gamma_{API}} - 1.7566$	Standing (1977)[4-2]
Gas-in-oil ratio	$R_s = 0.571 \cdot \gamma_g \cdot 10^{0.0151 \cdot \gamma_{API} - 0.00198 \cdot T} \cdot (0.797 \cdot p + 1.4)^{1.205}$	Standing (1977)[4-2]
Oil formation factor	$B_o = 0.9759 + 0.000952 \cdot \left[\left(\dfrac{\gamma_g}{\gamma_o}\right)^{0.5} \cdot R_s + 0.401 \cdot T - 103\right]^{1.2}$	Standing (1977)[4-2]
Gas formation factor	$B_g = 0.00351 \cdot \dfrac{T \cdot Z}{p}$	Definition
Oil-in-gas ratio	$r_s = 1.25 \cdot 10^{-6} \cdot R_S^* \cdot (0.08 + 4 \cdot 10^{-7} \cdot p^{2.5})$	Whitson (1994)[4-3]

Where

p	Fluid pressure [bara]
R_S	Gas solubility [Sm³/Sm³]
R_S^*	Gas solubility @ 345 bara [Sm³/Sm³]
T	Fluid temperature [K]
Z	Generalized compressibility factor [-]
γ_{API}	API gravity [-]
γ_o	Stock tank oil gravity [-]

As in the case of the BO tables, the given expressions for R_S, B_o, B_g and r_s describe the behavior of the undersaturated region. The first step is then, with the given GOR, calculate the saturation pressure (e.g. bubble pressure) at the given temperature. If the pressure of interest is below the saturation pressure, the correlations are used as shown. Otherwise, an expression for undersaturated BO properties has to be used.

As mentioned earlier, tuning parameters can be introduced in the BO correlations to match test or field data. This is usually done (in commercial software) by introducing two constants:

$$value^c \cdot A + B = value^m$$

<div align="right">EQ. 4-1</div>

Where:

A	Tuning multiplier
B	Tuning shifting
$value^c$	Calculated property (using correlation)
$value^m$	Measured property

These parameters A and B are changed by an optimization engine to minimize the difference between the test or field data and the correlation output.

4.5.   BO PROPERTIES IN PRODUCTION CALCULATIONS

The most typical use of BO properties in production system calculations is to convert from standard conditions rates to local rates and vice-versa. The local rates are used for pressure drop calculations, flow assurance analysis, among others. Figure 4-20 presents the relationship between standard conditions rates and local conditions rates and vice versa using a BO transformation matrix. These expressions assume that water is not soluble in oil nor gas.

$$\begin{bmatrix} q_{\bar{g}} \\ q_{\bar{o}} \\ q_{\bar{w}} \end{bmatrix} = \begin{bmatrix} \dfrac{1}{B_g} & \dfrac{R_s}{B_o} & 0 \\ \dfrac{r_s}{B_g} & \dfrac{1}{B_o} & 0 \\ 0 & 0 & \dfrac{1}{B_w} \end{bmatrix}_{(p,T)} \cdot \begin{bmatrix} q_g \\ q_o \\ q_w \end{bmatrix}$$	$$\begin{bmatrix} q_g \\ q_o \\ q_w \end{bmatrix} = \begin{bmatrix} \dfrac{B_g}{1 - R_s \cdot r_s} & \dfrac{-R_s \cdot B_g}{1 - R_s \cdot r_s} & 0 \\ \dfrac{-B_o.r_s}{1 - R_s \cdot r_s} & \dfrac{B_o}{1 - R_s \cdot r_s} & 0 \\ 0 & 0 & B_w \end{bmatrix}_{(p,T)} \cdot \begin{bmatrix} q_{\bar{g}} \\ q_{\bar{o}} \\ q_{\bar{w}} \end{bmatrix}$$
Standard conditions calculated from local conditions	Local conditions calculated from standard conditions

FIGURE 4-20. TRANSFORMATION MATRIXES TO TAKE STANDARD CONDITIONS RATES TO LOCAL CONDITIONS AND VICE VERSA

A similar relationship can be developed between the local and surface condition densities (Figure 4-21).

$$\begin{bmatrix} \rho_{\bar{g}} \\ \rho_{\bar{o}} \\ \rho_{\bar{w}} \end{bmatrix} = \begin{bmatrix} \dfrac{B_g}{1 - R_s \cdot r_s} & \dfrac{-r_s \cdot B_g}{1 - R_s \cdot r_s} & 0 \\ \dfrac{-R_s.B_g}{1 - R_s \cdot r_s} & \dfrac{B_o}{1 - R_s \cdot r_s} & 0 \\ 0 & 0 & B_w \end{bmatrix}_{(p,T)} \cdot \begin{bmatrix} \rho_g \\ \rho_o \\ \rho_w \end{bmatrix}$$	$$\begin{bmatrix} \rho_g \\ \rho_o \\ \rho_w \end{bmatrix} = \begin{bmatrix} \dfrac{1}{B_g} & \dfrac{r_s}{B_o} & 0 \\ \dfrac{R_s}{B_o} & \dfrac{1}{B_o} & 0 \\ 0 & 0 & \dfrac{1}{B_w} \end{bmatrix}_{(p,T)} \cdot \begin{bmatrix} \rho_{\bar{g}} \\ \rho_{\bar{o}} \\ \rho_{\bar{w}} \end{bmatrix}$$
Standard conditions calculated from local conditions	Local conditions calculated from standard conditions

FIGURE 4-21. TRANSFORMATION MATRIXES TO TAKE STANDARD CONDITIONS DENSITIES TO LOCAL CONDITIONS AND VICE VERSA

This expression assumes that:

· The density of the surface oil coming from local oil ($\rho_{\bar{o}o}$) is the same as the surface oil coming from local gas ($\rho_{\bar{o}g}$) and

· The density of surface gas coming from local gas ($\rho_{\bar{g}g}$) is the same as surface gas coming from local oil ($\rho_{\bar{g}o}$).

Application example of BO properties: Separation of oil and gas

Consider an stream with standard condition rates of gas ($q_{\bar{g}}$) and oil ($q_{\bar{o}}$), entering a gravity separator as indicated in Figure 4-22.
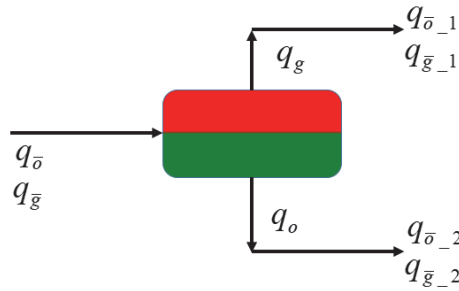
FIGURE 4-22. Sketch depicting a 2 phase (oil and gas) gravity separator with inlet and outlet streams

To find the volumetric rates of oil and gas separated (assuming the separator is 100% efficient, i.e. all free gas and free oil will be separated), the black oil properties are used (Figure 4-20):

$$q_o = \frac{-B_o \cdot r_s}{1-R_s \cdot r_s} \cdot q_{\bar{g}} + \frac{B_o}{1-R_s \cdot r_s} \cdot q_{\bar{o}}$$

$$q_g = \frac{B_g}{1-R_s \cdot r_s} \cdot q_{\bar{g}} - \frac{B_g \cdot R_s}{1-R_s \cdot r_s} \cdot q_{\bar{o}}$$

EQ. 4-2

The standard conditions rates of the gas outlet are then calculated by:

$$q_{\bar{g}\_1} = \frac{1}{B_g} \cdot q_g = \frac{1}{1-R_s \cdot r_s} \cdot q_{\bar{g}} - \frac{R_s}{1-R_s \cdot r_s} \cdot q_{\bar{o}}$$

$$q_{\bar{o}\_1} = \frac{r_s}{B_g} \cdot q_g = \frac{r_s}{1-R_s \cdot r_s} \cdot q_{\bar{g}} - \frac{r_s \cdot R_s}{1-R_s \cdot r_s} \cdot q_{\bar{o}}$$

EQ. 4-3

And the standard condition rates of oil and gas for the oil outlet are calculated by:

$$q_{\bar{g}\_2} = \frac{R_s}{B_o} \cdot q_o = \frac{-r_s \cdot R_s}{1-R_s \cdot r_s} \cdot q_{\bar{g}} + \frac{R_s}{1-R_s \cdot r_s} \cdot q_{\bar{o}}$$

$$q_{\bar{o}\_2} = \frac{1}{B_o} \cdot q_o = \frac{-r_s}{1-R_s \cdot r_s} \cdot q_{\bar{g}} + \frac{1}{1-R_s \cdot r_s} \cdot q_{\bar{o}}$$

EQ. 4-4

If r_s = 0 then the expressions become:

$$q_{\bar{g}\_1} = q_{\bar{g}} - R_s \cdot q_{\bar{o}}$$

$$q_{\bar{o}\_1} = 0$$

$$q_{\bar{g}\_2} = R_s \cdot q_{\bar{o}}$$

$$q_{\bar{o}\_2} = q_{\bar{o}}$$

EQ. 4-5

4.6.   ESTIMATION OF A NEW COMPOSITION WHEN THE WELL GOR CHANGES

In some occasions, it is desirable to estimate the well or stream composition given a producing GOR, for example when the producing GOR of the well changes in time and no sampling has been performed or when reservoir simulations are not available. The new composition can usually determine by recombining some "source" oil and gas at different proportions (as shown in Figure 4-23, using the β multiplier). This setup can be modeled in any PVT calculator and the parameter beta varied until a match is obtained with the new GOR.
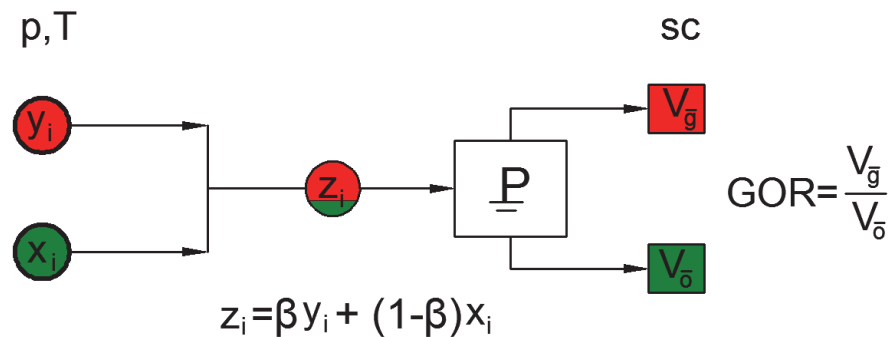
FIGURE 4-23. RECOMBINATION OF SOURCE GAS AND OIL TO YIELD STREAM COMPOSITION

There are two methods generally accepted to obtain source compositions of oil and gas: 1) separator oil and gas generated after passing a measured composition through the surface process use and 2) Using the last known measured composition, take it from the reservoir depletion state when it was measured to the current reservoir depletion state. This should be performed using the process with approximates the best the actual process that undergoes in the reservoir (e.g. CVD, CCE).

Note that on some occasions the GOR is measured by means of a test separator thus the surface process to employ must be different than the surface process used during normal production.

4.7.   WATER-RELATED PROPERTIES

In some cases, it is necessary to account for the content of water in gas and gas in water. (e.g. condensation of water in natural gas production systems or liberation of gas in water-dominated flow). Two factors are typically employed for this purpose: r_{sw} (p,T) that provides the water content in gas when the gas is fully saturated with water at a given pressure and temperature, and R_{sw}, that provides the gas content in water when the water is fully saturated with gas at a given pressure and temperature.

Despite often being expressed as a ratio of standard conditions volumes, r_{sw} and R_{sw} are **not calculated** considering the surface process or by taking the saturated mixture of gas and water to standard conditions. They are calculated by first computing the mole fraction of water in the gas and water mixture (or gas in the

water and gas mixture) and then converting the mole fraction to a volume fraction, with conversion factors (i.e. molar densities) calculated at standard conditions of pressure and temperature.

Despite this caveat, r_{sw} and R_{sw} can still be used to compute local rates of water or gas along the production system, just like black oil properties. For example, consider a gas well, where the gas entering the wellbore is saturated with water at T_R, p_R conditions, and there is no free water entering the well. To calculate local rates of water at any p,T combination in the tubing, one can use the following expression:

$$q_w = max\{0, r_{sw@(p_R, T_R)} - r_{sw@(p,T)}\} \cdot q_{\bar{g}} \cdot B_w(p,T)$$

EQ. 4-6

The difference in r_{sw} could be positive or negative. If positive, it means that the gas has lowered its water content (capacity of carrying dissolved water) and therefore some water will condense out of the gas as a liquid phase. If negative, it means that the gas has increased its capacity of carrying dissolved water and could take more water than what currently has, i.e. there is no water out of solution as a liquid phase. However, as there is no more water available to go into the gas, a lower limit of zero is imposed to the expression.

When there is free water entering the flow system besides water-saturated gas, then the equation must be modified as follows:

$$q_w = max\left\{0, \frac{q_{w,inj}}{B_w(p_{inj}, T_{inj})} + \left(r_{sw@(p_1, T_1)} - r_{sw@(p,T)}\right) \cdot q_{\bar{g}}\right\} \cdot B_w(p,T)$$

EQ. 4-7

Where inj is the water injection point, and 1 is the conditions at which the gas was saturated with water. The "max" function is used here again in case all the injected free water vaporizes into the gas, because of the increase in r_{sw}.

Figure 4-24 shows a color map of r_{sw} as a function of pressure and temperature. r_{sw} is inversely proportional to pressure and directly proportional to temperature.
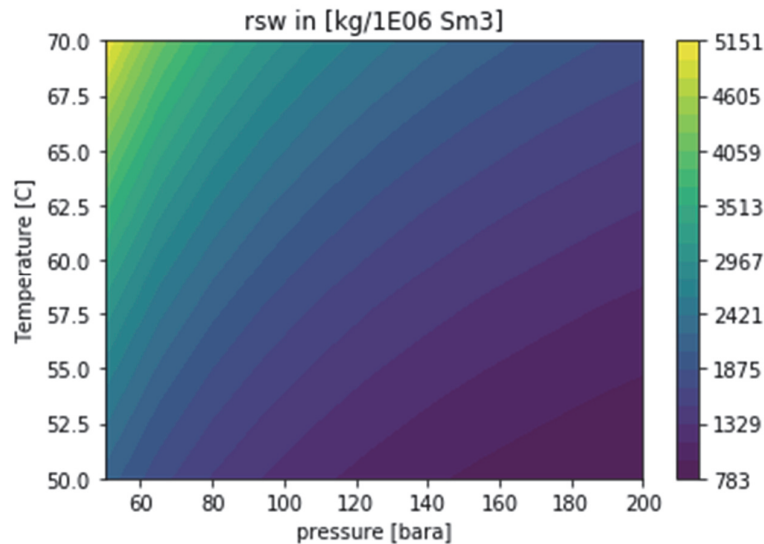
FIGURE 4-24. COLOR MAP OF r_{sw} AS A FUNCTION PF PRESSURE AND TEMPERATURE

Corrosion or liquid loading but no free water, how is this possible?

In pipe and wellbore flow there could be some situations where there is no free water at the inlet and outlet of the conduit, but there is free water some place in between. This is because values of r_{sw} at the inlet and outlet are greater than the r_{sw} content of the inlet gas, but at some point in the conduit, r_{sw} values go below

this value. To exemplify this situation, three possible paths (linear) of evolution of temperature and pressure in the conduit are over-imposed to the color map in Figure 4-25.

The yellow line represents a situation in which there is a significant pressure drop but a modest drop in temperature. In this case the r_{sw} will increase along the conduit and free water will therefore never be found along the conduit.

The red line represents a case in which there is a modest pressure drop but a significant drop in temperature along the conduit. In this case the r_{sw} will decrease along the conduit and water could drop out at some point in the conduit. However, in this case, there will be free water at the outlet of the conduit also.

The light blue line represents a case in which there is a significant pressure and temperature drop. In this case the r_{sw} will first decrease and then increase, exhibiting a local minimum. If, at some point, the value of r_{sw} goes below the r_{sw} content of the inlet gas, then free water will form.
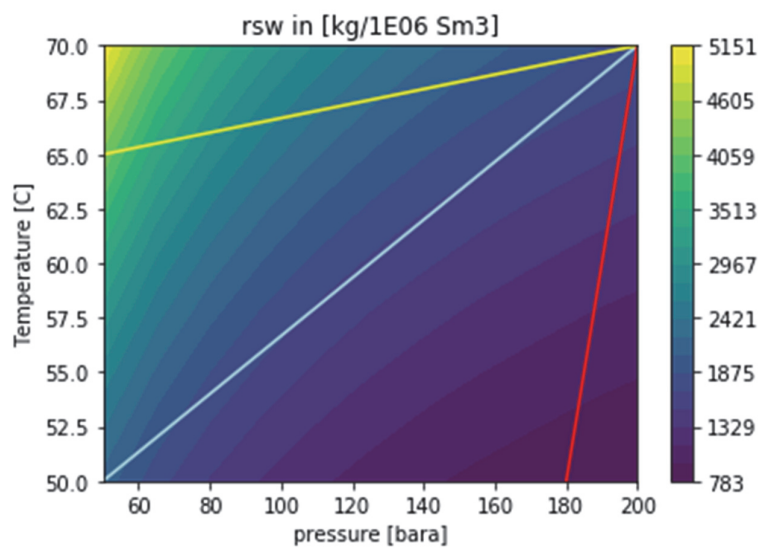
FIGURE 4-25. COLOR MAP OF r_{sw} AS A FUNCTION OF PRESSURE AND TEMPERATURE DEPICTING THREE POSSIBLE TRAJECTORIES OF PRESSURE AND TEMPERATURE IN A CONDUIT (DEPARTING FROM AN INLET PRESSURE AND TEMPERATURE OF 200 BARA AND 70 °C)

REFERENCES

[4-1] Whitson, C.H. & Brule, M.R. (2000). *Phase Behavior*. Society of Petroleum Engineers. 978-1-55563-087-4.

[4-2] Standing, M.B. (1977). *Volumetric and Phase Behavior of Oil Field Hydrocarbon Systems*. 8th printing, Society of Petroleum Engineers, Dallas.

[4-3] Whitson, C. H. (1998). *PVT Analysis Manual*. Chapter 3. Norsk Hydro.

5.   THE FIELD DEVELOPMENT PROCESS

The design of an optimum development plan of an offshore hydrocarbon field aims to maximize its economic value to the stakeholders while producing the resources in a safe and environmentally responsible manner. This while subjected to variety of socio-economic, political and regulatory constraints. The challenge is that most factors contributing to the value of the project are dynamic in nature and are continuously changing over the lifetime of the field. The evolution and behavior of the physical system (e.g. reservoir and production system) can be somewhat predicted or controlled but other factors, related to regional and global factors might change abruptly and unexpectedly as evidenced by historical trends. Some examples of such factors are cost, consumption, revenue, demands (quantity and quality), political climate and socio-economic development.

The field planning process aims to maximize value by performing an educated and robust "guess" of most of these factors for all available development alternatives. This is done to help taking important decisions that entail heavy investment and expenditure that must be taken upfront with limited data available (collected mainly by geophysical and seismic surveys and a few exploration and appraisal wells). The final "truth" however is always revealed much later, during the execution and operations phase.

Figure 5-1 shows the typical lifecycle of a hydrocarbon field focusing on the field design phase. Initially, the value chain model is established, consisting of several critical components that are traditionally considered and that are of concern for the particular case (to keep simplicity, only a few are shown in the figure). All components are usually interdependent but the subsurface (reservoir) is central. There are some components where physical models are defined and used typically to compute their behavior with time with some particular input (e.g. production profiles). There are other components that require estimating or defining some key parameters (scheduling, topside structures). There are other components (e.g. economics) where calculations are performed based on the input from other components and making assumptions of some required factors (e.g. oil price). A more detailed diagram showing some of the main components considered in the value chain is shown in Figure 5-2.

Due to the variety of components considered in the value chain of the project, this usually requires the involvement and cooperation between several specialists, typically: project management and engineering, oceanography, marine geo-technology, engineering geology, marine structures, pipeline engineering, marine operations, subsea technology, subsea facilities, process technology, top-side facilities engineering, technical safety, cost engineering, geography and impacts analyst (environmental, socio-economical, impact on fishery), field architecture, etc.
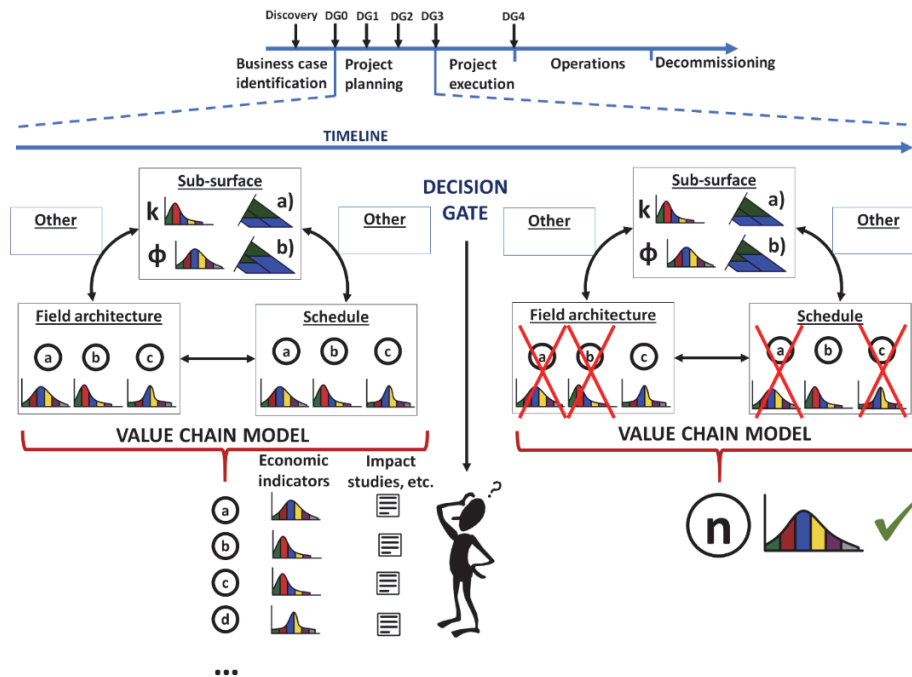
FIGURE 5-1. FIELD DEVELOPMENT TIMELINE AND THE EVOLUTION OF THE VALUE CHAIN MODEL AFTER DECISION ARE MADE
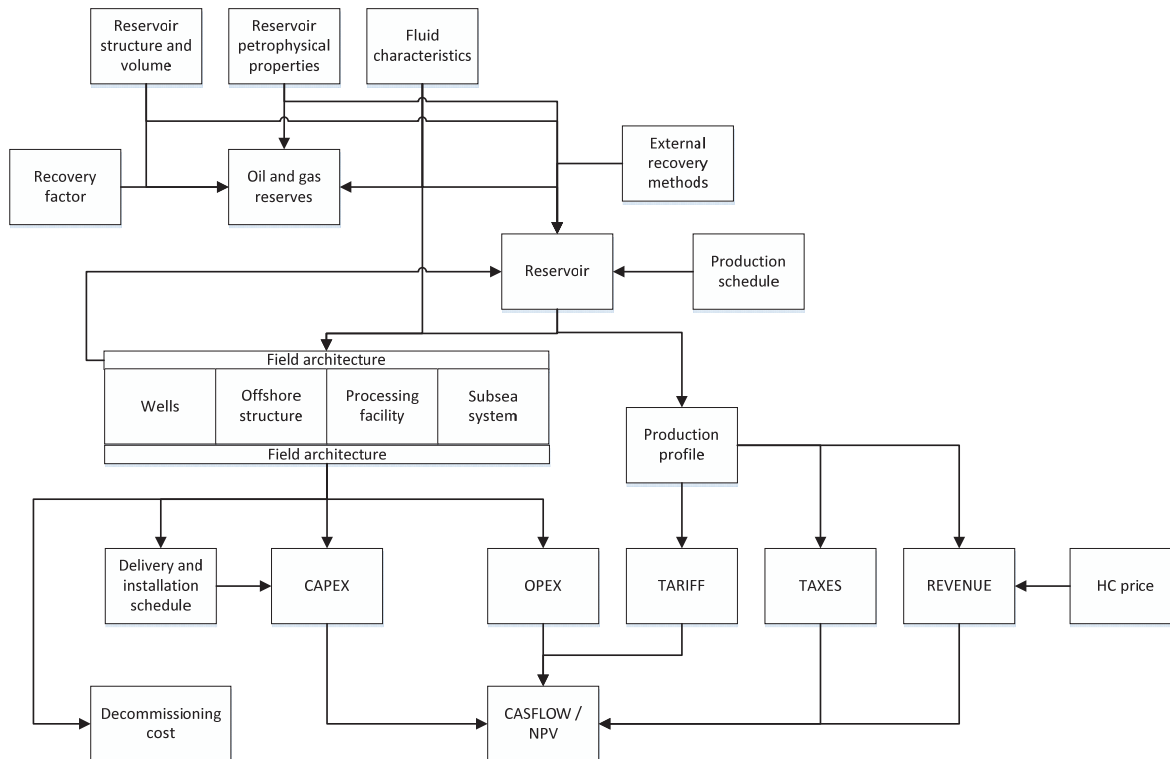
FIGURE 5-2. DETAILED VALUE CHAIN COMPONENTS

During early phases of field planning some components will have several possible alternatives (e.g. offshore structures, scheduling) that in turn affect other components. Additionally, most parameters will have an associated uncertainty (that is often described statistically). With the value chain model, it is possible to establish all development options and further calculate their associated economic indicators, impact and risks. The field design process progresses by gradually discarding non-attractive alternatives and narrowing further

the alternatives, factors and details in each individual component. This is typically done through decision gates (DG).

The field design process aims to find an optimum balance between flexibility and cost for the particular asset under study. High flexibility is desirable to cope with future changes, field expansion, market fluctuations; however, it usually comes at a very high cost. For example, oversizing the processing facilities to allow production ramp-ups entrains big investments that would likely affect negatively the net present value of the project. Low flexibility gives less costs but it makes the system very rigid to absorb future changes. The optimum lies someplace in between.

The decision-making process within field design should be done leaving an appropriate amount of flexibility and options open in each stage. This to allow adapting to new information gathered at a later stage and have the possibility to execute changes when necessary. It also should carry further all relevant uncertainties that could impact the value of the project.

During the design process the company has the crucial role to look at the solutions proposed by the vendor, verify their purpose and determine their relevance and applicability for the particular case. Pre-packaged solutions that have high flexibility and multiple components are easier to handle from the contracting point of view but they might cause extra expenses that affect negatively the economic value of the asset. Strong cooperation between company and vendor and performing third party "fit for purpose" reviews are ways to ensure that the solutions offered are applicable and necessary for the particular field development.

Oil and gas companies usually have an internal project development process similar to the one shown in Figure 5-3. Along the process there are decision gates (DG, usually located between phases) where the status of the project is reviewed and decisions are made to continue, review or terminate it. A brief description of each phase is given next.
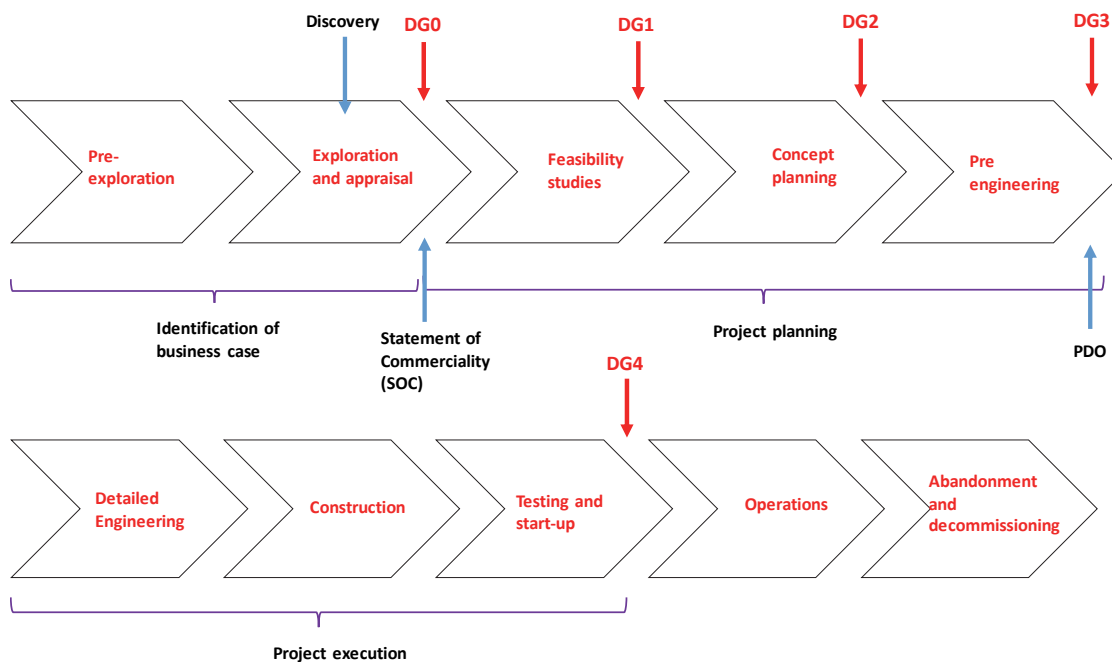
FIGURE 5-3. FIELD DEVELOPMENT PROCESS

5.1.   BUSINESS CASE IDENTIFICATION

The main goal of this step is to prove economic potential of the discovery and quantify and reduce the uncertainty in the estimation of reserves.

It usually involves the following steps:

· Pre-exploration – scouting: collecting information on areas of interests. In this step technical, political, geological, geographical, social, environmental considerations are taken into account. E.g. expected size of reserves, political regime, government stability, technical challenges of the area, taxation regime, personnel security, environmental sensitivity, previous experience in the region, etc.

· Getting pre-exploration access – The exploration license (usually non-exclusive). In the NCS only seismic and shallow wells are allowed. This is usually done by specialized companies selling data to oil companies.

· Identify prospects.

· Apply and obtain exclusive production license. In the NCS[28]: Licensing rounds (frontier areas) or Awards in predefined areas (APA). The current fees are 34.000 NOK/km^2 for the first year, 68.000 NOK/km^2 for the second year and 137.000 NOK/km^2 per year thereafter.

· Exploration. Perform geological studies, geophysical surveys, seismic, exploration drilling (Well cores, wall cores, cuttings samples, fluid samples, wireline logs, productivity test).

· Discovery.

· Assessment of the discovery and the associated uncertainty. Risk management.

· Probabilistic reserve estimation. Identify and assess additional segments.
  o Perform simplified economic valuation of the resources.
  o Field appraisal to reduce uncertainty: more exploration wells and seismic to determine for example: fault communication, reservoir extent, aquifer behavior, location of water oil contact or gas oil contact.

Possible outcomes of DG0 are:

· Issue a SOC (Statement of Commerciality) and proceed with development.
· Continue with more appraisal
· Sell the discovery.
· Do nothing (wait)
· Relinquish to the government

5.1.1. RESERVE ESTIMATION USING PROBABILISTIC ANALYSIS

A typical problem in field development is estimating initial hydrocarbon in place. For example, consider the simple expression to compute initial oil in place (N) of a clean (no shale) undersaturated oil layer:

$$N = \frac{V_R \cdot \phi \cdot (1 - S_W)}{B_o}$$

EQ. 5-1

Where:

V_R Rock volume (in m^3)

ϕ Porosity (fraction)

S_w Water saturation (fraction)

---

[28] NCS. Norwegian Continental Shelf

B_o Oil formation volume fraction

The input to this equation is often not a unique set of values but rather a range. This could be due to uncertainty: e.g. lack of more detailed information, errors in measurement, or simply due to natural variability of the parameters. Additionally, often within this range there are some values that have a higher probability of occurrence than others. Therefore, input is typically characterized with a probability distribution defined between a lower and upper limit and that provides a probability for values of the variable. Examples of distributions are uniform (all values have the same probability), normal, triangular (both exhibit a peak).

The variability in the input often causes the output to be variable, and, a priori, uncertain (rather than a unique value, when the input are single numbers). This is shown in Figure 5-4. For our example on initial oil in place estimation, Y is N and X1, X2, X3 and X4 are porosity, rock volume, water saturation and oil formation volume factor. The "model" is simply Eq. 5-1. However, the ellipse in Figure 5-4 can also represent the result of solving a system of equations, a simulator, a process, etc.
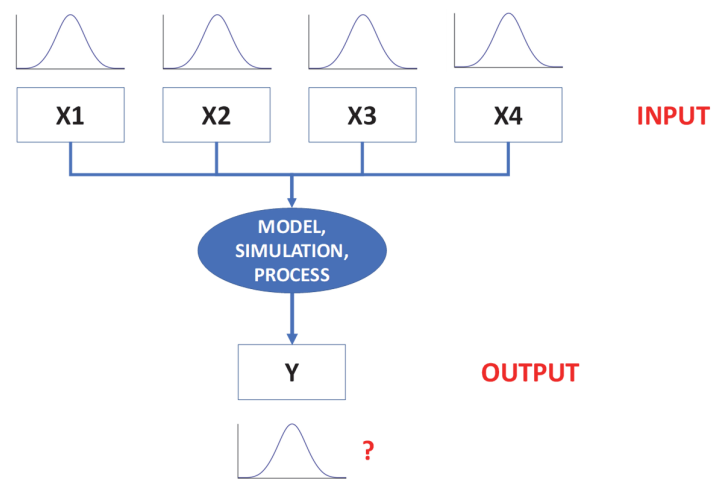
FIGURE 5-4. MODEL OR SIMULATION WITH UNCERTAINTY IN ITS INPUT PARAMETERS

To quantify and analyze the uncertainty in the output one can employ sampling methods. The goal of sampling methods is to compute several values that are the "most representative" of the function of interest and perform a frequency analysis on them to compute its probability distribution. Even though it is impossible to sample all possible values of the function (this will require an infinite number of samples to map thoroughly the output domain), if the number of samples taken is high enough (or properly distributed), it should be a good estimate of the "real" probability distribution of the function.

With the probability distribution of the function, one can then estimate the mean, the expected "spread" of the distribution and other useful quantities such as percentiles (the most common are P10, P50 and P90). The percentiles are found from the cumulative probability plot by intersecting the percent value with the curve and reading the value on the x axis. For example, if the cumulative probability plot was found by compounding probabilities from largest to lowest value, a value of P50 means that there is 50% probability that the variable is equal or greater than P50. On the contrary, if the cumulative probability curve was found by compounding probabilities from smallest to largest, a value of P50 means that there is 50% probability that the variables is equal or smaller than P50.

Sampling is typically performed by generating sets of input variables that represent the variability of the input. These sets are further input to the model individually, the model is executed (this is often referred to as a

"simulation") and all outputs are recorded. A frequency analysis is then executed on the output to find the probability distribution.

One popular sampling method is Monte Carlo. This method consists of choosing randomly a value of the cumulative distribution function (cdf) of each input variable (if using a continuous probability function), obtain a value of the variable and combine it with random values of other variables. It is advantageous to sample on the cumulative distribution function as the number is bounded between 0 and 1. It also guarantees the resulting sample of the input exhibits the same trend as the original probability distribution.

As an example, Figure 5-5 shows the result of a Monte Carlo simulation[29] of Eq. 5-1, with increasing number of samples. Above 1000 samples, the frequency distribution changes very little. By increasing the number of samples, the probability distribution converges to a unique (the real) distribution.
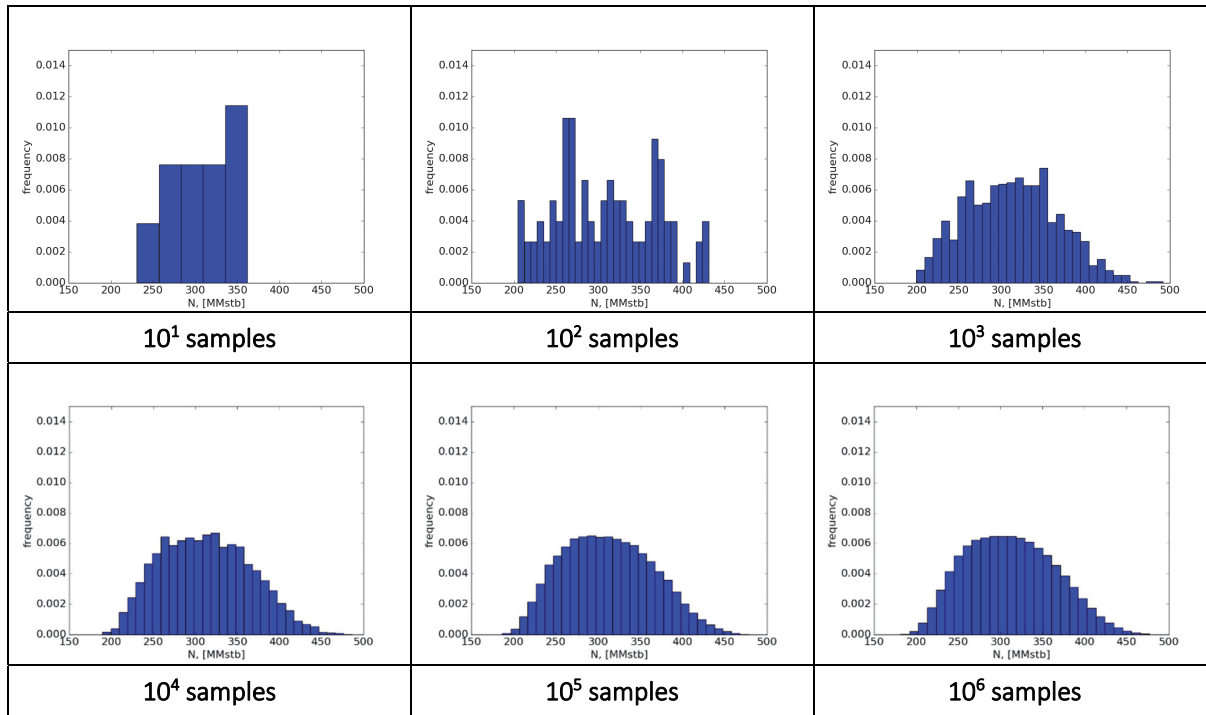
FIGURE 5-5. PROBABILITY DISTRIBUTION OF INITIAL OIL IN PLACE CALCULATED WITH MONTE CARLO SIMULATION AND DIFFERENT NUMBER OF SAMPLES

To estimate the required number of iterations to perform in the Monte Carlo method, one uses statistical inference. Consider that the probability distribution function of N is known and it displays a normal probability distribution with mean μ. If a sample of size "n" is taken from that "real" distribution (this is what Monte Carlo does), the quantity T.

$$T = \frac{(\overline{X} - \mu)}{\frac{S}{\sqrt{n}}}$$

EQ. 5-2

---

[29] Using uniform distribution for porosity (0.18-0.3), rock volume (2000-2500 MMbbl), oil saturation (0.8-0.9) and oil formation volume factor (1.35-1.6)

will be t-distributed[30] symmetrically around zero, with n-1 degrees of freedom. $\overline{X}$ is the mean of the sample and S is the standard deviation of the sample.

One can define an "interval of confidence" for T (Eq. 5-3). For example, if 25 samples were taken (24 degrees of freedom) and A is 2.064, this means that 95% of the times the interval limits are calculated, T will be located within the interval. This is often referred to as a 95% confidence interval. The higher the confidence level, the larger A must be.

$$-A \leq T \leq A$$

<div align="right">EQ. 5-3</div>

The value A (often referred to as $t_{\alpha/2}$, with α in this case being 100-95=5) is affected by the number of samples and by the confidence level, and it can be computed from the cdf of the t-distribution. However, for a large number of samples (e.g. more than 30), the t-distribution tends to overlap with a normal distribution with zero mean and a standard deviation of one.

Substituting the expression of T in Eq. 5-3, and rearranging terms:

$$\overline{X} + t_{\alpha/2} \cdot \frac{S}{\sqrt{n}} \geq \mu \geq \overline{X} - t_{\alpha/2} \cdot \frac{S}{\sqrt{n}}$$

<div align="right">EQ. 5-4</div>

Eq. 5-4 then defines a range for the real (unknown) mean μ if the confidence interval (A) is provided.

As an example, consider a normal distribution of N, with real (unknown) mean of 660 MMstb and standard deviation of 150 stb. Figure 5-6 shows the mean and confidence interval (for a confidence level of 95 %) of a sample of varying sizes. The confidence interval gets smaller and smaller as the number of samples is increased and the distribution of the sample resembles closer the "real" distribution.

---

[30] https://en.wikipedia.org/wiki/Student%27s_t-distribution
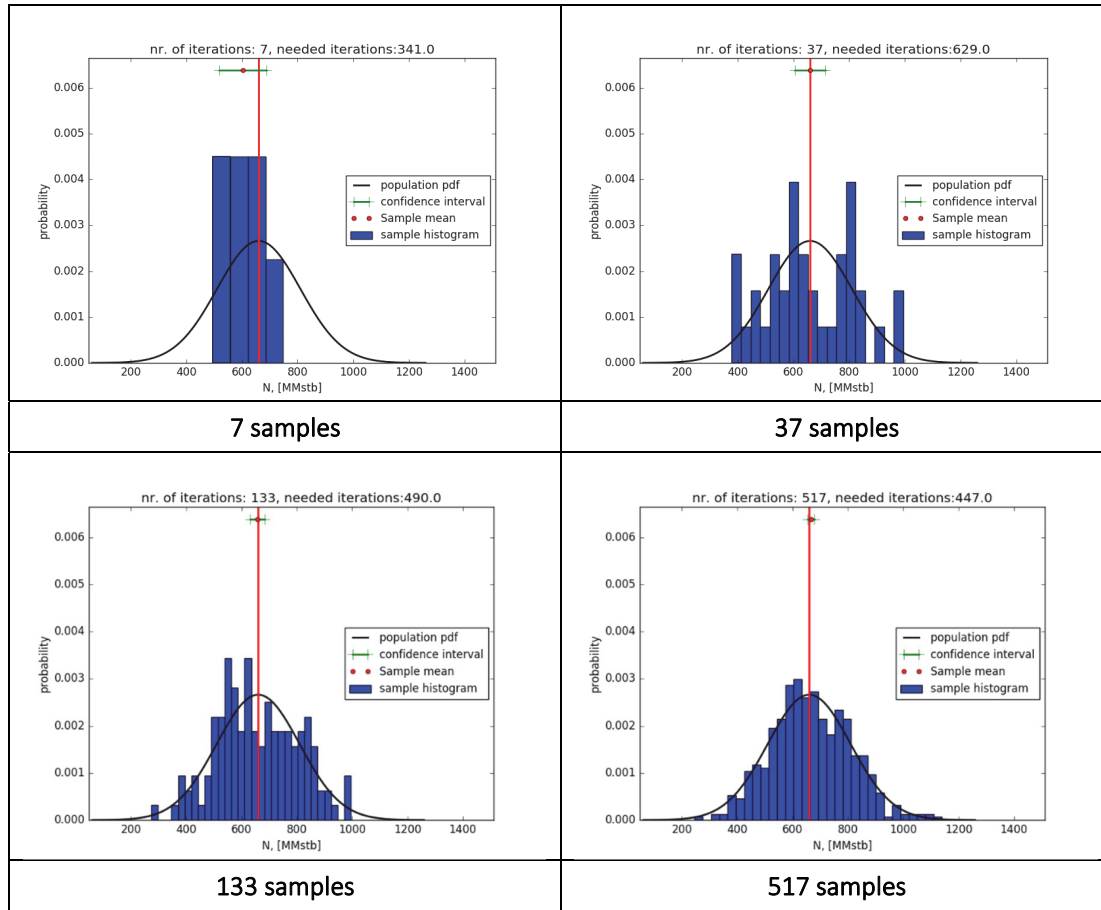
FIGURE 5-6. PROBABILITY DISTRIBUTION OF INITIAL OIL IN PLACE SAMPLED FROM A NORMAL DISTRIBUTION FOR DIFFERENT NUMBER OF SAMPLES

To estimate the number of samples required in Monte Carlo, one can modify Eq. 5-4 by specifying the error (e) one wishes to achieve.

$$e = t_{\alpha/2} \cdot \frac{S}{\sqrt{n}}$$

EQ. 5-5

e is the absolute error, and it is often expressed in terms of the mean of the sample, $\overline{X}$, for example, by multiplying it with a fraction F (between 0-1). By substituting this in Eq. 5-5, and clearing "n" it yields

$$n = \left(t_{\alpha/2} \cdot \frac{S}{F \cdot \overline{X}} \right)^2$$

EQ. 5-6

To estimate a value of n, one must have performed at least one iteration, and S and $\overline{X}$ should be available. There will be a new value of n for each iteration and one stops when n estimated is smaller than the actual sample size.

Sometimes the number of iterations required for the Monte Carlo method to achieve an acceptable error are too large to be practical, especially if the simulation running time is high. There are other methods that perform a smarter sampling of the function (instead of random), that require less iterations. One of this methods is Latin hypercube sampling. In Latin Hypercube sampling the steps are:

- Define the number of samples "n" to use.
- Subdivide the pdf of each input variable in "n" intervals of equal probability.

- Create a set of "n" values for each variable by picking a random number in each interval (using the cdf of each interval, just like in Monte Carlo).
- Create "n" input sets by picking randomly a value of each variable set. It is not allowed to pick the same value twice.
- Run the simulations with the "n" input sets and apply a frequency analysis to the results.

5.2. PROJECT PLANNING

The main goal of the planning phase is to perform a systematic screening of concepts, to define a preferred development concept and to evaluate its profitability, technical feasibility and HSE within acceptable levels of uncertainty. Furthermore, to document the solution for delivery to the authorities managing the production license.

5.2.1. FEASIBILITY STUDIES

The main goal of this step is to justify further development of the project, finding one or more concepts that are technically, commercially and organizationally feasible. Some specific tasks of this phase are:

·   Define objectives of the development in line with the corporate strategy.
·   Establish feasible development scenarios.
·   Create a project timeline and a workplan.
·   Identify possible technology gaps and blockers.
·   Identify the needs for new technology.
·   Identify added value opportunities.
·   Cost evaluation for all options.

5.2.2. CONCEPT PLANNING (LEADING TO DG2)

Identify development concepts, rank them and select and document a viable concept (Base Case Scenario).

·   Evaluate and compare alternatives for development and screen out non-viable options.
·   Elaborate a Project Execution Plan (PEP) which describes the project and management system.
·   Define the commercial aspects, legislation, agreements, licensing, financing, marketing and supply, taxes.
·   Create and refine a static and a dynamic model of reservoir. Define the depletion and production strategy.
·   Define an HSE program.
·   Flow assurance evaluation. Identification of challenged related with fluid properties, multiphase handling and driving pressure.
·   Drilling and well planning.
·   Pre-design of facilities.
·   Planning of operations, start-up and maintenance.
·   Cost and manpower estimates of the best viable concept.

5.2.3. FIELD PRODUCTION PROFILE AND ECONOMIC VALUE

During the concept phase, one of the main tasks is to define the field production schedule that provides the maximum economic value for the project. The economic value of the project could be estimated using different financial evaluation approaches; one of the approaches is the net present value (NPV), calculated on a yearly basis, which is defined as:

$$NPV = \sum_{t=1}^{n} \frac{CF_t}{(1+i)^t}$$

EQ. 5-7

Where:

i Discount rate (usually a value in the range 5-12%)

t Integer counter for the number of years

n Total number of years

CF_t Cash flow of year "t"

Neglecting royalties and tax payments (which vary from country to country, or even on license type), the cashflow for the project can be expressed as:

$$CF_t = Revenue_t - OPEX_t - DRILLEX_t - CAPEX_t$$

EQ. 5-8

During the first years of the project, when the field is under construction and there is no production, only drilling expenditures (also known as DRILLEX) and capital expenditures (CAPEX) are considered. CAPEX are expenditures to acquire, design, manufacture and transport physical assets such as an offshore structure, topside facilities, subsea system, etc. For later years, when the field is producing only revenue and operating expenditures (OPEX) are considered.

The CAPEX related with the offshore structure and topside facilities depends strongly on the type and weight of units and equipment that will be placed on the offshore structure. The type of units and equipment depend on the treatment processes required for reservoir fluids, while the weight is given mainly by the maximum liquid and gas processing capacities. Therefore, the offshore structure and topside CAPEX is a function of the maximum field liquid rate ($q_{l,max}$) and the maximum field gas rate ($q_{g,max}$) produced during the life of the field. The relationship is sometimes assumed linear, as shown in equation Eq. 5-9.

$$CAPEX_{top+off} = C_1 \cdot q_{l,max} + C_2 \cdot q_{g,max} + C_3$$

EQ. 5-9

For some offshore structures that "house" wells (for example jackets, gravity-based platforms, tension leg platforms with dry Christmas trees), the CAPEX of offshore and topside also depends strongly on the number of wells.

The subsea system CAPEX depends on several factors: number of wells, number of subsea manifolds and flowlines, umbilicals, water depth, etc. Despite showing dependencies on these many factors, the subsea CAPEX can sometimes be expressed as function of the number of wells:

$$CAPEX_{subsea} = C_4 + C_5 \cdot N_w$$

EQ. 5-10

Where:

N_w Number of wells

DRILLEX is sometimes computed the well cost times the number of wells:

$$DRILLEX = N_w \cdot P_w$$

EQ. 5-11

Where:

P_w Cost of drilling a well

Yearly OPEX depends on the producing rates of oil, gas and water, and the number of wells in operation in year "t". Additionally, there are other yearly costs such as energy usage, insurance, transportation of goods and personnel to and from the field, consumption of chemicals, among others. The relationship is sometimes assumed linear:

$$OPEX_t = O_1 \cdot q_{l,t} + O_2 \cdot q_{g,t} + O_3 \cdot N_{w,t} + O_4$$

<div align="right">EQ. 5-12</div>

The revenue function will be discussed next with an example. Due to the discounting factor, the production in later years typically contributes less to the NPV than production in earlier years. Thus, one usually tends to favor production in earlier years against production in later years.

Estimating the NPV of the revenue, case study: oil or gas field with a linear production potential curve, operating in plateau mode

Assume the field exhibits the following dimensionless production potential linear equation for oil (or gas) production (please refer to Eq. 1-12, Eq. 1-18):

$$\bar{q}_{pp} = 1 - \alpha \cdot \frac{Q_p}{Q}$$

<div align="right">EQ. 5-13</div>

Here Q is used instead of N (oil) or G (gas).

The production potential is then:

$$q_{pp} = q_{ppo,field} \cdot \left(1 - \alpha \cdot \frac{Q_p}{Q}\right)$$

<div align="right">EQ. 5-14</div>

If there are several identical producing wells in the production systems that are independent from each other[31], then $q_{ppo,field}$ is:

$$q_{ppo,field} = N_{prod\ wells} \cdot q_{ppo,well}$$

<div align="right">EQ. 5-15</div>

If the field is produced at plateau and then decline, the plateau duration (in years) can be calculated with the following equation:

$$\Delta t_p = \frac{Q}{\alpha \cdot t_{uptime}} \cdot \left(\frac{1}{q_{p,f}} - \frac{1}{q_{ppo,field}}\right)$$

<div align="right">EQ. 5-16</div>

To derive an expression of field production rate versus time, we follow a similar procedure to the one presented in Example 1 of section 1.6, assuming the field is produced in plateau mode and then declines, and that production starts at t_{ini}, instead of at zero the field rate is given by:

$$for\ t < t_{ini} \qquad\qquad q_f = 0$$

<div align="right">EQ. 5-17</div>

$$for\ t_{ini} \leq t < t_{ini} + \Delta t_p \qquad\qquad q_f = q_{p,f}$$

<div align="right">EQ. 5-18</div>

$$for\ t \geq t_{ini} + \Delta t_p \qquad\qquad q_f = q_{p,f} \cdot e^{-\frac{\alpha \cdot q_{ppo,field} \cdot t_{uptime}}{Q} \cdot (t - \Delta t_p - t_{ini})}$$

<div align="right">EQ. 5-19</div>

Here t is input in years.

Introducing the parameter m:

---

[31] Alternatively, if there are interactions between wells, one could use Eq. 1-25.

$$m = \frac{\alpha \cdot q_{ppo,field} \cdot t_{uptime}}{Q}$$

EQ. 5-20

The recovery factor can be computed with:

$$R_f = \frac{1}{Q} \left(\int_{t_{ini}}^{t_{ini}+\Delta t_p} q_{p,f} \cdot t_{uptime} \cdot dt + \int_{\Delta t_p + t_{ini}}^{t} q_{p,f} \cdot t_{uptime} \cdot e^{-m \cdot (t - \Delta t_p - t_{ini})} dt \right)$$

EQ. 5-21

Which gives the following expression:

$$R_f = \frac{q_{p,f} \cdot t_{uptime}}{Q} \cdot \left[\Delta t_p + \frac{1}{m} \cdot \left(1 - e^{-m \cdot (t - \Delta t_p - t_{ini})} \right) \right]$$

EQ. 5-22

Returning to the expression of the project net present value:

$$NPV = \sum_{t=1}^{N} \frac{CF_t}{(1+i)^t} = \sum_{t=1}^{N} \frac{Revenue_t - OPEX_t - DRILLEX_t - CAPEX_t}{(1+i)^t}$$

EQ. 5-23

If we separate each term in the sum:

$$NPV = \sum_{t=1}^{N} \frac{Revenue_t}{(1+i)^t} - \sum_{t=1}^{N} \frac{OPEX_t}{(1+i)^t} - \sum_{t=1}^{N} \frac{DRILLEX_t}{(1+i)^t} - \sum_{t=1}^{N} \frac{CAPEX_t}{(1+i)^t}$$

EQ. 5-24

Each term is renamed as follows:

$$NPV = NPV_{rev} - NPV_{OPEX} - NPV_{DRILLEX} - NPV_{CAPEX}$$

EQ. 5-25

To find an analytical equation for the NPV_{rev}, we will use continuous discounting instead of yearly discounting. The discrete discount factor (DF) is:

$$DF(t) = (1+i)^t$$

EQ. 5-26

If discounting is made over "x" discrete periods within the year, the expression must be modified as follows:

$$DF(t) = \left(1 + \frac{i}{x} \right)^{x \cdot t}$$

EQ. 5-27

The limit when x is large yields:

$$\lim_{x \to \infty} DF(t) = \lim_{x \to \infty} \left(1 + \frac{i}{x} \right)^{x \cdot t} = e^{i \cdot t}$$

EQ. 5-28

Assuming that there are sales of both oil and gas, at a constant price of P_o, P_g respectively, assuming the field will produce a constant gas-oil ratio (in case of an oil field, R_p) or a constant condensate gas ratio (in case of a gas field, C_{gr}), and using a continuous discounting with the exponential function and discount rate "i" the net present value of the revenue stream at a given time "t" is calculated by:

$$NPV_{rev} = \int_{t_{ini}}^{t} q_f(t) \cdot t_{uptime} \cdot K \cdot e^{-i \cdot t} dt$$

EQ. 5-29

Where $K = \left(P_o + R_p \cdot P_g\right)$ or $K = \left(P_g + C_{gr} \cdot P_o\right)$ if an oil or gas field respectively.

Expanding the expression for the plateau and post-plateau periods:

$$NPV_{rev} = \int_{t_{ini}}^{t_{ini}+\Delta t_p} q_{p,f} \cdot t_{uptime} \cdot K \cdot e^{-i \cdot t} dt$$
$$+ \int_{t_{ini}+\Delta t_p}^{t} q_{p,f} \cdot t_{uptime} \cdot e^{-m \cdot (t-\Delta t_p - t_{ini})} \cdot K \cdot e^{-i \cdot t} dt$$

EQ. 5-30

Solving the integral for the plateau period:

$$NPV_{rev} = q_{p,f} \cdot K \cdot t_{uptime} \cdot \left[\frac{e^{-i \cdot t_{ini}} - e^{-i \cdot (t_{ini}+\Delta t_p)}}{i} \right] + q_{p,f} \cdot K \cdot t_{uptime} \cdot e^{m \cdot (\Delta t_p + t_{ini})}$$
$$\cdot \int_{t_{ini}+\Delta t_p}^{t} e^{-(m+i) \cdot t} dt$$

EQ. 5-31

Solving the integral for the decline period:

$$NPV_{rev} = q_{p,f} \cdot K \cdot t_{uptime} \cdot \left[\frac{e^{-i \cdot t_{ini}} - e^{-i \cdot (t_{ini}+\Delta t_p)}}{i} \right] + q_{p,f} \cdot K \cdot t_{uptime} \cdot e^{m \cdot (\Delta t_p + t_{ini})}$$
$$\cdot \left[\frac{e^{-(m+i) \cdot (t_{ini}+\Delta t_p)} - e^{-(m+i) \cdot t}}{(m+i)} \right]$$

EQ. 5-32

Rearranging terms:

$$NPV_{rev} = q_{p,f} \cdot K \cdot t_{uptime}$$
$$\cdot \left\{ \left[\frac{e^{-i \cdot t_{ini}} - e^{-i \cdot (t_{ini}+\Delta t_p)}}{i} \right] + \left[\frac{e^{-i \cdot (t_{ini}+\Delta t_p)} - e^{-(m+i) \cdot t + m \cdot (\Delta t_p + t_{ini})}}{(m+i)} \right] \right\}$$

EQ. 5-33

To study the behavior of NPV_{rev}, and oil field is considered and the following values are used (some taken from Nunes[5-1]):

- $t_{production\ horizon}$ = 25 years
- N = $2.19E09\ stb$
- $q_{ppo,well}$ = 20 000 stb/d
- i = 0.09
- $\alpha = 4$
- $P_o = 50\ [USD/stb]$
- $P_g = 0.004\ [USD/scf]$
- R_p = 200 scf/stb
- $t_{uptime} = 352\ d/year$
- t_{ini} = 5 years

NPV_{rev} is calculated until abandonment time, which, considering initial time, is:

$$t_{abandonment} = t_{ini} + t_{production\ horizon}$$

EQ. 5-34

Using these values, the calculation of the revenue net present value is depicted in Figure 5-7 for two (2) number of producing wells and several values of oil field plateau rate. The function has been plotted up to the maximum oil plateau rate that it is physically possible to produce from the field (e.g. 240 000 for 12 wells and 300 000 for 15 wells respectively).
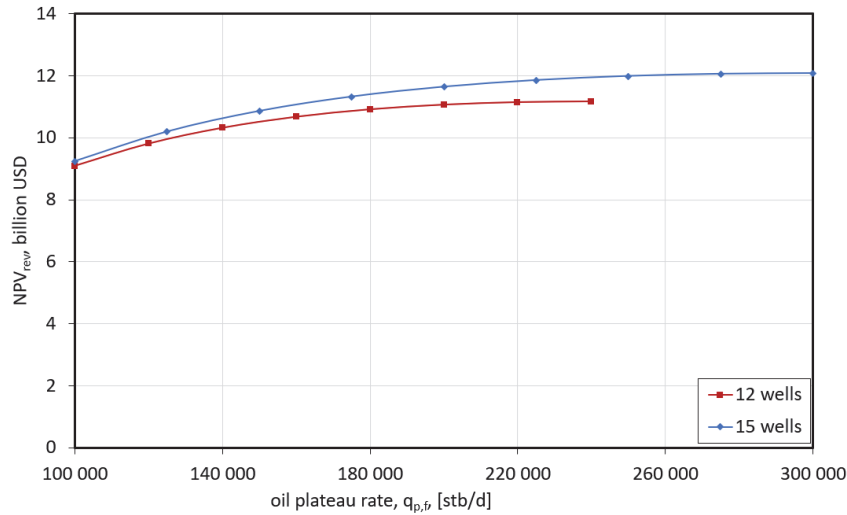
FIGURE 5-7. BEHAVIOR OF THE NET PRESENT VALUE OF THE REVENUE VERSUS OIL PLATEAU RATE FOR TWO NUMBERS OF WELLS

The function "growth" slows down when the oil plateau rates approaches its upper bound. This indicates that the production strategy to produce as much as possible as early as possible indeed does increase the revenue present value, but its effect becomes weaker and weaker as the rate approaches the maximum rate the field can produce.

Abandonment time

Abandonment time is often calculated when cash flow becomes negative. At late times, there are no more capital expenditures, only operational expenditures, and the field is usually in its decline phase. Calculating field revenue at abandonment time using the decline phase field rate equation versus time (Eq. 5-19), and making it equal to OPEX[32] at abandonment time "t", gives:

$$OPEX_{@t_{abandonment}} = q_{p,f} \cdot e^{-m \cdot (t_{abandonment} - \Delta t_p - t_{ini})} \cdot K$$

EQ. 5-35

If one assumes daily OPEX at abandonment is known, then it is possible to clear explicitly from the equation the abandonment time:

$$t_{abandonment} = \frac{1}{m} \cdot ln\left(\frac{q_{p,f} \cdot K}{OPEX_{@t_{abandonment}}}\right) + \Delta t_p + t_{ini}$$

EQ. 5-36

In some cases, for example gas field producing associated liquid, there is a minimum gas rate required to ensure stable production ($q_{f,minimum}$, for example to avoid well liquid loading or large slugs in subsea

---

[32] In this equation, to ensure units consistency, the term $OPEX_{@t_{abandonment}}$ must be given in units of USD/d (daily operational expenditures).

transportation pipelines). Therefore, abandonment won't occur when cash flow becomes negative, but rather when the minimum field gas flow rate is reached. Abandonment time for this case can be computed with:

$$t_{abandonment} = \frac{1}{m} \cdot ln\left(\frac{q_{p,f}}{q_{f,minimum}}\right) + \Delta t_p + t_{ini}$$

EQ. 5-37

Estimating the NPV, case study: offshore oil field with a linear production potential curve, operating in plateau mode

The behavior of NPV, i.e. when combining revenues and expenses in a cash flow and discounting in time will be discussed next with an example.

In this case we will use some data presented by Nunes[5-1]. We make the following assumptions:

- CAPEX and DRILLEX are paid at initial time, thus it is not necessary to discount them.
- The maximum liquid capacity is taken as equal to the oil plateau rate, i.e., no water will be produced from the field.
- Each producer well has an associated water injector, thus the total number of wells N_w is equal to $2 \cdot N_{prod,wells}$
- All wells are drilled before production starts.

The capital expenditures of the topside facilities and the offshore structure can be estimated with the following expression, using the oil plateau rate (maximum oil rate expected), and assuming that the producing gas-oil ratio, R_p is constant:

$$CAPEX_{top+off} = C_1 \cdot q_{p,f} + C_2 \cdot q_{g,max,f} \cdot R_p + C_3 = C_1 \cdot q_{p,f} + C_2 \cdot q_{p,f} \cdot R_p + C_3$$

EQ. 5-38

With:

- C_1=1.2 E03 USD/stb/d
- C_2=6.6 USD/scf/d
- C_3=1.07 E09 USD

The capital expenditures of the subsea system can be estimated with the following expression. The last term is the cost of a subsea manifold assuming that there is a maximum of 4 wells per manifold.

$$CAPEX_{subsea} = C_4 + C_5 \cdot N_w + C_6 \cdot roundup\left(\frac{N_w}{4}\right)$$

EQ. 5-39

- C_4=130 E06 USD
- C_5=66.1 E06 USD/well
- C_6=32 E06 USD/manifold

The cost of each well is P_w=150 E06 USD/well

OPEX is varying in time, as a function of the oil and gas rate in time. The following expression will be assumed:

$$OPEX(t) = O_1 \cdot q_f(t) + O_2 \cdot q_g(t) + O_3 \cdot N_w + O_4$$
$$= O_1 \cdot q_f(t) + O_2 \cdot q_f(t) \cdot R_p + O_3 \cdot N_w + O_4$$

EQ. 5-40

With:

- O_1=400 USD/stb/d
- O_2=0 USD/scf/d

- O_3=0.7 E06 USD/well
- O_4=80 E06 USD

OPEX will be discounted continuously, in a similar manner as the revenue:

$$NPV_{OPEX} = \int_{t_{ini}}^{t} OPEX(t) \cdot e^{-i \cdot t} dt$$

EQ. 5-41

The derivation gives:

$$
\begin{aligned}
NPV_{OPEX} = q_{p,f} \cdot &\left(O_1 + O_2 \cdot R_p\right) \\
&\cdot \left\{ \left[\frac{e^{-i \cdot t_{ini}} - e^{-i \cdot (t_{ini}+\Delta t_p)}}{i} \right] + \left[\frac{e^{-i \cdot (t_{ini}+\Delta t_p)} - e^{-(m+i) \cdot t + m \cdot (\Delta t_p + t_{ini})}}{(m+i)} \right] \right\} \\
&+ (O_3 \cdot N_w + O_4) \frac{\left(e^{-i \cdot t_{ini}} - e^{-i \cdot t}\right)}{i}
\end{aligned}
$$

EQ. 5-42

The expression is similar to the one obtained or NPV$_{REV}$, thus it is possible to combine both into one:

$$
\begin{aligned}
NPV_{rev+OPEX} = q_{p,f} \cdot &\left[\left(P_o + R_p \cdot P_g\right) \cdot t_{uptime} - \left(O_1 + O_2 \cdot R_p\right) \right] \\
&\cdot \left\{ \left[\frac{e^{-i \cdot t_{ini}} - e^{-i \cdot (t_{ini}+\Delta t_p)}}{i} \right] + \left[\frac{e^{-i \cdot (t_{ini}+\Delta t_p)} - e^{-(m+i) \cdot t + m \cdot (\Delta t_p + t_{ini})}}{(m+i)} \right] \right\} \\
&- (O_3 \cdot N_w + O_4) \frac{\left(e^{-i \cdot t_{ini}} - e^{-i \cdot t}\right)}{i}
\end{aligned}
$$

EQ. 5-43

Figure 5-8 shows, for 12 producers (24 wells in total) the NPV$_{rev}$, NPV$_{OPEX}$, the project NPV, and the CAPEX+DRILLEX versus the oil field plateau rate.
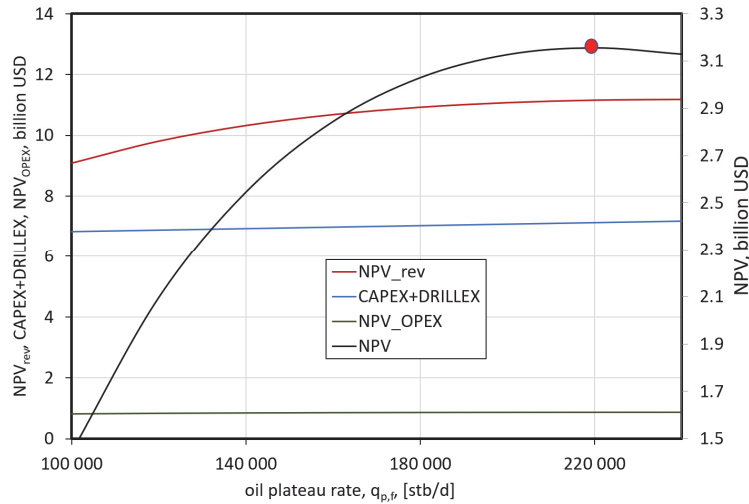
FIGURE 5-8. PROJECT NPV, NPV$_{REV}$, NPV$_{OPEX}$, AND CAPEX+DRILLEX FOR 12 PRODUCER WELLS VERSUS OIL PLATEAU RATE.

The NPV curve shows a maximum at around 220 000 stb/d. This maximum corresponds to the point where:

$$\frac{\partial NPV}{\partial q_{p,f}} = 0$$

EQ. 5-44

As mentioned earlier, the NPV is a function of revenue, CAPEX, OPEX, therefore:

$$\frac{\partial NPV_{rev}}{\partial q_{p,f}} - \frac{\partial CAPEX}{\partial q_{p,f}} - \frac{\partial DRILLEX}{\partial q_{p,f}} - \frac{\partial NPV_{OPEX}}{\partial q_{p,f}} = 0 \qquad \text{EQ. 5-45}$$

As we have assumed the CAPEX is a linear function of the plateau oil production, the maximum of NPV is given when:

$$\frac{\partial NPV_{rev+OPEX}}{\partial q_{p,f}} = C_1 + C_2 \cdot R_p \qquad \text{EQ. 5-46}$$

Effect of water production

In practice, the field could also produce associated water. Considering this, it is possible to express the CAPEX as a function of both water and hydrocarbon flowrates using the water cut (W_C), as shown in Eq. 5-47

$$CAPEX_{TOP+OFF} = C_1 \cdot \frac{q_{o,f}}{(1 - W_c)} + C_2 \cdot q_{o,f} \cdot R_p + C_3 \qquad \text{EQ. 5-47}$$

The maximum liquid and gas rates often occur during the plateau period, therefore:

$$CAPEX_{TOP+OFF} = C_1 \cdot \frac{q_{p,f}}{(1 - W_c)} + C_2 \cdot q_f \cdot R_p + C_3 \qquad \text{EQ. 5-48}$$

To calculate the slope of the CAPEX function, Eq. 5-48 is differentiated once.

$$\frac{\partial CAPEX_{TOP+OFF}}{\partial q_{p,f}} = \frac{C_1}{(1 - W_c)} + C_2 \cdot R_p \qquad \text{EQ. 5-49}$$

This function will give another maximum and optimum oil plateau rate of the NPV function compared with the one given in Eq. 5-9. The CAPEX slope will be higher, thus the optimum plateau rate will be lower than for the case without water production.

Effect of number of producers

Figure 5-9 shows NPV values calculated for number of producer wells between 1 and 20 and oil plateau rates between 5 000 and 400 000 stb/d. The white space are plateau rates that are not feasible because they exceed the maximum production possible by the number of producers specified. The NPV exhibits a global maximum indicated with the blue dot (9 producers, oil plateau rate 170 186 stb/d). The black line depicts combinations that give a NPV of zero.
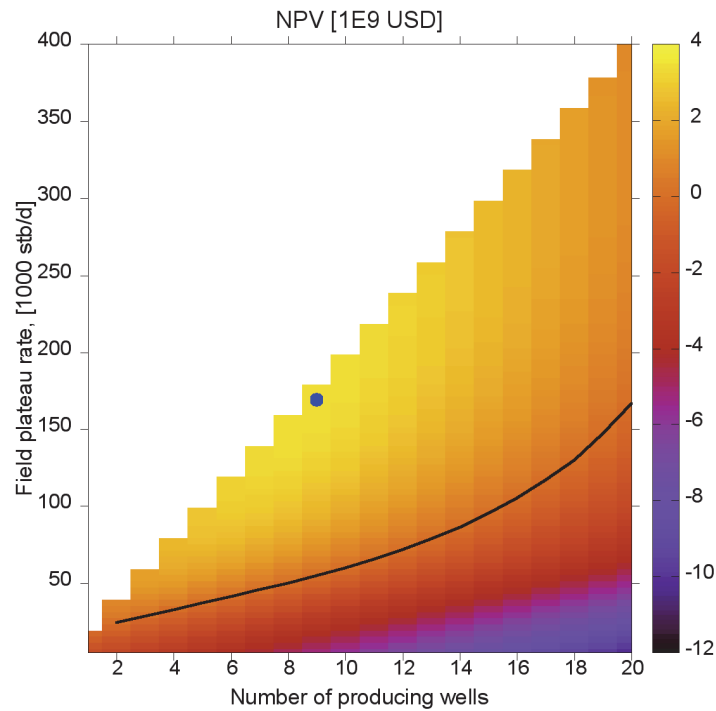
FIGURE 5-9. COLOR CONTOUR OF NPV VERSUS NUMBER OF PRODUCING WELLS AND FIELD PLATEAU RATE

Effect of initial oil in place

Figure 5-10 shows NPV values calculated for number of producer wells between 1 and 20 and oil plateau rates between 5 000 and 400 000 stb/d, for three different values of initial oil in place (base case, 40% less and 40% more). The white space are plateau rates that are not feasible because they exceed the maximum production possible by the number of producers specified. The NPV exhibits a global maximum indicated with the blue dots:

- An N value 40% smaller than the base gives an optimum at 5 producers, oil plateau rate 95 127 stb/d.
- An N value 40% bigger than the base gives an optimum at 12 producers, oil plateau rate 227 814 stb/d.

a) N= 0.6·base   b) N= base   c) N= 1.4·base
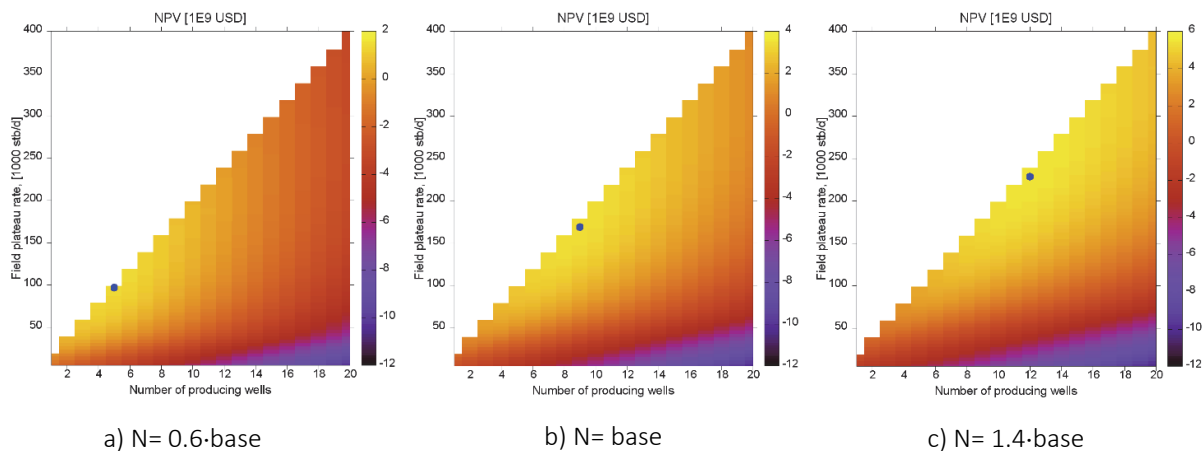
FIGURE 5-10. COLOR MAP OF NPV VERSUS NUMBER OF PRODUCING WELLS AND FIELD PLATEAU RATE, FOR THREE VALUES OF INITIAL OIL IN PLACE. THE BLUE DOT INDICATES THE OPTIMAL COMBINATION OF NUMBER OF PRODUCERS AND OIL PLATEAU RATE

Effect of oil price

Figure 5-11 shows NPV values calculated for number of producer wells between 1 and 20 and oil plateau rates between 5 000 and 400 000 stb/d, for two values of oil price, 50 and 70 USD/stb. The white space are plateau rates that are not feasible because they exceed the maximum production possible by the number of producers specified. The NPV for the oil price of 70 USD/stb exhibits a global maximum at 12 producers, oil plateau rate 225 291 stb/d.

a) P_O= 50 USD/stb   b) P_O= 70 USD/stb
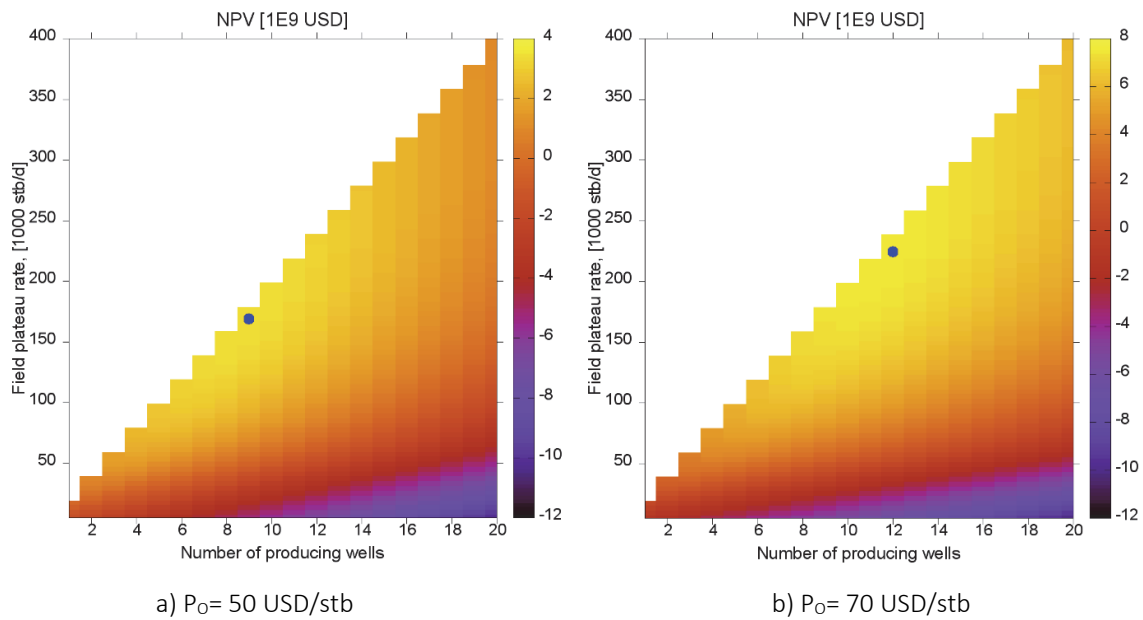
FIGURE 5-11. COLOR MAP OF NPV VERSUS NUMBER OF PRODUCING WELLS AND FIELD PLATEAU RATE, FOR OIL PRICE 50 USD/STB AND 70 USD/STB.

5.2.4. PRE-ENGINEERING (LEADING TO DG3)

Further mature, define and document the development solution based on the selected concept. Some specific tasks are:

· Selection of the final technical solution. Decide and define all remaining critical technical alternatives.
· Execute Front-End Engineering Design (FEED): determine technical requirements (arranged in packages) for the project based on the final solution chosen. Estimate cost of each package.
· Plan and prepare the execution phase.
· Prepare for submission of the application to the authorities.
· Perform the Environmental impact assessment.
· Establish the basis for awarding contracts.

The outcome of DG3 is[5-2]:

· Issue plan for development and operations (PDO), plan for Installation and Operation of Facilities for transport and utilization of petroleum (PIO), and Impact assessment report.

5.3. PROJECT EXECUTION

If the plan for development and operations is approved by the authorities, the project execution phase starts.

5.3.1. DETAILED ENGINEERING, CONSTRUCTION, TESTING AND STARTUP

· Detailed design, procurement of the construction materials, construction, installation and commissioning of the agreed facilities. This can be done in two ways:

- o **Individual contracts**
- o Detailed engineering
- o Bids, contracts
- o Construction, fabrication
- o Installation
- o Commissioning (Cold or Hot)
- o **Or using an EPCM** (Engineering, procurement, construction, and management contract) with one main contractor.
- Constructing wells.
- Perform hand over to asset, operations
- Prepare for start-up, operation and maintenance

5.4. OPERATIONS

- Production startup, Build-up phase, Plateau phase, decline phase, Tail production, Field shut-down.
- Maintenance.
- Planning Improved Oil recovery methods.
- Allocation and metering.
- De-bottlenecking.
- Troubleshooting.

5.5. DECOMMISSIONING AND ABANDONMENT

- Engineering "down and clean": flushing and cleaning tanks, processing equipment, piping.
- Coordinate with relevant environmental and governmental authorities.
- Well plugging and abandonment (P&A)
- Cut and remove well conductor and casing.
- Remove topside equipment.
- Removal of the offshore structure: Lifting operations and transport
- Remove or bury subsea pipelines
- Mark and register leftover installations on marine maps
- Monitoring
- Recovery of material: Scrap (steel) and recycling equipment (Gas turbines, separators, heat exchangers, pumps, processing equipment)
- Disposal of residues

REFERENCES

[5-1] Nunes, G. C.; Da Silva, A. H & Esch, L.G. (2018). A Cost Reduction Methodology for Offshore Projects. OTC-28898-MS. *Offshore Technology Conference*. Houston.

[5-2] Norwegian Petroleum Directorate. *Guidelines for PDO and PIO*. Retrieved from http://www.npd.no/Global/Engelsk/5-Rules-and-regulations/Guidelines/PDO-PIO-guidelines_2010.pdf, on Jan 9th, 2017.

[5-3] Presentation "Field Development and Portfolio Evaluation". Statoil. Retrieved from http://www.uio.no/studier/emner/matnat/math/MEK4450/h15/ppt/l1-2/10-field-development-and-cvp-process-august-2015.pdf on Jan 9th, 2017.

[5-4] Jahn, F., Cook, M. & Graham, M. (2008). *Hydrocarbon Exploration and Production.* 2nd edition. Elsevier Science. 978-0-08056-8836.

6.   OFFSHORE STRUCTURES FOR OIL AND GAS PRODUCTION

In this section a brief discussion will be made about offshore structures typically used for oil and gas production. Some particular offshore vessels and structures that are not discussed here are drilling vessels and platforms, well intervention vessels, vessels used to transport and lay down pipelines and equipment, supply vessels and tankers. Some fields can also be developed subsea and their production tied to shore (subsea-to-beach) or to existing installations. These cases are not discussed here. The current records of subsea tiebacks are the Penguin A-E field for oil (69.8 km) in the North Sea and the Tamar field offshore Israel (149.7 km).

Offshore structures for oil and gas production have, in general, some of the components provided in the list below:

- Facilities for drilling and full intervention. This includes drilling tower, BOP, drilling floor, mud package, cementing pumps, storage deck for drill pipes and tubulars, drilling risers.
- Facilities for light well intervention.
- Processing facilities: separator trains for primary oil, gas and water separation, gas processing train, water processing train.
- Gas injection system
- Gas compression units for pipeline transport
- Water injection system
- Living quarters
- Helideck.
- Power generation.
- Flare system.
- Utilities (hydraulic power fluid, compressed air, drinking water unit, air condition system, ventilation and heating system)
- Bay for wellheads and christmas trees
- Production manifolds
- Oil storage
- Facilities for oil offloading
- Control system
- Monitoring system
- System for storage, injection and recovery of production chemicals (wax, scale, hydrate or corrosion inhibitors)
- Repair workshop

Not every offshore production structure has all elements mentioned on the list. The required functionality will vary depending on the type and processing capacity required for reservoir fluids, number of wells required, the development plan and future modifications to be made, the architecture of the production system, among others. It is also not uncommon to have two structures or more in the field with complementary functionality.

Figure 6-1 shows some common types of marine structures that are typically used for offshore oil and gas exploitation classified under two main categories: Bottom-supported or floating.
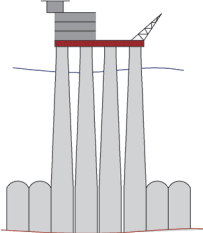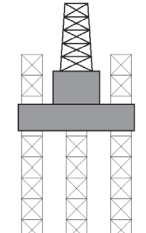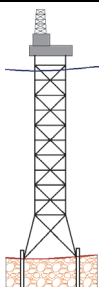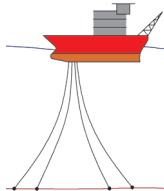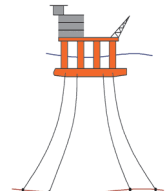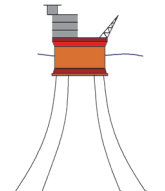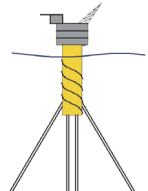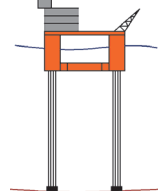
	Fixed			Compliant
BOTTOM-SUPPORTED	Jacket	Gravity-Based Structure	Jack-up	Compliant tower
	Neutrally buoyant			Positively buoyant
FLOATING	Ship FPSO	Semi-Sub	Sevan FPSO	Spar Tension Leg Platform (TLP)

FIGURE 6-1. SOME COMMON MARINE STRUCTURES FOR OIL AND GAS EXPLOITATION

Bottom-supported structures display reduced movement in the lateral and vertical direction. As the name indicates, most of the weight and the environmental loads on the structure are transferred to the seabed soil. Compliant towers have some lateral movement because they are allowed to rotate about their base.

Floating structures keep above the water level due to buoyancy and have relevant movement in the lateral and vertical direction due to environmental loads such as wind, current and waves. They are commonly moored to avoid drifting excessively with free hanging lines (steel catenary, Figure 6-2a), with pre-tensioned lines (taut, Figure 6-2b) or a combination of both. The buoyancy is controlled actively with ballast depending on the amount of fluids stored onboard.
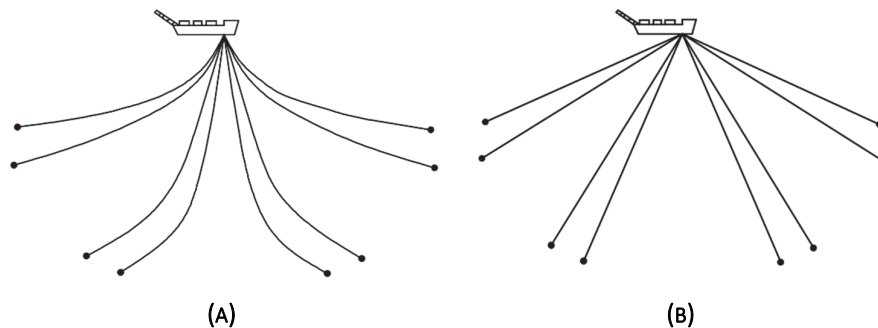
FIGURE 6-2. A) CATENARY MOORING, B) TAUT MOORING. (ADAPTED FROM CHAKRABARTI[6-5])

Naturally buoyant structures are usually subjected to substantial movement in the vertical and lateral directions. Spars, however, have significantly less movement (around 3 m of vertical stroke) because a big part of the hull is submerged (deep draft).

Positively buoyed structures are moored vertically and keep a pre-fix tension level. Whenever external loads try to displace it, the mooring lines create a lateral tension that brings the structure back in place. The vertical motion is therefore limited, but they are subjected to some displacement in the lateral direction.

6.1. SELECTION OF PROPER MARINE STRUCTURE

The selection of the marine structure to employ depends on multiple factors such as water depth, marine loads, reservoir structure, soil conditions, future development plans, well artificial lift, among others. Some of these factors will be described in more detail next.

6.1.1. WATER DEPTH

Figure 6-3 shows the water depth range of the most common offshore structures for hydrocarbon production. For shallow water depths (<450 m) the preferred and most economical option is usually a fixed structure such as steel jacket or Gravity Based structure. For medium to deep waters, floating structures are preferred such as TLPs, SPARs, FPSOs and Semi-Subs. For ultra-deep waters, FPSOs and Spars are more commonly used.
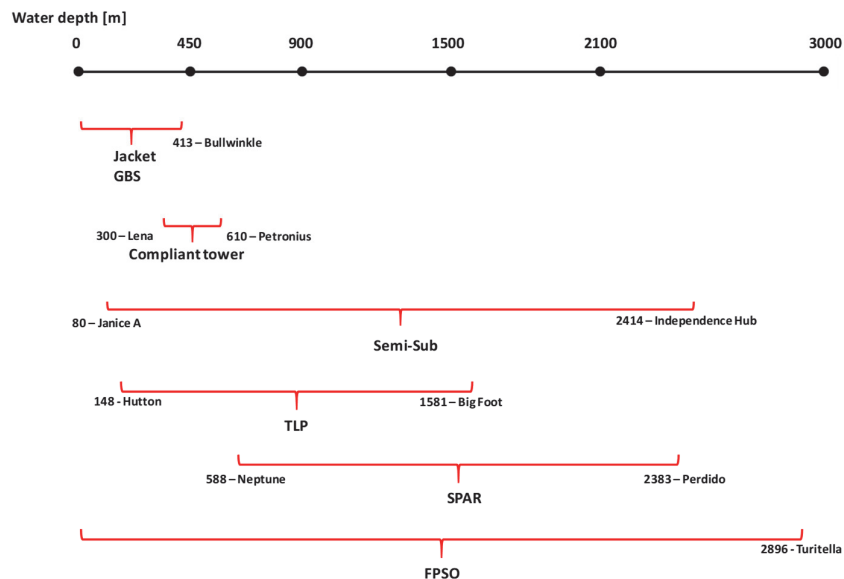
FIGURE 6-3. WATER DEPTH RANGE OF THE MOST COMMON OFFSHORE STRUCTURES FOR HYDROCARBON PRODUCTION

6.1.2. LOCATION OF THE CHRISTMAS TREE

There are two main alternatives where to place the well trees: above (dry), or below (wet) the waterline. This has a direct effect on the type of offshore structure to employ because only bottom-supported structures, TLPs and spars have a low enough motion range that is suitable for having dry trees. FPSOs and semi-subs use typically subsea wells (wet trees), the production is usually comingled with flowlines at the seabed and transported with risers to the deck. Field developments might employ only dry trees, only wet trees of a combination of both.

COMPLETION BITE: WELLHEAD ARCHITECTURE

The wellhead has the following main functions:

- Provides structural support (suspension point) for all casings and tubing strings. It transfers all loads to the ground through the conductor.

- It seals off each annulus at the top (at the bottom such seal is achieved by cementing). This is to avoid leakages and to avoid that an outer casing, of a smaller pressure rating, will be exposed to full reservoir pressure and therefore fail.
- Provide a connection point (interface) with the BOP and the Christmas tree.
- Provide annulus access and monitoring.

The procedure to deploy a wellhead during onshore drilling operations is described next. The focus is primarily on the wellhead thus some details about the drilling process are omitted. The mechanical details of wellhead components are simplified for clarity.

1. Dig the cellar, drill the conductor hole (typically 36 in), run the conductor (typically 30 in and length 40 m-120 m) and cement it. Cut the conductor to the desired height (such that the production master valve will be easy to operate at ground level).
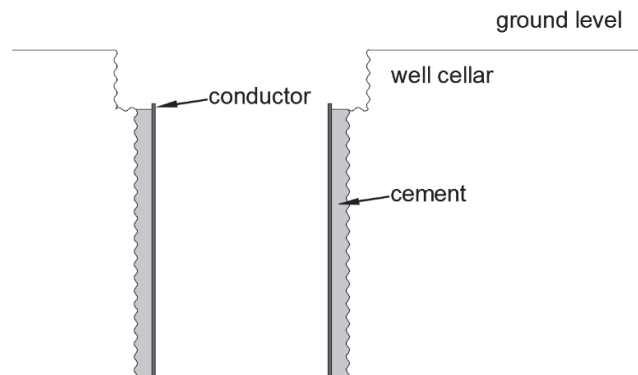
FIGURE 6-4. DEPLOYMENT OF THE CONDUCTOR

2. The BOP is placed, the surface casing hole is drilled (typically 24 in), the surface casing is run (typically 20 in) and cemented. The well is plugged and the BOP is removed. A baseplate is installed to transfer all loads to the conductor and the casing head. The casing head is attached to the surface casing by welding, threaded or with slips.
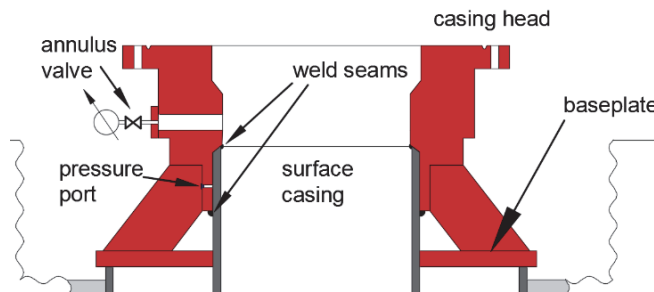
FIGURE 6-5. RUN OF THE SURFACE CASING AND CASING HEAD

The casing-casing head seal is positive-pressure tested from below with the pressure port.
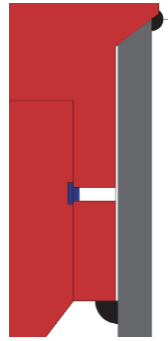
FIGURE 6-6. DETAILS OF THE PRESSURE PORT ON THE CASING HEAD TO MAKE THE PRESSURE TEST

3. The BOP is placed, the intermediate casing hole is drilled (typically 17 ½ in), the intermediate casing is run (typically 13 3/8 in) and cemented. The casing is hang on the casing head with the casing hanger (set of slips, wedge, elastomer and no-go shoulder).
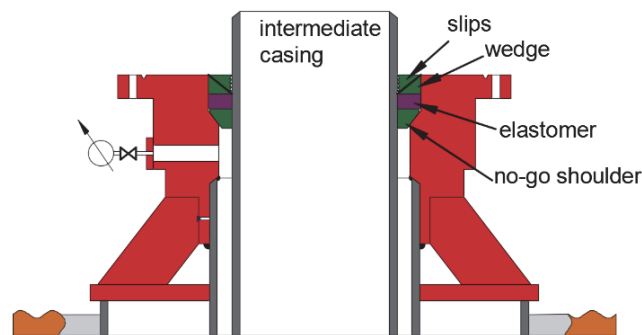
FIGURE 6-7. CASING HEAD WITH THE INTERMEDIATE CASING HANGED

The weight of the casing drives the slips down, presses the wedge that in turn squeezes the elastomer and activates the seal. Lockdown screws (that pass through the flange, not shown in the figure) are sometimes used to lock the upper part of the casing hanger and avoid unseating if the casing experiences thermal expansion.
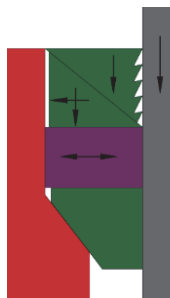
FIGURE 6-8. DETAILS OF THE CASING HANGER (SLIPS AND SEALS)

The casing hanger can also be screwed, instead of using slips (also known as mandrel-type hanger).

A negative pressure test is performed to ensure the casing hanger seal has been set properly.

4. The well is temporarily plugged, the BOP is removed and the casing spool for the intermediate casing is installed (flanged). The casing hanger seal and the gasket are positive-pressure tested from above using the pressure port.
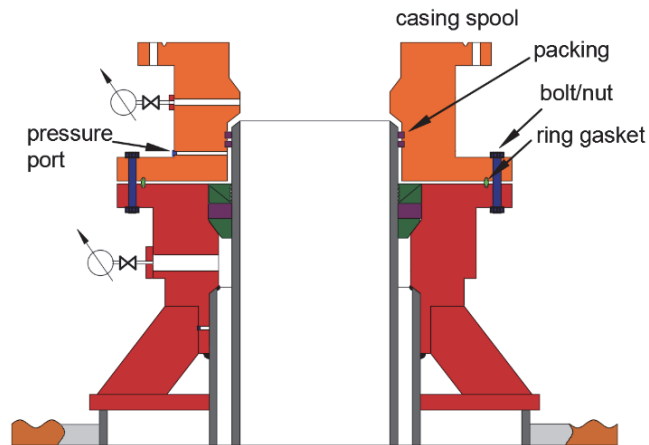
FIGURE 6-9. INSTALLATION OF THE CASING SPOOL TO THE CASING HEAD

Steps 3 and 4 are repeated as many times as number of intermediate casings are planned for the well.

5. After all casings are hanged on the wellhead, the tubing head is bolted to the last casing spool. The tubing is ran in hole and the tubing hanger is threaded to the last tubing joint. The tubing is then hanged on the tubing head. The seal of the tubing hanger is activated with the lockdown screws.

    Depending on the application, the tubing hanger may have a port for hydraulic lines (activation of SSSV, ICV), instrumentation line (pressure and temperature gauges), power lines (ESP), etc.
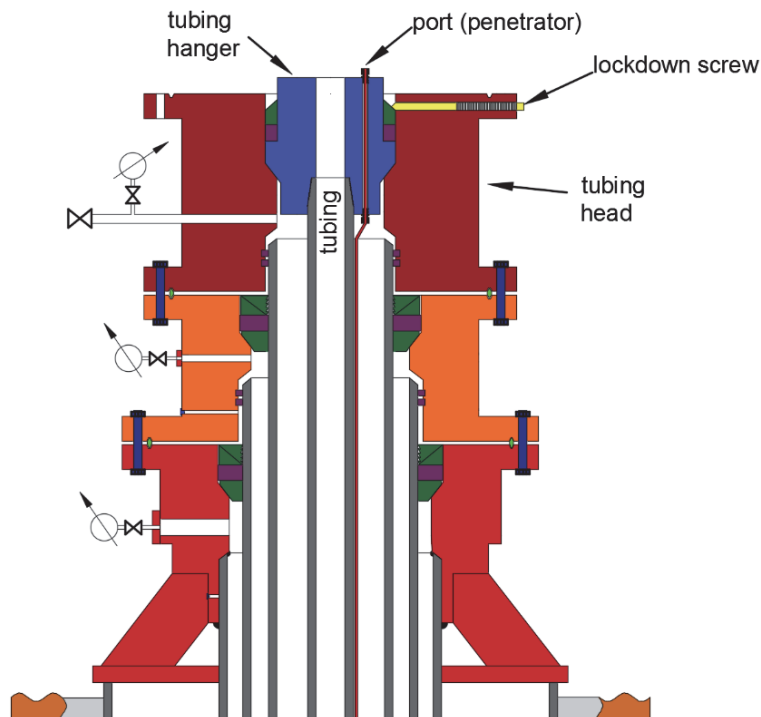
FIGURE 6-10. FINAL CONFIGURATION OF THE WELLHEAD

SAFETY STRATEGY FOR WELLS

·   There must be two pressure barriers between the reservoir and the surface (in series)

- No single event will compromise the two barriers at the same time (the barriers must be physically in different places)
- The two barriers must be functionally independent.
- The barriers must be always tested from the direction of flow. (or using a negative pressure test).
- In case of barrier failure, the barrier must be reinstated as soon as possible.

The selection of dry or wet trees is further influenced by the spread of the reservoir, the future drilling or well intervention plan and the water depth. For example, dry wells are preferred if it is feasible to produce a big part of the reservoir with wells drilled from a single location. Also, if regular well intervention or recompletion is expected during the life of the field. This is the case for example when wells are equipped with electric submersible pumps that have a limited lifetime (around 2 years). Contrastingly, subsea wells usually require intervention every 5 years.

Regarding water depth, dry tree systems have been used up to 1,700 m water depth.

If dry trees are used, the offshore structure has a well bay from where wells are drilled and completed and it is equipped with a drilling package. It is also possible to have structures with drilling package and subsea wells (e.g. Semi-Sub Njord in the Norwegian Continental Shelf) where the wells are located exactly beneath the structure. The size of the drilling package determines the drilling reach, a larger drilling package will allow to drill longer wells but the structure must be bigger and therefore more expensive.

In steel jackets and GBSs wells are drilled and completed in a similar manner as onshore, wellheads and Christmas trees are placed above the waterline. The well loads are supported by the soil and not the structure. In TLPs and Spars, the wellhead is located on the seabed and there is a flex joint connector and a riser. The riser ends further at the deck there is a secondary wellhead (with the tubing hanger) and the christmas tree. There is a dynamic tensioner or buoyancy cans that support the tree and the production riser (Figure 6-11a and Figure 6-11b).
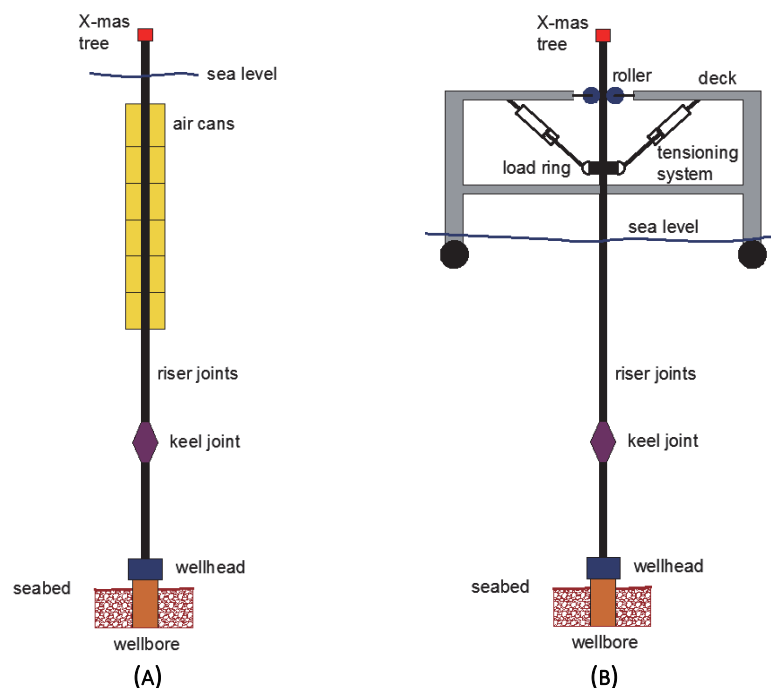
FIGURE 6-11. TOP TENSION SYSTEMS FOR PRODUCTION RISERS IN FLOATING STRUCTURES (ADAPTED FROM CHAKRABARTI[6-6])

Other considerations to take into account are:

· Dry well structures have usually a limited number of well slots available due to space constraints and load capacity. This makes the system less flexible for future expansion (infill drilling).
· Systems with subsea wells require special handling regarding flow assurance, to ensure the uninterrupted transport of hydrocarbons in the flowlines from the seabed to the facilities.
· In systems with subsea wells, production can usually occur as soon as the facilities are commissioned. New wells are tied-in to the system as they become available.
· Fiscal metering requirements might affect the type of well to use. If the only test method allowed is using a gravity vessel, then platform wells might be a better choice to avoid having several risers from subsea wells.

6.1.3. OIL STORAGE

While gas is typically reinjected into the formation or sent through a transportation pipeline, oil is usually transported from the field to the market using shuttle tankers. Sometimes it is desirable to store crude temporarily on site to avoid stopping production in case of delays in the tankers' trips due to external factors (e.g. harsh weather conditions, remote locations). Table 6-1 shows the storage capacities (qualitative) of the most common offshore structures used for hydrocarbon production.

TABLE 6-1. QUALITATIVE STORAGE CAPACITY OF COMMON OFFSHORE STRUCTURES

No or limited storage	Steel Jackets, Semi-subs, TLPs, Spars[33]
Medium - Large storage (up to 2.5000.000 STB)	FPSOs, GBS

6.1.4. MARINE LOADS ON THE OFFSHORE STRUCTURE

Offshore structures are subjected to 3 main types of external loads: wind, waves and currents. These three loads usually fluctuate with time and induce movements on the structure.
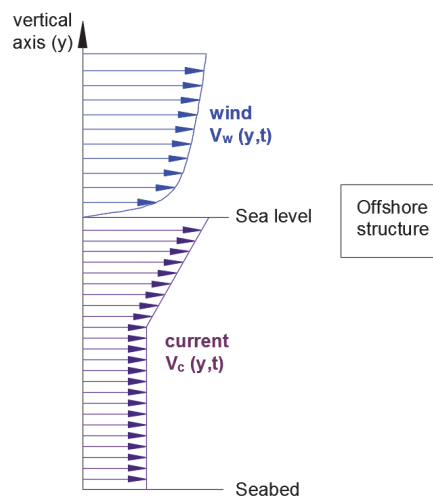
FIGURE 6-12. WIND AND CURRENT LOADS ON AN OFFSHORE STRUCTURE

---

[33] The Aasta Hansteen spar is the only spar up to date that has liquid (condensate) storing capacity of 150,000 STB.

The types of movement exhibited by an offshore structure can be roughly classified depending if they are floating or bottom-supported. Floating structures display boat-like motion with heave, yaw, sway, pitch, roll and surge (Figure 6-13a). Bottom fixed structures usually display deflections along its height similar to a long bar recessed into the seabed (Figure 6-13b).
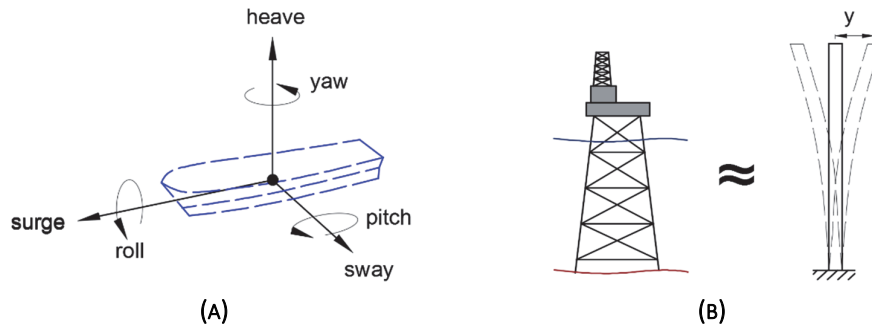
FIGURE 6-13. EXAMPLES OF TYPICAL MOVEMENTS EXHIBITED BY OFFSHORE STRUCTURES

During the design and selection process of the offshore structure displacement and stresses must be calculated based on the transient forces caused by wind, waves and currents. Some other considerations are:

- To determine the optimal location of flare of processing facilities to avoid fumes reaching the structure considering preferential wind directions.
- To determine required deck elevation to avoid waves reaching facilities (usually based on a 100-year wave).

The computation of displacement and stresses with time in such structures is done typically using numerical models (and often validated with scaled experimental prototypes). Forces are calculated from wave, wind and current loads and applied on the structure. Due to the variability of these loads, there are usually three main design approaches:

- **Design wave:** perform the analysis using the 100-year significant wave height ($H_{S,100}$) and a suitable range of wave periods. If more accurate estimates are not available, the Norwegian standard NORSOK N-003 suggests to take $H_{S,100}$ = *1.9 H_S* and vary the wave period between $\sqrt{6.5 \cdot H_{S,100}} \leq T \leq \sqrt{11 \cdot H_{S,100}}$
- **Short term design:** perform the analysis for a 100-year storm of specified duration (3-6 h) with an associated frequency spectrum. This is usually done to predict dynamic loads and stresses on critical load-bearing components.
- **Long term design:** This analysis takes into account the long-term varying weather conditions. This is important for fatigue design.

Resulting movement and stresses are time-varying thus also must be analyzed statistically.

Every offshore structure has a "natural frequency" value that depends, simply put, on their weight, flexibility and damping characteristics. If the structure is excited by external forces with a frequency that coincides with the natural frequency, it will exhibit maximum amplitudes (a phenomenon called resonance). Correspondingly, maximum amplitudes usually cause maximum loads and stresses on the structure thus most be avoided. This is a phenomenon that occurs for all relevant movements the structure might have (described in Figure 6-13).

A factor that is typically used in marine engineering is the Response Amplitude Operator (RAO). This value gives the relationship between the amplitude of the response and the amplitude of the excitation for a range of frequencies of the excitation force. As an example, consider the Heave RAO of a Sevan-type FPSO presented

in Figure 6-14. The RAO gives the ratio of the amplitude in vessel heave by the wave amplitude for a range of excitations periods. There is a very clear peak, around an 11 s period where the heave response is greatest.
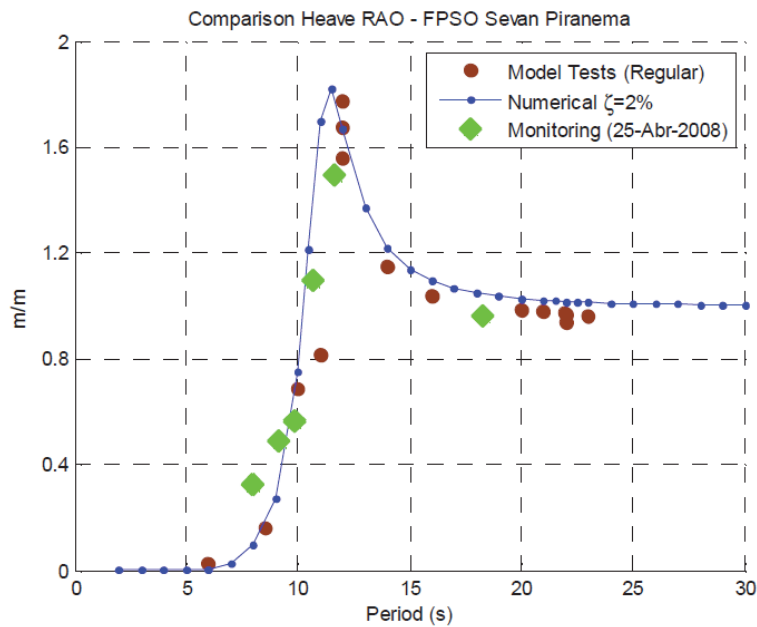
FIGURE 6-14. HEAVE RAO OF A SEVAN FPSO (TAKEN FROM SAAD ET AL. [6-7])

Figure 6-15 shows the natural periods of some offshore structures and the period range of some environmental loads. Structures might be subjected to resonance if these two values coincide.
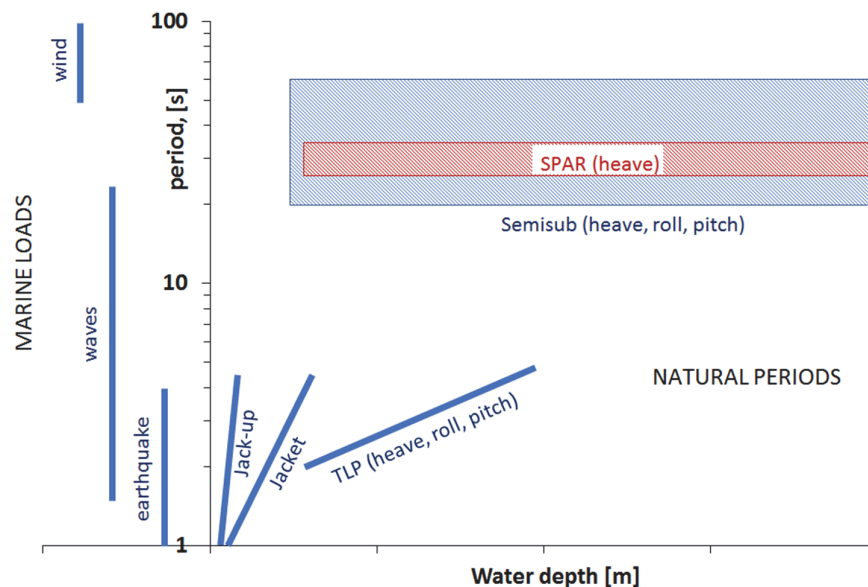
FIGURE 6-15. ILLUSTRATIVE FIGURE INDICATING NATURAL PERIODS OF SOME OFFSHORE STRUCTURES AND EXCITATION PERIODS OF SOME ENVIRONMENTAL LOADS

6.1.   TREATMENT OF WIND, WAVES AND CURRENTS

Wind and current consist of flow velocity profiles along the vertical direction impacting on the structure (V_W and V_C in Figure 6-12). The magnitude of the velocity usually fluctuates in time (currents typically fluctuate

with a period of hours and wind with a period between seconds and a minute). There are also some preferential directions that exhibit stronger magnitudes than others (as shown in Figure 6-16 for wind).
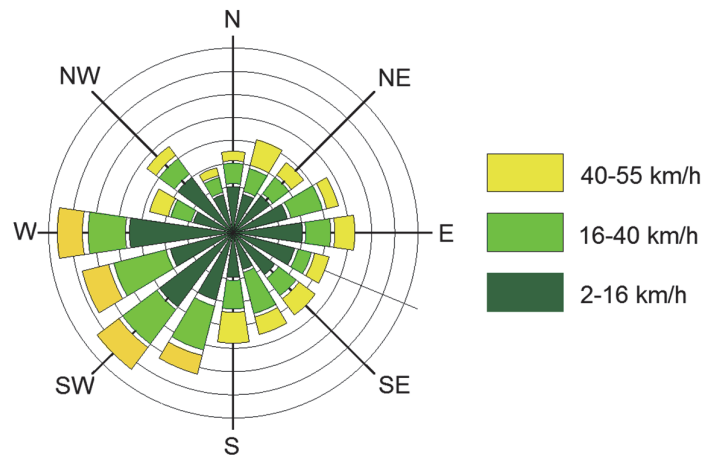
FIGURE 6-16. WIND ROSE, (ADAPTED FROM HTTPS://SUSTAINABILITYWORKSHOP.AUTODESK.COM/BUILDINGS/WIND-ROSE-DIAGRAMS)

During the design process of offshore structures, wind and currents are usually considered time invariant. Wind is considered uniform while the variability of current with depth is usually accounted for. The value used for design is the hundred-year value (value that on average is met or exceeded only once in a hundred years for a given location). An exception to this methodology is floating structures, where wind might have a more relevant effect and its variability must be taken into account.

Waves are fundamentally variations of the sea level in space and time caused by wind. Figure 6-17 shows a wave time profile that displays a random behavior.
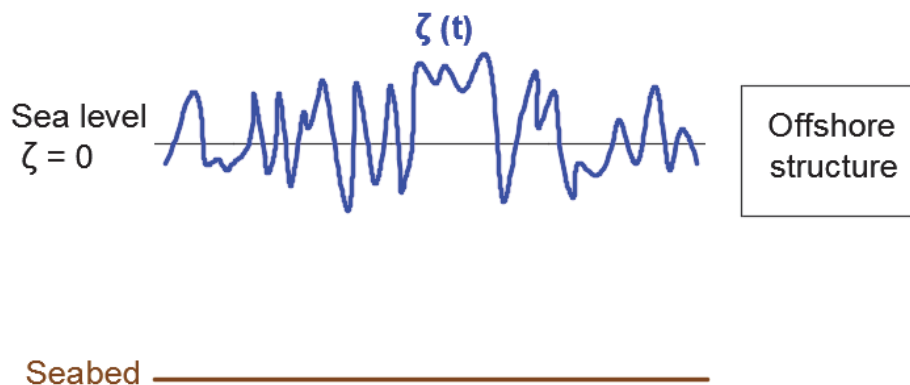
FIGURE 6-17. TWO-DIMENSIONAL RANDOM WAVE TIME PROFILE

Following Fourier's theorem, this complex wave signal can be decomposed as the sum of "N" sine or cosine functions each with an associated specific amplitude (ζ_{ai}), frequency (ω_i) and angle shift (ε_i). Please note that the frequency is the inverse of the period.
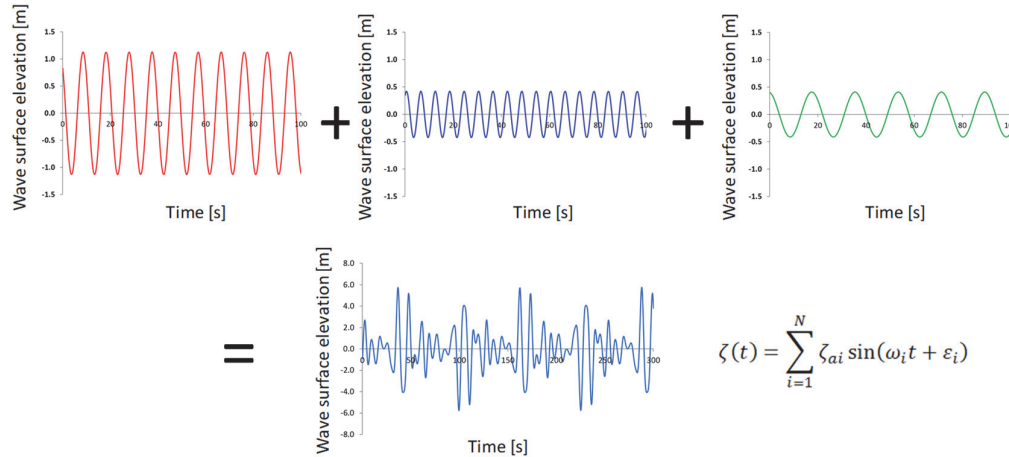
FIGURE 6-18. CONTRIBUTION OF INDIVIDUAL REGULAR WAVES

Information about the components that make up a particular signal is commonly displayed in a wave energy spectrum (Figure 6-19a). The spectrum is the result of applying a Fast Fourier Transform (FFT) to the wave signal and displays wave energy spectrum (S_ζ) vs frequency (ω). For particular case of a regular wave made of a single frequency component, the spectrum will display just a delta in the corresponding frequency. Common spectrum formulas are Pierson-Moskowitz (P-M) and JONSWAP.
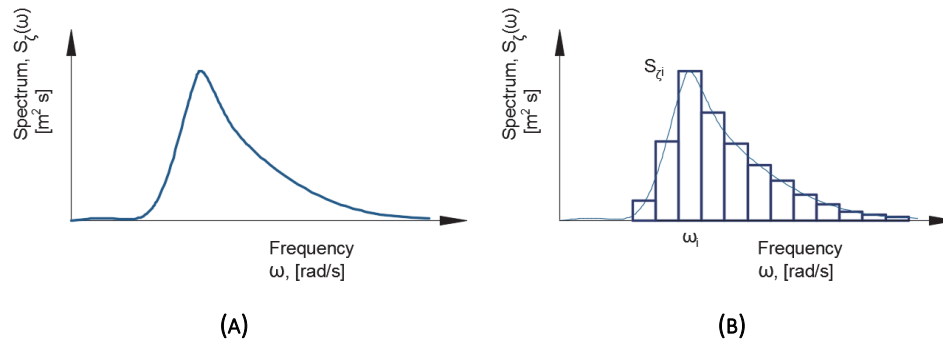
FIGURE 6-19. WAVE ENERGY SPECTRUM A) CONTINUOUS AND B) DISCRETIZED

The spectrum is often presented in a discretized manner (Figure 6-19b) where the frequency axis is split in segments (of width $\Delta\omega_i$) and each segment has an associated frequency value (ω_i) and wave energy value ($S_{\zeta i}$). The relationship between wave energy spectrum and wave elevation is shown in Eq. 6-1.

$$\varsigma_i = \sqrt{2 \cdot S_{\varsigma_i} \cdot \Delta\omega_i}$$

EQ. 6-1

In short periods of time (typically 3 hours, called "sea state") the spread in frequency is usually relatively low (there is one dominant period called the "mean" period T_Z) such that it is practically considered constant. The wave elevation is assumed to follow a Gaussian type probability density function (Figure 6-20a) and the wave height (H, distance between consecutive peak and valley) a Rayleigh distribution (Figure 6-20b).
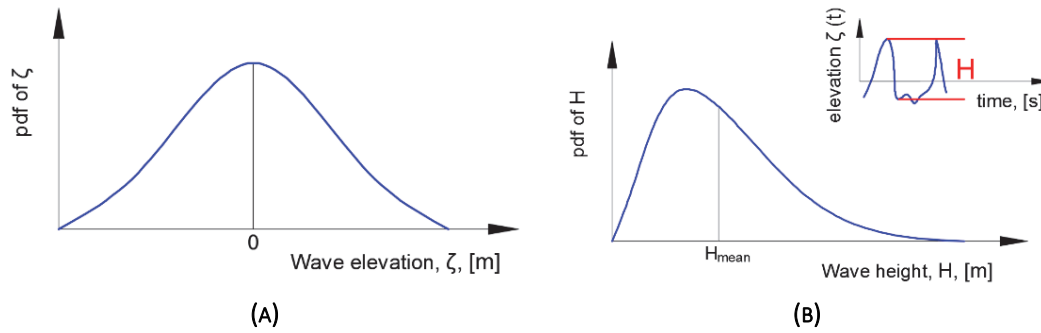
FIGURE 6-20. SHORT TERM PROBABILITY DENSITY FUNCTION OF WAVE ELEVATION (A) AND HEIGHT (B)

A parameter that is often used is the significant wave height H_s, defined as the average of the wave height in the range between the maximum wave height *(H_max)* and the wave height value for which 1/3 of all wave heights are greater or equal than it *(H_{1/3})*.

In design of offshore structures, it is desired to have accurate values of the expected wave characteristics during their lifetime (long term statistics of ocean waves). Historic wind and wave data is typically gathered with instrumentation located in weather and merchant ships, buoys, existing offshore structures, etc. To establish statistical information of the sea state parameters, waves have to be measured for at least a couple of years.

In such long periods of time, there will be a variation of the significant wave height and the mean period. The data is often presented in a scatter diagram (an example shown in Figure 6-21, gathered during a period of 15 years) that shows number of occurrences (Sea states) for a particular combination of significant wave height and mean period. The mean period is also called spectral peak period (T_p). The particular case shown, the sea displays a wave height between 1-14 m and a period between 3-20 s. The color red indicates combinations that occurred only a few times, yellow medium and green combinations that were more frequent. Generally speaking, in storms waves exhibit periods between 5-25 s.

Hs [m]	0-3	3-4	4-5	5-6	6-7	7-8	8-9	9-10	10-11	11-12	12-13	13-14	14-15	15-16	16-17	17-18	18-19	19-20	20-21	21-22	22-23	23-24	24-25	Sum
0-1	15	290	1367	2876	3716	3527	2734	1849	1138	656	362	192	101	52	26	13	7	3	2	1	0	0	0	18927
1-2	1	81	1153	5308	12083	17323	18143	15262	10980	7053	4169	2316	1229	631	315	155	75	36	17	8	4	5	1	96348
2-3	0	2	94	1050	4532	10304	15020	15953	13457	9752	5991	3403	1795	894	426	197	88	39	17	7	3	1	1	83026
3-4	0	0	2	72	686	2782	6171	8847	9189	7493	5082	2991	1577	762	345	148	61	24	9	4	1	0	0	46246
4-5	0	0	0	2	51	433	1645	3495	4807	4750	3638	2286	1229	584	251	100	37	13	5	1	0	0	0	23327
5-6	0	0	0	0	2	39	294	1037	2069	2664	2440	1709	968	463	193	72	25	8	2	1	0	0	0	11986
6-7	0	0	0	0	0	2	32	215	692	1264	1485	1228	767	382	159	57	18	5	1	0	0	0	0	6307
7-8	0	0	0	0	0	0	2	27	157	447	730	762	555	302	130	46	14	4	1	0	0	0	0	3177
8-9	0	0	0	0	0	0	0	2	23	112	276	392	355	223	104	38	11	3	1	0	0	0	0	1540
9-10	0	0	0	0	0	0	0	0	2	19	77	160	192	148	79	31	9	2	0	0	0	0	0	719
10-11	0	0	0	0	0	0	0	0	0	2	16	50	85	85	55	24	8	2	0	0	0	0	0	327
11-12	0	0	0	0	0	0	0	0	0	0	2	12	29	40	33	18	7	2	0	0	0	0	0	143
12-13	0	0	0	0	0	0	0	0	0	0	0	2	8	15	17	12	5	2	0	0	0	0	0	61
13-14	0	0	0	0	0	0	0	0	0	0	0	0	2	5	7	6	4	1	0	0	0	0	0	25
14-15	0	0	0	0	0	0	0	0	0	0	0	0	0	1	2	3	2	1	0	0	0	0	0	9
15-16	0	0	0	0	0	0	0	0	0	0	0	0	0	0	1	1	1	1	0	0	0	0	0	4
16-17	0	0	0	0	0	0	0	0	0	0	0	0	0	0	0	0	0	0	0	0	0	0	0	0
17-18	0	0	0	0	0	0	0	0	0	0	0	0	0	0	0	0	0	0	0	0	0	0	0	0
Sum	16	373	2616	9308	21070	34410	44041	46687	42514	34212	24268	15503	8892	4587	2143	921	372	146	55	22	8	6	2	292172

Spectral Peak period (T_p) [s]

FIGURE 6-21. SCATTER DIAGRAM OF LONG TERM WAVE STATISTICS

A number that is typically reported and used during the design process of offshore structures is the significant wave height that might be reached or exceeded during a period of 100 years ($H_{S,100}$). As data hasn't been collected for such long periods of time, an extrapolation of the wave data collected in the scatter diagram is performed. The extrapolation is done using a Semi-logarithmic distribution that relates the significant wave height versus the chance of exceedance.

$$\log\bigl(P(H)\bigr) = \frac{1}{a} \cdot H$$

<div align="right">EQ. 6-2</div>

The 100-year period is constituted by 292,000 "sea states" of 3 h duration (where the significant wave height and the period can be considered constant). The 100-year wave occurs is reached or exceeded only once, thus its probability is 1/292,000 i.e. 3.40×10^{-6}.

The data shown in Figure 6-21 has been gathered during a period of 15 years (probability of occurrence of a 15 years wave is 2.3×10^{-5}). If one particular spectral period range is chosen (e.g. 18-19) then the probability density of the wave height and the cumulative distribution can be computed. The significant wave height that will likely occur once in 15 years is then can be read from the cumulative distribution (16.5 m).
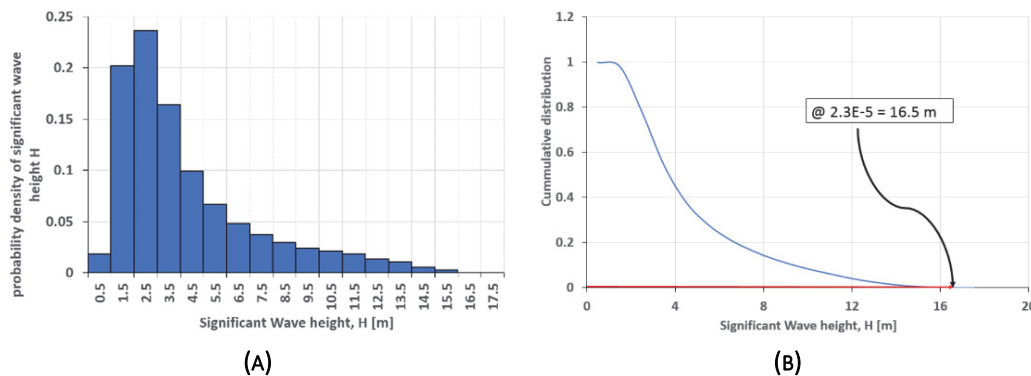
FIGURE 6-22. PDF AND CD OF SIGNIFICANT WAVE HEIGHT FOR SPECTRAL PERIOD RANGE 18-19 S

Then, it is possible to compute *a* from Eq. 6-2 (for the particular case *a = -3.5531*). The significant wave height of 100 years is then computed with Eq. 6-2 and a probability of 3.40×10^{-6}. The 100-year wave obtained is 19.4 m for the period range 18-19 s for the particular case. This value is often used to determine the required distance between the deck and the sea level.

REFERENCES

[6-1] Petrowiki. *Offshore and Subsea Facilities*. SPE publications. Retrieved from http://petrowiki.org/Offshore_and_subsea_facilities, on Jan 9th, 2017.

[6-2] Petrowiki. *Compliant and Floating systems*. SPE publications. Retrieved from http://petrowiki.org/Compliant_and_floating_systems, on Jan 9th, 2017.

[6-3] Offshore magazine. *2015 Deepwater Solutions and Records for Concept Selection*. Poster. Retrieved from http://www.offshore-mag.com/content/dam/offshore/print-articles/volume-75/05/0515-DeepwaterPoster040815ADS.pdf, on Jan 9th, 2017.

[6-4] Stell, J. *Wet tree vs. dry tree criteria*. OE Offshore engineer. Retrieved from http://www.oedigital.com/component/k2/item/9601-wet-tree-vs-dry-tree-criteria, on Jan 9th, 2017.

[6-5] Chakrabarti, S. (2005). *Handbook of Offshore Engineering*. Volume I. Elsevier.

[6-6] Chakrabarti, S. (2005). *Handbook of Offshore Engineering*. Volume II. Elsevier.

[6-7] Saad, A. C., Vilain, L., Loureiro, R., Brandao, R.M., Filho, R.Z. *Motion behavior of the Mono-Column FPSO Sevan Piranema in Brazilian Waters*. OTC paper 20139. Offshore Technology Conference, May, 2009.

7. FLOW ASSURANCE MANAGEMENT IN PRODUCTION SYSTEMS

Flow assurance consists in ensuring uninterrupted flow of hydrocarbon streams from the reservoir to the point of sale according to production plan. Flow assurance is particularly relevant for deep subsea systems with relatively long transportation distances (5-150 km) and low surrounding temperatures. If there is a problem intervention and remediation, these activities usually must be done remotely and are time consuming and expensive.

Flow assurance focuses on three main aspects:

1. Avoid flow restrictions (excessive pressure drop, blockage or intermittent production).
2. Safeguard the structural integrity of parts of the production system from damages caused by internal flow.
3. Maintain the functionality and operability of components in the production system.

There are multiple issues that are typically addressed in flow assurance:

· Formation and deposition of wax.
· Formation of hydrates.
· Formation and accumulation of scale
· Flow induced vibrations (FIV)
· Asphaltene formation and deposition
· Slugging
· Erosion
· Emulsion
· Corrosion
· Pressure surges during shutdown and startup.
· Naphtenates
· Foaming
· Liquid loading

Figure 7-1 shows where these issues usually occur in the production system.
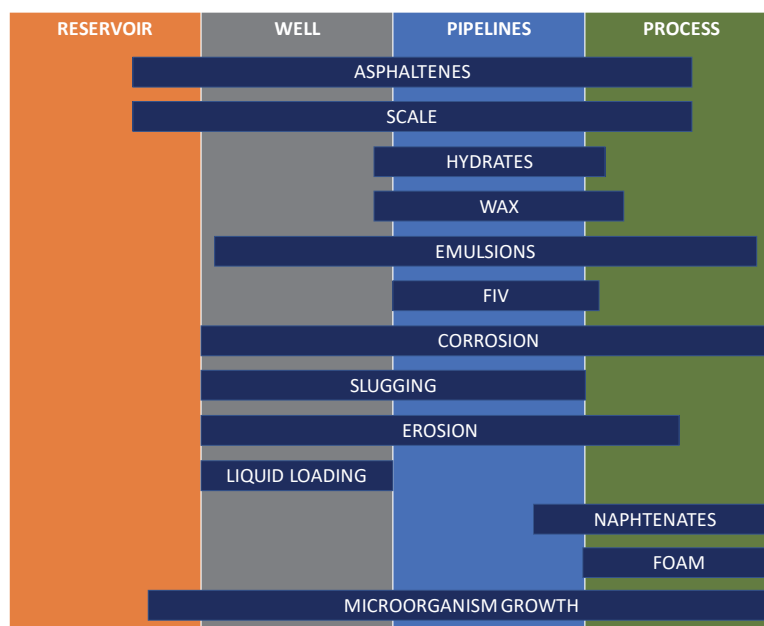
FIGURE 7-1. FLOW ASSURANCE PROBLEMS AND THEIR TYPICAL LOCATION IN THE PRODUCTION SYSTEM

An overview of some of these flow assurance issues is provided next.

7.1.   HYDRATES

Hydrates are solid substances where water molecules (in liquid phase) form a cage-like structure that hosts small (< 9 Å diameter) molecules (Figure 7-2). The small molecules are usually methane, ethane, propane, butane, carbon dioxide, nitrogen. The cage-type structure is formed due to hydrogen bonding of water molecules (the water molecule tends to spacially create two positives and a negative pole).

| (A) | (B) |
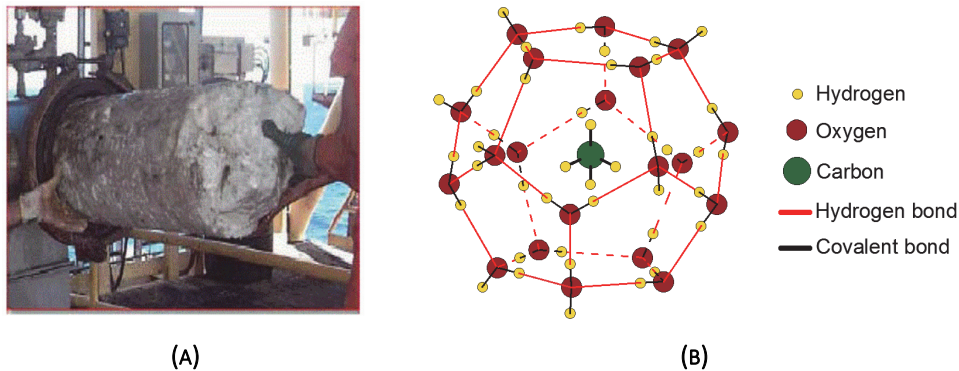
FIGURE 7-2. A) APPEARANCE OF A HYDRATE PLUG (PHOTO TAKEN FROM SCHROEDER ET AL[7-1]), B) MOLECULAR STRUCTURE OF A METHANE HYDRATE

Hydrates contains a much higher proportion of water than the hydrocarbon component. For example, a methane hydrate (called methane clathrate) with molecular formula $4CH_4 \cdot 23H_2O$ (M_W = 478 kmol/kg) has a molar proportion of 85% (23/27) water and 15% (4/27) methane.

However, this does not necessarily indicate that they contain small amounts of gas. For example, one cubic meter of methane clathrate (of an approximate density of 900 kg/m^3) contains 1.88 (900/478) kmol of hydrate, of which there are 7.53 (1.88 x 4) kmol of methane. 7.53 kmol of methane at standard conditions correspond to 178.4 Sm^3! ($V_{SC} = n_{moles} \cdot R \cdot T_{SC}/p_{SC}$). For a cubic meter to contain the same amount of gaseous methane at standard temperature, it would have to be compressed at 180.4 bara (*p= 7.53 kmol·R·T$_{SC}$/1 m^3*).

Hydrates form only if **ALL** following ingredients are present:

· Free water (in liquid phase)
· Small hydrocarbon molecules
· Particular range of pressure and temperature.

An example of the hydrate formation region is shown in Figure 7-3. The actual line depends mainly on the fluid composition, but, as a rule of thumb, it happens at high pressure and low temperatures. For example, at a pressure of 12 bar, the hydrate formation temperature is 4 °C.
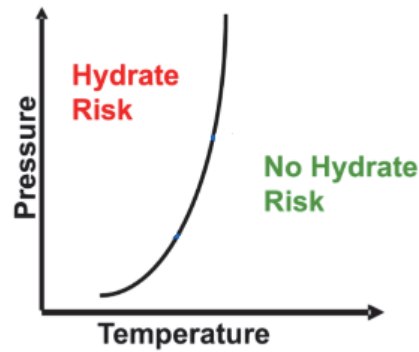
FIGURE 7-3. HYDRATE FORMATION REGION

The hydrate formation line can be predicted by empirical expressions (that are a function of the specific gravity of the gas) or using equilibrium calculations with an Equation of State. Hydrate equilibrium calculations resemble to Vapor Liquid equilibria by finding p and temperature conditions that make equal the chemical energy of the component in the hydrate phase and liquid and gas phases.

7.1.1. CONSEQUENCES

If the pressure and temperature of the fluid flowing along the production system falls inside the hydrate formation region, hydrates will start to form. Hydrates usually form at the liquid-gas interphase where free water and small hydrocarbon molecules are in contact. The mixing and turbulence of the flow further increases the contact between the two thus causing the formation of more hydrates. Hydrates then start to agglomerate until they eventually plug the pipe (Figure 7-4).
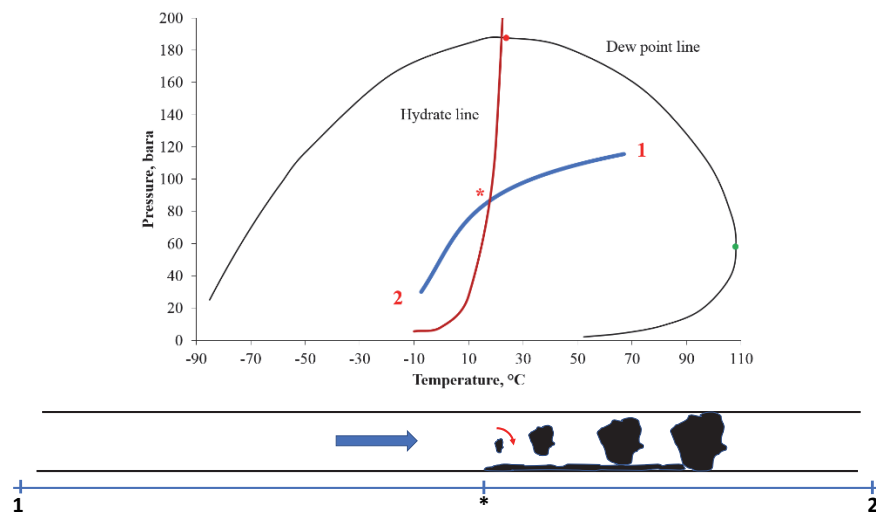
FIGURE 7-4. EVOLUTION OF P AND T OF THE FLUID WHEN FLOWING ALONG THE PRODUCTION SYSTEM

Hydrates can also form when the production is stopped and the stagnant fluid begins to cool by transferring heat with the environment.

7.1.2. MANAGEMENT

The traditional strategy to manage hydrates is to avoid their formation. There are two main techniques commonly used to prevent the formation of hydrates:

·   **Keep the fluid conditions out of the hydrate formation region.** This is done mainly by reducing the rate of temperature drop of the fluid (reducing the lateral spread of the blue line in Figure 7-4). This is achieved in practice by two methods: better insulation or electrical heating of the pipe.

Please note that insulation works effectively for a flowing system, but when production is stopped, usually some other control method must be used as the fluid will eventually cool down during a long period.

Electrical heating is usually not cost effective for long transportation distances.

·   **Reduce the hydrate formation region.** The equilibrium pressure and temperature of hydrate formation can be affected by adding liquid inhibitors (typically Mono-ethylene-glycol MEG, Tri-ethylene-glycol TEG or methanol MEOH) to the water phase. Inhibitors interfere with the formation of hydrogen bonds by keeping water molecules apart. As a consequence, the hydrate formation line will be shifted to the left (as shown in Figure 7-5).
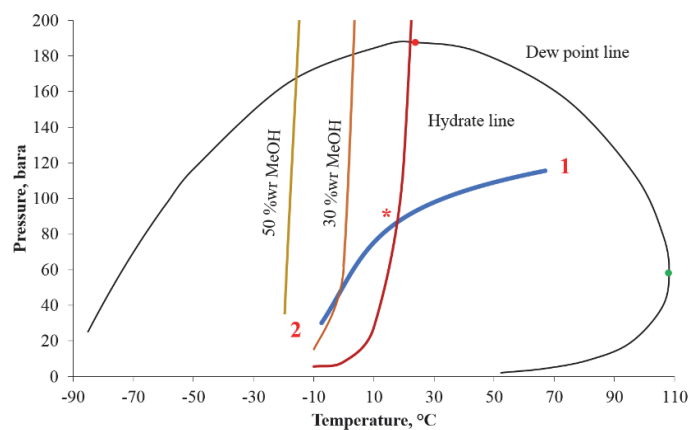
FIGURE 7-5. EFFECT OF INHIBITOR INJECTION ON THE HYDRATE LINE

Typical concentrations of inhibitors used are 30-60 in weight %. For example, the Snøhvit field has a Water Gas ratio of 6.00 x 10^{-6} Sm^3/Sm^3. The plateau production of the field is 20 MSm^3/d, thus it produces around 120 Sm^3/d of water, or, equivalently, 120,000 kg/d of water. If we assume that the inhibitor concentration used is 50 in weight %, then this gives 120,000 kg/d of MEG that must be continuously injected on the field. This represents a daily cost of 60,000 − 180,000 USD (assuming a MEG cost between 0.5 − 1.5 USD/kg). Therefore, MEG is usually reclaimed in the processing facilities.

The inhibitor must be present in the water phase for it to be effective, thus evaporation to the gas phase has to be taken into account when estimating the required amounts of inhibitor.

Inhibitors are also injected when preparing to shut down production, to make sure hydrates will not form due to the cooling of the fluid.

Figure 7-6 shows a flow schematic of a subsea production system highlighting the hydrate inhibitor injection system (in green color). The production system has 2 satellite wells, a manifold template, and two pipelines that transport reservoir fluids topside. The hydrate inhibitor is transported with an umbilical[34] from topside until the subsea distribution unit. In the subsea distribution unit, the hydrate inhibitor line in the umbilical is connected to a distribution manifold that is further connected to the wells with a separate flowline (if the distance is short) or with an umbilical.

---

[34] The umbilical is a flexible pipe-like structure that encloses other pipes that transport chemicals, hydraulic fluid to actuate valves, electrical cables, fiber optic lines, etc.
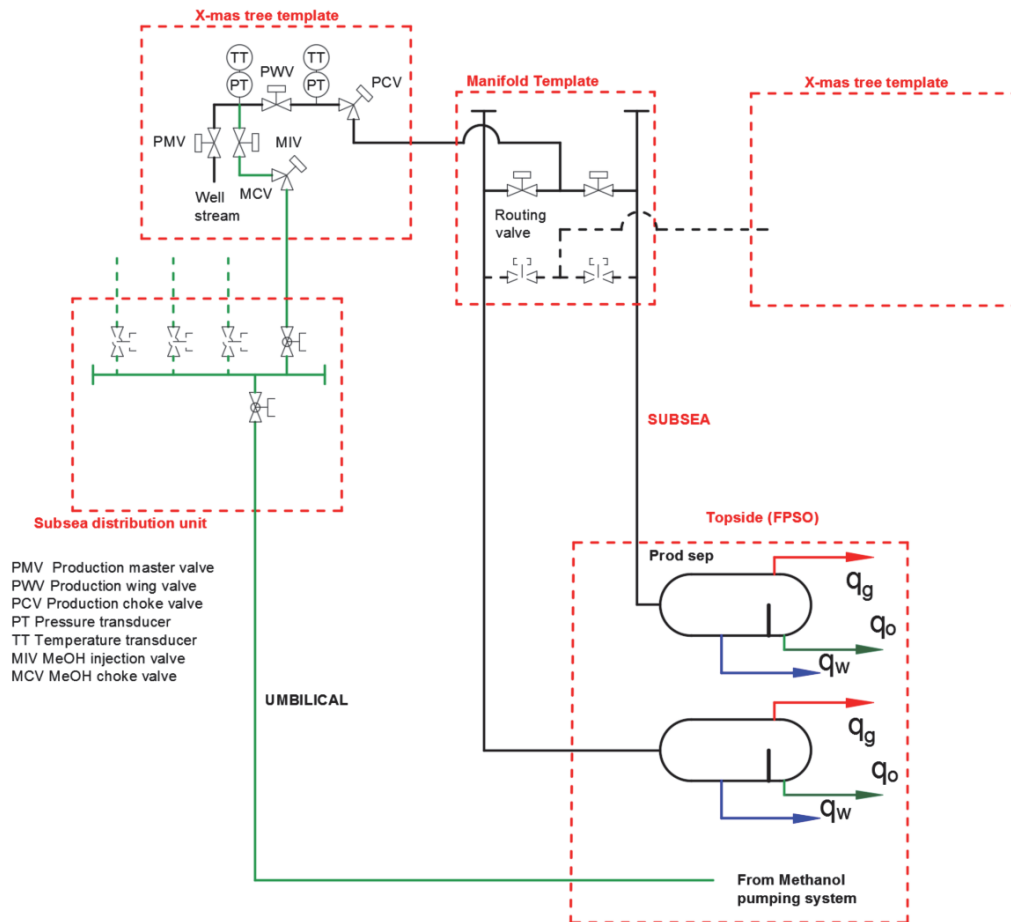
FIGURE 7-6. FLOW SCHEMATIC OF A SUBSEA PRODUCTION SYSTEM WITH HYDRATE INHIBITOR INJECTION SYSTEM

Figure 7-7 shows in more detail the pipe and cable splitting that occurs in the subsea distribution unit, the distribution manifold for the hydrate inhibitor and the isolation valves for each well (ROV operated). Figure 7-8 shows in more detail how is the hydrate inhibitor injection system integrated with the well tree.
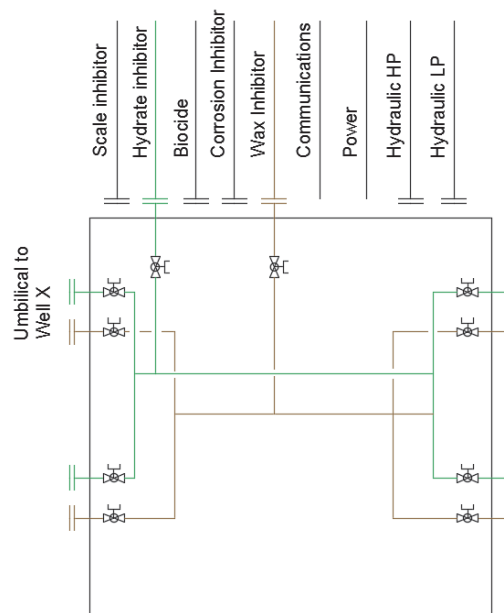
FIGURE 7-7. DETAILS OF A SUBSEA DISTRIBUTION UNIT.
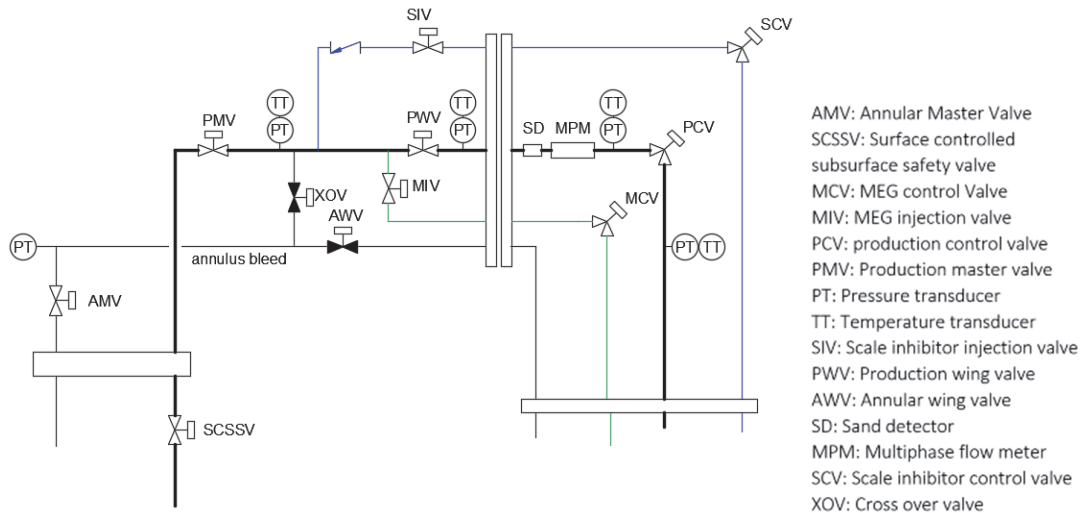
FIGURE 7-8. HYDRATE AND SCALE INHIBITOR INJECTION SYSTEM IN THE X-MAS TREE

In the last years, experts have proposed to use a less conservative hydrate control strategy where we allow hydrates to form but impede their agglomeration and carry the slurry together with the production fluids. This can be performed by injecting special types of chemicals, or by using cold flow. However, up to date there are limited field cases where this type of management is performed.

7.2.   SLUGGING

Slugging consists on intermittent flow of gas and liquid in the production system (Figure 7-9).
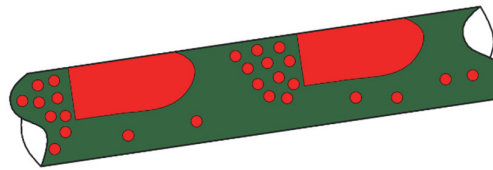
FIGURE 7-9. SLUG IN A PIPE SECTION

There are two main types of slugging:

· **Hydrodynamic slugging:** It occurs spontaneously at a particular combination of flow velocities of liquid and gas and it depends strongly on the fluid properties and pipe inclination. As an example, Figure 7-10 shows the flow pattern map for a horizontal pipe and certain fluid properties. There is a particular combination of operational velocities where the flow will arrange itself in a slug flow configuration.
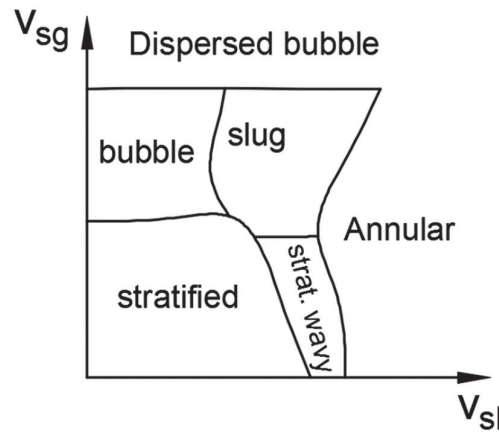
FIGURE 7-10. FLOW PATTERN MAP FOR A HORIZONTAL PIPE

- **Terrain slugging:** Terrain slugging is mainly due to cyclic accumulation of liquid in the production system (especially in lower points). This happens in undulating well trajectories, transportation flowlines with varying topology of the seabed and in risers.

An example of slugging in a s-shaped production riser is shown in Figure 7-11. Liquid accumulates in the lowest pipe section and blocks the flow of gas (a). The liquid level starts increasing and the gas pressure in the horizontal line also increases (b). Eventually, the liquid floods the second floor of the riser (c). Gas pressure increases until it is sufficient to flush out almost all the liquid in the riser (d).

(A)   (B)   (C)   (D)
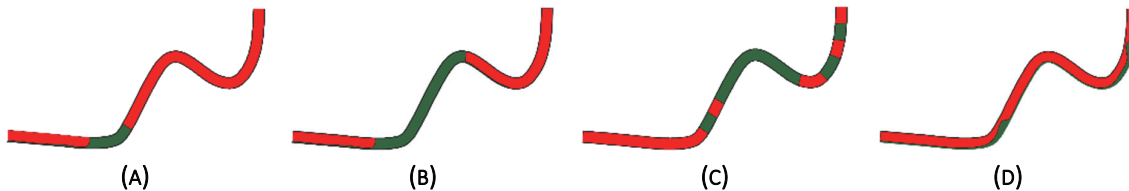
FIGURE 7-11. STAGES OF SEVERE SLUGGING IN AN S-SHAPED RISER

7.2.1. CONSEQUENCES

The main consequence of slugging is that production rates and pressures will fluctuate in time which is often detrimental to the proper operation of the downstream processing facilities. In gravity separators for example, a sudden inlet of liquid might increase significantly the liquid level, causing liquid carryover, activating the warnings for high liquid level and even triggering a shutdown alarm. The distance between the normal liquid level and the high alarm level should be big enough to accommodate the volume of the biggest liquid slug expected.

Slugging also causes vibration in flowlines, manifolds, risers which can develop in structural damages due to elevated stress levels and fatigue.

7.2.2. MANAGEMENT

Slugging can be, to some extent, predicted during the design phase of the field using commercial multiphase flow simulators such as LedaFlow, Olga and FlowManager. If it is detected and it has high severity (long slug lengths, frequencies that coincide with the natural frequency of the structure, relevant pressure fluctuations), potential solutions are to change the routing of the flowline, refill or dig some sections of the seabed that can cause liquid accumulation or changing the pipe diameter. Smaller pipe diameters increase the gas velocity,

increasing the drag of the gas on the liquid thus reducing the liquid deposition. However, too-small pipe diameters also cause higher pressure drops that reduce overall production rates.

If slugging is occurring in an existing production system, some approaches that have been used successfully in the past are to apply gas lift in the riser base or to use the topside choke to change dynamically the backpressure on the line and "control" the slug.

7.3. SCALING

Scaling is the precipitation of minerals compounds (constituted by Na, K, Mg, Ca, Ba, Sr, Fe, Cl) **from the produced water** and their deposition on pipe walls. Scale occurs when the solubility of the minerals in the water decreases due to changes in pressure and temperature, due to mixing of waters of different sources, injection of CO_2. Minerals usually deposit on surface areas that are rough or have irregularities (e.g. valve components).

FIGURE 7-12. SCALE ACCUMULATION IN CHOKE (IMAGE TAKEN FROM SANDENGEN[7-2])

There are two main types of scales that usually occur in production systems:

- **Carbonate scales.** These scales are formed when CO_2 dissolved in the water disassociates in carbonate ions CO_3^{-2} and join with some of the aforementioned minerals (typically calcite $CaCO_3$, Iron carbonate $FeCO_3$). Their precipitation is mainly due to reduction in pressure (due to flow in restrictions, valves, chokes) or increases in temperature. This type of scale can be removed with acid.
- **Sulphate scales:** These scales are formed by the sulphate ion SO_4^{-2} that is present in seawater (Barite $BaSO_4$, Gypsum $CaSO_4 \cdot 2H_2O$, Anhydrite $CaSO_4$, Celestite $SrSO_4$). It precipitates out of solution when waters from different sources are mixed (e.g. seawater used for injection and production water from the aquifer or formation). The pressure has little influence in the precipitation, but the increase in temperature can reduce further the solubility. This type of scale **must be** removed mechanically.

7.3.1. CONSEQUENCES

Scaling causes gradual blockage of the flow path and loss of functionality in production equipment (Subsurface safety valves, chokes).

7.3.2. MANAGEMENT

Studies are usually performed on the produced water to determine if it will be prone to form scale at the pressure and temperature conditions encountered in the production system. Moreover, special attention must be payed to situations where there is mixing of water from different sources, CO_2 injection.

Scaling is usually avoided by using chemicals (scale inhibitors) that attach themselves to the scale ions and impede growth. Coating can help to prevent deposition on the surfaces but when damaged (e.g. due to erosion) their effectivity is reduced dramatically.

If scale forms in a component of the production system, the removal technique depends on the type of scale. Carbonates can be removed by acid injection and sulphates can only be removed mechanically.

7.4.   EROSION

Erosion is the gradual damage and loss of material from the wall of components of the production system (valves, pipes, bends, etc. Figure 7-13) due to the repeated impingement of solid particles (sand) or droplets at high velocity.

FIGURE 7-13. EROSION DAMAGE IN A CAGE-TYPE CHOKE [SOURCE UNKNOWN)

7.4.1. CONSEQUENCES

Structural damage, vibration, leaks and corrosion (due to the removal of the protective coating).

7.4.2. MANAGEMENT

Erosion is usually accounted for in the field design phase. The design process sizes the equipment such that the velocities are below certain limit value that gives an acceptable erosional rate. These calculations usually consider the velocity of impingement, the angle of impingement, the concentration of solid particles and the wear resistance of the material.

There are some standards that give guidelines how to estimate erosive wear for common pipe components (e.g. DNV Recommended Practice RP O501). However, complex geometries usually require in-depth studies (e.g. using computational fluid dynamics, CFD) to estimate erosion-prone areas, fluid velocities, angle of impingement, etc. An example is shown in Figure 7-14.
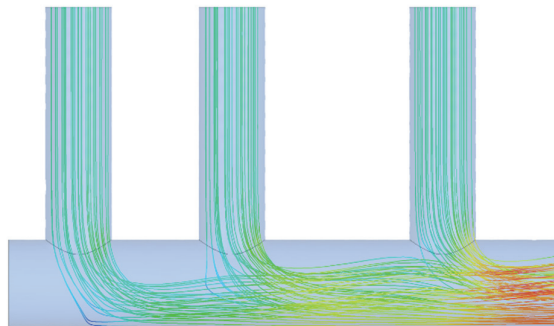
FIGURE 7-14. CFD SIMULATION OF EROSION IN A PRODUCTION HEADER

If erosion is detected in an existing production system then, when possible, components might be reevaluated and replaced with geometries that are less susceptible to erosion. Alternatively, if corrosion is due to excessive sand production from the reservoir, the only alternative is then reducing the well rate to limit sand production.

7.5. CORROSION

Corrosion is an electrochemical reaction where steel is converted to rust and occurs when metal is in contact with water. Two locations are established in the metal, a cathode and an anode. In the anode, iron loses electrons and becomes a positively charged ion. This ion further reacts with water and oxygen in the surrounding media to form rust. The cathode receives the electrons of the anode and generates by-products (such as hydrogen H_2) with other ions.

| (A) | (B) | (C) |
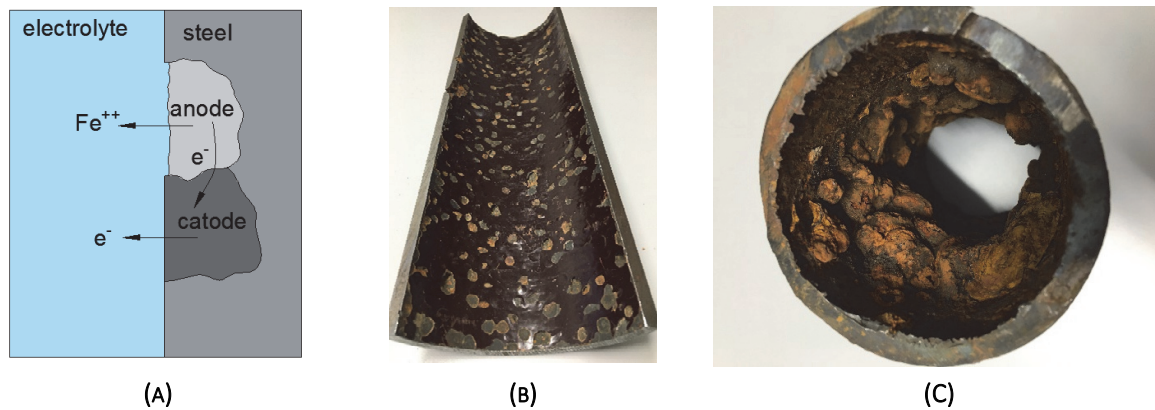
FIGURE 7-15. A) ILLUSTRATION OR A CORROSION REACTION B) CORROSION ON A CASING INSIDE SURFACE C) CORROSION ON TUBING

Corrosion can occur virtually anywhere in the production system where water is in contact with metal (casing, tubing, flowlines, pipelines, tanks, pumps, etc.). In transportation pipes, corrosion usually occurs at the pipe bottom where water is transported, in low pipe sections where water accumulates or at the top of the pipe due to splashing and condensation of water droplets (also known as TLC, Top of line corrosion).
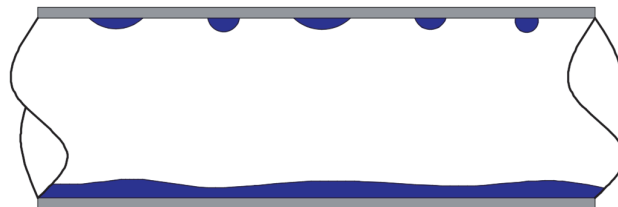
FIGURE 7-16. WET GAS FLOW IN A HORIZONTAL FLOWLINE DEPICTING TOP OF LINE CONDENSATION

Oxygen and acid gases such as CO_2 and H_2S contribute to corrosion.

7.5.1. CONSEQUENCES

Corrosion on an unprotected pipe can cause losses of 1-20 mm of pipe thickness per year, leading ultimately to structural damage and leakages. Rust particles can also travel downstream and cause problems such as plugging other components.

7.5.2. MANAGEMENT

The measures to mitigate corrosion can be divided into two main principles:

·   Eliminate the contact between water from steel. This can be done by applying a protective layer on the steel surface, for example with coating (which might be eventually damaged due to sand erosion), creating a layer of protective oxide on the steel (Figure 7-17a) or by using inhibitors (Figure 7-17b).

(A)   (B)
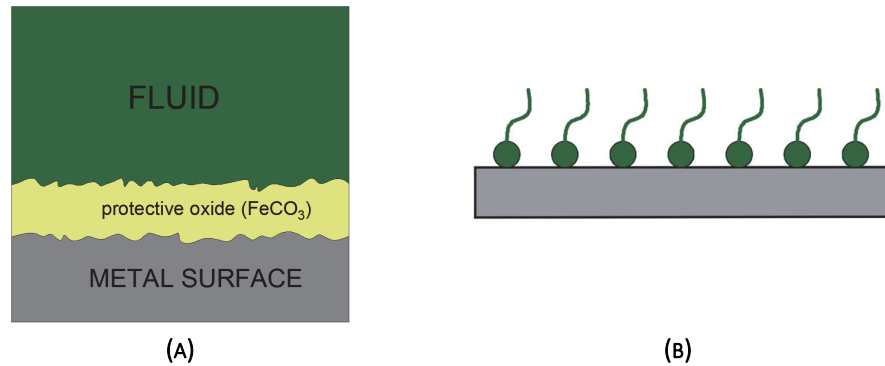
FIGURE 7-17. PROTECTIVE LAYER OF FeCO$_3$ FORMED ON THE METAL SURFACE B) INHIBITORS ATTACHED TO THE METAL SURFACE

· Use steel materials with higher resistance to corrosion. For example, alloy steels. This is usually feasible for wells, but it becomes too expensive for flowlines and pipelines.

7.6. WAX DEPOSITION

Wax deposition occurs when long alkane chains (C18+) precipitate out of solution from the oil, agglomerate and deposit on the pipe walls.

In a waxy crude, when temperature is reduced down to a certain value (for North sea crudes this happens around 30-40 C), some wax crystals will start to precipitate and become visible. The temperature when this occurs is called cloud point or WAT (wax appereance temperature).

(A)   (B)
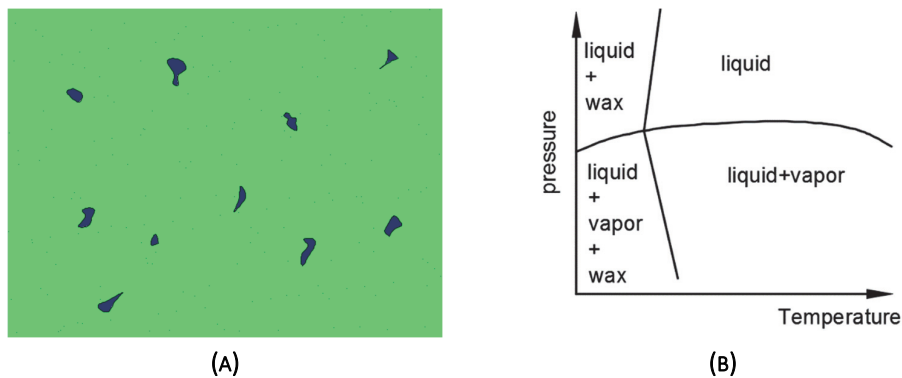
FIGURE 7-18. A) WAX CRYSTALS VISIBLE IN A CRUDE AT WAT, B) WATS AT DIFFERENT PRESSURES IN THE PHASE DIAGRAM

The WAT depends on oil composition, type and molar amounts of alkanes, pressure, cooling rate. Wax crystals typically attach to nucleating agents present in the oil (asphaltenes[35], fine sand, clay, water, salt), form wax "clusters" and grow.

If the temperature is reduced further down to the pour point, the oil becomes solid-like and stops flowing by gravity.

---

[35] Asphaltenes are coal-like solids that also have the tendency to precipitate out of the crude. They are high molecular weight compounds containing poly-aromatic carbon rings with nitrogen, sulphur, oxygen and heavy metals such as vanadium and nickel.
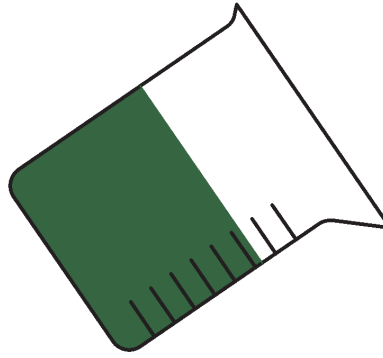
FIGURE 7-19. CRUDE OIL NOT FLOWING ONCE THE POUR POINT IS REACHED

Wax deposition occurs when **ALL** the following ingredients are present:

· Wax-prone components in the oil composition (long alkane chains).
· Temperature below WAT.
· Pipe wall colder than the fluid such that there is a temperature profile in the fluid reducing towards the pipe wall (temperature gradient).
· Irregularities on the wall where wax clusters attach.

Wax deposits age with time and become more rigid (thus more difficult to remove).

7.6.1. CONSEQUENCES

In flowlines and pipelines:

· Increases pressure drop due to the increase in pipe roughness.
· Reduction of cross section area.
· Pipe blockage.
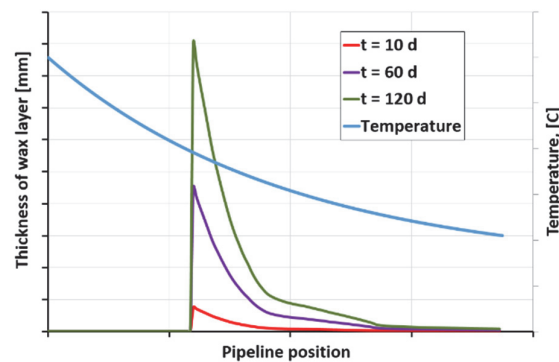
(A)   (B)

FIGURE 7-20. A) WAX PLUG RETRIEVED TOPSIDE (IMAGE TAKEN FROM LABES-CARRIER ET AL[7-3]), B) EVOLUTION OF THE WAX THICKNESS IN A PIPELINE WITH TIME

· The presence of wax crystals in the fluids changes its rheology (e.g. making it non-Newtonian or with a higher effective viscosity).
· During shut-downs, the temperature of the fluid can reach the pour point of the crude, causing it not to flow (gelling).

7.6.2. MANAGEMENT

The first step in developing a wax management strategy is to test the crude oil in the laboratory and measure and quantify all of its properties relevant for deposition.

A common management method for wax is to perform frequent pigging. Pigging consists in sending a device (pig) inside the pipe that scraps the wax deposits and pushes them forward. Pigs are usually sent and received from the processing facilities thus two pipelines must be installed. There are also subsea pig launchers, but this is economic only for systems with very low pigging frequency.

Figure 7-21 shows the flow schematics of a subsea production system with two satellite wells producing to a subsea manifold. There are two pipelines from the manifold to topside and there is a crossover valve on the subsea manifold (normally closed) that allows to communicate both. When performing pigging operations, the crossover valve is open and the pig is send through one pipeline with a pig launcher topside and received through the other end, on the pig receiver.
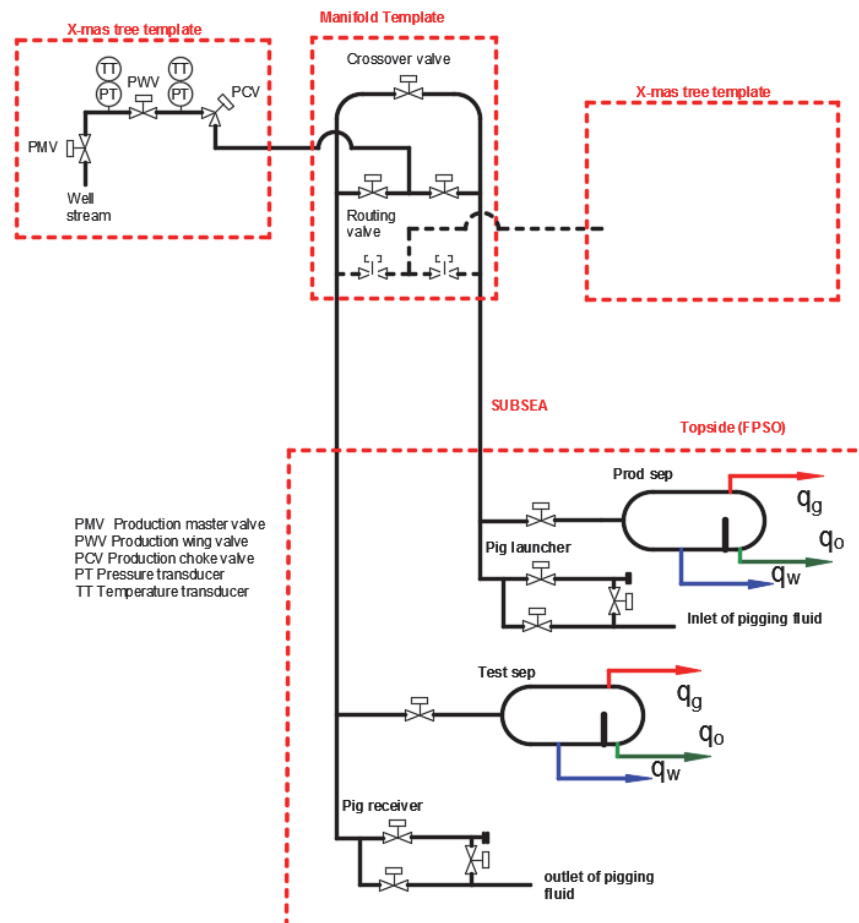
FIGURE 7-21. FLOW SCHEMATIC OF A SUBSEA PRODUCTION SYSTEM WITH FACILITIES FOR PIGGING AND INDIVIDUAL WELL TESTING

Pigging frequency is usually estimated by performing numerical simulations to compute the profile of deposited wax along the flowline with time. With this, the total amount of wax deposited in the system at any given time is estimated. There is a maximum length and weight of wax that can be pushed through the pipe, given by the maximum allowable pressure that the pipe can tolerate. The required pigging frequency is given by the time at which that wax amount is reached.

Other techniques used are keeping the fluid outside of the wax formation region. This is done by thermal insulation or electrical heating. However, for long flowlines, electrical heating is usually very expensive and insulation alone is not enough to keep temperature sufficiently high. Thus, in most cases insulation or electrical heating are often used to reduce wax deposition rates together with pigging.

Chemical inhibitors that are also often injected. Chemical inhibitors work by reducing the cloud point of the crude or by preventing further agglomeration of wax crystals. As with insulation, in many systems this does not eliminate completely the problem but it helps slowing down the deposition rate. Chemical inhibitors are typically expensive.

If the seabed temperature is below or equal the pour point of the oil, then it is necessary to inject chemical inhibitors before shutting down the system to avoid gelling.

In recent years pipe coating has been proposed as a technique to avoid wax attaching to pipe walls. However, it is not yet field tested.

In systems with wax-prone oils the pressure drop between end points of flowlines should be closely monitored. Any unexplained increase might indicate wax deposition and must be immediately addressed.

7.7.   OIL-WATER EMULSIONS

Oil-water emulsions are fine and stable dispersions of oil droplets in water or water droplets in oil (Figure 7-22). The formation of emulsions depends on a variety of factors such as the dynamics of multiphase flow, the properties of oil and water such as viscosity and interfacial tension, the shear stress (mixing) experienced by the mixture, chemical compounds present in the oil-water interface. In production systems, the mixing is typically generated when commingling production from different sources, due to the violent expansion across the choke, flow through multiphase pumps, etc.

(A)   (B)

FIGURE 7-22. A) OIL (RED) AND WATER (WHITE) ORIGINALLY SEPARATED, B) OIL AND WATER EMULSION AFTER VIGOROUS STIRRING IN A BLENDER. PHOTOS TAKEN BY HONG[7-4]

7.7.1. CONSEQUENCES

In pipe flow, emulsions often exhibit the behavior presented in Figure 7-23. For a fixed volumetric rate of the mixture ($q_o + q_w$), if one measures the pressure drop along a pipe segment for several water volume fractions, it will increase with water volume fraction until a maximum is reached and then it will decline abruptly. The water volume fraction that has the highest-pressure gradient is called the inversion point. The increase in pressure drop is usually significant (more 2.5 times the one for pure oil in the figure).

When increasing the water fraction, at the inversion point the dispersion changes from a water in oil dispersion to an oil in water dispersion.
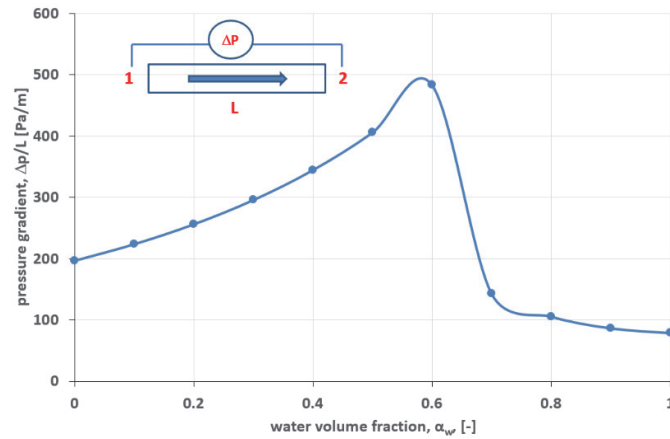
FIGURE 7-23. MEASURED PRESSURE DROP IN A HORIZONTAL PIPE KEEPING THE TOTAL FLOW RATE CONSTANT AND CHANGING WATER VOLUME FRACTION, $qw/(qw + qo)$

Figure 7-24 shows an oil-water flow pattern map depicting mixture velocity (total liquid rate divided by pipe cross section area) in the "x" axis, water cut in the "y" axis and the flow pattern regions in colors. The transition shown in Figure 7-23, from water volume fraction of zero to one at constant flow rate (mixture velocity) is plotted as a vertical line on the figure at mixture velocity approximately equal to 0.5 m/s (arbitrary value). Along the line the flow pattern changes from a dispersion of water in oil (Dw/o) to a dispersion of oil in water (Do/w) and the inversion point occurs at a water volume fraction of around 0.5.
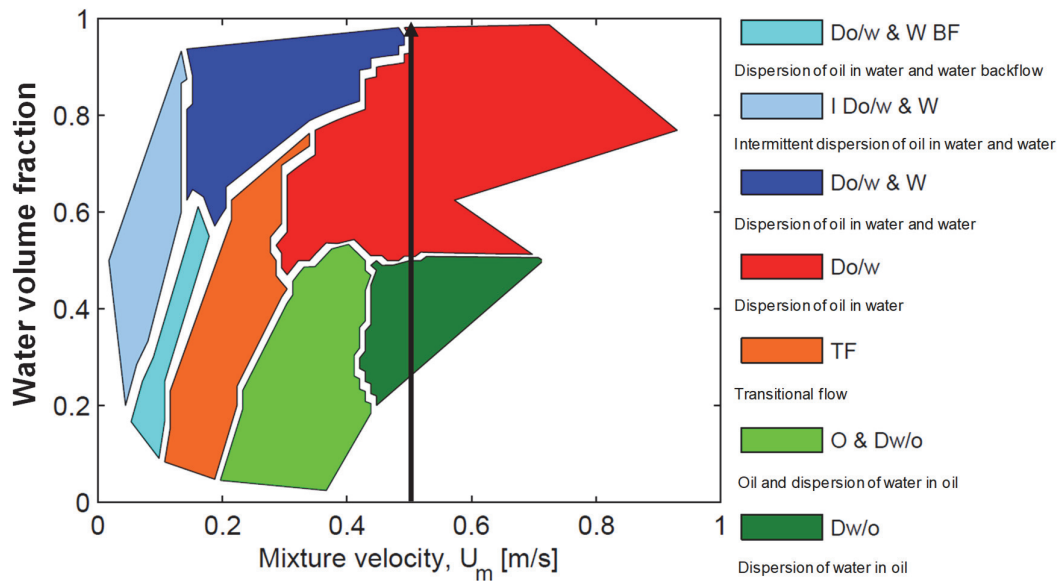
FIGURE 7-24. OIL-WATER FLOW PATTERN MAP OF WATER VOLUME FRACTION VERSUS MIXTURE VELOCITY FOR AN UPWARD PIPE INCLINATION OF 45°. FIGURE ADAPTED FROM RIVERA[7-5] [7-1] .

Using a homogeneous model (single fluid with average properties) one can back-calculate the effective mixture or "emulsion" viscosity that the mixture should have to provide the pressure drop measured (Figure 7-25). For the particular case, the emulsion viscosity at the inversion point (570 cP) is 7.1 times the viscosity of the oil (80 cP).
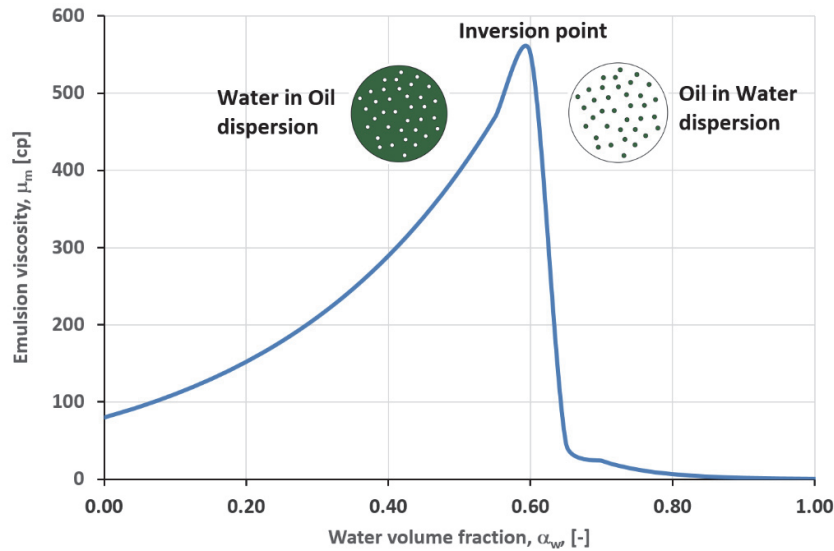
FIGURE 7-25. MIXTURE VISCOSITY BEHAVIOR VERSUS WATER VOLUME FRACTION EXHIBITED BY THE OIL WATER MIXTURE

There are many expressions used to represent the behavior shown in Figure 7-25 that are later used in emulsion pressure drop models. Most of them require data measured in the lab to tune their coefficients. As an example, the Richardson model is shown below.

For oil continuous $$\mu_m = \mu_o \cdot e^{n_o \cdot \alpha_w}$$ EQ. 7-1

For water continuous $$\mu_m = \mu_w \cdot e^{n_w \cdot (1 - \alpha_w)}$$ EQ. 7-2

Emulsions can cause excessive pressure drops in pipe segments and components, which can reduce dramatically production rates, pumping capacity of electric submersible pumps, etc. Moreover, stable emulsions are difficult to separate in processing facilities thus creating bottlenecks and fluid disposal problems.

7.7.2. MANAGEMENT

During the field design phase, the capacity oil and water system to form emulsions can be somewhat studied with laboratory tests (shaking bottle tests). However, these results have sometimes limited applicability partly because the shear magnitudes (mixing) applied in the laboratory conditions are very different from the mixing experienced in the field.

When there is mixing of streams with different water cut, the inversion point must be avoided.

Often, chemical substances such as demulsifiers and light oils (diluent) are injected into the stream to reduce the stability of the emulsion. Light oils reduce the viscosity of the formation oil, thus helping separation. Demulsifiers are chemicals that attach themselves to the interface between oil and water promoting separation.

7.1. SUMMARY TABLE

A summary table is provided describing briefly causes, potential consequences, prevention and solution measures and tools available for analysis for some flow assurance issues mentioned above.

TABLE 7-1. SUMMARY TABLE OF FLOW ASSURANCE ISSUES: CAUSES, POTENTIAL CONSEQUENCES, PREVENTION AND SOLUTION MEASURES AND TOOLS AVAILABLE FOR ANALYSIS

ISSUE	CAUSES	POTENTIAL CONSEQUENCES	PREVENTION/SOLUTION	TOOLS AVAILABLE FOR ANALYSIS
HYDRATES	• Small gas HC molecules • Free water • Begin to form at a given p and T (low T, high P) given by thermodynamic equilibrium of the hydrate phase.	• Blockage of flowlines and pipelines	Reduce the hydrate formation region: •Continuous or on-demand injection of chemical inhibitor (MEG or MEOH) Stay out of hydrate formation region: •Improve thermal insulation •Electric heating Others: •Cold flow* •Water removal and gas dehydration*	To determine hydrate formation conditions: •Laboratory tests •Empirical correlations •Thermodynamic simulators (e.g. Hysys, PVTsim, Unisim) To determine p and T along the pipe: •Multiphase simulator (Olga, LedaFlow). •Computational fluid dynamics (CFD)
WAX	• Composition of the crude oil • Begins to form at given p and T due to changes in solubility • Cold wall	In wells, flowlines and pipelines: •Increase of pressure drop (pipe roughness) •Reduces heat transfer •Reduction of cross section area •Pipe blockage •Changes fluid rheology •Gelling (problem for startup)	• Pigging • Thermal insulation • Electric heating • Chemical inhibitors • Chemical dissolvers • Pipe coating • Cold flow*	• Laboratory tests • Transient multiphase simulators (e.g. Olga, LedaFlow)
SLUGGING	• Dynamics of multiphase flow of liquid and gas • Reduction of rate • Liquid accumulation on low points of wells, flowlines and pipelines	• Fluctuating liquid and gas input to processing facilities In flowlines and pipelines: • Vibration • Added pressure drop • Fatigue	• Change separator size • Pipeline dimensioning • Maintain flow above minimum flow rate • Gas lift in riser base • Choking topside • Pipeline re-routing • Subsea separation*	• Transient multiphase simulator (OLGA, LEDA) • Structural analysis (usually with FEA, e.g. Ansys) • Laboratory experiments
SCALING	• Changes in solubility (e.g. changes in P and T conditions, changes in pH, mixing incompatible waters, CO2 injection). • Irregularities on surface	In wells, pipelines and flowlines: •Reduction of cross section area •Pipe blockage •Malfunctioning of valves and equipment	• Continuous injection of chemical inhibitors • Dilution by adding more water • Chemical dissolvers • Mechanical removal • Coating	• Laboratory tests • Simulation tools
EROSION	• Sand production • High flow velocities • Liquid droplets in the gas • Gas droplets in the liquid	In wells, pipelines and flowlines: •Structural damage •Vibration •Leaks •Corrosion	• Change geometry • Replacement and maintenance of components • Reduce flow rate (reduce formation drawdown) • Sand separation • Coatings	• Standards (DNV-RP-0501) • Computational fluid dynamics • Laboratory testing
CORROSION	• Metal in contact with water • Presence of O_2, CO_2, H_2S	• Leaks • Integrity	• Chemical inhibitor • Coatings • Material selection • Surface passivation	• Laboratory testing
EMULSIONS	• Emulsification agents in the crude • Mixing, shear when flowing through valves, chokes	• Added pressure drop • Increased separation time	• Injection of demulsifiers • Heating	• Laboratory tests • Multiphase models
ASPHALTENES	• Crude with asphaltenes • Pressure reduction • Add-up of light hydrocarbon components	• Blockage of formation, well, flowline and pipeline • Loss of equipment functionality • Promotes emulsification and foamification	• Mechanical removal • Chemical injection	• Laboratory tests • Some simulation tools

7.1. ABOUT CHEMICAL INJECTION

Many of the preventive and corrective measures against flow assurance issues involve the continuous or occasional injection of chemicals and substances to inhibit the precipitation or dissolve solids. Such chemicals often cannot be recovered and reused, but rather follow the produced oil, gas or water. Some of the chemicals employed are often damaging to the environment and therefore their usage must be strictly controlled, especially if they might end up in the environment (e.g. follow the disposed water).

In offshore installations, chemicals are classified in categories following applicable regulation (for example the OSPAR, convention for the protection of the marine environment of the North-East Atlantic). For example, color codes are used to classify substances:

- Green: substances which pose little or no risk to the environment.
- Yellow: substances that are not classified as green, red or black. Typically includes substances with low toxicity and that can be significantly degraded after 28 days.
- Red: substances that can accumulate in the environment and that have slow degradation times. Requires special permission to use and discharge to environment.

- Black: substances that do not degrade, that are poisonous and that accumulate in the environment. Permission to use and discharge is only given due to safety or critical technical reasons.

Some examples of red chemicals are emulsion inhibitors, wax inhibitors, anti-foamers. However, these substances are injected or accumulate main in the oil, and therefore will not end in the environment.

Some examples of yellow chemicals are scale inhibitors, biocides. These substances are soluble in water and will follow injection water or disposed produced water.

MEG is often classified a green-type substance. However, it is more economic to recover it from the production water for reuse.

References

[7-1] Schroeder, Jr.; Chitwood, J. Krasin, T.; Lee, B.; Krohn, D.; Huizinga, M.; Paramonoff, A.;Schroeder, C.; Gay, T.; Cercone, D.; Pappas, J. *Development and Qualification of a Subsea 3000 Barrel Pressure Compensated Chemical Storage and Injection System*. OTC paper 26966. Offshore Technology Conference, May, 2016.

[7-2] Sandengen, K. *Hydrates and Glycols MEG (Mono Ethylene Glycol) Injection and Processing*. Presentation at NTNU. September, 9. 2010.

[7-3] Labes-Carrier, C.; Rønningsen, H. P.; Kolnes, J.; Leporcher, E. *Wax Deposition in North Sea Gas Condensate and Oil Systems: Comparison Between Operational Experience and Model Prediction*. SPE paper 77573. SPE Annual Technical Conference and Exhibition. San Antonio, Texas. 2002.

[7-4] Hong, C. *Study on Ultrasonic Influence on Oil-Water Emulsion Separation*. Project Report. Norwegian University of Science and Technology. 2017.

[7-5] Rivera, R. *Water Separation from Wellstream in Inclined Separation Tube with Distributed Tapping*. PhD Thesis. Norwegian University of Science and Technology. 2011.

8.   HEAT TRANSFER FOR FLOW IN CONDUITS

The equation for conservation of energy for a section of a conduit is

$$\dot{Q} + \dot{W} = \dot{m} \cdot (e_{out} - e_{in})$$

EQ. 8-1

The specific energy that the stream has is usually split in internal energy (u), potential energy (z·g) and kinetic energy ($V^2/2$). In this equation, the sign convention for $\dot{Q}$ and $\dot{W}$ is when entering the pipe are positive, and when leaving the pipe are negative.

A conduit doesn't exchange work with the surroundings, but the fluid must perform work to enter and leave the system. This specific work is: $(p_{in} \cdot v_{in} - p_{out} \cdot v_{out})$ (Here v is specific volume).

By combining the inlet and outlet specific internal energy "u" with the specific work to enter and leave the system to obtain specific enthalpy, the energy conservation equation is written as:

$$\dot{Q} = \dot{m} \cdot \left(h_{out} + z_{out} \cdot g + \frac{(V_{out})^2}{2} - h_{in} - z_{in} \cdot g - \frac{(V_{in})^2}{2} \right)$$

EQ. 8-2

Or, alternatively

$$\dot{Q} = \dot{m} \cdot \left(\Delta h + \Delta z \cdot g + \frac{(V_{out})^2}{2} - \frac{(V_{in})^2}{2} \right)$$

EQ. 8-3

Here Δ represents outlet minus inlet.

In differential form (for an infinitesimally small length of pipe) the equation can be expressed as follows:

$$\frac{d\dot{Q}}{dL} = \dot{m} \cdot \left(\frac{dh}{dL} + g \cdot \frac{dz}{dL} + v \cdot \frac{dv}{dL} \right)$$

EQ. 8-4

Heat leaving the system is negative (the temperature of the outlet fluid is lower than the temperature at the inlet and the term Δh is usually negative). Heat entering the system is positive.

8.1.   ORDER OF MAGNITUDE ANALYSIS ON THE SPECIFIC ENERGY TERMS OF A STREAM

The energy conservation shown above is usually simplified by neglecting the changes in specific kinetic and potential energy. This is because changes in specific enthalpy are usually much larger than changes in specific kinetic and potential energy. To analyze this, we will compare the following three terms:

$$\Delta h, \Delta e_P = \Delta z \cdot g, \Delta e_K = \frac{(V_{out})^2 - (V_{in})^2}{2}$$

EQ. 8-5

Where Δe_P and Δe_K are changes in specific potential and kinetic energy respectively.

To perform this comparison, we will use as a reference a vertical pipe section with $\Delta z = 1\ m$, i.e. the change in specific potential energy is of order 10 m²/s² (9.81 m²/s²). We will also need some reference values on variation of pressure and temperature along the conduit. Table 8-1 shows some reference gradients of pressure and temperature that will be use as upper limit in the derivations.

TABLE 8-1. UPPER BOUNDS ON TEMPERATURE AND PRESSURE SPATIAL GRADIENTS.

Quantity	Value	Reference
$\Delta p/\Delta L$	-7848 Pa/m	Stagnant column of water
$\Delta T/\Delta L$	-0.03 °C/m	Geothermal gradient

8.1.1. COMPARISON BETWEEN THE SPECIFIC KINETIC AND POTENTIAL ENERGY TERMS

The change in specific kinetic energy can be neglected when it is equal to a fraction "x" (usually small) of the change in specific potential energy:

$$x \cdot (\Delta z \cdot g) = \frac{(V_{out})^2 - (V_{in})^2}{2}$$

EQ. 8-6

For this example, fraction "x" will be set to 0.1 (10%). Thus, the left side of the equation is 0.981 m²/s².

We now express the velocity downstream in terms of the velocity upstream and a factor F:

$$V_{out} = F \cdot V_{in}$$

EQ. 8-7

Then

$$x \cdot (\Delta z \cdot g) = \frac{(F \cdot V_{in})^2 - (V_{in})^2}{2} = \left(\frac{V_{in}}{\sqrt{2}}\right)^2 \cdot (F^2 - 1)$$

EQ. 8-8

The change in specific kinetic energy term depends on the inlet velocity of the fluid and the factor F. Figure 8-1 shows the required values of F to equal a change in specific potential energy of 0.981 m²/s² for different values of V_{in}.
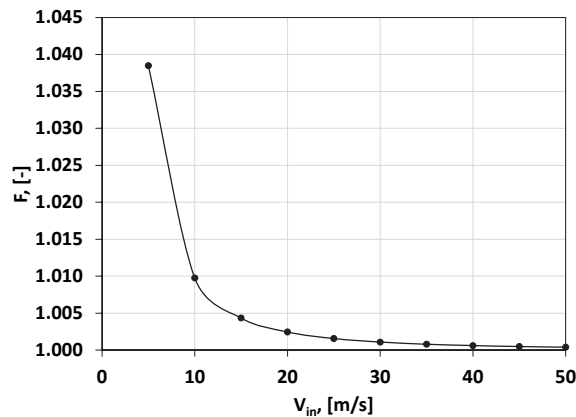
FIGURE 8-1. PLOT OF FACTOR F VERSUS INLET FLUID VELOCITY THAT GIVES A CHANGE IN SPECIFIC KINETIC ENERGY EQUAL TO 0.981 M²/S²

Higher values of V_{in} require lower variations between upstream and downstream velocity. In liquid flow, velocities in the conduit are usually below 5 m/s. For the specific kinetic energy term to be negligible when compared against the specific potential energy, the variation of velocity in one meter must be of around 3.8% or lower.

In gas flow, velocities in the conduit are usually below 30 m/s. For the specific kinetic energy term to be negligible when compared against the change in specific potential energy, the variation of velocity in one meter of pipe must be of around 0.1% or lower.

For steady-state conditions, the variation of velocity along the conduit is usually because of variations in density and phase change (condensation/vaporization). Neglecting phase change, and using mass conservation in a section of the conduit gives:

$$V_{in} \cdot A \cdot \rho_{in} = V_{out} \cdot A \cdot \rho_{out}$$

EQ. 8-9

Expressing the velocity downstream in terms of the velocity upstream (with the factor F) and simplifying terms gives:

$$\rho_{in} = F \cdot \rho_{out}$$

EQ. 8-10

This expression indicates that variations in downstream velocity are inversely proportional to variations in downstream density. For example, if velocity increases by 30%, then downstream density must have decreased by 30%. Variations in density are usually due to variations in pressure and temperature.

Using the values from the previous example (liquid velocity of 5 m/s), the change in specific kinetic energy will be negligible with respect to the change in specific potential energy if there is a reduction in density of 3.8% or lower, in a length of 1 m. In liquids, large variations in pressure are required to produce small variations in density. Consider the formula for compressibility:

$$\beta = \frac{1}{\rho} \cdot \left(\frac{\partial \rho}{\partial p} \right)$$

EQ. 8-11

Approximating the differentials by deltas, gives:

$$\beta = \frac{1}{\rho} \cdot \left(\frac{\Delta \rho}{\Delta p} \right) = \frac{\Delta \rho}{\rho} \cdot \left(\frac{1}{\Delta p} \right) = \varepsilon \cdot \left(\frac{1}{\Delta p} \right) \rightarrow \Delta p = \frac{\varepsilon}{\beta}$$

EQ. 8-12

To produce variation in density of 3.8 % ($\varepsilon = 0.038$) in 1 meter, the variation in pressure for kerosene[36] must be of around 500 bar. This is significantly higher than pressure drops typically encountered in petroleum production systems (usually below or slightly above the pressure gradient of a stagnant column of water, -7848 Pa/m).

Therefore, for liquids, and liquid-dominated flows, the specific kinetic energy is usually small when compared to the potential energy and can safely be neglected.

For gases, variations of pressure and temperature have a bigger effect on density. Additionally, the density variations required to achieve the same value of specific potential energy are smaller, because the inlet velocity is higher.

For gases, the density at the inlet can be expressed by the real gas equation:

$$p_{in} = \rho_{in} \cdot Z_{in} \cdot \frac{R_u}{M_w} \cdot T_{in}$$

EQ. 8-13

And the density at the outlet

---

[36] β=0.8 E-5 bar^{-1}

$$p_{out} = \rho_{out} \cdot Z_{out} \cdot \frac{R_u}{M_w} \cdot T_{out}$$

EQ. 8-14

If variations in temperature and gas deviation factor (Z) are considered small when compared to pressure, and dividing both equations, this gives:

$$\frac{p_{in}}{p_{out}} = \frac{\rho_{in}}{\rho_{out}} = F$$

EQ. 8-15

Or, equivalently,

$$p_{in} = F \cdot p_{out}$$

EQ. 8-16

The pressure drop along the pipe section can then be expressed as a function of F

$$\frac{\Delta p}{\Delta L} = \frac{(p_{out} - p_{in})}{\Delta L} = \frac{\left(\frac{p_{in}}{F} - p_{in}\right)}{\Delta L} = \frac{p_{in} \cdot \left(\frac{1-F}{F}\right)}{\Delta L}$$

EQ. 8-17

Figure 8-2 shows values of pressure gradient versus inlet pressure that give a change in specific kinetic energy equal to a change of specific potential energy of 0.981 m^2/s^2 for an inlet velocity of 30 m/s. At higher inlet pressure, the pressure gradient required is of bigger magnitude. Values of pressure gradient above the black line will cause the change in specific kinetic energy to be negligible.
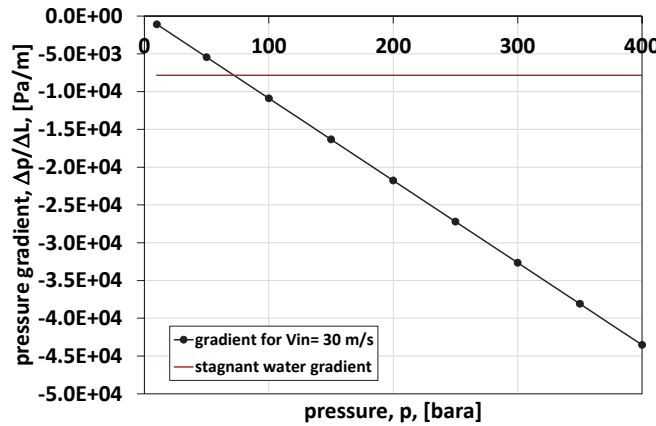
FIGURE 8-2. PLOT OF PRESSURE GRADIENT VERSUS INLET PRESSURE THAT GIVE A CHANGE IN SPECIFIC POTENTIAL ENERGY EQUAL TO 0.981 M^2/S^2, FOR V_{IN}=30 M/S

Consider the pressure gradient of a stagnant column of water: -7848 Pa/m (red line in Figure 8-2). Pressure drops in single and multiphase flow in conduits of petroleum production systems are usually above or slightly below this value. For most of the range of inlet pressure values (i.e. above 75 bara), values of pressure gradient (for the change in specific kinetic energy to be negligible with respect to changes in specific potential energy) are above it.

Figure 8-3 shows the values of inlet velocity required versus inlet pressure that cause the change in specific kinetic energy to be negligible when compared against the change in potential energy, for several values of pressure gradients. Lower pressure gradients require higher inlet velocities for the kinetic energy term to be negligible. For values in the upper part of the lines, the change in specific kinetic energy must likely be included.
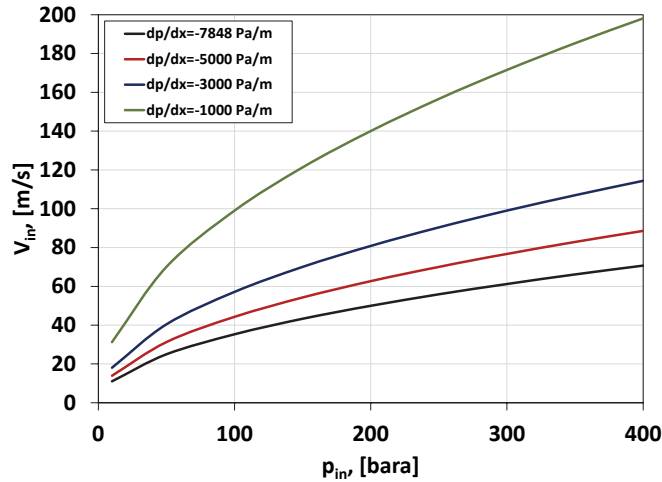
FIGURE 8-3. PLOT OF VALUES OF INLET VELOCITY VERSUS INLET PRESSURE THAT GIVE A CHANGE IN SPECIFIC KINETIC ENERGY EQUAL TO 0.981 M^2/S^2, FOR SEVERAL VALUES OF PRESSURE GRADIENT

Therefore, for gas and gas-dominated flow and operating conditions of low pressures and high velocities, the term of specific kinetic energy usually must be accounted for.

8.1.2. COMPARISON BETWEEN THE SPECIFIC ENTHALPY AND POTENTIAL ENERGY TERMS

An order of magnitude comparison between the specific enthalpy and potential energy terms is expressed mathematically as follows

$$O(\Delta z \cdot g) = O(\Delta h)$$

EQ. 8-18

The enthalpy difference is a function of the inlet and outlet pressure and temperature and the type of fluid. In this section, the outlet pressure and temperature will be expressed in terms of the inlet pressure and temperature and the temperature ($\Delta T/\Delta L$) and pressure ($\Delta p/\Delta L$) gradients.

For liquids, the following approximation for enthalpy is often used:

$$\Delta h = C_p \cdot (\Delta T)$$

EQ. 8-19

C_p usually falls within the range between 1000-4000 J/kg K (oil-water).

Consider the reference vertical pipe section with $\Delta z = 1\ m$ (change in specific potential energy equal to 9.81 m^2/s^2). For the change in specific enthalpy to be of the same order of magnitude the temperature gradient $\Delta T/\Delta L$ must equal or below values in the range -0.01 to -0.002 C/m. For the change in specific enthalpy to be equal to 98.1 m^2/s^2 (10 times larger than 9.81 m^2/s^2), the temperature gradient must be equal or less than values in the range -0.1 to -0.03 C/m.

In wells and pipelines, the temperature gradient along the pipe is usually higher than -0.03 °C/m (geothermal temperature gradient). Therefore, for liquids and liquid-dominated flows, it is often necessary to include the term of change in specific potential energy, especially for liquids with low heat capacity values and when the temperature gradient is low.

For gases, enthalpy h is affected by both temperature and pressure. For methane, in the range of pressure and temperature between 1 to 400 bara and 15 to 200 °C, the partial derivatives of enthalpy with respect to temperature and pressure are in the ranges 2225 to 3560 J/kg/C and between -1.2e-2 and -6.4e-5 J/kg/Pa

respectively. Note that the gradients with respect to pressure and temperature have different signs. So, for flow in pipe where both pressure and temperature are reduced, their effect will usually counteract.

Consider the reference vertical pipe section with $\Delta z = 1\ m$ (change in specific potential energy equal to 9.81 m^2/s^2). For the change in specific enthalpy to be equal to 98.1 m^2/s^2 (10 times larger than 9.81 m^2/s^2), the pressure gradient (keeping temperature constant) must be equal or lower than values between -1.5e-6 and -8077 Pa/m. When comparing against a reference pressure gradient of stagnant water (-7848 Pa/m) these values are quite low.

For the change in specific enthalpy to be equal or higher than 98.1 m^2/s^2 (10 times larger than 9.81 m^2/s^2), the temperature gradient (keeping pressure constant) must be equal or lower than values in the range -0.03 and -0.04 C/m. When comparing against a reference temperature gradient of geothermal gradient (-0.03 C/m) these values are quite low.

Therefore, for gases and gas-dominated flows, it is often also necessary to include the term of change in specific potential energy, especially for liquids with low heat capacity values and when the temperature gradient is low.

Please note that the examples presented above were made for a vertical pipe section of 1 m. However, if the pipe is inclined, the term of specific potential energy will be smaller (due to scaling $\Delta e_P = sin(\alpha) \cdot \Delta z \cdot g$, with α being the angle between the pipe and the horizontal) and results and limit values presented in the discussion will be different.

8.2.   HEAT TRANSFER WITH THE ENVIRONMENT

In a conduit there are usually several heat transfer mechanisms between the fluid and the ambient. For example, there is forced convection between the fluid and the inner pipe wall, conduction in the pipe wall, cement, insulation layer or soil, free convection in liquid trapped in the annulus, or with the external air or water. There is also radiation in the annular space, but this is often neglected.

The heat is usually expressed in terms of an overall heat transfer coefficient, a pipe surface area, and the temperature differential between the ambient and the fluid:

$$\dot{Q} = -2 \cdot \pi \cdot L \cdot r \cdot U \cdot \left(T_f - T_\infty\right)$$ EQ. 8-20

Where:

r reference radius [m]

U Overall heat transfer coefficient, expressed in terms of the reference radius r [W/m^2.K]

T_∞ Mean ambient temperature [K or °C]

T_f Mean fluid temperature in the section [K or °C]

In this section we will work with the heat by unit of conduit length $\frac{\dot{Q}}{L} = \frac{d\dot{Q}}{dL}$.

In Eq. 8-20 the sign if positive if the temperature of the ambient is greater than the fluid while negative if otherwise. This is consistent with the sign convention for heat (heat entering the system is positive and heat leaving the system is negative).

The overall heat transfer coefficient U is a function of the reference radius and the number of layers and heat transfer mechanisms between the fluid and the ambient. To explain the calculation procedure, we will consider two cases:

Case 1. A subsea pipeline with four layers between the fluid and the ambient (from innermost to outer most):

- Forced convection inside the pipe
- Conduction in pipe wall
- Conduction in insulation layer
- Free/forced convection with surrounding air (or water)

Case 2. A wellbore with 7 layers between the fluid and the formation sand face (from innermost to outer most):

- Forced convection inside the tubing
- Conduction in the tubing wall
- Free convection in the annulus between the tubing and the production casing
- Conduction in the production casing wall
- Conduction in the cement between the production and intermediate casing
- Conduction in the intermediate casing wall
- Conduction in the cement between the intermediate casing and the formation

8.2.1. CASE 1. SUBSEA PIPELINE

A sketch of the configuration to study is shown in Figure 8-4.
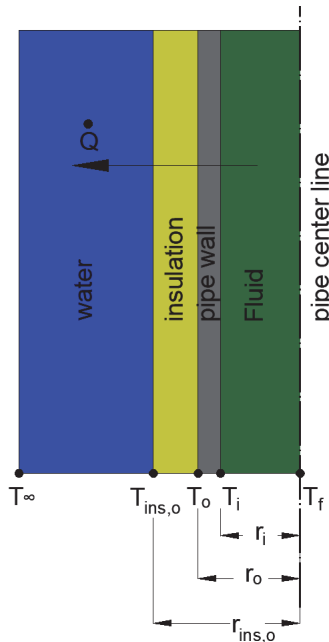
FIGURE 8-4. SKETCH SHOWING THE SIDE VIEW OF A SUBSEA PIPELINE WITH INNER FORCED CONVECTION, CONDUCTION IN PIPE WALL AND INSULATION AND FREE CONVECTION WITH WATER

We will first write the expressions to calculate heat transfer in each layer.

Forced convection inside the pipe

The heat transfer in the interior of the flowing pipe can be expressed as follows:

$$\frac{d\dot{Q}}{dL} = -2 \cdot \pi \cdot r_i \cdot h_i \cdot (T_f - T_i)$$

EQ. 8-21

Where:

r_i Pipe inner radius [m]

h_i Convective coefficient, inner fluid [W/m^2.K]

T_f Fluid temperature [K or °C]

T_i Temperature, inner pipe wall [K or °C]

The convective heat transfer coefficient h_i, depends on the fluid and wall temperatures, velocities and distribution of phases inside the pipe, variables which are the result of pressure and temperature drop calculations. It is often calculated from the Nusselt number (ratio of convective and conductive heat transfer h·L /k). The Nusselt number is often expressed as a function of the Reynolds number and the Prandtl number (μ·C$_p$ / k).

Therefore, the estimation of h_i is often an implicit calculation (because fluid and wall temperature and velocities are not known a priori). Initially a value is assumed, pressure and temperature are calculated in the conduit, and then a new value of h_i is estimated. The process is repeated iteratively until convergence is achieved.

Conduction in pipe wall

The heat transfer in the metal wall of the pipe can be expressed with the following expression:

$$\frac{d\dot{Q}}{dL} = -2 \cdot \pi \cdot k_p \cdot \frac{(T_i - T_o)}{\ln\left(\frac{r_o}{r_i}\right)}$$

EQ. 8-22

Where:

r_i Pipe inner radius [m]

r_o Pipe outer radius [m]

k_p Pipe material thermal conductivity [W/m.K]

T_i temperature, inner pipe wall [K or °C]

T_o temperature, outer pipe wall [K or °C]

Conduction in insulating layer

Similar to the heat transfer in the metal wall of the pipe, the heat transfer in the insulation layer can be expressed with the following expression:

$$\frac{d\dot{Q}}{dL} = -2 \cdot \pi \cdot k_{ins} \cdot \frac{(T_o - T_{ins,o})}{\ln\left(\frac{r_{ins,o}}{r_o}\right)}$$

EQ. 8-23

Where:

$r_{ins,o}$ Insulation outer radius [m]

r_o Pipe outer radius [m]

k_{ins} Insulation material thermal conductivity [W/m.K]

T_o Temperature, outer pipe wall [K or °C]

$T_{ins,o}$ Temperature, outer insulation wall [K or °C]

Free-forced convection with air (or water)

The heat transfer (free and forced convection) with external air (or water) can be expressed with the following expression:

$$\frac{d\dot{Q}}{dL} = -2 \cdot \pi \cdot r_{ins,o} \cdot h_o \cdot \left(T_{ins,o} - T_\infty\right)$$

<div style="text-align:right">EQ. 8-24</div>

Where:

$r_{ins,o}$ Insulation outer radius [m]

h_o Convective coefficient, outer fluid [W/m^2.K]

T_∞ Ambient temperature (sea water) [K or °C]

$T_{ins,o}$ Temperature, outer insulation wall [K or °C]

Similar to the heat transfer inside the pipe, this heat transfer mechanism is usually a combination of free convection (the flow is induced by the temperature difference) and forced convection (there is an external current e.g. wind or marine current). The convective heat transfer coefficient h_o depends on the fluid and wall temperatures, velocities and distribution of phases inside the pipe, variables which are the result of pressure and temperature drop calculations and are not known a priori. It is often calculated from the Nusselt number (ratio of convective and conductive heat transfer h·L /k). The Nusselt number is often expressed as a function of the Reynolds number, the Prandtl number (μ·C$_p$ /k) and the Grashoff number (g·ρ^2·|ΔT|·L^3·|β| /μ^2). β is the thermal volumetric expansion coefficient at constant temperature, equal to $\frac{1}{\rho} \cdot \frac{\partial \rho}{\partial T}\Big|_{p=const}$

Therefore, the estimation of h_o often requires an implicit calculation where a value is assumed, pressure and temperature are calculated in the conduit, and then a new value of h_o is estimated. The process is repeated iteratively until convergence is achieved.

Overall heat transfer coefficient

The overall heat transfer coefficient is estimated by clearing temperature difference and summing up all expressions (Eq. 8-21, Eq. 8-22, Eq. 8-23, and Eq. 8-24):

$$\left(T_f - T_i\right) + \left(T_i - T_o\right) + \left(T_o - T_{ins,o}\right) + \left(T_{ins,o} - T_\infty\right)$$
$$= \frac{-\frac{d\dot{Q}}{dL}}{2 \cdot \pi \cdot r_i \cdot h_i} + \frac{-\frac{d\dot{Q}}{dL}}{\frac{2 \cdot \pi \cdot k_p}{\ln\left(\frac{r_o}{r_i}\right)}} + \frac{-\frac{d\dot{Q}}{dL}}{\frac{2 \cdot \pi \cdot k_{ins}}{\ln\left(\frac{r_{ins,o}}{r_o}\right)}} + \frac{-\frac{d\dot{Q}}{dL}}{2 \cdot \pi \cdot r_{ins,o} \cdot h_o}$$

<div style="text-align:right">EQ. 8-25</div>

Clearing the temperature difference between fluid and environment:

$$\left(T_f - T_\infty\right) = -\frac{d\dot{Q}}{dL} \cdot \left[\frac{1}{2 \cdot \pi \cdot r_i \cdot h_i} + \frac{1}{\frac{2 \cdot \pi \cdot k_p}{\ln\left(\frac{r_o}{r_i}\right)}} + \frac{1}{\frac{2 \cdot \pi \cdot k_{ins}}{\ln\left(\frac{r_{ins,o}}{r_o}\right)}} + \frac{1}{2 \cdot \pi \cdot r_{ins,o} \cdot h_o}\right]$$

<div style="text-align:right">EQ. 8-26</div>

If the inner pipe radius will be used as reference radius, we then divide Eq. 8-26 by the inner pipe perimeter:

EQ. 8-27

$$\left(T_f - T_\infty\right) = -\frac{d\dot{Q}}{dL} \cdot \frac{1}{2 \cdot \pi \cdot r_i} \cdot \left[\frac{1}{h_i} + \frac{1}{\frac{k_p}{r_i \cdot \ln\left(\frac{r_o}{r_i}\right)}} + \frac{1}{\frac{k_{ins}}{r_i \cdot \ln\left(\frac{r_{ins,o}}{r_o}\right)}} + \frac{1}{\frac{r_{ins,o}}{r_i} \cdot h_o}\right]$$

The overall heat transfer coefficient based on the pipe inner area is defined as:

EQ. 8-28

$$U = \left(\frac{1}{h_i} + \frac{r_i \cdot \ln\left(\frac{r_o}{r_i}\right)}{k_p} + \frac{r_i \cdot \ln\left(\frac{r_{ins,o}}{r_o}\right)}{k_{ins}} + \frac{r_i}{r_{ins,o} \cdot h_o}\right)^{-1}$$

There are some cases where a few terms in this expression are much larger than others, thus a few can be safely neglected:

- Inner forced convection: The inner forced-convection coefficient (h_i) is usually in the range 100-50 000 W/m^2 K.[37] It is lower for low velocities and for gas flow. This gives a term in the range O(1E-5) to O(1E-2).
- Conduction in metal: Inner radii of well tubulars and pipelines are usually in the range 0.01-0.25 m. The ratio between inner and outer radius is usually between 1.05-1.3 (thickest pipe walls are usually for the small pipe diameters), thus the natural log of it is between 0.04-0.24. Lastly, the conductivity of the steel is around 45 W/m^2 K. This gives a term O(1E-4).
- Conduction in the insulating layer: Inner radii of well tubulars and pipelines are usually in the range 0.01-0.25 m. The ratio between inner and outer radius of the insulating layer is usually around 2, thus the natural log is around 0.6. The conductivity of the insulating layer is usually around 0.2-0.3 W/m^2 K (polypropylene). This gives a term in the range O(1E-2) to O(1).
- Free/forced outer convection: The ratio between the inner pipe wall and the outermost radius is more than 2. The free convection coefficient is usually a number between 1-400 W/m^2 K (for air, it is lower, and for water it is higher, and for moving fluids it is higher, while for stagnant fluids it is lower). This gives a term between O(1E-3) and O(1E-1).

In this case, the most important contribution to the overall heat transfer coefficient comes from the conduction in the insulation layer and (maybe) inner and outer convection. This is important to consider when modeling temperature and pressure drop of multiphase flow in wellbores, flowlines and pipelines, to avoid performing implicit calculations. If it is found that the inner or outer convection coefficient will not contribute significantly to the overall heat transfer coefficient, then can often be neglected and the calculation executed explicitly thus avoiding iteration.

If the outer area is used instead of the inner area, then the overall heat transfer coefficient based on the outer area is the following:

EQ. 8-29

$$U = \left(\frac{r_{ins,o}}{r_i \cdot h_i} + \frac{r_{ins,o} \cdot \ln\left(\frac{r_o}{r_i}\right)}{k_p} + \frac{r_{ins,o} \cdot \ln\left(\frac{r_{ins,o}}{r_o}\right)}{k_{ins}} + \frac{1}{h_o}\right)^{-1}$$

The relationship between the overall heat transfer coefficient based on inner area (U_i) and the overall heat transfer coefficient based on outer area (U_o) is :

---

[37] https://www.engineeringtoolbox.com/convective-heat-transfer-d_430.html

$$\frac{U_o}{U_i} = \frac{r_i}{r_{ins,o}}$$

<div align="right">EQ. 8-30</div>

8.2.1. CASE 2. HEAT TRANSFER IN WELLBORE

A sketch of the configuration to study is shown in Figure 8-5.
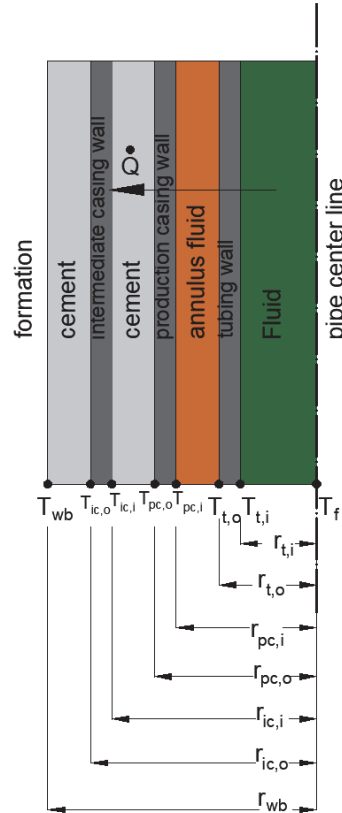
FIGURE 8-5. SKETCH SHOWING THE SIDE VIEW OF A WELLBORE WITH INNER FORCED CONVECTION, CONDUCTION IN TUBING WALL, FREE CONVECTION IN ANNULUS, CONDUCTION IN WALL OF PRODUCTION CASING, CONDUCTION IN CEMENT LAYER BETWEEN PRODUCTION CASING AND INTERMEDIATE CASING, CONDUCTION IN WALL OF INTERMEDIATE CASING, CONDUCTION IN CEMENT LAYER BETWEEN FORMATION AND INTERMEDIATE CASING

Where:

$r_{t,i}$	Tubing inner radius [m]
$r_{t,o}$	Tubing outer radius [m]
$r_{pc,i}$	Production casing inner radius [m]
$r_{pc,o}$	Production casing outer radius [m]
$r_{ic,i}$	Intermediate casing inner radius [m]
$r_{ic,o}$	Intermediate casing outer radius [m]
r_{wb}	Wellbore radius [m]
$T_{t,i}$	Temperature at tubing inner radius [m]
$T_{t,o}$	Temperature at tubing outer radius [m]

$T_{pc,i}$ Temperature at production casing inner radius [m]

$T_{pc,o}$ Temperature at production casing outer radius [m]

$T_{ic,i}$ Temperature at intermediate casing inner radius [m]

$T_{ic,o}$ Temperature at intermediate casing outer radius [m]

T_{wb} Temperature at wellbore radius [m]

We will first write the expressions to calculate heat transfer in each layer. The expressions for forced convection inside the tubing, conduction in the tubing wall, in the production casing wall, in the cement between the intermediate and production casing and in the cement between the intermediate casing and formation are similar to the ones presented earlier for the case of the subsea pipeline and won't be repeated.

Free convection in the annulus

The heat transfer (free convection) in the annulus fluid can be expressed with the following expression:

$$\frac{d\dot{Q}}{dL} = -2 \cdot \pi \cdot r_{t,o} \cdot h_{ann} \cdot (T_{t,o} - T_{ic,i})$$

EQ. 8-31

Where:

$r_{t,o}$ Tubing outer radius [m]

h_{ann} Free convection coefficient, annulus [W/m^2.K]

$T_{t,o}$ Temperature of outer wall of tubing [K or °C]

$T_{ic,in}$ Temperature of inner wall of intermediate casing [or °C]

This heat transfer mechanism is usually free convection (the flow is induced by the temperature difference). The convective heat transfer coefficient h_{ann} depends on the fluid and wall temperatures, variables which are the result of pressure and temperature drop calculations and are not known a priori. It is often calculated from the Nusselt number (ratio of convective and conductive heat transfer h·L /k). The Nusselt number is often expressed as a function of the Reynolds number, the Prandtl number (μ·C$_p$ /k) and the Grashoff number (g·ρ^2·|ΔT|·L^3·|β| /μ^2). β is the thermal volumetric expansion coefficient at constant temperature, equal to $\frac{1}{\rho} \cdot \frac{\partial \rho}{\partial T}\Big|_{p=const}$

Therefore, the estimation of h_{ann} often requires an implicit calculation where a value is assumed, pressure and temperature are calculated in the conduit, and then a new value of h_{ann} is estimated. The process is repeated iteratively until convergence is achieved.

Overall heat transfer coefficient

The overall heat transfer coefficient is estimated by clearing temperature difference and summing up all expressions, as done previously:

$$(T_f - T_{t,i}) + (T_{t,i} - T_{t,o}) + (T_{t,o} - T_{pc,i}) + (T_{pc,i} - T_{pc,o}) + (T_{pc,o} - T_{ic,i}) + (T_{ic,i} - T_{ic,o})$$
$$+ (T_{ic,o} - T_{wb})$$

$$= \frac{-\frac{d\dot{Q}}{dL}}{2 \cdot \pi \cdot r_{t,i} \cdot h_i} + \frac{-\frac{d\dot{Q}}{dL}}{\frac{2 \cdot \pi \cdot k_t}{\ln\left(\frac{r_{t,o}}{r_{t,i}}\right)}} + \frac{-\frac{d\dot{Q}}{dL}}{2 \cdot \pi \cdot r_{t,o} \cdot h_{ann}} + \frac{-\frac{d\dot{Q}}{dL}}{\frac{2 \cdot \pi \cdot k_{pc}}{\ln\left(\frac{r_{pc,o}}{r_{pc,i}}\right)}} + \frac{-\frac{d\dot{Q}}{dL}}{\frac{2 \cdot \pi \cdot k_c}{\ln\left(\frac{r_{ic,i}}{r_{pc,o}}\right)}}$$

$$+ \frac{-\frac{d\dot{Q}}{dL}}{\frac{2 \cdot \pi \cdot k_{ic}}{\ln\left(\frac{r_{ic,o}}{r_{ic,i}}\right)}} + \frac{-\frac{d\dot{Q}}{dL}}{\frac{2 \cdot \pi \cdot k_c}{\ln\left(\frac{r_{wb}}{r_{ic,o}}\right)}}$$

EQ. 8-32

Clearing the temperature difference between fluid and wellbore wall:

$$(T_f - T_{wb}) = -\frac{d\dot{Q}}{dL}$$

$$\cdot \left[\frac{1}{2 \cdot \pi \cdot r_{t,i} \cdot h_i} + \frac{1}{\frac{2 \cdot \pi \cdot k_t}{\ln\left(\frac{r_{t,o}}{r_{t,i}}\right)}} + \frac{1}{2 \cdot \pi \cdot r_{t,o} \cdot h_{ann}} + \frac{1}{\frac{2 \cdot \pi \cdot k_{pc}}{\ln\left(\frac{r_{pc,o}}{r_{pc,i}}\right)}} + \frac{1}{\frac{2 \cdot \pi \cdot k_c}{\ln\left(\frac{r_{ic,i}}{r_{pc,o}}\right)}} \right.$$

$$\left. + \frac{1}{\frac{2 \cdot \pi \cdot k_{ic}}{\ln\left(\frac{r_{ic,o}}{r_{ic,i}}\right)}} + \frac{1}{\frac{2 \cdot \pi \cdot k_c}{\ln\left(\frac{r_{wb}}{r_{ic,o}}\right)}} \right]$$

EQ. 8-33

If the inner tubing radius will be used as reference radius, we then we divide by the inner perimeter of the inner tubing:

$$(T_f - T_{wb}) = -\frac{d\dot{Q}}{dL} \cdot \frac{1}{2 \cdot \pi \cdot r_{t,i}}$$

$$\cdot \left[\frac{1}{h_i} + \frac{r_{t,i} \cdot \ln\left(\frac{r_{t,o}}{r_{t,i}}\right)}{k_t} + \frac{r_{t,i}}{r_{t,o} \cdot h_{ann}} + \frac{r_{t,i} \cdot \ln\left(\frac{r_{pc,o}}{r_{pc,i}}\right)}{k_{pc}} + \frac{r_{t,i} \cdot \ln\left(\frac{r_{ic,i}}{r_{pc,o}}\right)}{k_c} \right.$$

$$\left. + \frac{r_{t,i} \cdot \ln\left(\frac{r_{ic,o}}{r_{ic,i}}\right)}{k_{ic}} + \frac{r_{t,i} \cdot \ln\left(\frac{r_{wb}}{r_{ic,o}}\right)}{k_c} \right]$$

EQ. 8-34

The overall heat transfer coefficient expressed in terms of the inner radius of the tubing is:

$$U = \left(\frac{1}{h_i} + \frac{r_{t,i} \cdot \ln\left(\frac{r_{t,o}}{r_{t,i}}\right)}{k_t} + \frac{r_{t,i}}{r_{t,o} \cdot h_{ann}} + \frac{r_{t,i} \cdot \ln\left(\frac{r_{pc,o}}{r_{pc,i}}\right)}{k_{pc}} + \frac{r_{t,i} \cdot \ln\left(\frac{r_{ic,i}}{r_{pc,o}}\right)}{k_c} + \frac{r_{t,i} \cdot \ln\left(\frac{r_{ic,o}}{r_{ic,i}}\right)}{k_{ic}} \right.$$

$$\left. + \frac{r_{t,i} \cdot \ln\left(\frac{r_{wb}}{r_{ic,o}}\right)}{k_c} \right)^{-1}$$

EQ. 8-35

Where:

h_i Convective coefficient, inner fluid [W/m^2.K]

k_t Thermal conductivity of tubing [W/m.K]

h_{ann} Free convection coefficient, annulus [W/m^2.K]

k_c Thermal conductivity of cement [W/m.K]

k_{pc} Thermal conductivity of production casing [W/m.K]

k_{ic} Thermal conductivity of intermediate casing [W/m.K]

As mentioned earlier for the case of the subsea pipeline, the terms for metal conduction (tubing and casing wall) are usually small and can be neglected (terms 2, 4 and 6). The term of forced convection in the pipe might be in the range O(1E-5) to O(1E-2) and could be neglected.

Free convection in the annulus (Term 3): The free convection coefficient in the annulus usually has values around 100 W/m^2 K. The ratio between outer and inner tubing diameter can range from 1.05 to 1.3. Therefore, this term is usually O(1E-2).

Conduction in cement (terms 5 and 7): The thermal conductivity of cement (k_c) is usually in the range between 0.3 to 2 W/m K. The ratio between the outer and inner diameter of the annular space is usually around 1.2. The inner tubing diameter is usually 0.02-0.2. Therefore, this term is usually O(1E-2).

Heat transfer in formation or soil

In the previous derivation, we were assuming that the temperature of the sandface of the formation is constant. However, this is often not the case when the well is producing or injecting. In these situations, the temperature of the formation near the wellbore will change (will be warmed up or cooled down) and the undisturbed formation temperature (geothermal) will be located farther away from the wellbore. For large times, a steady state will be reached where the temperature distribution in the soil will not change any longer.

The heat transfer in the formation is a transient problem and is often described with the following partial differential equation (here T$_e$ is soil temperature and r is radius):

$$\frac{\partial^2 T_e}{\partial r^2} + \frac{1}{r} \cdot \frac{\partial T_e}{\partial r} = \frac{c_e \cdot \rho_e}{k_e} \cdot \frac{\partial T_e}{\partial t}$$

EQ. 8-36

Where:

k_e Thermal conductivity, soil [W/m.K]

C_e Specific heat capacity, soil [J/K.kg]

t Time [s]

This equation is made for a given vertical position and is considering the heat transfer is mostly radial.

This equation has often the following initial conditions and boundary conditions:

$$T_e(r, t = 0) = T_{ei}$$

EQ. 8-37

$$\frac{\partial T_e}{\partial r}(r \to \infty, t) = 0$$

EQ. 8-38

$$\frac{d\dot{Q}}{dz} = -2 \cdot \pi \cdot k_e \cdot r_{wb} \cdot \frac{\partial T_e}{\partial r}\bigg|_{r=r_{wb}}$$

EQ. 8-39

The last boundary condition represents the heat transfer (per unit length) that is transferred with the well.

Several exact and approximate solutions have been proposed to this equation. An approach consists of defining a dimensionless temperature:

$$T_D = \frac{2 \cdot \pi \cdot k_e}{\frac{d\dot{Q}}{dz}}(T_{wb} - T_{ei})$$

EQ. 8-40

The behavior of dimensionless temperature with time can be approximated with the following expressions[8-1]:

$$T_D = 1.1281 \cdot \sqrt{t_D} \cdot (1 - 0.3 \cdot \sqrt{t_D}), \qquad for \quad t_D \leq 1.5$$

EQ. 8-41

$$T_D = \left(0.4063 + 0.5 \cdot \ln(t_D)\right)\left(1 + \frac{0.6}{t_D}\right) \quad for \quad t_D > 1.5$$

EQ. 8-42

With:

Dimensionless time, $t_D = \frac{\alpha_e \cdot t}{r_{wb}^2}$

And α_e is the thermal diffusivity of the soil, [m2/s], equal to $\frac{k_e}{\rho_e \cdot C_e}$

The solution above provides an expression of the temperature of the sandface (T_{wb}) with time, if the heat rate per unit length ($\frac{d\dot{Q}}{dz}$) is provided.

Now we will include the effect of the soil transient in the wellbore heat transfer equation. The heat transfer equation considering all heat transfer mechanisms from fluid to wellbore (sandface) is:

$$\frac{d\dot{Q}}{dL} = -2 \cdot \pi \cdot r_{t,i} \cdot U \cdot \left(T_f - T_{wb}\right)$$

EQ. 8-43

Clearing out the temperature of the sandface (T$_{wb}$):

$$T_{wb} = T_f + \frac{d\dot{Q}}{dL} \cdot \frac{1}{2 \cdot \pi \cdot r_{t,i} \cdot U}$$

EQ. 8-44

This expression is now substituted in the definition of dimensionless temperature, T$_D$:

$$T_D = \frac{2 \cdot \pi \cdot k_e}{\frac{d\dot{Q}}{dz}}\left(T_f + \frac{d\dot{Q}}{dL} \cdot \frac{1}{2 \cdot \pi \cdot r_{t,i} \cdot U} - T_e\right)$$

EQ. 8-45

The wellbore usually has some inclination, and therefore the vertical and along the pipe coordinates do not overlap. However, it is often assumed that this difference can be neglected and the terms $\frac{d\dot{Q}}{dL}$ and $\frac{d\dot{Q}}{dz}$ have the same magnitude. However, they have different signs ($\frac{d\dot{Q}}{dL} = -\frac{d\dot{Q}}{dz}$). For the wellbore, if the fluid is hotter than

the formation, the heat is lost to the formation, therefore the sign is negative. For the formation, if the fluid is hotter than the formation, the heat enters the formation, so the sign is positive.

Simplifying terms and rearranging:

$$T_D + \frac{k_e}{r_{t,i} \cdot U} = -\frac{2 \cdot \pi \cdot k_e}{\frac{d\dot{Q}}{dL}} \left(T_f - T_e\right)$$

EQ. 8-46

Clearing out the heat rate per unit length

$$\frac{d\dot{Q}}{dL} = -\frac{2 \cdot \pi \cdot k_e}{\frac{k_e}{r_{t,i} \cdot U} + T_D} \left(T_f - T_e\right)$$

EQ. 8-47

Separating terms to obtain the inner perimeter of tubing

$$\frac{d\dot{Q}}{dL} = -2 \cdot \pi \cdot r_{t,i} \cdot \left(\frac{U \cdot k_e}{k_e + T_D \cdot r_{t,i} \cdot U}\right)\left(T_f - T_e\right)$$

EQ. 8-48

This equation shows that the transient in the formation causes the effective overall heat transfer coefficient to be modified according to the following expression:

$$U_{eff}(t) = \left(\frac{U \cdot k_e}{k_e + T_D \cdot r_{t,i} \cdot U}\right)$$

EQ. 8-49

The thermal conductivity of the formation (k_e) is usually a number around 3 W/mK. Dimensionless temperature (T_D) is usually a number between 0 (early times) to 7 (late times). The inner tubing radius is usually ranging from 0.05 to 0.23 m. Overall heat transfer coefficient for wellbores are usually in the range 3-15 W/m2 K. Therefore, for late times, the effective overall heat transfer coefficient is usually lower than the overall heat transfer coefficient neglecting the formation. This means that the hot formation region around the wellbore with time acts as an insulating layer.

8.3.   BEHAVIOR OF SPECIFIC ENTHALPY OF OIL AND GAS VERSUS PRESSURE AND TEMPERATURE FOR MULTI-COMPONENT HYDROCARBON MIXTURES

Figure 8-6 presents a sketch of the variation of the oil and gas specific enthalpy properties versus pressure for three temperatures of the hydrocarbon mixture shown in Figure 8-7. At the given temperatures, single phase oil will be formed for pressures equal or greater than the bubble point pressures.
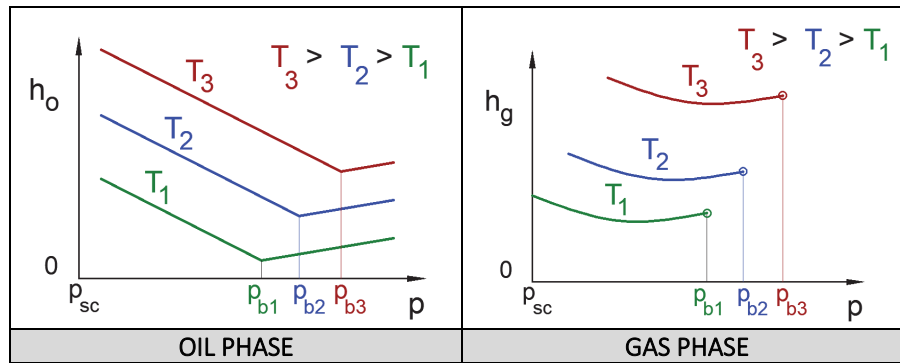
FIGURE 8-6. BEHAVIOR OF SPECIFIC ENTHALPY OF GAS AND OIL VS. PRESSURE FOR THREE TEMPERATURES
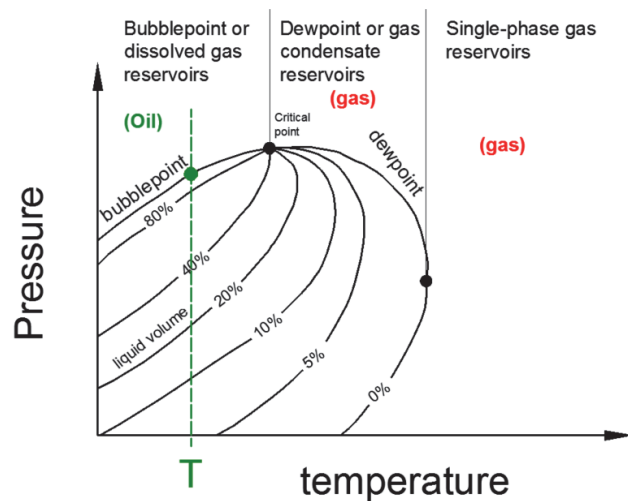
FIGURE 8-7. PHASE DIAGRAM OF THE HYDROCARBON MIXTURE USED IN FIGURE 8-6

Figure 8-8 presents a sketch of the variation of the oil and gas specific enthalpy properties versus pressure for three temperatures of the hydrocarbon mixture shown in Figure 8-9. At the given temperatures, single phase gas will be formed for pressures equal or greater than the dew point pressures.
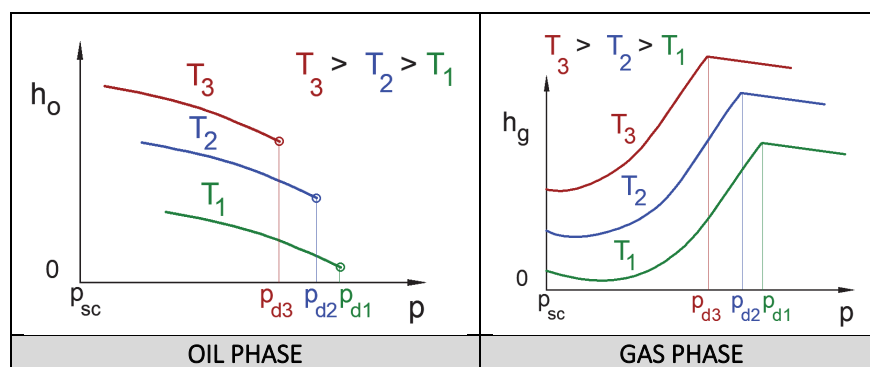
FIGURE 8-8. BEHAVIOR OF SPECIFIC ENTHALPY OF GAS AND OIL VS. PRESSURE FOR THREE TEMPERATURES
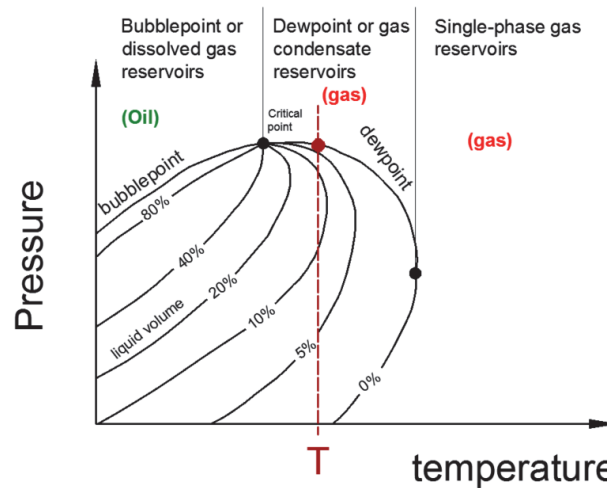
FIGURE 8-9. PHASE DIAGRAM OF THE HYDROCARBON MIXTURE USED IN FIGURE 8-8

The behavior shown in the figure corresponds to multi-component mixtures. For fluids consisting of pure components, the behavior in the single-phase region (liquid or gas) is similar, but in the saturation region it isn't, since there is only one saturation temperature ($T_{bubblepoint} = T_{dewpoint}$) at a given pressure. Therefore, in saturation, a pressure-temperature combination could give you several values of specific enthalpy.

8.4.   PROCEDURE TO ESTIMATE TEMPERATURE DROP IN A CONDUIT

Split the conduit in intervals and start your computations from a boundary point of known temperature. For every interval in the conduit, the temperature at the other end of the interval can be computed as follows:

- The heat exchanged by the section is computed using the temperature difference between the known temperature at one end of the interval (T_{in} or T_{out}) and the temperature of the environment (T_{amb}) at the corresponding end. The calculation requires the overall heat transfer coefficient of the section (U), the pipe inner diameter (ϕ) and the length of the interval (ΔL).

$$\dot{Q} = -(T_{in} - T_{amb@in}) \cdot U \cdot \pi \cdot \phi \cdot \Delta L \qquad \text{EQ. 8-50}$$

- The enthalpy at the other end of the interval is calculated with the energy equation, neglecting changes in specific kinetic energy

$$(\Delta h + \Delta z \cdot g) \cdot \dot{m} = \dot{Q} \;\; \rightarrow \;\; h_{out} = (h_{in} - \Delta z \cdot g) \cdot \dot{m} + \dot{Q} \qquad \text{EQ. 8-51}$$

- The temperature at the other pipe end is calculated with the PVT model, the value of specific enthalpy and the pressure. This usually requires some iteration to converge, e.g. assume a value of temperature, compute enthalpy with the PVT model, the pressure and assumed temperature and then verify that the computed enthalpy is equal than the one obtained with the energy balance.

This procedure assumes that pressure is known at the end of the segment. However, pressure calculations in a conduit also require a temperature input. Therefore, these must often be executed simultaneously.

REFERENCES

[8-1] Hasan, A.R.; Kabir, C.S. *Heat Transfer During Two-Phase Flow in Wellbores: Part I – Formation Temperature*. SPE paper 22866. 66th Annual Technical Conference and Exhibition. Dallas, October, 1991.

9.   GAS WELL LIQUID LOADING

Liquid loading is a phenomenon that occurs in gas wells producing associated liquid (e.g. condensate, water) whose symptoms are a sharp decline in production, intermittent production and presence of stagnant liquids in the wellbore. A liquid loaded well will eventually be unable to flow unaided.

It is commonly accepted that liquid loading occurs when the flow pattern of part of the wellbore starts transitioning from gas-dominated to liquid-dominated. Usually slug, churn and bubble are considered as liquid-dominated flow patterns and mist, annular as gas-dominated.

Figure 9-1 shows the flow pattern map of vertical upward flow in pipe for a specific set of fluid properties and pipe diameter. Gas-dominated flow patterns require high superficial velocities[38] of gas and relatively low superficial velocities of liquid.

Note the transitions are often not sharp as drawn in the figure, but gradual (e.g. in bands instead of lines). Additionally, visual classification of flow regimes can be highly subjective.
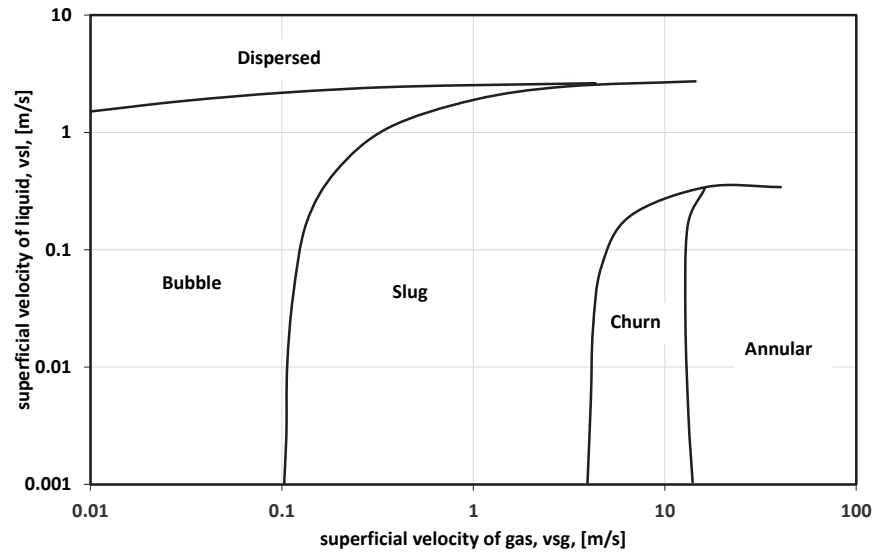
FIGURE 9-1. SAMPLE FLOW PATTERN MAP FOR VERTICAL (90°) UPWARD FLOW OF GAS AND LIQUID

Transition criteria for liquid loading is often built based on determining when the liquid phase will start to flow downwards starting from a gas-dominated flow pattern. For example, if one assumes that most of the liquid is transported in droplets, then liquid loading will occur when the gas is not able to drag droplets upwards and start traveling downwards. If, on the contrary, one assumes that most of the liquid is transported as a liquid on the wall, then liquid loading will occur when the velocity of the liquid at the film starts pointing downwards (Figure 9-2).

---

[38] Local rate of gas divided by the total pipe cross section area
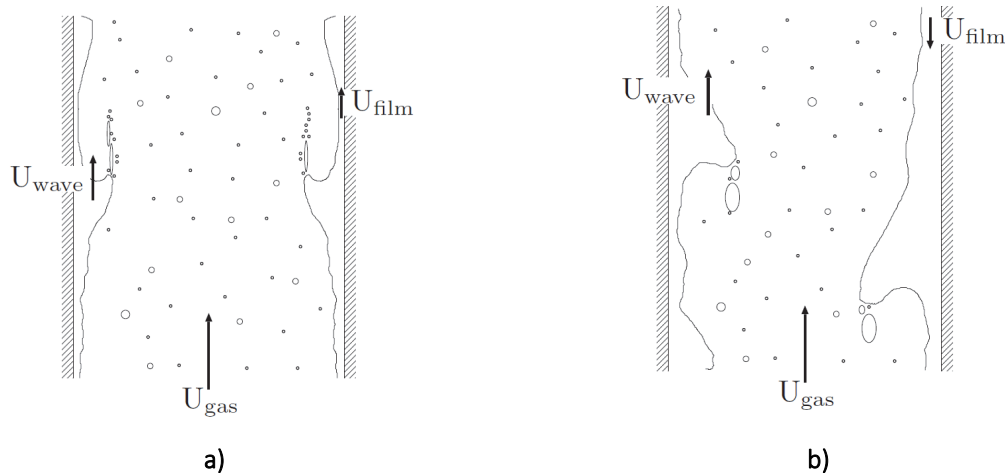
FIGURE 9-2. VISUALIZATION OF LIQUID LOADING TRANSITION CRITERIA WHEN THE LIQUID IS TRANSPORTED MAINLY AS A FILM ON THE PIPE WALL. A) REPRESENTS AN UNLOADED CONDITION (ANNULAR FLOW) AND B) REPRESENTS A LOADED CONDITION (CHURN-ANNULAR). TAKEN FROM VAN'T WESTENDE[7-3]

When loading occurs, it does not imply that the flow pattern will change immediately from gas to liquid dominated. It usually takes some further reduction in gas rate (or increase in the liquid rate) to fully achieve the transition.

The scientific and technical community has done extensive work in the past years to develop mechanistic and empirical models to estimate accurately the point where loading occurs. Some focus issues are how is the liquid distributed in the pipe (in droplets entrained in the gas or transported as a film on wall, or both) and the effect of pipe inclination on the asymmetry of the wall liquid film.

A typical procedure to determine if a well has liquid loading problems is to perform temperature and pressure drop calculations along the wellbore for its current operating conditions and apply a liquid loading criterion at all depths. Alternatively, to determine the flow pattern for all depths.

The onset of liquid loading is typically determined by finding the critical gas standard condition rate that causes the wellbore to exhibit liquid loading (or a liquid-dominated flow pattern) at least in one location.

As an example, consider a vertical gas well producing with a constant wellhead pressure of 14.8 bara, that has a total depth of 3 000 m, and inner tubing diameter of 0.15 m. The well is producing water, has a water gas ratio (WGR) of 5 stb/1E06 scf[39] and a condensate-gas ratio of 0 stb/1E06 scf. In this example, water is used instead of condensate, to partly remove the complexity of change in the mass rate of condensate along the tubing due to condensation or evaporation. The model did not consider vaporization of water in the gas. Multiphase flow calculations are made with a mechanistic model.

Figure 9-3 shows the calculated flow pattern along the tubing for several values of gas rate (at standard conditions). A TVD value of 0 m is the wellhead, and a TVD value of 3000 m is the bottom-hole. When the gas rate is reduced (from left to right) the wellbore transitions from flow patterns that are gas dominated (annular) to flow patterns that are liquid dominated (slug).

---

[39] Here field units are used because they are easier to remember

If one sets that the flow pattern "slug" is considered as liquid loaded, then the gas flow rate of 0.24 E06 Sm^3/d will be the critical loading gas flow rate, because that is the first rate for which a location in the tubing exhibits loading. To have an "unloaded" well, one must produce the well above this rate.
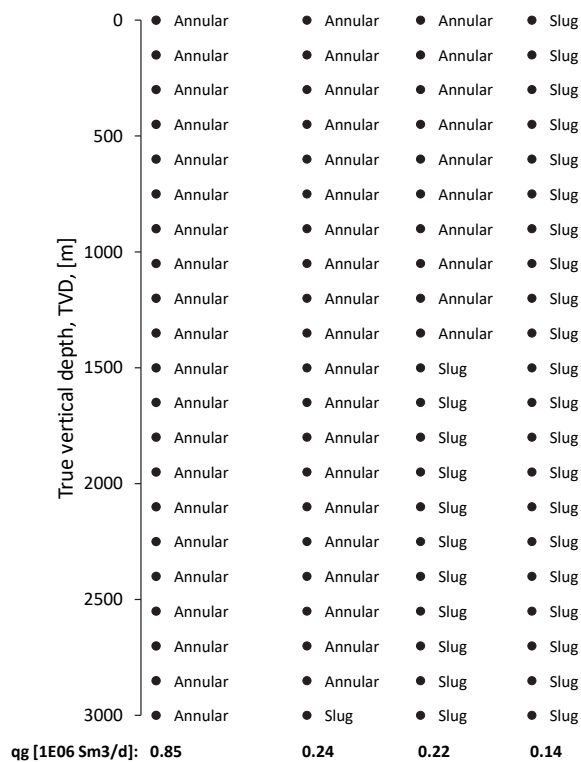
FIGURE 9-3. FLOW PATTERNS ALONG THE TUBING FOR THE TEST WELL FOR SEVERAL VALUES OF GAS RATE

The gas rate of a gas well will usually diminish with time, due to depletion. When this happens the gas well usually transitions from an unloaded to a loaded condition. The bottom of the well is usually the place where liquid loading occurs first. This is because the pressure is highest, the volumetric local rate of gas is smaller, and therefore the gas velocity (and superficial velocity) is highest.

However, the liquid rate also affects the flow pattern and liquid loading (ref. Figure 9-1). In some gas wells, due to condensation at low pressure and temperature, there is usually more free liquid at the wellhead than at the bottom-hole. Therefore, in these cases liquid loading occurs usually in the shallow part of the wellbore, despite the high gas velocities.

Figure 9-4 shows the flowing bottom-hole pressure and the percentage of wellbore volume occupied by the liquid versus standard conditions gas rates for the example case discussed earlier. The gas rate at which the "slug" flow pattern is detected in the tubing is marked with a vertical discontinuous violet line. For values of gas rates below the critical, the flowing bottom-hole pressure and percent of wellbore filled by the liquid start to increase abruptly. In this case, liquid loading is detrimental for well performance, because the pressure drop in the tubing increases with reduction in gas rate.
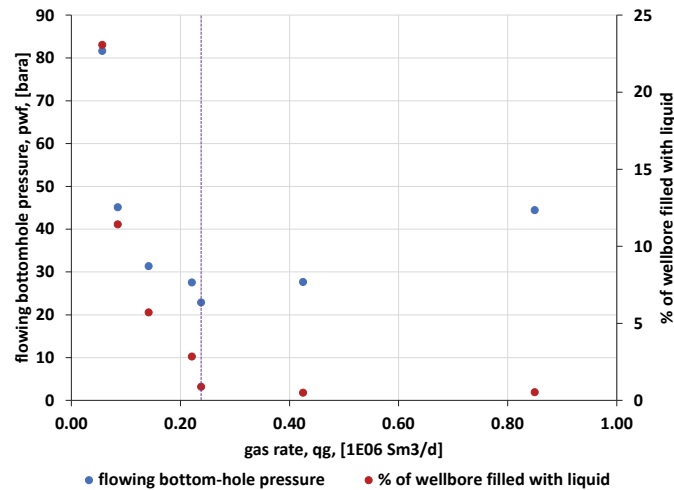
FIGURE 9-4. FLOWING BOTTOM-HOLE PRESSURE AND PERCENTAGE OF WELLBORE VOLUME OCCUPIED BY THE LIQUID VERSUS STANDARD CONDITIONS GAS RATE

9.1.   LIQUID LOADING MAPS

Liquid loading maps are plots that display the relationship between condensate gas ratio (or gas-oil ratio, GOR, or gas liquid ratio, GLR) and critical loading gas rate. Figure 9-5 shows a liquid loading map calculated for the example discussed earlier. This liquid loading map is made for a constant wellhead pressure. The critical gas rate is computed using the bisection method, starting with two extreme values: a very low gas rate (that will give loaded conditions) a very high gas rate (that will give unloaded conditions). The condensate-gas ratio is equal to 0 stb/1E06 scf. As mentioned earlier, WGR is used instead of CGR to remove complexities due to phase change. The model did not consider vaporization of water in the gas.

For this example, we are considering the flow pattern "slug" as liquid loaded.
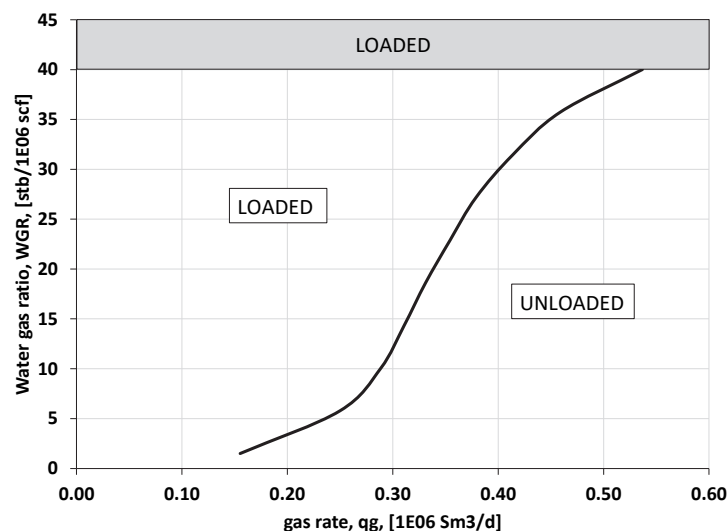
FIGURE 9-5. CURVES OF CRITICAL GAS RATE VERSUS WATER GAS RATIO FOR A WELLHEAD PRESSURE OF 14.8 BARA.

This figure shows that the critical gas rate increases with the WGR. This is because when the amount of liquid in the tubing increases, the superficial velocity of the liquid increases, and it is more likely the gas-liquid superficial velocity combination will fall in a liquid-dominated flow pattern region. However, when the WGR is greater than 40 stb/1E06 scf, no matter what gas rate the well is produced at, the well will always be loaded.

This could be explained by using at the flow map shown in Figure 9-1. For $u_{sl} > 0.2$ m/s, the flow pattern will always be slug, no matter how high the gas u_{sg} is.

Figure 9-6 shows the curves of critical gas rate versus condensate gas ratio for 3 values of wellhead pressure. Higher wellhead pressures have higher critical gas rates than lower wellhead pressures. This is because the gas volumetric rate is reduced at high pressure, and therefore superficial gas velocity will also be less.
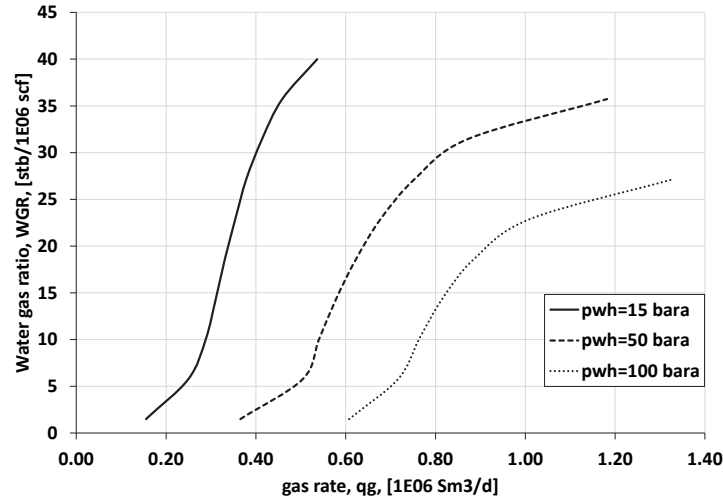
FIGURE 9-6. CURVES OF CRITICAL GAS RATE VERSUS WATER GAS RATIO FOR SEVERAL VALUES OF WELLHEAD PRESSURE

Figure 9-7 shows curves of WGR and critical gas rate for 3 values of tubing inner diameter at a constant wellhead pressure of 14.8 bara. Smaller tubing diameters move the curve to the left (require lower values of critical gas rates). This is because the superficial gas velocity is greater for lower diameters.
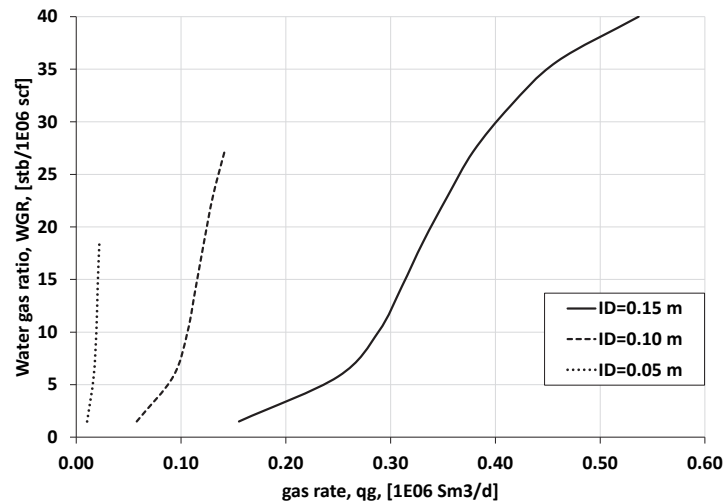
FIGURE 9-7. CURVES OF CRITICAL GAS RATE VERSUS WATER GAS RATIO FOR SEVERAL VALUES OF TUBING INNER DIAMETER

Liquid loading maps can be used to predict when a well will enter in liquid loading (e.g. by plotting the predicted pairs of CGR-qg and determine when they cross the boundary). Also, to determine what kind of changes can be done to the well (e.g. change tubing size, install a velocity string, change the wellhead pressure by choking, apply gas-lift etc.) to move the operational conditions from a loading state to a unloaded state.

9.1.1. ESTIMATING LIQUID LOADING MAP CURVES WITH REFERENCE POINTS

After inspection of Figure 9-6 and Figure 9-7, it seems it should be possible to find a liquid loading curve for a given diameter and wellhead pressure, by scaling the curve of a reference diameter and a wellhead pressure by a factor. The factor should involve the given and reference diameter and the given and reference wellhead pressure.

Estimating liquid loading map curves for a new diameter with a reference diameter

Table 9-1 shows a collection of data points representing a liquid loading curve at one reference tubing diameter (ϕ_{ref}) and a reference wellhead pressure ($\boldsymbol{p_{wh,ref}}$).

TABLE 9-1. DATA POINTS REPRESENTING A LIQUID LOADING CURVE AT ONE REFERENCE TUBING DIAMETER $\boldsymbol{\phi_{ref}}$ AND REFERENCE WELLHEAD PRESSURE $\boldsymbol{p_{wh,ref}}$.

Gas rate, $q_{\bar{g}}$	Liquid gas ratio, L_{gr}
$q_{\bar{g},1}$	$L_{gr,1}$
$q_{\bar{g},2}$	$L_{gr,2}$
$q_{\bar{g},3}$	$L_{gr,3}$
$q_{\bar{g},4}$	$L_{gr,4}$
$q_{\bar{g},5}$	$L_{gr,5}$

The liquid loading curve for a given diameter ϕ_1, and for the same reference wellhead pressure $p_{wh,ref}$ is calculated by applying the following transformation to the points provided in Table 9-1.

$$\left(q_{\bar{g},1}\right)_{@\phi_1} = \left(q_{\bar{g},1}\right)_{@\phi_{ref}} \cdot \left(\frac{\phi_1}{\phi_{ref}}\right)^{2.46} \qquad \text{EQ. 9-1}$$

$$\left(L_{gr,1}\right)_{@\phi_1} = \left(L_{gr,1}\right)_{@\phi_{ref}} \qquad \text{EQ. 9-2}$$

This scaling procedure does not account for the fact that liquid loading curves at different diameters will have different values of $L_{gr,max}$. For this reason, to avoid missing parts of the curve during the scaling process is recommended to use as reference curve one that covers the highest range in L_{gr}, i.e. the one for the largest diameter. The value of $L_{gr,max}$ for a given diameter ϕ_1 (at a constant wellhead pressure $\boldsymbol{p_{wh,ref}}$) can be obtained from the following equation:

$$\frac{\left(L_{gr,max}\right)_{@\phi_1,\boldsymbol{p_{wh,ref}}}}{\left(L_{gr,max}\right)_{@\phi_{ref},\boldsymbol{p_{wh,ref}}}} = 0.48 \cdot \left(\frac{\phi_1}{\phi_{ref}}\right)^2 + 0.16 \cdot \left(\frac{\phi_1}{\phi_{ref}}\right) + 0.36 \qquad \text{EQ. 9-3}$$

Estimating liquid loading map curves for a new wellhead pressure with a reference wellhead pressure

The value of $L_{gr,max}$ for a given wellhead pressure $p_{wh,1}$ (and a reference diameter ϕ_{ref}), can be obtained from the following equation:

$$\frac{\left(L_{gr,max}\right)_{@\phi_{ref},p_{wh,1}}}{\left(L_{gr,max}\right)_{@\phi_{ref},p_{wh,ref}}} = -0.0032 \cdot \left(\frac{p_{wh,1}}{p_{wh,ref}}\right)^2 - 0.031 \cdot \left(\frac{p_{wh,1}}{p_{wh,ref}}\right) + 1.0342 \qquad \text{EQ. 9-4}$$

The reader is adviced that the values of the constants given in this section depend on the actual system modeled and shouldn't be generalized for all cases.

9.2.   "TRANSIENTNESS" OF LIQUID LOADING

Not so transient after all?

As shown in the previous sections, when the well gas rate is reduced (or the CGR increases) this usually leads to an increase in the liquid content of the wellbore. For this to occur, there must a transient liquid buildup process from a condition 1 (CGR_1, q_{g1}) to a condition 2 (CGR_2, q_{g2}) where part of the reservoir liquids will not be produced to surface but will be gradually "retained" in the wellbore. However, such liquid volumes and usually small and the accumulation process occurs gradually over long time (days-weeks-months). Therefore, the evolution of the wellbore conditions in time can often be properly approximated by a sequence of steady states.

Transition criteria for liquid loading is often built based on determining when the liquid phase will start to flow downwards considering a gas-dominated flow pattern. However, this does not mean that the net flow of liquid will be downwards once the well is loaded (e.g. the liquid will drip and accumulate at the bottom of the wellbore and never flows to surface). When liquid starts traveling downwards in a mist/annular flow pattern, the flow pattern will eventually change to churn/intermittent flow, characterized by quick transients with upwards and downwards flow of pockets of gas, slugs of liquid and liquid waves in a chaotic manner. In these flow patterns, the net liquid and gas flux over a sufficiently long time (seconds/minutes) are still upwards, but there are some short quick periods where there the flow is downwards or there might be part of the cross-section area with fluid recirculation. Intermittent flow patterns such as slug and churn can still be modeled with steady state approximations.

When churn and slug flow occur at the bottom of the well, there will be a significant pressure gradient along the sand face. Due to this, and if the perforated interval is long, the inflow will usually be unevenly distributed, exhibiting low velocities at the bottom and high velocities at the top (even to the extreme of flow back to the formation). When this occurs, the gas velocities at the lower part of the wellbore might not enough to lift the liquid upwards. Figure 9-8 shows an example of such a case. In the configuration shown, a liquid column is established at the well bottom. Part of the liquid flows back into the formation and gas and liquid enter through mainly through the top part of the interval.
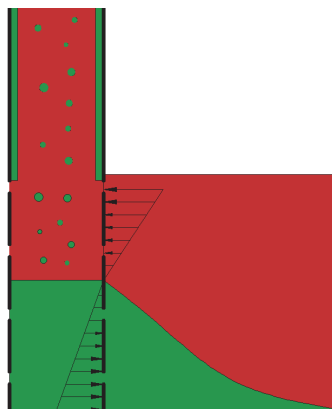
FIGURE 9-8. SKETCH SHOWING A CONFIGURATION AT WELL BOTTOM WITH DISTRIBUTED INFLOW WITH DOWNHOLE LIQUID SEPARATION AND BACK-SEEPAGE FROM WELLBORE TO THE FORMATION

The configuration shown in Figure 9-8 can still be modeled with a steady-state approximation.

Some transient situations

There could be some situations for which a steady-state approximation does not work. For example, situations where part of the liquid does not flow upwards with the gas and accumulates at the bottom of the well (e.g. in a stagnant column). However, for this situation to occur, the gas velocity must usually be very low (which imply very low gas production rates) and the well gets filled with liquid very quickly. In these cases, one should notice a significant drop in the liquid production of the well (e.g. a reduction in the producing WGR, CGR or LGR).

Churn and slug flow can create transient rapid pressure fluctuations that can cause liquid flowback to the formation and transient conditions downhole, especially if the inflow is distributed over a distance.

There could be some cases where liquid loaded wells exhibit transient production in large time scales (hours). Some examples are listed next:

- If the well is deviated, has a horizontal section, or has a high degree of tortuosity in the horizontal section, a phenomenon similar to severe slugging in risers and pipeline is triggered due to the accumulation of liquids in low points. A cyclic pressure build-up and blow down occurs that drives liquids upwards cyclically.
- Cyclic wellbore-formation interaction, due to, for example liquid accumulation in the near wellbore region (condensation banking).

DELIQUIFICATION METHODS SPOTLIGHT: PLUNGER LIFT

Plunger lift is a deliquification method used to remove liquids accumulated at the bottom of the well and improve production. It is often used to counteract liquid loading issues. A schematic of a well with plunger lift installed is shown in Figure 9-9 below:
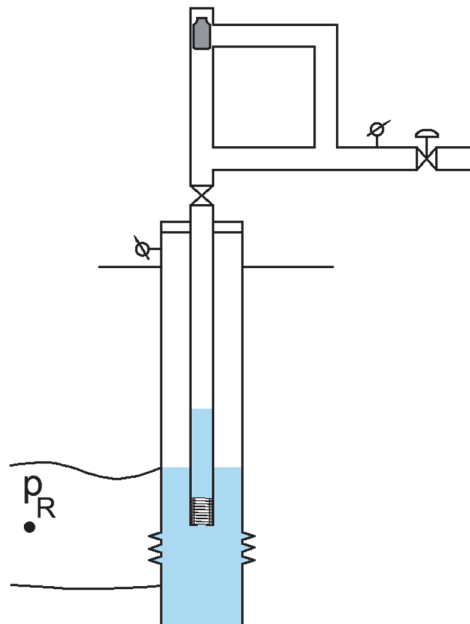
FIGURE 9-9. SKETCH SHOWING THE CONFIGURATION OF A PLUNGER LIFTED WELL

There is a plunger (gray color) which, simply put, is a cylindrical piston that travels up and down the tubing. The plunger actuation is controlled by the opening and closing of the motorized valve located at the surface. Plunger lift consists of 4 "stages":

- **Stage 1, well shut-in.** The well is shut in with the motorized valve, gas production at the surface and in the tubing is interrupted. Liquids slide down and accumulate at the bottom, the plunger drops and travels to the bottom of the tubing (stops at a bumper spring). The velocity of the plunger is maybe 5 m/s or less (for example when passing through the liquid), so, for a 2 000 m-long tubing, it will take around 6 minutes (or more) to reach the bottom. The pressure at the bottom-hole increases due to reservoir influx and gas is stored in the annulus.
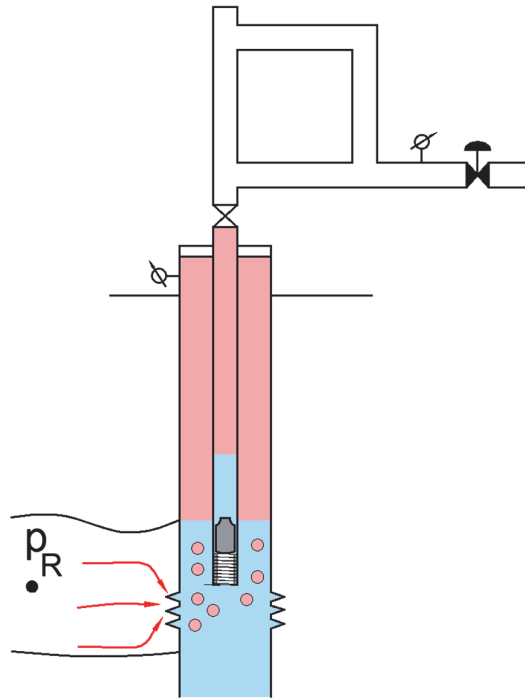
FIGURE 9-10. SKETCH SHOWING STAGE 1 OF A PLUNGER LIFT CYCLE, SHUT-IN. MOTORIZED VALVE IS CLOSED, PLUNGER DROPS AT THE BOTTOM OF THE TUBING.

- **Stage 2, pressure build-up.** The well is often kept shut-in for a long period (hrs), to allow bottom-hole pressure to increase and achieve better liquid displacement and higher gas rates when the well is put to production again.
- **Stage 3, production start.** The motorized valve is opened. The plunger is pushed upwards by the gas in the near wellbore and the gas in the casing. The average velocity of the plunger might be something in the vicinity of 5-10 m/s (higher at the beginning of the cycle and slower later). For a 2 000 m long tubing this means it takes between 3-6 min to reach the top of the well. During this stage, all the gas that is above the liquid slug pushed by the plunger is produced (and maybe some gas bypasses the plunger and liquid slug).
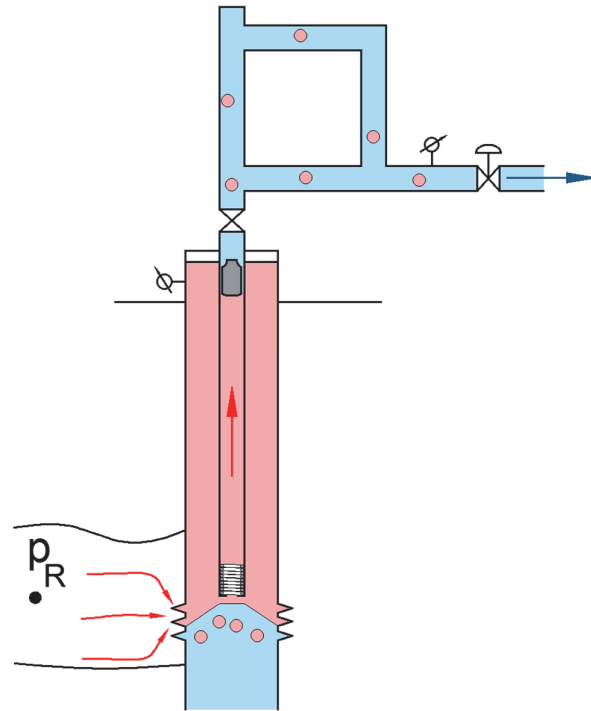
FIGURE 9-11. SKETCH SHOWING STAGE 3 OF A PLUNGER LIFT CYCLE, PRODUCTION START. MOTORIZED VALVE IS OPEN, PLUNGER IS PUSHED BY CASING AND FORMATION GAS UPWARDS, DISPLACING THE LIQUID ABOVE.

- **Stage 4, production.** The plunger reaches the top and is parked. The gas flowing behind is deviated to a bypass line, which is usually accompanied by a modest increase in the gas rate, since it doesn't have to push plunger and liquid slug any longer, it is flowing through unobstructed pipe and the wellbore is liquids free.
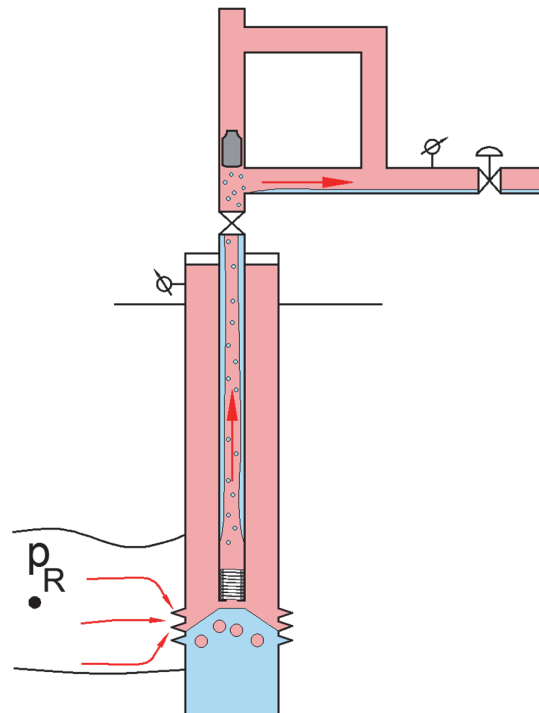
FIGURE 9-12. SKETCH SHOWING STAGE 4 OF A PLUNGER LIFT CYCLE, PRODUCTION.

For the rest of stage 4, reservoir gas and liquid enter the wellbore. Most of the liquid stays behind being accumulated at the bottom of the well. The duration of this stage is usually short (maybe a few hours) because the liquid fills up the tubing quite quickly, but it depends on the liquid gas ratio of the well and size of tubing and casing.
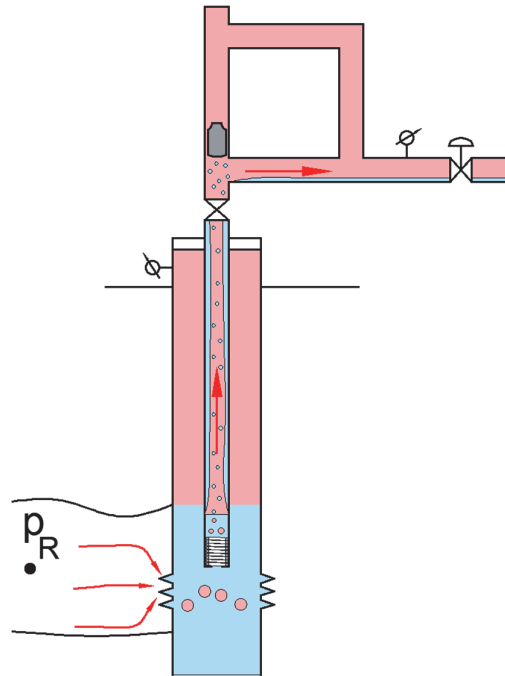
FIGURE 9-13. SKETCH SHOWING STAGE 4 OF A PLUNGER LIFT CYCLE, PRODUCTION. THERE STARTS TO BE LIQUID ACCUMULATION IN THE TUBING AND BOTTOM-HOLE.

- The cycle is repeated (back to stage 1)

Figure 9-14 show the evolution of the well gas rate (dark red dots), the well reservoir influx (bright red line) and bottom-hole pressure (blue line) in the 4 stages, and the flowing bottom-hole pressure (in solid green).
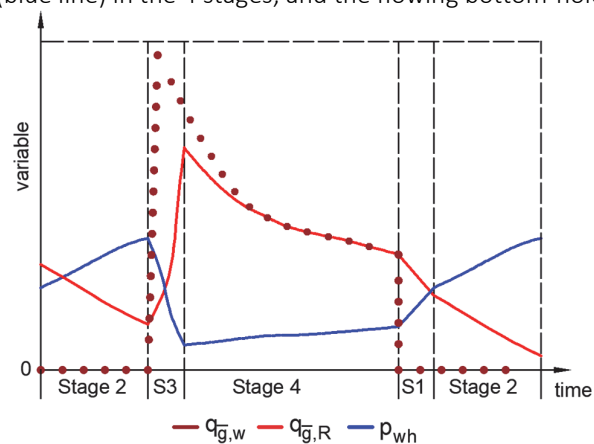
FIGURE 9-14. SKETCH SHOWING THE BEHAVIOR OF BOTTOM-HOLE FLOWING PRESSURE, GAS STANDARD CONDITIONS RATE AT WELLHEAD, GAS STANDARD CONDITIONS RATE PRODUCED BY FORMATION FOR ALL STAGES OF PLUNGER LIFT.

References

[9-1] Barnea, D. (1986), "Transition from annular flow and from dispersed bubble flow-unified models for the whole range of pipe inclinations", International journal of multiphase flow 12(5), 733-744.

[9-2] Turner, R., Hubbard, M. and Dukler, A. (1969), "Analysis and prediction of minimum flow rate for the continuous removal of liquids from gas wells", Journal of Petroleum Technology 21(11), 1-475.

[9-3] Van't Westende, J. M. C. (2008), "Droplets in annular-dispersed gas-liquid pipe-flows", PhD thesis, Delft University of Technology, Netherlands.

10. CO$_2$ TRANSPORT AND STORAGE

Disclaimer: the values given in this section should be taken with a grain of salt, since significant approximations are made to get ballpark numbers to use in the discussion.

10.1. INTRODUCTION AND BACKGROUND

Carbon dioxide is often produced by the combustion of hydrocarbons to generate energy. The energy released by combustion is often used for the generation of heat, electricity or shaft power. As an example, consider the chemical reaction that occurs when combusting methane:

$$CH_4 + 2 \cdot O_2 \rightarrow CO_2 + 2 \cdot H_2O$$

EQ. 10-1

1 mol of methane (16 g) gives 1 mol of CO$_2$ (44 g). There is therefore a mass ratio of 2.75 between CO$_2$ and hydrocarbons. This ratio will change slightly depending on which hydrocarbon is being combusted (for example for pentane it is around 3).

Reality check

Consider you are evaluating developing a CO$_2$ capture system for your combustion engine car (which might have a tank of around 50 l, or ca 38 kg of gasoline). If you plan to refuel and dispose CO$_2$ when the tank is half full (19 kg) you must plan to carry in the car ca. 3·19 = 57 kg of CO$_2$ in the car + the associated capture equipment. This is significant weight, that will negatively affect the fuel efficiency and size of the vehicle.

For natural gas (which is mainly methane) often the unit of Sm^3 is used, and metric tons (t, 1000 kg) for CO$_2$. Assuming a natural gas standard condition density of 0.65 kg/m^3, and using the mass ratio of 2.75 found above, this gives 1.788 E-3 t CO$_2$/Sm^3 of natural gas when combusted (or, alternatively, 1.788 kg CO$_2$/Sm^3).

To do the equivalent calculation for oil, let's assume it is possible to use an equivalency between a Sm^3 of gas and a Sm^3 of oil equivalent (o.e.). The Norwegian Offshore directorate specifies[40] that 1 000 Sm^3 of natural gas are equivalent to 1 Sm^{3}o.e. Therefore, using this relationship, an oil equivalent standard cubic meter emits 1.788 t CO$_2$ if/when combusted (for example if used as gasoline in a combustion engine vehicle).

There are 3 main categories of Green House Gas emissions of an entity[41]:

- Scope 1. Emissions that the entity makes directly during operations.
- Scope 2 Emissions that the entity makes indirectly during operations (emitted by services acquired by the company)
- Scope 3. Emissions that are emitted by the products sold (when costumers use the product) and acquired (when manufactured) by the entity.

In the oil and gas industry, some examples of scope 1 CO$_2$ emissions are:

- Natural gas burning in gas turbines for generation of electricity and shaft power
- Combustion of hydrocarbons for heat generation
- Transport

---

[40] https://www.sodir.no/en/about-us/use-of-content/conversion-table/

[41] https://www2.deloitte.com/uk/en/focus/climate-change/zero-in-on-scope-1-2-and-3-emissions.html

- Drilling, completion and intervention

Regarding Scope 1 emissions, an indicator that is typically used to quantify it is the amount of CO$_2$ emitted to produce a unit of oil equivalent, also known as carbon intensity. The average for Norway in 2018 was 0.0503 t CO$_2$/Sm^3.o.e. This value is usually related with the amount of energy required to produce the oil and gas and it varies significantly by field, type of energy source and stage in the field life[42].

Regarding scope 3 emissions, the estimation of the indicator CO$_2$ emitted/unit of oil equivalent produced requires a comprehensive tracking of the CO$_2$ emissions produced by the oil and gas sold to the market and its final uses (and tedious and lengthy calculations). However, usually a significant portion of the oil and gas is combusted to generate energy for vehicles, electricity, heat, and industry[43] so the value is somewhat similar to the previous number estimated above (1.788 t CO$_2$/ Sm^3 o.e.). Using values for 2023 published by Equinor[44] the value obtained is, in fact, surprisingly similar (2 t CO$_2$/ Sm^3 o.e.).

Reality check

In the oil and gas industry, Scope 3 emissions are several times larger than Scope 1 emissions (using 1.788 t CO$_2$/ Sm^3 o.e./ 0.0503 t CO$_2$/Sm^3.o.e gives ca **35 larger**). Therefore, when tackling Greenhouse Gas (GHG) emissions, the most important action is to mitigate the emissions generated by the combustion of oil and gas products.

More details about Scope 1 emissions

It is often reported[45] that most (**80%+**) of the Scope 1 emissions of the Norwegian oil and gas industry come from gas turbines. Consider a gas turbine of 45 MW[46]. Gas turbines for offshore applications have efficiencies of 40-50%. Consider the following approximation to define gas turbine efficiency:

$$\eta = \frac{\dot{W}_{out}}{\dot{m}_g \cdot C_v}$$ EQ. 10-2

Where $\dot{W}_{out}$ is the power produced by the turbine, while the denominator is the total energy released by the combustion (gas mass flow times the calorific value). The energy content (calorific value or heat of combustion) of natural gas (which is mainly methane) varies between 42-55 MJ/kg[47] (or ca 12-15 kWh/kg). If one assumes

---

[42] The energy required by the field varies somewhat with the produced rates, but there is always a constant base load. At initial times, the oil and gas rates are high, and energy required to produce, and associated CO$_2$ emissions are high. At late times, oil and gas rates are low and energy required to produce, and associated CO$_2$ emissions are still medium-high.

[43] https://www.epa.gov/ghgemissions/global-greenhouse-gas-overview

[44] https://sustainability.equinor.com/climate-tables

[45] https://www.sodir.no/en/whats-new/publications/reports/resource-report/resource-report-2019/emissions-discharges-and-the-environment/

[46] https://www.havtil.no/contentassets/3391c6686b2b4265abe8585294151335/2020_1862_rapport-equinor-hammerfest-lng-gransking.pdf

[47] https://group.met.com/en/media/energy-insight/calorific-value-of-natural-gas The differences are usually due to composition changes and also to the state of the water at the end of the reaction (in vapor or liquid).

a natural gas standard condition density of 0.65 kg/m^3, this gives between ca 27-36 MJ/Sm^3 (or ca 7.6-10 kWh/Sm^3). The amount of gas burned is therefore[48]:

$$\dot{m}_g = \frac{\dot{W}_{out}}{\eta \cdot C_v} = \frac{40\ MW}{0.45 \cdot 7.6\ E-3\ MWh/Sm^3} = 280\ 702\ Sm^3/d \qquad \text{Eq. 10-3}$$

Which is around 280 702 Sm^3/d · 1.788 E-3 t CO₂/Sm^3 = 502 t CO₂/d.

With these values, we obtain the following approximate relationship for gas turbines: 1 MWh electricity generated → 300 Sm^3 of natural gas → 0.5 t CO₂. These values are similar to values reported elsewhere[49] and can be used as a proxy for power generation offshore using gas turbines.

This relationship (1 MWh electricity generated → 0.5 t CO₂) together with the emissions indicator (0.0503 t CO₂/Sm^3.o.e.) can be used to obtain the required amount of energy to produce a Sm^3 o.e (energy intensity). This assuming all the energy comes from gas turbines, which it is not always accurate. This gives 100 kWh/Sm^3.o.e[50]. This value is several times smaller than the amount of energy contained in the oil equivalent. If we use the conversion between natural gas and oil equivalent (1000 Sm^3 of natural gas are 1 Sm^3 o.e.), natural gas has an energy content of 7.6-10 kWh/Sm^3, therefore oil equivalent energy content is ca. 7581-9927 kWh/Sm^3 o.e. This gives a ratio of 75 between energy contained in the oil equivalent versus energy required to produce it.

However, as mentioned earlier, energy intensity and carbon intensity values vary widely during the life of the field. Using data for the Wisting field[51] one finds a variation from early time to late time for the carbon intensity from 0.022-0.12 t CO₂/Sm^3.o.e. and 75-460 kWh/ Sm^3.o.e for the energy intensity.

10.1. THE CO₂ CAPTURE AND SUBSURFACE STORAGE VALUE CHAIN

One method to reduce the amount of CO₂ that ends up in the atmosphere is to capture it (for example, from exhaust of combustion chambers), making it purer, transport it to an injection location and store it underground. This method is, in essence, waste management (there is practically no end use or economic value for the large amounts of CO₂ captured). The only reason why it is applied is due to regulation, or because it is more economical than paying for economic penalties associated with CO₂ emissions to the atmosphere[52].

Therefore, it is necessary to make it very efficient and low cost. Additionally, it is important to do it safe as large CO₂ leakages and high CO₂ concentrations can also cause human losses.

---

[48] The gas standard condition rate required (280 702 Sm^3/d) is not much for a big offshore gas producer (with production in the order of 3 E06 Sm^3/d). But it could be equivalent to the production of some medium-size onshore gas producers.

[49] https://www.rte-france.com/en/eco2mix/co2-emissions

[50] As a reference, the battery of an electric SUV is of around 100 kWh.

[51] https://www.equinor.com/content/dam/statoil/documents/impact-assessment/wisting/equinor-wisting-forslag-til-ku-program-05-01-21.pdf

[52] Measures that are put in place to ultimately avoid damage to the environment

10.1.1. THE NORWEGIAN CONTEXT

It has been estimated[53] that Norway has a CO$_2$ storage capacity in the Norwegian continental shelf (NCS) or around 70 Gt of CO$_2$. To put this number in perspective, consider the following numbers:

- Norway's CO$_2$ emissions in 2022 where 0.031 Gt.
- Norwegian oil and gas production in 2022 was 232.8 MSm^3 o.e. The scope 3 CO$_2$ emissions associated with this production could be estimated as 1.788 t/Sm3 o.e. · 232.8 MSm^3 o.e. = 0.4 Gt CO$_2$.
- Norwegian oil and gas production from start until 2023 has been 8489 MSm^3 o.e. The scope 3 CO$_2$ emissions associated with this production could be estimated as 1.788 t/Sm3 o.e. · 8489 MSm^3 o.e. = 15 Gt CO$_2$.

It is planned that each Norwegian CO$_2$ injection well will have a capacity of 1.5 Mt/y. If one assumes each well has a lifetime of ca. 70 years, then this gives each well will be able to store, in average, 0.105 Gt.

To exploit all the storage available in the NCS, a total number of 667 wells are needed. To make the Norwegian oil and gas carbon neutral and compensate for scope 3, CO$_2$ emissions, a total of 278 wells would be currently needed in the NCS. To put this number in perspective, as of July 2024, according to the website of the Norwegian offshore directorate, there are a total of 7619 exploration and production wells (active and inactive), and a total of 207 wells were drilled in 2023.

10.1.2. CO$_2$ CAPTURE

The capture and purification process must remove other components that are unnecessary to store (e.g. nitrogen, methane, carbon monoxide, which are typical products of air combustion) and components that could cause issues (e.g. material integrity) in the transportation and storing system. Current CO$_2$ specifications for transport, injection and storage are quite strict. For example, the Northern Lights[54] project, which considers CO$_2$ transport by tanker, requires a minimum CO$_2$ content of 99.81% mol-% and less than 30 ppm-mol of water, among many other requirements. The CO$_2$ Aramis specification[55] for pipeline transport requires a minimum CO$_2$ content of 95% mol-% and less than 70 ppm-mol of water, among many other requirements. These requirements must be achieved using specialized processing equipment that are costly and energy intensive.

The cost of CO$_2$ capture is often expressed in terms of monetary unit per ton of CO$_2$. This cost value often includes lifetime costs, including, among others capital expenditures to design and build the capture facility, operational expenditures, etc. The cost depends strongly on the concentration of CO$_2$ in the inlet stream to the capture facility (low concentration gives high cost). As an example, for capture from power generation, where the exhaust has a low CO$_2$ concentration[56], the number ranges from 50-100 USD/t CO$_2$[57].

Regarding energy intensity, numbers vary widely depending on the application, but we could use a figure of 300-400 kWh/t CO$_2$[58] as a reference.

---

[53] https://www.sodir.no/en/whats-new/publications/co2-atlases/co2-storage-atlas-norwegian-north-sea/

[54] https://norlights.com/wp-content/uploads/2024/02/Northern-Lights-GS-co2-Spec2024.pdf

[55] https://www.aramis-ccs.com/files/ARM-CPT-BB8-PRO-MEM-0033-rev-6.2-public-version-NEW.pdf

[56] Considering combustion of methane and air, the mass percent of CO$_2$ in the exhaust will be of around 15%. However, combustion is usually done on excess air, thus the actual mass % could be much lower.

[57] https://www.iea.org/commentaries/is-carbon-capture-too-expensive

[58] https://www.shareyourgreendesign.com/energy-fundamentals-of-carbon-capture/

Simple energy accountancy of CCS – thought experiment

An issue that must be considered when evaluating CCS, is the amount of energy that is needed. We want to avoid the situation in which more energy is invested in capturing and storing the CO$_2$ than what we get out of the hydrocarbon combustion.

Consider the hypothetical scenario in which scope 1 and scope 3 emissions of the oil and gas industry will be compensated by using CO$_2$ capture, transport and injection (The oil and gas industry will be carbon neutral). Using the CO$_2$ energy intensity value provided above (neglecting energy expenses during transportation and injection which are usually much less than the capture requirements) and the scope 1 and 3 carbon intensities given earlier (for scope 1, 0.0503 t CO$_2$/Sm^3.o.e, for scope 3, 1.788 t CO$_2$/ Sm^3 o.e.) one can compute a CCS-related energy intensity per standard cubic meter of oil equivalent of 551-735 kWh/Sm^3[59].

Let's assume that the energy intensity due to oil and gas production is in the range 75-460 kWh/ Sm^3.o.e[60]. So, the total energy intensity of oil equivalent, considering carbon capture and production could be in the range 626-1195 kWh/ Sm^3.o.e. As a comparison, the energy contained in the oil could be in the range: 7581-9927 kWh/Sm^3 o.e. Therefore, it seems we will still get many times more energy from hydrocarbons even if we apply CCS.

10.1.1. CO$_2$ TRANSPORT

The current approach chosen for future large-scale disposal of CO$_2$ in Norway is transport via tanker or pipeline from Europe and onshore Norway and further injection in subsurface reservoirs. Tankers will be used initially, until pipeline infrastructure is built.

It is usually desirable to transport CO$_2$ in liquid phase, since the density is high (similar to water), it allows to transport more mass in the same volume and to use liquid pumps instead of compressors and reduce energy requirements. In tankers, high density is achieved by liquefaction, lowering temperature (e.g. around -30 °C). Pressure is kept relatively low (15 barg), which allows to use thinner vessel walls and reduce weight. When offloading to the riser that connects to the subsea injection system, pressure and temperature are increased (e.g. to around 60 bar and °0 C) by means of a pump and heater.

In pipelines and subsea distribution systems, due to the long distances, the CO$_2$ usually reaches thermal equilibrium with the seafloor temperature, which is usually at temperatures in the range 4-8 °C, depending on depth and location. At these temperatures, the saturation pressure of pure CO$_2$ is around 40 bara, which means that liquid will form at higher values. Pressure in the transportation pipelines will be in the range of 80-200 bara, to compensate for friction pipe losses and have sufficient pressure to inject into the formation.

In the well, the temperature of the CO$_2$ will increase due to heating up from the formation. The temperature of the formation depends on the depth, but if one assumes a 3 °C/100 m gradient, then this gives that the reservoir temperature might be around 30-40 °C for a 1000 m-deep well.

---

[59] (0.0503 t+1.788 t CO$_2$/Sm^3.o.e) · (300-400 kWh/t CO$_2$)

[60] Values calculated for the Wisting field https://www.equinor.com/content/dam/statoil/documents/impact-assessment/wisting/equinor-wisting-forslag-til-ku-program-05-01-21.pdf

Figure 10-1 below shows values of density and viscosity of pure CO$_2$ for the range of temperatures and pressures encountered in Norwegian injection systems.

density [kg/m3]	T [C] 0	10	20	30	40	50		viscosity [Pa s]	T [C] 0	10	20	30	40	50
50	940	587	144	125	114	105		50	1.04E-04	5.92E-05	1.66E-05	1.67E-05	1.70E-05	1.74E-05
60	948	882	567	175	150	136		60	1.07E-04	8.83E-05	5.11E-05	1.79E-05	1.78E-05	1.80E-05
70	955	893	808	487	201	173		70	1.09E-04	9.10E-05	7.29E-05	3.80E-05	1.92E-05	1.89E-05
80	962	903	827	692	287	221		80	1.11E-04	9.36E-05	7.66E-05	5.52E-05	2.25E-05	2.04E-05
90	968	912	843	743	482	288		90	1.13E-04	9.59E-05	7.97E-05	6.22E-05	3.49E-05	2.30E-05
100	974	920	856	771	620	387		100	1.15E-04	9.82E-05	8.25E-05	6.66E-05	4.70E-05	2.82E-05
110	980	928	868	792	682	499		110	1.17E-04	1.00E-04	8.50E-05	7.02E-05	5.41E-05	3.60E-05
120	985	935	878	809	717	582		120	1.19E-04	1.02E-04	8.74E-05	7.32E-05	5.88E-05	4.33E-05
130	990	942	887	823	743	635		130	1.21E-04	1.04E-04	8.96E-05	7.59E-05	6.25E-05	4.88E-05
140	995	948	896	836	763	672		140	1.22E-04	1.06E-04	9.17E-05	7.84E-05	6.57E-05	5.32E-05
150	1000	954	904	847	780	699		150	1.24E-04	1.08E-04	9.37E-05	8.07E-05	6.84E-05	5.67E-05
160	1004	960	911	857	795	722		160	1.26E-04	1.10E-04	9.56E-05	8.28E-05	7.10E-05	5.98E-05
170	1008	965	918	866	808	741		170	1.27E-04	1.11E-04	9.74E-05	8.48E-05	7.33E-05	6.26E-05
180	1012	970	925	875	819	757		180	1.29E-04	1.13E-04	9.92E-05	8.67E-05	7.54E-05	6.50E-05
190	1017	975	931	883	830	771		190	1.31E-04	1.15E-04	1.01E-04	8.86E-05	7.75E-05	6.73E-05
200	1021	980	937	891	840	784		200	1.32E-04	1.16E-04	1.03E-04	9.03E-05	7.94E-05	6.95E-05

FIGURE 10-1. DENSITIES AND VISCOSITIES OF PURE CO$_2$ FOR THE TEMPERATURE RANGE 0-50 °C AND PRESSURE RANGE 50-200 BARA.

For most of the points (specially at 80 bara+ and 0-10 °C, conditions occurring during subsea pipeline transport), the density is water-like, while the viscosity is gas-like[61]. This is advantageous for two reasons: low viscosity gives low frictional pressure drop in the pipe and high density gives additional pressure buildup due to transport from a high elevation (shore or ship) to a low elevation (seabed and reservoir). It is usually such that the gains in pressure due to the elevation difference counter the drop in pressure due to friction.

Multiphase flow in a CO$_2$ injection system?

It is often mentioned that there could be situations in which there is simultaneous flow of liquid and vapor CO$_2$ in the pipe and well, and that this could create multiphase flow-related challenges (e.g. slugging, separation, instabilities). Therefore, a lot of research and funding is dedicated to improving predictability and accuracy of multiphase flow models for CO$_2$, usually using expensive experimental setups.

Consider the equation provided below that predicts saturation pressure in bara, if saturation temperature, in °C, is provided. This equation is valid in the range T$_{sat}$ -45 °C to 30.978 °C (critical temperature, p$_c$ = 73.773 bara).

$$p_{sat} = 8.3468E - 3 \cdot T_{sat}^{2} + 0.95321 \cdot T_{sat} + 35.069$$

EQ. 10-4

As mentioned earlier, the temperature of CO$_2$ in subsea transport systems is in equilibrium with the seabed, which in the North Sea might be in the range 4-8 °C. At these temperatures the pressure must be greater than ca. 40 bara for the CO$_2$ to be in single phase. A multiphase flow situation could occur if, for example, it is sufficient with having a wellhead pressure of 40 bara (or lower) to inject CO$_2$ into the formation. In that case, there will be vapor released by the liquid at the wellhead. The multi-phase flow could continue inside the well also, as the pressure increases inside the well due to the hydrostatic column but also the temperature due to the heat exchange with the formation, giving out higher saturation pressures.

---

[61] As a reference, the viscosity of air and water at 20 °C and 1.01325 bara are 1.825 E-5 Pa/s and 1.0016 E-3 Pa/s respectively.

Consider an injection configuration with a flowline, a wellhead choke, and a CO$_2$ injection well. Assume flowline pressure is 90 bara (or higher) and temperature is 4 °C. Two phase flow arises at the choke downstream if saturation conditions are reached at the choke outlet. Since in a choke the enthalpy downstream is equal to the enthalpy upstream, to find the outlet conditions, one can then search for saturation pressure where the enthalpy of the saturated liquid is equal to the inlet enthalpy. For pure CO$_2$, this gives around 37 bara, and 2 °C. If the wellhead pressure required to inject is any lower, there will be vaporization across the choke and CO$_2$ two-phase flow at the wellhead (and significantly more cooling). We can refer to this pressure as the minimum wellhead pressure required to ensure single phase flow in the wellbore ($p_{wh,min}$).

The minimum bottom-hole pressure to ensure single phase flow in the wellbore can be estimated by using the following expression:

$$p_{wf,min} = p_{wh,min} + \frac{\rho \cdot TVD \cdot g}{1E5}$$

EQ. 10-5

This expression assumes the following:

- Frictional losses are negligible when compared against the hydrostatic pressure change. This is usually the case in CO$_2$ injection wells, due to the low velocity and low viscosity. For example, for a 7" tubing, mass rate of 1.5 E06 t/y, and density of 900 kg/m^3, velocities in the tubing will be of around 2 m/s. For a 4.5" tubing, velocities in the tubing could be around 5 m/s.
- There is only single liquid phase flow in the tubing. This is reasonable since pressure will increase with depth for locations downstream the wellhead, and then p>p$_{sat}$.

The chart below shows the p-T phase envelope of CO$_2$, the values of p-T pairs at pipeline, wellhead, and bottom-hole conditions and the p-T evolution in the wellbore[62].
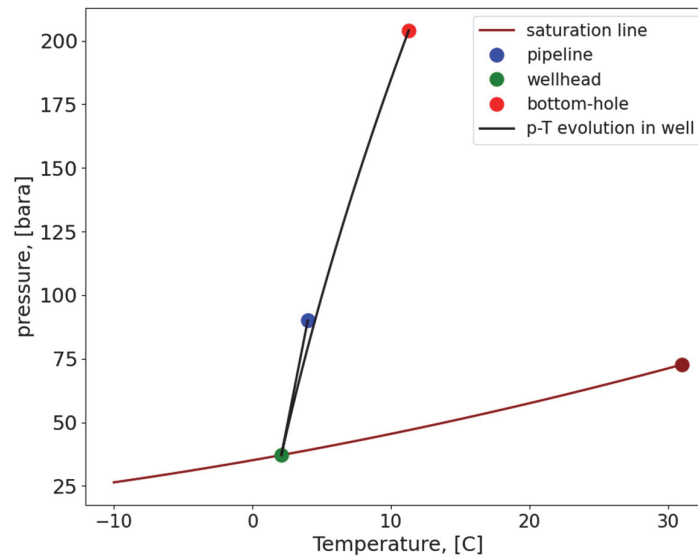
FIGURE 10-2. P-T PHASE ENVELOPE OF PURE CO$_2$ WITH MAIN P-T CONDITIONS IN A CO$_2$ INJECTION WELL AND EVOLUTION OF P-T IN WELLBORE.

---

[62] The values used to compute this chart were: vertical well, injection interval at 1800 m TVD, reservoir temperature 65 °C, linear geothermal gradient from 4 °C to 65 °C. Wellbore overall heat transfer coefficient: 10 W/m^2 K. Average heat capacity at constant pressure: 2312 J/kg K, average density: 946 kg/m^3, mass flow: 1.5 E6 t/y, ID= 0.168 m. Temperature evolution in the wellbore was calculated using Eq. C-24.

To relate the minimum bottom-hole pressure required to ensure single phase flow in the wellbore with the injectivity index and reservoir pressure, we use the inflow performance relationship:

$$\dot{m}_g = J \cdot \left(p_{wf} - p_R\right)$$

EQ. 10-6

Clearing out the flowing bottom-hole pressure, and adding the condition that it should be greater than the minimum bottom-hole pressure derived above gives:

$$p_R + \frac{\dot{m}_g}{J} \geq p_{wf,min}$$

EQ. 10-7

Substituting the definition of minimum bottom-hole pressure gives:

$$p_R + \frac{\dot{m}_g}{J} \geq p_{wh,min} + \frac{\rho \cdot TVD \cdot g}{1E5}$$

EQ. 10-8

Clearing out the injectivity index gives:

$$J \leq \frac{\dot{m}_g}{p_{wh,min} + \frac{\rho \cdot TVD \cdot g}{1E5} - p_R}$$

EQ. 10-9

Using a mass rate of 1.5E06 t/y and $p_{wh,min}$ = 37 bara, the equation gives:

$$J \leq \frac{4110 \; t/d}{37 \; bara + \frac{\rho \cdot TVD \cdot g}{1E5} - p_R}$$

EQ. 10-10

A plot of Eq. 10-10 is shown in the figure below. As reservoir pressure increases, the value of injectivity index required to have two-phase flow in the wellbore becomes bigger.
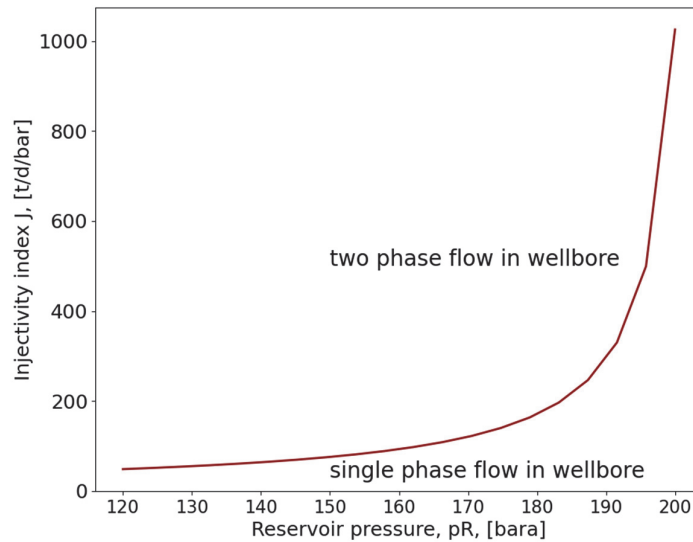
FIGURE 10-3. CRITERIA FOR SINGLE- OR TWO-PHASE FLOW IN WELLBORE BASED ON THE RELATIONSHIP BETWEEN INJECTIVITY INDEX AND RESERVOIR PRESSURE FOR A 1800 M DEEP RESERVOIR.

Impurities

Another issue that could cause the appearance of multiphase flow is the presence of impurities in the stream. Impurities cause the transformation of the vapor-liquid equilibrium line into a region, where higher saturation pressures are required to be in liquid phase. A phase envelope with for example 4 mole % of an impurity like methane cause the saturation pressure to be around 8 bara higher at 4-8 °C.

Could we model pipe flow of liquid/dense CO$_2$ using the dry gas flow equation?

The dry gas flow equation is commonly used for dry gas flow in wells and transportation systems:

$$q_{sc} = C_T \cdot \left[\left(\frac{p_1^2}{e^S} - p_2^2 \right) \right]^{0.5}$$

EQ. 10-11

Here 1 is pipe inlet and 2 is pipe outlet. With:

$$C_T = \left(\frac{\pi}{4} \right) \cdot \left(\frac{R}{M_{air}} \right)^{0.5} \cdot \left(\frac{T_{sc}}{p_{sc}} \right) \cdot \left(\frac{D^5}{f_M \cdot L \cdot \gamma_g \cdot Z_{av} \cdot T_{av}} \right)^{0.5} \cdot \left(\frac{S \cdot e^S}{e^S - 1} \right)^{0.5}$$

$$S = 2 \cdot \frac{28.97 \cdot \gamma_g \cdot g}{Z_{av} \cdot R \cdot T_{av}} \cdot L \cdot \cos(\alpha)$$

$$f_M = \frac{0.0077}{D^{0.224}}$$

α is the angle between the vertical axis and the pipe.

In this equation, one should have a good estimate for the value of Z_{av} and T_{av} to calculate the value of S and C$_T$. If the actual inlet and outlet conditions are very different from the values that were used to estimate S and C$_T$ originally, the values of S and C$_T$ should be updated (and some converging process might be required). Luckily, in dry gases the equation often exhibits a fair accuracy even for conditions that are significantly different from the ones used to calculate the constants.

Consider a case in which temperature does not change along the pipe. Consider the real gas equation, clearing out the value of the deviation factor Z:

$$Z = \frac{p \cdot M_w}{\rho \cdot R \cdot T}$$

EQ. 10-12

In gases, density is greatly affected by pressure. In liquids, not so much. Therefore, when pressure varies in liquids, the value of Z must change accordingly, to ensure variation in density remains modest. This is not the case in gases, where when pressure varies, density also varies and variations in deviation factor Z could in result be more modest than in liquids.

As an example, consider a hydrostatic 1000 m column of CO$_2$ with 90 bara and 4 °C conditions at the top. Density is 947 kg/m^3 and Z = 0.18153. The pressure at the bottom of the column can be estimated by

$$p_{bottom} = p_{top} + \frac{\rho \cdot H \cdot g}{1E5} = 183 \ bara$$

EQ. 10-13

Now let's use the dry gas equation. Calculating S using the conditions at the top gives:

$$S = 2 \cdot \frac{28.97 \cdot \gamma_g \cdot g}{Z_{top} \cdot R \cdot T} \cdot L \cdot \cos(\alpha) = 2.06 \qquad \text{EQ. 10-14}$$

Using the dry gas flow equation

$$q_{sc} = 0 = C_T \cdot \left[\left(\frac{p_1^2}{e^S} - p_2^2 \cdot \right) \right]^{0.5}$$

$$\left(\frac{p_1^2}{e^S} - p_2^2 \right) = 0$$

$$p_2 = \frac{p_1}{e^{S/2}} = \frac{90}{e^{2.06/2}} = 252.6 \; bara$$

Which is a number significantly different than the one obtained with the liquid column approximation. At this pressure and 4 °C, the deviation factor is Z = 0.47066, which means that a Z_{av} = 0.3261 should have been used instead of $Z_{av} = Z_{top}$ = 0.18153. Repeating this process **7 times(!)** finally gives a value like the one obtained with the liquid column approximation $p_2 = \frac{90}{e^{1.41/2}} = 182 \; bara$

Therefore, if using the dry gas equation to estimate pressure drop in CO₂ liquid flow, it is extremely important to perform a convergence process recalculating the value of S and C$_T$, since the deviation factor Z will vary significantly with pressure.

Another aspect of using the dry gas equation is that the friction factor is assumed to be a function of relative roughness only. The chart below shows the Moody friction factor diagram. In red lines and shaded red area are the relative roughnesses typically encountered in the oil and gas industry (corresponding to inner diameters 0.05 to 0.5 m). The area with green stripes indicates the region where using the friction factor equation of Smith gives within 5% deviation of the real friction factor value.
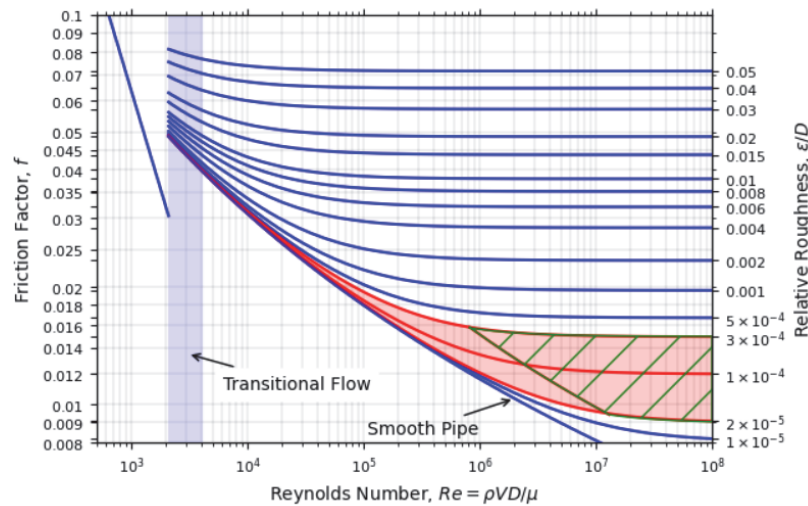
FIGURE 10-4. MOODY FRICTION FACTOR DIAGRAM INDICATING RELATIVE ROUGHNESS REGION ENCOUNTERED IN THE OIL AND GAS INDUSTRY (IN RED COLOR) AND A REGION WHERE THE DEVIATION BETWEEN THE SMITH FRICTION FACTOR CORRELATION AND THE ACTUAL VALUE OF THE FRICTION VALUE IS BELOW 5% (GREEN)

Calculating the Reynolds number for a CO2 injection well:

$$R_e = \frac{V \cdot \rho \cdot D}{\mu} = \frac{3 \frac{m}{s} \cdot 900 \; kg/m^3 \cdot 0.15 \; m}{0.1E - 3 \; Pa \; s} = 4.5 \; E06$$

Relative roughness for a 0.15 m ID pipe is ca 9E-5 (ref Eq. A-34). This combination falls into the green region, where the approximation of friction factor as a function of relative roughness only could be reasonable.

Vapor-liquid phase segregation in CO$_2$ injection well during shut-in

It is often of interest to compute, after the well is shut-in, the depth (location) of the liquid-vapor interface (if any). This is because residual molecules like NO$_x$ and SO$_x$, tend to partition more readily into the gas phase, and can potentially cause material issues to the well tubulars (like corrosion, when e.g. formation water diffuses from the formation and upwards into the wellbore). It is therefore of practical interest to determine what parts of the well will be exposed to vapor during shut-in and the potential impact of the exposure.

Assuming the well reaches equilibrium with the surrounding formation, the fluid in the well will exhibit the geothermal temperature distribution:

$$T = T_{seabed} + TVD \cdot G$$

EQ. 10-15

This equation gives temperature for a given well depth, TVD (in m), with G is the formation geothermal gradient in °C/m, and T$_{seabed}$ is the temperature of the seabed in °C. With temperature, it is possible to compute a saturation pressure at each depth using e.g. Eq. 10-4 (if pure CO$_2$).

The pressure in the liquid column can be calculated from bottom-hole and upwards:

$$p = p_R - \frac{\rho \cdot (TVD_R - TVD) \cdot g}{1E5}$$

EQ. 10-16

Where p$_R$ is reservoir pressure in bara, ρ is average density of CO$_2$ in the liquid column, TVD$_R$ is the total vertical depth of the formation, g is gravitational acceleration in m/s^2.

The gas-liquid contact will occur at a depth TVD_{glc} when:

$$p = p_{sat}$$

EQ. 10-17

Substituting Eq. 10-15 in Eq. 10-4 and making it equal to Eq. 10-16:

$$
\begin{aligned}
p_R &- \frac{\rho \cdot \left(TVD_R - TVD_{glc}\right) \cdot g}{1E5} \\
&= 8.3468E - 3 \cdot \left[T_{seabed} + TVD_{glc} \cdot G\right]^2 + 0.95321 \\
&\cdot \left(T_{seabed} + TVD_{glc} \cdot G\right) + 35.069
\end{aligned}
$$

EQ. 10-18

Simplifying and grouping terms gives:

$$
\begin{aligned}
0 \leq\; & TVD_{glc}{}^2 \cdot (8.3468E - 3 \cdot G^2) + TVD_{glc} \\
& \cdot \left(8.3468E - 3 \cdot 2 \cdot G \cdot T_{seabed} + 0.95321 \cdot G - \frac{\rho \cdot g}{1E5}\right) \\
& + \left(8.3468E - 3 \cdot T_{seabed}{}^2 + 0.95321 \cdot T_{seabed} + 35.069 - p_R \right. \\
& \left. + \frac{\rho \cdot TVD_R \cdot g}{1E5}\right)
\end{aligned}
$$

EQ. 10-19

Using the quadratic formula, it is possible to clear out the depth of the gas-liquid contact in the well as a function of reservoir pressure, formation geothermal gradient, formation depth, seabed temperature:

$$TVD_{glc} = \frac{-b - \sqrt{b^2 - 4 \cdot a \cdot c}}{2 \cdot a}$$

<div align="right">EQ. 10-20</div>

With

- $a = (8.3468E - 3 \cdot G^2)$
- $b = \left(8.3468E - 3 \cdot 2 \cdot G \cdot T_{seabed} + 0.95321 \cdot G - \frac{\rho \cdot g}{1E5}\right)$
- $c = \left(8.3468E - 3 \cdot T_{seabed}^2 + 0.95321 \cdot T_{seabed} + 35.069 - p_R + \frac{\rho \cdot TVD_R \cdot g}{1E5}\right)$

As an example, Figure 10-5 show Eq. 10-20 plotted versus reservoir pressure keeping all other parameters constant. The depth of the liquid-vapor contact is inversely proportional to reservoir pressure. For a value of reservoir pressure equal to 198 bara, no gas will form in the well when shut-in. For a value of reservoir pressure equal to 118.4 bara, the well will contain gas only.
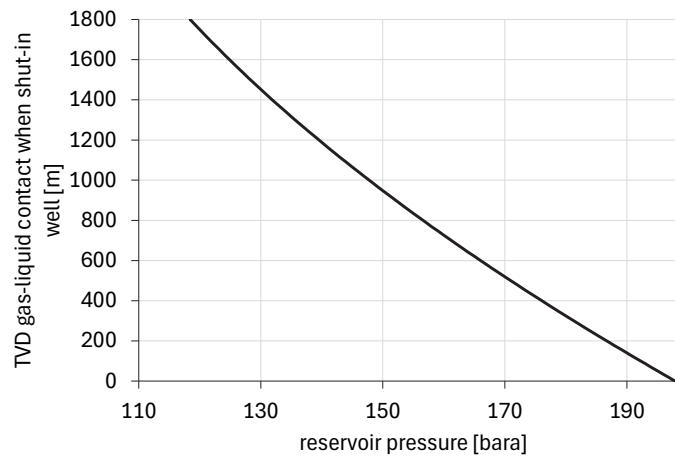
FIGURE 10-5. TRUE VERTICAL DEPTH OF VAPOR-LIQUID INTERFACE IN A STAGNANT PURE CO$_2$ INJECTION WELL THAT HAS REACHED THERMAL EQUILIBRIUM WITH THE FORMATION. VERTICAL WELL, RESERVOIR DEPTH: 1800 M, SEABED TEMPERATURE: 4 °C, GEOTHERMAL GRADIENT 0.03 °C/M.

Optimal placement of a downhole choke in a CO$_2$ injection well to avoid two-phase flow in the wellbore while injecting

A strategy proposed to avoid the formation of two-phase flow in CO$_2$ injection wells during operation is to place a downhole choke as part of the tubing string (or lower completion) instead of a wellhead choke.

Consider that there is liquid CO$_2$ upstream and downstream of the choke, and that the choke is located at a depth TVD$_c$. The pressure downstream the choke can be computed from the bottom-hole flowing pressure (neglecting frictional pressure drop):

$$p_{dc} = p_{wf} - \frac{\rho \cdot (TVD_R - TVD_c) \cdot g}{1E5}$$

<div align="right">EQ. 10-21</div>

Where p$_{dc}$ is pressure downstream the choke in bara, p$_{wf}$ is flowing bottom-hole pressure in bara, ρ is average density of CO$_2$ in the liquid column, TVD$_R$ is the total vertical depth of the formation, g is gravitational acceleration in m/s^2.

The injector IPR equation (Eq. 10-6) is used to express the flowing bottom-hole pressure as a function of injection rate, injectivity index and reservoir pressure.

$$p_{dc} = p_R + \frac{\dot{m}_g}{J} - \frac{\rho \cdot (TVD_R - TVD_c) \cdot g}{1E5}$$

EQ. 10-22

The pressure upstream the choke (p_{uc}, in bara) can be computed from wellhead pressure and neglecting frictional losses. Wellhead pressure is equal to pipeline (supply) pressure, since wellhead choke is fully open.

$$p_{uc} = p_{wh} + \frac{\rho \cdot TVD_c \cdot g}{1E5}$$

EQ. 10-23

The pressure drop to be provided by the choke is therefore:

$$\Delta p_c = p_{wh} + \frac{\rho \cdot TVD_c \cdot g}{1E5} - p_R - \frac{\dot{m}_g}{J} + \frac{\rho \cdot (TVD_R - TVD_c) \cdot g}{1E5}$$

$$\Delta p_c = p_{wh} - p_R - \frac{\dot{m}_g}{J} + \frac{\rho \cdot TVD_R \cdot g}{1E5}$$

EQ. 10-24

Which is independent of choke depth.

To avoid the formation of vapor in the wellbore, the pressure at each wellbore location should be higher than the vapor pressure at the temperature of each wellbore location. The place where the pressure is lowest, and is therefore most critical, is downstream the choke.

$$p_{dc} = p_R + \frac{\dot{m}_g}{J} - \frac{\rho \cdot (TVD_R - TVD_c) \cdot g}{1E5} \geq p_{sat@T_{dc}}$$

EQ. 10-25

The temperature at a given wellbore depth[63] can be computed with Eq. C-24[64], which assumes incompressible liquid flow, linear geothermal gradient and constant overall heat transfer coefficient U.

$$T(TVD) = (T_{wh} - T_{seabed}) \cdot e^{-\frac{TVD}{A}} + (T_{seabed} + G \cdot TVD) + \frac{g}{C_p} \cdot A \cdot \left(1 - e^{-\frac{TVD}{A}}\right) - G \cdot A$$
$$\cdot \left(e^{-\frac{TVD}{A}} - 1\right)$$

EQ. 10-26

With C_p specific heat capacity in J/kg K, T_{wh}, wellhead temperature in °C, and

- $A = \frac{\dot{m} \cdot C_p}{2 \cdot \pi \cdot r_{ref} \cdot U}$

$\dot{m}$ is mass flow rate, in kg/s, r_{ref} is reference radius for the overall heat transfer coefficient U.

Applying Eq. 10-26 at the depth of the downhole choke, assuming $T_{uc} \approx T_{dc}$, and substituting the resulting expression in Eq. 10-4 (valid for pure CO₂) gives the vapor pressure at the choke downstream ($p_{sat@T_{dc}}$). The expression can be compared then with Eq. 10-25 to verify that there is no vaporization of CO₂ occurring.

---

[63] In reality, the CO₂ experiences some cooling when flowing across the choke, but the temperature change is often modest for liquid CO₂ (for example an expansion of pure CO₂ from 90 bara and 4 °C to 37 bara, gives a temperature change of 2 °C). But a lower temperature at the choke discharge will give a lower saturation pressure, therefore it will be a less strict condition on the pressure downstream the choke.

[64] Since it is a vertical injector well, the angle the well forms with the horizontal θ is equal to -90 °.

As an example, following a similar procedure, but iterating on the TVD of the downhole choke, Figure 10-6 shows the minimum required value of TVD of downhole choke to avoid vaporization versus reservoir pressure, for three values of formation injectivity. When reservoir pressure is high, the downhole choke can be placed closer to the surface, until there comes a point where it is sufficient to install a wellhead choke. When reservoir pressure is low, then the downhole choke must be placed deeper into the well to ensure single phase liquid flow. A higher injectivity index will require to install the choke deeper into the well.
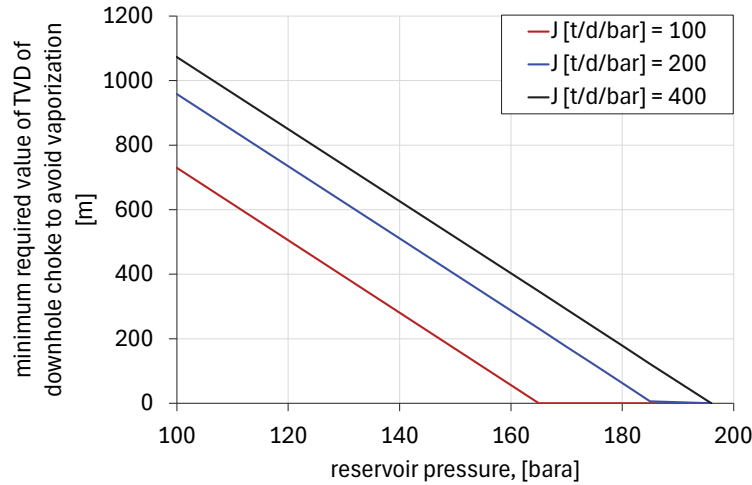
FIGURE 10-6. MINIMUM REQUIRED VALUE OF TVD OF DOWNHOLE CHOKE TO AVOID VAPORIZATION OF CO$_2$ IN THE WELLBORE, VERSUS RESERVOIR PRESSURE AND FOR THREE VALUES OF INJECTIVITY INDEX. VERTICAL WELL, RESERVOIR DEPTH: 1800 M, SEABED TEMPERATURE: 4 °C, WELLHEAD TEMPERATURE: 4 °C, GEOTHERMAL GRADIENT 0.03 °C/M, OVERALL HEAT TRANSFER COEFFICIENT: 10 W/M^2 K, MASS FLOW 1.5 MT/Y, CO$_2$ LIQUID DENSITY: 946 KG/M^3, SPECIFIC HEAT CAPACITY C$_P$: 2312 J/KG K.

Figure 10-7 shows required choke pressure drop versus reservoir pressure for 3 values of injectivity index, considering maximum wellhead pressure available of 80 bara. Higher values of reservoir pressure require less choking. Higher values of injectivity index require more choking.
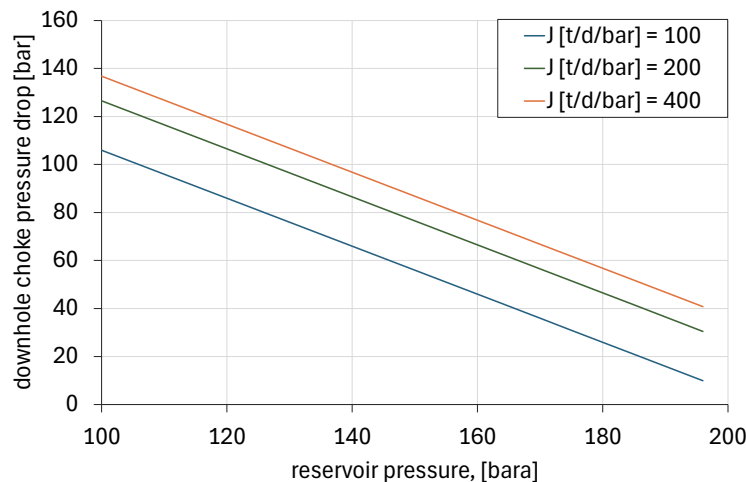
FIGURE 10-7. REQUIRED PRESSURE DROP ACROSS DOWNHOLE CHOKE TO AVOID VAPORIZATION OF CO$_2$ IN THE WELLBORE, VERSUS RESERVOIR PRESSURE AND FOR THREE VALUES OF INJECTIVITY INDEX. VERTICAL WELL, RESERVOIR DEPTH: 1800 M, SEABED TEMPERATURE: 4 °C, WELLHEAD TEMPERATURE: 4 °C, GEOTHERMAL GRADIENT 0.03 °C/M, OVERALL HEAT TRANSFER COEFFICIENT: 10 W/M^2 K, MASS FLOW 1.5 MT/Y, CO$_2$ LIQUID DENSITY: 946 KG/M^3, SPECIFIC HEAT CAPACITY C$_P$: 2312 J/KG K, MAXIMUM WELLHEAD PRESSURE: 80 BARA.

10.1.1. CO₂ STORAGE

There are two main candidate reservoir types, saline aquifers and depleted gas reservoirs.

Saline aquifers have the advantage that are usually shallow (e.g. in the range 800-1000 m), thus wells are somewhat less costly. Also, in contrast with oil and gas reservoirs that usually the developer must deal with what he/she gets, one can explore for saline aquifers that have more convenient properties for storing CO_2 (location, size, depth, etc.).

An issue in saline aquifers is management of the injection pressure (the highest pressure is usually experienced at the well bottom-hole) to avoid fracking the formation and cap rock, losing reservoir integrity. As the reservoir fills up, reservoir pressure increases, thus the required well bottom injection pressure increases as well. Water has very little compressibility, so at some point it could be necessary to remove water from the reservoir using producers, to make more place to store CO_2 and reduce the increase of reservoir pressure and well bottom-hole pressure. Another issue could be containment, making sure that CO_2 does not leave the reservoir through a spill point.

Regarding the cost of CO_2 storage offshore, this source[65] indicates cost values range from 6-20 USD/t CO_2.

10.1.2. SIMPLE ECONOMICS OF CO₂ VALUE CHAIN

Table 10-1 shows the approximate cost figures for capture, transport and storage given in the previous sections and adding them up to obtain a total cost for CO_2 capture, transport and storage. To put this number in perspective, in Norway there are two taxes on CO_2 emissions[66]. The Norwegian tax, which in 2023, was of around 761 NOK/t CO_2 (ca 71 USD/t CO_2) and the European tax, which in 2023, was approximately 92 USD/t CO_2. When combined, this gives around 150 USD/t CO_2. The CO_2 tax is often used as a mechanism to promote companies to reduce their emissions.

Table 10-1. Details and total cost of CO_2 capture, transport and storage

Cost of capture* [USD/t CO₂]	Cost of Transport** [USD/t CO₂]	Cost of storage*** [USD/t CO₂]	Total cost [USD/t CO₂]
50-100	6.5-22	6-20	62.5-142

*Capture from combustion exhaust
**Transport or large quantities of CO_2 offshore by ship or pipeline of a distance of up to 500 km.
***In offshore saline aquifers

Thought experiment

Consider the hypothetical scenario in which scope 1 and scope 3 emissions of the oil and gas industry will be compensated by using CO_2 capture, transport and injection (the oil and gas industry will be carbon neutral). Using the total cost for capture, transport and estimated above and the scope 1 and 3 carbon intensities given

---

[65] https://zeroemissionsplatform.eu/wp-content/uploads/Overall-CO2-Costs-Report.pdf

[66] https://www.norskpetroleum.no/en/environment-and-technology/emissions-to-air/

earlier (for scope 1, 0.0503 t CO$_2$/Sm^3.o.e, for scope 3, 1.788 t CO$_2$/ Sm^3 o.e.), this gives a total CCS-related cost per standard cubic meter of oil equivalent of 115-261 USD/Sm^3 o.e[67], or 18-41 USD/bbl.

The cost of producing the oil varies widely by country and field, but some values reported[68] are between 8-50 USD/bbl. So, considering CCS costs and producing costs, breakeven oil prices could range between 26-91 USD/bbl, which, given historic prices, seems to be somewhat feasible while protecting the environment? (however the profit margins will be reduced considerably).

Despite being a waste product, a lot of effort, resources and energy must be allocated to dispose of CO2.

---

[67] (0.0503 t+1.788 t CO$_2$/Sm^3.o.e) · (62.5-142 USD/t CO$_2$)

[68] https://www.statista.com/statistics/597669/cost-breakdown-of-producing-one-barrel-of-oil-in-the-worlds-leading-oil-producing-countries/

APPENDICES

A. THE TUBING RATE EQUATION IN VERTICAL AND DEVIATED GAS-WELLS

Author: Prof. Michael Golan, with modifications and additions by Milan Stanko

DERIVATION FROM FIRST PRINCIPLES (PURE SI SYSTEM)

Neglecting the acceleration term in the momentum equation, the pressure gradient at any point in the pipe is the sum of the hydrostatic and the frictional gradients:

$$-\frac{dp}{dl} = \rho \cdot g \cdot \cos(\alpha) + f_M \cdot \frac{\rho \cdot u^2}{2 \cdot D}$$

EQ. A-1

Where:

f It could be Moody or Fanning friction factor (f_M or f_F)[69]

α Inclination angle from the vertical direction

When the units are in British Engineering unit system, the equation becomes:

$$-\frac{dp}{dl} = \rho \cdot \frac{g}{g_c} \cdot \cos(\alpha) + f_M \cdot \frac{\rho \cdot u^2}{2 \cdot g_c \cdot D}$$

and in oil field unit system, where pressure is expressed in psia, it is written as

$$-144 \cdot \frac{dp}{dl} = \rho \cdot \frac{g}{g_c} \cdot \cos(\alpha) + f_M \cdot \frac{\rho \cdot u^2}{2 \cdot g_c \cdot D}$$

Returning to the SI equation, expressing the density in terms of the compressibility factor, and the flow velocity in terms of mass flow rate, $u = \frac{\dot{m}}{\rho \cdot A}$, gives:

$$-\frac{dp}{dl} = \frac{p \cdot M_g}{Z \cdot R \cdot T} \cdot g \cdot \cos(\alpha) + \frac{8 \cdot f_M \cdot \dot{m}^2}{\pi^2 \cdot D^5} \cdot \frac{Z \cdot R \cdot T}{p \cdot M_g}$$

EQ. A-2

Defining:

$$C_a = \frac{M_g}{Z \cdot R \cdot T} \cdot g \cdot \cos(\alpha)$$

EQ. A-3

And

$$C_b = \frac{8 \cdot f_M \cdot \dot{m}^2}{\pi^2 \cdot D^5} \cdot \frac{Z \cdot R \cdot T}{M_g}$$

EQ. A-4

and substituting Eq. A-3 and Eq. A-4 into Eq. A-2 gives

$$-dp = (C_a \cdot p + \frac{C_b}{p}) \cdot dl$$

EQ. A-5

Or

$$dl = \frac{-dp}{(C_a \cdot p + \frac{C_b}{p})} = -\frac{p \cdot dp}{(C_a \cdot p^2 + C_b)}$$

EQ. A-6

---

[69] The Fanning friction factor is defined as $f_F = \frac{2 \cdot \tau}{\rho \cdot u^2}$ and the Moody friction factor $f_M = \frac{8 \cdot \tau}{\rho \cdot u^2}$, thus $f_M = 4 \cdot f_F$

To integrate this equation a new variable U, is defined,

$$U = C_a \cdot p^2 + C_b \qquad \text{EQ. A-7}$$

$$dU = 2 \cdot C_a \cdot p \cdot dp \qquad \text{EQ. A-8}$$

The U and dU substituted into Eq. A-6 give:

$$dl = -\frac{1}{2 \cdot C_a} \cdot \frac{dU}{U} \qquad \text{EQ. A-9}$$

Integrating Eq. A-9 between two points in the pipe 1 and 2, assuming that parameters C_a and C_b are constant[70] between 1-2:

$$\int_1^2 dl = -\frac{1}{2 \cdot C_a} \cdot \int_1^2 \frac{dU}{U} \qquad \text{EQ. A-10}$$

This integral gives

$$l_2 - l_1 = L = -\frac{1}{2 \cdot C_a} \cdot \ln\left(\frac{U_2}{U_1}\right) = -\frac{1}{2 \cdot C_a} \cdot \ln\left(\frac{C_a \cdot p_2^2 + C_b}{C_a \cdot p_1^2 + C_b}\right) \qquad \text{EQ. A-11}$$

Or:

$$e^{-2 \cdot L \cdot C_a} = \frac{C_a \cdot p_2^2 + C_b}{C_a \cdot p_1^2 + C_b} \qquad \text{EQ. A-12}$$

Defining:

$$S = 2 \cdot L \cdot C_a = 2 \cdot \frac{M_g}{Z_{av} \cdot R \cdot T_{av}} \cdot L \cdot g \cdot \cos(\alpha) = 2 \cdot \frac{28.97 \cdot \gamma_g \cdot g}{Z_{av} \cdot R \cdot T_{av}} \cdot L \cdot \cos(\alpha) \qquad \text{EQ. A-13}$$

Eq. A-12 becomes:

$$e^{-S} = \frac{C_a \cdot p_2^2 + C_b}{C_a \cdot p_1^2 + C_b} \qquad \text{EQ. A-14}$$

Which can be rearranged such that:

$$p_1^2 = p_2^2 \cdot e^S + \left(\frac{C_b}{C_a}\right) \cdot (e^S - 1) \qquad \text{EQ. A-15}$$

Dividing Eq. A-4 by Eq. A-3 gives:

$$\frac{C_b}{C_a} = \frac{8 \cdot f_{M,av} \cdot \dot{m}^2}{\pi^2 \cdot D^5 \cdot g \cdot \cos(\alpha)} \cdot \left(\frac{Z_{av} \cdot R \cdot T_{av}}{M_g}\right)^2 \qquad \text{EQ. A-16}$$

Converting the mass flow rate to volumetric flow-rate expressed at standard conditions using Eq. A-17

$$\dot{m} = \rho_{sc} \cdot q_{sc} = \left(\frac{p}{T}\right)_{sc} \cdot \frac{M_g}{R} \cdot q_{sc} \qquad \text{EQ. A-17}$$

---

[70]Evaluated with average deviation factor $Z_{av} = 0.5 \cdot (Z_1 + Z_2)$, average temperature and average friction factor

results in:

$$\frac{C_b}{C_a} = \frac{8 \cdot f_{M,av} \cdot (Z_{av} \cdot T_{av})^2}{\pi^2 \cdot D^5 \cdot g \cdot \cos(\alpha)} \cdot \left(\frac{p}{T}\right)^2_{sc} \cdot q^2_{sc}$$

EQ. A-18

Substituting Eq. A-18 into Eq. A-15:

$$p^2_{wf} = p^2_t \cdot e^S + \frac{8 \cdot f_M}{\pi^2 \cdot D^5 \cdot g \cdot \cos(\alpha)} \cdot \left(\frac{p}{T}\right)^2_{sc} \cdot (Z_{av} \cdot T_{av})^2 \cdot (e^S - 1) \cdot q^2_{sc}$$

EQ. A-19

Substituting the values for the constants:

$$p^2_{wf} = p^2_t \cdot e^S + \frac{8}{9.81 \cdot \pi^2} \cdot \left(\frac{10^5}{293}\right)^2_{sc} \cdot f_M \cdot (Z_{av} \cdot T_{av})^2 \cdot \frac{(e^S - 1)}{D^5 \cdot \cos(\alpha)} \cdot q^2_{sc}$$

EQ. A-20

Gives

$$p^2_{wf} = p^2_t \cdot e^S + 9624 \cdot f_M \cdot (Z_{av} \cdot T_{av})^2 \cdot \frac{(e^S - 1)}{D^5 \cdot \cos(\alpha)} \cdot q^2_{sc}$$

EQ. A-21

When converting to practical metric units, Sm³/d, bara, m, the equation becomes

$$p^2_{wf} = p^2_t \cdot e^S + \frac{9624}{(10^5 \cdot 86400)^2} \cdot f_M \cdot (Z_{av} \cdot T_{av})^2 \cdot \frac{(e^S - 1)}{D^5 \cdot \cos(\alpha)} \cdot q^2_{sc}$$

EQ. A-22

Simplifying the constants gives:

$$p^2_{wf} = p^2_t \cdot e^S + 1.295 \cdot 10^{-16} \cdot f_M \cdot (Z_{av} \cdot T_{av})^2 \cdot \frac{(e^S - 1)}{D^5 \cdot \cos(\alpha)} \cdot q^2_{sc}$$

EQ. A-23

Another version of the equation often used is obtained by multiplying and dividing the second term on the right-hand side of Eq. A-19 with S:

$$p^2_{wf} = p^2_t \cdot e^S + \left(\frac{16}{\pi^2}\right) \cdot \frac{28.97}{R} \cdot \left(\frac{p}{T}\right)^2_{sc} f_M \cdot L \cdot \gamma_g \cdot Z_{av} \cdot T_{av} \cdot \frac{(e^S - 1)}{S \cdot D^5} \cdot q^2_{sc}$$

EQ. A-24

Simplifying the constants in Eq. A-24:

$$p^2_{wf} = p^2_t \cdot e^S + 658 \cdot f_M \cdot L \cdot \gamma_g \cdot Z_{av} \cdot T_{av} \cdot \frac{(e^S - 1)}{S \cdot D^5} \cdot q^2_{sc}$$

EQ. A-25

When converting to practical metric units, Sm³/d, bara, m, the equation becomes:

$$p^2_{wf} = p^2_t \cdot e^S + 8.8 \cdot 10^{-18} \cdot f_M \cdot L \cdot \gamma_g \cdot Z_{av} \cdot T_{av} \cdot \frac{(e^S - 1)}{S \cdot D^5} \cdot q^2_{sc}$$

EQ. A-26

Another version of the equation often used is obtained by clearing out the flow rate in Eq. A-24:

$$q_{sc} = \left(\frac{\pi}{4}\right) \cdot \left(\frac{R}{M_{air}}\right)^{0.5} \cdot \left(\frac{T_{sc}}{p_{sc}}\right) \cdot \left(\frac{D^5}{f_M \cdot L \cdot \gamma_g \cdot Z_{av} \cdot T_{av}}\right)^{0.5} \cdot \left[(p^2_{wf} - p^2_t \cdot e^S) \cdot \left(\frac{S}{e^S - 1}\right)\right]^{0.5}$$

EQ. A-27

This equation relates the pressure at the top and the bottom of the tubing.

By defining the tubing constant C_T:

$$C_T = \left(\frac{\pi}{4}\right) \cdot \left(\frac{R}{M_{air}}\right)^{0.5} \cdot \left(\frac{T_{sc}}{p_{sc}}\right) \cdot \left(\frac{D^5}{f_M \cdot L \cdot \gamma_g \cdot Z_{av} \cdot T_{av}}\right)^{0.5} \cdot \left(\frac{S \cdot e^S}{e^S - 1}\right)^{0.5} \qquad \text{EQ. A-28}$$

This yields a more compact form of the tubing equation:

$$q_{sc} = C_T \cdot \left[\left(\frac{p_{wf}^2}{e^S} - p_t^2 \cdot\right)\right]^{0.5} \qquad \text{EQ. A-29}$$

In fully turbulent flow (high Reynolds numbers), the friction factor depends essentially on the relative roughness of the pipe, ε/D, and becomes independent of the Reynolds number.
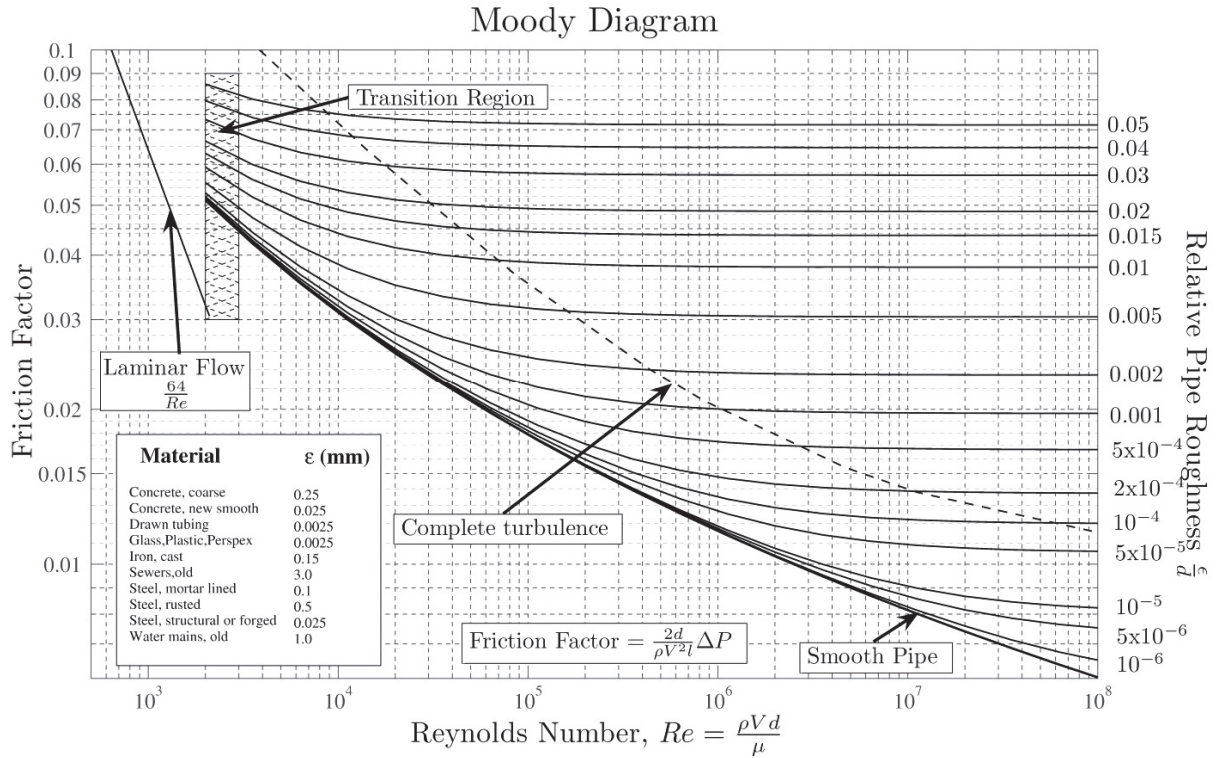
FIGURE A-1. MOODY FRICTION FACTOR DIAGRAM. AT HIGH REYNOLDS NUMBERS, THE FRICTION FACTOR BECOMES A FUNCTION OF RELATIVE PIPE ROUGHNESS ONLY. SOURCE: S BECK AND R COLLINS, UNIVERSITY OF SHEFFIELD, WIKIPEDIA.

An equation that expresses the condition to obtain complete turbulence, where friction factor is a function of relative roughness only, is given below:

$$Re \geq 217.85 \cdot e^{-1.2468} \qquad \text{EQ. A-30}$$

Measurements in gas wells conducted by R.V.Smith, (1950), yielded a correlation for friction factor in tubings that became the norm for most equations used by the gas industry, and which appear in engineering handbooks. Smith's measurements are expressed in terms of friction factor as:

$$f_M = \frac{0.01748}{D^{0.224} \cdot \left(|1\,m| \cdot \left|\frac{39.37\,in}{1\,m}\right|\right)^{0.224}} = \frac{0.0077}{D^{0.224}} \qquad \text{EQ. A-31}$$

Using Figure A-1, an expression for the relationship between Moody friction factor and relative roughness ($e = \epsilon/D$) in the fully turbulent region is:

260

$$f_M = \left(2 \cdot log \left(\frac{3.71}{e} \right) \right)^{-2}$$

<div align="right">EQ. A-32</div>

Using this expression, one can back-calculate the relationship between relative roughness and diameter found by R.V.Smith, (1950):

$$f_M = \left(2 \cdot log \left(\frac{3.71}{e} \right) \right)^{-2} = 0.0077 \cdot D^{-0.224}$$

<div align="right">EQ. A-33</div>

Clearing out the relative roughness as a function of diameter gives:

<div align="right">EQ. A-34</div>

$$e = \frac{3.71}{10^{5.69803 \cdot D^{0.112}}}$$

This expression roughly matches an expression for honed bare carbon steel found by fitting the data presented by Farshad et al (2005):

$$e = 1.2894E - 5 \cdot D^{-1.0036}$$

<div align="right">EQ. A-35</div>

The comparison is shown in the plot below:
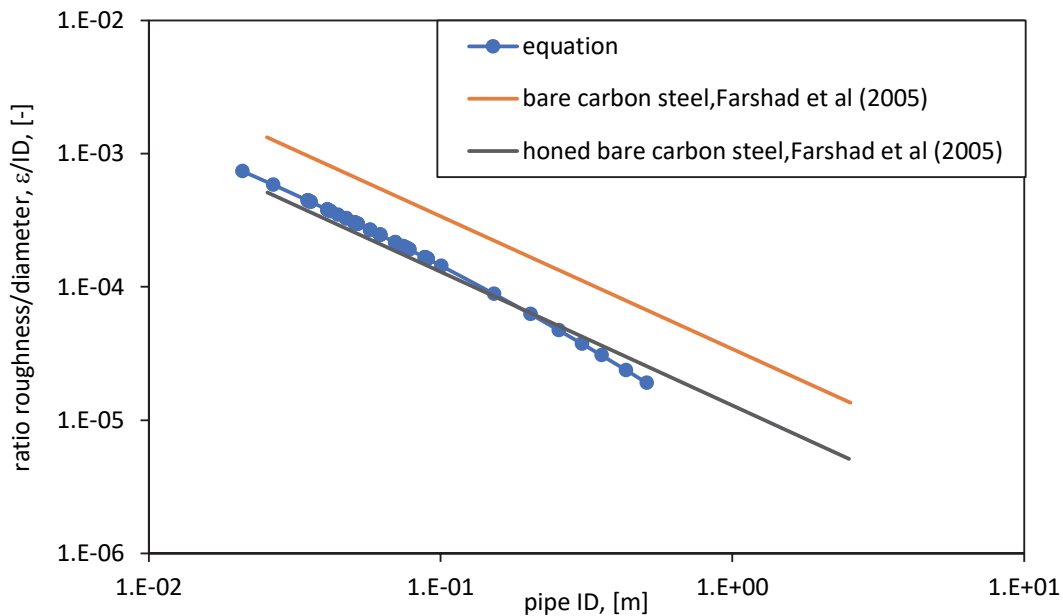
FIGURE A-2. RELATIONSHIP BETWEEN RELATIVE ROUGHNESS AND INTERNAL PIPE DIAMETER, DATA PRESENTED BY FARSHAD ET AL. AND EQUATION BACKCALCULATED FROM THE SMITH FRICTION FACTOR CORRELATION

The chart below shows the Moody friction factor diagram. In red lines and shaded red area are the relative roughnesses typically encountered in the oil and gas industry (corresponding to inner diameters 0.05 to 0.5 m and using the equation derived earlier). The area with green stripes indicates the region where using the friction factor equation of Smith gives within 5% deviation of the real friction factor value.
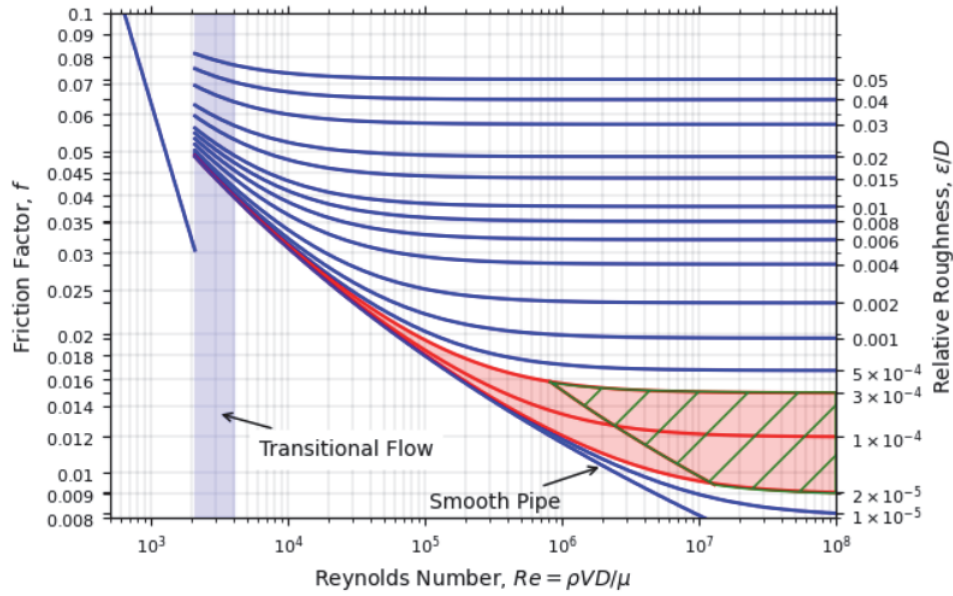
FIGURE A-3. MOODY FRICTION FACTOR DIAGRAM INDICATING RELATIVE ROUGHNESS REGION ENCOUNTERED IN THE OIL AND GAS INDUSTRY (IN RED COLOR) AND A REGION WHERE THE DEVIATION BETWEEN THE SMITH FRICTION FACTOR CORRELATION AND THE ACTUAL VALUE OF THE FRICTION VALUE IS BELOW 5% (GREEN)

The tubing gas equation expressed in terms of the bottom-hole pressure translated to wellhead datum level (Fetkovich approach)

In integrated gas field studies, it is convenient to analyze the flow of the entire production system using the wellhead or the top of the well as a reference datum level. Mike Fetkovich has suggested this approach in a 1975 paper. He rearranged Eq. A-27 as follows:

$$q_{sc} = \left(\frac{\pi}{4}\right) \cdot \left(\frac{R}{M_{air}}\right)^{0.5} \cdot \left(\frac{T_{sc}}{p_{sc}}\right) \cdot \left(\frac{D^5}{f_M \cdot L \cdot \gamma_g \cdot Z_{av} \cdot T_{av}}\right)^{0.5} \cdot \left[\left(\frac{p_{wf}^2}{e^S} - p_t^2\right) \cdot \left(\frac{S \cdot e^S}{e^S - 1}\right)\right]^{0.5} \qquad \text{EQ. A-36}$$

Substituting $\frac{p_{wf}^2}{e^S} = p_w^2$

$$q_{sc} = \left(\frac{\pi}{4}\right) \cdot \left(\frac{R}{M_{air}}\right)^{0,5} \cdot \left(\frac{T_{sc}}{p_{sc}}\right) \cdot \left(\frac{D^5}{f_M \cdot L \cdot \gamma_g \cdot Z_{av} \cdot T_{av}}\right)^{0.5} \cdot \left[(p_w^2 - p_t^2) \cdot \left(\frac{S \cdot e^S}{e^S - 1}\right)\right]^{0.5} \qquad \text{EQ. A-37}$$

Where p_w represents the flowing bottom hole pressure expressed at wellhead datum level. The quantity, p_w is actually the bottom-hole flowing pressure minus the hydrostatic pressure of the gas column.

Substituting the definition of S (Eq. A-13) (all in pure SI system):

$$q_{sc} = \left(\frac{\pi}{4}\right) \cdot \left(\frac{T_{sc}}{p_{sc}}\right) \cdot (2 \cdot g \cdot \cos{(\alpha)})^{0.5} \cdot \left(\frac{D^5}{f_M}\right)^{0.5} \cdot \frac{e^{S/2}}{Z_{av} \cdot T_{av} \cdot \sqrt{e^S - 1}} \cdot (p_w^2 - p_t^2)^{0.5} \qquad \text{EQ. A-38}$$

In practical metric units, where: q_{sc} in [Sm^3/d], pressure in [bara], length in [m] and temperature in [K], the equation becomes:

$$q_{sc} = \frac{86400 \cdot \pi}{4} \cdot (2 \cdot 9.81 \cdot \cos{(\alpha)})^{0.5} \cdot \frac{288}{1} \cdot \left(\frac{D^5}{f_M}\right)^{0.5} \cdot \frac{e^{S/2}}{Z_{av} \cdot T_{av} \cdot \sqrt{e^S - 1}} \\ \cdot (p_w^2 - p_t^2)^{0.5}$$

EQ. A-39

Or

$$q_{sc} = 86.56 \cdot 10^6 \cdot \cos{(\alpha)}^{0.5} \cdot \left(\frac{D^5}{f_M}\right)^{0.5} \cdot \frac{e^{S/2}}{Z_{av} \cdot T_{av} \cdot \sqrt{e^S - 1}} \cdot (p_w^2 - p_t^2)^{0.5}$$

EQ. A-40

In vertical wells $H = L$, and $cos(\alpha) = 1$. When substituting into the rate equation, together with the expression for fully turbulent friction factor (Eq. A-31) gives:

$$q_{sc} = 0.986 \cdot 10^9 \cdot \frac{D^{2.612} \cdot e^{S/2}}{Z_{av} \cdot T_{av} \cdot \sqrt{e^S - 1}} \cdot (p_w^2 - p_t^2)^{0.5}$$

EQ. A-41

This is the metric version of the rate equation suggested by Fetkovich for integrated field studies.

In oilfield units (psia, MSCFD, ft, R), the datum corrected rate equation (Eq. A-38) is:

$$q_{sc} = 86.4 \cdot \frac{\pi}{4} \cdot \left(\frac{520}{14.7}\right) \cdot (2 \cdot 32.17 \cdot \cos{(\alpha)})^{0.5} \cdot \left(\frac{D^5}{12^5 \cdot f_M}\right)^{0.5} \cdot \frac{e^{S/2}}{Z_{av} \cdot T_{av} \cdot \sqrt{e^S - 1}} \\ \cdot (p_w^2 - p_t^2)^{0.5}$$

EQ. A-42

Substituting the expression for fully turbulent Moody friction factor (Eq. A-31):

$$q_{sc} = 693.034 \cdot \frac{\pi}{4} \cdot \left(\frac{520}{14.7}\right) \cdot \cos{(\alpha)}^{0.5} \cdot \left(\frac{D^{5.224}}{12^5 \cdot 0.01748}\right)^{0.5} \cdot \frac{e^{S/2}}{Z_{av} \cdot T_{av} \cdot \sqrt{e^S - 1}} \\ \cdot (p_w^2 - p_t^2)^{0.5}$$

EQ. A-43

Which finally gives:

$$q_{sc} = 292.9 \cdot \frac{D^{2.612} \cdot e^{S/2}}{Z_{av} \cdot T_{av} \cdot \sqrt{e^S - 1}} \cdot (p_w^2 - p_t^2)^{0.5}$$

EQ. A-44

RELATIONSHIP BETWEEN FETKOVICH RATE EQUATION AND THE EQUATION IN THE IOCC MANUAL

The equation used by Fetkovich in his 1975 paper is derived from the IOCC manual and is (rate is in MSCFD):

$$q_{sc} = \frac{31.62 \cdot e^{S/2}}{F_r \cdot Z_{av} \cdot T_{av} \cdot \sqrt{e^S - 1}} \cdot (p_w^2 - p_t^2)^{0.5}$$

EQ. A-45

where $F_r = \frac{0.10797}{D^{2.612}}$

The relationship between F_r[71] and the friction factors is, by definition:

$$F_r{}^2 = \frac{2.6665 \cdot f_F \cdot q^2}{D^5} = \frac{2.6665 \cdot \frac{f_M}{4} \cdot q^2}{D^5}$$

EQ. A-46

---

[71] The dimensional expression Fr has been introduced originally by Cullender and Smith (1956) to facilitate another method to calculated bottom hole pressure accounting for changes in temperature and compressibility factor. The IOCC preferred to apply it in its manual rather than the dimensionless friction factor (Oklahoma City People versus the rest of the world).

Where D is inner tubing diameter, in and q is the gas rate in MMSCFD.

By substituting the empirical value of F_r to the rate equation it becomes:

$$q_{sc} = 292.9 \cdot \frac{D^{2.612} \cdot e^{S/2}}{Z_{av} \cdot T_{av} \cdot \sqrt{e^S - 1}} \cdot (p_w^2 - p_t^2)^{0.5} \qquad \text{EQ. A-47}$$

In practical metric units

$$q_{sc} = 292.9 \cdot \frac{1000}{1} \cdot \frac{1}{35.14} \cdot \frac{(39.37 \cdot D)^{2.612} \cdot e^{S/2}}{Z_{av} \cdot 1.8 \cdot T_{av} \cdot \sqrt{e^S - 1}} \cdot \frac{14.7}{1} (p_w^2 - p_t^2)^{0.5} \qquad \text{EQ. A-48}$$

Or:

$$q_{sc} = 0.986 \cdot 10^9 \cdot \frac{D^{2.612} \cdot e^{S/2}}{Z_{av} \cdot T_{av} \cdot \sqrt{e^S - 1}} \cdot (p_w^2 - p_t^2)^{0.5} \qquad \text{EQ. A-49}$$

The relationship between f_M and the F_r in the IOCC equation: *Interstate Oil Compact Commission "manual of Backpressure Testing of Gas Wells", Oklahoma City, Oklahoma*

Cullender and Smith (1956) introduced originally the dimensional expression F_r. It is a function of f_M, flow rate, and pipe diameter. Back calculating the friction factor from the F_r used in the IOCC equation yields

$$f_F = \frac{0.00437}{D^{0.224}} \qquad \text{EQ. A-50}$$

$$f_M = \frac{0.01748}{D^{0.224}} \qquad \text{EQ. A-51}$$

Starting with the IOCC equation[72] as listed in Fetkovich's paper from 1975 (before dividing by e^S for datum change):

$$p_{wf}^2 = p_t^2 \cdot e^S + \frac{q \cdot F_r \cdot T_{av} \cdot Z_{av}}{31.62} \cdot (e^S - 1) \qquad \text{EQ. A-52}$$

Rearranging:

$$p_{wf}^2 = p_t^2 \cdot e^S + \left(\frac{F_r \cdot T_{av} \cdot Z_{av}}{31.62}\right)^2 \cdot (e^S - 1) \cdot q_{sc}^2 \qquad \text{EQ. A-53}$$

where:

$F_r = \frac{0.10797}{D^{2.612}}$, pipe diameter D in inch, and the gas rate in MSCFD.

For comparison, taking any of the widely used engineering equations, for example in the **SPE –Petroleum Engineering Handbook** (Chapter 34 "Wellbore Hydraulics" by Bertuzzi, Fetkovich, Poettmann and Thomas, equation 44) which applies Moody friction factor f_m:

---

[72] (Note: there is an error in the pressure equation in the original 1975 paper where the equations are hand written, there the number 31.62 is wrongly written as 1.000. The error has been corrected in later prints of the paper. Also be aware that the rate equation in most gas engineering manuals is reported in MMSCFD, Fetkovich uses MSCFD in his analysis)

$$p_1^2 = p_2^2 \cdot e^S + 25 \cdot f_m \cdot H \cdot \gamma_g \cdot Z \cdot T \cdot \frac{(e^S - 1)}{S \cdot D^5} \cdot q_{sc}^2$$

EQ. A-54

or, by substituting the expression for S:

$$p_1^2 = p_2^2 \cdot e^S + 25 \cdot f_m \cdot (Z_{av} \cdot T_{av})^2 \cdot \frac{(e^S - 1)}{0.0375 \cdot D^5} \cdot q_{sc}^2$$

EQ. A-55

or in the **The Canadian Energy Resource Conservation Board Manual (ERCB) on gas well testing** which applies Fanning friction factor (note that Moody factor is 4 times Fanning factor):

$$p_1^2 = p_2^2 \cdot e^S + 100 \cdot f_F \cdot H \cdot \gamma_g \cdot Z_{av} \cdot T_{av} \cdot \frac{(e^S - 1)}{S \cdot D^5} \cdot q_{sc}^2$$

EQ. A-56

The units in these two equations are: p in [psia], vertical depth H in [ft], q = flow-rate in [MMSCFD], d in [in], friction factor f [-], and S is expressed by the following expression:

$$S = 2 \cdot \frac{28.97 \cdot \gamma_g \cdot g}{Z_{av} \cdot T_{av} \cdot R} \cdot H = 2 \frac{28.97 \cdot 32.174}{10.732 \cdot 144 \cdot 32.174} \cdot \frac{\gamma_g}{Z_{av} \cdot T_{av}} \cdot H$$
$$= 0.0375 \cdot \frac{\gamma_g}{Z_{av} \cdot T_{av}} \cdot H$$

EQ. A-57

To back-calculate the friction factor as implied by the IOCC equation, a comparison is made between the second terms on the right-hand side of the IOCC and the ERCB equations (converting it from MMSCFD to MSCFD as used by the IOCC).

$$\left(\frac{F_r \cdot Z_{av} \cdot T_{av}}{31.62}\right)^2 \cdot (e^S - 1) \cdot q_{sc}^2 = 100 \cdot f_F \cdot H \cdot \gamma_g \cdot Z_{av} \cdot T_{av} \cdot \frac{(e^S - 1)}{S \cdot D^5} \cdot q_{sc}^2 \cdot (10^{-6})$$

EQ. A-58

Substituting s in the denominator of the right-hand side gives:

$$1000 \cdot (F_r \cdot Z_{av} \cdot T_{av})^2 \cdot (e^S - 1) \cdot q_{sc}^2$$
$$= 100 \cdot f_F \cdot H \cdot \gamma_g \cdot Z_{av} \cdot T_{av} \cdot \frac{(e^S - 1)}{\left(0.0375 \cdot \frac{\gamma_g \cdot H}{Z_{av} \cdot T_{av}}\right) \cdot D^5} \cdot q_{sc}^2$$

EQ. A-59

which, when compared with the relevant term in IOCC equation gives:

$$(F_r)^2 = 0.1 \cdot f_F \cdot \frac{1}{0.0375 \cdot D^5}$$

EQ. A-60

Solving for the Fanning Friction factor, f_F

$$f_F = 0.375 \cdot D^5 \cdot (F_r)^2$$

EQ. A-61

and substituting $F_r = \frac{0.10797}{D^{2.612}}$ gives:

$$f_F = 0.375 \cdot D^5 \cdot \left(\frac{0.10797}{D^{2.612}}\right)^2 = \frac{0.00437}{D^{0.224}}$$

EQ. A-62

which is equivalent to:

$$f_M = 4 \cdot \left(\frac{0.10797}{D^{2.612}}\right)^2 \cdot 0.375 \cdot D^5 = \frac{0.0174}{D^{0.224}}$$

EQ. A-63

The diameter, D, in both expressions is in inch (While the pipe length in the equation is in ft).

REFERENCES

- Katz, D.L., Cornel, D., Kobayashi, R., Poetmann, F.H., Vary, J.A. Elenbass, J.R., Weinaug, C.F. (1959). *Handbook of Natural Gas Engineering*. McGraw-Hill Publishing Company.
- Smith, R.V. (1950). Determining Friction Factors for Measuring Productivity of Gas Wells. *Trans AIME* **189** (73).
- Energy Resources Conservation Board (ERCB) (1975). *Theory and Practice of the Testing of Gas Wells*. ERCB 73-34, Third Edition, 1975.
- Katz, D.L., & Lee, R.L., (1990). *Natural Gas Engineering-Production and Storage.* McGraw-Hill Publishing Company.
- Young, K.L. (1966). *Effect of Assumptions Used to Calculate Bottom-Hole Pressures in Gas Wells*. SPE-1626. Society of Petroleum Engineers
- Smith, R.V., Williams R.H., & Dewees, E.J. (1954). Measurements of Resistance to Flow of Fluids in Natural Gas Wells. *Trans AIME* **201**, pp. 279
- Cullender M.H. & Smith R.V. (1956) Practical solution of the Gas Flow Equations for Wells and Pipelines with Large Temperature Gradients. *Trans AIME* **207** pp. 281-287.
- Farshad, Fred F., and H.H. Rieke. "Technology Innovation for Determining Surface Roughness in Pipes." J Pet Technol 57 (2005): 82–85. doi: https://doi.org/10.2118/79123-JPT

B. CHOKE EQUATIONS

UNDERSATURATED OIL FLOW

Based on a frictionless flow contraction from an upstream point 1 to a downstream point 2.

The single-phase Bernoulli equation for steady state frictionless flow along a streamline, neglecting elevation changes, is:

$$\frac{dp}{\rho} + V \cdot dV = 0$$

EQ. B-1

Where:

p Pressure

ρ Density

V Velocity

Integrating Eq. B-1 from point 1 to 2:

$$\int_{p_1}^{p_2} \frac{dp}{\rho} + \int_{V_1}^{V_2} V \cdot dV = 0$$

EQ. B-2

Assuming incompressible flow:

$$\frac{p_2 - p_1}{\rho} + \frac{V_2^2 - V_1^2}{2} = 0$$

EQ. B-3

The mass is conserved in the choke, thus:

$$V_1 \cdot A_1 = V_2 \cdot A_2$$

EQ. B-4

The area upstream the choke can be expressed with the diameter of the pipe upstream the choke:

$$A_1 = \frac{\pi \cdot \emptyset_1^2}{4}$$

EQ. B-5

In a similar way, the cross-section area of 2:

$$A_2 = \frac{\pi \cdot \emptyset_2^2}{4}$$

EQ. B-6

Using Eq. B-4, Eq. B-5 and Eq. B-6, it is possible to express V_1 as a function of V_2:

$$V_1 = V_2 \cdot \frac{A_2}{A_1} = V_2 \cdot \frac{\emptyset_2^2}{\emptyset_1^2}$$

EQ. B-7

To simplify the nomenclature, the ratio between the diameters is named beta (which, in a contraction, is always less than 1):

$$\beta = \frac{\emptyset_2}{\emptyset_1}$$

EQ. B-8

Substituting Eq. B-7 in Eq. B-3:

$$\frac{p_2 - p_1}{\rho} + \frac{V_2^2 - V_2^2 \cdot \beta^4}{2} \qquad \text{EQ. B-9}$$

Clearing V_2 in Eq. B-9:

$$V_2 = \sqrt{\frac{2 \cdot (p_2 - p_1)}{\rho \cdot (1 - \beta^4)}} \qquad \text{EQ. B-10}$$

For petroleum production calculations, we often require the oil rate at standard conditions, not the velocity, thus, multiplying Eq. B-10 by A_2 and the oil volume factor $B_{o,@2}$:

$$q_{\bar{o}} = \frac{A_2}{B_{o,@2}} \cdot \sqrt{\frac{2 \cdot (p_2 - p_1)}{\rho \cdot (1 - \beta^4)}} \qquad \text{EQ. B-11}$$

Where $B_{o,@2}$ and ρ are evaluated at p_2 and T_2.

As mentioned earlier, due to the "vena contracta" effect, the effective area at the throat is not exactly A_2, but slightly less. Thus, a correction factor called the flow coefficient is introduced in Eq. B-11:

$$q_{\bar{o}} = \frac{A_2 \cdot C_d}{B_{o,@2}} \cdot \sqrt{\frac{2 \cdot (p_2 - p_1)}{\rho \cdot (1 - \beta^4)}} \qquad \text{EQ. B-12}$$

Relationship between C_v and C_d

The definition of C_v of a valve is:

$$q = \frac{C_V \cdot \sqrt{(p_1 - p_2) \cdot 1.450377E - 4}}{15850.32} \qquad \text{EQ. B-13}$$

Here q is in m^3/s and p is in Pa. The work fluid is water.

Making q equal in both equations

$$C_V \cdot \sqrt{(p_1 - p_2)} \cdot 7.59805E - 7 = A_2 \cdot C_d \cdot \sqrt{\frac{2}{\rho \cdot \left(1 - \left(\frac{\emptyset_2}{\emptyset_1}\right)^4\right)}} \cdot \sqrt{(p_1 - p_2)} \qquad \text{EQ. B-14}$$

Gives the following relationship between Cv and Cd:

$$C_d = \frac{C_V}{A_2} \cdot 7.59805E - 7 \cdot \sqrt{\frac{\rho \cdot \left(1 - \left(\frac{\emptyset_2}{\emptyset_1}\right)^4\right)}{2}} \qquad \text{EQ. B-15}$$

DRY GAS FLOW

(based on a frictionless flow contraction from an upstream point 1 to a downstream point 2)

Using Eq. B-2 as the starting point, the term related to pressure and density remains valid; however, in gas flow the velocity downstream is usually much higher than the velocity upstream, thus $V_2^2 \gg V_1^2$:

$$\int_{p_1}^{p_2} \frac{dp}{\rho} + \frac{V_2^2}{2} = 0$$

EQ. B-16

The density will vary inside the choke. An assumption commonly used is that the contraction process is adiabatic (with an exponent k, the ratio between the specific heats of the gas):

$$p \cdot \rho^{-k} = C$$

EQ. B-17

Where C is a constant. Substituting Eq. B-17 in Eq. B-16:

$$C^{\frac{1}{k}} \cdot \int_{p_1}^{p_2} \frac{dp}{p^{\frac{1}{k}}} + \frac{V_2^2}{2} = 0$$

EQ. B-18

Solving the integral:

$$C^{\frac{1}{k}} \cdot \frac{k}{k-1} \cdot \left(p_2^{\frac{k-1}{k}} - p_1^{\frac{k-1}{k}} \right) + \frac{V_2^2}{2} = 0$$

EQ. B-19

The constant C is expressed in terms of the inlet conditions:

$$C^{\frac{1}{k}} = \frac{p_1^{\frac{1}{k}}}{\rho_1}$$

EQ. B-20

Substituting Eq. B-20 in Eq. B-19 and introducing the pressure ratio $y = p_2/p_1$:

$$\frac{p_1^{\frac{1}{k}}}{\rho_1} \cdot \frac{k}{k-1} \cdot p_1^{\frac{k-1}{k}} \cdot \left(y^{\frac{k-1}{k}} - 1 \right) + \frac{V_2^2}{2} = 0$$

EQ. B-21

Clearing V_2 and simplifying p_1:

$$V_2 = \sqrt{2 \cdot \frac{p_1}{\rho_1} \cdot \frac{k}{k-1} \cdot \left(1 - y^{\frac{k-1}{k}} \right)}$$

EQ. B-22

Expressing ρ_1 with the real gas equation:

$$\rho_1 = \frac{p_1 \cdot M_w}{Z_1 \cdot R \cdot T_1}$$

EQ. B-23

Where:

M_w Molecular weight of the gas

R Universal gas constant

Z Generalized compressibility factor

Substituting Eq. B-23 in Eq. B-22:

$$V_2 = \sqrt{2 \cdot \frac{Z_1 \cdot R \cdot T_1}{M_w} \cdot \frac{k}{k-1} \cdot \left(1 - y^{\frac{k-1}{k}} \right)}$$

EQ. B-24

For petroleum production calculations, we often require the gas rate at standard conditions, not the velocity, thus, multiplying Eq. B-24 by the "effective" cross-section area of 2 gives the local volume rate:

$$q_{g2} = A_2 \cdot C_d \cdot \sqrt{2 \cdot \frac{Z_1 \cdot R \cdot T_1}{M_w} \cdot \frac{k}{k-1} \cdot \left(1 - y^{\frac{k-1}{k}}\right)}$$

<div align="right">EQ. B-25</div>

The local volumetric rate at point 2 is related to the rate at standard conditions by the following equation:

$$q_{g2} \cdot \rho_2 = q_{\bar{g}} \cdot \rho_{sc}$$

<div align="right">EQ. B-26</div>

Substituting Eq. B-26 in Eq. B-25 gives:

$$q_{\bar{g}} = \frac{\rho_2 \cdot A_2 \cdot C_d}{\rho_{sc}} \cdot \sqrt{2 \cdot \frac{Z_1 \cdot R \cdot T_1}{M_w} \cdot \frac{k}{k-1} \cdot \left(1 - y^{\frac{k-1}{k}}\right)}$$

<div align="right">EQ. B-27</div>

ρ_2 is related with ρ_1 by Eq. B-20:

$$\frac{p_2^{\frac{1}{k}}}{\rho_2} = \frac{p_1^{\frac{1}{k}}}{\rho_1}$$

<div align="right">EQ. B-28</div>

Clearing ρ_2 from Eq. B-28 and substituting in Eq. B-27, and using the real gas equation to express the gas density at standard conditions:

$$q_{\bar{g}} = \frac{\rho_1 \cdot p_2^{\frac{1}{k}} \cdot R \cdot T_{sc} \cdot A_2 \cdot C_d}{p_1^{\frac{1}{k}} \cdot p_{sc} \cdot M_w} \cdot \sqrt{2 \cdot \frac{Z_1 \cdot R \cdot T_1}{M_w} \cdot \frac{k}{k-1} \cdot \left(1 - y^{\frac{k-1}{k}}\right)}$$

<div align="right">EQ. B-29</div>

Introducing Eq. B-23 for ρ_1:

$$q_{\bar{g}} = \frac{p_1 \cdot M_w \cdot p_2^{\frac{1}{k}} \cdot R \cdot T_{sc} \cdot A_2 \cdot C_d}{Z_1 \cdot R \cdot T_1 \cdot p_1^{\frac{1}{k}} \cdot p_{sc} \cdot M_w} \cdot \sqrt{2 \cdot \frac{Z_1 \cdot R \cdot T_1}{M_w} \cdot \frac{k}{k-1} \cdot \left(1 - y^{\frac{k-1}{k}}\right)}$$

<div align="right">EQ. B-30</div>

Simplifying and rearranging terms[73]:

$$q_{\bar{g}} = \frac{p_1 \cdot T_{sc} \cdot A_2 \cdot C_d}{p_{sc}} \cdot \sqrt{2 \cdot \frac{R}{Z_1 \cdot T_1 \cdot M_w} \cdot \frac{k}{k-1} \cdot \left(y^{\frac{2}{k}} - y^{\frac{k+1}{k}}\right)}$$

<div align="right">EQ. B-31</div>

C_d depends on the geometry of the restriction, the Reynolds number and the ratio between the upstream and downstream diameters. If no information is available, a value of 0.865 can be used.

Eq. B-31 is valid only for the subcritical range. To predict the rate in the critical range the critical pressure ratio (y_c) must be used, instead of the actual pressure ratio.

For gas, the critical pressure ratio can be predicted as:

$$y_c = \left(\frac{2}{k+1}\right)^{\frac{k}{k-1}}$$

<div align="right">EQ. B-32</div>

---

[73] Be aware there is an inconsistency in this model. When deriving the pressure-density relationship, assumptions of ideal gas and calorically perfect gas were done, but later the density at the inlet is expressed with real gas equation including the gas deviation factor.

LIQUID-GAS MIXTURES – RELATIONSHIP BETWEEN PRESSURE, TEMPERATURE AND DENSITY

Often there is a mixture of oil, gas and water circulating through the choke. To estimate fluid properties at the choke outlet or at the throat, an assumption that is typically made is that the mixture undergoes an adiabatic expansion. Using the first law of the thermodynamics and assuming piston work yields:

$$du = -p \cdot dv_m$$

EQ. B-33

Where:

u Specific internal energy

p Pressure

v_m Specific volume of the mixture

The variation in specific internal energy is expressed in terms of the specific heat at constant volume:

$$du = \left(x_o \cdot C_{v,o} + x_g \cdot C_{v,g} + x_w \cdot C_{v,w} \right) \cdot dT$$

EQ. B-34

Where:

x_i Molar fraction of phase "i"

$C_{v,i}$ Specific heat at constant volume of phase "i"

T Temperature

Or, introducing the specific heat at constant volume of the mixture:

$$du = C_{v,m} \cdot dT$$

EQ. B-35

The specific volume of the mixture is expressed in terms of the mixture density:

$$dw = p \cdot dv_m = -\frac{p}{\rho_m{}^2} \cdot d\rho_m$$

EQ. B-36

Substituting Eq. B-35 and Eq. B-36 in equation Eq. B-33 yields:

$$C_{v,m} \cdot dT = \frac{p}{\rho_m{}^2} \cdot d\rho_m$$

EQ. B-37

We wish to express temperature as a function of pressure and mixture density. The density of the mixture is:

$$\rho_m = \frac{1}{\dfrac{x_g}{\rho_g} + \dfrac{x_o}{\rho_o} + \dfrac{x_w}{\rho_w}}$$

EQ. B-38

Clearing the gas density:

$$\frac{1}{\rho_g} = \frac{1}{x_g} \cdot \left(\frac{1}{\rho_m} - \frac{x_o}{\rho_o} - \frac{x_w}{\rho_w} \right)$$

EQ. B-39

Substituting the ideal gas equation:

$$T = \frac{p}{R \cdot x_g} \cdot \left(\frac{1}{\rho_m} - \frac{x_o}{\rho_o} - \frac{x_w}{\rho_w} \right)$$

EQ. B-40

Deriving the expression (assuming that oil and water densities and molar fractions remain constant during the choke expansion):

$$dT = \frac{dp}{R \cdot x_g} \cdot \left(\frac{1}{\rho_m} - \frac{x_o}{\rho_o} - \frac{x_w}{\rho_w}\right) - \frac{p}{R \cdot x_g} \cdot \frac{1}{\rho_m^2} \cdot d\rho_m$$

EQ. B-41

Substituting in Eq. B-37 yields:

$$C_{v,m} \cdot \frac{dp}{R \cdot x_g} \cdot \left(\frac{1}{\rho_m} - \frac{x_o}{\rho_o} - \frac{x_w}{\rho_w}\right) - \frac{p}{R \cdot x_g} \cdot \frac{1}{\rho_m^2} \cdot d\rho_m = \frac{p}{\rho_m^2} \cdot d\rho_m$$

EQ. B-42

Rearranging terms (all that is related to pressure to the right side and with density to the left):

$$\rho_w \cdot \rho_o \cdot \left(1 + \frac{R \cdot x_g}{C_{v,m}}\right) \cdot \frac{d\rho_m}{\rho_w \cdot \rho_o \cdot \rho_m - x_o \cdot \rho_m^2 \cdot \rho_w - x_w \cdot \rho_m^2 \cdot \rho_o} = \frac{dp}{p} \cdot$$

EQ. B-43

Performing an indefinite integration on both sides and subsequently taking the exponential:

$$p \cdot \left(\frac{\rho_m}{\rho_w \cdot \rho_o - x_o \cdot \rho_m \cdot \rho_w - x_w \cdot \rho_m \cdot \rho_o}\right)^{-\frac{R \cdot x_g + C_{v,m}}{C_{v,m}}} = c \cdot$$

EQ. B-44

Where c is a constant.

Substituting the definition of specific heat at constant volume of the mixture (Eq. B-35):

$$p \cdot \left(\frac{\rho_m}{\rho_w \cdot \rho_o - x_o \cdot \rho_m \cdot \rho_w - x_w \cdot \rho_m \cdot \rho_o}\right)^{-\frac{R \cdot x_g + x_o \cdot C_{v,o} + x_g \cdot C_{v,g} + x_w \cdot C_{v,w}}{x_o \cdot C_{v,o} + x_g \cdot C_{v,g} + x_w \cdot C_{v,w}}} = c \cdot$$

EQ. B-45

And using the relationship between the gas specific heat at constant volume, specific heat at constant pressure and the universal gas constant:

$$R = C_p - C_v$$

EQ. B-46

Yields:

$$p \cdot \left(\frac{\rho_m}{\rho_w \cdot \rho_o - x_o \cdot \rho_m \cdot \rho_w - x_w \cdot \rho_m \cdot \rho_o}\right)^{-\frac{x_o \cdot C_{v,o} + x_g \cdot C_{p,g} + x_w \cdot C_{v,w}}{x_o \cdot C_{v,o} + x_g \cdot C_{v,g} + x_w \cdot C_{v,w}}} = c$$

EQ. B-47

Eq. B-39 is rearranged to express the density of the gas as a function of the density of the mixture:

$$\frac{\rho_g}{x_g \cdot \rho_o \cdot \rho_w} = \frac{\rho_m}{\rho_w \cdot \rho_o - x_o \cdot \rho_m \cdot \rho_w - x_w \cdot \rho_m \cdot \rho_o} = c$$

EQ. B-48

Substituting Eq. B-48 in Eq. B-47 yields:

$$p \cdot \left(\frac{\rho_g}{x_g \cdot \rho_o \cdot \rho_w}\right)^{-\frac{x_o \cdot C_{v,o} + x_g \cdot C_{p,g} + x_w \cdot C_{v,w}}{x_o \cdot C_{v,o} + x_g \cdot C_{v,g} + x_w \cdot C_{v,w}}} = c$$

EQ. B-49

The gas mole fraction, oil density and water density are assumed to remain constant during the choke expansion, therefore:

$$p \cdot (v_g)^{\frac{x_o \cdot C_{v,o} + x_g \cdot C_{p,g} + x_w \cdot C_{v,w}}{x_o \cdot C_{v,o} + x_g \cdot C_{v,g} + x_w \cdot C_{v,w}}} = c$$

EQ. B-50

This equation resembles a polytropic process across the choke.

If one considers pressure and temperature, the relationship becomes

$$p^{1-n} \cdot T^n = c$$

EQ. B-51

Or, equivalently, when applied between choke inlet and generic position x:

$$\frac{T_x}{T_1} = \left(\frac{p_x}{p_1}\right)^{\frac{n-1}{n}}$$

EQ. B-52

With

$$n = \frac{x_o \cdot C_{v,o} + x_g \cdot C_{p,g} + x_w \cdot C_{v,w}}{x_o \cdot C_{v,o} + x_g \cdot C_{v,g} + x_w \cdot C_{v,w}}$$

EQ. B-53

The author calculated values of n for several combinations of pressure (in the range 2-400 bara), temperature (5-100 C), GOR (50 to 10000 Sm3/Sm3) and water cut (0-90%), using black oil correlations and correlations for heat capacity of oil, gas and water. Values obtained varied between 1-1.3.

C. TEMPERATURE DROP IN CONDUIT FOR LIQUID FLOW

GENERAL EXPRESSION

Departing from the general steady state energy equation in one dimension:

$$\frac{d\dot{q}}{dL} = \dot{m} \cdot \left(\frac{dh}{dL} + v \cdot \frac{dv}{dL} + g \cdot \frac{dz}{dL} \right)$$

EQ. C-1

The heat transfer can be expressed with the overall heat transfer coefficient (U), based on a reference conduit radius (heat entering to the system is positive, heat leaving negative, thus a negative sign must be placed in front of the expression):

$$\dot{q} = -2 \cdot \pi \cdot L \cdot r_{ref} \cdot U \cdot \left(T_f - T_\infty \right)$$

EQ. C-2

Where:

r_{ref} Reference radius (in pipelines it is often insulation outer radius, in wells it is often tubing inner diameter [m]

U Overall heat transfer coefficient [W/m².K]

T_∞ Mean ambient temperature [K or °C]

T_f Mean fluid temperature in the section [K or °C]

Differentiating Eq. C-2:

$$d\dot{q} = -2 \cdot \pi \cdot r_{ref} \cdot U \cdot \left(T_f - T_\infty \right) \cdot dL$$

EQ. C-3

Making $T_f = T$ and neglecting velocity changes $\frac{dv}{dL} \approx 0$, Eq. C-1 becomes:

$$-2 \cdot \pi \cdot r_{ref} \cdot U \cdot (T - T_\infty) = \dot{m} \cdot \left(\frac{dh}{dL} + g \cdot \frac{dz}{dL} \right)$$

EQ. C-4

DERIVATION FOR LIQUIDS

For liquids, assuming incompressibility, enthalpy can be expressed in terms of the specific heat capacity at constant pressure:

$$dh = C_p \cdot dT$$

EQ. C-5

Where:

C_p Specific heat capacity [J/kg.K]

Substituting in the energy conservation equation

$$.-2 \cdot \pi \cdot r_{ref} \cdot U \cdot (T - T_\infty) = \dot{m} \cdot \left(C_p \cdot \frac{dT}{dL} + g \cdot \sin(\theta) \right)$$

EQ. C-6

Where:

θ Angle between pipe and horizontal [rad]

Expanding the expression:

$$-T \cdot 2 \cdot \pi \cdot r_{ref} \cdot U + T_\infty \cdot 2 \cdot \pi \cdot r_{ref} \cdot U = \dot{m} \cdot C_p \cdot \frac{dT}{dL} + \dot{m} \cdot g \cdot \sin(\theta)$$

EQ. C-7

$$\frac{dT}{dL} + T \cdot \frac{2 \cdot \pi \cdot r_{ref} \cdot U}{\dot{m} \cdot C_p} - \frac{T_\infty \cdot 2 \cdot \pi \cdot r_{ref} \cdot U}{\dot{m} \cdot C_p} + \frac{g \cdot \sin(\theta)}{C_p} = 0$$

EQ. C-8

For simplicity, we define the variable A:

$$A = \frac{\dot{m} \cdot C_p}{2 \cdot \pi \cdot r_{ref} \cdot U}$$

EQ. C-9

$$\frac{dT}{dL} + T \cdot \frac{1}{A} - \frac{T_\infty}{A} + \frac{g \cdot \sin(\theta)}{C_p} = 0$$

EQ. C-10

To solve the differential equation, and approach is to using $u = e^{\frac{x}{A}}$ and multiplying it by the above expression:

$$u \cdot \frac{dT}{dL} + u \cdot T \cdot \frac{1}{A} = u \cdot \left(\frac{T_\infty}{A} - \frac{g \cdot \sin(\theta)}{C_p} \right)$$

EQ. C-11

The product differentiating rule is defined as:

$$\frac{d(w(x) \cdot v(x))}{dx} = \frac{dw(x)}{dx} \cdot v(x) + w(x) \cdot \frac{dv(x)}{dx}$$

EQ. C-12

Using the result from Eq. C-12, it is possible to group Eq. C-11 as follows:

$$\frac{d(u \cdot T)}{dL} = u \cdot \left(\frac{T_\infty}{A} - \frac{g \cdot \sin(\theta)}{C_p} \right)$$

EQ. C-13

The resulting expression can be integrated by separating variables between the initial position "0" to a generic position x in the pipe. This assumes that T_∞, A, θ and C_p remain constant along the pipe length:

$$e^{\frac{x}{A}} \cdot T \Big|_{T_0}^{T(x)} = \int_0^x \left(\frac{T_\infty}{A} - \frac{g \cdot \sin(\theta)}{C_p} \right) \cdot e^{\frac{x}{A}} \cdot dx$$

EQ. C-14

$$e^{\frac{x}{A}} \cdot T \Big|_{T_0}^{T(x)} = \left(\frac{T_\infty}{A} - \frac{g \cdot \sin(\theta)}{C_p} \right) \cdot A \cdot e^{\frac{x}{A}} \Big|_0^x$$

EQ. C-15

Where:

T_0 Temperature of the fluid at pipe inlet $(T(x = 0)$),[K or °C]

Evaluating at the integration limits and rearranging:

$$e^{\frac{x}{A}} \cdot T(x) - T_0 = \left(\frac{T_\infty}{A} - \frac{g \cdot \sin(\theta)}{C_p} \right) \cdot A \cdot \left(e^{\frac{x}{A}} - 1 \right)$$

EQ. C-16

$$T(x) = T_0 \cdot e^{\frac{-x}{A}} + \left(\frac{T_\infty}{A} - \frac{g \cdot \sin(\theta)}{C_p} \right) \cdot A \cdot \left(1 - e^{\frac{-x}{A}} \right)$$

EQ. C-17

This gives:

$$T(x) = T_\infty + (T_0 - T_\infty) \cdot e^{\frac{-x}{A}} - \frac{1}{C_p} \cdot g \cdot \sin(\theta) \cdot A \cdot (1 - e^{\frac{-x}{A}})$$

EQ. C-18

WITH VARIABLE AMBIENT TEMPERATURE

Ambient temperature could be variable, e.g. in a vertical tubing or casing along a formation. In this case, T_∞ must be substituted by a function of x. Assuming a linear temperature gradient, T_∞ can be expressed as:

$$T_\infty(x) = T_\infty|_{x=0} + \sin(\theta) \cdot x \cdot G \qquad \text{EQ. C-19}$$

Where:

G Linear temperature gradient [K/m] (negative if temperature is reduced with $\sin(\theta) \cdot x$)

$T_\infty|_{x=0}$ Temperature of the environment at the beginning of the section [K or °C]

Substituting in Eq. C-14

$$e^{\frac{x}{A}} \cdot T\Big|_{T_0}^{T(x)} = \int_0^x \left(\frac{T_\infty|_{x=0}}{A} + \frac{\sin(\theta) \cdot x \cdot G}{A} - \frac{g \cdot \sin(\theta)}{C_p} \right) \cdot e^{\frac{x}{A}} \cdot dx \qquad \text{EQ. C-20}$$

Solving:

$$e^{\frac{x}{A}} \cdot T(x) - T_0 = \left(\frac{T_\infty|_{x=0}}{A} - \frac{g \cdot \sin(\theta)}{C_p} \right) \cdot A \cdot \left(e^{\frac{x}{A}} - 1 \right) + \frac{\sin(\theta) \cdot G}{A} \cdot \int_0^x x \cdot e^{\frac{x}{A}} \cdot dx \qquad \text{EQ. C-21}$$

.

$$e^{\frac{x}{A}} \cdot T(x) - T_0 = \left(\frac{T_\infty|_{x=0}}{A} - \frac{g \cdot \sin(\theta)}{C_p} \right) \cdot A \cdot \left(e^{\frac{x}{A}} - 1 \right) + \sin(\theta) \cdot G \cdot \left(e^{\frac{x}{A}} \cdot (x - A) \right)\Big|_0^x \qquad \text{EQ. C-22}$$

.

$$e^{\frac{x}{A}} \cdot T(x) - T_0 = \left(\frac{T_\infty|_{x=0}}{A} - \frac{g \cdot \sin(\theta)}{C_p} \right) \cdot A \cdot \left(e^{\frac{x}{A}} - 1 \right) + \sin(\theta) \cdot G \qquad \text{EQ. C-23}$$
$$\cdot \left(e^{\frac{x}{A}} \cdot (x - A) + A \right)$$

Gives:

$$T(x) = (T_0 - T_\infty|_{x=0}) \cdot e^{-\frac{x}{A}} + (T_\infty|_{x=0} + \sin(\theta) \cdot G \cdot x) - \frac{g \cdot \sin(\theta)}{C_p} \cdot A \cdot \left(1 - e^{-\frac{x}{A}} \right) \qquad \text{EQ. C-24}$$
$$+ \sin(\theta) \cdot G \cdot A \cdot \left(e^{-\frac{x}{A}} - 1 \right)$$

D. DERIVATION OF MULTIPHASE FLOW EXPRESSIONS

RELATIONSHIP BETWEEN LIQUID HOLDUP (H_L), SLIP RATIO (S) AND NON-SLIP LIQUID VOLUME FRACTION (λ_L)

Using the relationship between real (u_g) and superficial (u_{sg}) gas velocities:

$$u_g \cdot A \cdot (1 - H_L) = u_{sg} \cdot A \qquad \text{EQ. D-1}$$

Where:

A Pipe cross-section

Using the relationship between real (u_l) and superficial (u_{sl}) liquid velocities:

$$u_l \cdot A \cdot H_L = u_{sl} \cdot A \qquad \text{EQ. D-2}$$

Dividing Eq. D-1 by Eq. D-2 gives:

$$\frac{u_g \cdot A \cdot (1 - H_L)}{u_l \cdot A \cdot H_L} = \frac{u_{sg} \cdot A}{u_{sl} \cdot A} \qquad \text{EQ. D-3}$$

Simplifying and introducing the definition of the slip ratio $S = u_g / u_l$:

$$\frac{S \cdot (1 - H_L)}{H_L} = \frac{u_{sg}}{u_{sl}} \qquad \text{EQ. D-4}$$

The non-slip liquid volume fraction is defined as:

$$\lambda_L = \frac{u_{sl}}{u_{sl} + u_{sg}} \qquad \text{EQ. D-5}$$

or, alternatively,

$$\lambda_L = \frac{1}{1 + \dfrac{u_{sg}}{u_{sl}}} \qquad \text{EQ. D-6}$$

Clearing out $\frac{u_{sg}}{u_{sl}}$ gives

$$\frac{u_{sg}}{u_{sl}} = \frac{1 - \lambda_L}{\lambda_L} \qquad \text{EQ. D-7}$$

Substituting Eq. D-7 into Eq. D-4 gives

$$\frac{S \cdot (1 - H_L)}{H_L} = \frac{1 - \lambda_L}{\lambda_L} \qquad \text{EQ. D-8}$$

RELATIONSHIP BETWEEN HOLDUP (H_L), SLIP RATIO (S) AND QUALITY (x)

Using Eq. D-4, the ratio of superficial velocities is expressed using the total mass flow rate ($\dot{m}$) and the quality (gas mass fraction, x) and the densities of gas and liquid (ρ_l, ρ_g). The resulting expression is simplified:

$$S \cdot (1 - H_L) \over H_L = {\dfrac{\dot{m} \cdot x}{\rho_g \cdot A}} \over {\dfrac{\dot{m} \cdot (1-x)}{\rho_l \cdot A}} = \frac{x \cdot \rho_l}{\rho_g \cdot (1-x)}$$

EQ. D-9

Clearing H_L from Eq. D-9:

$$\frac{S \cdot (1 - H_L)}{H_L} = S \cdot \left(\frac{1}{H_L} - 1 \right) = \frac{x \cdot \rho_l}{\rho_g \cdot (1-x)}$$

EQ. D-10

$$\frac{1}{H_L} = \frac{x \cdot \rho_l}{S \cdot \rho_g \cdot (1-x)} + 1$$

EQ. D-11

$$\frac{1}{H_L} = \frac{x \cdot \rho_l + S \cdot \rho_g \cdot (1-x)}{S \cdot \rho_g \cdot (1-x)}$$

EQ. D-12

$$H_L = \frac{S \cdot \rho_g \cdot (1-x)}{x \cdot \rho_l + S \cdot \rho_g \cdot (1-x)}$$

EQ. D-13

HOLDUP AVERAGE MIXTURE DENSITY (ρ_m)

The holdup average mixture density can be expressed as function of slip ratio (S), quality (gas mass fraction x) and the densities of gas and liquid (ρ_l, ρ_g). The density of the mixture is defined:

$$\rho_m = (1 - H_L) \cdot \rho_g + H_L \cdot \rho_l$$

EQ. D-14

Substituting the holdup from Eq. D-13 in Eq. D-14:

$$\rho_m = \left[1 - \frac{S \cdot \rho_g \cdot (1-x)}{x \cdot \rho_l + S \cdot \rho_g \cdot (1-x)} \right] \cdot \rho_g + \frac{S \cdot \rho_g \cdot (1-x)}{x \cdot \rho_l + S \cdot \rho_g \cdot (1-x)} \cdot \rho_l$$

EQ. D-15

Simplifying:

$$\rho_m = \frac{x \cdot \rho_l}{x \cdot \rho_l + S \cdot \rho_g \cdot (1-x)} \cdot \rho_g + \frac{S \cdot \rho_g \cdot (1-x)}{x \cdot \rho_l + S \cdot \rho_g \cdot (1-x)} \cdot \rho_l$$

EQ. D-16

$$\rho_m = \frac{x + S \cdot (1-x)}{\dfrac{x}{\rho_g} + \dfrac{S}{\rho_l} \cdot (1-x)}$$

EQ. D-17

EFFECTIVE MOMENTUM DENSITY

$$\frac{\dot{m}^2}{\rho_e \cdot A} = \dot{m}_g \cdot u_g + \dot{m}_l \cdot u_l$$

EQ. D-18

$$\frac{1}{\rho_e} = \frac{A}{\dot{m}^2} \cdot \left(\dot{m}_g \cdot u_g + \dot{m}_l \cdot u_l \right)$$

EQ. D-19

$$\frac{1}{\rho_e} = \frac{A}{\dot{m}} \cdot \left(x \cdot u_g + (1-x) \cdot u_l \right)$$

EQ. D-20

$$\frac{1}{\rho_e} = \frac{A}{\dot{m}} \cdot u_l \cdot (x \cdot S + (1-x))$$

EQ. D-21

$$\frac{1}{\rho_e} = \frac{A}{\dot{m}} \cdot u_l \cdot S \cdot \left[x + \frac{(1-x)}{S} \right]$$

EQ. D-22

The holdup can be introduced in the right-hand side term using the following equation:

$$\frac{A}{\dot{m}} \cdot u_l \cdot S = \frac{A}{\dot{m}} \cdot u_g = \frac{m_g}{m} \cdot \frac{1}{(1 - H_L) \cdot \rho_g} = x \cdot \frac{1}{(1 - H_L) \cdot \rho_g}$$

EQ. D-23

Expressing the liquid holdup in terms of Eq. D-13, Eq. D-23 can be rewritten as:

$$\frac{A}{\dot{m}} \cdot u_l \cdot S = x \cdot \frac{1}{\left[1 - \dfrac{S \cdot \rho_g \cdot (1 - x)}{x \cdot \rho_l + S \cdot \rho_g \cdot (1 - x)}\right] \cdot \rho_g} = x \cdot \frac{1}{\dfrac{x \cdot \rho_l}{x \cdot \rho_l + S \cdot \rho_g \cdot (1 - x)} \cdot \rho_g}$$

EQ. D-24

$$\frac{A}{\dot{m}} \cdot u_l \cdot S = \frac{x \cdot \rho_l + S \cdot \rho_g \cdot (1 - x)}{\rho_l \cdot \rho_g} = \frac{x}{\rho_g} + \frac{S \cdot (1 - x)}{\rho_l}$$

EQ. D-25

Substituting Eq. D-25 in Eq. D-22:

$$\frac{1}{\rho_e} = \left[\frac{x}{\rho_g} + \frac{S \cdot (1 - x)}{\rho_l}\right] \cdot \left[x + \frac{(1 - x)}{S}\right]$$

EQ. D-26

KINETIC ENERGY-AVERAGE MIXTURE DENSITY

$$\frac{\dot{m}^2}{2 \cdot \rho_k^2 \cdot A^2} = x \cdot \frac{u_g^2}{2} + (1 - x) \cdot \frac{u_l^2}{2}$$

EQ. D-27

$$\frac{1}{\rho_k} = \sqrt{\frac{2 \cdot A^2}{\dot{m}^2} \cdot \left(x \cdot \frac{u_g^2}{2} + (1 - x) \cdot \frac{u_l^2}{2}\right)}$$

EQ. D-28

$$\frac{1}{\rho_k} = \sqrt{\frac{A^2 \cdot u_g^2}{\dot{m}^2} \cdot \left(x + \frac{(1 - x)}{S^2}\right)}$$

EQ. D-29

$$\frac{1}{\rho_k} = \sqrt{\frac{\dot{m}_g^2}{\dot{m} \cdot (1 - H_L)^2 \cdot \rho_g^2} \cdot \left(x + \frac{(1 - x)}{S^2}\right)}$$

EQ. D-30

$$\frac{1}{\rho_k} = \sqrt{\frac{x^2}{(1 - H_L)^2 \cdot \rho_g^2} \cdot \left(x + \frac{(1 - x)}{S^2}\right)}$$

EQ. D-31

Using Eq. D-13, as a definition for the liquid holdup and substituting in Eq. D-31:

$$\frac{1}{\rho_k} = \sqrt{\frac{x^2}{\left[1 - \dfrac{S \cdot \rho_g \cdot (1 - x)}{x \cdot \rho_l + S \cdot \rho_g \cdot (1 - x)}\right]^2 \cdot \rho_g^2} \cdot \left(x + \frac{(1 - x)}{S^2}\right)}$$

EQ. D-32

$$\frac{1}{\rho_k} = \sqrt{\frac{x^2}{\left[\dfrac{x \cdot \rho_l \cdot \rho_g}{x \cdot \rho_l + S \cdot \rho_g \cdot (1 - x)}\right]^2} \cdot \left(x + \frac{(1 - x)}{S^2}\right)}$$

EQ. D-33

$$\frac{1}{\rho_k} = \sqrt{\left[\frac{x \cdot \rho_l + S \cdot \rho_g \cdot (1 - x)}{\rho_l \cdot \rho_g}\right]^2 \cdot \left(x + \frac{(1 - x)}{S^2}\right)}$$

EQ. D-34

$$\frac{1}{\rho_k} = \left|\frac{x \cdot \rho_l + S \cdot \rho_g \cdot (1 - x)}{\rho_l \cdot \rho_g}\right| \cdot \sqrt{x + \frac{(1 - x)}{S^2}}$$

EQ. D-35

EQ. D-36

$$\frac{1}{\rho_k} = \left| \frac{x}{\rho_g} + \frac{S \cdot (1-x)}{\rho_l} \right| \cdot \sqrt{x + \frac{(1-x)}{S^2}}$$

E. OIL & GAS PROCESSING DIAGRAMS
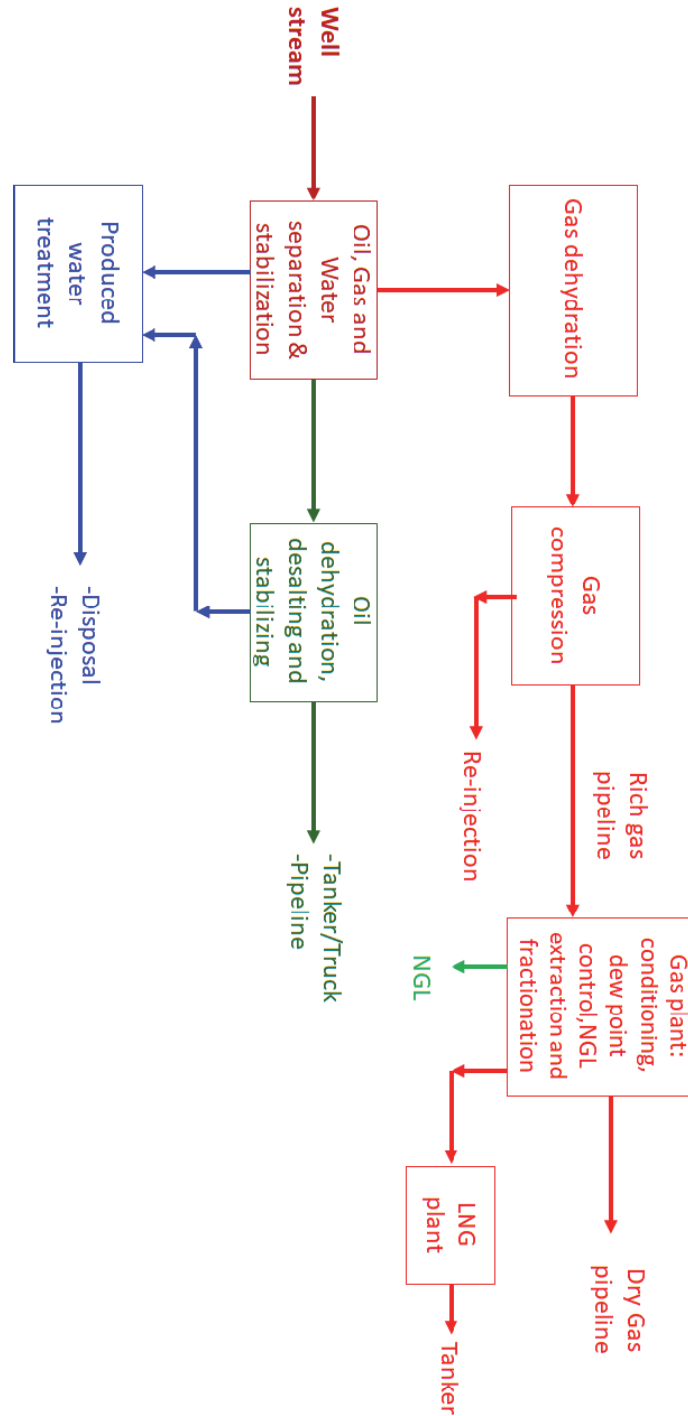
FIGURE E-1. GAS PROCESSING FROM WELL TO SALES

Well stream

1800–750 psig

Multi-stage separation (1-2 trains, 1-4 stages) with interstage compression and cooling

OiW : 500–1000 ppmw

- Hydrocyclones +
- Flotation
- Hydrocyclones+
degassing
- Skim tanks+flotation
- treatment

-TEG contactor
1000-1200 psig
-TEG regeneration
(400 F)

WiO : 1–3 %v

-Electrostatic coalescer.
-Desalter
-Heater

-Disposal: <40 ppmw OiW
-Re-injection

API: 8-65
WiO < 0.5-1% , < 2 % (N)
-Tanker/Truck: < 11 psia RVP
-Pipeline: 111 psia RVP, 150 psia TVD (N)
Salt: 10-30 PTB
H2S: 10-100 ppmw

Gas compression

100-200 barg
-Water dew point-18@ 69 barg
-WiG < 4 lb/MMscf
-CO2 2.5 mole%
-H2S < 5 ppm
-Cricondenbar:<105 barg
-Cricondenterm <40C

Re-injection

-JT expansion,
Turboexpander or refrigeration.
-NGL fractionation

NGL

-Dew point <-10 C (50 barg)
-Water Dew point -18@ 69 barg
-CO2 < 2.5 mole%
-H2S < 5 ppm
-Calorificvalue
-Wobbe index

LNG plant

Tanker

FIGURE E-2. GAS PROCESSING FROM WELL TO SALES (INCLUDING TYPICAL OPERATING VALUES)

F. DERIVATION OF LOCAL MASS AND VOLUME FRACTIONS OF OIL GAS AND WATER AS A FUNCTION OF BLACK OIL PROPERTIES

GAS, OIL AND WATER MASS FRACTIONS

Expressing the local gas volumetric rate in terms of the standard conditions rates and black oil properties:

$$q_g = q_{\bar{g}} \cdot \frac{B_g}{1 - R_s \cdot r_s} - \frac{R_s \cdot B_g}{1 - R_s \cdot r_s} \cdot q_{\bar{o}} \qquad \text{EQ. F-1}$$

The local mass flow rate of gas in terms of the local gas volumetric rate and the gas density:

$$\dot{m}_g = q_g \cdot \rho_g = \left[q_{\bar{g}} \cdot \frac{B_g}{1 - R_s \cdot r_s} - \frac{R_s \cdot B_g}{1 - R_s \cdot r_s} \cdot q_{\bar{o}} \right] \cdot \rho_g \qquad \text{EQ. F-2}$$

Similarly for the oil and water mass rates:

Local oil volumetric rate:

$$q_o = -q_{\bar{g}} \cdot \frac{B_o . r_s}{1 - R_s \cdot r_s} + \frac{B_o}{1 - R_s \cdot r_s} \cdot q_{\bar{o}} \qquad \text{EQ. F-3}$$

Local mass rate of oil:

$$\dot{m}_o = q_o \cdot \rho_o = \left[-q_{\bar{g}} \cdot \frac{B_o \cdot r_s}{1 - R_s \cdot r_s} + \frac{B_o}{1 - R_s \cdot r_s} \cdot q_{\bar{o}} \right] \cdot \rho_o \qquad \text{EQ. F-4}$$

Local water volumetric rate

$$q_w = B_w \cdot q_{\bar{w}} \qquad \text{EQ. F-5}$$

Local mass rate of water:

$$\dot{m}_w = q_w \cdot \rho_w = B_w \cdot q_{\bar{w}} \cdot \rho_w \qquad \text{EQ. F-6}$$

The gas mass fraction is then expressed as:

$$x_g = \frac{\dot{m}_g}{\dot{m}_g + \dot{m}_o + \dot{m}_w} \qquad \text{EQ. F-7}$$

Substituting Eq. F-2, Eq. F-4, Eq. F-6 in Eq. F-7 gives:

$$x_g = \frac{\left[q_{\bar{g}} \cdot \frac{B_g}{1 - R_s \cdot r_s} - \frac{R_s \cdot B_g}{1 - R_s \cdot r_s} \cdot q_{\bar{o}} \right] \cdot \rho_g}{\left[q_{\bar{g}} \cdot \frac{B_g}{1 - R_s \cdot r_s} - \frac{R_s \cdot B_g}{1 - R_s \cdot r_s} \cdot q_{\bar{o}} \right] \cdot \rho_g + \left[-q_{\bar{g}} \cdot \frac{B_o \cdot r_s}{1 - R_s \cdot r_s} + \frac{B_o}{1 - R_s \cdot r_s} \cdot q_{\bar{o}} \right] \cdot \rho_o + B_w \cdot q_{\bar{w}} \cdot \rho_w} \qquad \text{EQ. F-8}$$

Simplifying terms:

$$x_g = \frac{\left[q_{\bar{g}} \cdot B_g - R_s \cdot B_g \cdot q_{\bar{o}} \right] \cdot \rho_g}{\left[q_{\bar{g}} \cdot B_g - R_s \cdot B_g \cdot q_{\bar{o}} \right] \cdot \rho_g + \left[-q_{\bar{g}} \cdot B_o \cdot r_s + B_o \cdot q_{\bar{o}} \right] \cdot \rho_o + (1 - R_s \cdot r_s) \cdot B_w \cdot q_{\bar{w}} \cdot \rho_w} \qquad \text{EQ. F-9}$$

$$x_g = \frac{\left[q_{\bar{g}} \cdot B_g - R_s \cdot B_g \cdot q_{\bar{o}}\right]}{\left[q_{\bar{g}} \cdot B_g - R_s \cdot B_g \cdot q_{\bar{o}}\right] + \left[-q_{\bar{g}} \cdot B_o \cdot r_s + B_o \cdot q_{\bar{o}}\right] \cdot \frac{\rho_o}{\rho_g} + (1 - R_s \cdot r_s) \cdot B_w \cdot q_{\bar{w}} \cdot \frac{\rho_w}{\rho_g}}$$

EQ. F-10

Local densities of oil, gas and water are:

$$\rho_g = \frac{1}{B_g} \cdot \rho_{\bar{g}} + \frac{r_s}{B_o} \cdot \rho_{\bar{o}}$$

EQ. F-11

$$\rho_o = \frac{R_s}{B_o} \cdot \rho_{\bar{g}} + \frac{1}{B_o} \cdot \rho_{\bar{o}}$$

EQ. F-12

$$\rho_w = \frac{1}{B_w} \cdot \rho_{\bar{w}}$$

EQ. F-13

The density ratios are:

$$\frac{\rho_o}{\rho_g} = \frac{\frac{R_s}{B_o} \cdot \rho_{\bar{g}} + \frac{1}{B_o} \cdot \rho_{\bar{o}}}{\frac{1}{B_g} \cdot \rho_{\bar{g}} + \frac{r_s}{B_o} \cdot \rho_{\bar{o}}}$$

EQ. F-14

$$\frac{\rho_w}{\rho_g} = \frac{\frac{1}{B_w} \cdot \rho_{\bar{w}}}{\frac{1}{B_g} \cdot \rho_{\bar{g}} + \frac{r_s}{B_o} \cdot \rho_{\bar{o}}}$$

EQ. F-15

Substituting Eq. F-14 and Eq. F-15 in Eq. F-10 gives:

$$x_g = \frac{\left[q_{\bar{g}} \cdot B_g - R_s \cdot B_g \cdot q_{\bar{o}}\right]}{\left[q_{\bar{g}} \cdot B_g - R_s \cdot B_g \cdot q_{\bar{o}}\right] + \left[-q_{\bar{g}} \cdot B_o \cdot r_s + B_o \cdot q_{\bar{o}}\right] \cdot \left(\frac{\frac{R_s}{B_o} \cdot \rho_{\bar{g}} + \frac{1}{B_o} \cdot \rho_{\bar{o}}}{\frac{1}{B_g} \cdot \rho_{\bar{g}} + \frac{r_s}{B_o} \cdot \rho_{\bar{o}}}\right) + (1 - R_s \cdot r_s) \cdot B_w \cdot q_{\bar{w}} \cdot \left(\frac{\frac{1}{B_w} \cdot \rho_{\bar{w}}}{\frac{1}{B_g} \cdot \rho_{\bar{g}} + \frac{r_s}{B_o} \cdot \rho_{\bar{o}}}\right)}$$

EQ. F-16

Using:

$$q_{\bar{g}} = R_p \cdot q_{\bar{o}}$$

EQ. F-17

and

$$q_{\bar{w}} = \frac{W_c}{1 - W_c} \cdot q_{\bar{o}}$$

EQ. F-18

Gives:

$$x_g = \frac{\left[R_p \cdot q_{\bar{o}} \cdot B_g - R_s \cdot B_g \cdot q_{\bar{o}}\right]}{\left[R_p \cdot q_{\bar{o}} \cdot B_g - R_s \cdot B_g \cdot q_{\bar{o}}\right] + \left[-R_p \cdot q_{\bar{o}} \cdot B_o \cdot r_s + B_o \cdot q_{\bar{o}}\right] \cdot \left(\frac{\frac{R_s}{B_o} \cdot \rho_{\bar{g}} + \frac{1}{B_o} \cdot \rho_{\bar{o}}}{\frac{1}{B_g} \cdot \rho_{\bar{g}} + \frac{r_s}{B_o} \cdot \rho_{\bar{o}}}\right) + (1 - R_s \cdot r_s) \cdot B_w \cdot \frac{W_c}{1 - W_c} \cdot q_{\bar{o}} \cdot \left(\frac{\frac{1}{B_w} \cdot \rho_{\bar{w}}}{\frac{1}{B_g} \cdot \rho_{\bar{g}} + \frac{r_s}{B_o} \cdot \rho_{\bar{o}}}\right)}$$

EQ. F-19

Simplifying terms:

$$x_g = \frac{[R_p \cdot B_g - R_s \cdot B_g]}{[R_p \cdot B_g - R_s \cdot B_g] + [-R_p \cdot B_o \cdot r_s + B_o] \cdot \left(\dfrac{\dfrac{R_s}{B_o} \cdot \rho_{\bar{g}} + \dfrac{1}{B_o} \cdot \rho_{\bar{o}}}{\dfrac{1}{B_g} \cdot \rho_{\bar{g}} + \dfrac{r_s}{B_o} \cdot \rho_{\bar{o}}}\right) + (1 - R_s \cdot r_s) \cdot \dfrac{W_c}{1 - W_c} \cdot \left(\dfrac{\rho_{\bar{w}}}{\dfrac{1}{B_g} \cdot \rho_{\bar{g}} + \dfrac{r_s}{B_o} \cdot \rho_{\bar{o}}}\right)}$$

EQ. F-20

Finally gives:

$$x_g = \frac{[R_p - R_s]}{[R_p - R_s] + [-R_p \cdot r_s + 1] \cdot \left(\dfrac{R_s \cdot \rho_{\bar{g}} + \rho_{\bar{o}}}{\rho_{\bar{g}} + \dfrac{B_g}{B_o} \cdot r_s \cdot \rho_{\bar{o}}}\right) + (1 - R_s \cdot r_s) \cdot \dfrac{W_c}{1 - W_c} \cdot \left(\dfrac{\rho_{\bar{w}}}{\rho_{\bar{g}} + \dfrac{B_g}{B_o} \cdot r_s \cdot \rho_{\bar{o}}}\right)}$$

EQ. F-21

For oil:

$$x_o = \frac{[-R_p \cdot r_s + 1] \cdot \left(\dfrac{R_s \cdot \rho_{\bar{g}} + \rho_{\bar{o}}}{\rho_{\bar{g}} + \dfrac{B_g}{B_o} \cdot r_s \cdot \rho_{\bar{o}}}\right)}{[R_p - R_s] + [-R_p \cdot r_s + 1] \cdot \left(\dfrac{R_s \cdot \rho_{\bar{g}} + \rho_{\bar{o}}}{\rho_{\bar{g}} + \dfrac{B_g}{B_o} \cdot r_s \cdot \rho_{\bar{o}}}\right) + (1 - R_s \cdot r_s) \cdot \dfrac{W_c}{1 - W_c} \cdot \left(\dfrac{\rho_{\bar{w}}}{\rho_{\bar{g}} + \dfrac{B_g}{B_o} \cdot r_s \cdot \rho_{\bar{o}}}\right)}$$

EQ. F-22

For water:

$$x_w = \frac{(1 - R_s \cdot r_s) \cdot \dfrac{W_c}{1 - W_c} \cdot \left(\dfrac{\rho_{\bar{w}}}{\rho_{\bar{g}} + \dfrac{B_g}{B_o} \cdot r_s \cdot \rho_{\bar{o}}}\right)}{[R_p - R_s] + [-R_p \cdot r_s + 1] \cdot \left(\dfrac{R_s \cdot \rho_{\bar{g}} + \rho_{\bar{o}}}{\rho_{\bar{g}} + \dfrac{B_g}{B_o} \cdot r_s \cdot \rho_{\bar{o}}}\right) + (1 - R_s \cdot r_s) \cdot \dfrac{W_c}{1 - W_c} \cdot \left(\dfrac{\rho_{\bar{w}}}{\rho_{\bar{g}} + \dfrac{B_g}{B_o} \cdot r_s \cdot \rho_{\bar{o}}}\right)}$$

EQ. F-23

If one assumes $r_s = 0$, then the expressions are simplified as follows:

$$x_g = \frac{[R_p - R_s]}{\left[R_p + \dfrac{\rho_{\bar{o}}}{\rho_{\bar{g}}} + \dfrac{W_c}{1 - W_c} \cdot \left(\dfrac{\rho_{\bar{w}}}{\rho_{\bar{g}}}\right)\right]}$$

EQ. F-24

$$x_o = \frac{\left[R_s + \dfrac{\rho_{\bar{o}}}{\rho_{\bar{g}}}\right]}{\left[R_p + \dfrac{\rho_{\bar{o}}}{\rho_{\bar{g}}} + \dfrac{W_c}{1 - W_c} \cdot \left(\dfrac{\rho_{\bar{w}}}{\rho_{\bar{g}}}\right)\right]}$$

EQ. F-25

$$x_w = \frac{\dfrac{W_c}{1 - W_c} \cdot \left(\dfrac{\rho_{\bar{w}}}{\rho_{\bar{g}}}\right)}{\left[R_p + \dfrac{\rho_{\bar{o}}}{\rho_{\bar{g}}} + \dfrac{W_c}{1 - W_c} \cdot \left(\dfrac{\rho_{\bar{w}}}{\rho_{\bar{g}}}\right)\right]}$$

EQ. F-26

GAS, OIL AND WATER VOLUME FRACTIONS

The gas volume fraction is defined as:

$$\alpha_g = \frac{q_g}{q_g + q_o + q_w} \qquad \text{EQ. F-27}$$

Expressing local volumetric rates of gas, oil and water in terms of standard conditions rates and BO properties:

$$\alpha_g = \frac{\left[q_{\bar{g}} \cdot \frac{B_g}{1 - R_s \cdot r_s} - \frac{R_s \cdot B_g}{1 - R_s \cdot r_s} \cdot q_{\bar{o}} \right]}{\left[q_{\bar{g}} \cdot \frac{B_g}{1 - R_s \cdot r_s} - \frac{R_s \cdot B_g}{1 - R_s \cdot r_s} \cdot q_{\bar{o}} \right] + \left[-q_{\bar{g}} \cdot \frac{B_o.r_s}{1 - R_s \cdot r_s} + \frac{B_o}{1 - R_s \cdot r_s} \cdot q_{\bar{o}} \right] + B_w \cdot q_{\bar{w}}} \qquad \text{EQ. F-28}$$

Using:

$$q_{\bar{g}} = R_p \cdot q_{\bar{o}} \qquad \text{EQ. F-29}$$

and

$$q_{\bar{w}} = \frac{W_c}{1 - W_c} \cdot q_{\bar{o}} \qquad \text{EQ. F-30}$$

And simplifying, gives:

$$\alpha_g = \frac{[R_p - R_s]}{[R_p - R_s] + \frac{B_o}{B_g} \cdot [-R_p \cdot r_s + 1] + (1 - R_s \cdot r_s) \cdot \frac{W_c}{1 - W_c} \cdot \frac{B_w}{B_g}} \qquad \text{EQ. F-31}$$

For oil:

$$\alpha_o = \frac{\frac{B_o}{B_g} \cdot [-R_p \cdot r_s + 1]}{[R_p - R_s] + \frac{B_o}{B_g} \cdot [-R_p \cdot r_s + 1] + (1 - R_s \cdot r_s) \cdot \frac{W_c}{1 - W_c} \cdot \frac{B_w}{B_g}} \qquad \text{EQ. F-32}$$

For water

$$\alpha_w = \frac{(1 - R_s \cdot r_s) \cdot \frac{W_c}{1 - W_c} \cdot \frac{B_w}{B_g}}{[R_p - R_s] + \frac{B_o}{B_g} \cdot [-R_p \cdot r_s + 1] + (1 - R_s \cdot r_s) \cdot \frac{W_c}{1 - W_c} \cdot \frac{B_w}{B_g}} \qquad \text{EQ. F-33}$$

If one assumes $r_s = 0$, then the expressions are simplified as follows:

$$\alpha_g = \frac{[R_p - R_s]}{[R_p - R_s] + \frac{B_o}{B_g} + \frac{W_c}{1 - W_c} \cdot \frac{B_w}{B_g}} \qquad \text{EQ. F-34}$$

$$\alpha_o = \frac{\dfrac{B_o}{B_g}}{[R_p - R_s] + \dfrac{B_o}{B_g} + \dfrac{W_c}{1 - W_c} \cdot \dfrac{B_w}{B_g}}$$

EQ. F-35

$$\alpha_w = \frac{\dfrac{W_c}{1 - W_c} \cdot \dfrac{B_w}{B_g}}{[R_p - R_s] + \dfrac{B_o}{B_g} + \dfrac{W_c}{1 - W_c} \cdot \dfrac{B_w}{B_g}}$$

EQ. F-36

The volume fraction of oil in liquid:

$$\alpha_{o,l} = \frac{q_o}{q_o + q_w} = \frac{-q_{\bar{g}} \cdot \dfrac{B_o.r_s}{1 - R_s \cdot r_s} + \dfrac{B_o}{1 - R_s \cdot r_s} \cdot q_{\bar{o}}}{-q_{\bar{g}} \cdot \dfrac{B_o.r_s}{1 - R_s \cdot r_s} + \dfrac{B_o}{1 - R_s \cdot r_s} \cdot q_{\bar{o}} + B_w \cdot q_{\bar{w}}}$$

EQ. F-37

Using:

$$q_{\bar{g}} = R_p \cdot q_{\bar{o}}$$

EQ. F-38

and

$$q_{\bar{w}} = \frac{W_c}{1 - W_c} \cdot q_{\bar{o}}$$

EQ. F-39

Gives:

$$\alpha_{o,l} = \frac{-R_p \cdot q_{\bar{o}} \cdot \dfrac{B_o.r_s}{1 - R_s \cdot r_s} + \dfrac{B_o}{1 - R_s \cdot r_s} \cdot q_{\bar{o}}}{-R_p \cdot q_{\bar{o}} \cdot \dfrac{B_o.r_s}{1 - R_s \cdot r_s} + \dfrac{B_o}{1 - R_s \cdot r_s} \cdot q_{\bar{o}} + B_w \cdot \dfrac{W_c}{1 - W_c} \cdot q_{\bar{o}}}$$

EQ. F-40

Simplifying terms:

$$\alpha_{o,l} = \frac{-R_p \cdot B_o.r_s + B_o}{-R_p \cdot B_o.r_s + B_o + (1 - R_s \cdot r_s) \cdot B_w \cdot \dfrac{W_c}{1 - W_c}}$$

EQ. F-41

Gives finally:

$$\alpha_{o,l} = \frac{-R_p \cdot r_s + 1}{-R_p \cdot r_s + 1 + (1 - R_s \cdot r_s) \cdot \dfrac{B_w}{B_o} \cdot \dfrac{W_c}{1 - W_c}}$$

EQ. F-42

If one assumes $r_s = 0$, then the expression is simplified as follows:

$$\alpha_{o,l} = \frac{B_o}{B_o + B_w \cdot \dfrac{W_c}{1 - W_c}}$$

EQ. F-43

Liquid density for a mixture of oil and water (assuming $r_s = 0$):

$$\rho_l = \left(\frac{B_o}{B_o + B_w \cdot \frac{W_c}{1 - W_c}} \right) \cdot \rho_o + \left(\frac{B_w}{B_o + B_w \cdot \frac{W_c}{1 - W_c}} \right) \cdot \rho_w \qquad \text{EQ. F-44}$$

Using Eq. F-12 and Eq. F-13 gives:

$$\rho_l = \left(\frac{B_o}{B_o + B_w \cdot \frac{W_c}{1 - W_c}} \right) \cdot \left(\frac{R_s}{B_o} \cdot \rho_{\bar{g}} + \frac{1}{B_o} \cdot \rho_{\bar{o}} \right) + \left(\frac{B_w \cdot \frac{W_c}{1 - W_c}}{B_o + B_w \cdot \frac{W_c}{1 - W_c}} \right) \cdot \frac{1}{B_w} \cdot \rho_{\bar{w}} \qquad \text{EQ. F-45}$$

simplifying:

$$\rho_l = \left(\frac{R_s \cdot \rho_{\bar{g}} + \rho_{\bar{o}} + \rho_{\bar{w}} \cdot \frac{W_c}{1 - W_c}}{B_o + B_w \cdot \frac{W_c}{1 - W_c}} \right) \qquad \text{EQ. F-46}$$

G. DERIVATION OF THE EXPRESSION OF FIELD PRODUCING GAS-OIL RATIO AS A FUNCTION OF MOBILITIES OF OIL AND GAS AND BLACK OIL PROPERTIES

The producing gas oil ratio (R_p) can be expressed as the ratio between standard conditions rates of gas and oil:

$$R_p = \frac{q_{\bar{g}g} + q_{\bar{g}o}}{q_{\bar{o}o} + q_{\bar{o}g}}$$

EQ. G-1

Neglecting the oil condensing from the gas ($q_{\bar{o}g} = 0$):

$$R_p = \frac{q_{\bar{g}g} + q_{\bar{g}o}}{q_{\bar{o}o}} = \frac{q_{\bar{g}g}}{q_{\bar{o}o}} + \frac{q_{\bar{g}o}}{q_{\bar{o}o}}$$

EQ. G-2

The second term in the equation is the solution gas oil ratio (R_s). The first term can be expressed as a local rate of oil or gas times the oil volume factor and the gas volume factor.

$$R_p = \frac{\frac{q_g}{B_g}}{\frac{q_o}{B_o}} + R_s$$

EQ. G-3

The local flow rates depend on the IPR of each phase (and integrating the pressure function from p_wf to p_R). However, as a simplification, if one considers the reservoir as a tank with uniform pressure p_R then the integral and well geometric effects disappear, and each rate will be proportional to k_r/μ. Therefore:

$$R_p = \left(\frac{\frac{k_{rg}}{\mu_g \cdot B_g}}{\frac{k_{ro}}{\mu_o \cdot B_o}} \right)_{p_R} + R_s$$

EQ. G-4

The producing gas oil ratio (R_p) can be related to the solution gas-oil ratio (R_s) and solution oil-gas ratio (r_s) by introducing both definitions in Eq. G-1:

$$R_p = \frac{q_{\bar{g}g} + q_{\bar{g}o}}{q_{\bar{o}o} + q_{\bar{o}g}} = \frac{q_{\bar{g}g} + R_s \cdot q_{\bar{o}o}}{q_{\bar{o}o} + q_{\bar{g}g} \cdot r_s} = \frac{1 + R_s \cdot \frac{q_{\bar{o}o}}{q_{\bar{g}g}}}{\frac{q_{\bar{o}o}}{q_{\bar{g}g}} + r_s}$$

EQ. G-5

Defining a factor "a":

$$a = \frac{q_{\bar{o}o}}{q_{\bar{g}g}}$$

EQ. G-6

This factor indicates how is the ratio between surface oil coming from reservoir oil and surface gas coming from reservoir gas. For example, when a is infinite, it means that there is no surface gas coming from reservoir gas, therefore the producing gas oil ratio should be equal to the solution gas-gas ratio:

$$\lim_{a \to \infty} R_p = \lim_{a \to \infty} \frac{1 + R_s \cdot a}{a + r_s} = R_s$$

EQ. G-7

when a is zero, it means that there is no surface oil coming from reservoir oil, therefore the producing gas oil ratio should be equal to the inverse of the solution oil-gas ratio:

$$\lim_{a \to 0} R_p = \lim_{a \to 0} \frac{1 + R_s \cdot a}{a + r_s} = \frac{1}{r_s}$$

EQ. G-8

H. GAS LIFT OPTIMIZATION

Example 1: Single well, unconstrained maximization of economic revenue by adjusting gas injection rate

A simple but very typical revenue function is defined by Eq. H-1:

$$f_{rev}(q_{g,inj}) = q_o \cdot P_o - q_{g,inj} \cdot P_g = f(q_{g,inj}) \cdot P_o - q_{g,inj} \cdot P_g \qquad \text{EQ. H-1}$$

Where:

P_o Oil price [USD/stb/d, USD/Sm^3/d]

P_g Cost of injection gas [USD/MMSCFD, USD/MSm^3/d]

f_{rev} Revenue function

Deriving the function with respect to the adjustable variable:

$$\frac{df_{rev}(q_{g,inj})}{dq_{g,inj}} = \frac{df(q_{g,inj})}{dq_{g,inj}} \cdot P_o - P_g = 0 \Rightarrow \frac{df(q_{g,inj})}{dq_{g,inj}} = \frac{P_g}{P_o} \qquad \text{EQ. H-2}$$

The maximum revenue is therefore achieved for the point in the gas lift performance curve where the derivative is exactly equal to the ratio between the injection gas cost and the oil price. In general, the gas price is much smaller than the oil price, yielding that the derivative must be very close to zero.

Example 2: Single well, maximization of oil production with limited gas injection rate available

To include the limitation on injection gas available ($q_{g,inj} \leq q_{g,inj\ TOT}$) the Lagrange function[3-2] is created:

$$L(q_{g,inj}) = f(q_{g,inj}) - \lambda \cdot (q_{g,inj} - q_{g,inj\ TOT}) \qquad \text{EQ. H-3}$$

The maximum is given when the derivative of the function with respect to the adjustable variable is equal to zero (Eq. H-4) and when the additional conditions (Eq. H-5, Eq. H-6, Eq. H-7) are met:

$$\frac{dL(q_{g,inj})}{dq_{g,inj}} = \frac{df(q_{g,inj})}{dq_{g,inj}} - \lambda = 0 \Rightarrow \frac{df(q_{g,inj})}{dq_{g,inj}} = \lambda \qquad \text{EQ. H-4}$$

$$\lambda \cdot (q_{g,inj} - q_{g,inj\ TOT}) = 0 \qquad \text{EQ. H-5}$$

$$\lambda \geq 0 \qquad \text{EQ. H-6}$$

$$(q_{g,inj} - q_{g,inj\ TOT}) \leq 0 \qquad \text{EQ. H-7}$$

There are two possible solutions:

Solution 1: $\lambda = 0, \dfrac{df(q_{g,inj})}{dq_{g,inj}} = 0$ Valid only if there is enough gas available ($q_{g,inj} \leq q_{g,inj\ TOT}$)

Solution 2: $\lambda > 0, \dfrac{df(q_{g,inj})}{dq_{g,inj}} = \lambda$ Valid only if all the gas available is used ($q_{g,inj} = q_{g,inj\ TOT}$). Please note that due to the condition (Eq. H-6) on lambda, the derivative MUST NOT be negative.

Example 3: Single well, maximization of revenue with limited gas injection rate.

The Lagrange function is created:

$$L(q_{g,inj}) = f_{rev}(q_{g,inj}) - \lambda \cdot (q_{g,inj} - q_{g,inj\ TOT}) \qquad \text{EQ. H-8}$$

The maximum is given when the derivative of the function with respect to the adjustable variable is equal to zero (Eq. H-9) and when the additional conditions (Eq. H-10, Eq. H-11, Eq. H-12) are met:

$$\frac{\partial L(q_{g,inj})}{\partial q_{g,inj}} = \frac{df_{rev}(q_{g,inj})}{dq_{g,inj}} - \lambda = 0 \Rightarrow \frac{df(q_{g,inj})}{dq_{g,inj}} \cdot P_o - P_g = \lambda \Rightarrow \frac{df(q_{g,inj})}{dq_{g,inj}} = \frac{\lambda + P_g}{P_o} \qquad \text{EQ. H-9}$$

$$\lambda \cdot (q_{g,inj} - q_{g,inj\ TOT}) = 0 \qquad \text{EQ. H-10}$$

$$\lambda \geq 0 \qquad \text{EQ. H-11}$$

$$(q_{g,inj} - q_{g,inj\ TOT}) \leq 0 \qquad \text{EQ. H-12}$$

There are two possible solutions:

Solution 1:	$\lambda = 0, \dfrac{df(q_{g,inj})}{dq_{g,inj}} = \dfrac{P_g}{P_o}$	Valid only if there is enough gas available ($q_{g,inj} \leq q_{g,inj\ TOT}$)
Solution 2:	$\lambda > 0, \dfrac{df(q_{g,inj})}{dq_{g,inj}} = \dfrac{\lambda + P_g}{P_o}$	Valid only if all the gas available is used ($q_{g,inj} = q_{g,inj\ TOT}$).

Example 4: unconstrained oil production maximization on a group of wells by adjusting the individual well gas lift injection rate

The present development assumes that the operation of an individual well is independent from the others (the operating wellhead pressure remains constant despite of the operating conditions of the individual wells). This is because the mathematical procedure employed requires the objective function (e.g. total oil production) to be additively separable (a function that can expressed as the summation of two or more functions each one depending on only one variable).

The total oil production function (F) is the sum of the individual (i) well oil production (f_i). The total number of wells is N.

$$F(q_{g,inj1}, q_{g,inj2}, q_{g,inj3}, \dots) = \sum_{i=1}^{N} f_i(q_{g,inji}) \qquad \text{EQ. H-13}$$

F is a multivariate (N) additively separable scalar function. A necessary condition for this function to be maximum is that the elements of its gradient must be equal to zero:

$$\frac{\partial F(q_{g,inj1}, q_{g,inj2}, q_{g,inj3}, \dots)}{\partial q_{g,inji}} = \frac{\partial f_i(q_{g,inji})}{\partial q_{g,inji}} = 0 \qquad \text{EQ. H-14}$$

The maximum of the compound oil production is when all the oil production of the individual wells is also maximum.

Example 5: Revenue maximization on a group of wells by adjusting the gas lift injection rate

The total revenue function (f_{revTOT}) is the sum of the individual well oil production ($f_{rev,i}$). The total number of wells is N.

$$f_{revTOT}(q_{g,inj1}, q_{g,inj2}, q_{g,inj3}, \dots) = \sum_{i=1}^{N} f_{rev,i}(q_{g,inji}) \qquad \text{EQ. H-15}$$

f_{revTOT} is a multivariate (N) additively separable scalar function. A necessary condition for this function to be maximum is that the elements of its gradient must be equal to zero:

$$\frac{\partial f_{revTOT}(q_{g,inj1}, q_{g,inj2}, q_{g,inj3}, \dots)}{\partial q_{g,inji}} = \frac{\partial f_{rev,i}(q_{g,inji})}{\partial q_{g,inji}} = \left(\frac{\partial f_i(q_{g,inji})}{\partial q_{g,inji}} \cdot P_o - P_g\right) = 0 \qquad \text{EQ. H-16}$$

The maximum of the compound revenue is achieved when all the revenues of the individual wells are also maximum.

Example 6: revenue maximization of a group of wells by adjusting the gas lift injection rate with limited gas

The total revenue function (f_{revTOT}) is the sum of the individual well oil production ($f_{rev,i}$). The total number of wells is N.

$$f_{revTOT}(q_{g,inj1}, q_{g,inj2}, q_{g,inj3}, \dots) = \sum_{i=1}^{N} f_{rev,i}(q_{g,inji}) \qquad \text{EQ. H-17}$$

f_{revTOT} is a multivariate (N) additively separable scalar function. In order to include the limitation on injection gas available ($\sum q_{g,inj} < q_{g,inj\,TOT}$) the method of Lagrange multipliers is used. The Lagrange function is created:

$$L(q_{g,inj1}, q_{g,inj2}, q_{g,inj3}, \dots) = \sum_{i=1}^{N} f_{rev,i}(q_{g,inji}) - \lambda \cdot (\sum_{i=1}^{N} q_{g,inji} - q_{g,inj\,TOT}) \qquad \text{EQ. H-18}$$

A necessary condition for this function to be maximum is that the elements of its gradient must be equal to zero (Eq. H-19) and when the additional conditions (Eq. H-20, Eq. H-21, Eq. H-22) are met:

$$\frac{\partial L(q_{g,inj1}, q_{g,inj2}, q_{g,inj3}, \dots)}{\partial q_{g,inji}} = \frac{\partial f_{rev,i}(q_{g,inji})}{\partial q_{g,inji}} - \lambda = 0 \Rightarrow \frac{\partial f_i(q_{g,inji})}{\partial} = \frac{\lambda + P_g}{P_o} \qquad \text{EQ. H-19}$$

$$\lambda \cdot \left(\sum_{i=1}^{N} q_{g,inji} - q_{g,injTOT}\right) = 0 \qquad \text{EQ. H-20}$$

$$\lambda \geq 0 \qquad \text{EQ. H-21}$$

$$\sum_{i=1}^{N} q_{g,inji} < q_{g,injTOT} \qquad \text{EQ. H-22}$$

There are two possible solutions:

Solution 1: $\lambda = 0, \dfrac{\partial f_i(q_{g,inj})}{\partial q_{g,inj}} = \dfrac{P_g}{P_o}$ — All the wells are operating in their maximum revenue point. Valid only if there is enough gas available ($\sum q_{g,inj} < q_{g,inj\,TOT}$)

Solution 2: $\lambda > 0, \dfrac{\partial f_i(q_{g,inj})}{\partial q_{g,inj}} = \dfrac{\lambda + P_g}{P_o}$ — All wells are operating at the same derivative in the gas lift performance curve. Valid only if all the gas available is used ($\sum q_{g,inj} - q_{g,inj\,TOT} = 0$)

The procedure described is also applicable for any situation where the well (or group of wells) has a concave performance curve of oil production vs an adjustable parameter. For example, ESP lifted wells with diluent injection at the ESP suction also exhibit a similar performance curve.

I. ANALYTICAL EXPRESSION OF REVENUE NPV CONSIDERING A LINEAR DIMENSIONLESS PRODUCTION POTENTIAL, CONTINUOUS DISCOUNTING AND OIL PRICE VARYING LINEARLY IN TIME. CASE STUDY: OIL OFFSHORE FIELD.

Assume the oil price shows a linear behavior with time:

$$P_o(t) = P_1 + m_1 \cdot t$$

EQ. I-1

This gives the following expression for the revenue NPV:

$$
\begin{aligned}
NPV_{rev} = {} & q_{p,f} \cdot P_1 \cdot t_{uptime} \\
& \cdot \left\{ \left[\frac{e^{-i \cdot t_{ini}} - e^{-i \cdot (t_{ini} + \Delta t_p)}}{i} \right] + \left[\frac{e^{-i \cdot (t_{ini} + \Delta t_p)} - e^{-(m+i) \cdot t + m \cdot (\Delta t_p + t_{ini})}}{(m+i)} \right] \right\} \\
& + t_{uptime} \cdot \int_{t_{ini}}^{t_{ini} + \Delta t_p} q_{p,f} \cdot m_1 \cdot t \cdot e^{-i \cdot t} dt + t_{uptime} \\
& \cdot \int_{t_{ini} + \Delta t_p}^{t} q_{p,f} \cdot e^{-m \cdot (t - \Delta t_p - t_{ini})} \cdot m_1 \cdot t \cdot e^{-i \cdot t} dt
\end{aligned}
$$

EQ. I-2

Solving the second-to-last integral and factorizing the last integral:

$$
\begin{aligned}
NPV_{rev} = {} & q_{p,f} \cdot P_1 \cdot t_{uptime} \\
& \cdot \left\{ \left[\frac{e^{-i \cdot t_{ini}} - e^{-i \cdot (t_{ini} + \Delta t_p)}}{i} \right] + \left[\frac{e^{-i \cdot (t_{ini} + \Delta t_p)} - e^{-(m+i) \cdot t + m \cdot (\Delta t_p + t_{ini})}}{(m+i)} \right] \right\} \\
& + q_{p,f} \cdot m_1 \cdot t_{uptime} \cdot \left(-\frac{e^{-i \cdot t}}{i} \left[t + \frac{1}{i} \right] \right) \bigg|_{t_{ini}}^{t_{ini} + \Delta t_p} + q_{p,f} \cdot m_1 \cdot t_{uptime} \\
& \cdot e^{m \cdot (\Delta t_p + t_{ini})} \cdot \int_{t_{ini} + \Delta t_p}^{t} e^{-t \cdot (m+i)} \cdot t \cdot dt
\end{aligned}
$$

EQ. I-3

Solving the last integral and evaluating the second-to-last integral:

$$
\begin{aligned}
NPV_{profit} = {} & q_{p,f} \cdot P_1 \cdot t_{uptime} \\
& \cdot \left\{ \left[\frac{e^{-i \cdot t_{ini}} - e^{-i \cdot (t_{ini} + \Delta t_p)}}{i} \right] + \left[\frac{e^{-i \cdot (t_{ini} + \Delta t_p)} - e^{-(m+i) \cdot t + m \cdot (\Delta t_p + t_{ini})}}{(m+i)} \right] \right\} \\
& + q_{p,f} \cdot m_1 \cdot t_{uptime} \\
& \cdot \left\{ -\frac{e^{-i \cdot (t_{ini} + \Delta t_p)}}{i} \left[t_{ini} + \Delta t_p + \frac{1}{i} \right] + -\frac{e^{-i \cdot t_{ini}}}{i} \left[t_{ini} + \frac{1}{i} \right] \right\} + q_{p,f} \cdot \\
& \cdot t_{uptime} \cdot e^{m \cdot (\Delta t_p + t_{ini})} \cdot \left(-\frac{e^{-(m+i) \cdot t}}{(m+i)} \left[t + \frac{1}{(m+i)} \right] \right) \bigg|_{t_{ini} + \Delta t_p}^{t}
\end{aligned}
$$

EQ. I-4

Evaluating the last integral:

$$NPV_{profit} = q_{p,f} \cdot P_1 \cdot t_{uptime}$$

$$\cdot \left\{ \left[\frac{e^{-i \cdot t_{ini}} - e^{-i \cdot (t_{ini} + \Delta t_p)}}{i} \right] + \left[\frac{e^{-i \cdot (t_{ini} + \Delta t_p)} - e^{-(m+i) \cdot t + m \cdot (\Delta t_p + t_{ini})}}{(m+i)} \right] \right\}$$

$$+ q_{p,f} \cdot m_1 \cdot t_{uptime}$$

$$\cdot \left\{ -\frac{e^{-i \cdot (t_{ini} + \Delta t_p)}}{i} \left[t_{ini} + \Delta t_p + \frac{1}{i} \right] + -\frac{e^{-i \cdot t_{ini}}}{i} \left[t_{ini} + \frac{1}{i} \right] \right\} + q_{p,f} \cdot$$

$$\cdot t_{uptime} \cdot e^{m \cdot (\Delta t_p + t_{ini})}$$

$$\cdot \left(-\frac{e^{-i \cdot t}}{(m+i)} \left[t + \frac{1}{(m+i)} \right] + -\frac{e^{-i \cdot (t_{ini} + \Delta t_p)}}{(m+i)} \left[t_{ini} + \Delta t_p + \frac{1}{(m+i)} \right] \right)$$

EQ. I-5

J. SOME STYLE COMMENTS FOR TECHNICAL COMMUNICATION (PARAPHRASING THE NOTES OF M. STANDING AND M. GOLAN)

- Introduce smoothly the topic to the reader. Use as many aids as possible to accomplish that.
- Think of what you want to communicate with the sentence before writing it.
- Use active verbs.
- Give the most important information at the beginning of the sentence. It must be clear and objective.
- Differentiate between "observed", "calculated", "assumed", "guessed".
- Limit sentences to 30 words.
- Avoid clichés, watery and loaded statements that do not add any important information.
- Reference properly your statements.
- Give the proper context and take enough time when introducing and discussing a figure or a diagram.
- All figures and tables should be discussed in the text.
- Use proper English, select the right words and verbs.
- Your statements should be, as much as possible, defendable in a court of Law.